Electronic Supplementary Material (ESI) for Green Chemistry.

Synthesis, Characterisation and Carbon Dioxide Capture Capacities of Hierarchically Porous Starbons®

Supporting Information

Han Li, Cheng Li, Vitaliy L. Budarin, James H. Clark,* Michael North,* Jinxiu Wang and Xiao Wu

The original data used to generate the results reported in this manuscript and supporting information are freely available at
DOI: 10.15124/f3451289-dcf9-45b2-802e-7175aa073538

Contents

Procedures for the synthesis of activated Starbons®

Unactivated Starbons® (X300 and X800) were prepared by the freeze drying method as previously reported (A. Borisova, M. De Bruyn, V. L. Budarin, P. S. Shuttleworth, J. R. Dodson, M. L. Segatto and J. H. Clark, *Macromol. Rapid Commun.* 2015, **36**, 774–779).

KOH activated Starbons®

Starbon® X300 (1 g) was impregnated with KOH (KOH:X300, 1:1 to 5:1, w:w) using a solution of KOH (100 mL) in EtOH:H_2O (95:5, v:v) and stirred overnight at room temperature. The solvent was then evaporated at 60 ^oC under vacuum using a rotary evaporator and the resulting mixture was dried in a vacuum oven at 80 ^oC for 24 hours. Activation was then carried out by heating the resulting powder in a ceramic crucible placed in a HORIBA Scientific tube furnace under a flow of pure N_2 (100 cm^3 min^{-1}) with a heating rate of 2 ^oC min^{-1} to the final temperature of 600, 800 or 1000 ^oC. The temperature was held at the final temperature for 1 hour, then allowed to cool to room temperature. The residue was then washed first with 2M HCl and then with distilled water until the pH of the filtrate was approximately 7.0, to remove excess KOH and other potassium salts. Residual solvent was removed by centrifugation followed by drying at 80 ^oC for 24 hours to leave the KOH activated Starbons as black powders.

Sample	Yield (g)		Sample	Yield (g)		Sample	Yield (g)
S800K1	0.265		A800K1	0.270		P800K2	0.344
S800K2	0.432		A800K2	0.372		P800K3	0.227
S800K3	0.498		A800K3	0.325		P800K5	0.119
S800K4	0.284		A800K4	0.262			
S800K5	0.252		A800K5	0.144			
S600K4	0.390		A600K2	0.379			
S1000K4	0.171		A1000K2	0.319			

CO_2 activated Starbons®

CO_2 activation was carried out in a NETZSCH STA409 coupled to a Bruker Equinox 55 FTIR. Starbon® X800 were used as the starting materials. The burn-off wt% of the X800 was monitored by the thermogravimetric instrument and the composition of the gases from the reaction of carbon with CO_2 were analysed in real time using FTIR during the activation process.

X800 (100 mg) was placed in a ceramic cup and heated from room temperature to the required temperature (700 to 1000 ^oC) with a heating rate of 10 ^oC min^{-1} under a flow of pure CO_2 (flow rate 50 cm^3 min^{-1}). The maximum temperature was maintained for the specified period of time (0 to 2 hours). At the end of the activation period, the sample was cooled under a flow of pure N_2 (flow rate 50 cm^3 min^{-1}) to give the CO_2 activated Starbons® as black powders.

Sample	Yield (mg)		Sample	Yield (mg)		Sample	Yield (mg)
S800C15	85.3		S900C90	55.8		A750C45	73.8
S850C15	83.4		S900C120	48.5		A750C60	70.0
S900C15	77.5		S950C30	53.1		A750C90	61.8
S950C15	67.6		S950C60	36.0		A900C0	63.8
S1000C15	34.1		S950C90	29.4		A900C10	31.7
S900C30	74.0		S950C120	17.5		P700C50	64.5
S900C60	63.0					P900C0	27.1

O_2 activated Starbons®

O_2 activation was carried out in a NETZSCH STA409 coupled to a Bruker Equinox 55 FTIR. Starbon® X800 were used as the starting materials. The burn-off wt% of the X800 was monitored by the thermogravimetric instrument and the composition of the gases from the reaction of carbon with O_2 was analysed in real time using FTIR during the activation process.

X800 (100 mg) was placed in a ceramic cup, subjected to a flow of 200 cm^3 min^{-1} N_2 and 20 cm^3 min^{-1} air (overall O_2=2%) and heated from room temperature to the required temperature (400 to 800 ^oC) with a heating rate of 10 ^oC min^{-1}. The maximum temperature was maintained for the specified period of time (0 to 1 hour). At the end of the activation period, the sample was cooled under a flow of pure N_2 (flow rate 50 cm^3 min^{-1}) to give the O_2 activated Starbons® as black powders.

Sample	**Yield (mg)**		**Sample**	**Yield (mg)**		**Sample**	**Yield (mg)**
S700O0	81.6		A500O30	83.1		P400O50	74.5
S750O0	74.5		A500O60	66.9		P500O30	74.3
S800O0	70.6		A750O0	77.9		P750O0	71.7
S750O40	49.9						
S750O56	39.9						

Methodology for the characterisation of Starbons®

Porosimetry

The textural properties of all samples were investigated by measuring nitrogen adsorption-desorption isotherms on a Micromeritics ASAP 2020 volumetric adsorption analyser at 77 K. Before the analyses, the powdered samples (~0.1g) were degassed at 200 ^{o}C for 8 hours to remove moisture and other contaminants. The BET model was applied for the determination of surface area and the BET surface area was calculated from the nitrogen adsorption data at a relative pressure range of 0.01-0.2; the total pore volume (V_{total}) was estimated at a relative pressure of 0.99; the Barrett-Joyner-Halenda (BJH) method was used for determination of mesopore volume and mesopore size distribution. The HK method for carbon materials with slit-shaped pores was applied for the determination of micropore volume (V_{micro}), ultramicropore volume ($V_{ultramicro}$) and micropore size distribution. The DFT method assuming a slit pore model and a non-local DFT method (NLDFT) assuming a non-homogeneous fluid at a solid interface in a slit pore model were also applied for the characterisation of the pore volumes in the activated Starbons®.

ICP-OES analysis

ICP-OES analysis of the elemental composition of Starbon® samples was carried out by the Biorenewables Development Centre using an Agilent 7700 series inductively coupled plasma-optical emission spectrometry (ICP-OES). Samples (~50 mg) were digested by a solution of nitric acid and hydrogen peroxide (10 mL, 4:1, v:v). The mixture was microwave heated to 200 ^{o}C over 30 minutes, and the temperature was held at 200 ^{o}C for 15 minutes. After cooling down, the mixtures transferred into 100 mL conical flasks and diluted to up to the mark with distilled water and then analysed. The results for each element were fitted onto a calibration curve. The results recorded were then multiplied by the dilution factor, to produce the concentration for each element in the samples.

CHN analysis

The quantity of carbon, hydrogen and nitrogen in Starbon® samples were determined by the CHN analysis service of the University of York using an Exeter Analytical Inc. CE-440 analyser and a high temperature combustion method.

XPS analysis

Surface characterization by XPS analysis was performed by the UK national XPS service at the University of Cardiff using a Thermo K-Alpha+ XPS fitted with a monochromated Al kα X-ray source. Data were collected at a pass energy of 2150 eV for survey spectra and 40 eV for high-resolution scans. The spectra were collected at a pressure below 10^{-7} Torr and a temperature of 294 K. Peaks were fit with a Shirley background prior to component analysis. Data was analysed using CasaXPS (v2.3.34) after subtraction of the background and using modified sensitivity factors as supplied.

SEM imaging

The morphology of samples was studied using a scanning electron microscope (SEM, JEOL 7800F) at an accelerating voltage of 5 kV and a working distance of 10 mm with a LED detector. Energy dispersive X-ray spectrometry (EDS) analysis was performed by setting the accelerating voltage to 15 kV. The sample was mounted on an aluminium plate and coated with carbon to increase the conductivity prior to analysis.

TEM imaging

The morphology of samples was also observed using transmission electron microscopy (JEOL 2011 TEM) at an accelerating voltage of 100 kV. Samples were prepared by sonicating the material in ethanol and depositing it on a holey carbon support film on a 300 mesh copper grid.

CO_2 adsorption studies

CO_2/N_2 composition swing

The CO_2 adsorption of samples was investigated using a STA 625 thermal analyser with a gas composition swing method. Before each measurement, the sample (~10.0 mg) was heated at 373 K for 1 hour under a flow of N_2 (60 ml min^{-1}) to ensure the removal of residual water and impurities. After cooing to room temperature under N_2, the sample was heated to 308 K at 1 ^oC min^{-1} under a flow of N_2 (60 ml min^{-1}) and then the temperature was kept at 308 K during remainder of the analysis. A three-way valve was employed to switch the gas flow between pure CO_2 (60 ml min^{-1}) and pure N_2 (60 ml min^{-1}) for CO_2 adsorption and desorption, respectively. For experiments carried out using CO_2 partial pressures of 0.15-0.83 bar instead of pure CO_2, the three-way valve was set to give the appropriate CO_2 and N_2 flow rates whilst keeping the total gas flow rate constant at 60 ml min^{-1}. The changes in mass and heat flow were recorded by the TGA and DSC capabilities of the STA 625 respectively. Multiple adsorption and desorption cycles were run to determine the reproducibility of the data and the regenerability of the samples. Calculations of adsorption capacities and enthalpies of adsorption were carried out on the basis that the observed changes in mass and heat flow were entirely due to adsorption or desorption of carbon dioxide as other experiments (nitrogen porosimetry at 35 ^oC, volumetric N_2 adsorption, and the high CO_2 to N_2 selectivities determined volumetrically) showed that at 35 ^oC, adsorption of N_2 onto these materials was negligible relative to the amount of CO_2 adsorbed.

CO_2 and N_2 adsorption isotherm studies

The adsorption isotherms of pure CO_2 and N_2 for selected Starbon® samples were measured volumetrically at Fudan University, using a Quantachrome Isorb HP2 instrument. Before measurement, all samples were degassed under vacuum at 473 K for 8 hours. The CO_2 and N_2 adsorptions were performed under the same conditions in the range of 0 to 10 bar at 273, 298 and 323 K. For measurements at 273 and 298K, the stainless-steel sample holder was connected to an external circulating cooling device filled with an aqueous solution of ethylene glycol (1:3,v/v) to keep the temperature constant (within a variation of ± 0.02 ^oC). For measurements at 323K, the temperature control system was switched to an external heating package.

TGA-FTIR plots for starch derived CO_2 activated Starbons®

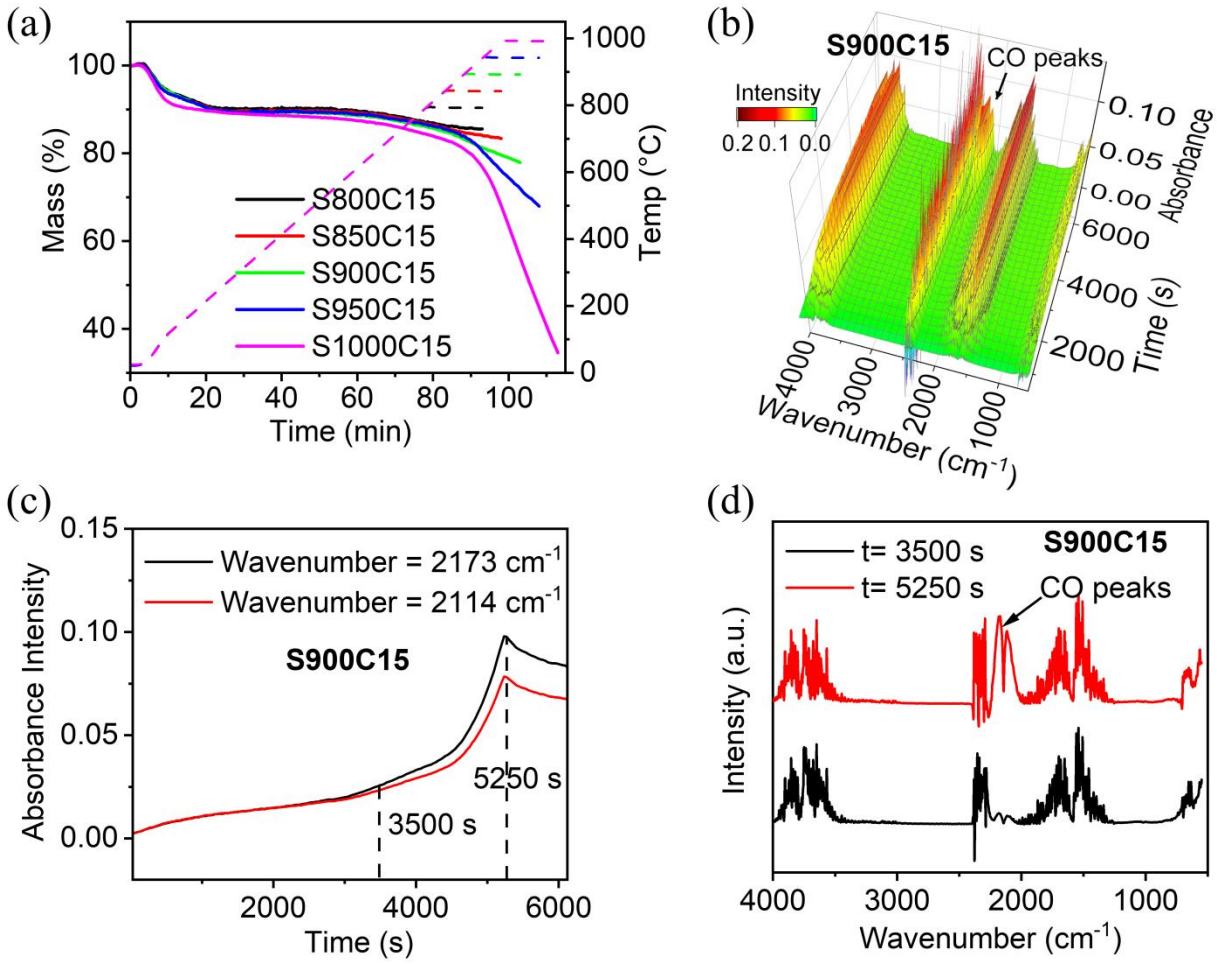

(a) TGA curves of activation time versus temperature and burn-off wt% for CO_2 activation of S800 as the temperature increases from 20 ^{o}C. The ca 10% mass loss in the first 10 minutes (up to 100 ^{o}C) corresponds to desorption of water and CO_2 from the S800.
(b) Real-time FTIR spectra of the off-gases from the preparation of S900C15 showing that formation of CO becomes pronounced at about 5250 seconds which corresponds to 900 ^{o}C.
(c) Change of absorbance with time of the FTIR spectral peaks of CO from the preparation of S900C15 showing that CO formation starts at about 3500 seconds (corresponding to 600 ^{o}C) and becomes more pronounced at about 5250 seconds (corresponding to 900 ^{o}C).
(d) FTIR spectra at 3500 (black) and 5250 seconds (red) from the preparation of S900C15 showing the change in intensity of the CO peaks.

TGA-plots for the synthesis of S900C15 with different flow rates of CO_2

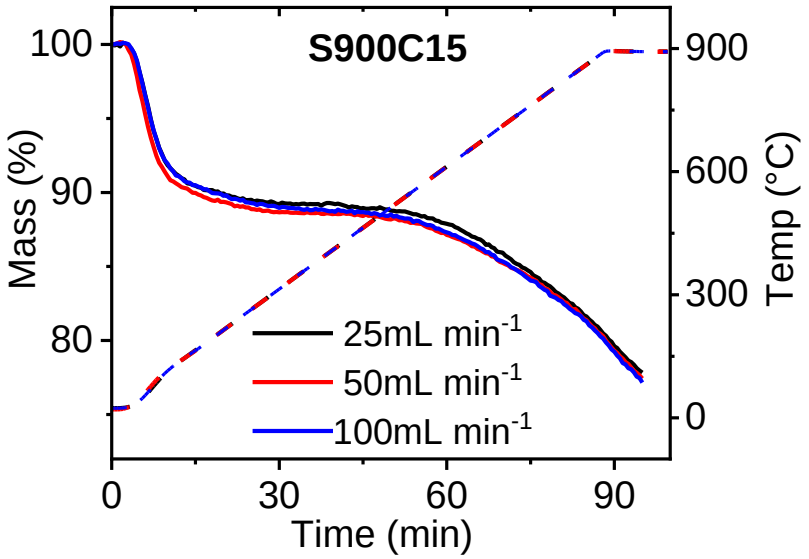

TGA-plots for the synthesis of S900C15–120 and S950C30–120

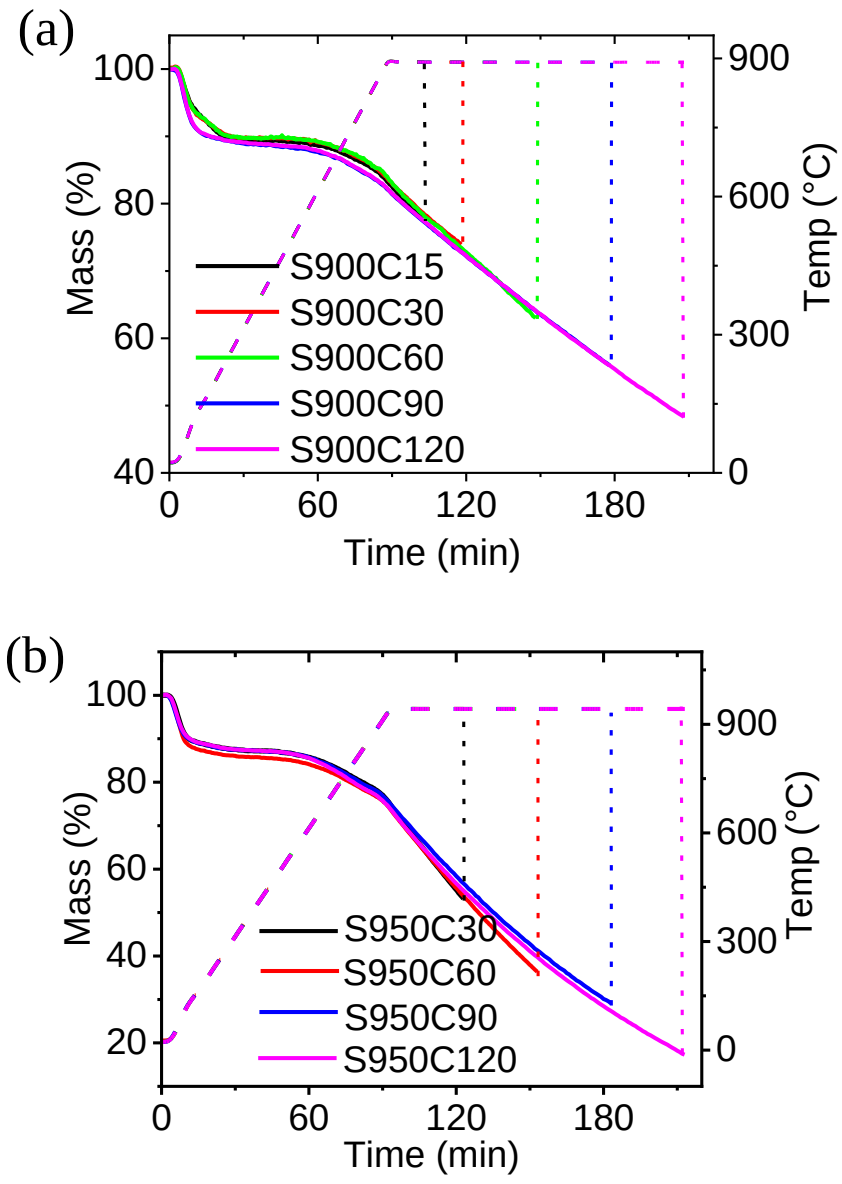

TGA-FTIR plots for alginic acid and pectin derived CO_2 activated Starbons®

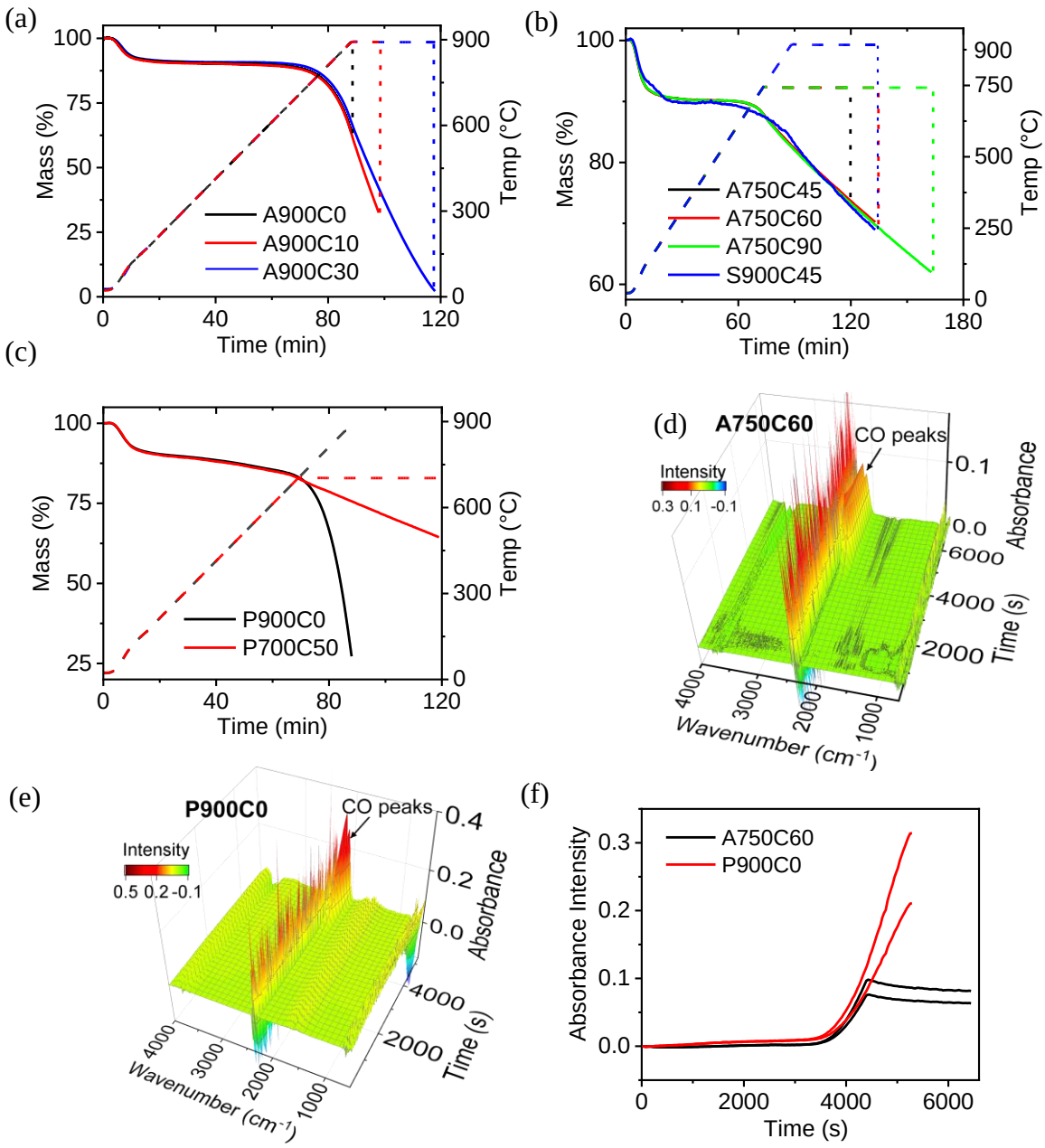

(a,b) TGA curves of activation time versus temperature and burn-off wt% for CO_2 activation of A800 as the temperature increases from 20 °C to 900 °C (a) or 750 °C (b). Plot (b) also shows data for S900C45 to illustrate that aliginic acid derived Starbons® are more readily activated with CO_2 than starch derived Starbons®. The ca 10% mass loss in the first 10 minutes (up to 100 °C) corresponds to desorption of water and CO_2 from the A800.

(c) TGA curves of activation time versus temperature and burn-off wt% for CO_2 activation of P800 as the temperature increases from 20 °C. The ca 10% mass loss in the first 10 minutes (up to 100 °C) corresponds to desorption of water and CO_2 from the P800. Comparison of the P900C0 curve in plot (c) with the A900C0 curve in plot (a) shows that pectin derived Starbons® are more readily activated with CO_2 than alginic acid derived Starbons®.

(d,e) Real-time FTIR spectra of the off-gases from the preparation of A750C60 and P900C0 showing that formation of CO becomes pronounced at about 4400 seconds which corresponds to 750 °C.

(f) Change of absorbance with time of the FTIR spectral peaks of CO during the synthesis of A700C60 and P900C0 showing that CO formation starts at about 3500 seconds (corresponding to 600 °C).

TGA-FTIR plots for starch derived O_2 activated Starbons®

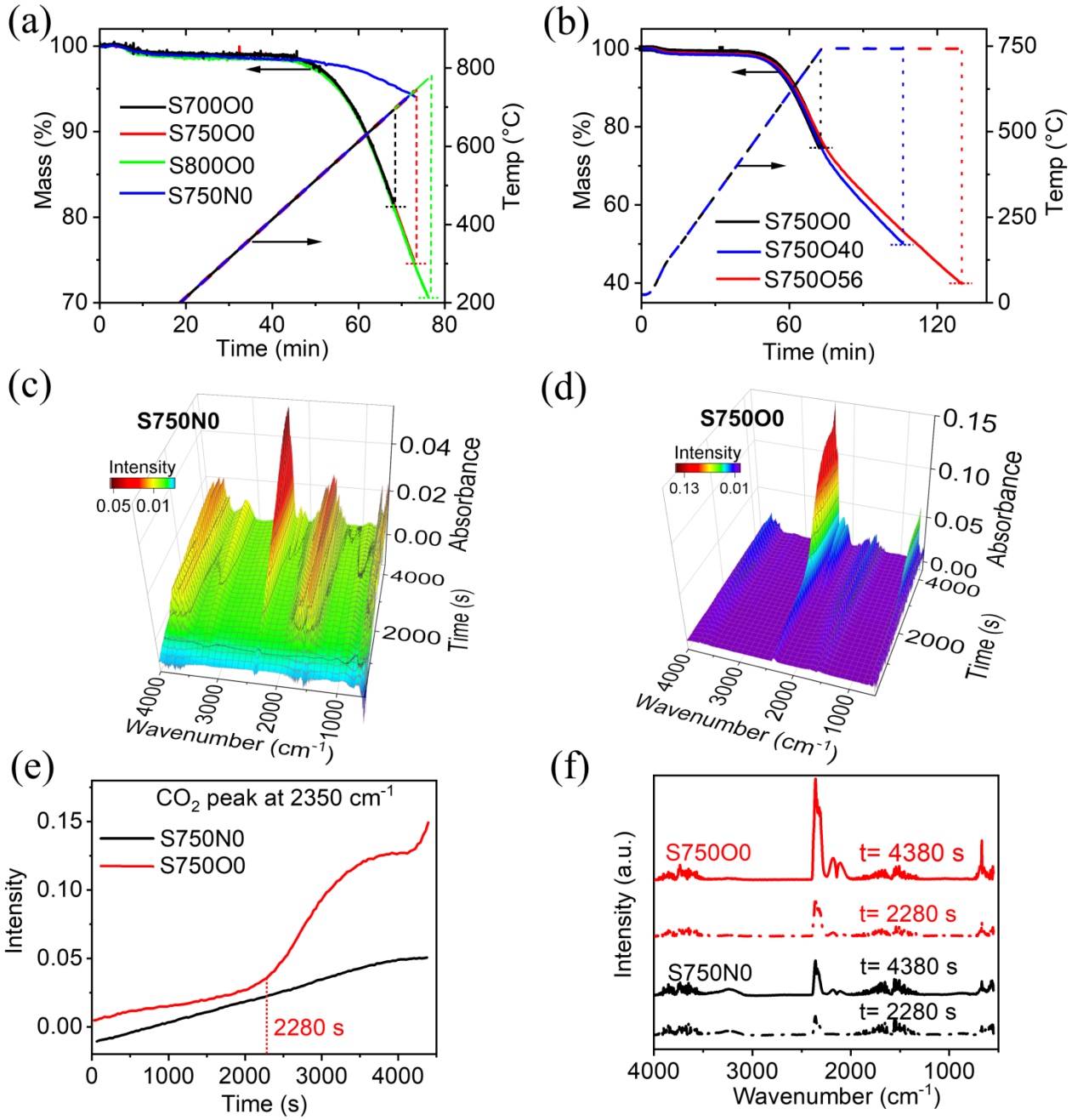

(a) TGA curves of activation time versus temperature and burn-off wt% for CO_2 activation of S800 as the temperature increases from 20 °C to 700–800 °C. A control experiment (S750N0) in which S800 was heated to 750 °C under nitrogen is also included for comparison. The small mass loss in the first 10 minutes (up to 100 °C) corresponds to desorption of water from the S800.
(b) TGA curves of activation time versus temperature and burn-off wt% for CO_2 activation of S800 as the temperature increases from 20 °C to 750 °C with hold times of 0–56 minutes at 750 °C. The small mass loss in the first 10 minutes (up to 100 °C) corresponds loss of water from the S800.
(c,d) Real-time FTIR spectra of the off-gases from the TGA experiments of heating S800 to 750 °C under nitrogen (c) and oxygen (d). Note the three-fold difference in absorbance intensity scales between the spectra in plots (c) and (d).
(e) The change of absorbance at 2350 cm^{-1} (CO_2 stretch) with time of the FTIR spectra of the off-gases obtained when S800 was heated to 750 °C under nitrogen and oxygen. In the latter case, CO_2 evolution increases markedly at 38 minutes which corresponds to 400 °C.
(f) FTIR spectra recorded of the off-gases obtained at 2280 s and 4380 s when S800 was heated to 750 °C under nitrogen and oxygen.

TGA-FTIR plots for alginic acid and pectin derived O_2 activated Starbons®

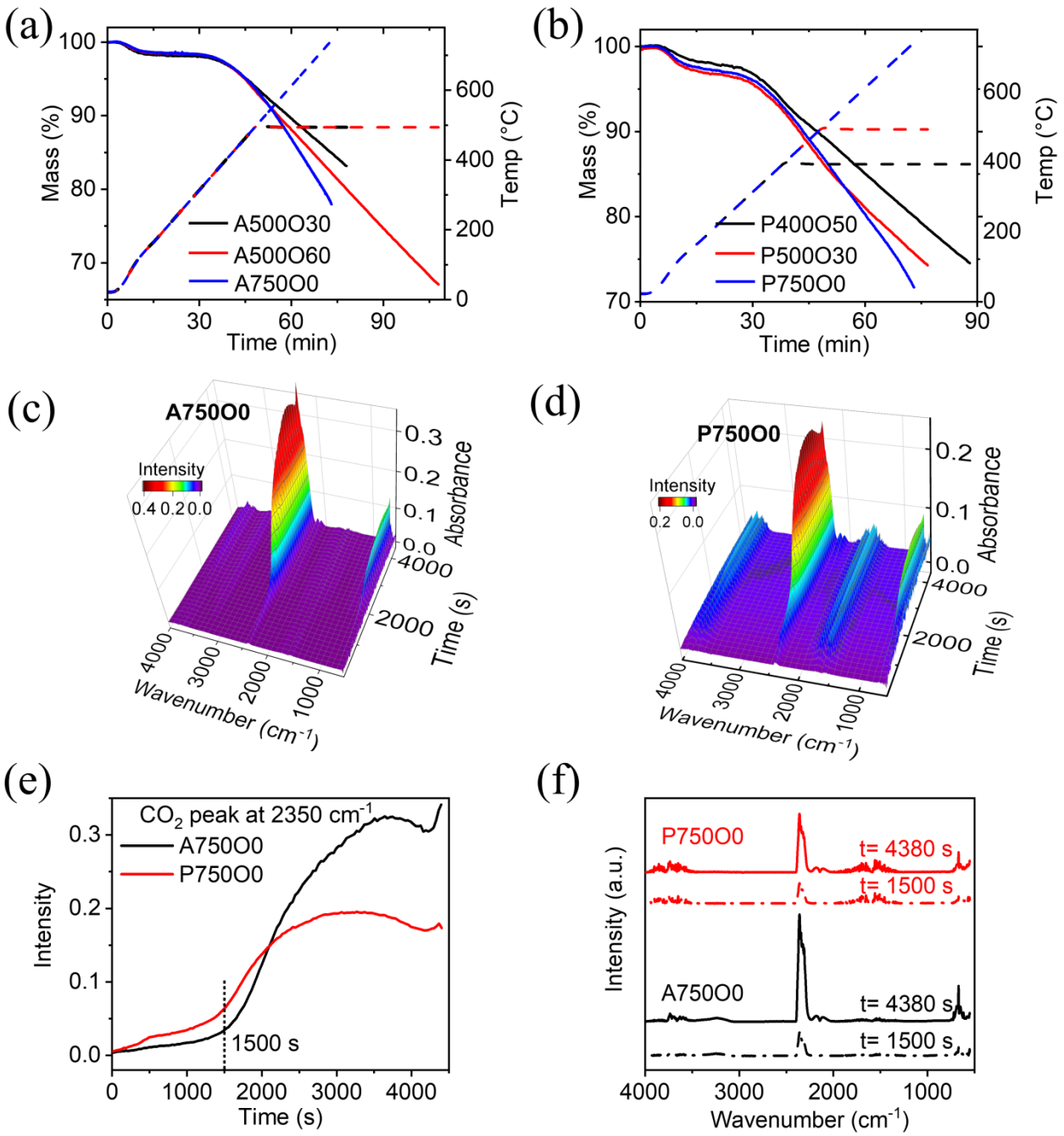

(a,b) TGA curves of activation time versus temperature and burn-off wt% for O_2 activation of A800 (a) or P800 (b) as the temperature increases from 20 °C to 750 °C.
(c,d) Real-time FTIR spectra of the off-gases from the preparation of A750O0 and P750O0 showing that formation of CO_2 becomes pronounced at about 1500 seconds which corresponds to 270 °C.
(e) The change of absorbance at 2350 cm^{-1} (CO_2 stretch) with time of the FTIR spectra of the off-gases obtained when A800 and P800 were heated to 750 °C under oxygen. CO_2 evolution increases markedly at 1500 seconds which corresponds to 270 °C.
(f) FTIR spectra recorded of the off-gases obtained at 1500 s and 4380 s when A800 and P800 were heated to 750 °C under oxygen.

Nitrogen adsorption isotherm and pore distribution plots for S300

Nitrogen adsorption isotherm (77K)

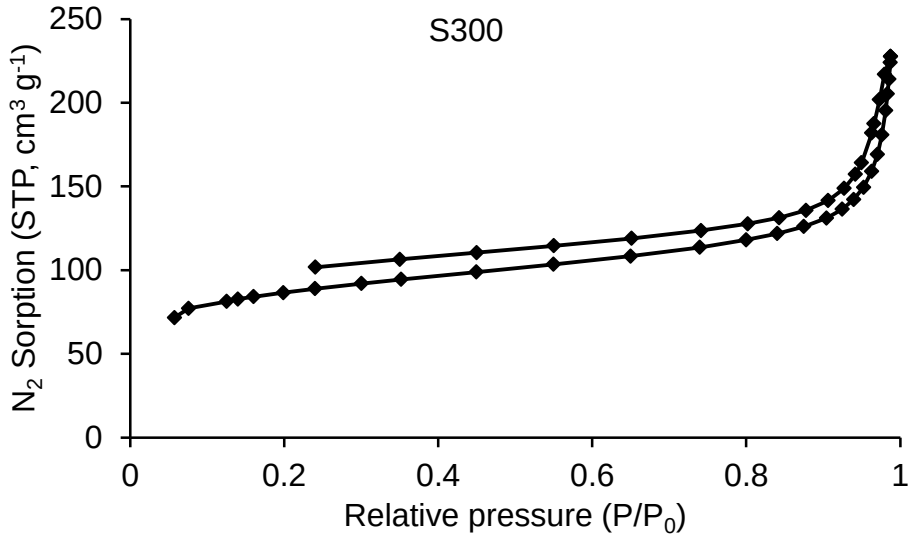

Pore distribution in the mesopore region (BJH method)

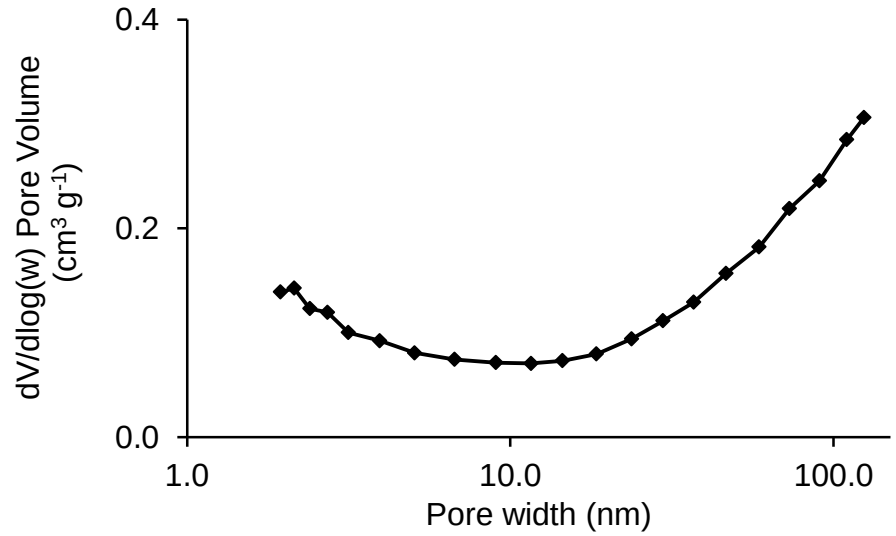

Nitrogen adsorption isotherm and pore distribution plots for A300

Nitrogen adsorption isotherm (77K)

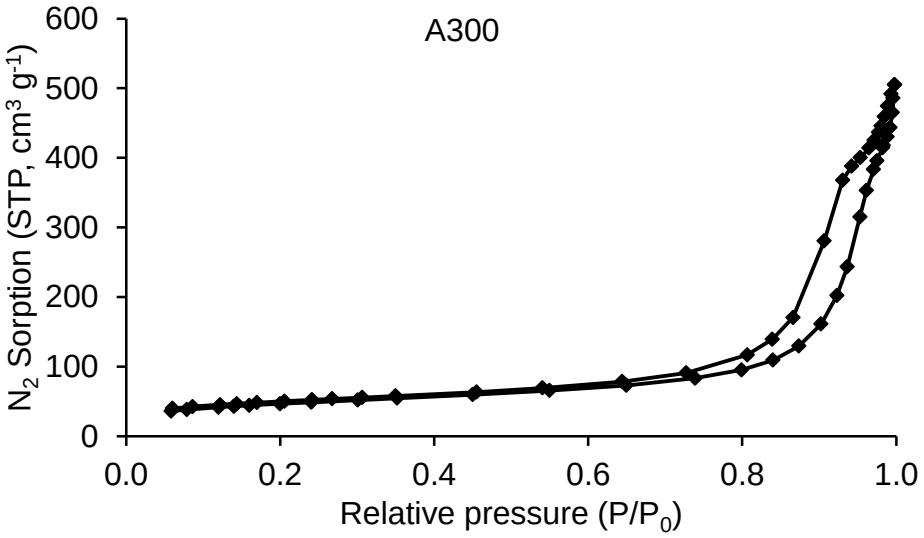

Pore distribution in the mesopore region (BJH method)

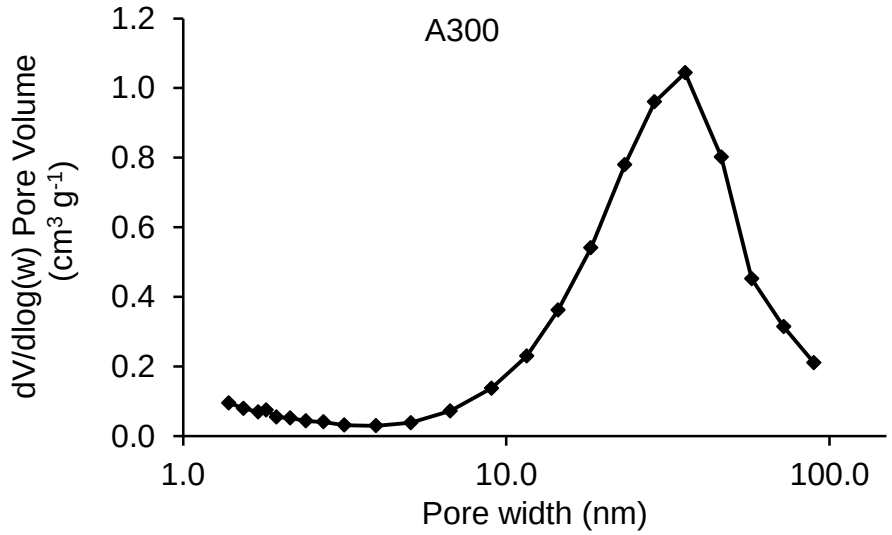

Nitrogen adsorption isotherm and pore distribution plots for P300

Nitrogen adsorption isotherm (77K)

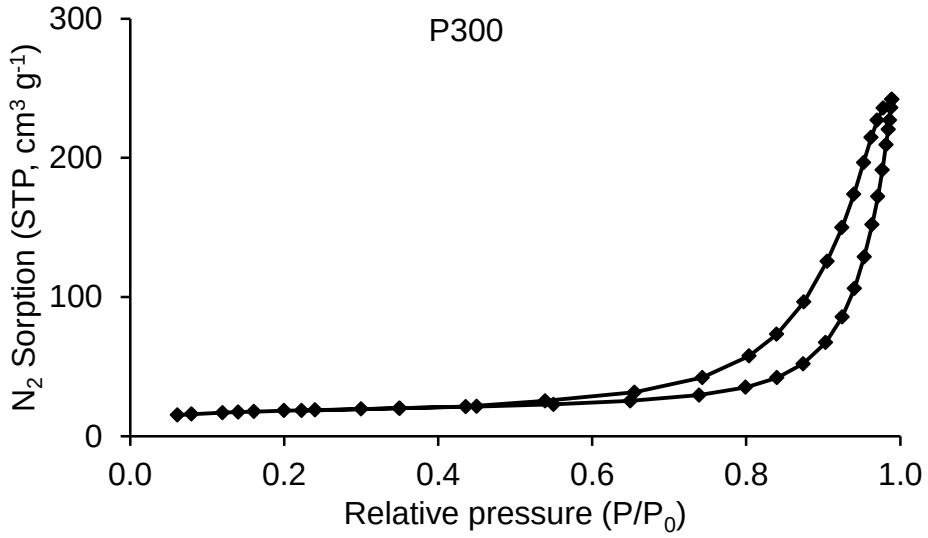

Pore distribution in the mesopore region (BJH method)

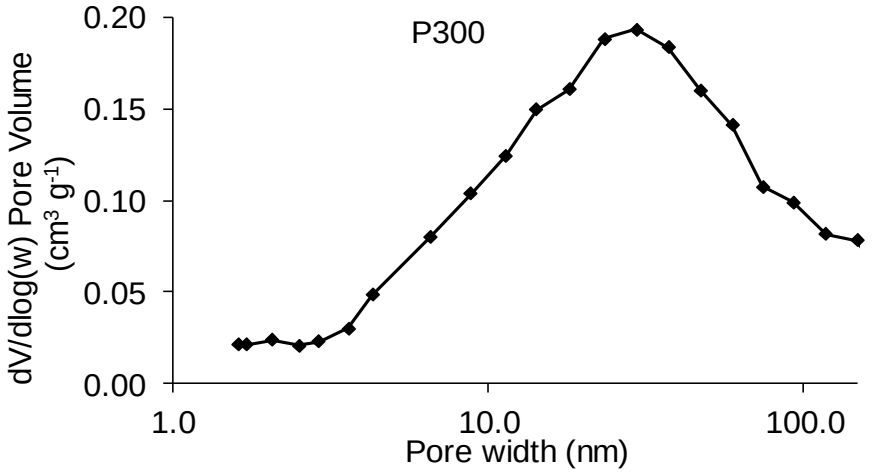

Nitrogen adsorption isotherm and pore distribution plots for S600

Nitrogen adsorption isotherm (77K)

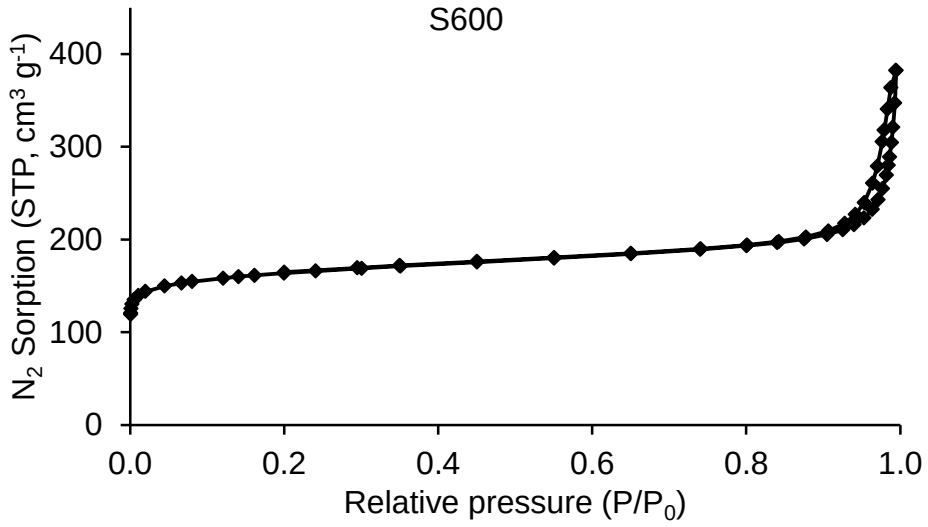

Pore distribution in the mesopore region (BJH method)

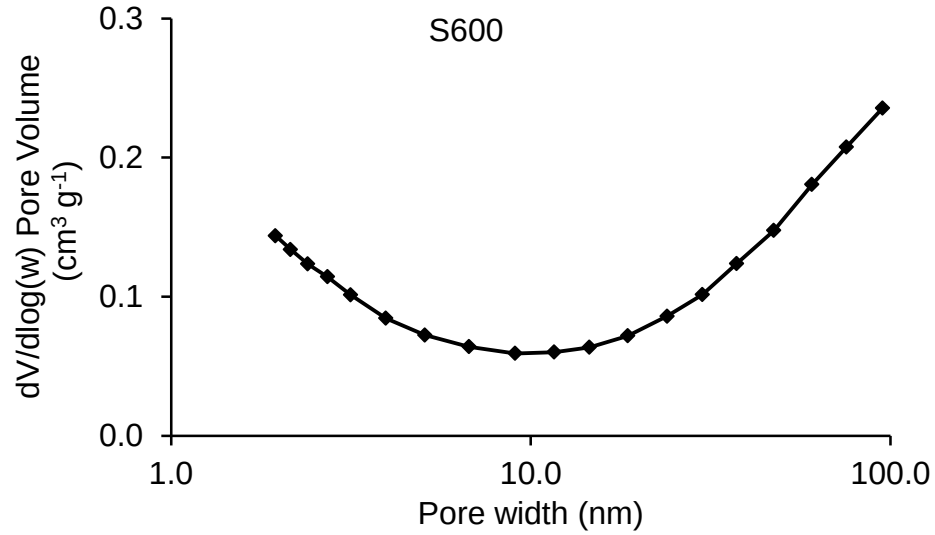

Pore distribution in the micropore region (HK method)

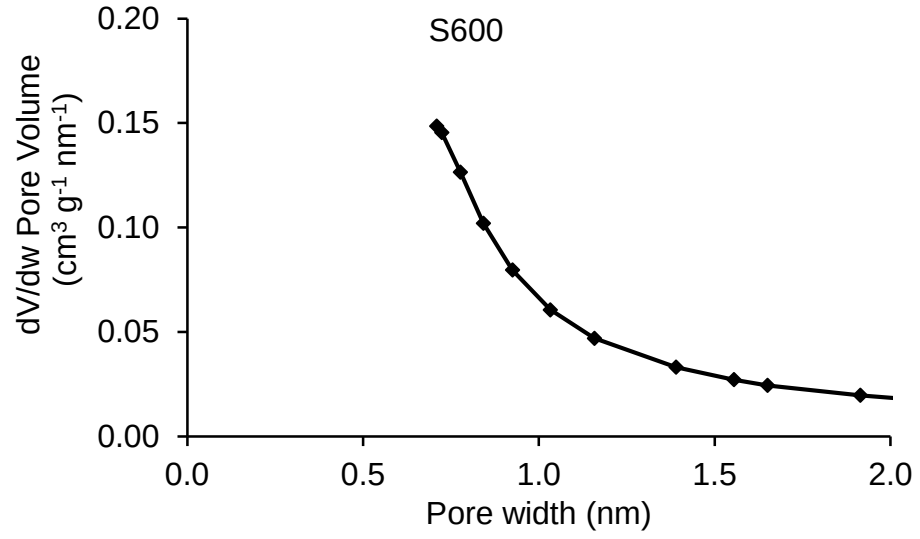

Nitrogen adsorption isotherm and pore distribution plots for S800

Nitrogen adsorption isotherm (77K)

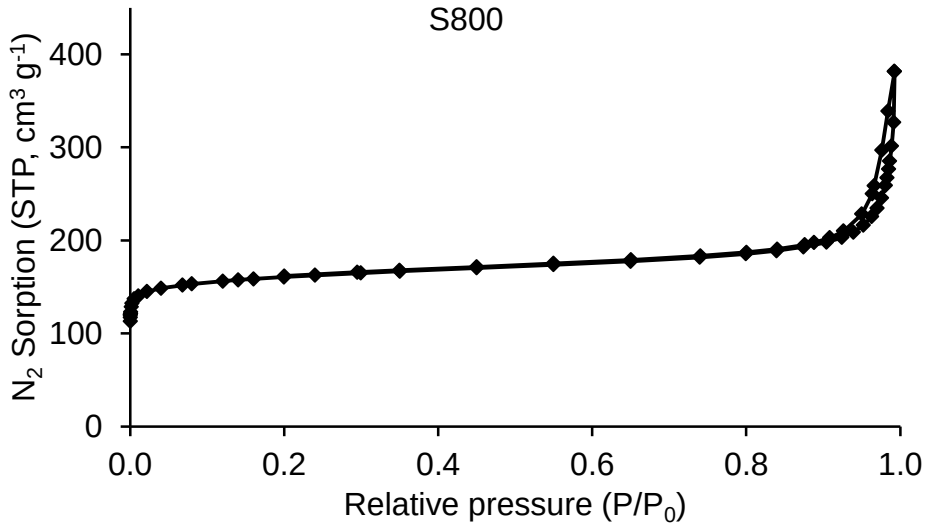

Pore distribution in the mesopore region (BJH method)

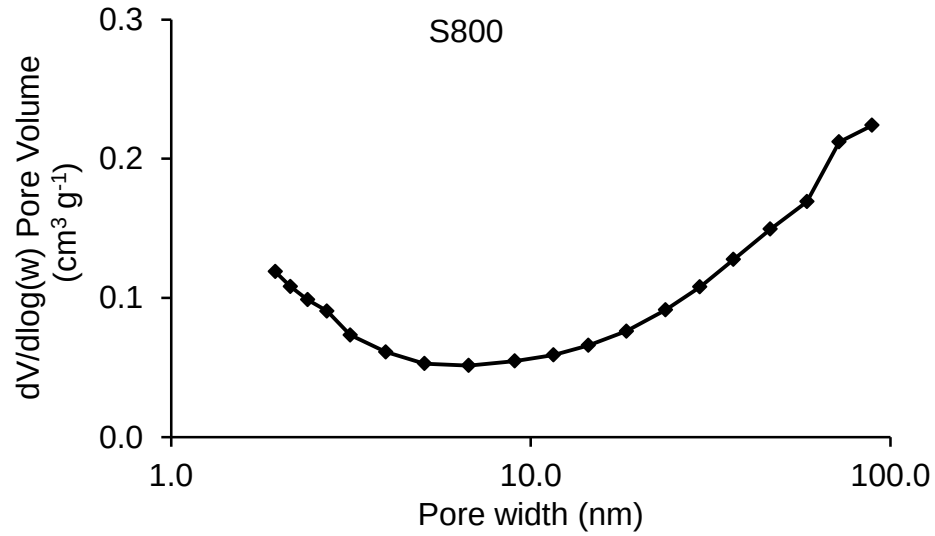

Pore distribution in the micropore region (HK method)

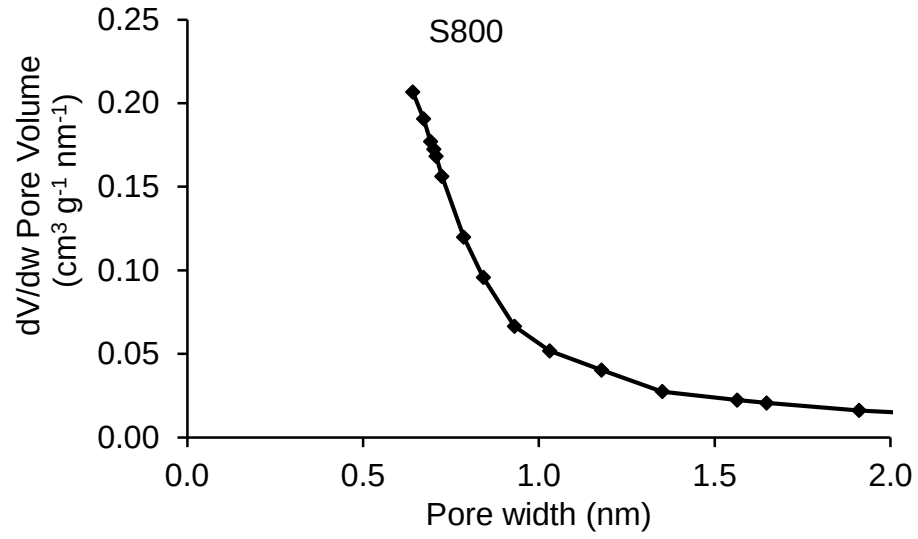

Nitrogen adsorption isotherm and pore distribution plots for A800

Nitrogen adsorption isotherm (77K)

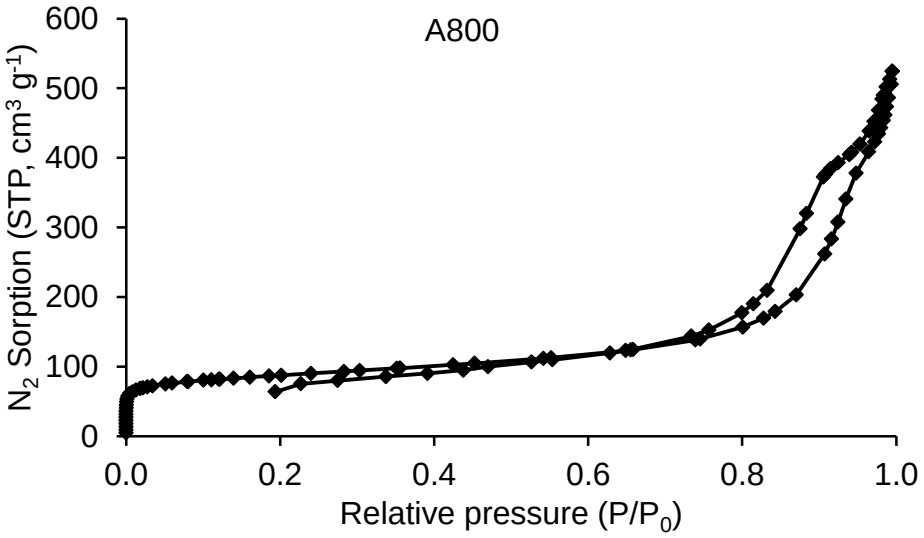

Pore distribution in the mesopore region (BJH method)

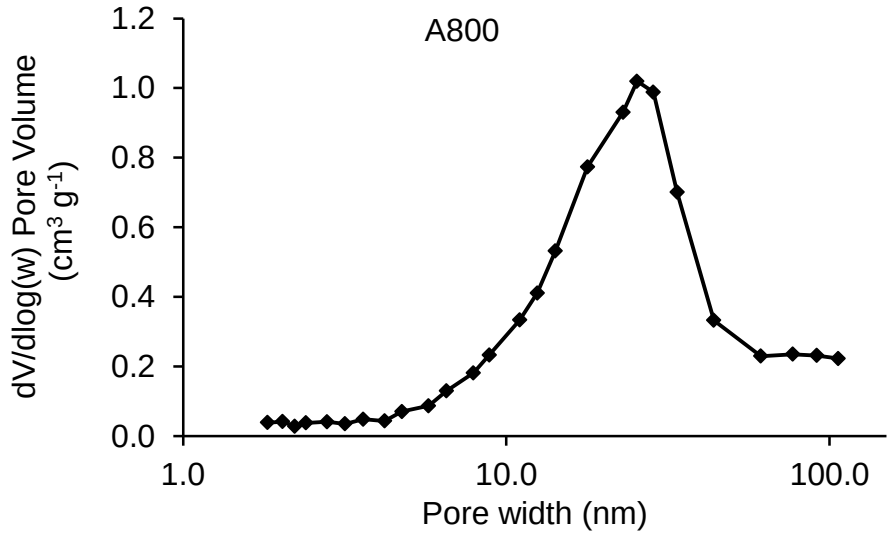

Pore distribution in the micropore region (HK method)

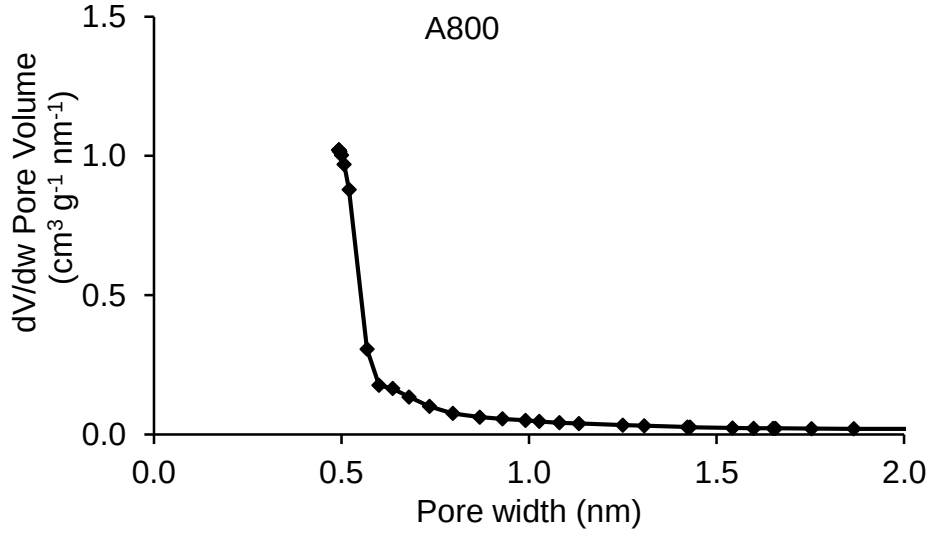

Nitrogen adsorption isotherm and pore distribution plots for P800

Nitrogen adsorption isotherm (77K)

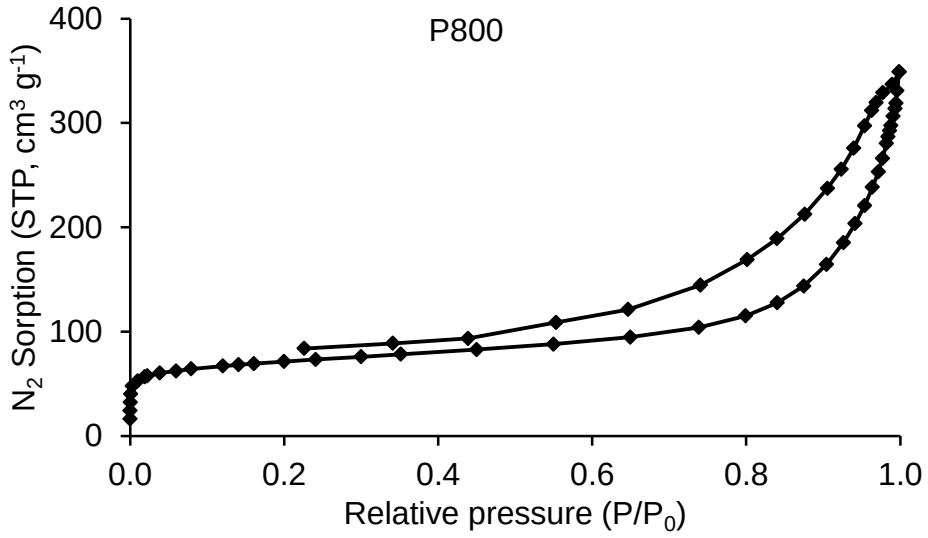

Pore distribution in the mesopore region (BJH method)

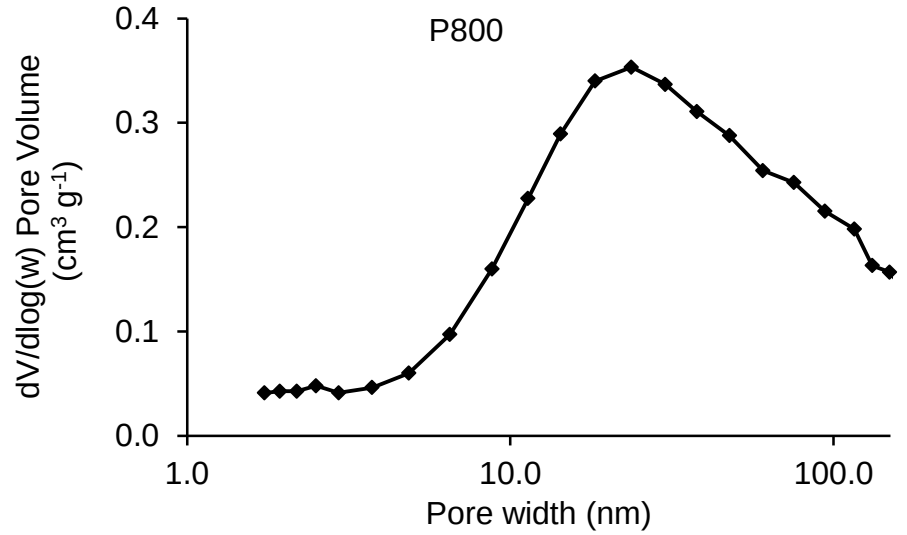

Pore distribution in the micropore region (HK method)

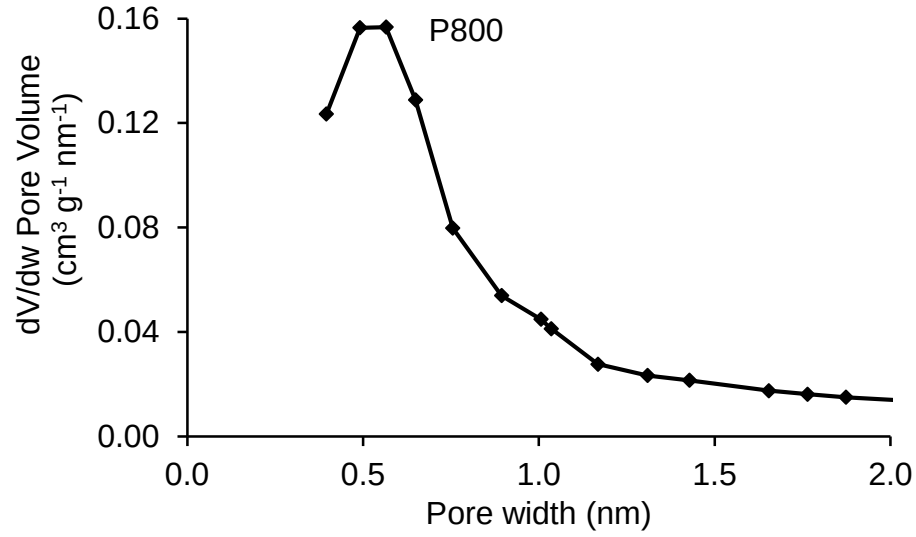

Nitrogen adsorption isotherm and pore distribution plots for S1000

Nitrogen adsorption isotherm (77K)

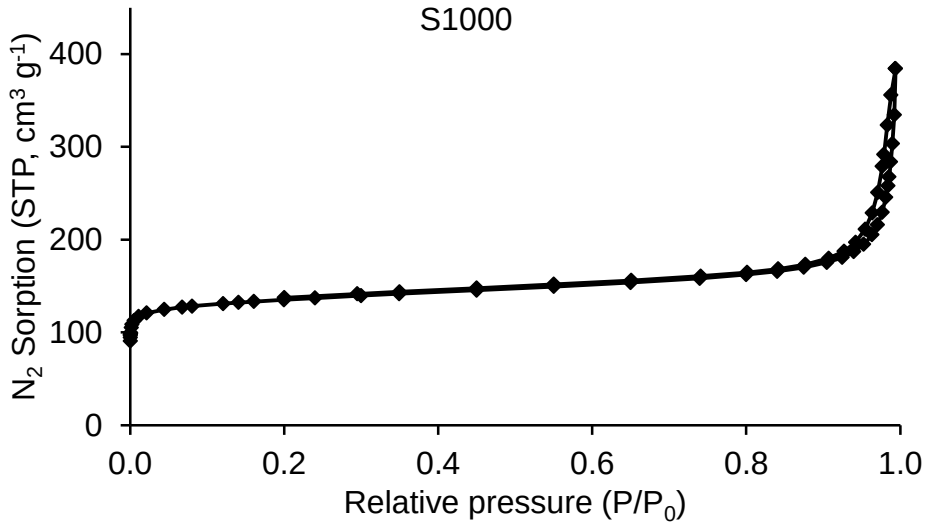

Pore distribution in the mesopore region (BJH method)

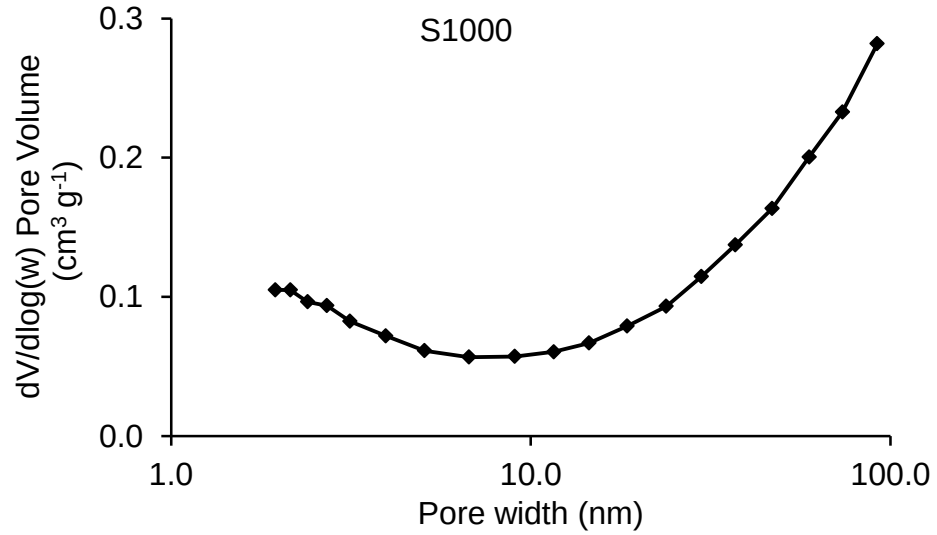

Pore distribution in the micropore region (HK method)

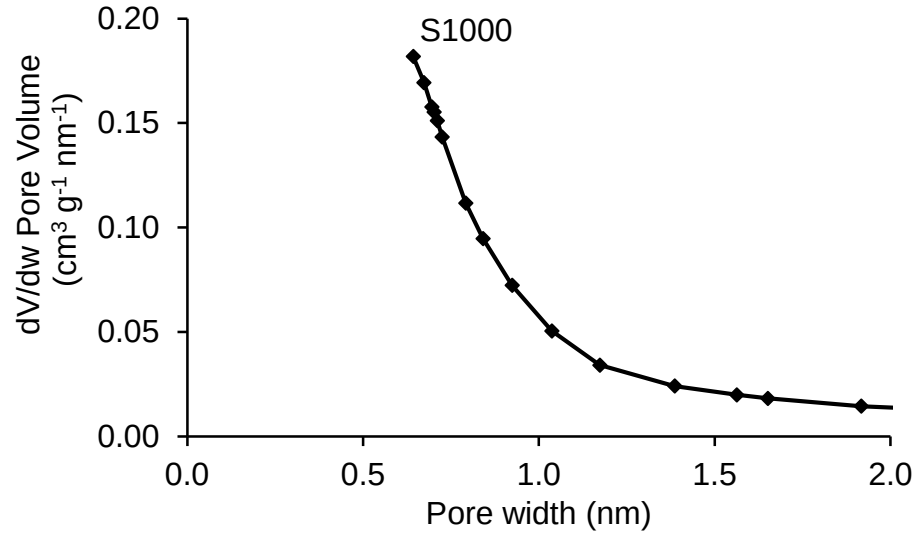

Nitrogen adsorption isotherm and pore distribution plots for S800K1

Nitrogen adsorption isotherm (77K)

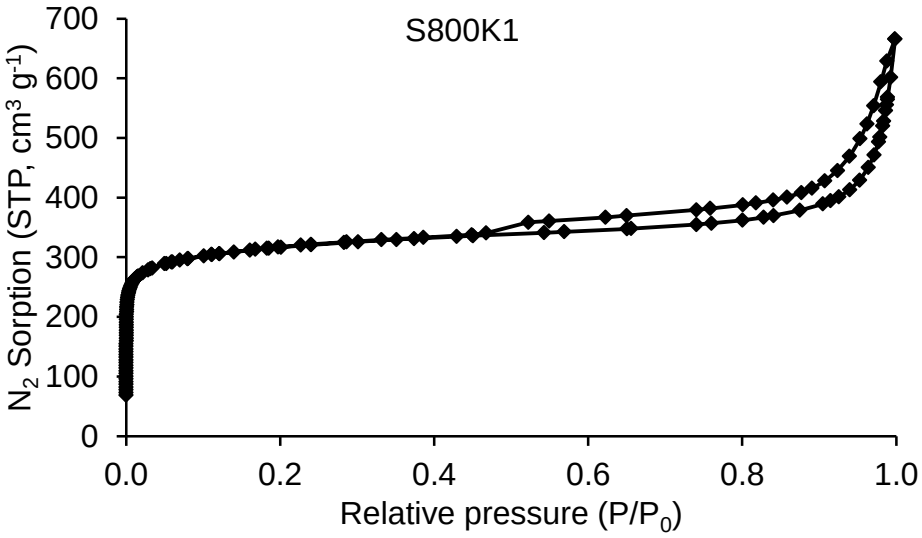

Pore distribution in the mesopore region (BJH method)

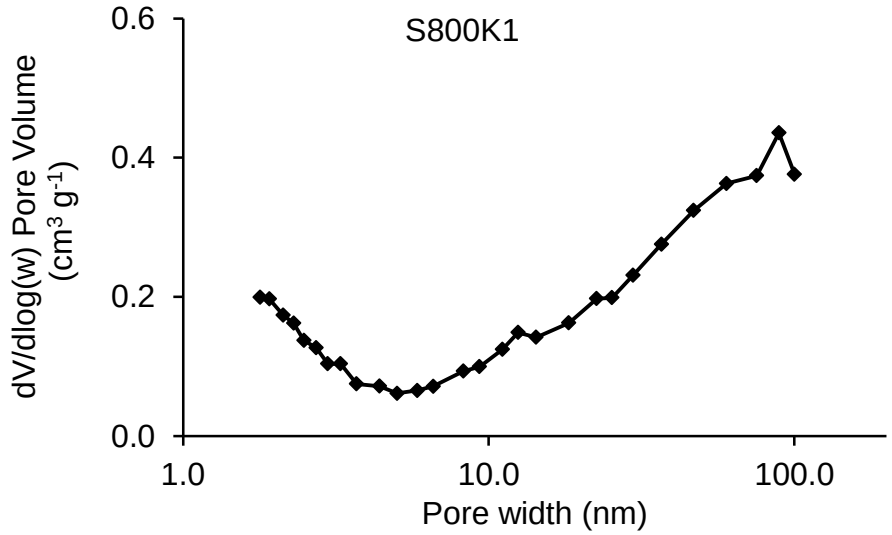

Pore distribution in the micropore region (HK method)

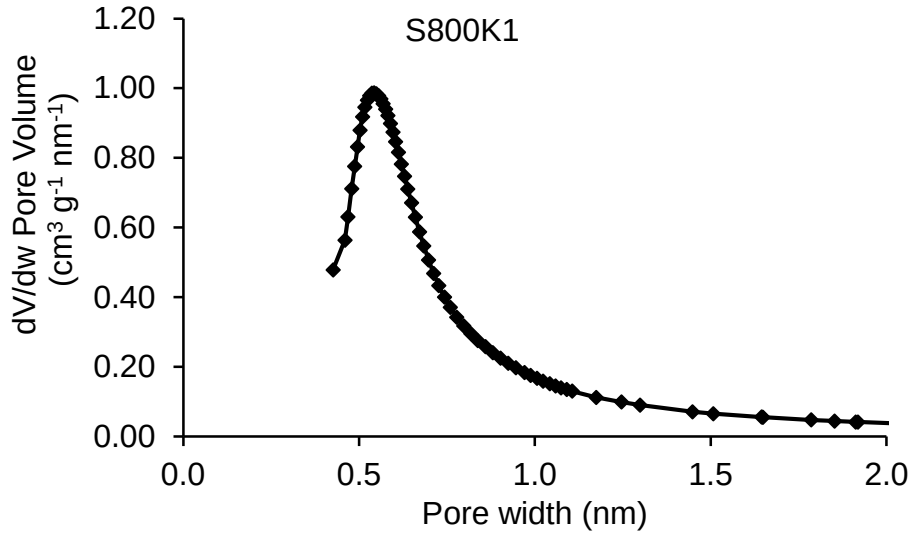

Nitrogen adsorption isotherm and pore distribution plots for S800K2

Nitrogen adsorption isotherm (77K)

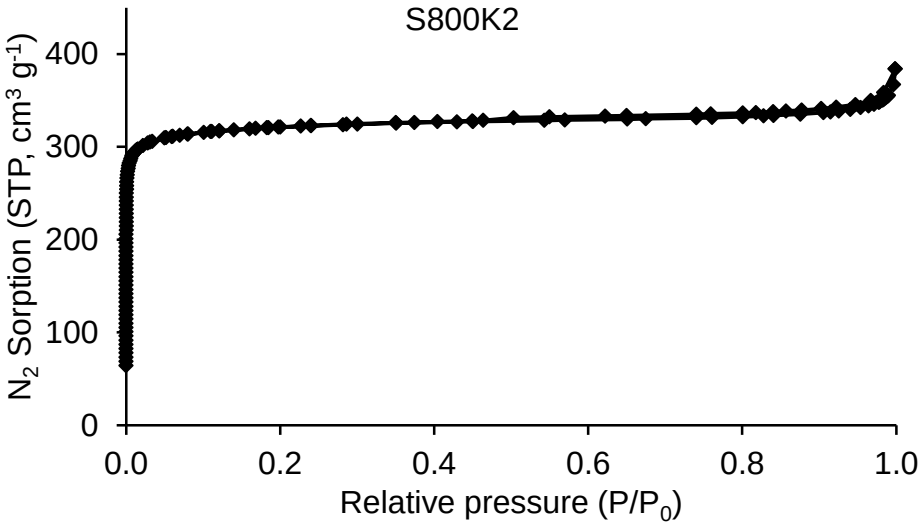

Pore distribution in the mesopore region (BJH method)

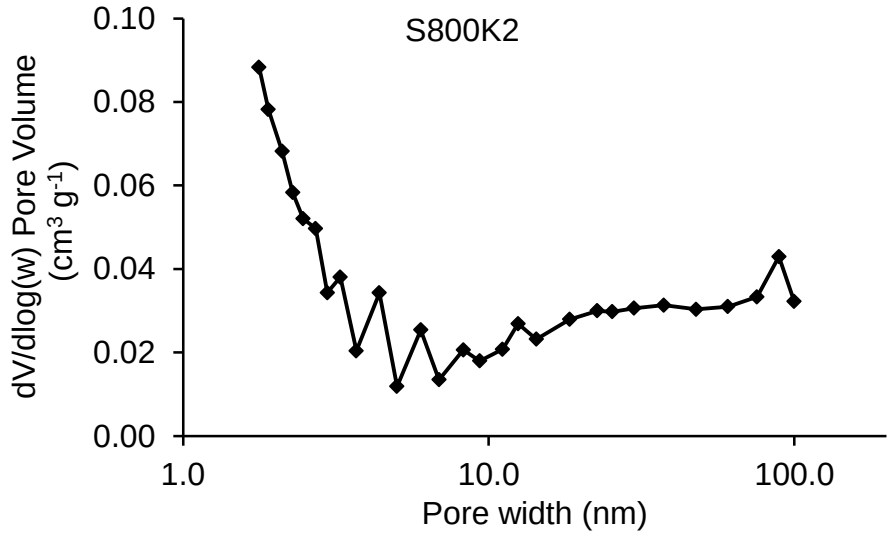

Pore distribution in the micropore region (HK method)

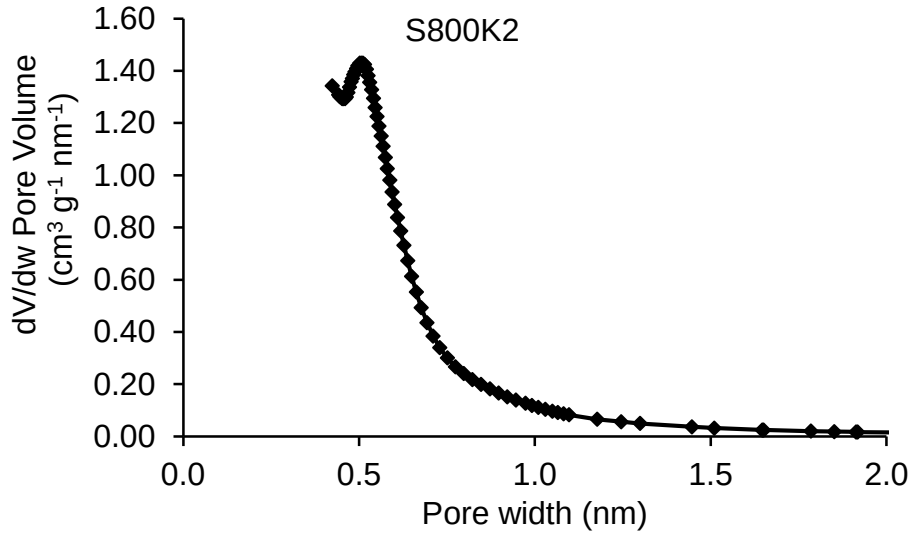

Nitrogen adsorption isotherm and pore distribution plots for S800K3

Nitrogen adsorption isotherm (77K)

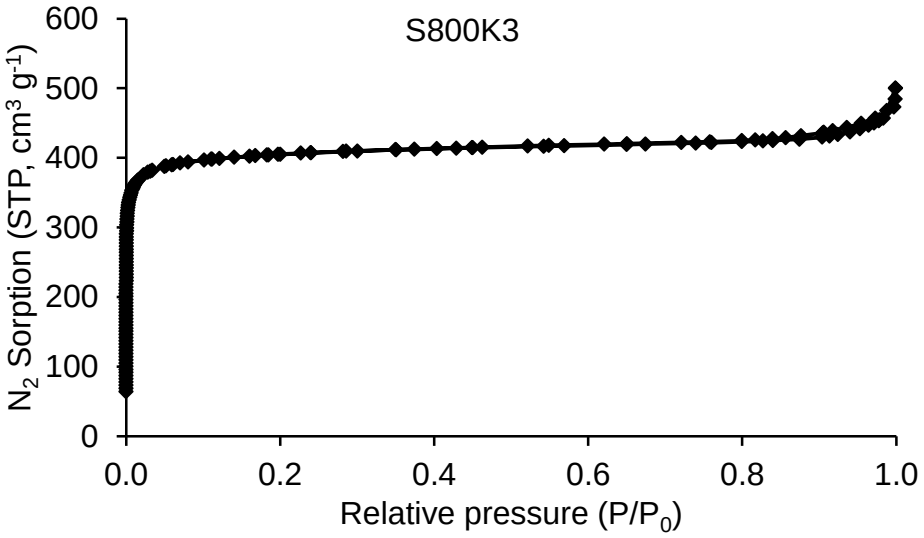

Pore distribution in the mesopore region (BJH method)

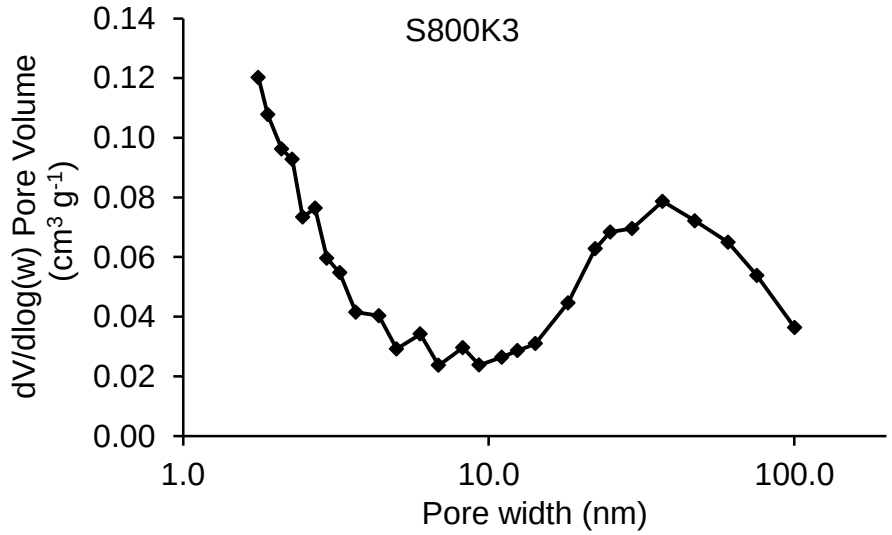

Pore distribution in the micropore region (HK method)

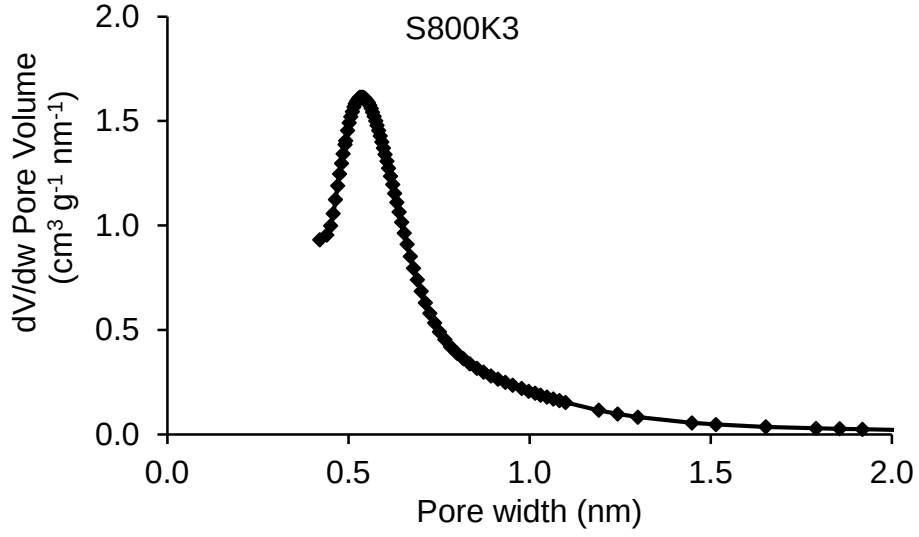

Nitrogen adsorption isotherm and pore distribution plots for S800K4

Nitrogen adsorption isotherm (77K)

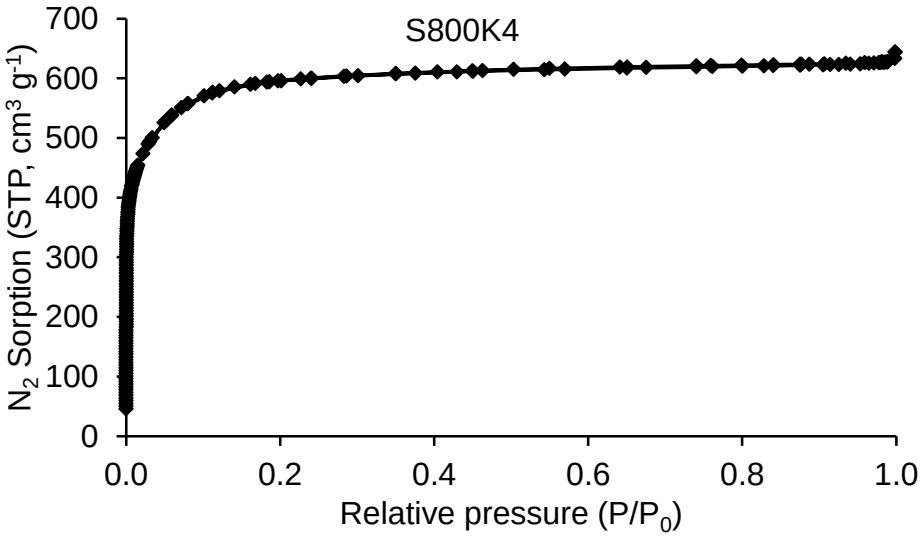

Pore distribution in the mesopore region (BJH method)

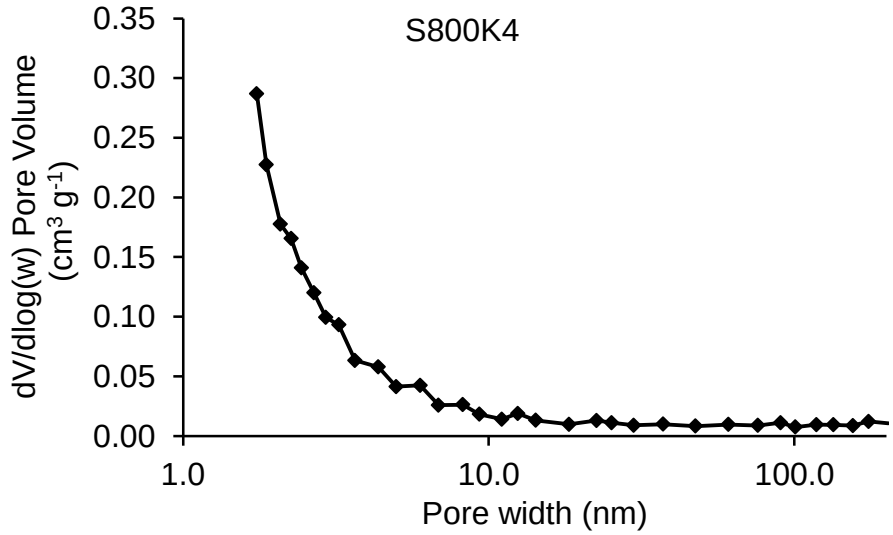

Pore distribution in the micropore region (HK method)

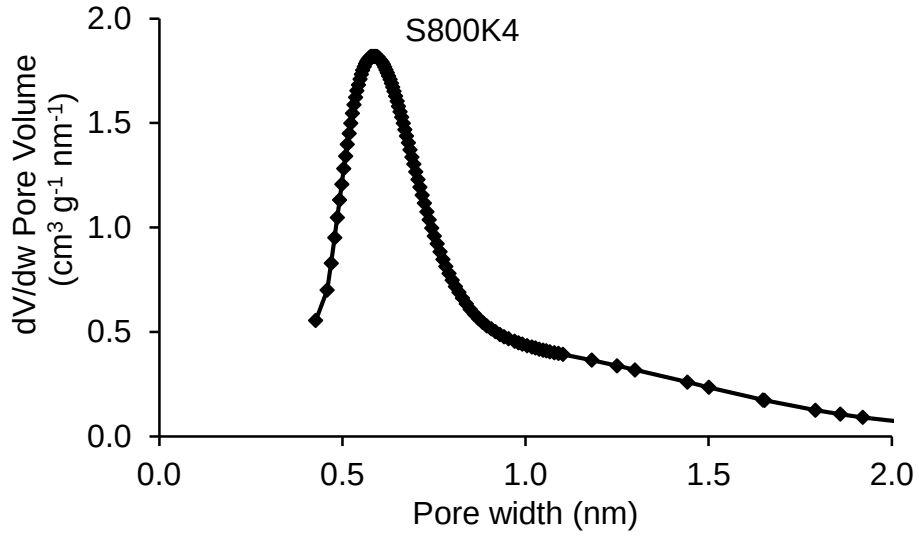

Nitrogen adsorption isotherm and pore distribution plots for S800K5

Nitrogen adsorption isotherm (77K)

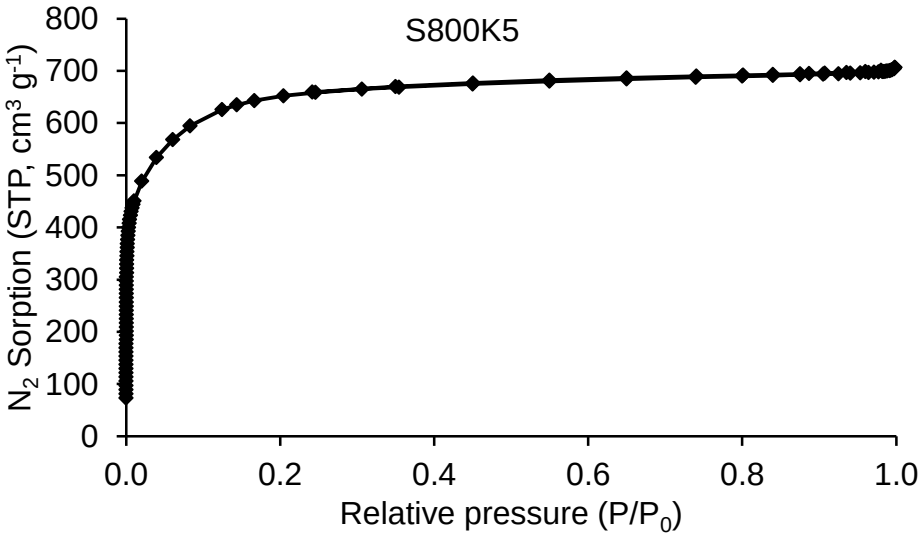

Pore distribution in the mesopore region (BJH method)

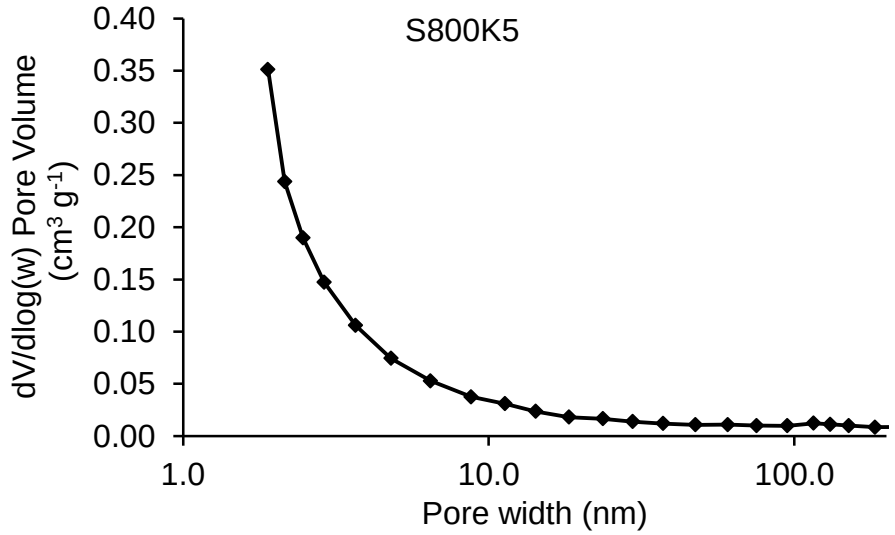

Pore distribution in the micropore region (HK method)

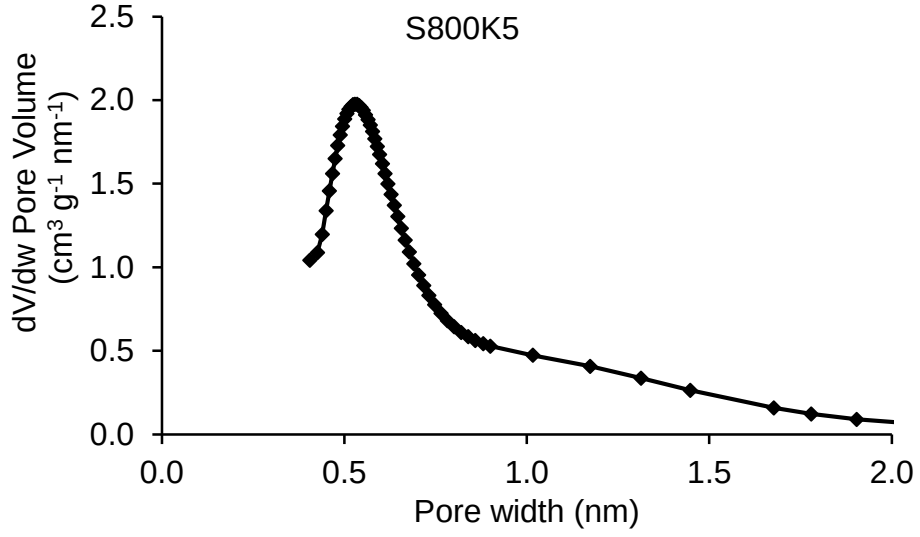

Nitrogen adsorption isotherm and pore distribution plots for S600K4

Nitrogen adsorption isotherm (77K)

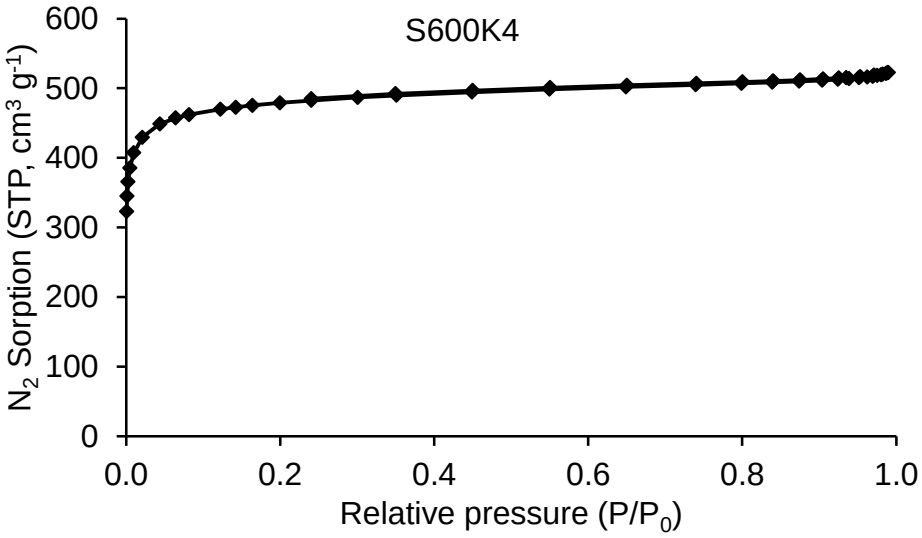

Pore distribution in the mesopore region (BJH method)

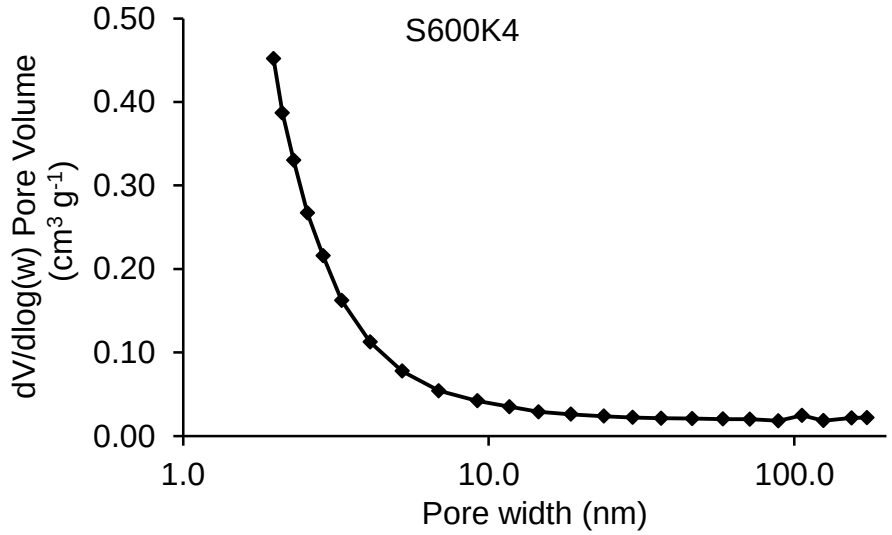

Pore distribution in the micropore region (HK method)

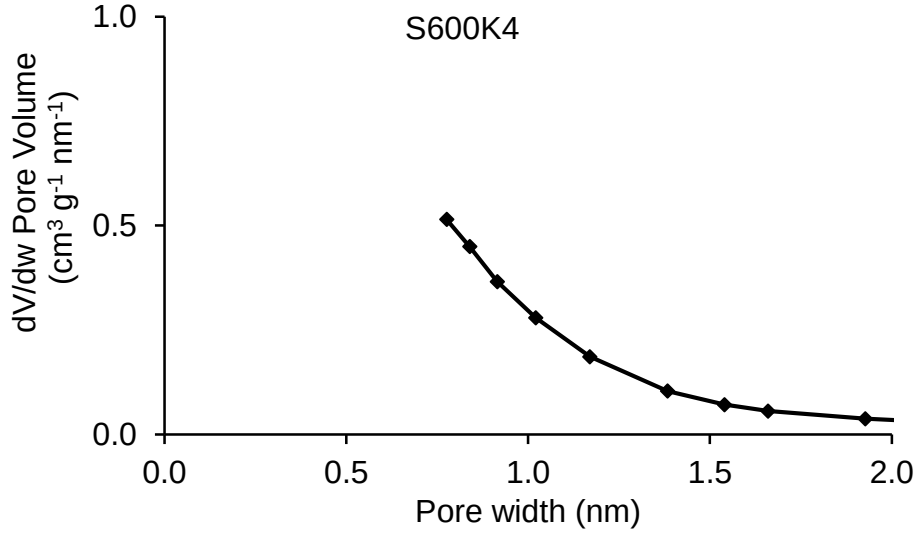

Nitrogen adsorption isotherm and pore distribution plots for S1000K4

Nitrogen adsorption isotherm (77K)

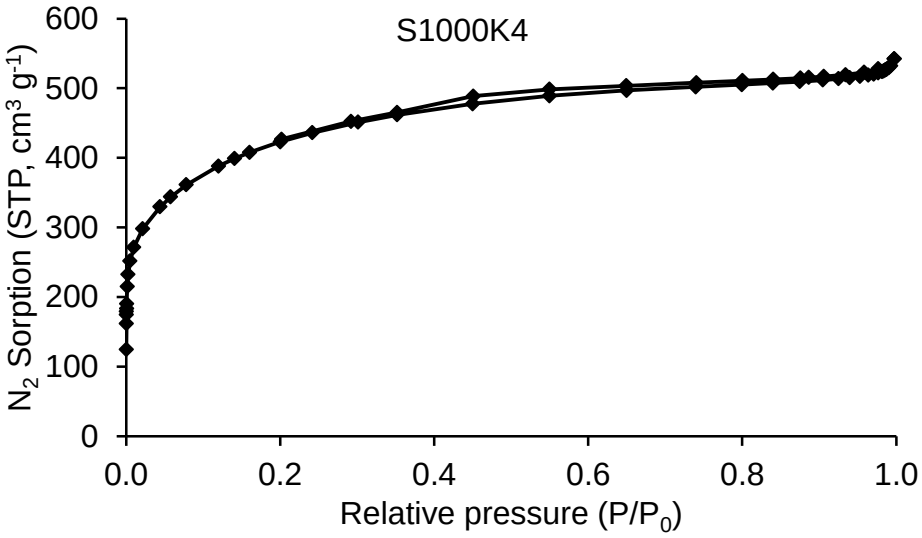

Pore distribution in the mesopore region (BJH method)

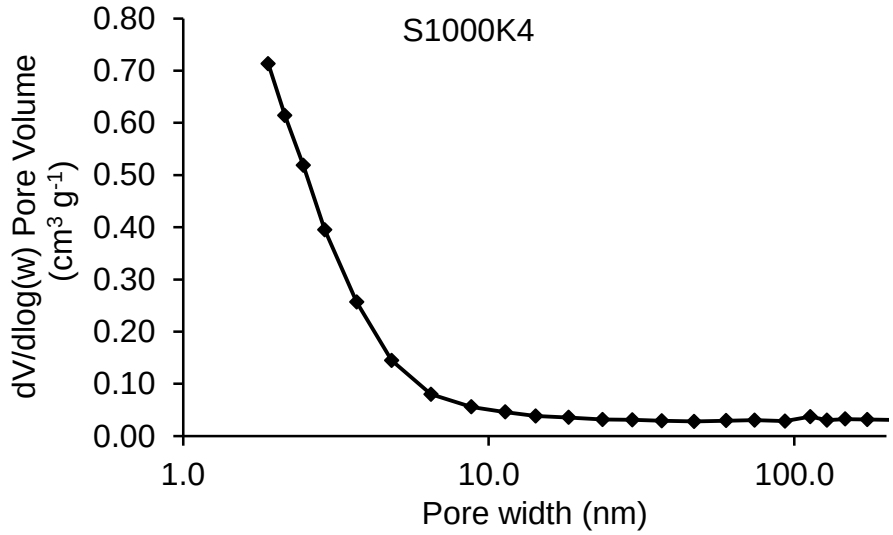

Pore distribution in the micropore region (HK method)

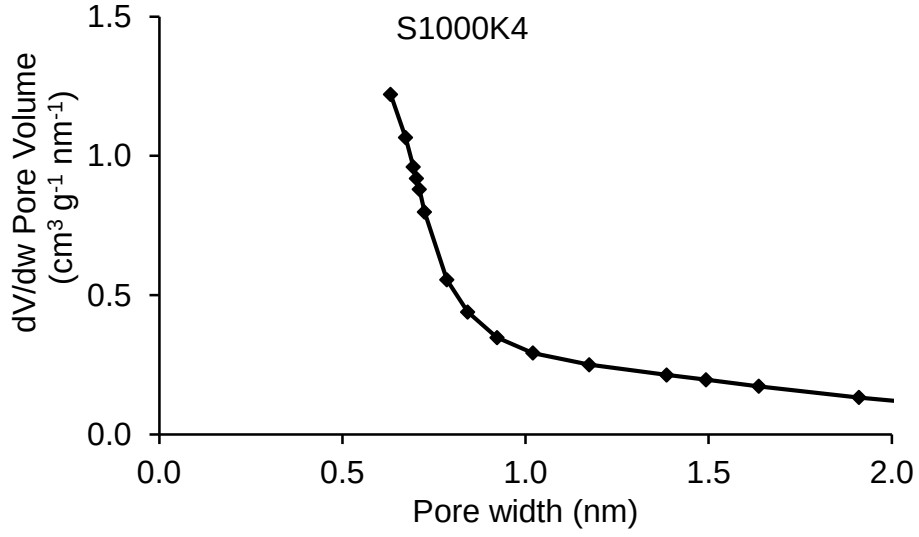

Nitrogen adsorption isotherm and pore distribution plots for A800K1

Nitrogen adsorption isotherm (77K)

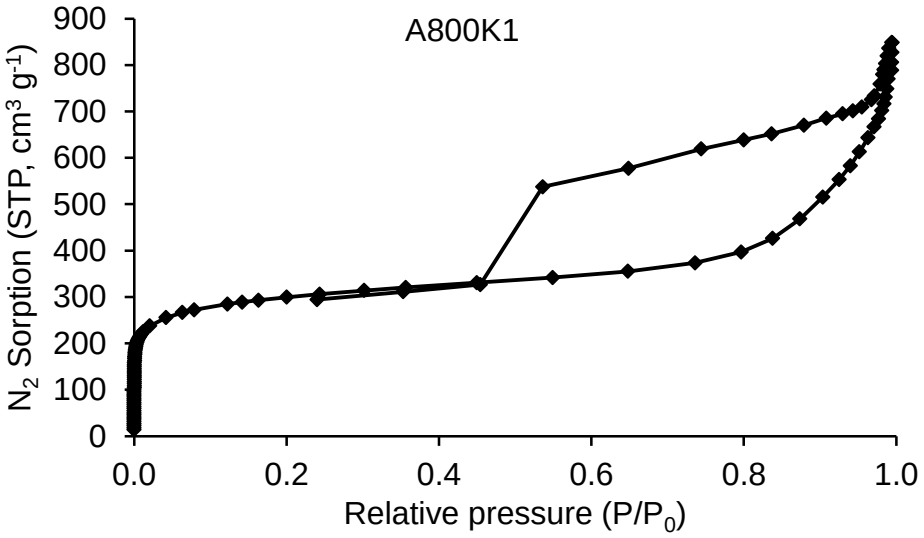

Pore distribution in the mesopore region (BJH method)

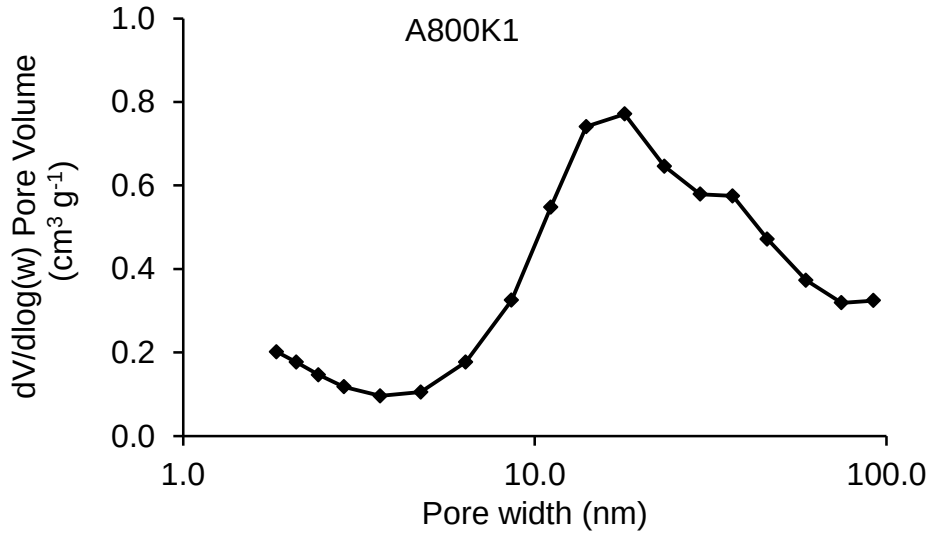

Pore distribution in the micropore region (HK method)

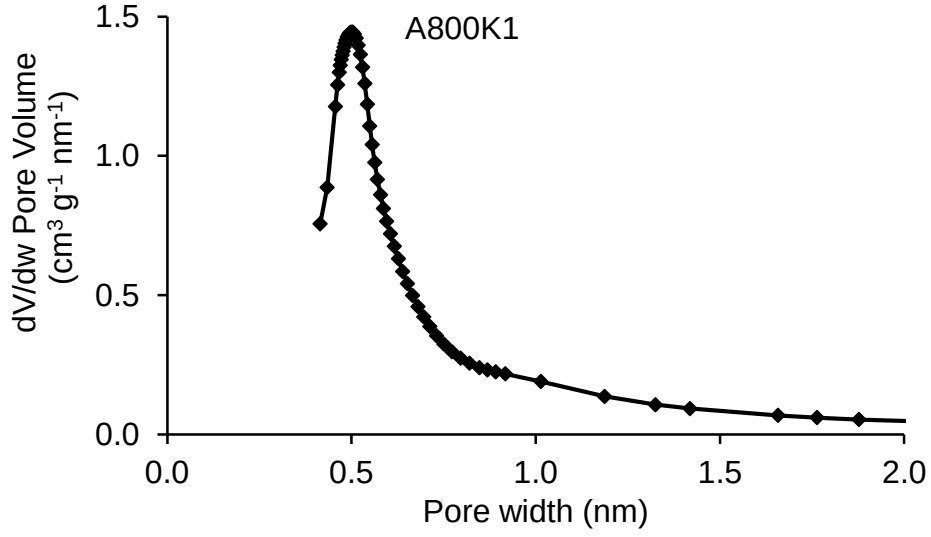

Nitrogen adsorption isotherm and pore distribution plots for A800K2

Nitrogen adsorption isotherm (77K)

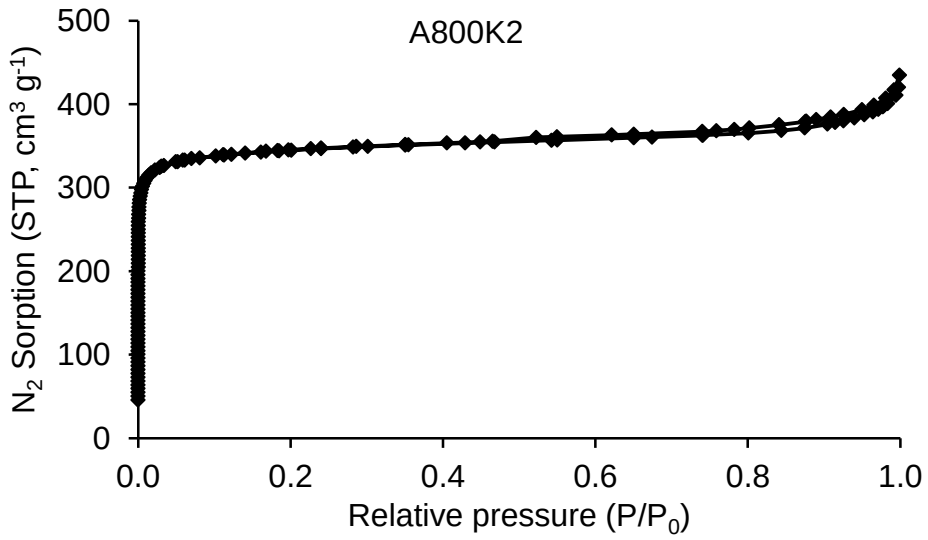

Pore distribution in the mesopore region (BJH method)

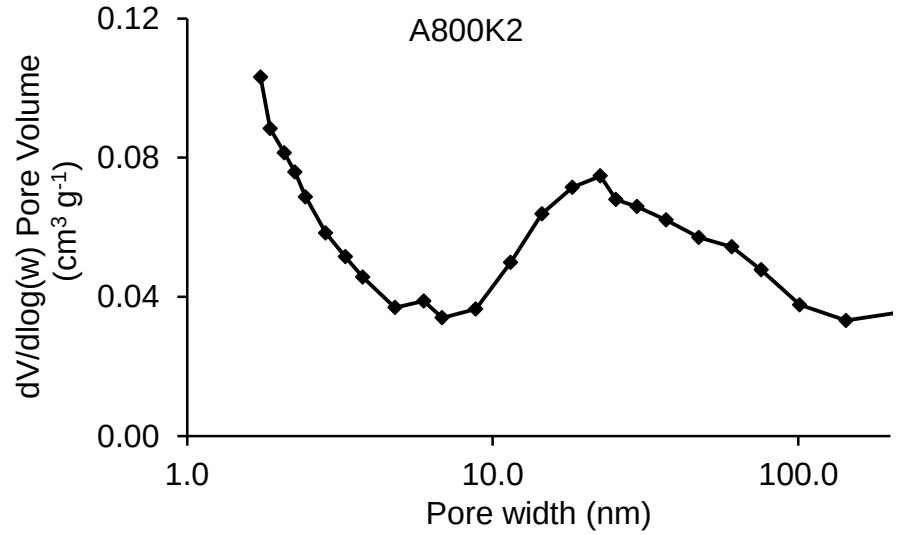

Pore distribution in the micropore region (HK method)

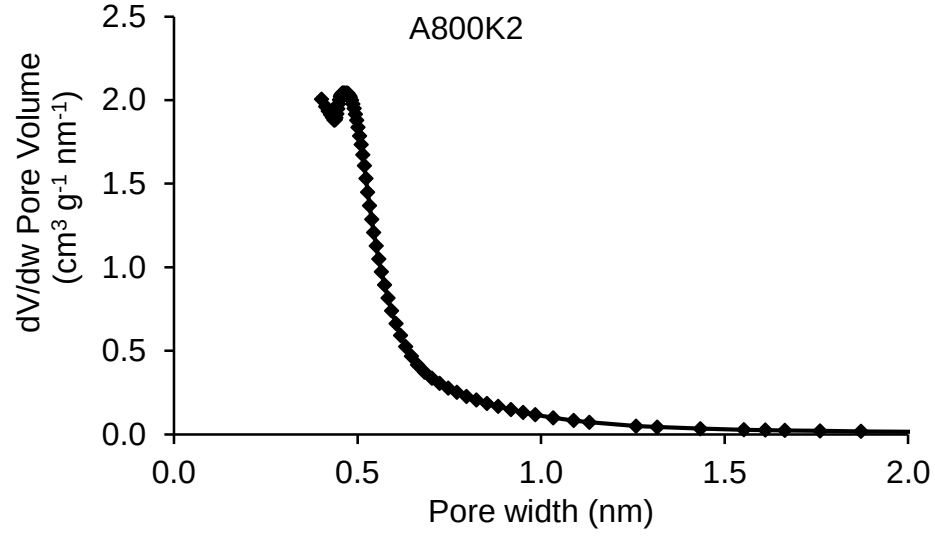

Nitrogen adsorption isotherm and pore distribution plots for A800K3

Nitrogen adsorption isotherm (77K)

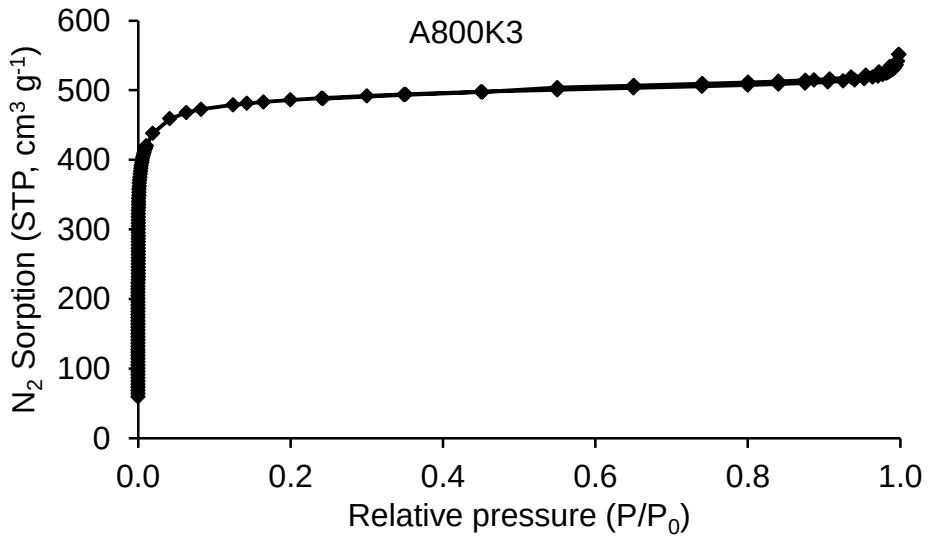

Pore distribution in the mesopore region (BJH method)

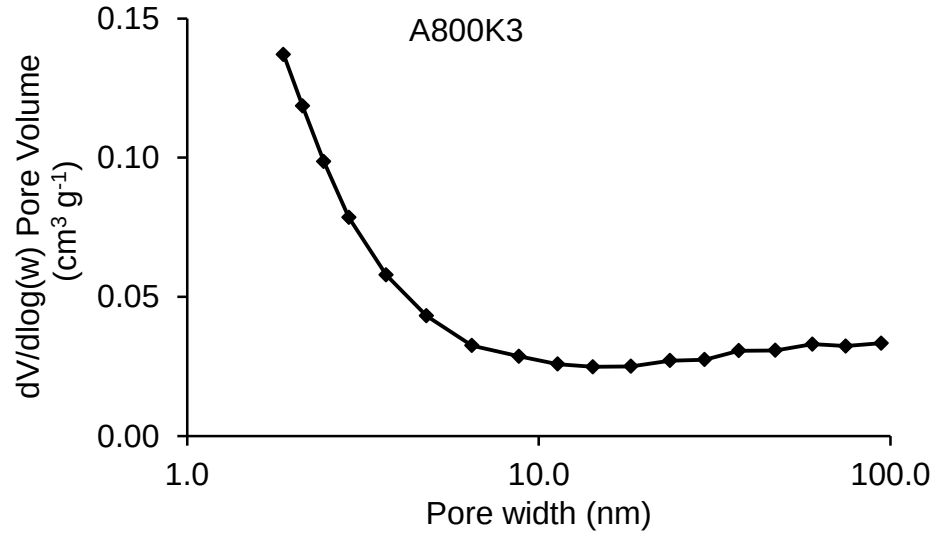

Pore distribution in the micropore region (HK method)

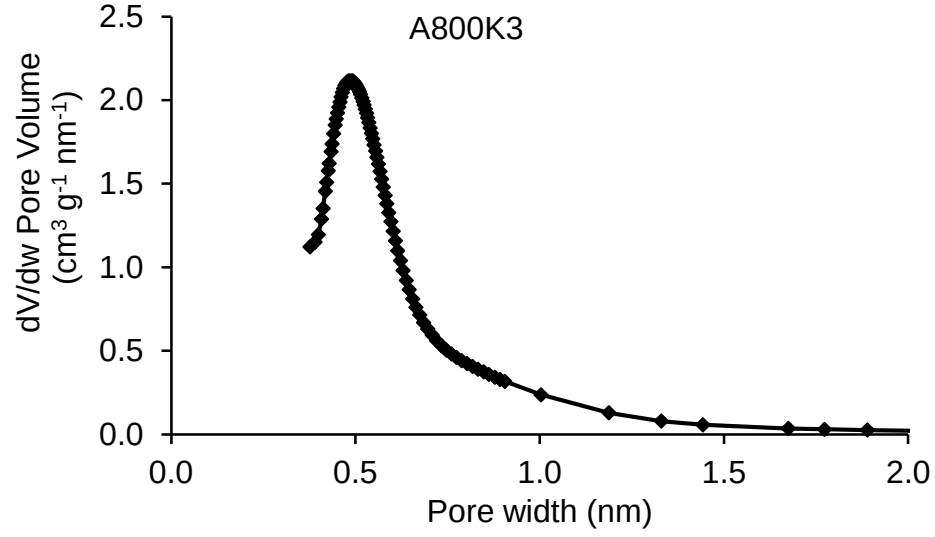

Nitrogen adsorption isotherm and pore distribution plots for A800K4

Nitrogen adsorption isotherm (77K)

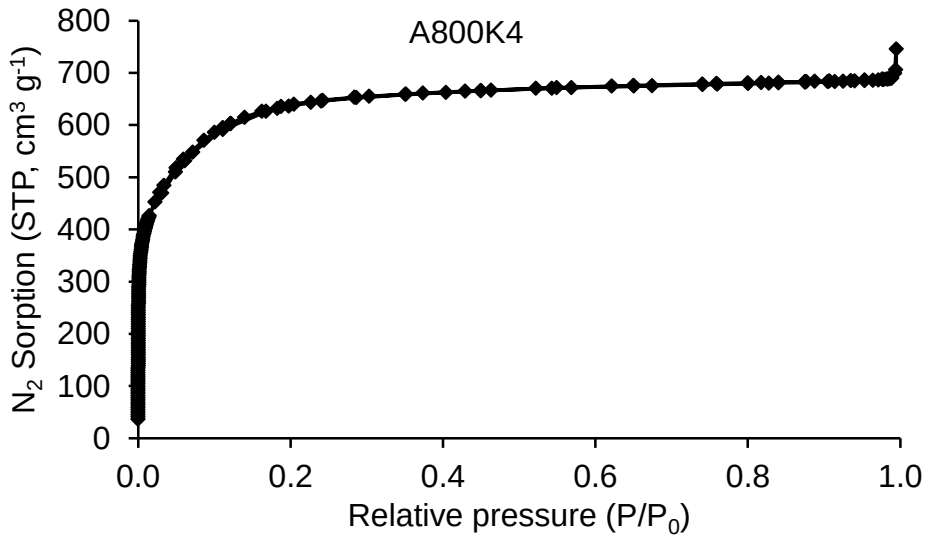

Pore distribution in the mesopore region (BJH method)

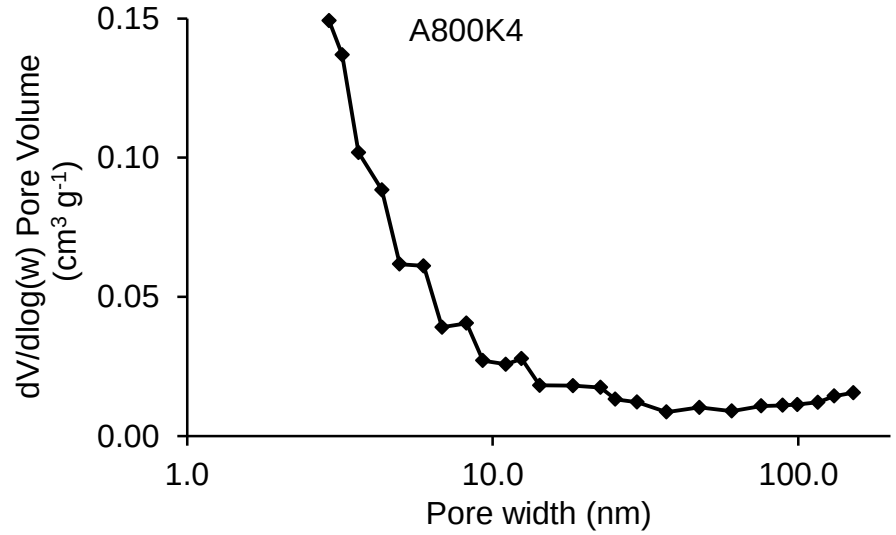

Pore distribution in the micropore region (HK method)

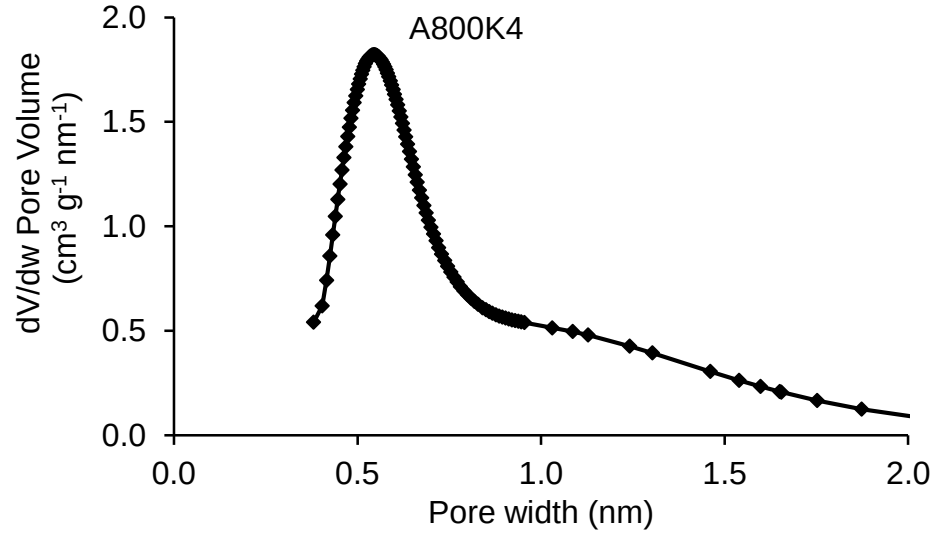

Nitrogen adsorption isotherm and pore distribution plots for A800K5

Nitrogen adsorption isotherm (77K)

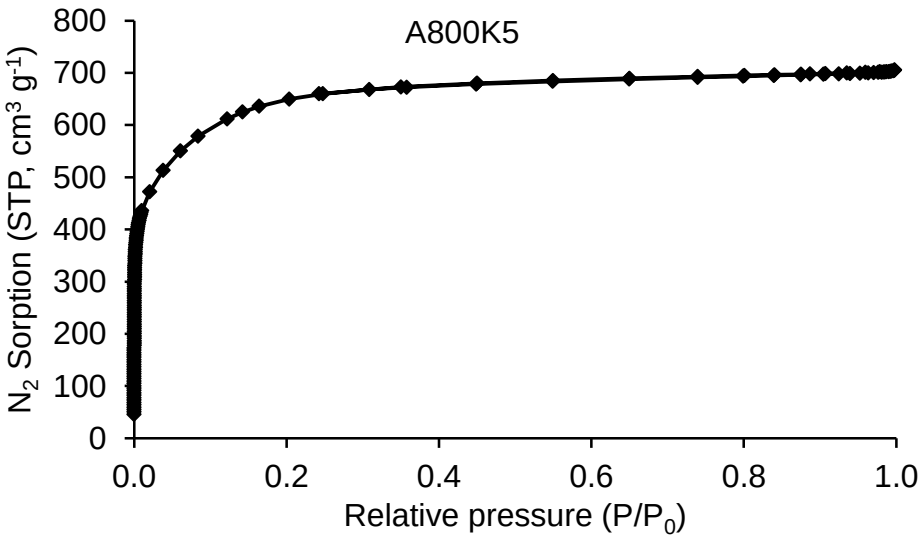

Pore distribution in the mesopore region (BJH method)

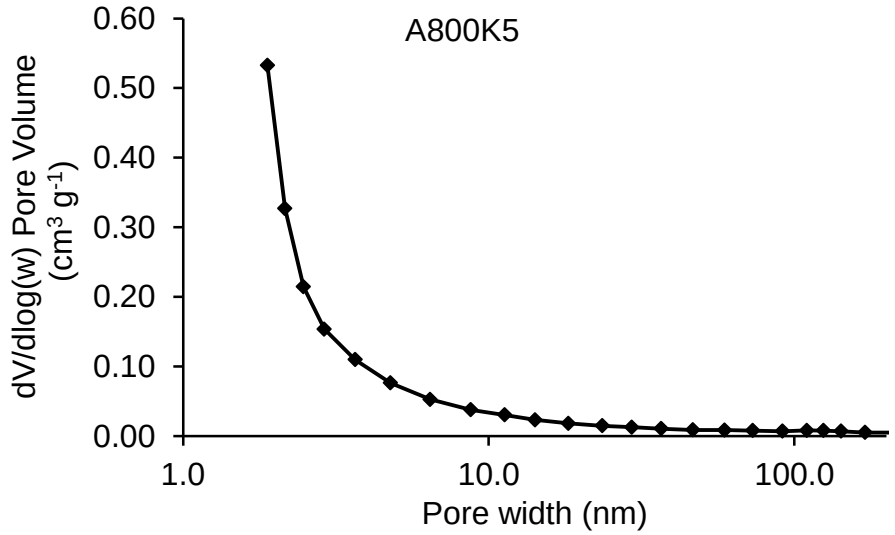

Pore distribution in the micropore region (HK method)

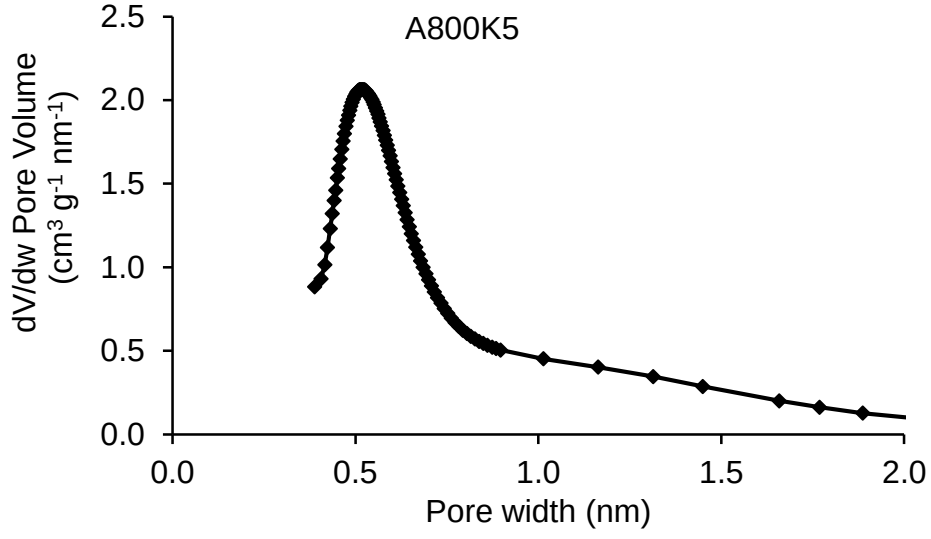

Nitrogen adsorption isotherm and pore distribution plots for A600K2

Nitrogen adsorption isotherm (77K)

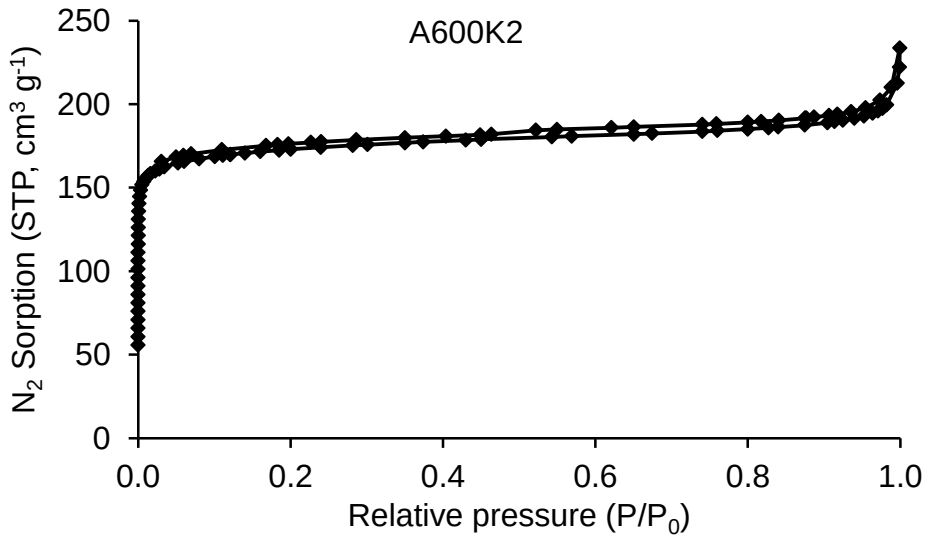

Pore distribution in the mesopore region (BJH method)

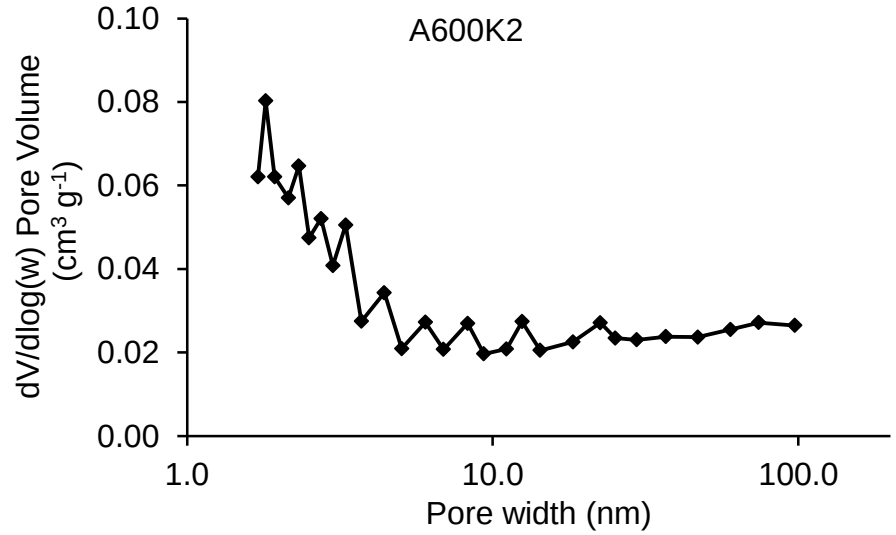

Pore distribution in the micropore region (HK method)

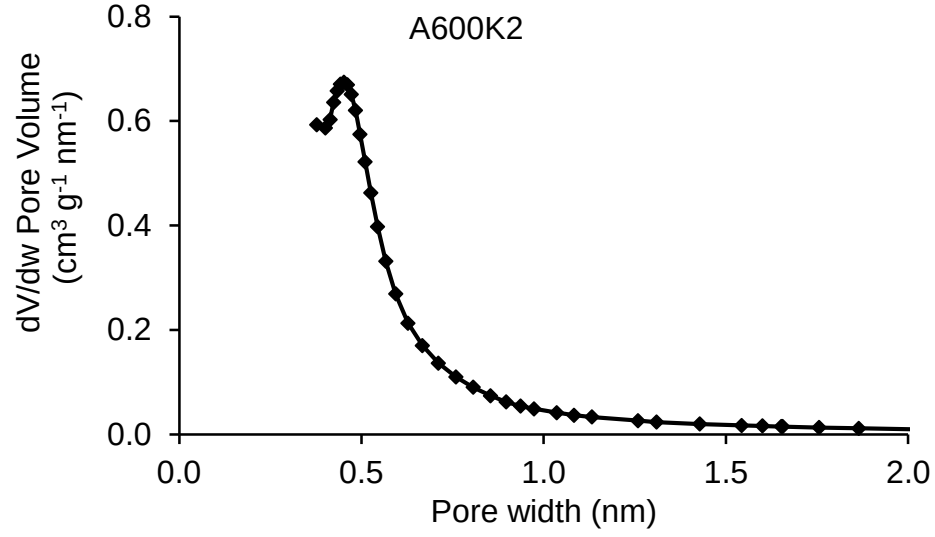

Nitrogen adsorption isotherm and pore distribution plots for A1000K2

Nitrogen adsorption isotherm (77K)

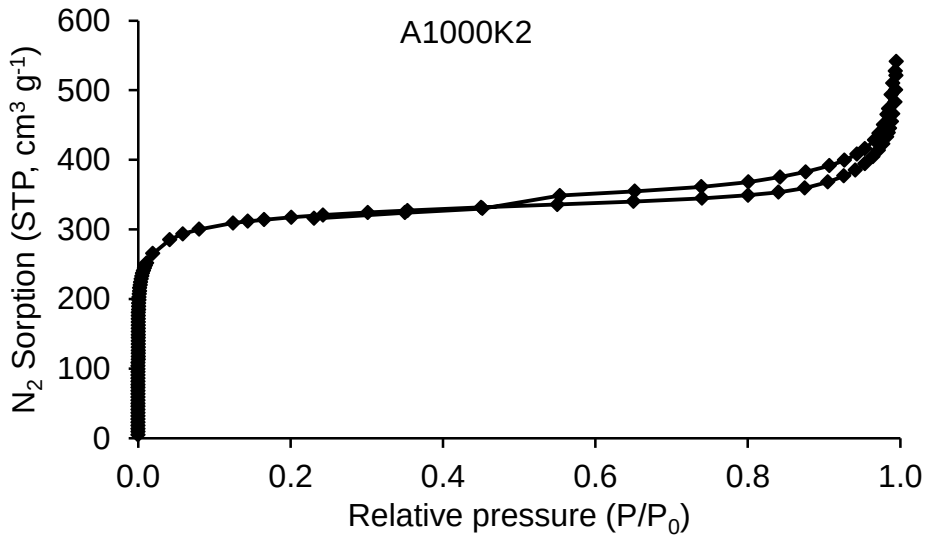

Pore distribution in the mesopore region (BJH method)

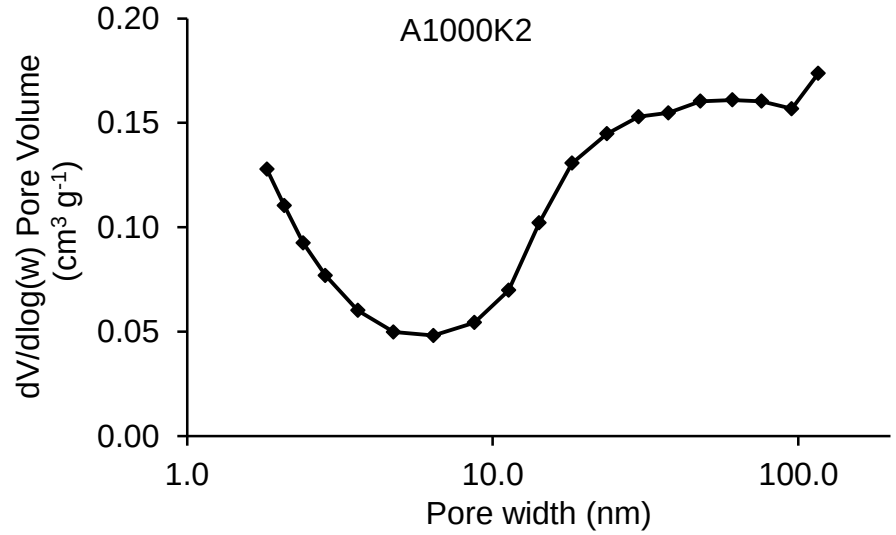

Pore distribution in the micropore region (HK method)

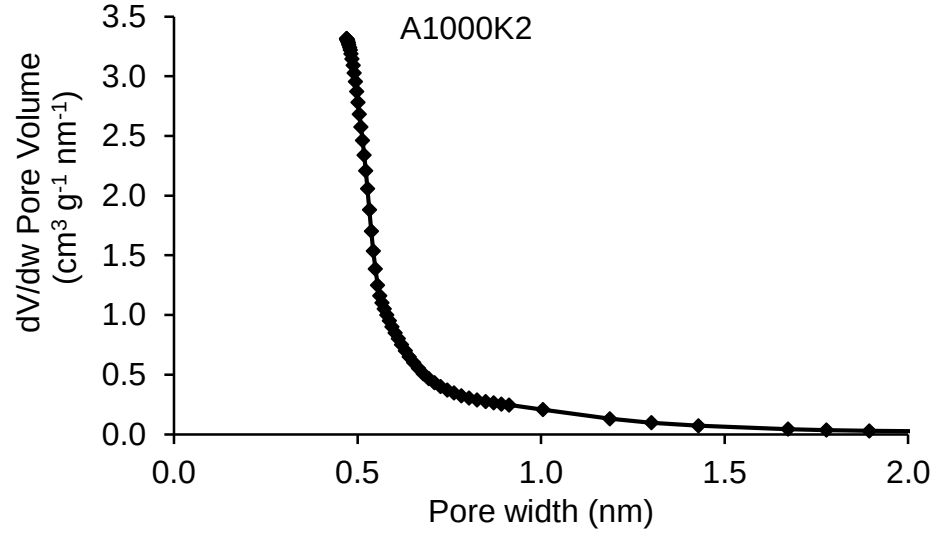

Nitrogen adsorption isotherm and pore distribution plots for P800K2

Nitrogen adsorption isotherm (77K)

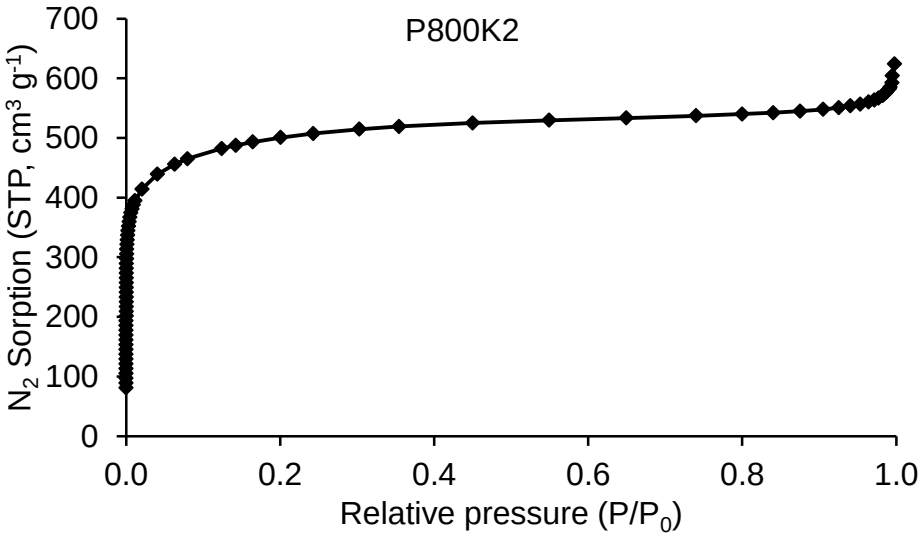

Pore distribution in the mesopore region (BJH method)

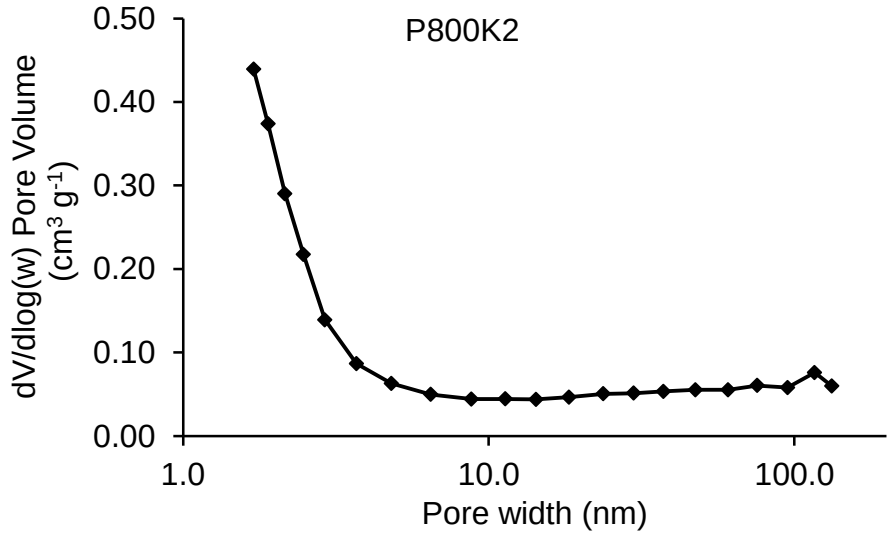

Pore distribution in the micropore region (HK method)

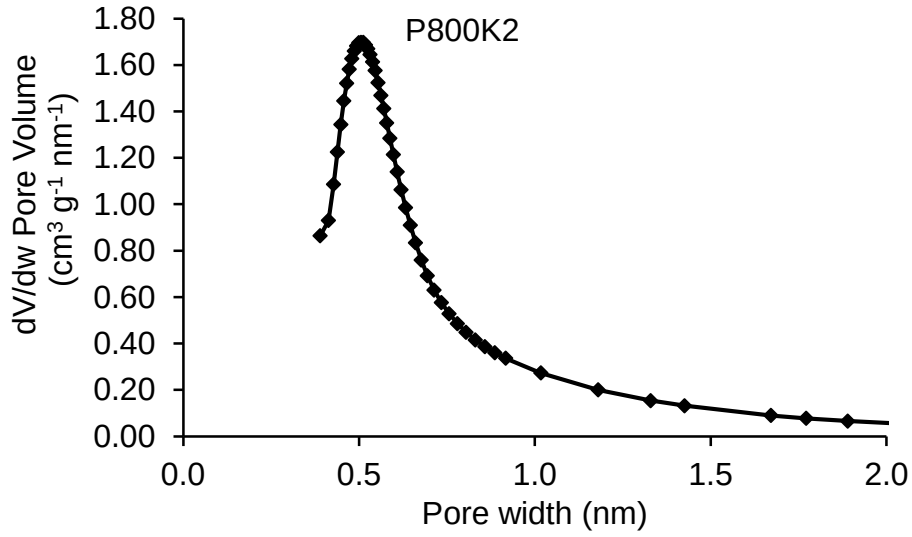

Nitrogen adsorption isotherm and pore distribution plots for P800K3

Nitrogen adsorption isotherm (77K)

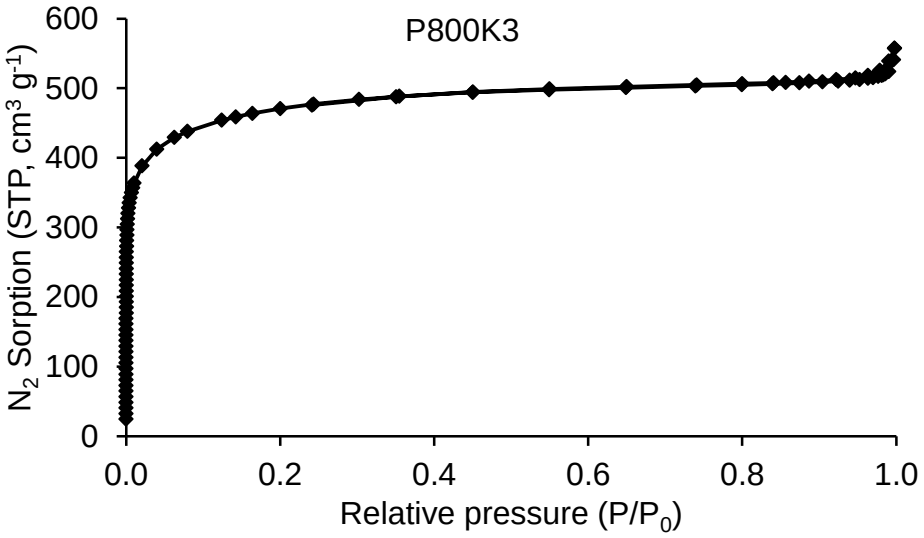

Pore distribution in the mesopore region (BJH method)

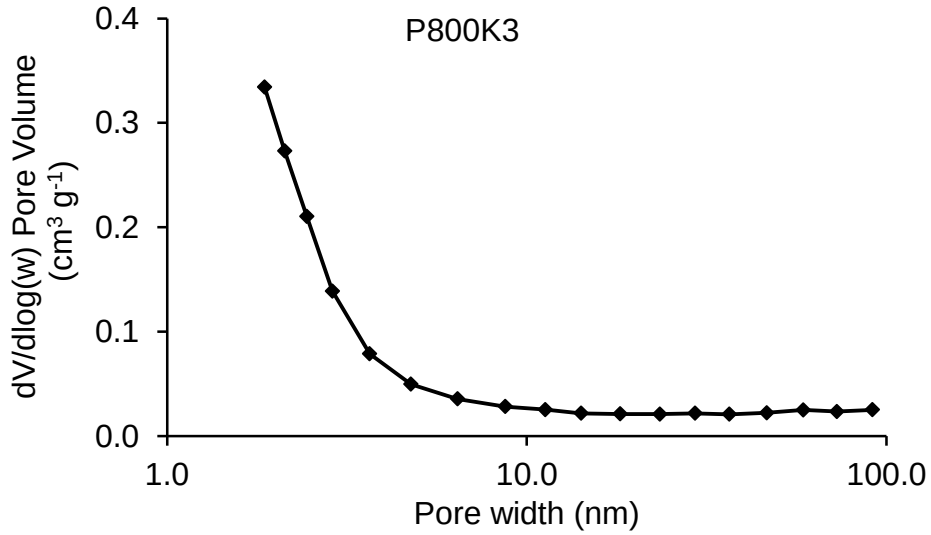

Pore distribution in the micropore region (HK method)

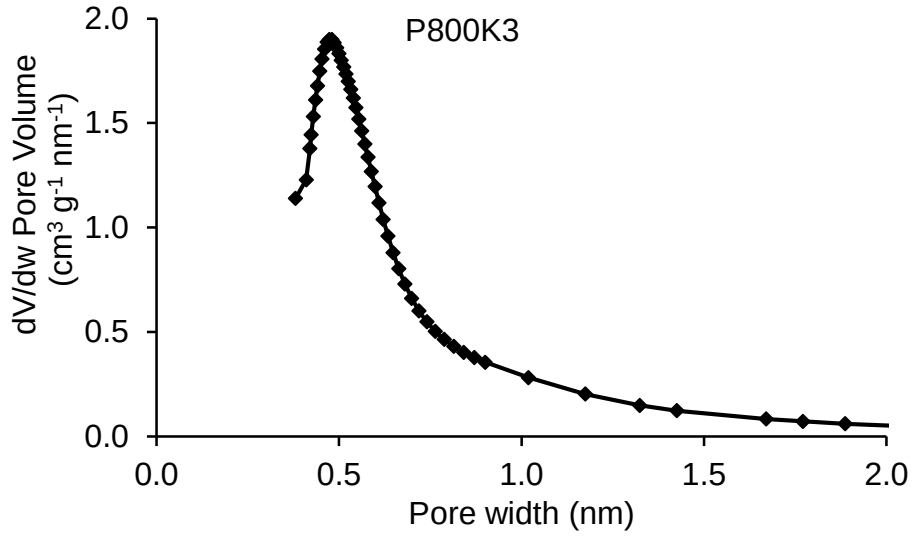

Nitrogen adsorption isotherm and pore distribution plots for P800K5

Nitrogen adsorption isotherm (77K)

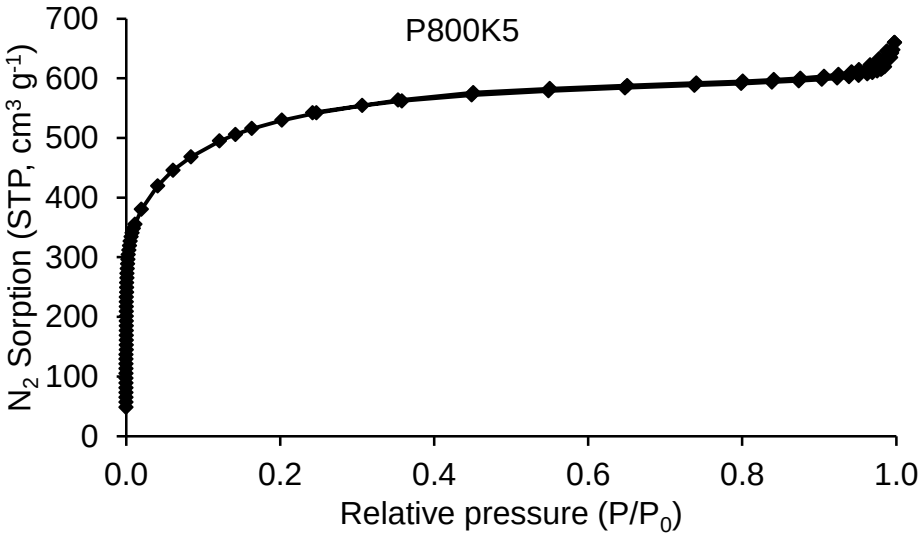

Pore distribution in the mesopore region (BJH method)

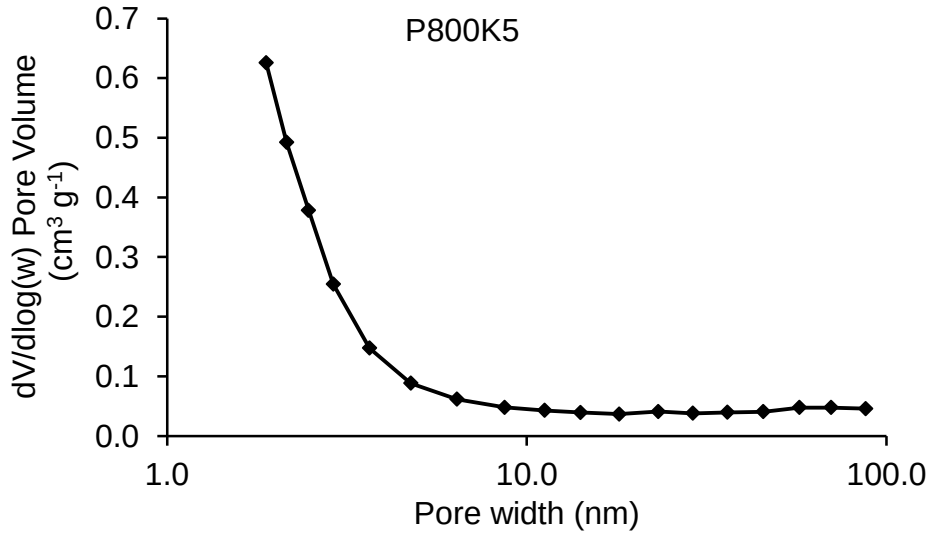

Pore distribution in the micropore region (HK method)

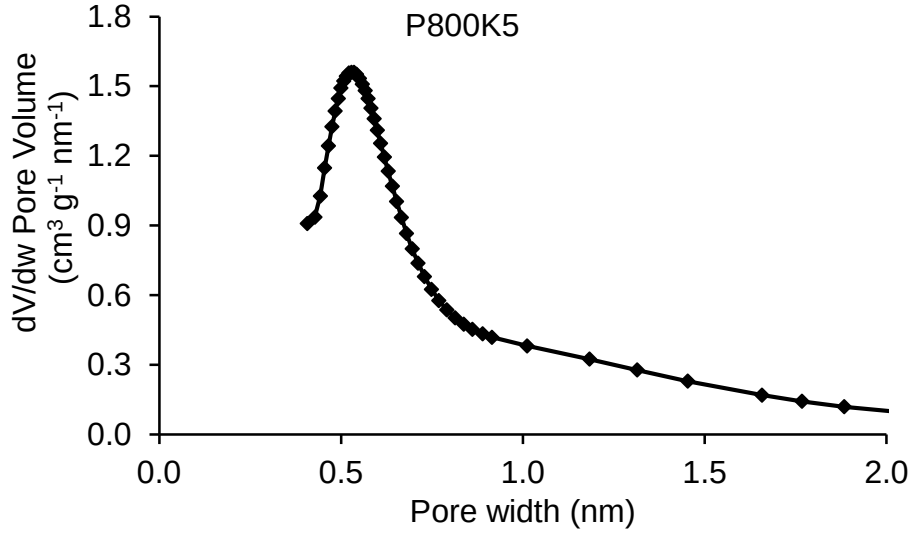

Nitrogen adsorption isotherm and pore distribution plots for S800C15

Nitrogen adsorption isotherm (77K)

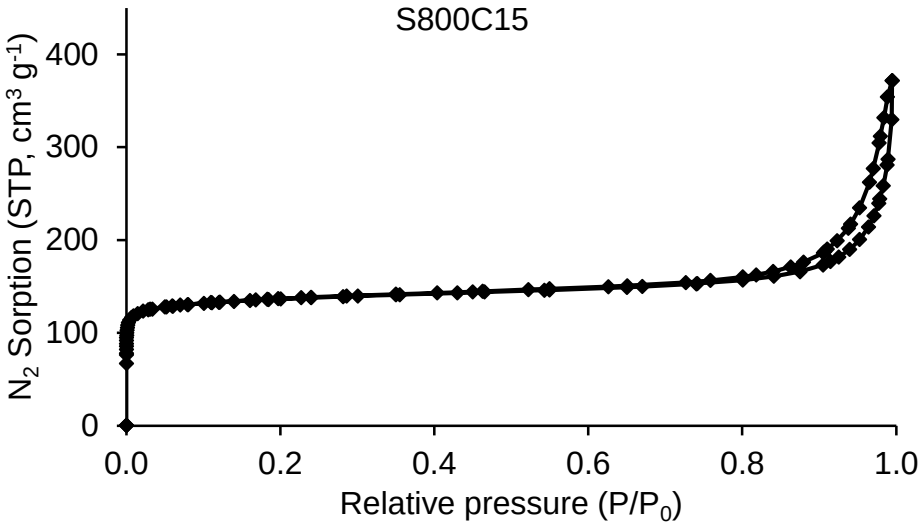

Pore distribution in the mesopore region (BJH method)

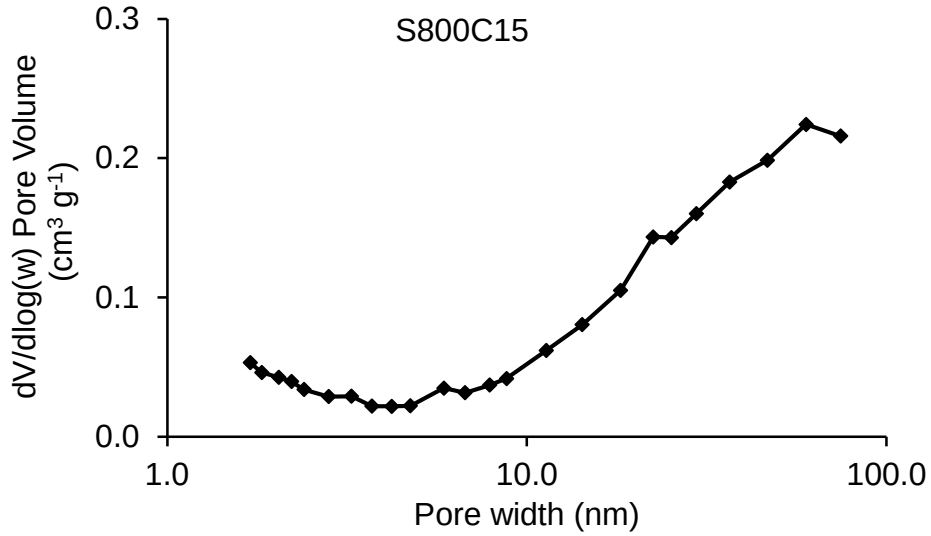

Pore distribution in the micropore region (HK method)

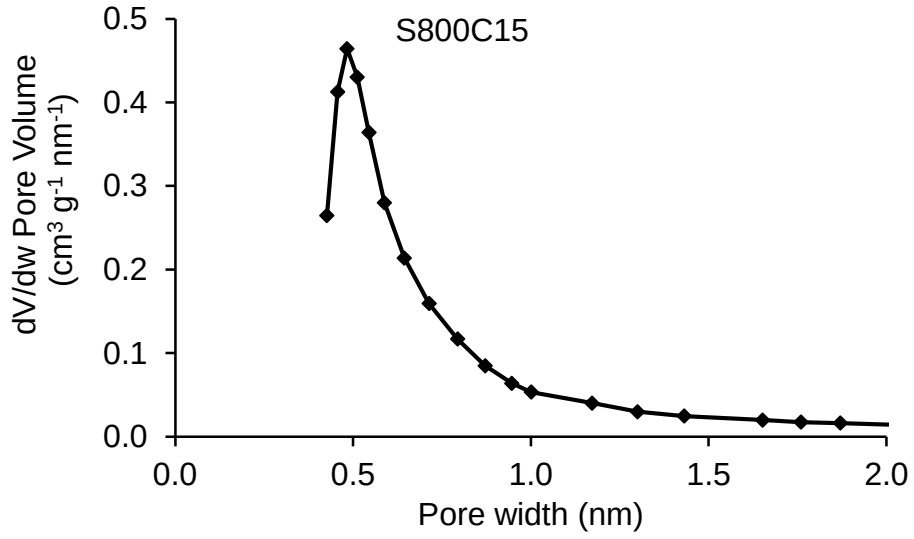

Nitrogen adsorption isotherm and pore distribution plots for S850C15

Nitrogen adsorption isotherm (77K)

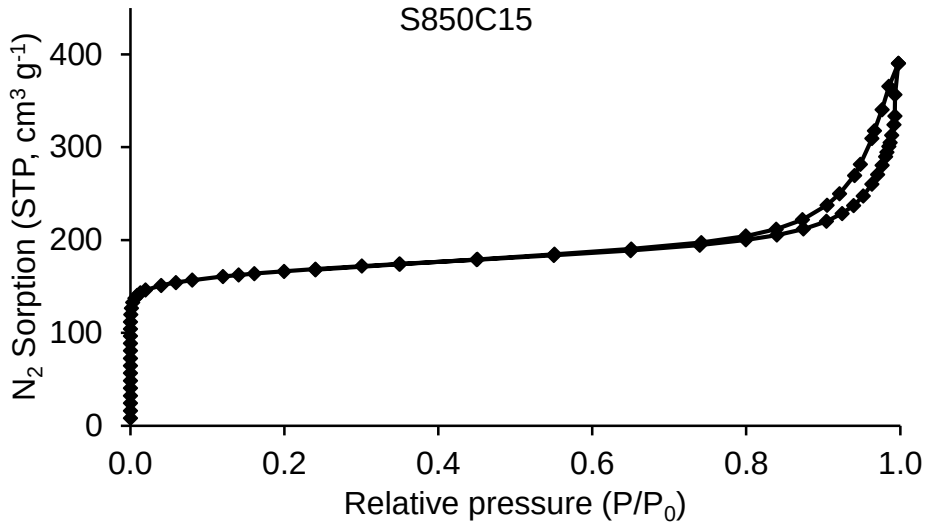

Pore distribution in the mesopore region (BJH method)

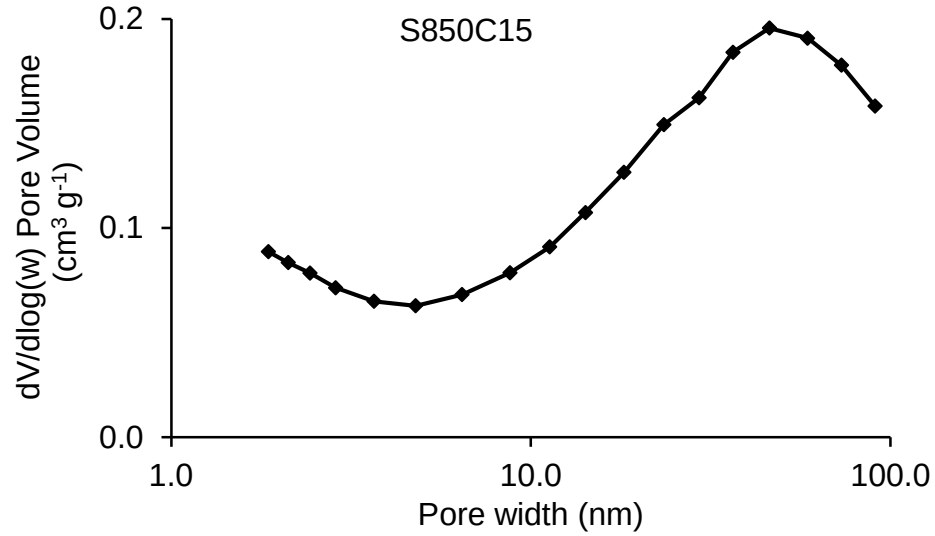

Pore distribution in the micropore region (HK method)

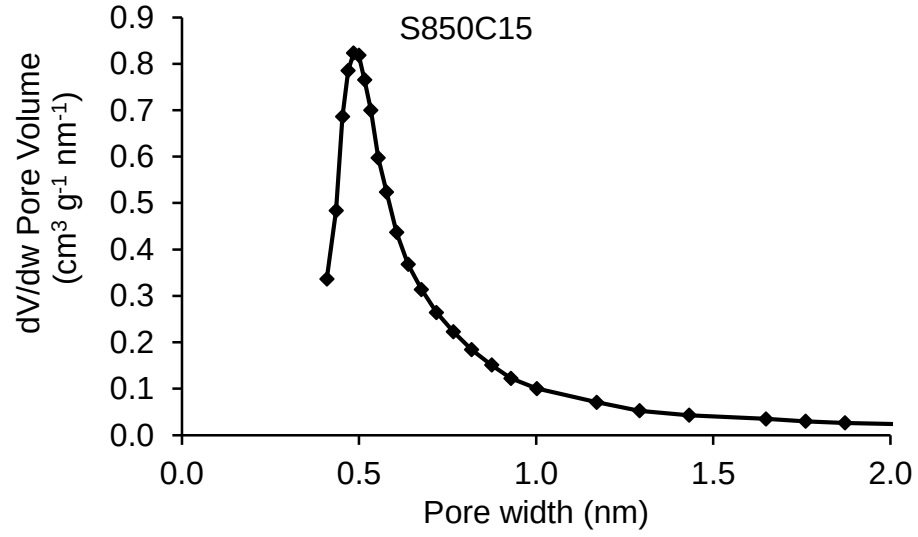

Nitrogen adsorption isotherm and pore distribution plots for S900C15 with a CO_2 flow rate of 25 mL min^{-1}

Nitrogen adsorption isotherm (77K)

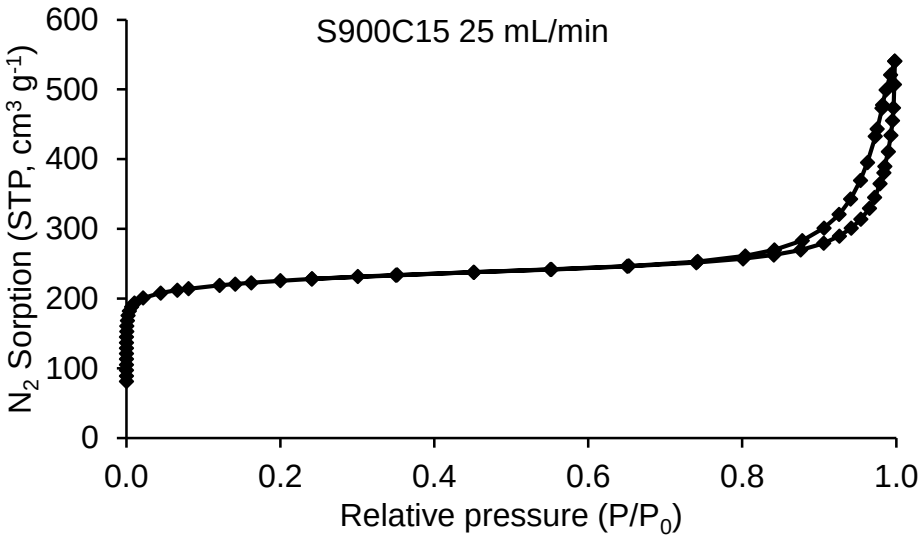

Pore distribution in the mesopore region (BJH method)

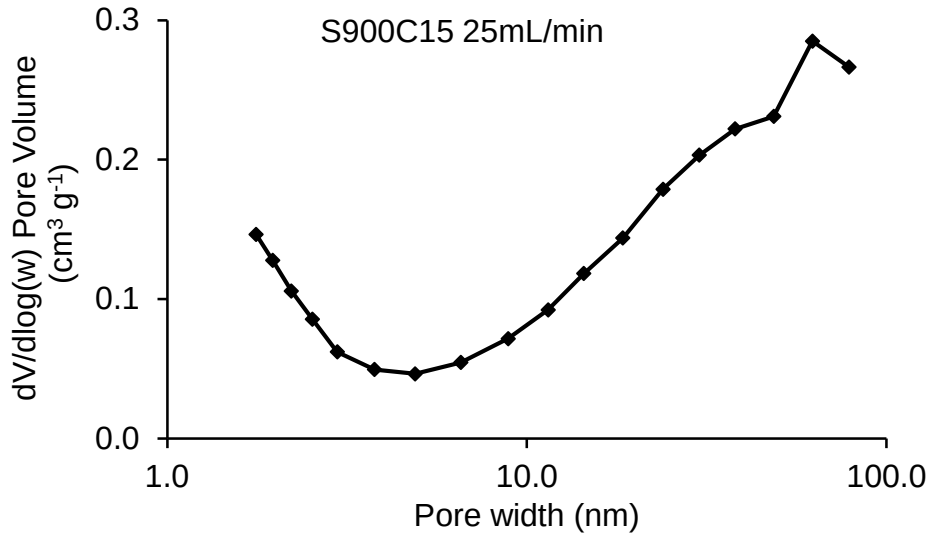

Pore distribution in the micropore region (HK method)

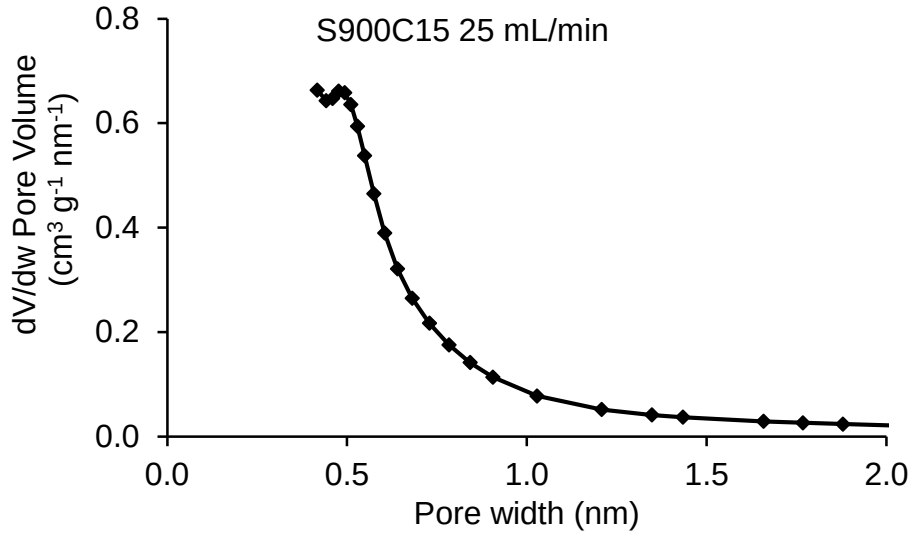

Nitrogen adsorption isotherm and pore distribution plots for S900C15 with a CO_2 flow rate of 50 mL min^{-1} (standard flow rate)

Nitrogen adsorption isotherm (77K)

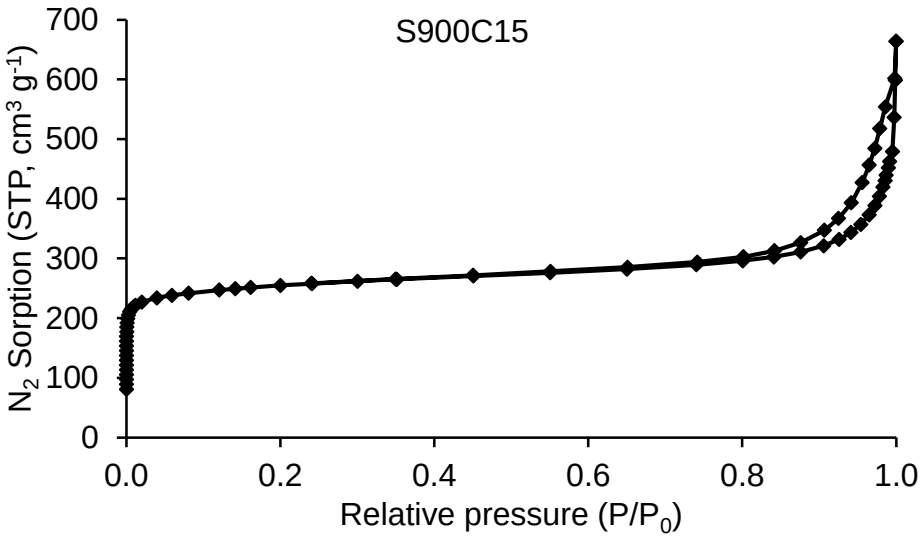

Pore distribution in the mesopore region (BJH method)

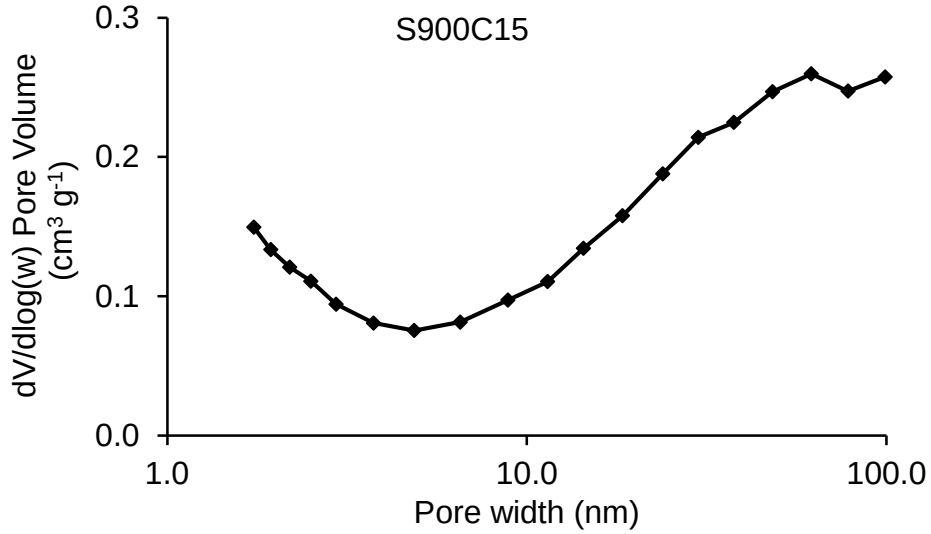

Pore distribution in the micropore region (HK method)

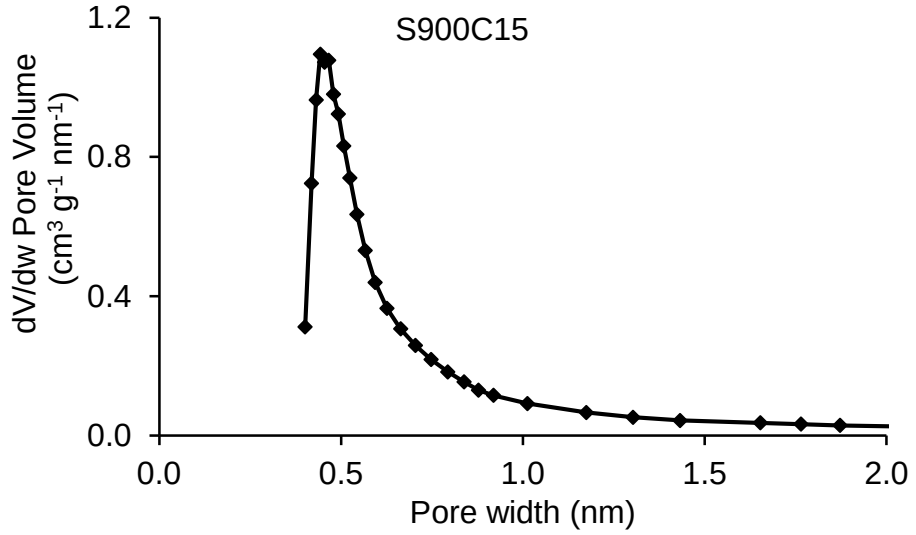

Nitrogen adsorption isotherm and pore distribution plots for S900C15 with a CO_2 flow rate of 100 mL min^{-1}

Nitrogen adsorption isotherm (77K)

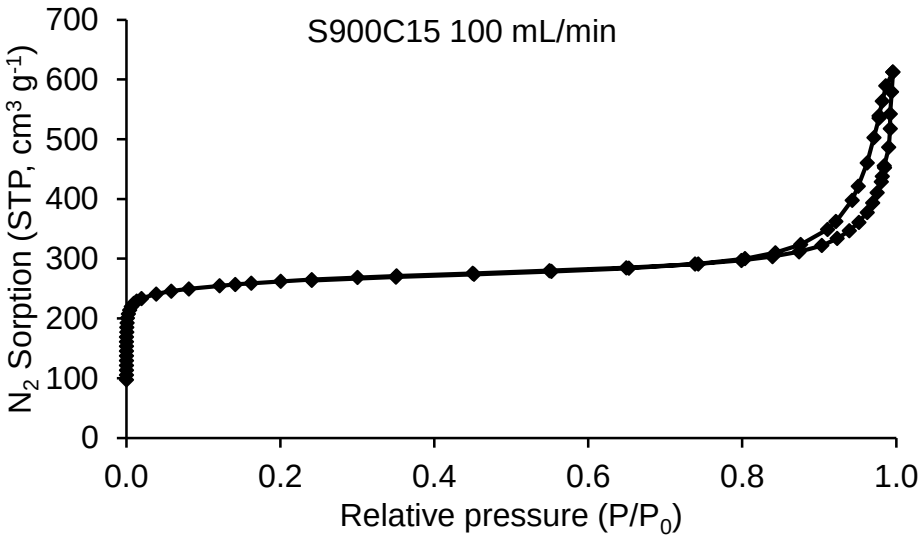

Pore distribution in the mesopore region (BJH method)

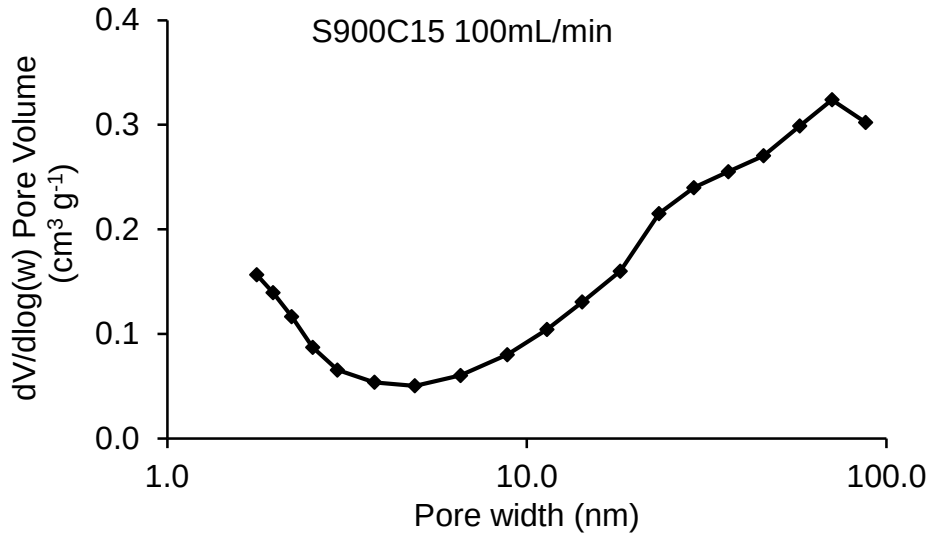

Pore distribution in the micropore region (HK method)

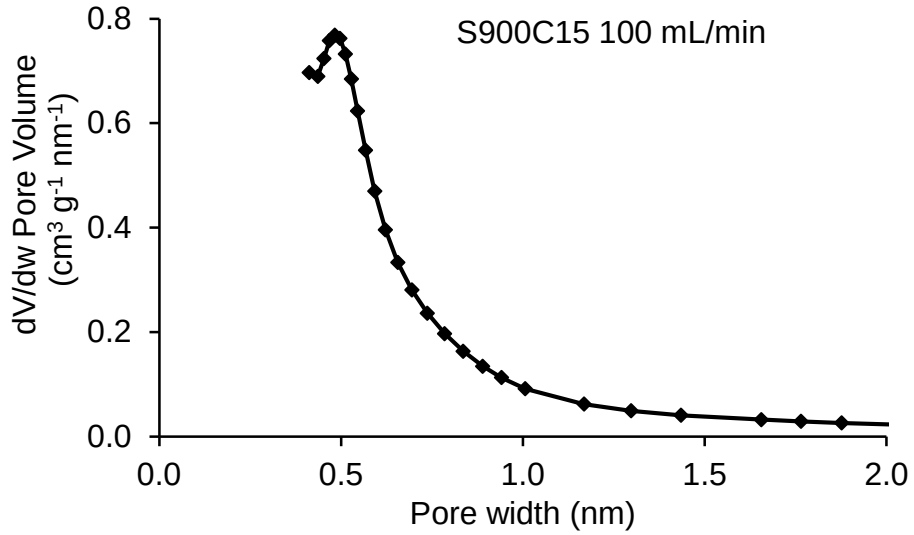

Nitrogen adsorption isotherm and pore distribution plots for S950C15

Nitrogen adsorption isotherm (77K)

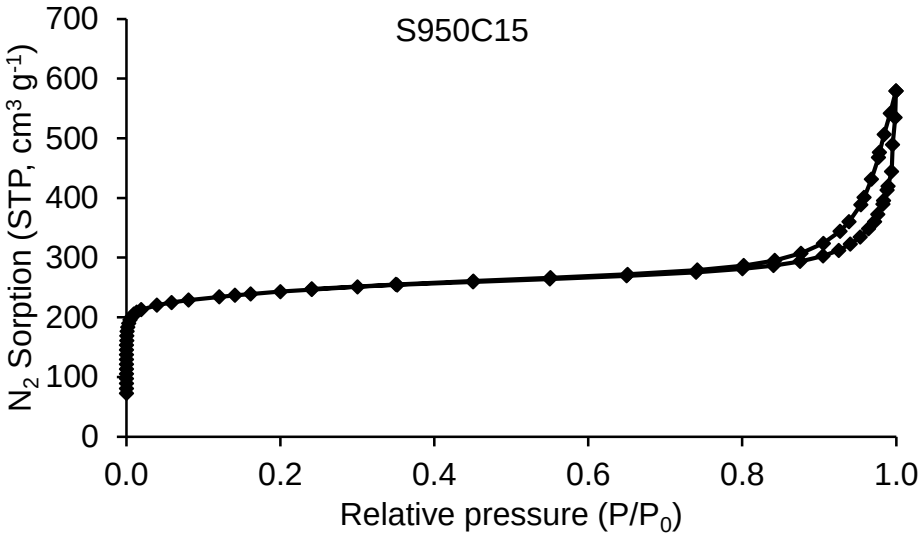

Pore distribution in the mesopore region (BJH method)

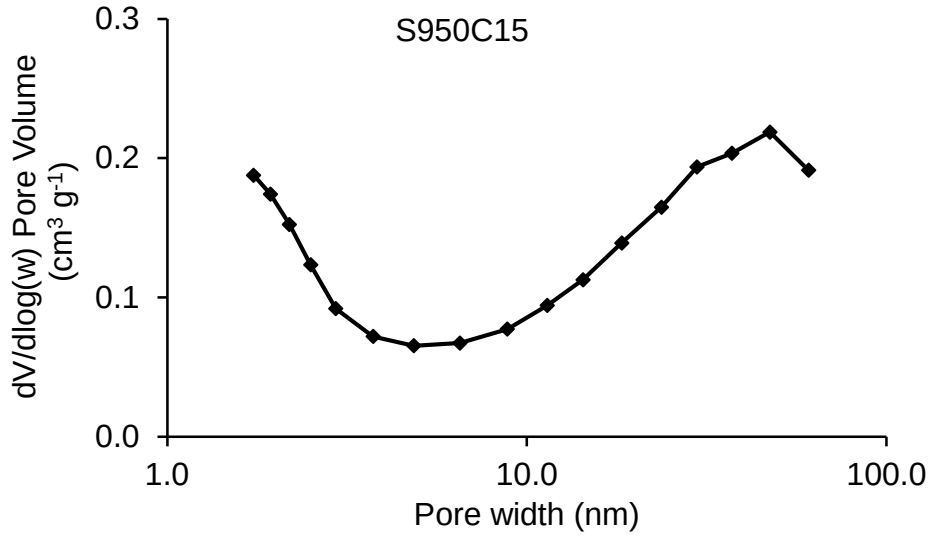

Pore distribution in the micropore region (HK method)

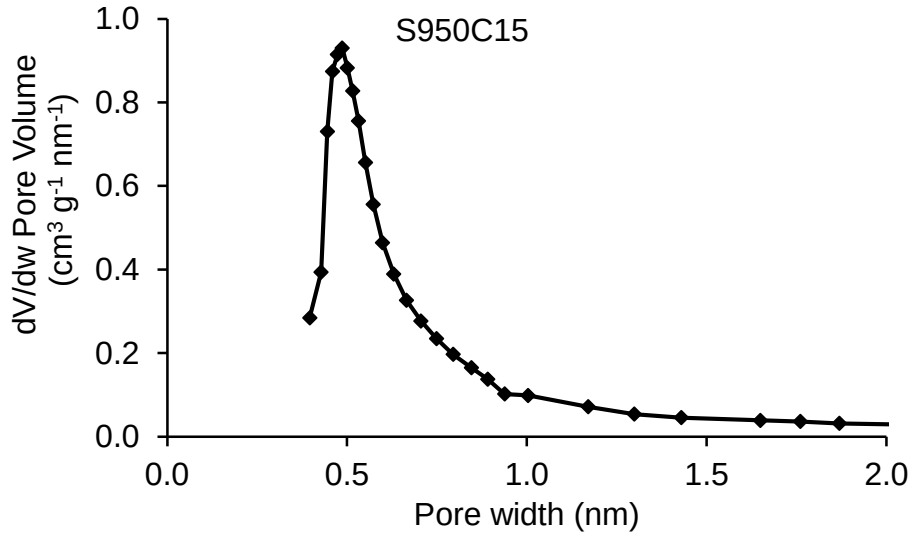

Nitrogen adsorption isotherm and pore distribution plots for S1000C15

Nitrogen adsorption isotherm (77K)

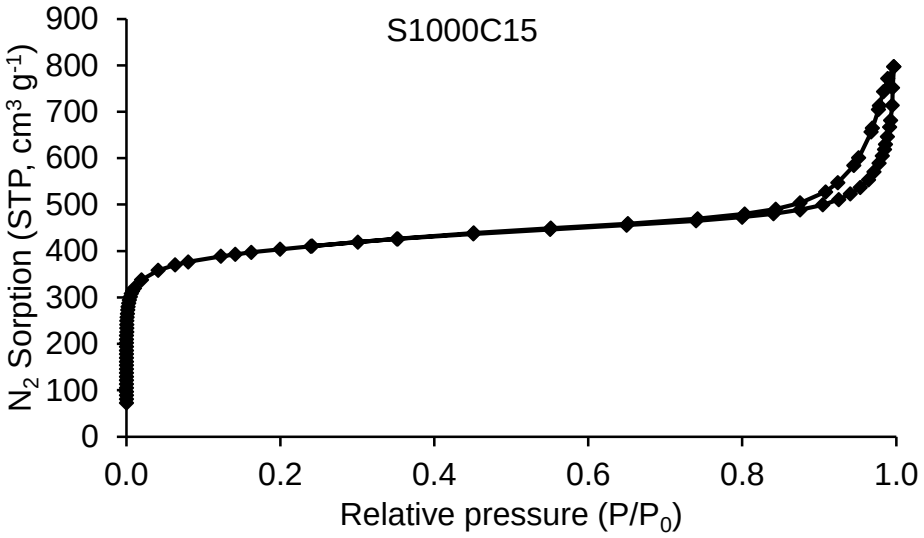

Pore distribution in the mesopore region (BJH method)

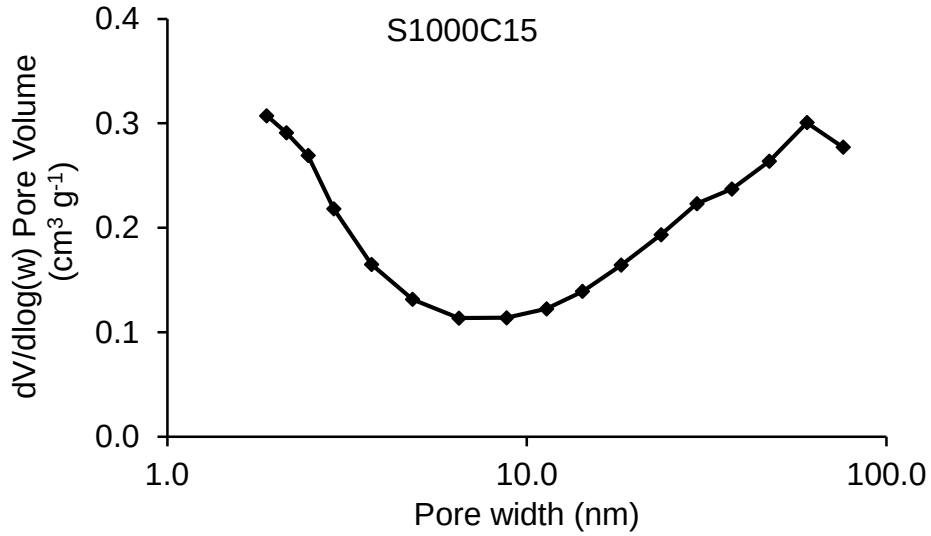

Pore distribution in the micropore region (HK method)

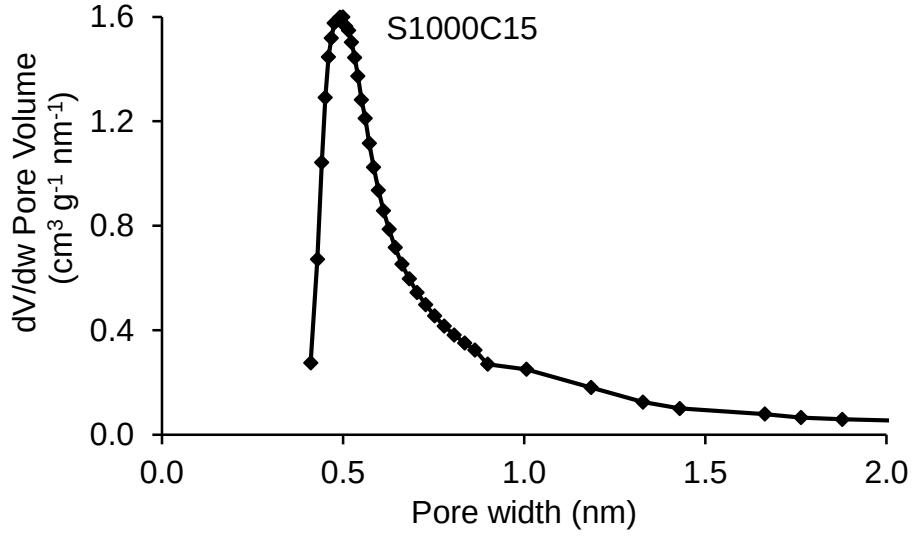

Nitrogen adsorption isotherm and pore distribution plots for S900C30

Nitrogen adsorption isotherm (77K)

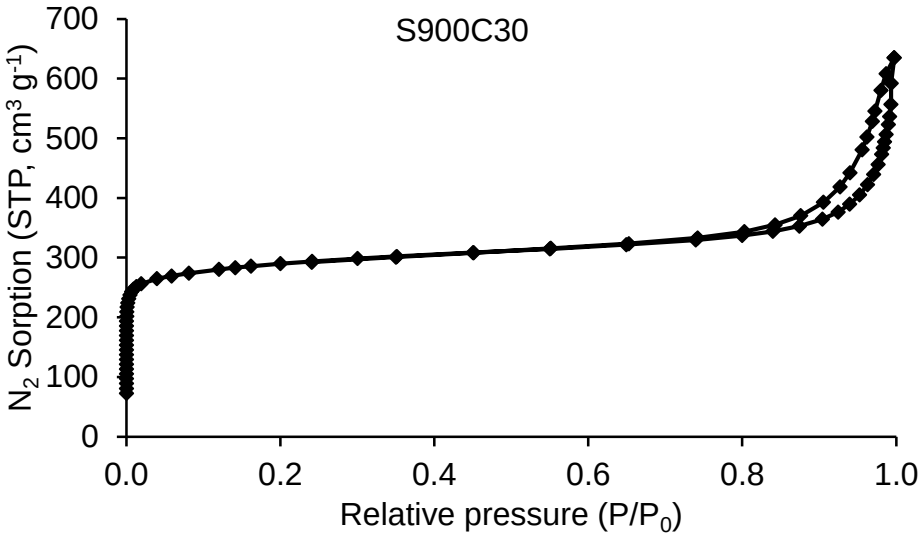

Pore distribution in the mesopore region (BJH method)

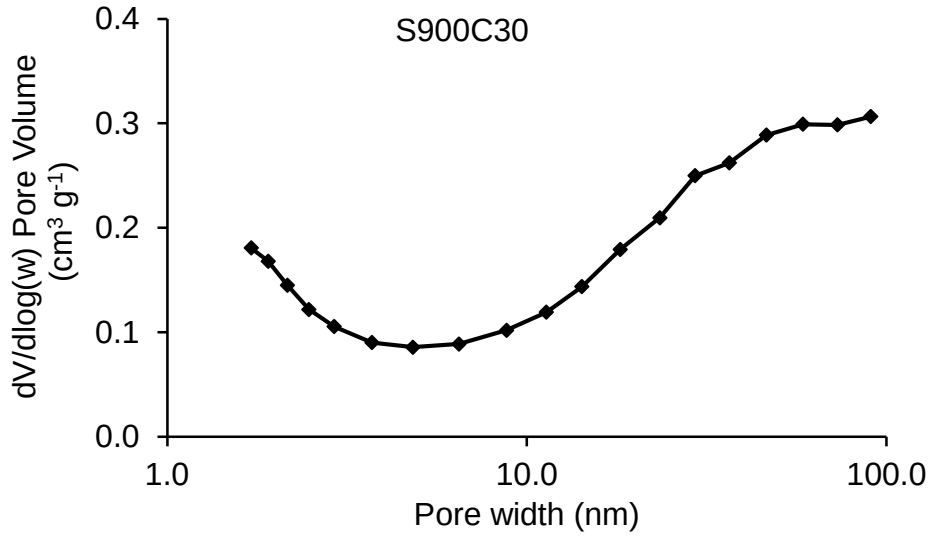

Pore distribution in the micropore region (HK method)

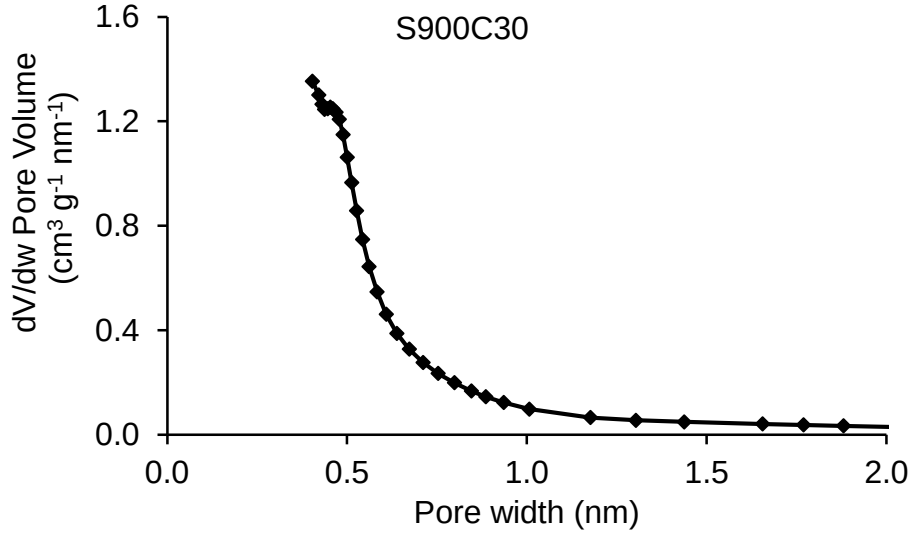

Nitrogen adsorption isotherm and pore distribution plots for S900C60

Nitrogen adsorption isotherm (77K)

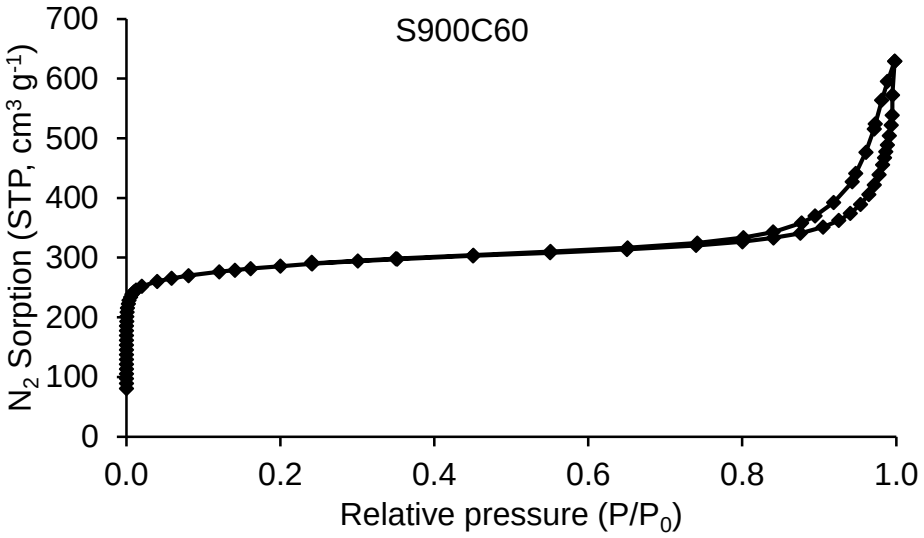

Pore distribution in the mesopore region (BJH method)

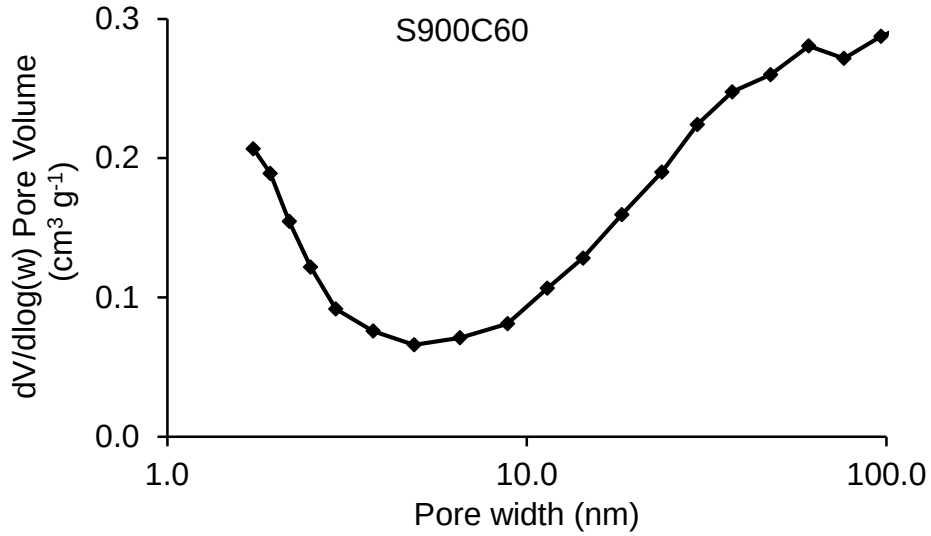

Pore distribution in the micropore region (HK method)

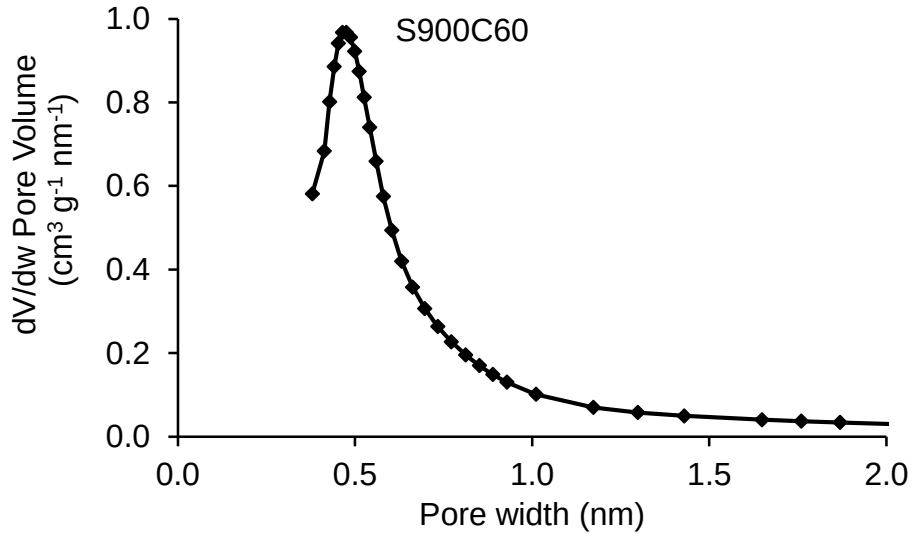

Nitrogen adsorption isotherm and pore distribution plots for S900C90

Nitrogen adsorption isotherm (77K)

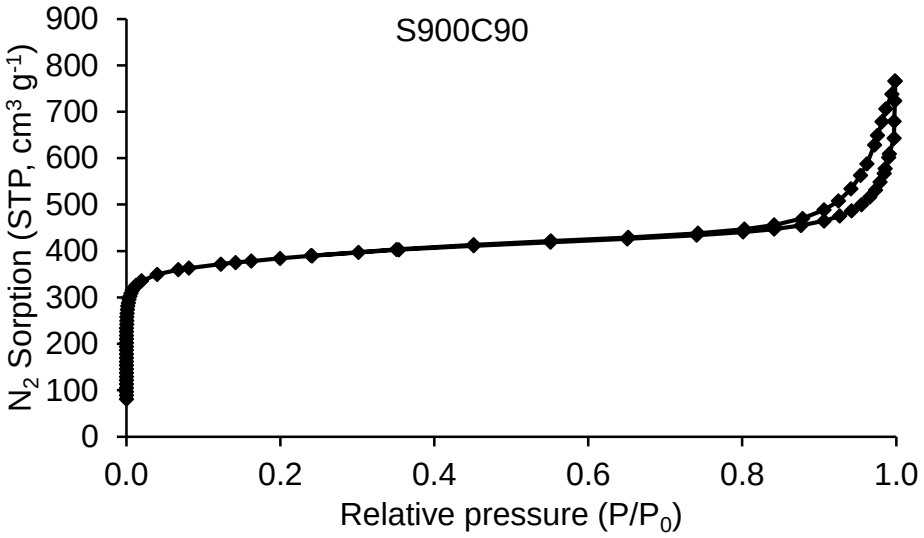

Pore distribution in the mesopore region (BJH method)

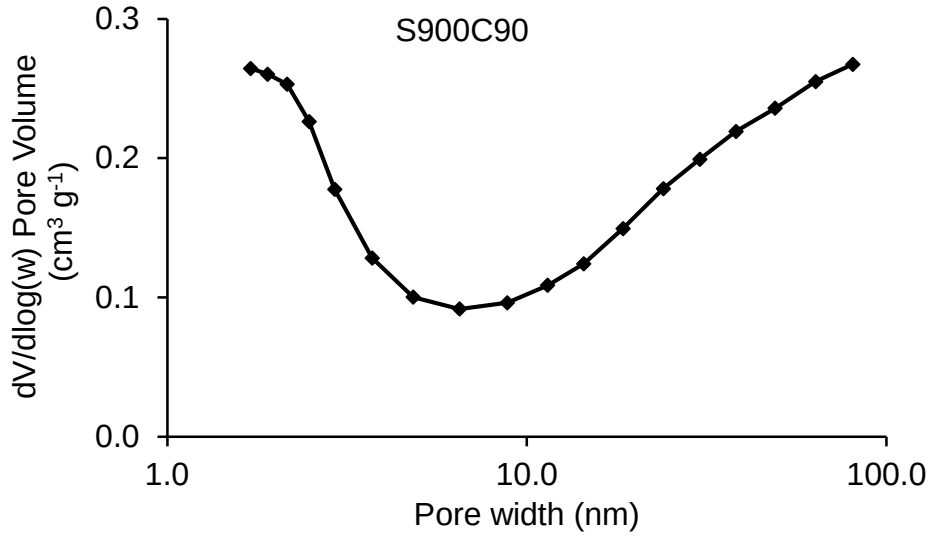

Pore distribution in the micropore region (HK method)

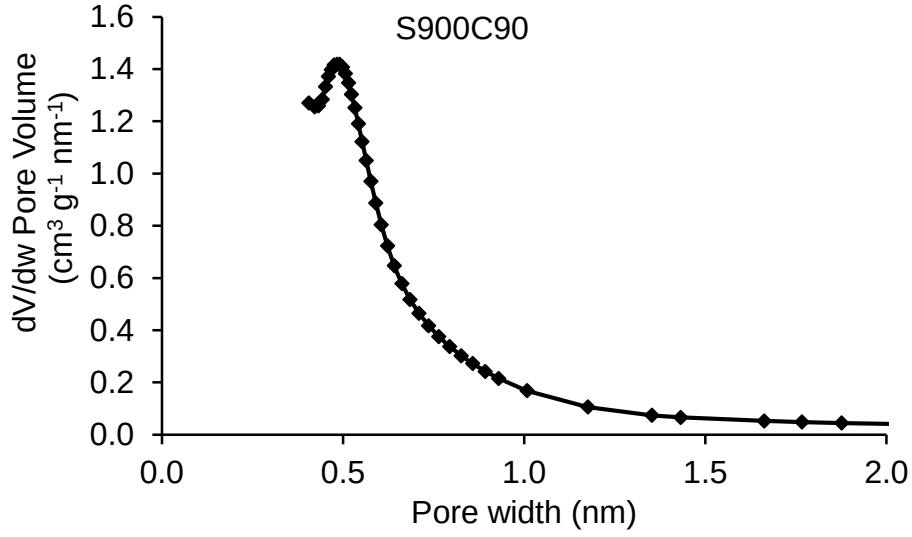

Nitrogen adsorption isotherm and pore distribution plots for S900C120

Nitrogen adsorption isotherm (77K)

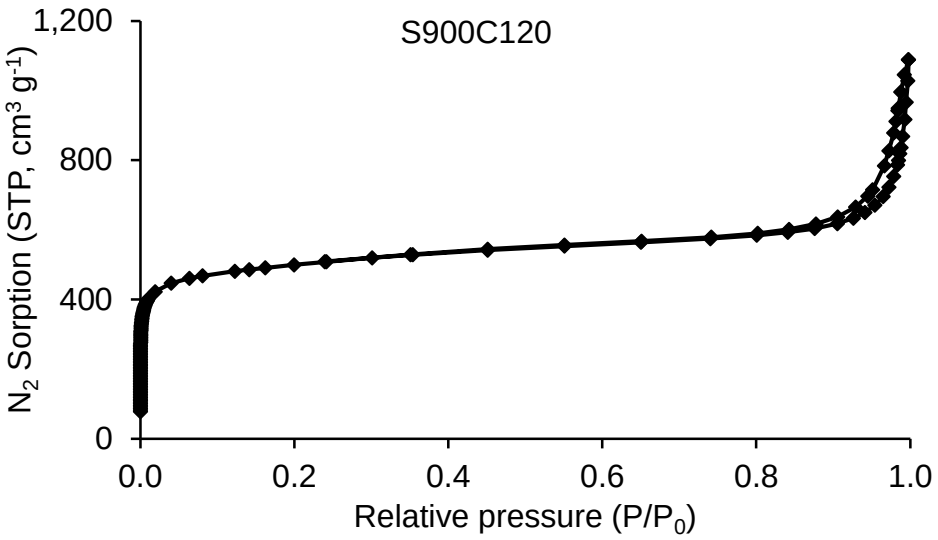

Pore distribution in the mesopore region (BJH method)

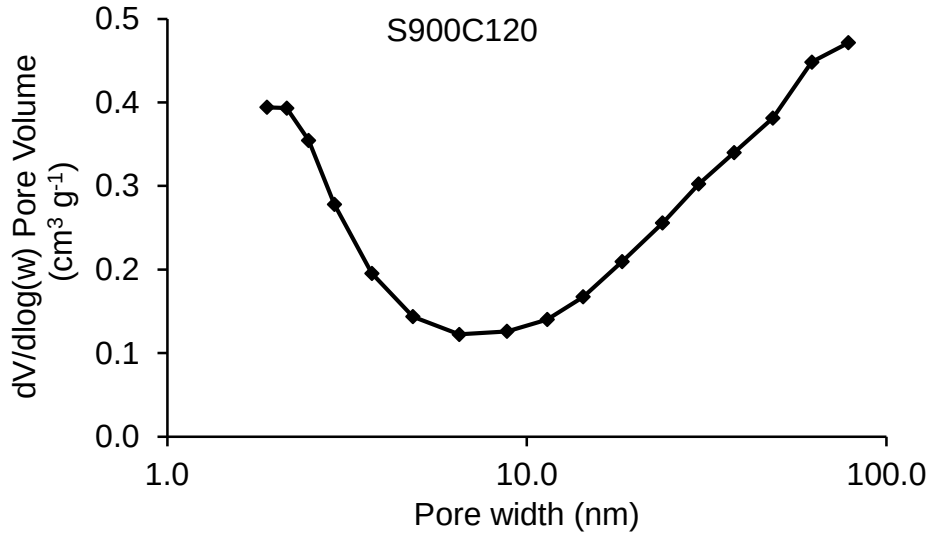

Pore distribution in the micropore region (HK method)

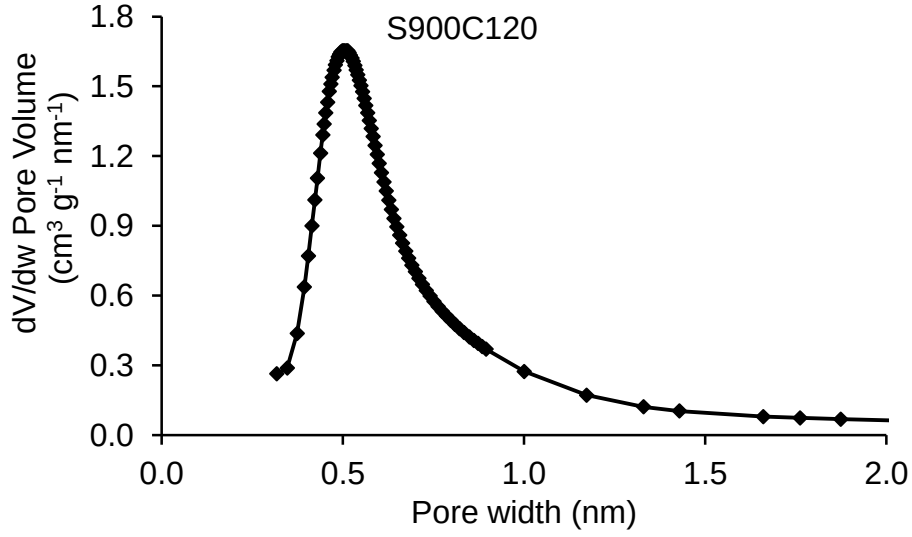

Nitrogen adsorption isotherm and pore distribution plots for S950C30

Nitrogen adsorption isotherm (77K)

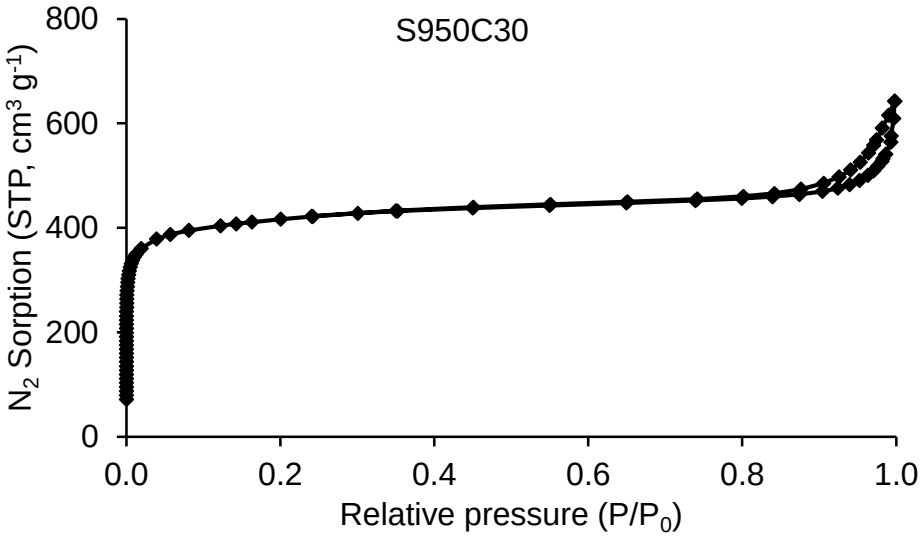

Pore distribution in the mesopore region (BJH method)

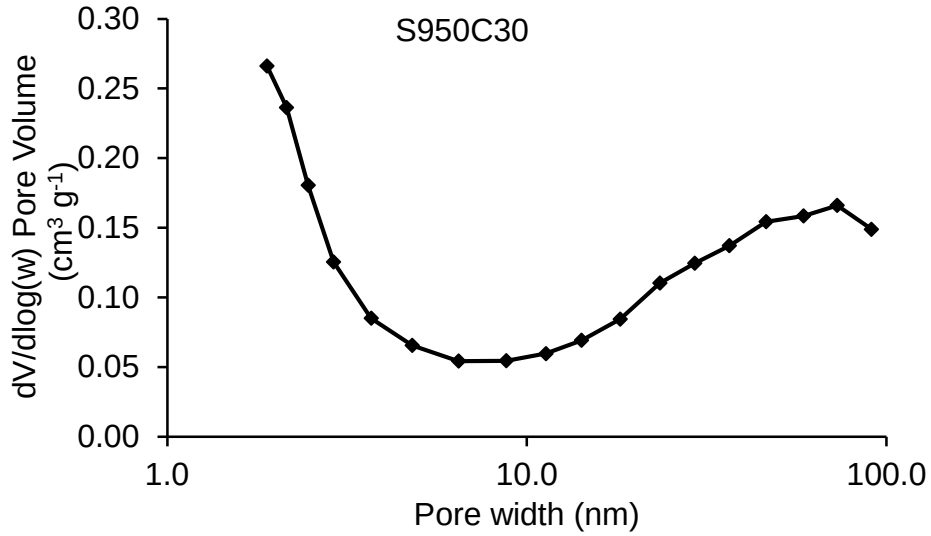

Pore distribution in the micropore region (HK method)

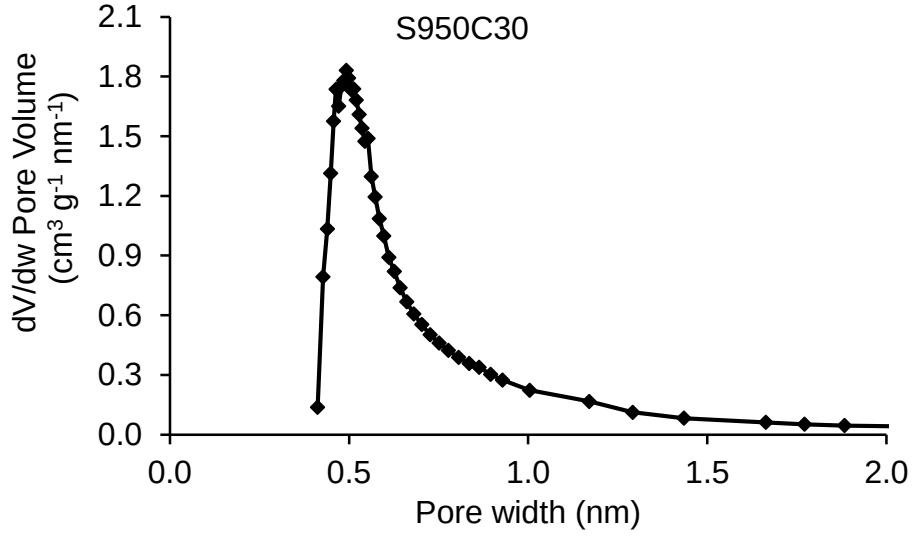

Nitrogen adsorption isotherm and pore distribution plots for S950C60

Nitrogen adsorption isotherm (77K)

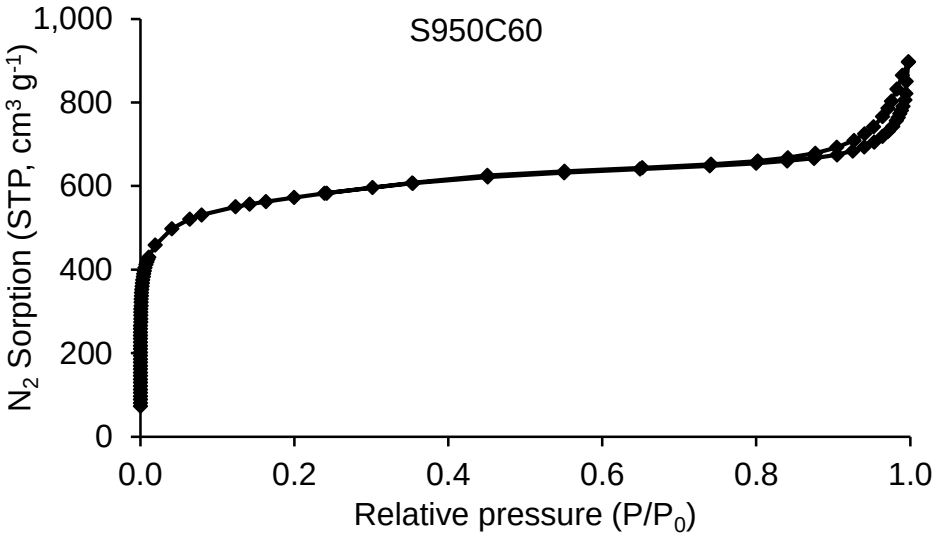

Pore distribution in the mesopore region (BJH method)

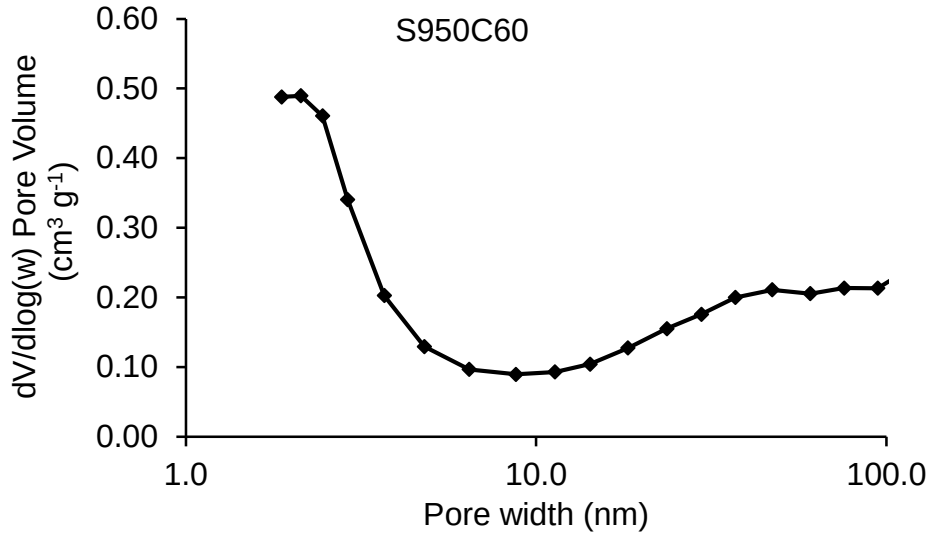

Pore distribution in the micropore region (HK method)

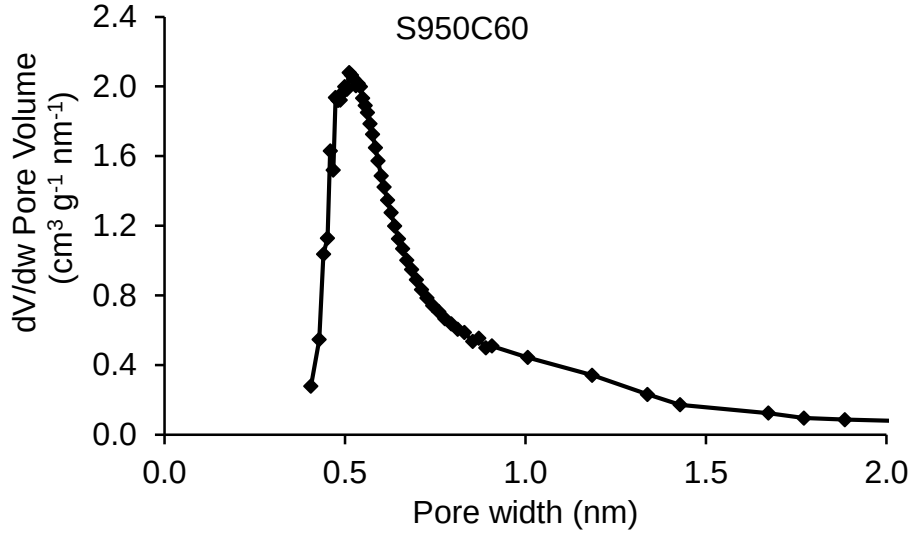

Nitrogen adsorption isotherm and pore distribution plots for S950C90

Nitrogen adsorption isotherm (77K)

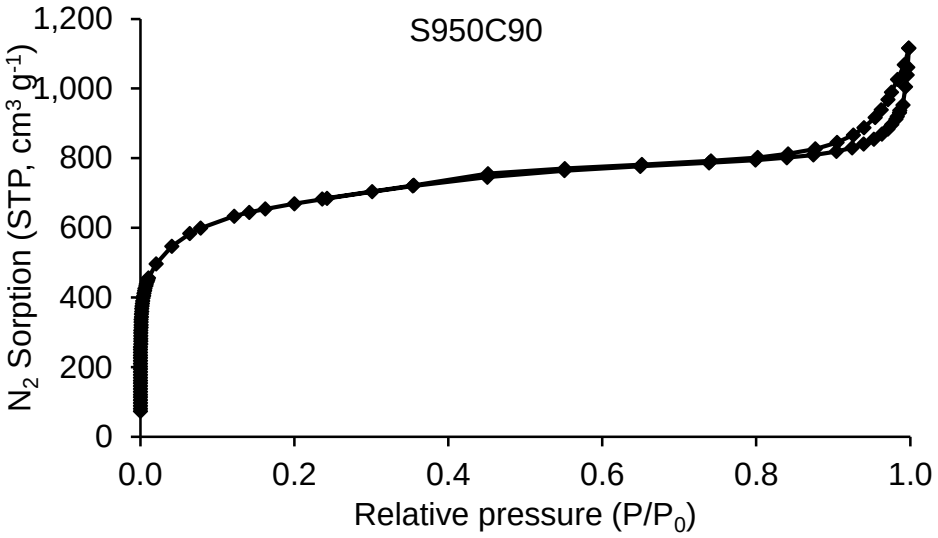

Pore distribution in the mesopore region (BJH method)

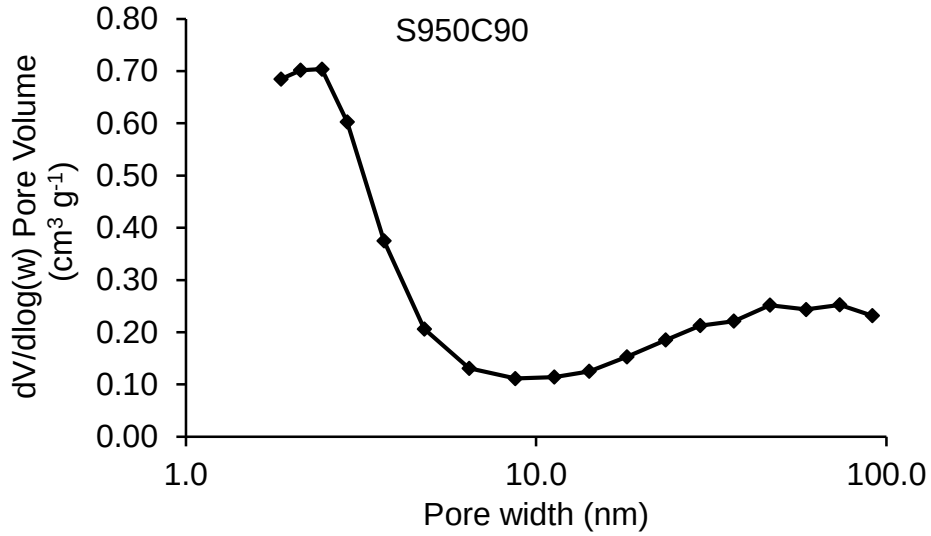

Pore distribution in the micropore region (HK method)

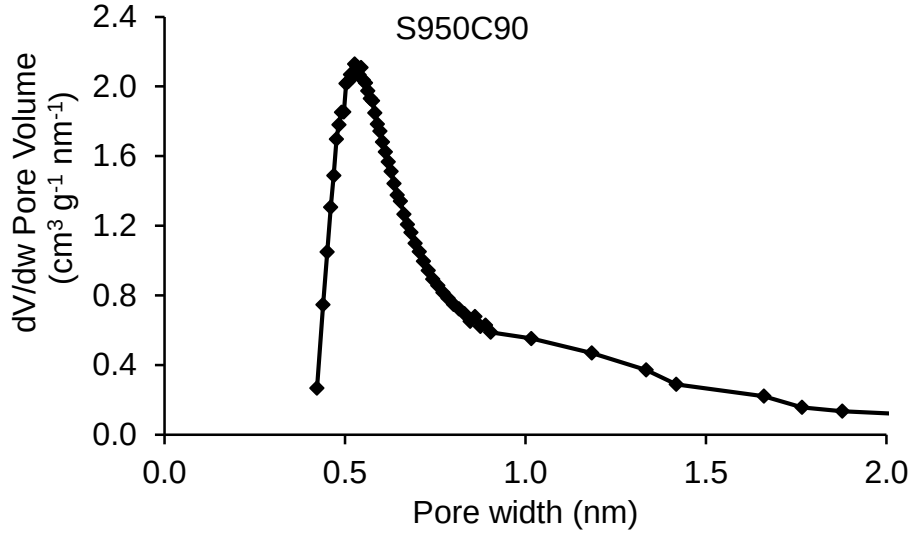

Nitrogen adsorption isotherm and pore distribution plots for S950C120

Nitrogen adsorption isotherm (77K)

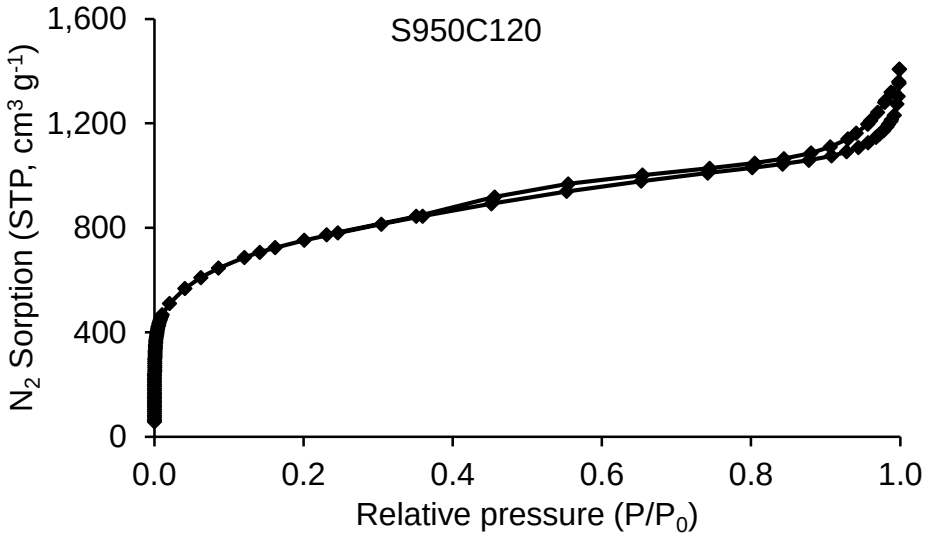

Pore distribution in the mesopore region (BJH method)

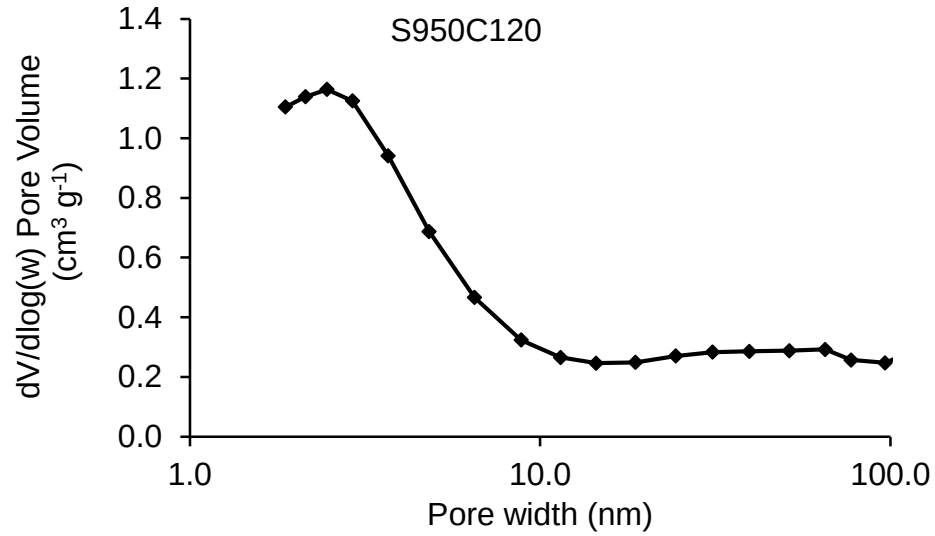

Pore distribution in the micropore region (HK method)

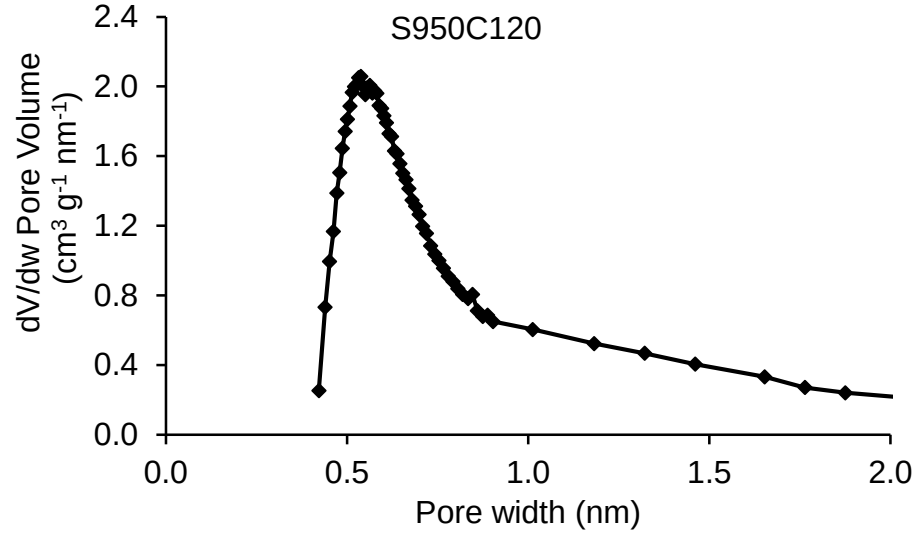

Nitrogen adsorption isotherm and pore distribution plots for A750C45

Nitrogen adsorption isotherm (77K)

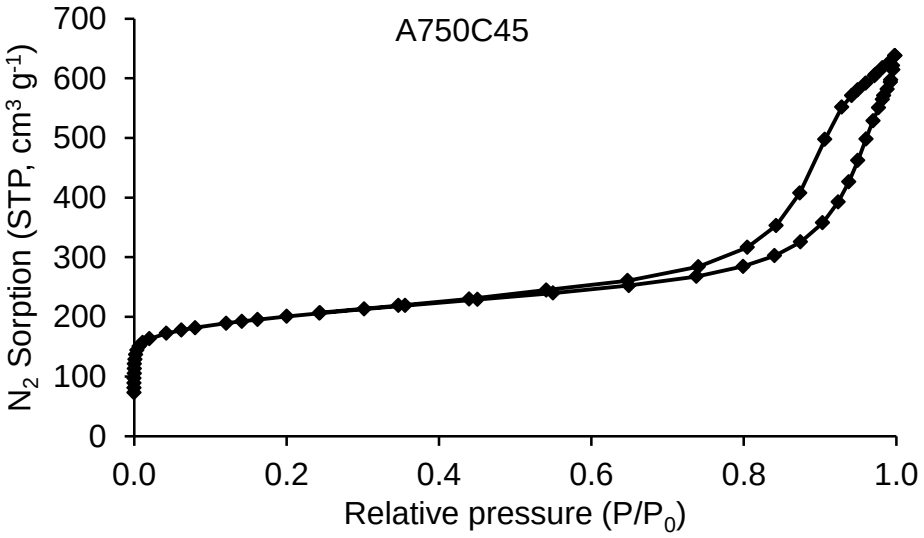

Pore distribution in the mesopore region (BJH method)

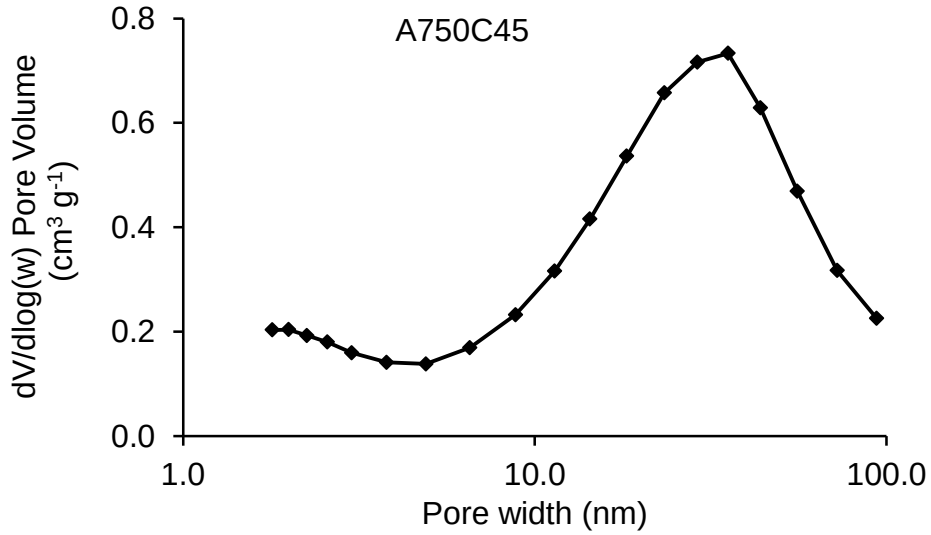

Pore distribution in the micropore region (HK method)

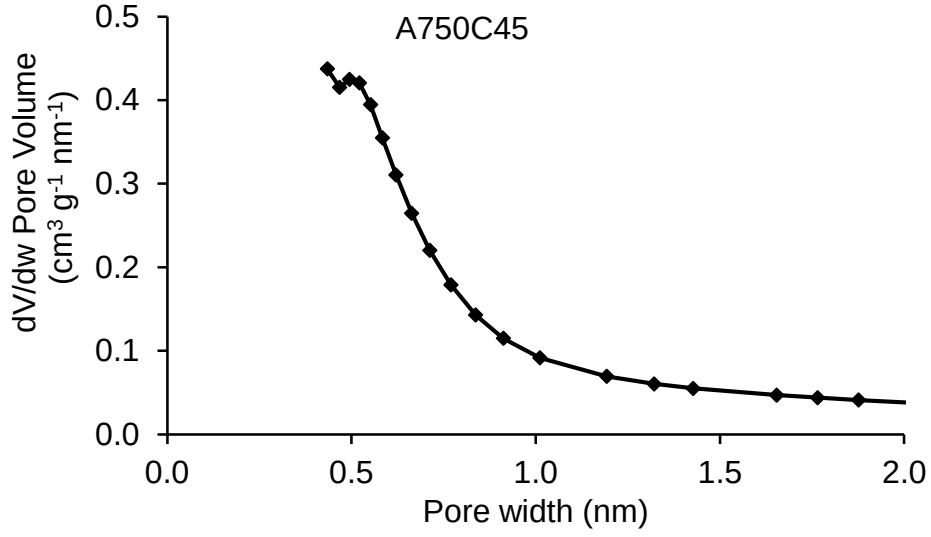

Nitrogen adsorption isotherm and pore distribution plots for A750C60

Nitrogen adsorption isotherm (77K)

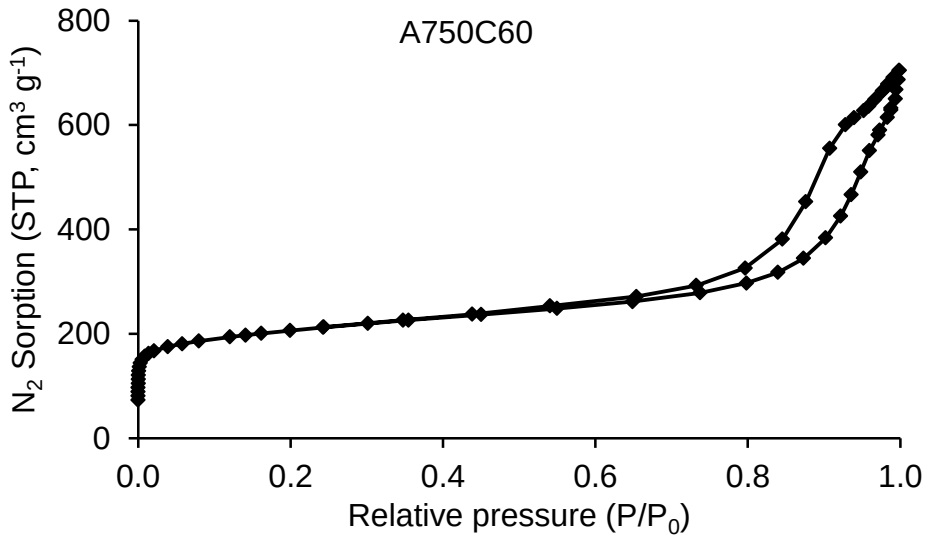

Pore distribution in the mesopore region (BJH method)

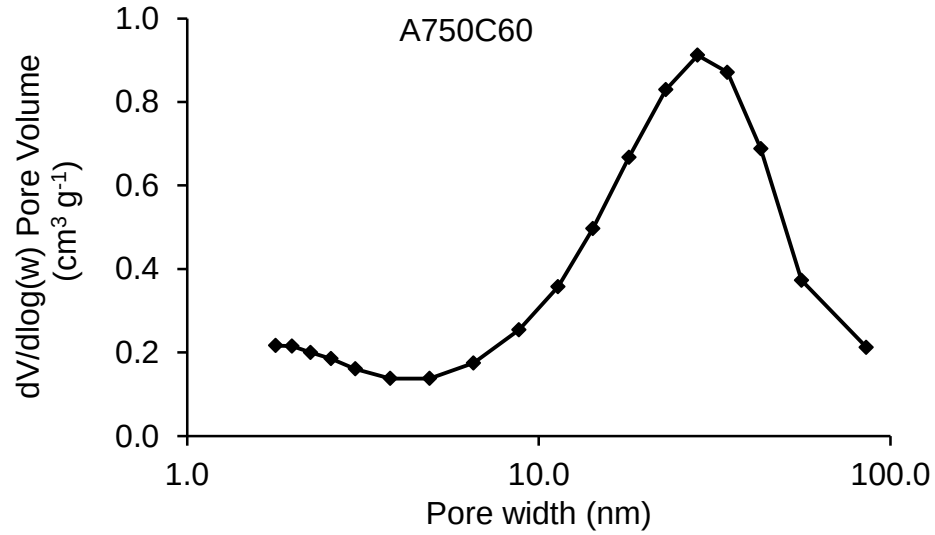

Pore distribution in the micropore region (HK method)

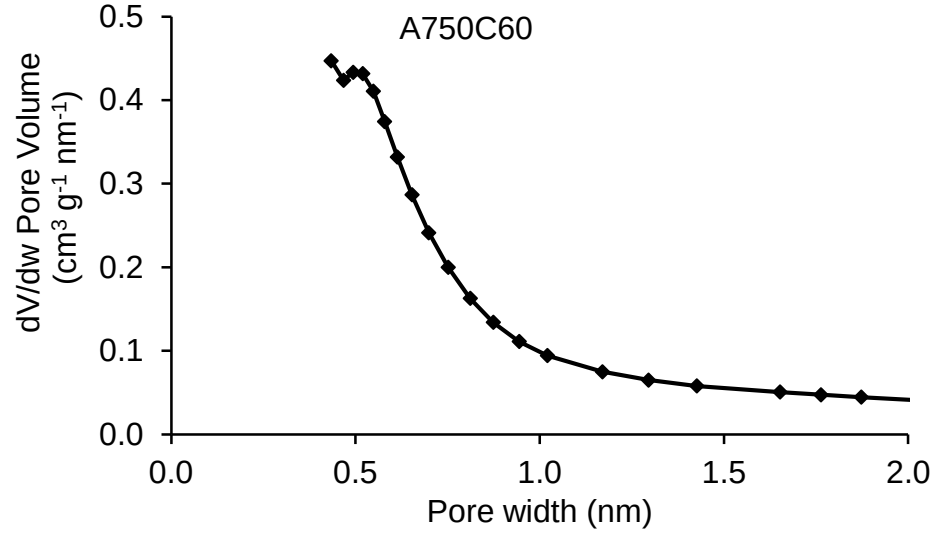

Nitrogen adsorption isotherm and pore distribution plots for A750C90

Nitrogen adsorption isotherm (77K)

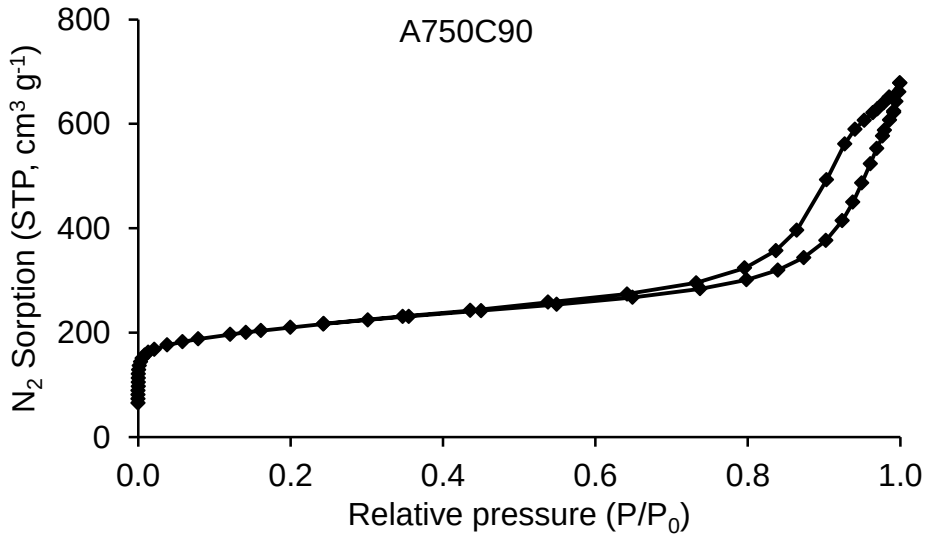

Pore distribution in the mesopore region (BJH method)

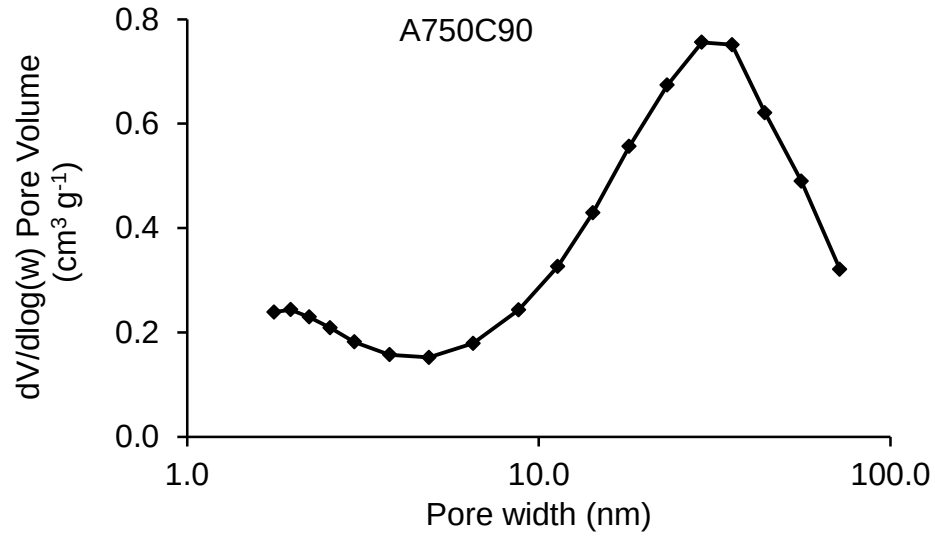

Pore distribution in the micropore region (HK method)

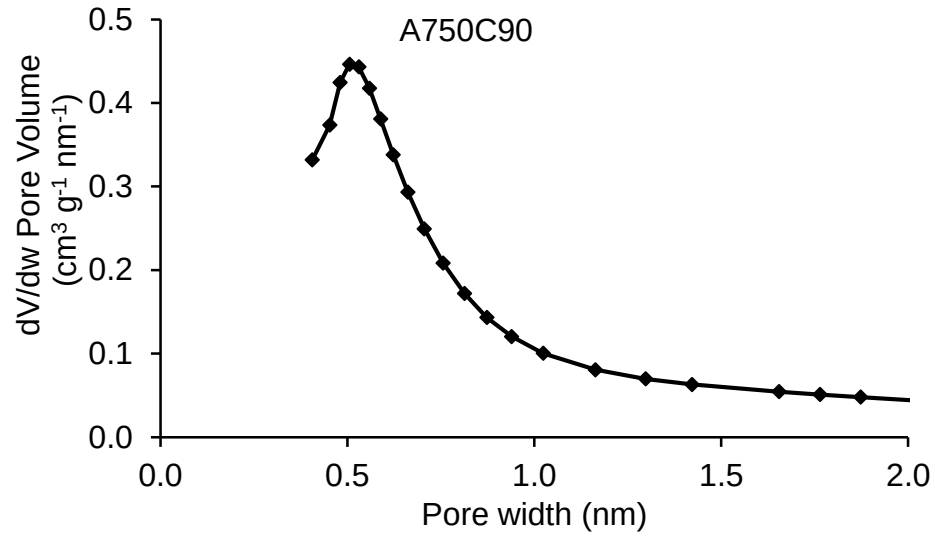

Nitrogen adsorption isotherm and pore distribution plots for A900C0

Nitrogen adsorption isotherm (77K)

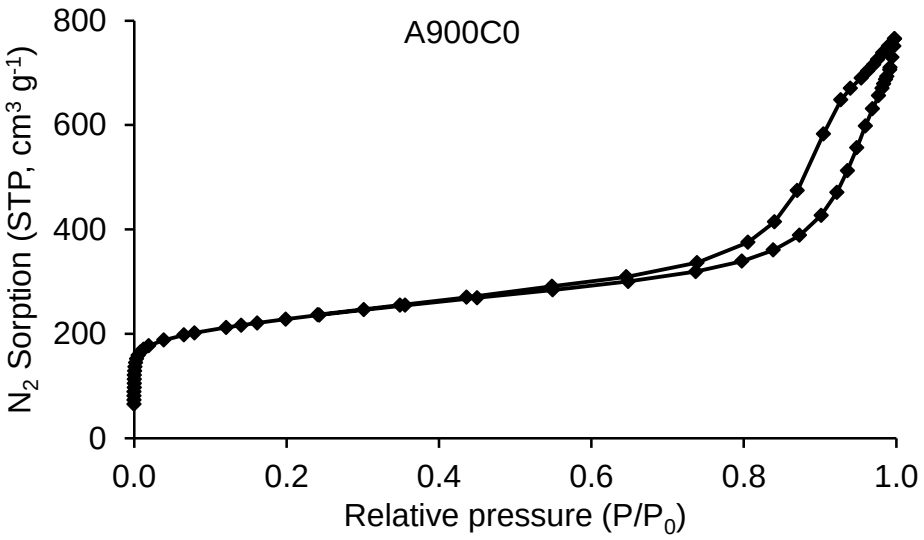

Pore distribution in the mesopore region (BJH method)

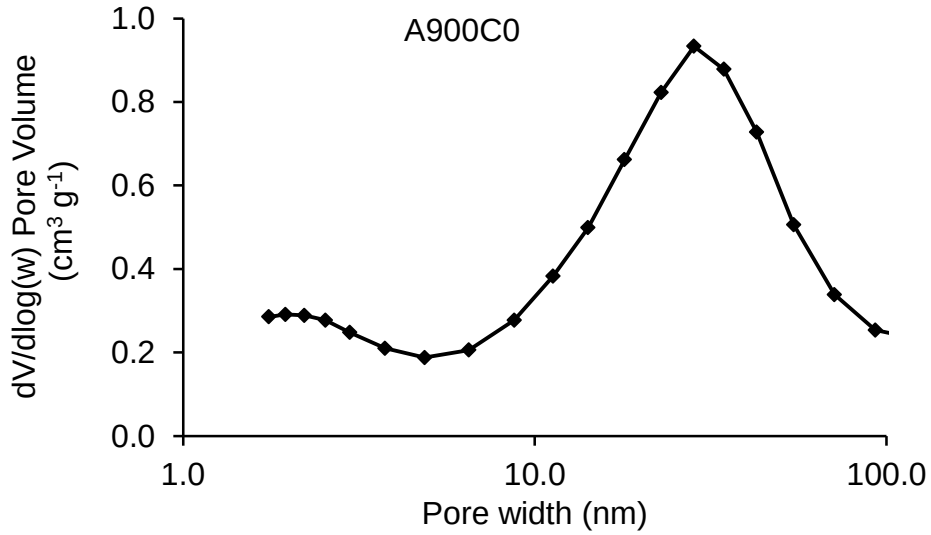

Pore distribution in the micropore region (HK method)

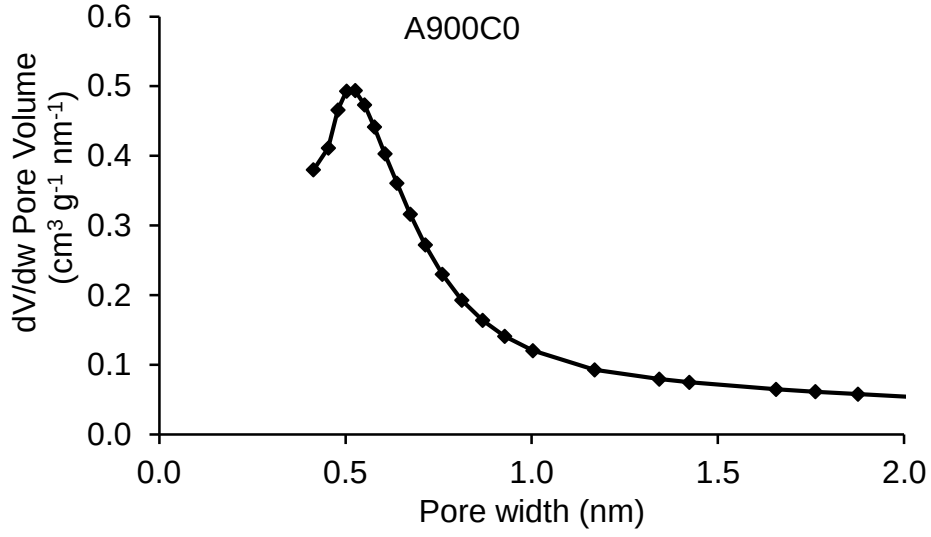

Nitrogen adsorption isotherm and pore distribution plots for A900C10

Nitrogen adsorption isotherm (77K)

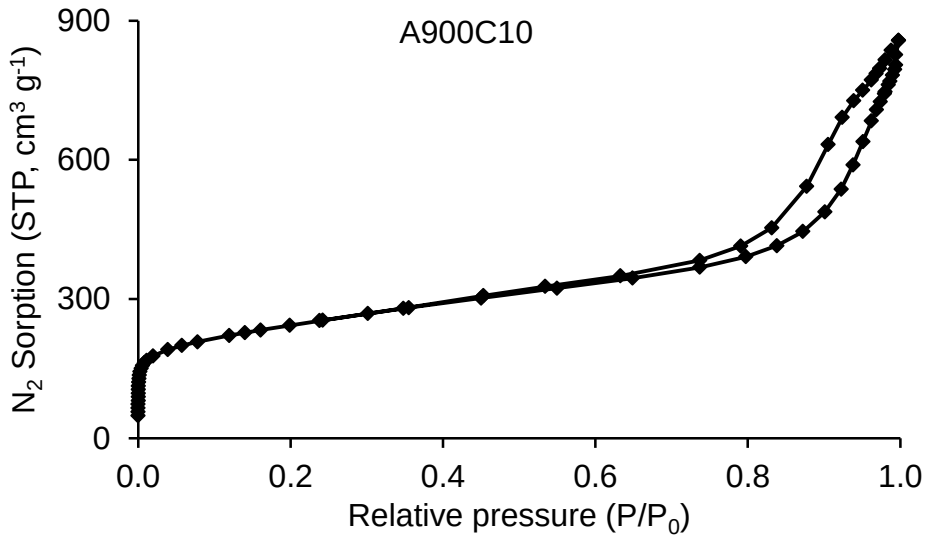

Pore distribution in the mesopore region (BJH method)

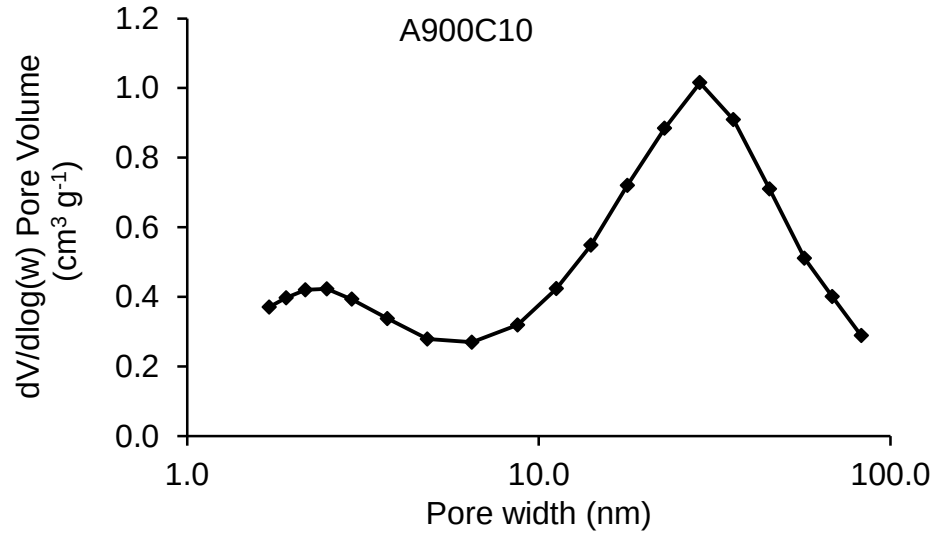

Pore distribution in the micropore region (HK method)

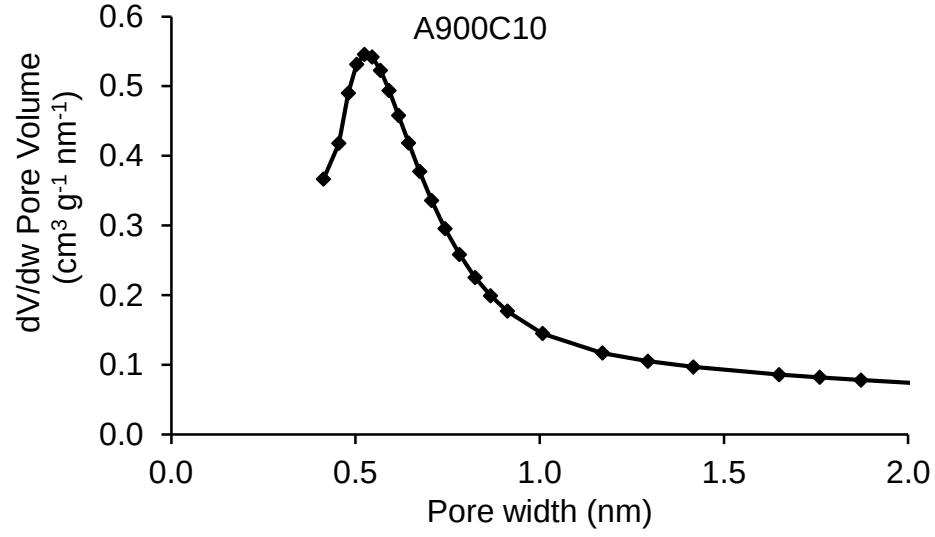

Nitrogen adsorption isotherm and pore distribution plots for P700C50

Nitrogen adsorption isotherm (77K)

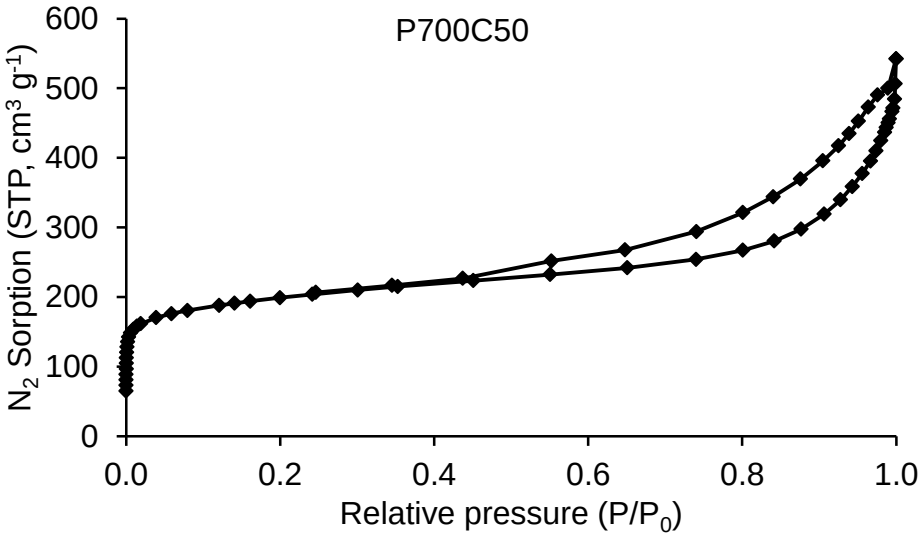

Pore distribution in the mesopore region (BJH method)

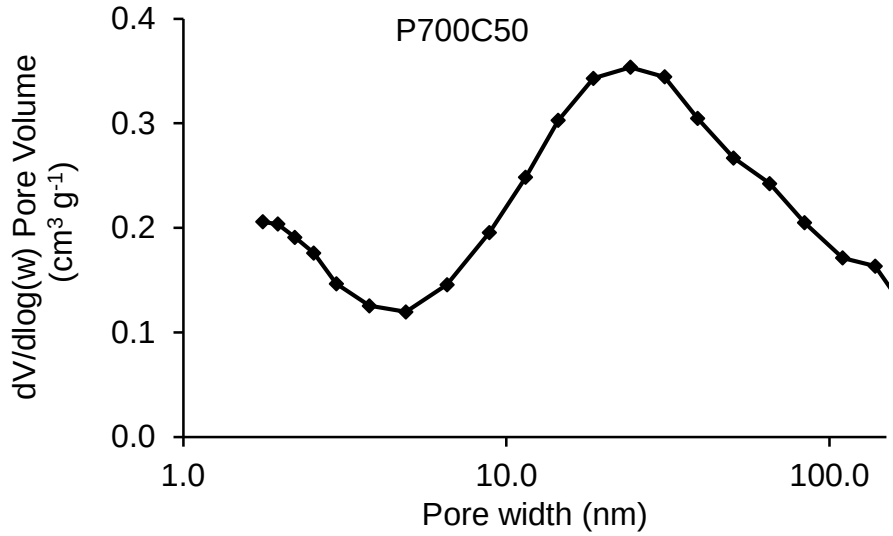

Pore distribution in the micropore region (HK method)

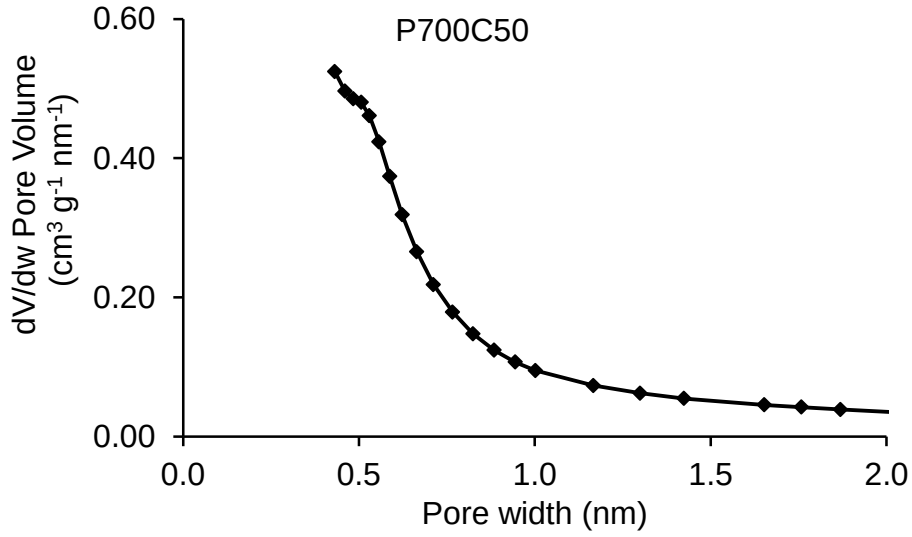

Nitrogen adsorption isotherm and pore distribution plots for P900C0

Nitrogen adsorption isotherm (77K)

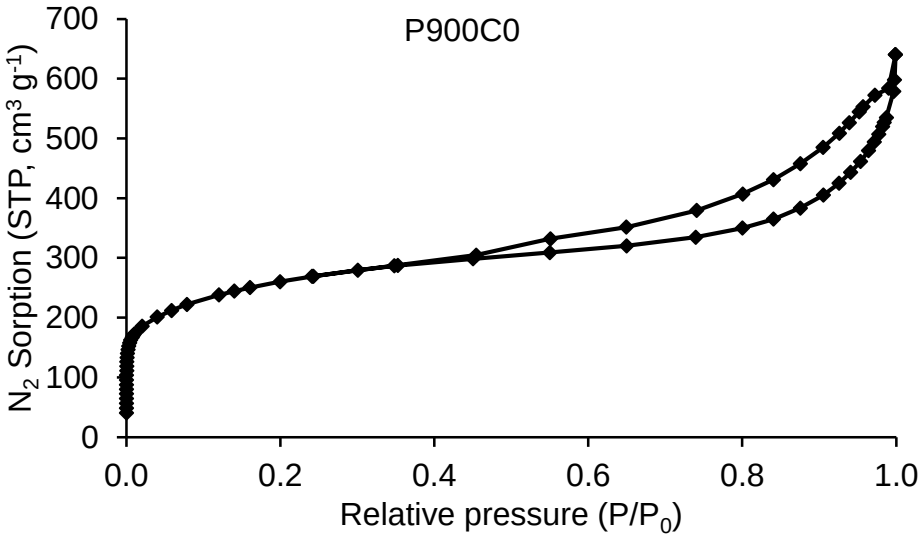

Pore distribution in the mesopore region (BJH method)

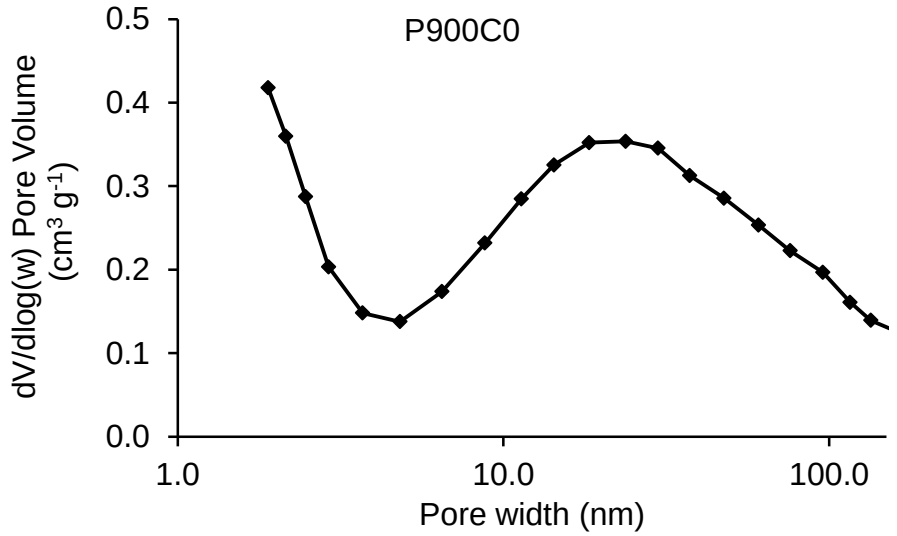

Pore distribution in the micropore region (HK method)

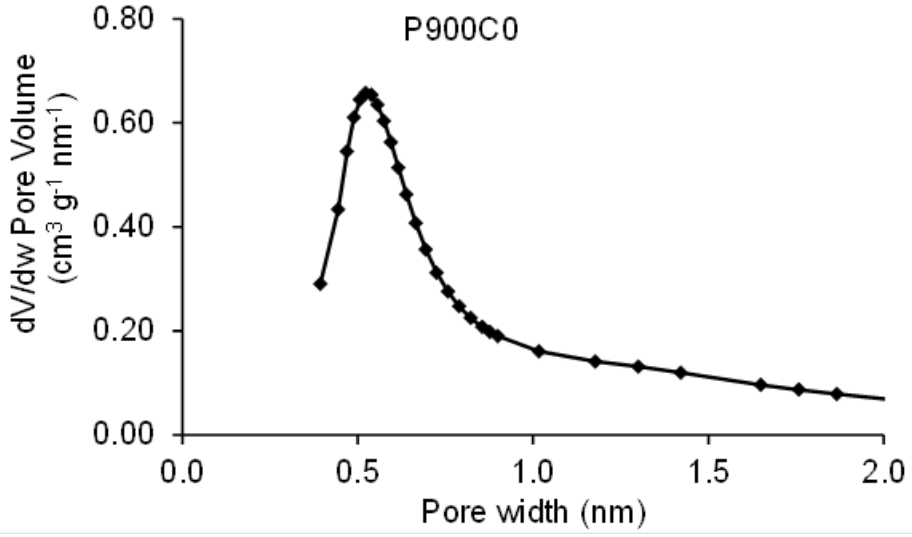

Nitrogen adsorption isotherm and pore distribution plots for S700O0

Nitrogen adsorption isotherm (77K)

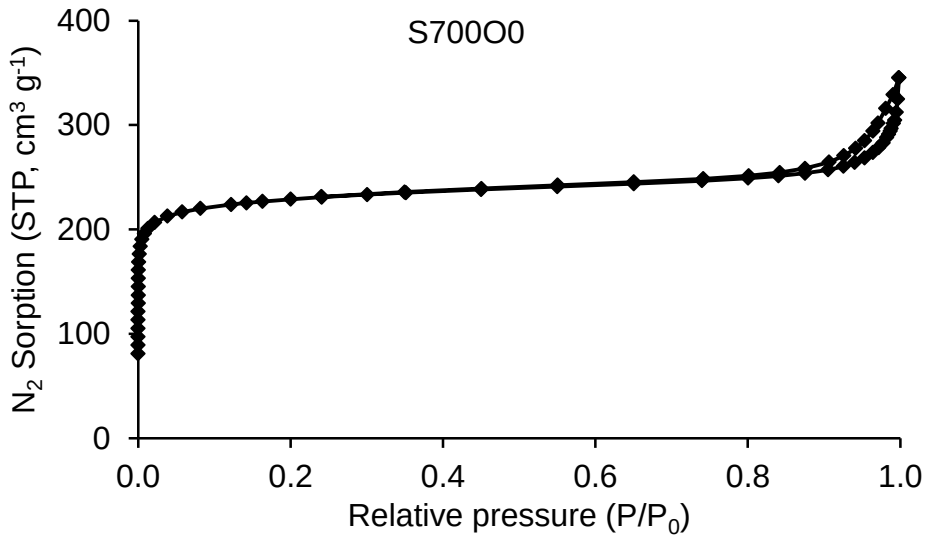

Pore distribution in the mesopore region (BJH method)

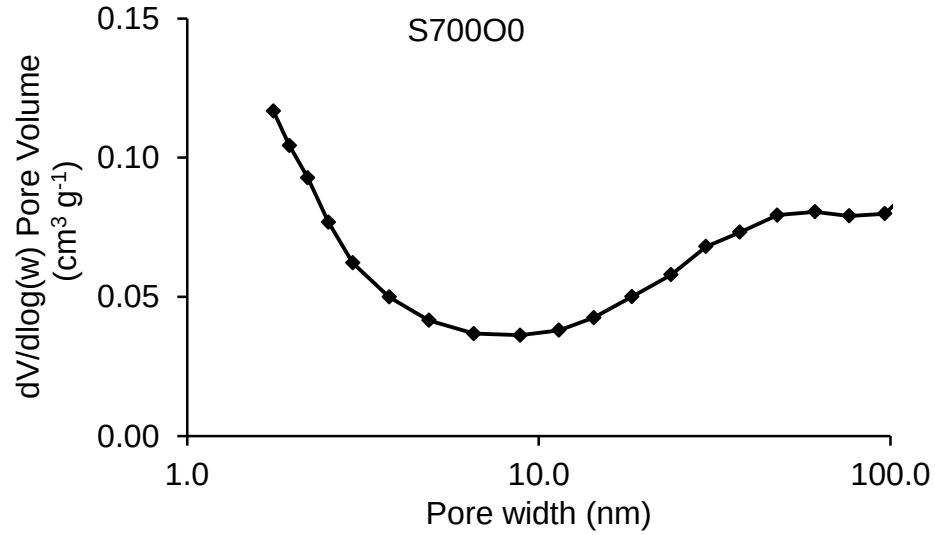

Pore distribution in the micropore region (HK method)

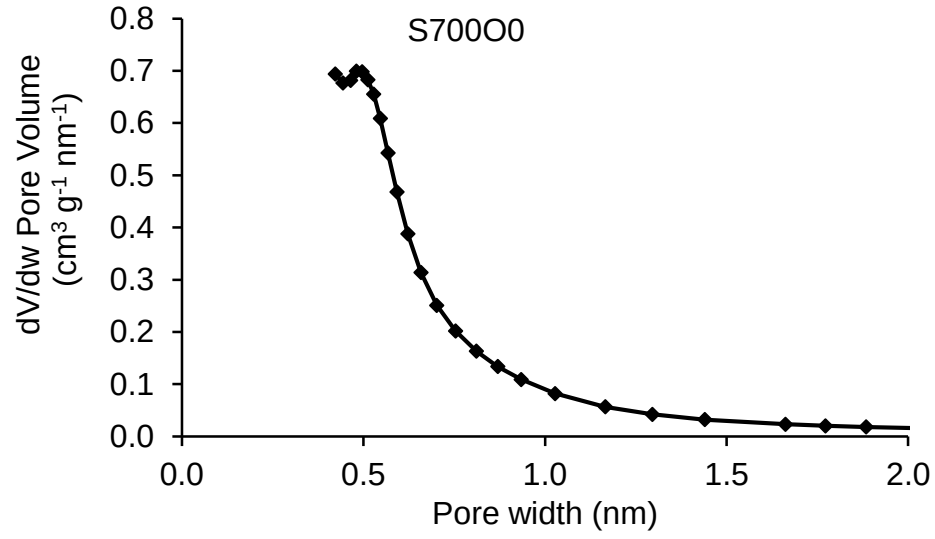

Nitrogen adsorption isotherm and pore distribution plots for S750O0

Nitrogen adsorption isotherm (77K)

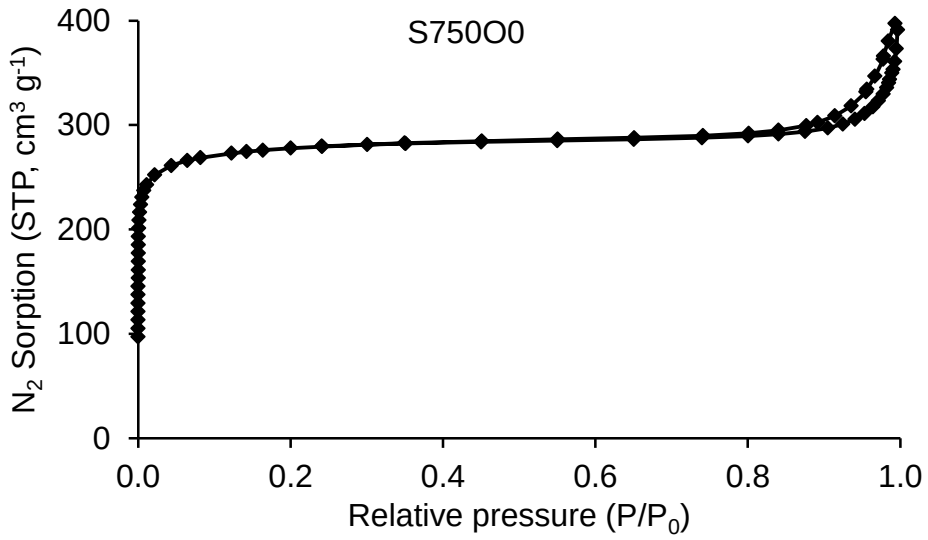

Pore distribution in the mesopore region (BJH method)

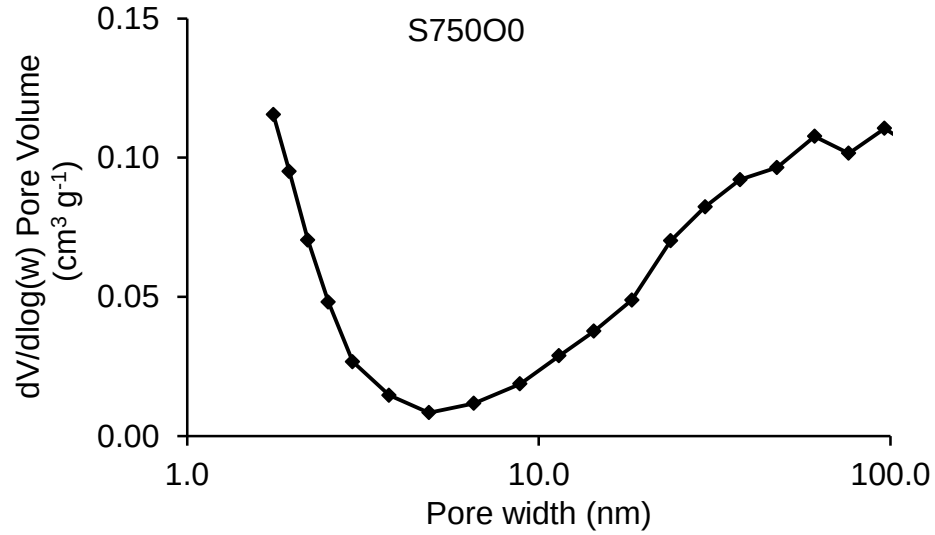

Pore distribution in the micropore region (HK method)

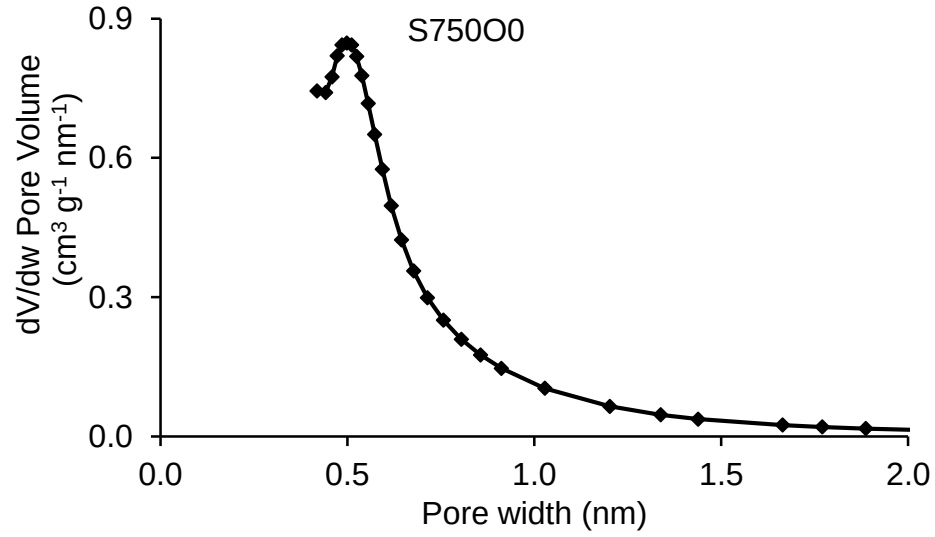

Nitrogen adsorption isotherm and pore distribution plots for S800O0

Nitrogen adsorption isotherm (77K)

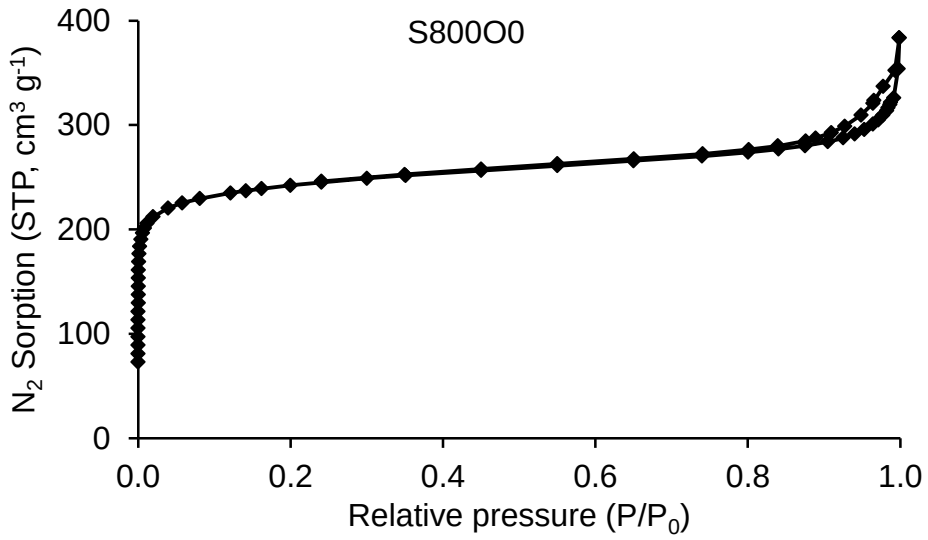

Pore distribution in the mesopore region (BJH method)

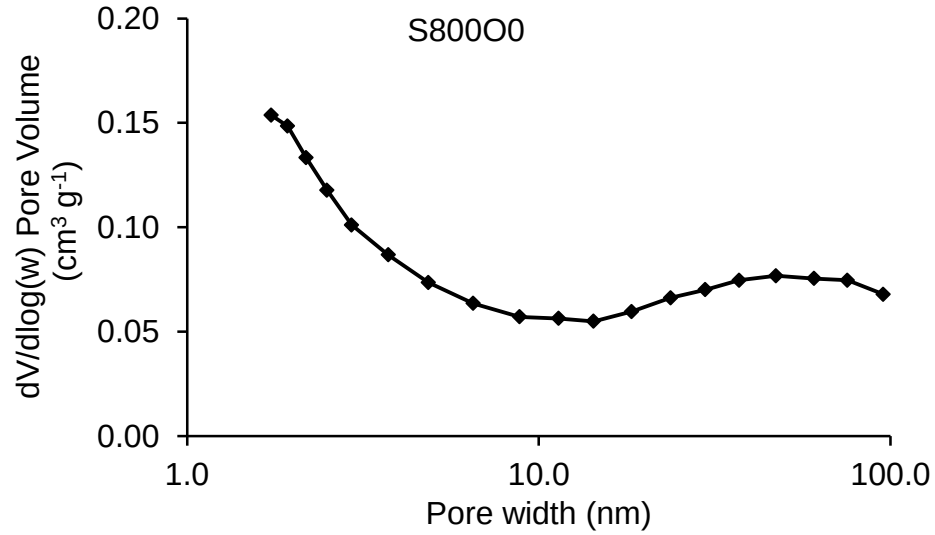

Pore distribution in the micropore region (HK method)

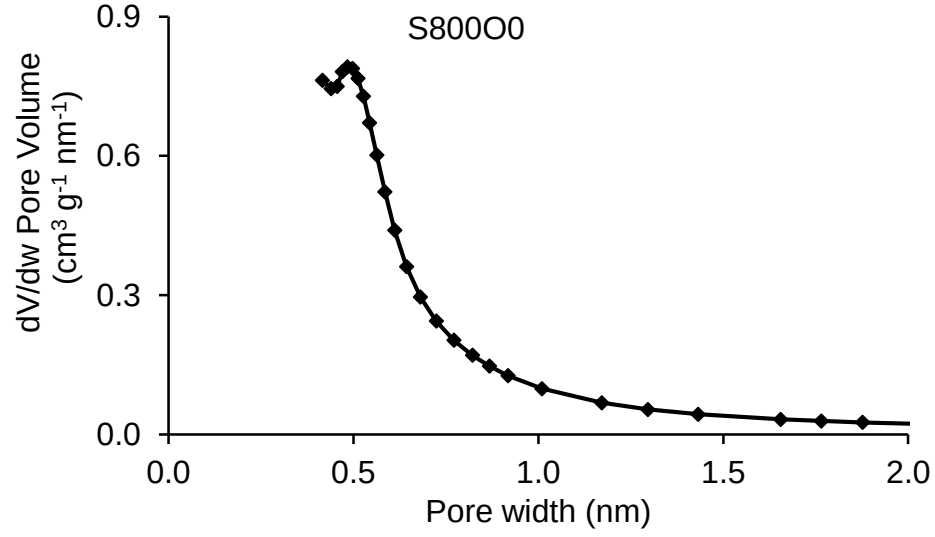

Nitrogen adsorption isotherm and pore distribution plots for S750O40

Nitrogen adsorption isotherm (77K)

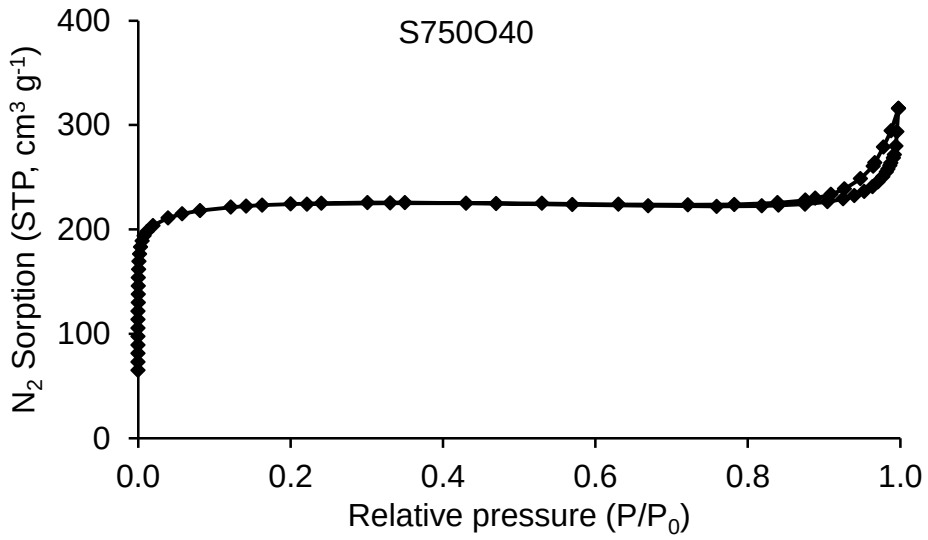

Pore distribution in the mesopore region (BJH method)

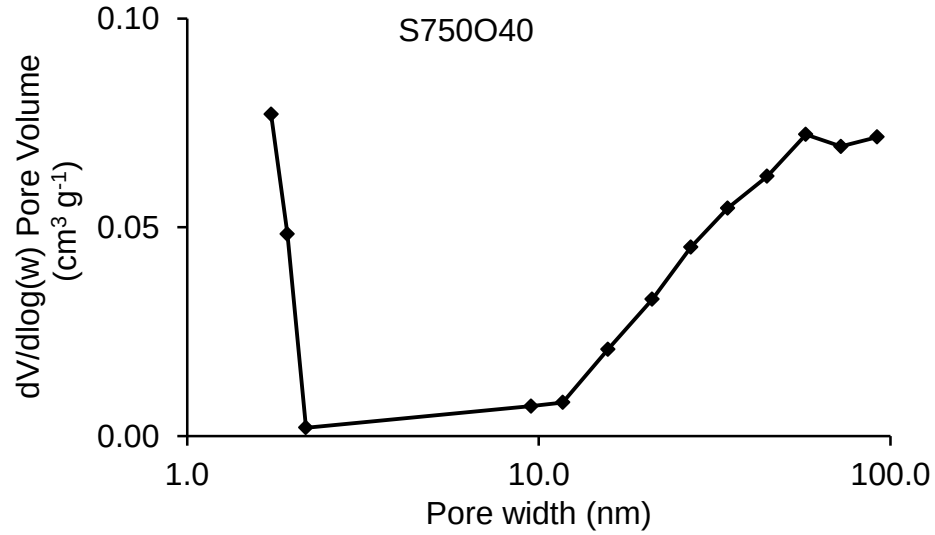

Pore distribution in the micropore region (HK method)

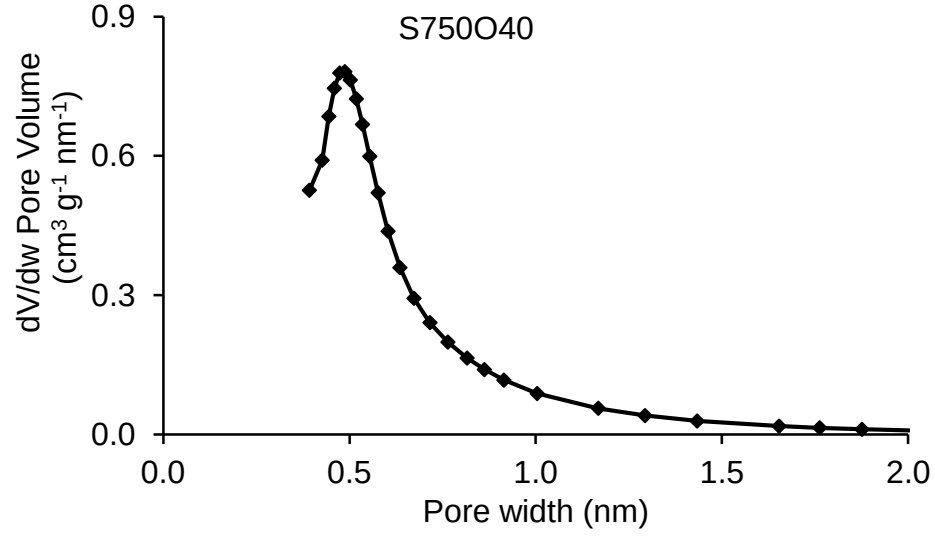

Nitrogen adsorption isotherm and pore distribution plots for S750O56

Nitrogen adsorption isotherm (77K)

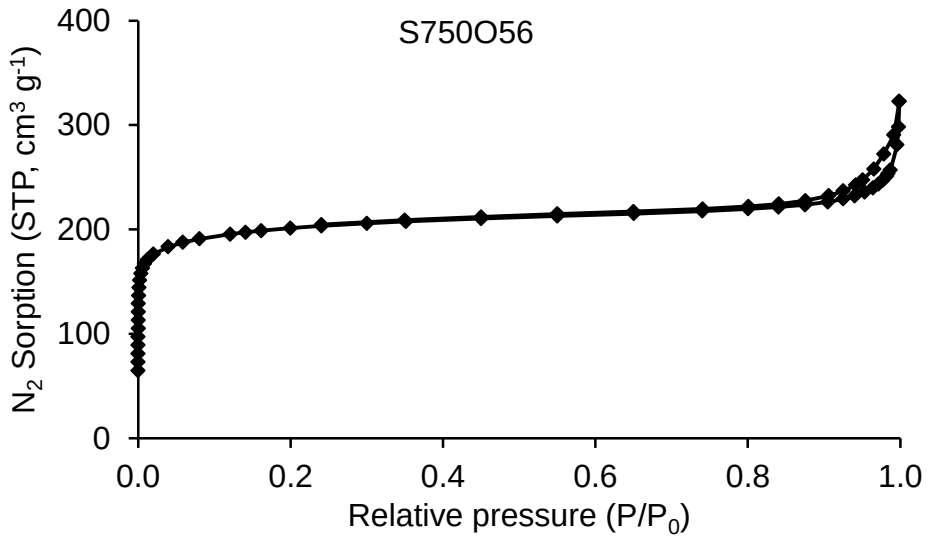

Pore distribution in the mesopore region (BJH method)

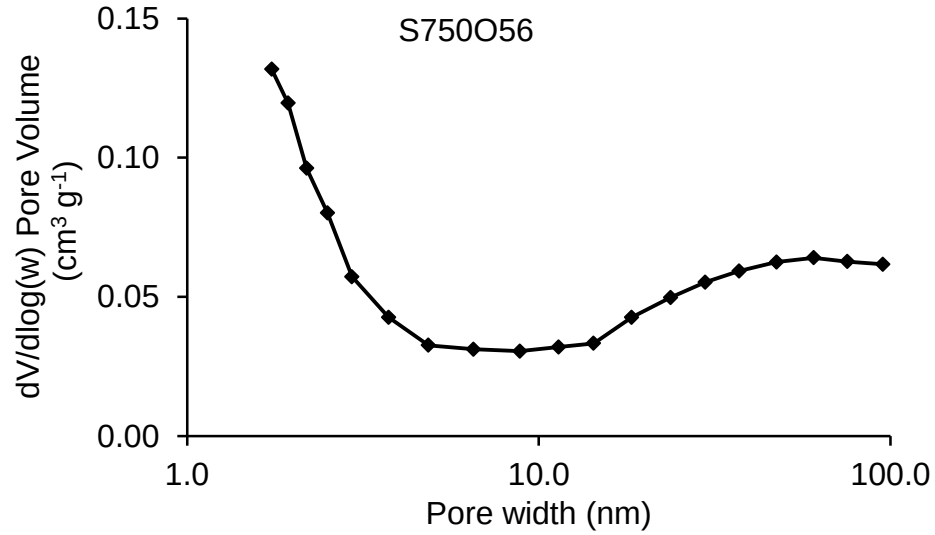

Pore distribution in the micropore region (HK method)

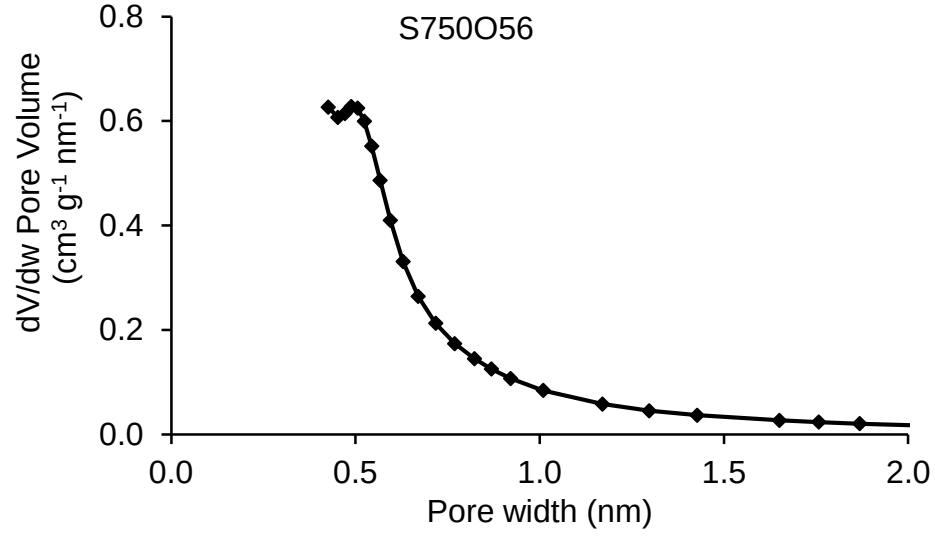

Nitrogen adsorption isotherm and pore distribution plots for A500O30

Nitrogen adsorption isotherm (77K)

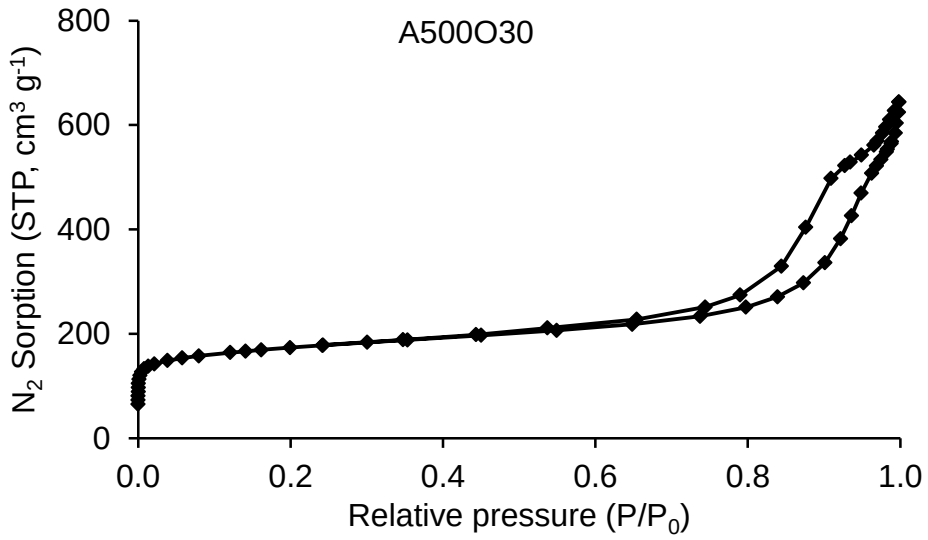

Pore distribution in the mesopore region (BJH method)

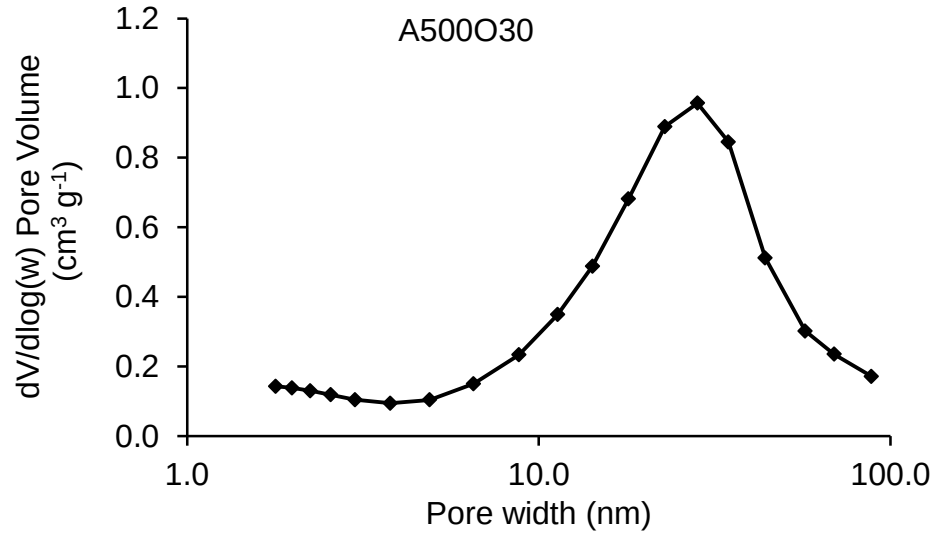

Pore distribution in the micropore region (HK method)

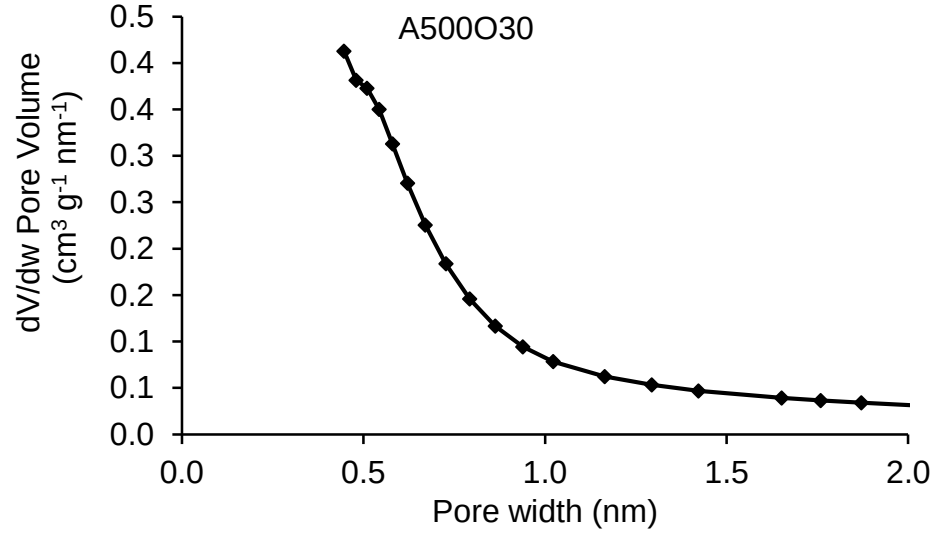

Nitrogen adsorption isotherm and pore distribution plots for A500O60

Nitrogen adsorption isotherm (77K)

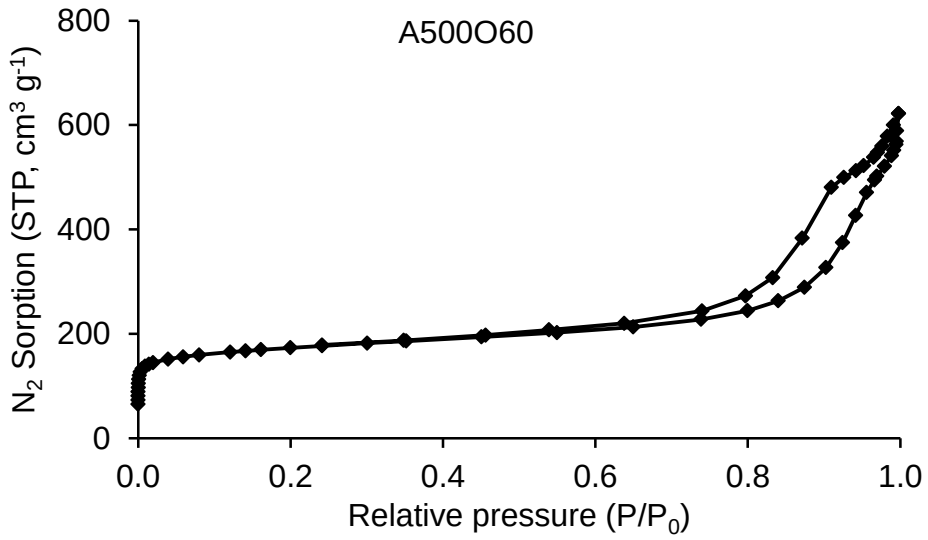

Pore distribution in the mesopore region (BJH method)

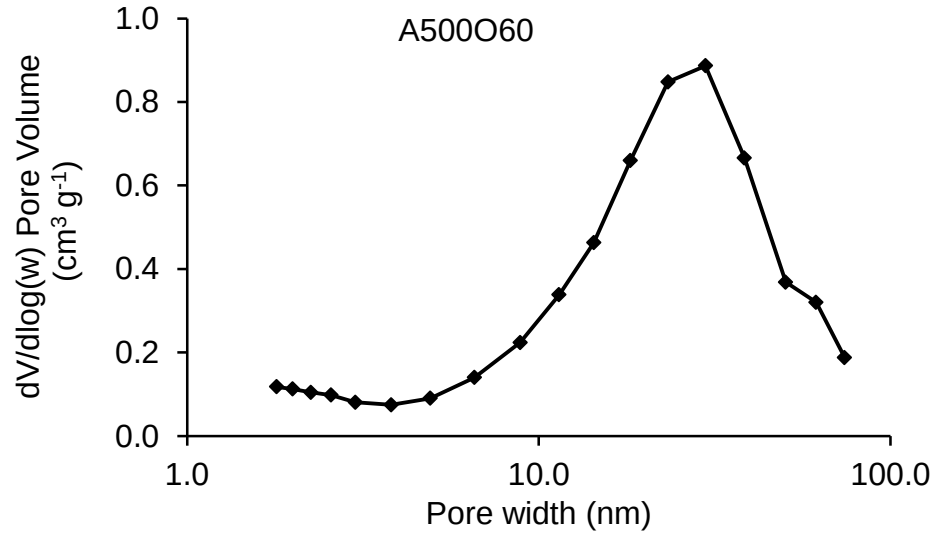

Pore distribution in the micropore region (HK method)

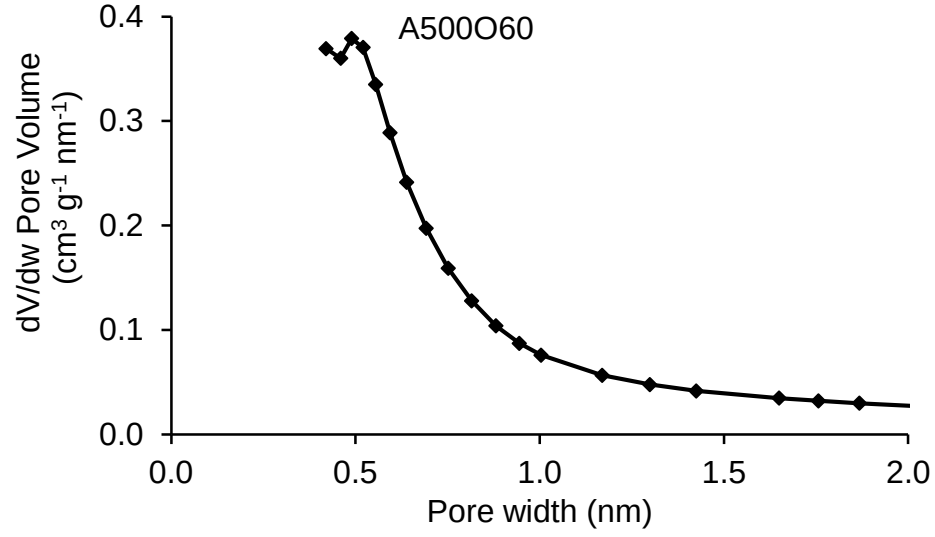

Nitrogen adsorption isotherm and pore distribution plots for A750O0

Nitrogen adsorption isotherm (77K)

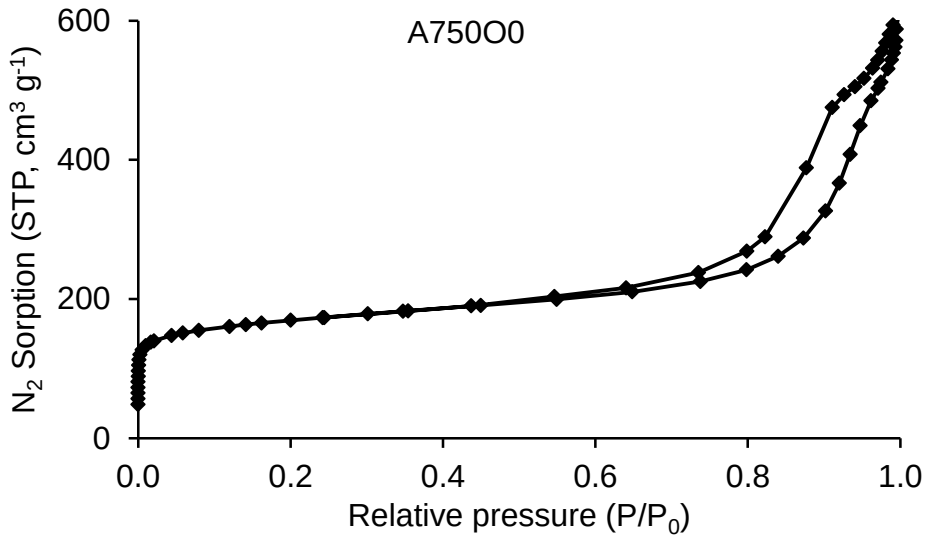

Pore distribution in the mesopore region (BJH method)

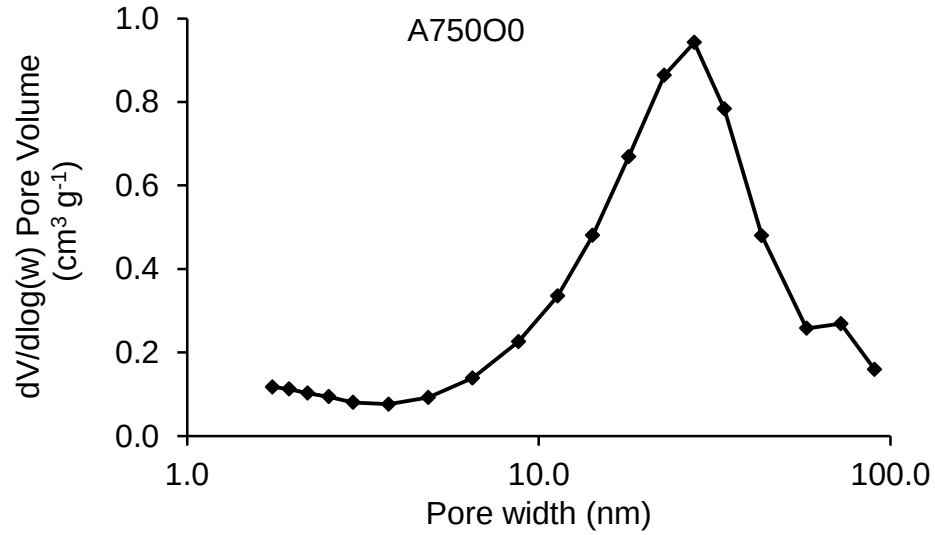

Pore distribution in the micropore region (HK method)

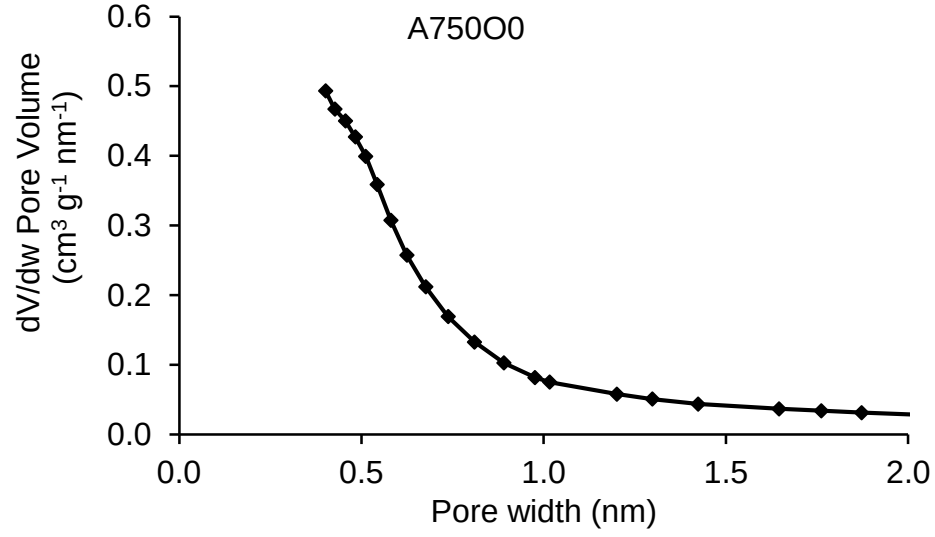

Nitrogen adsorption isotherm and pore distribution plots for P400O50

Nitrogen adsorption isotherm (77K)

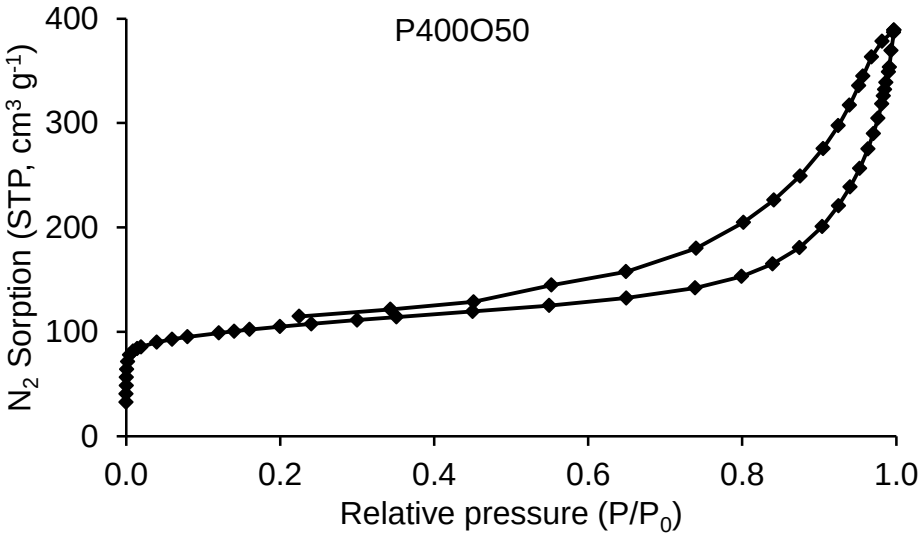

Pore distribution in the mesopore region (BJH method)

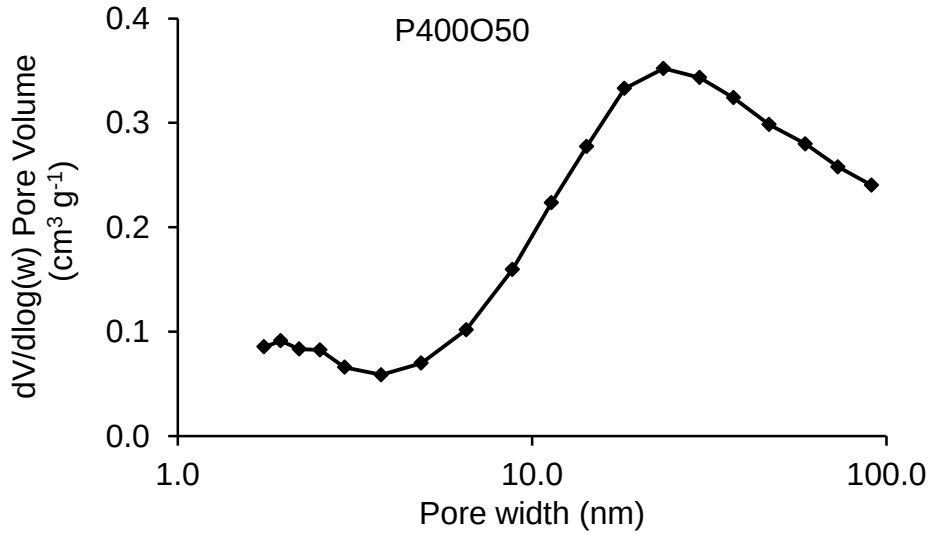

Pore distribution in the micropore region (HK method)

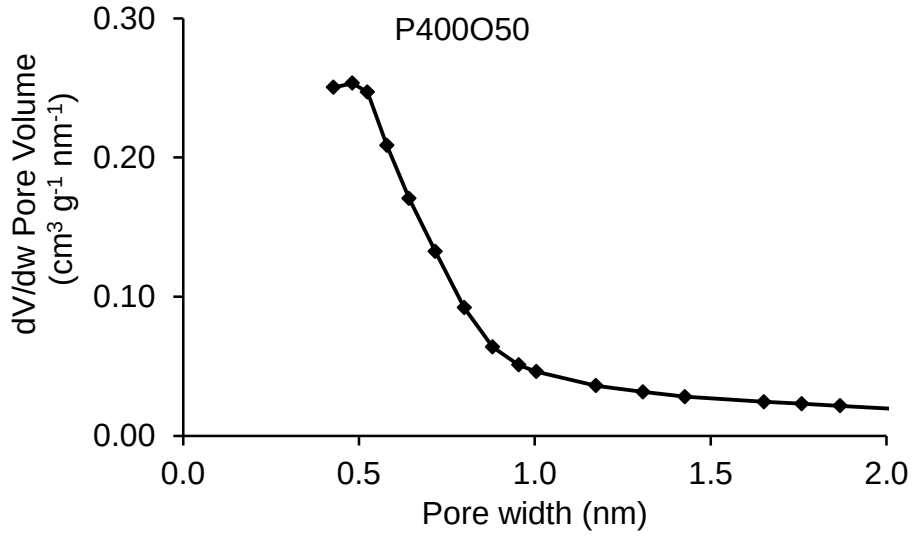

Nitrogen adsorption isotherm and pore distribution plots for P500O30

Nitrogen adsorption isotherm (77K)

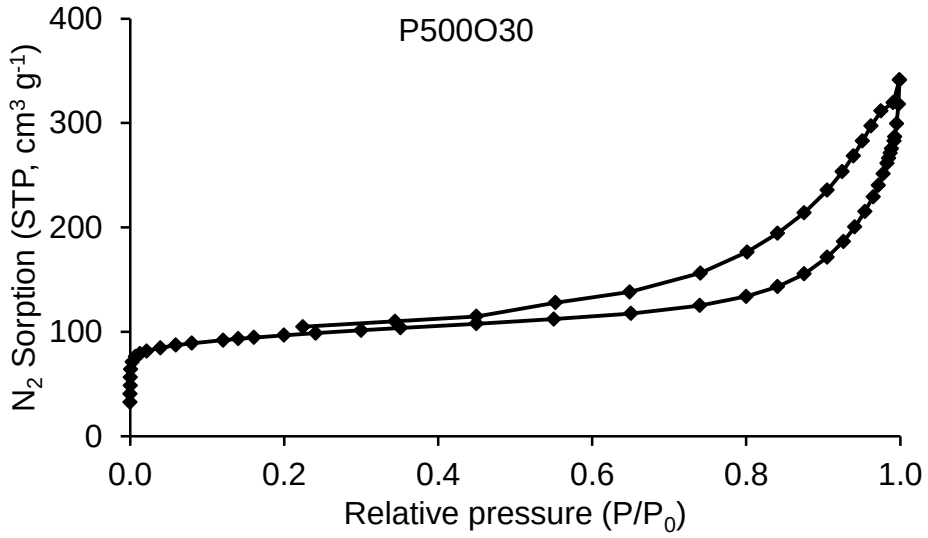

Pore distribution in the mesopore region (BJH method)

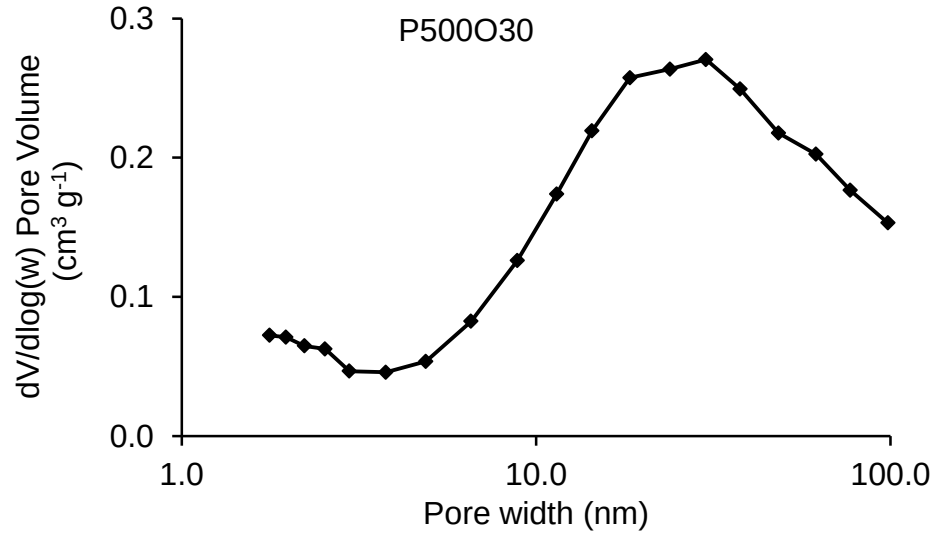

Pore distribution in the micropore region (HK method)

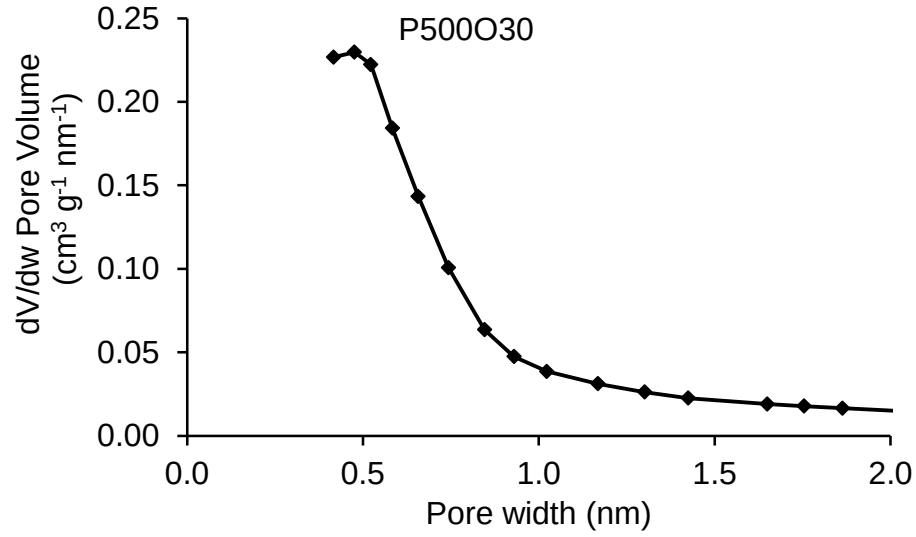

Nitrogen adsorption isotherm and pore distribution plots for P750O0

Nitrogen adsorption isotherm (77K)

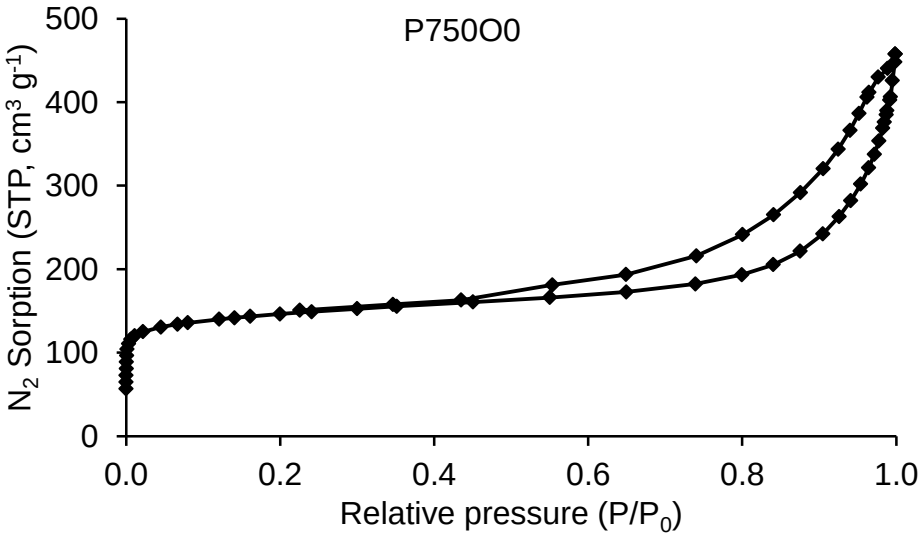

Pore distribution in the mesopore region (BJH method)

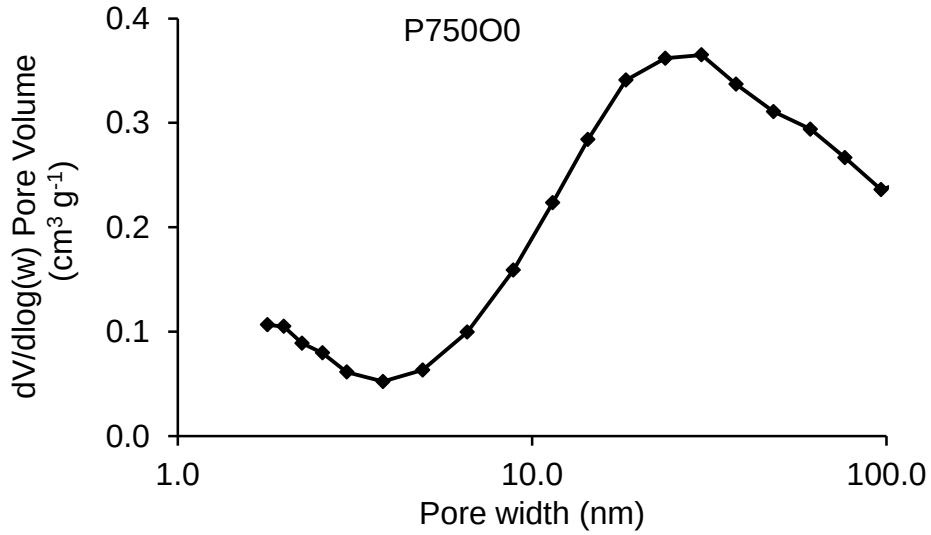

Pore distribution in the micropore region (HK method)

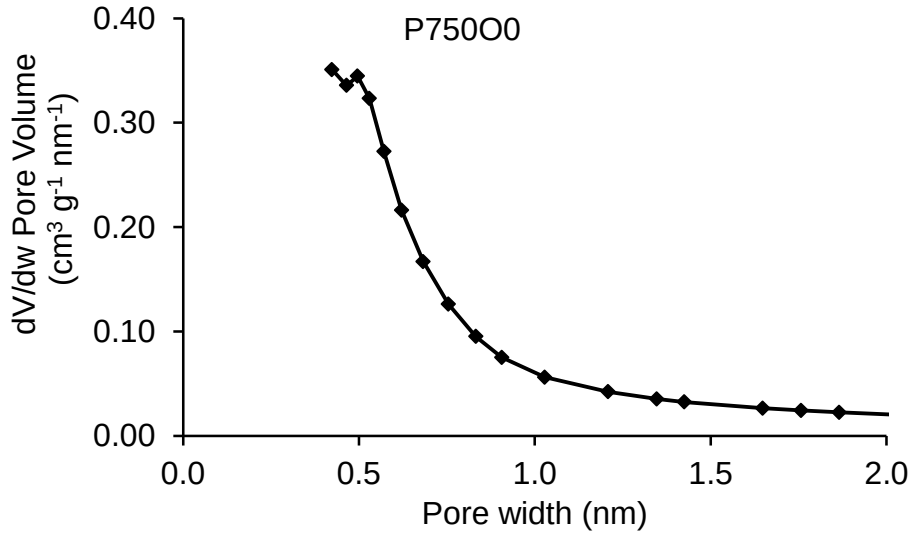

BET-surface areas and pore volumes for S900C15 prepared using different flow rates of CO_2

CO_2 flow rate (cm^3 min^{-1})	S_{BET} (m^2 g^{-1})	V_{micro} (cm^3 g^{-1})[a,b]	$V_{ultramicro}$ (cm^3 g^{-1})[a]	V_{meso} (cm^3 g^{-1})[c]	V_{total} (cm^3 g^{-1})[d]	micropore (%)[e]	ultramicropore (%)
25	873	0.35	0.27	0.35	0.70	50.0	38.6
50	983	0.39	0.31	0.38	0.77	50.6	40.3
100	1,020	0.41	0.31	0.52	0.94	43.6	33.0

a) Calculated based on the HK model.
b) Includes the ultramicropore volume.
c) Calculated based on the BJH model.
d) Determined from nitrogen adsorbed at P/P_0=0.99.
e) Includes the ultramicropore %.

Comparison of various isotherm models

Determination of V_{micro} ($cm^3\ g^{-1}$)

Material	t-plot	HK	DFT	NLDFT
S800	0.15	0.20	0.14	0.18
S600K4	0.70	0.73	0.64	0.70
S800K4	0.69	0.91	0.78	0.87
S1000K4	0.52	0.62	0.45	0.53
S800K1	0.35	0.48	0.39	0.44
S800K2	0.44	0.49	0.43	0.49
S800K3	0.55	0.62	0.54	0.60
S800K5	0.75	1.00	0.82	0.93
A800	0.06	0.13	0.06	0.08
A600K2	0.23	0.27	0.23	0.26
A800K2	0.47	0.53	0.44	0.49
A1000K2	0.36	0.49	0.40	0.45
A800K1	0.25	0.46	0.33	0.37
A800K3	0.64	0.75	0.64	0.72
A800K4	0.57	0.95	0.76	0.89
A800K5	0.43	1.01	0.77	0.90
P800	0.05	0.11	0.07	0.08
P800K2	0.49	0.77	0.63	0.72
P800K3	0.47	0.73	0.58	0.66
P800K5	0.32	0.82	0.61	0.71
S800C15	0.17	0.21	0.16	0.17
S850C15	0.18	0.26	0.20	0.23
S900C15 (25cm^3/min)	0.26	0.35	0.29	0.32
S900C15 (50cm^3/min)	0.29	0.39	0.32	0.36
S900C15 (100cm^3/min)	0.30	0.41	0.33	0.38
S950C15	0.26	0.38	0.29	0.35
S1000C15	0.41	0.62	0.49	0.55
S900C30	0.32	0.45	0.35	0.40
S900C60	0.31	0.44	0.36	0.41
S900C90	0.43	0.59	0.48	0.54
S900C120	0.52	0.77	0.61	0.68
S950C30	0.47	0.64	0.53	0.58
S950C60	0.55	0.89	0.70	0.79
S950C90	0.49	1.04	0.78	0.84
S950C120	0.28	1.16	0.74	0.91
A750C45	0.16	0.31	0.20	0.25
A750C60	0.16	0.32	0.20	0.25
A750C90	0.15	0.32	0.20	0.26
A900C0	0.14	0.35	0.21	0.27
A900C10	0.10	0.38	0.20	0.26
P700C50	0.16	0.31	0.22	0.26
P900C0	0.10	0.40	0.26	0.32
S700O0	0.28	0.35	0.30	0.34
S750O0	0.36	0.43	0.36	0.42
S800O0	0.27	0.37	0.31	0.35

Material	t-plot	HK	DFT	NLDFT
S750O40	0.30	0.35	0.28	0.32
S750O56	0.23	0.31	0.26	0.29
A500O30	0.14	0.27	0.17	0.22
A500O60	0.16	0.27	0.18	0.22
A750O0	0.15	0.26	0.17	0.21
P400O50	0.09	0.16	0.11	0.13
P500O30	0.09	0.15	0.10	0.12
P750O0	0.14	0.23	0.17	0.19

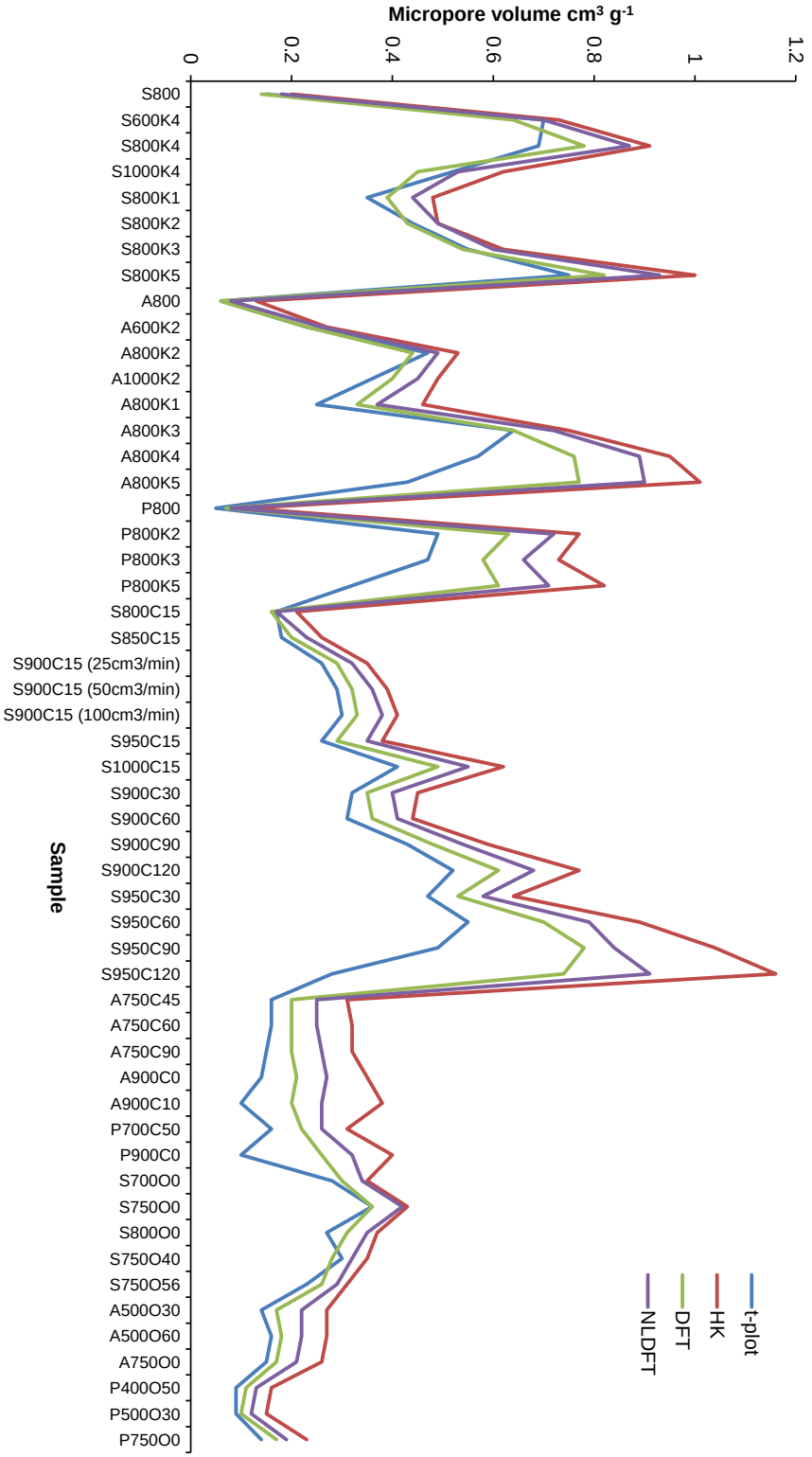

Determination of V_{meso} ($cm^3\ g^{-1}$)

Material	BJH	DFT	NLDFT
S800	0.36	0.22	0.26
S600K4	0.13	0.01	0.04
S800K4	0.04	0.04	0.01
S1000K4	0.23	0.28	0.21
S800K1	0.58	0.54	0.41
S800K2	0.10	0.06	0.04
S800K3	0.14	0.09	0.08
S800K5	0.11	0.11	0.06
A800	0.71	0.62	0.65
A600K2	0.08	0.06	0.05
A800K2	0.15	0.10	0.09
A1000K2	0.30	0.23	0.22
A800K1	0.82	0.75	0.76
A800K3	0.09	0.07	0.04
A800K4	0.18	0.21	0.07
A800K5	0.10	0.16	0.09
P800	0.43	0.43	0.38
P800K2	0.18	0.20	0.12
P800K3	0.13	0.13	0.08
P800K5	0.20	0.27	0.18
S800C15	0.37	0.31	0.24
S850C15	0.31	0.36	0.24
S900C15 (25cm^3/min)	0.35	0.41	0.30
S900C15 (50cm^3/min)	0.38	0.43	0.33
S900C15 (100cm^3/min)	0.52	0.41	0.35
S950C15	0.34	0.43	0.29
S1000C15	0.52	0.64	0.41
S900C30	0.50	0.55	0.38
S900C60	0.40	0.53	0.33
S900C90	0.45	0.42	0.34
S900C120	0.71	0.85	0.58
S950C30	0.27	0.32	0.21
S950C60	0.41	0.53	0.35
S950C90	0.59	0.71	0.76
S950C120	0.96	1.07	0.87
A750C45	0.68	0.71	0.64
A750C60	0.76	0.79	0.72
A750C90	0.74	0.74	0.68
A900C0	0.86	0.87	0.79
A900C10	0.98	1.04	0.92
P700C50	0.47	0.47	0.42
P900C0	0.54	0.57	0.49
S700O0	0.14	0.16	0.10
S750O0	0.14	0.18	0.10
S800O0	0.20	0.17	0.13
S750O40	0.09	0.13	0.06
S750O56	0.15	0.13	0.09

Material	BJH	DFT	NLDFT
A500O30	0.70	0.73	0.65
A500O60	0.66	0.71	0.61
A750O0	0.67	0.72	0.62
P400O50	0.44	0.47	0.40
P500O30	0.32	0.35	0.30
P750O0	0.47	0.46	0.41

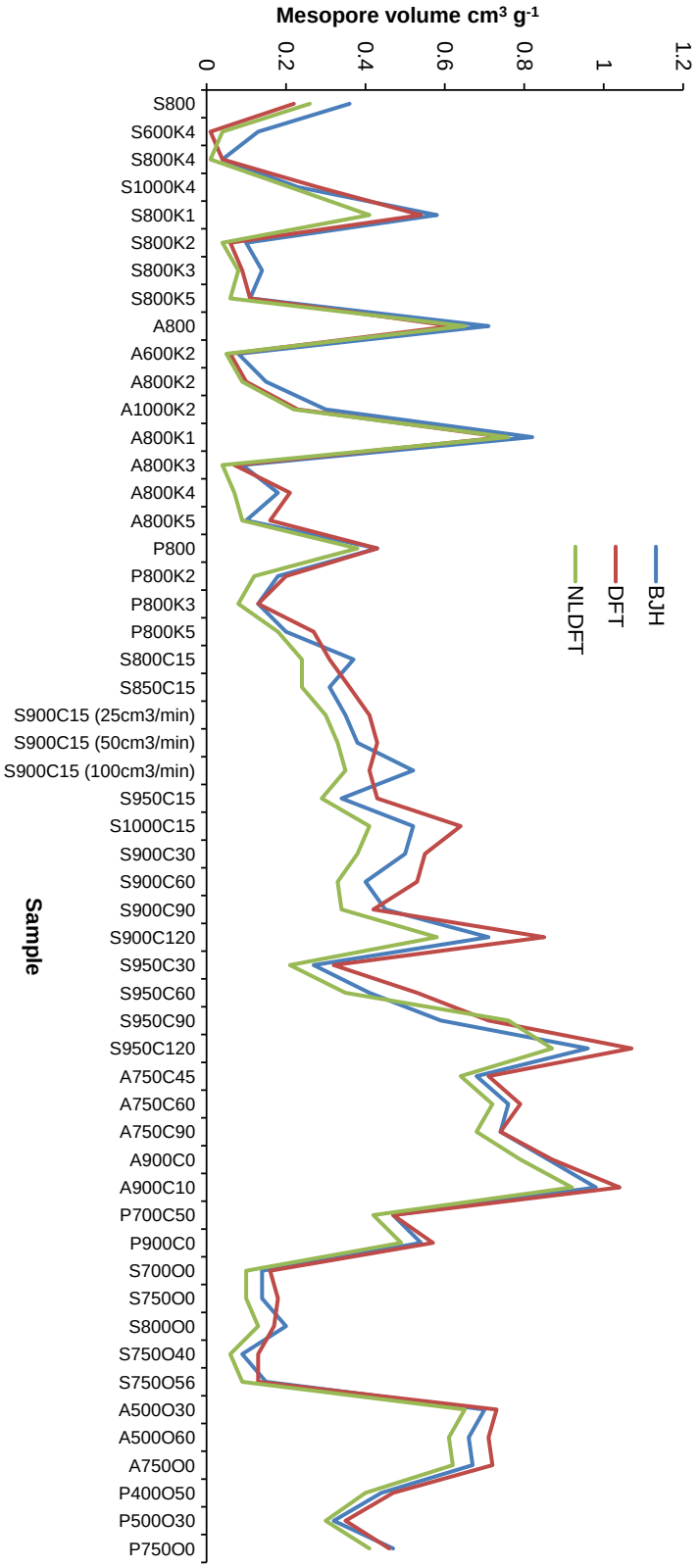

Determination of V_{total} ($cm^3\ g^{-1}$)

Material	P/P_0=0.99	DFT	NLDFT
S800	0.55	0.36	0.44
S600K4	0.81	0.65	0.74
S800K4	0.95	0.78	0.82
S1000K4	0.84	0.73	0.74
S800K1	1.03	0.93	0.85
S800K2	0.59	0.49	0.53
S800K3	0.77	0.63	0.68
S800K5	1.09	0.93	0.99
A800	0.81	0.68	0.73
A600K2	0.36	0.29	0.31
A800K2	0.67	0.54	0.58
A1000K2	0.84	0.63	0.67
A800K1	1.31	1.08	1.13
A800K3	0.85	0.71	0.76
A800K4	1.15	0.97	0.96
A800K5	1.09	0.93	0.99
P800	0.54	0.50	0.46
P800K2	0.97	0.83	0.84
P800K3	0.86	0.71	0.74
P800K5	1.02	0.88	0.89
S800C15	0.58	0.47	0.41
S850C15	0.60	0.56	0.47
S900C15 (25cm^3/min)	0.70	0.70	0.62
S900C15 (50cm^3/min)	0.74	0.75	0.69
S900C15 (100cm^3/min)	0.94	0.74	0.73
S950C15	0.76	0.72	0.64
S1000C15	1.16	1.13	0.95
S900C30	0.98	0.90	0.78
S900C60	0.89	0.89	0.74
S900C90	1.05	0.90	0.88
S900C120	1.49	1.46	1.26
S950C30	0.94	0.85	0.79
S950C60	1.32	1.23	1.14
S950C90	1.64	1.49	1.60
S950C120	2.09	1.81	1.78
A750C45	0.99	0.91	0.89
A750C60	1.09	0.99	0.97
A750C90	1.05	0.94	0.94
A900C0	1.18	1.08	1.06
A900C10	1.33	1.24	1.18
P700C50	0.78	0.69	0.68
P900C0	0.93	0.83	0.81
S700O0	0.50	0.46	0.44
S750O0	0.58	0.54	0.52
S800O0	0.57	0.48	0.48
S750O40	0.45	0.41	0.38
S750O56	0.46	0.39	0.38

Material	P/P_0=0.99	DFT	NLDFT
A500O30	0.97	0.90	0.87
A500O60	0.96	0.89	0.83
A750O0	0.94	0.89	0.83
P400O50	0.60	0.58	0.53
P500O30	0.49	0.45	0.42
P750O0	0.71	0.63	0.60

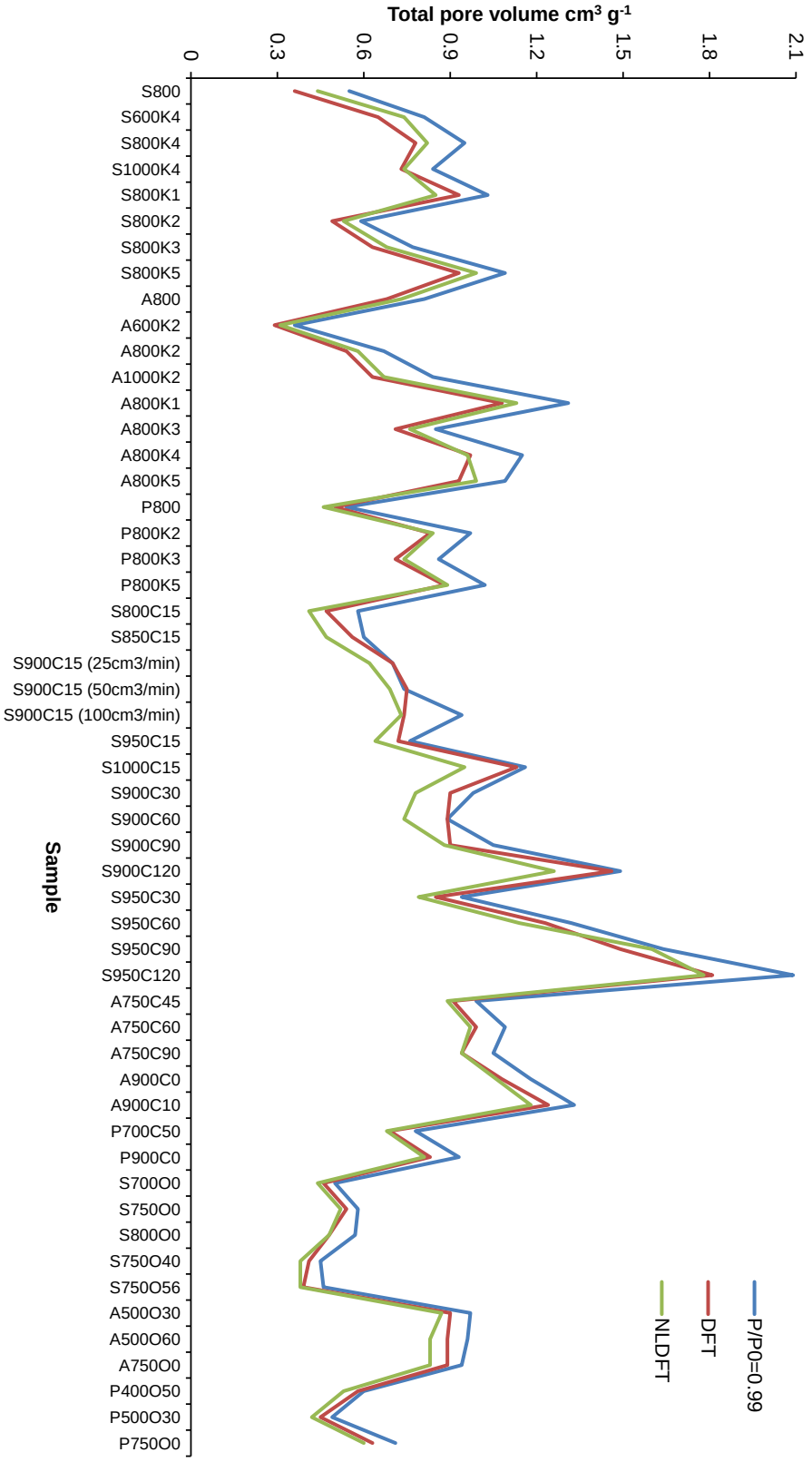

SEM Images for S800

S800 x300 magnification and particle size distribution plot

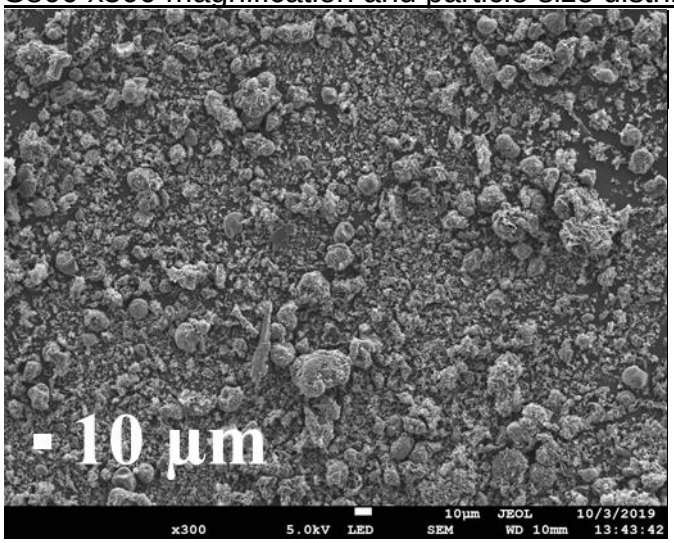

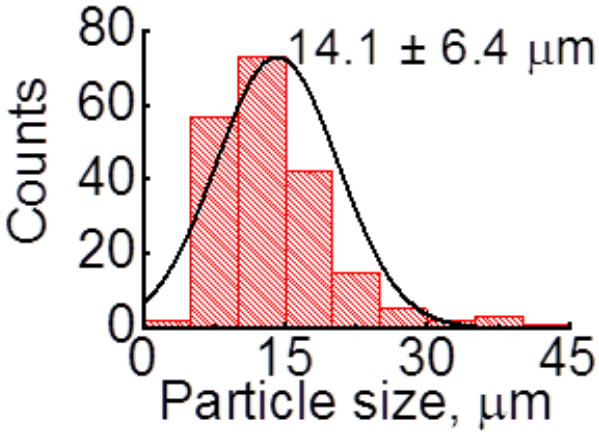

S800 x10,000 magnification

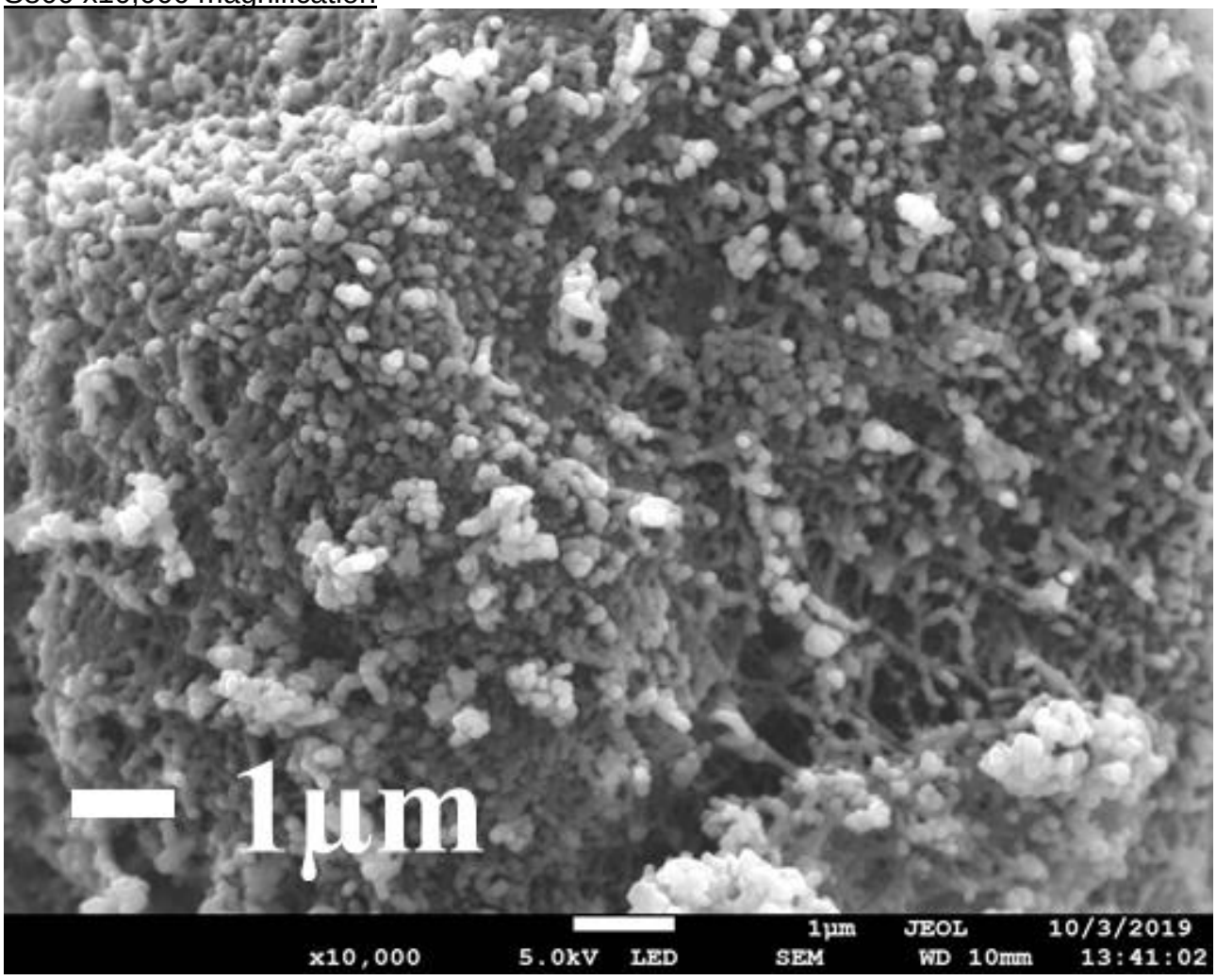

SEM Images for A800

A800 x100 magnification and particle size distribution plot

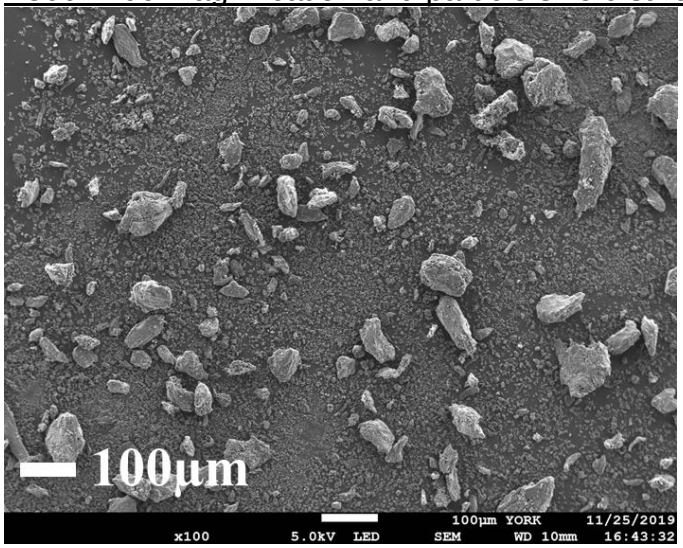

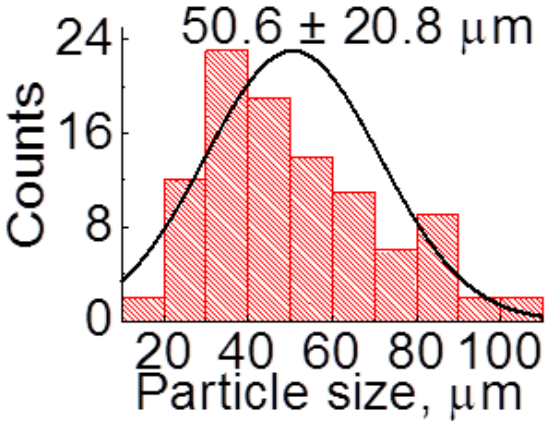

A800 x10,000 magnification

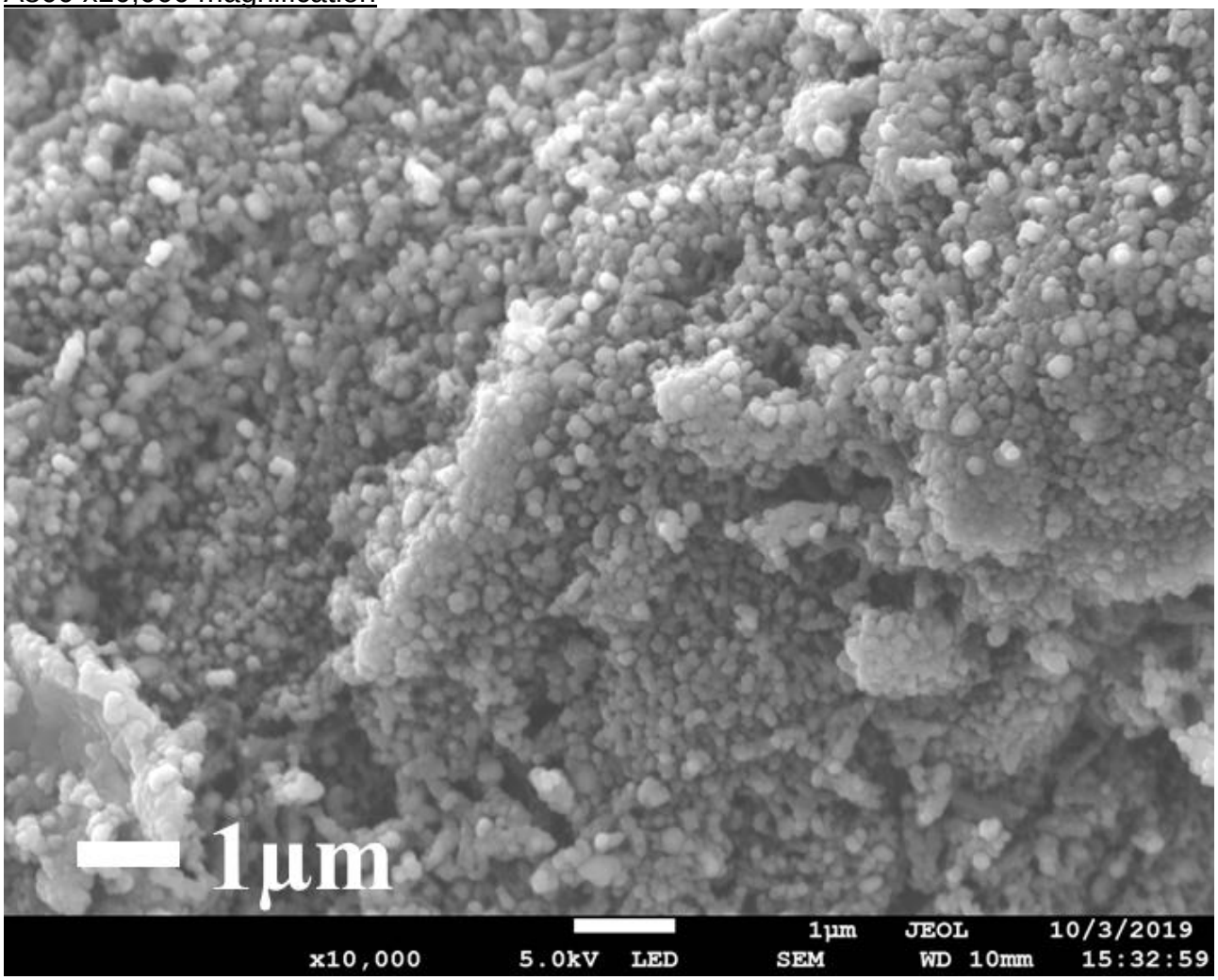

SEM Images for P800

P800 x500 magnification and particle size distribution plot

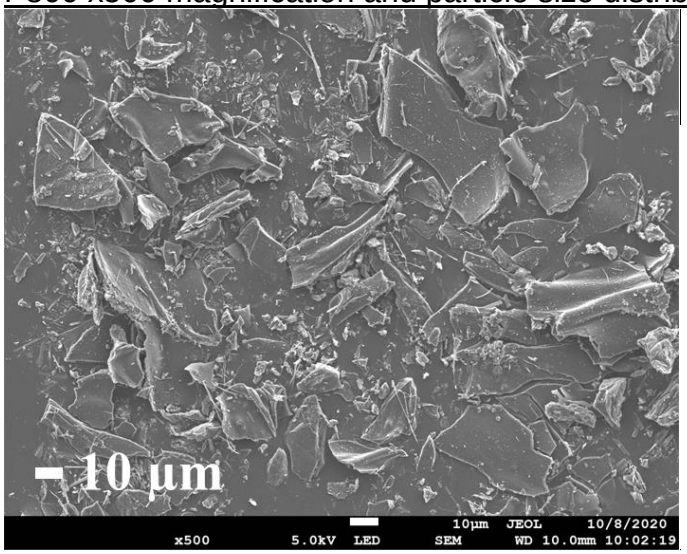

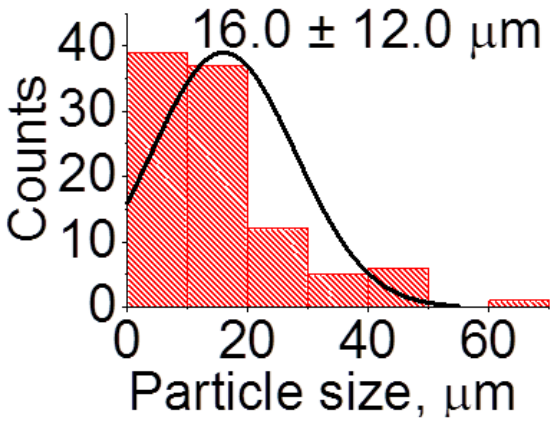

P800 x10,000 magnification

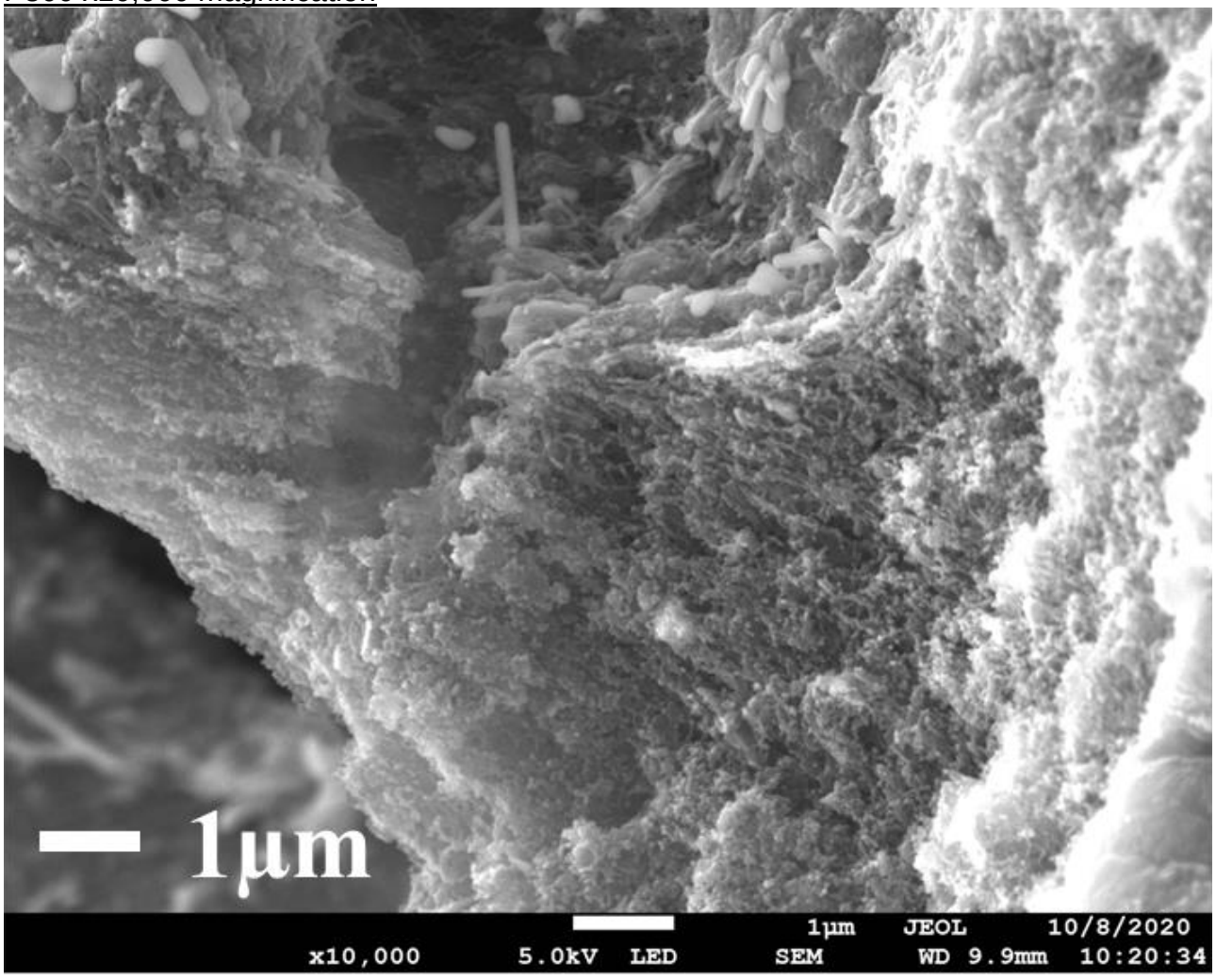

SEM Images for S800K1

S800K1 x200 magnification and particle size distribution plot

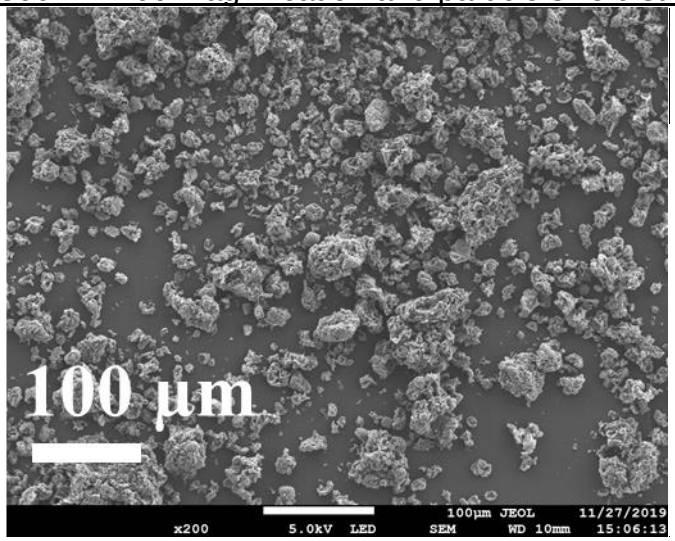

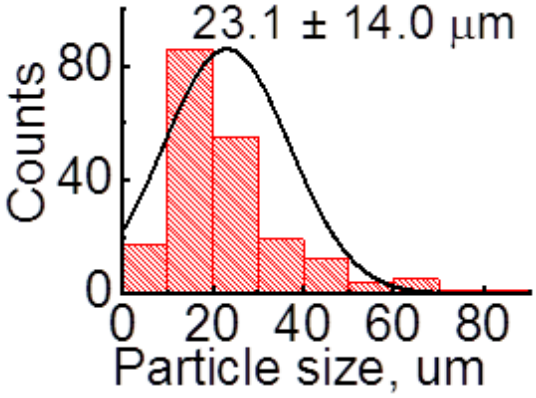

S800K1 x10,000 magnification

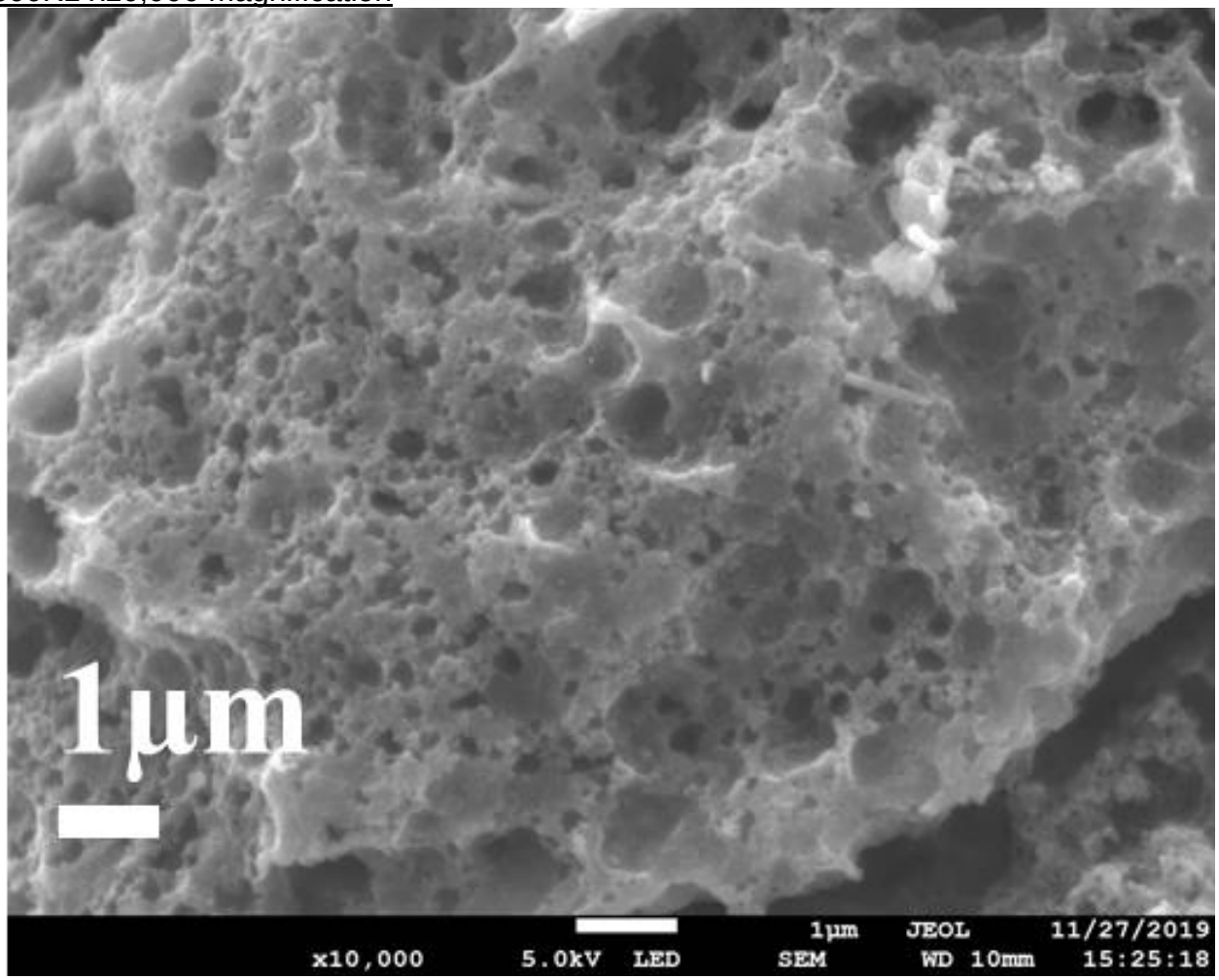

SEM Images for S800K2

S800K2 x200 magnification and particle size distribution plot

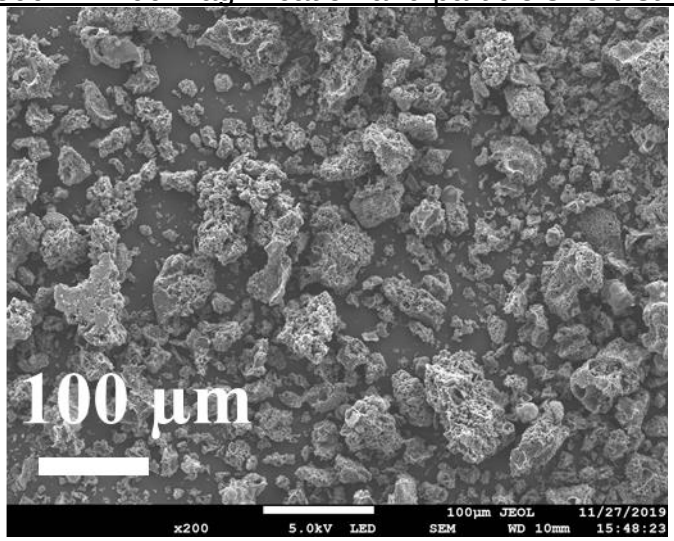

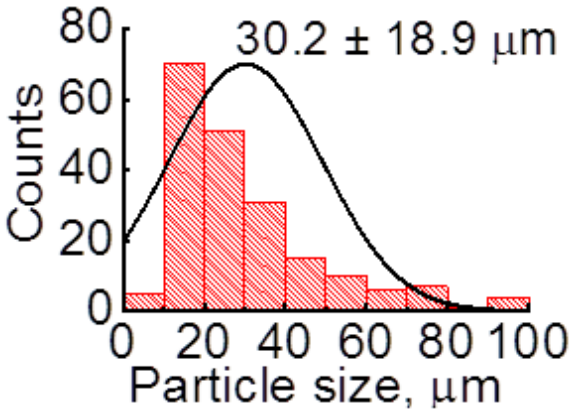

S800K2 x10,000 magnification

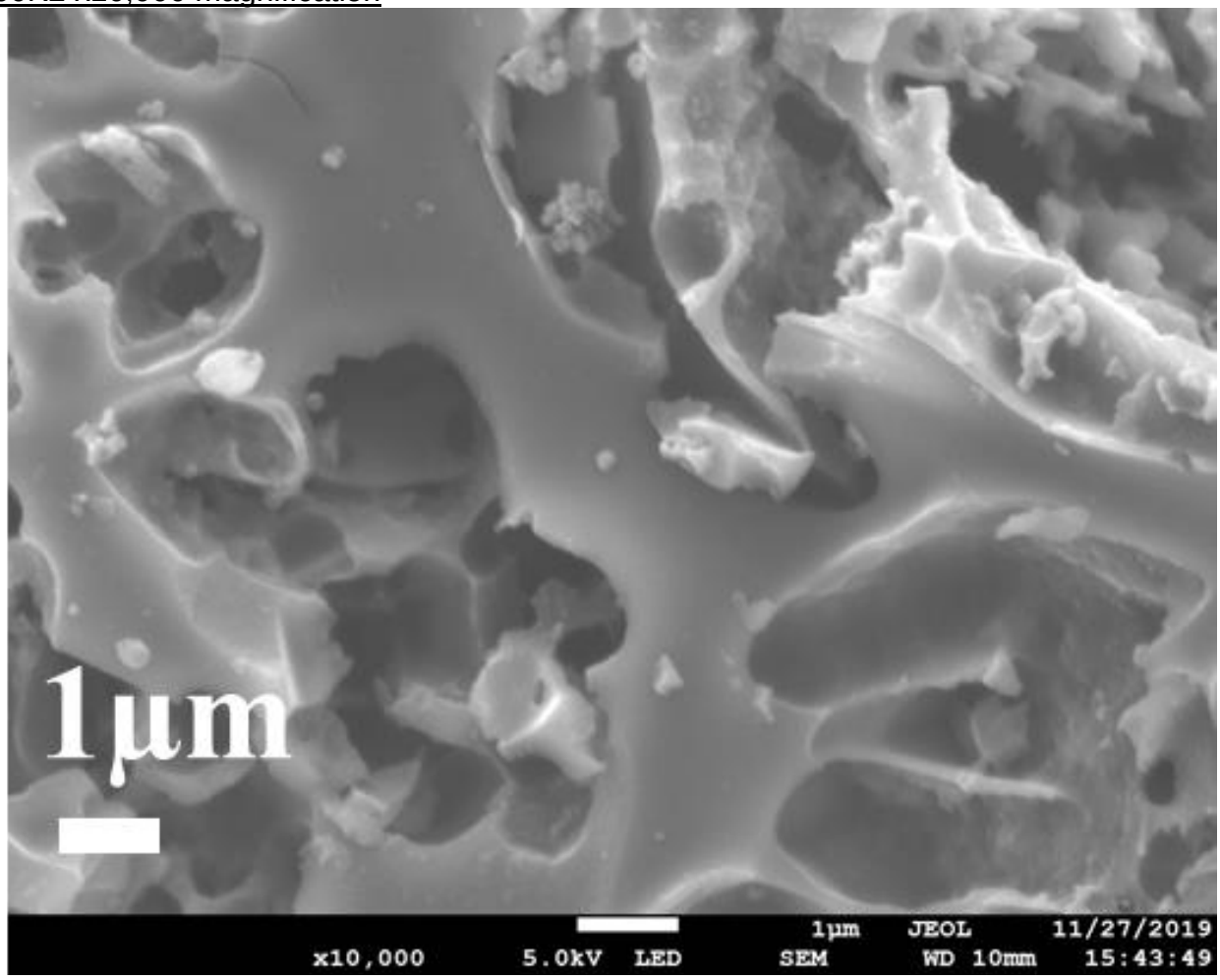

SEM Images for S800K3

S800K3 x200 magnification and particle size distribution plot

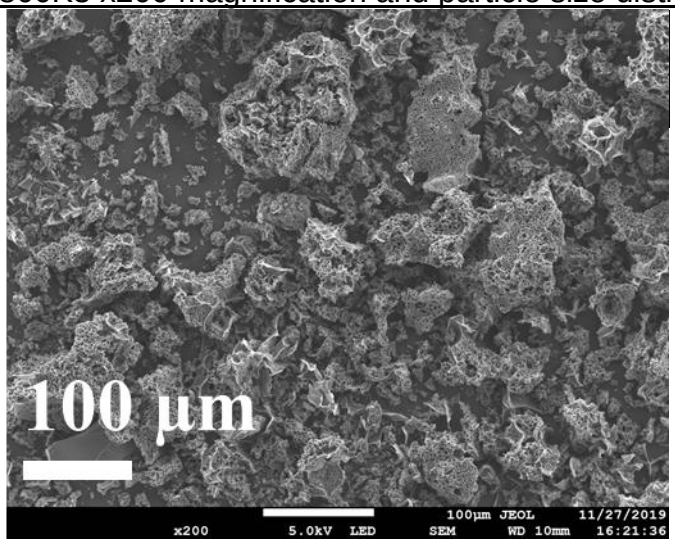

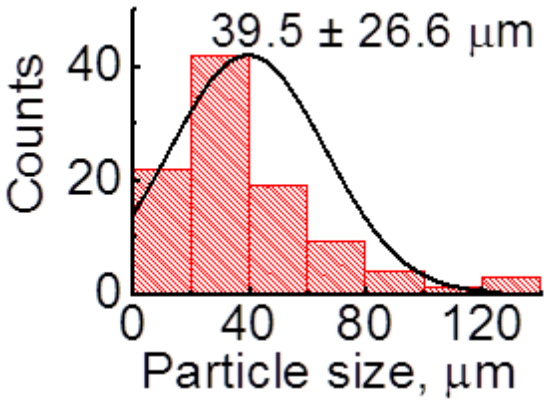

S800K3 x10,000 magnification

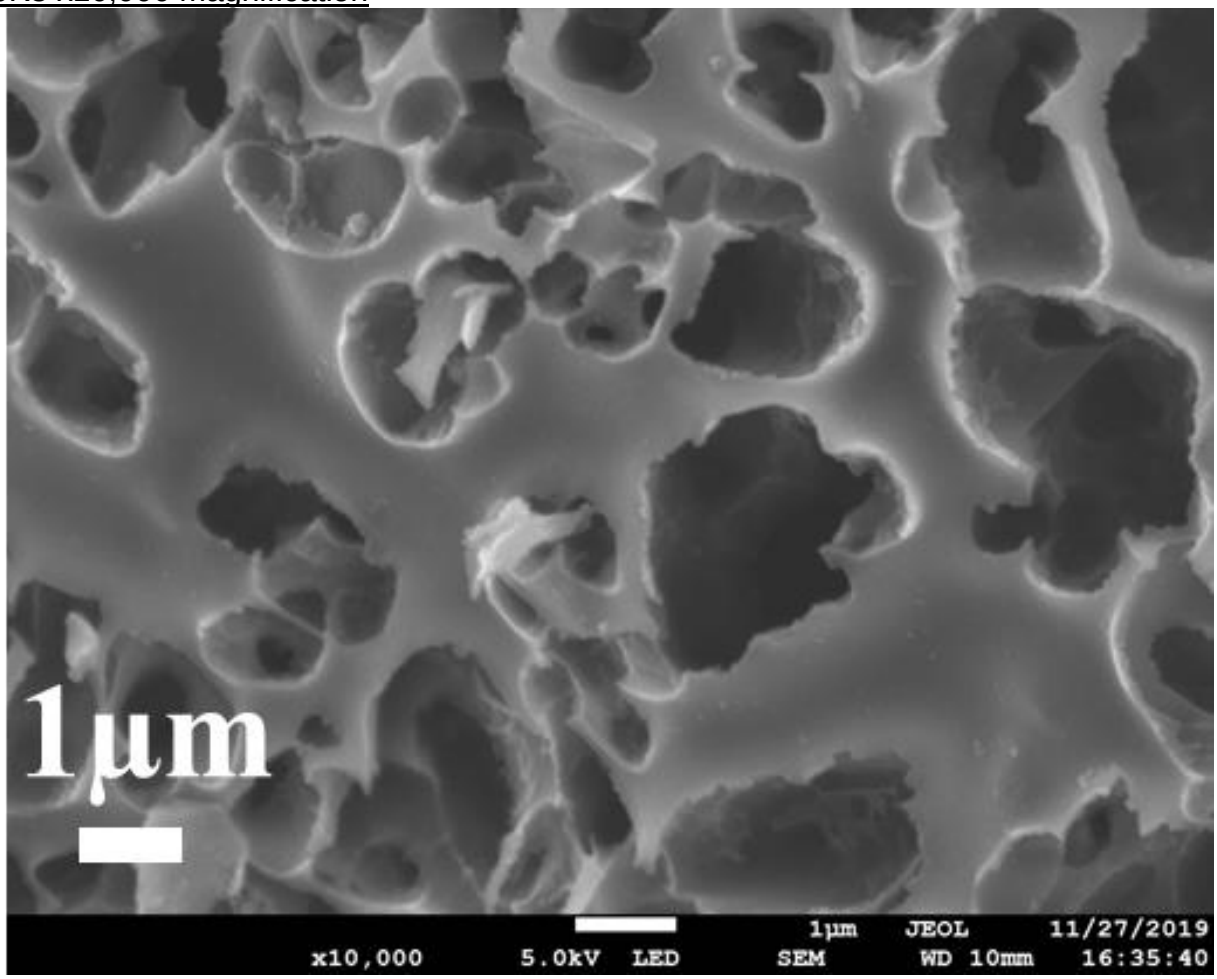

SEM Images for S800K4

S800K4 x200 magnification and particle size distribution plot

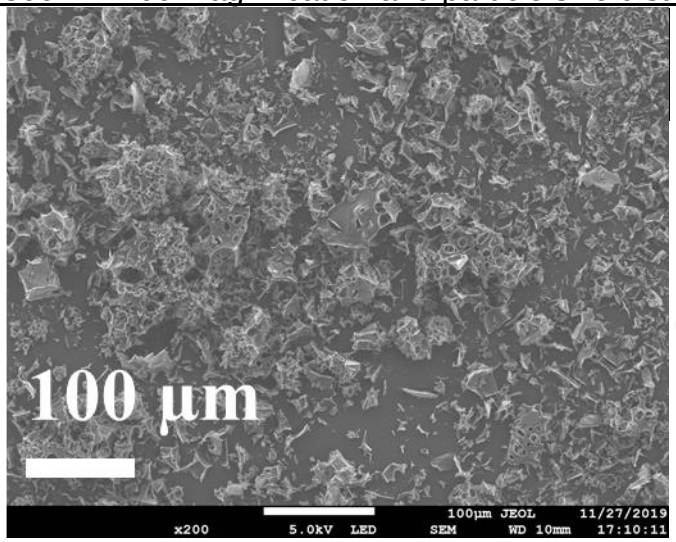

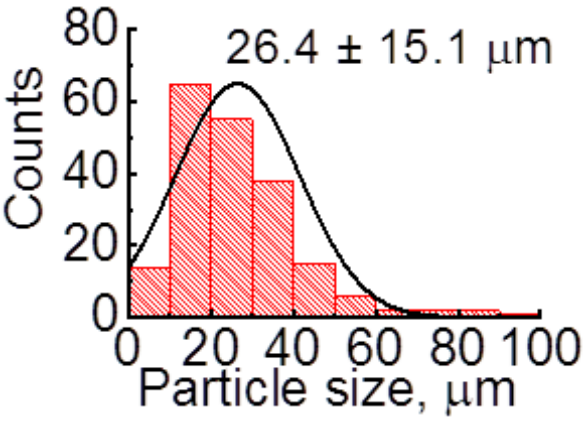

S800K4 x10,000 magnification

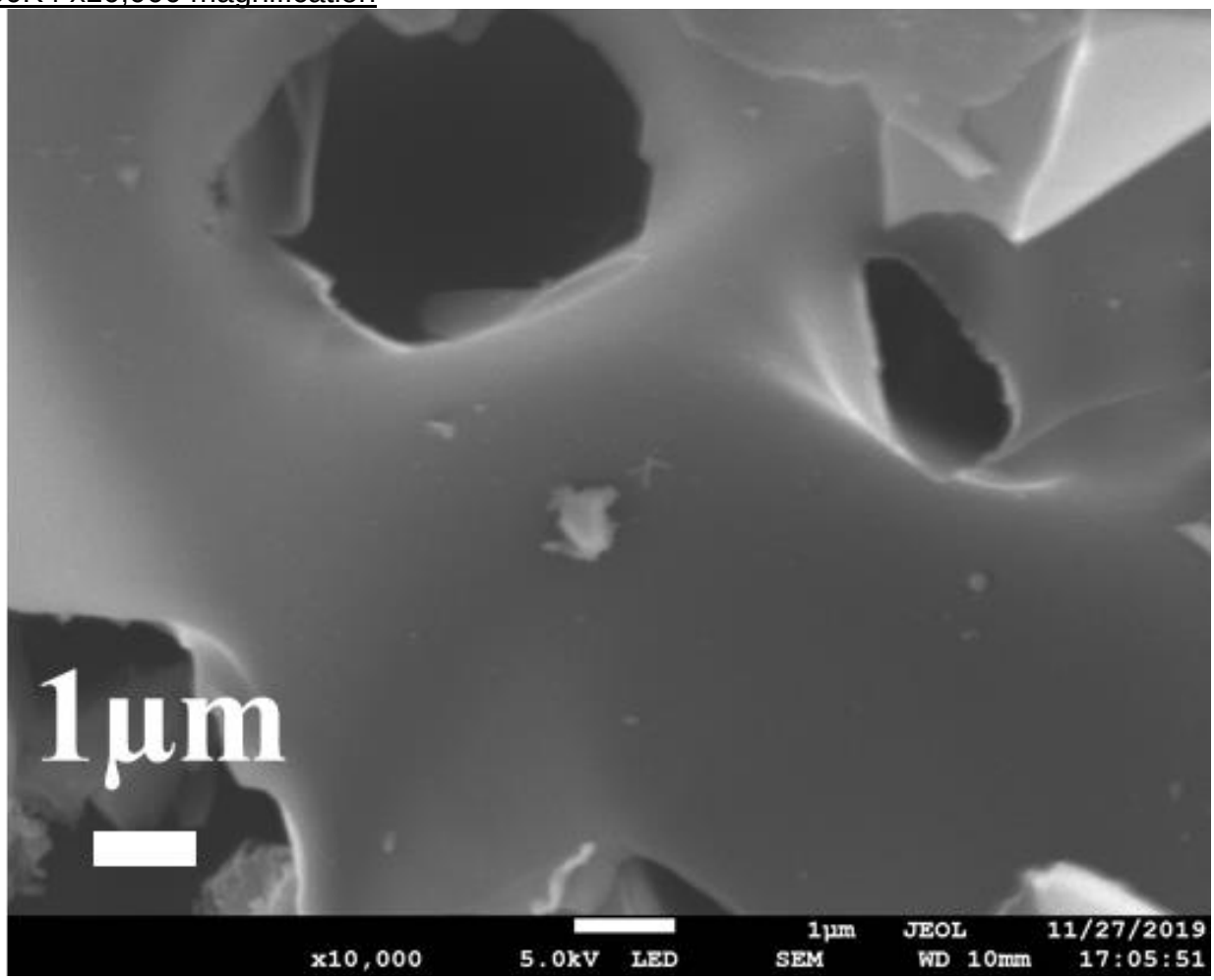

SEM Images for S800K5

S800K5 x200 magnification and particle size distribution plot

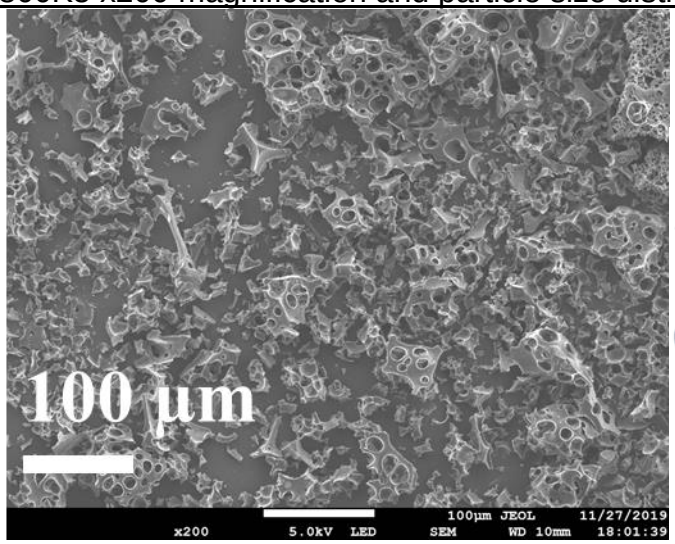

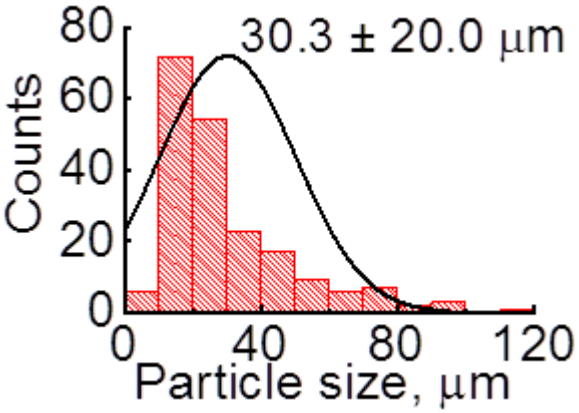

S800K5 x30,000 magnification

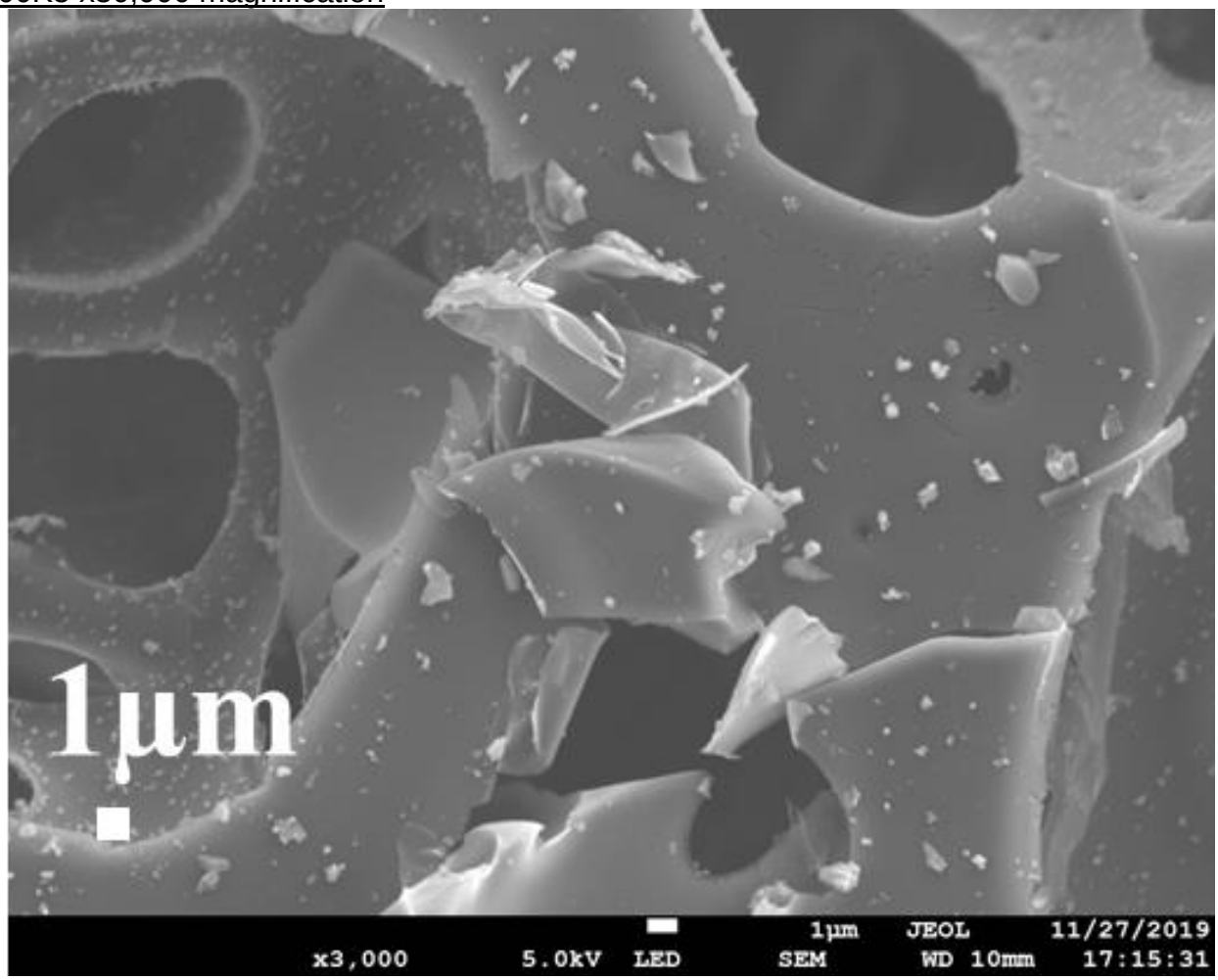

SEM Images for A800K1

A800K1 x100 magnification and particle size distribution plot

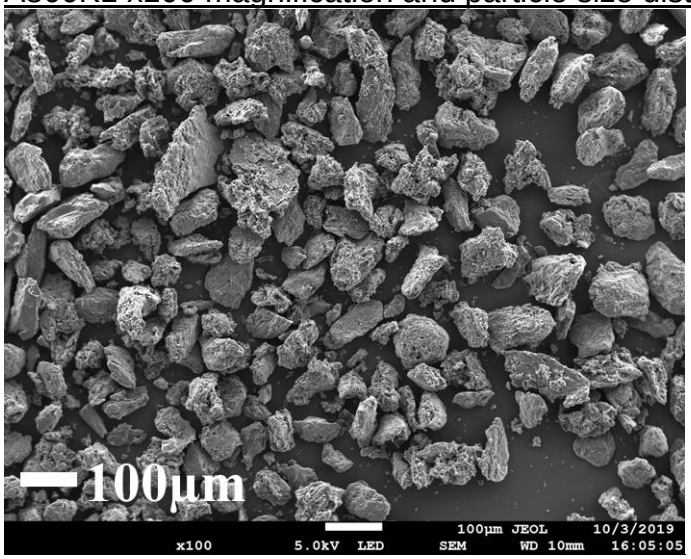

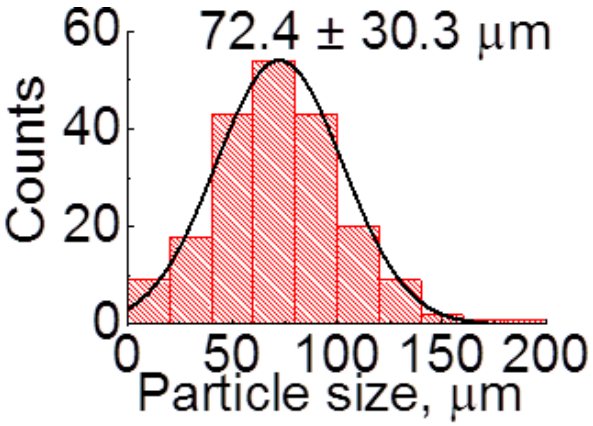

A800K1 x10,000 magnification

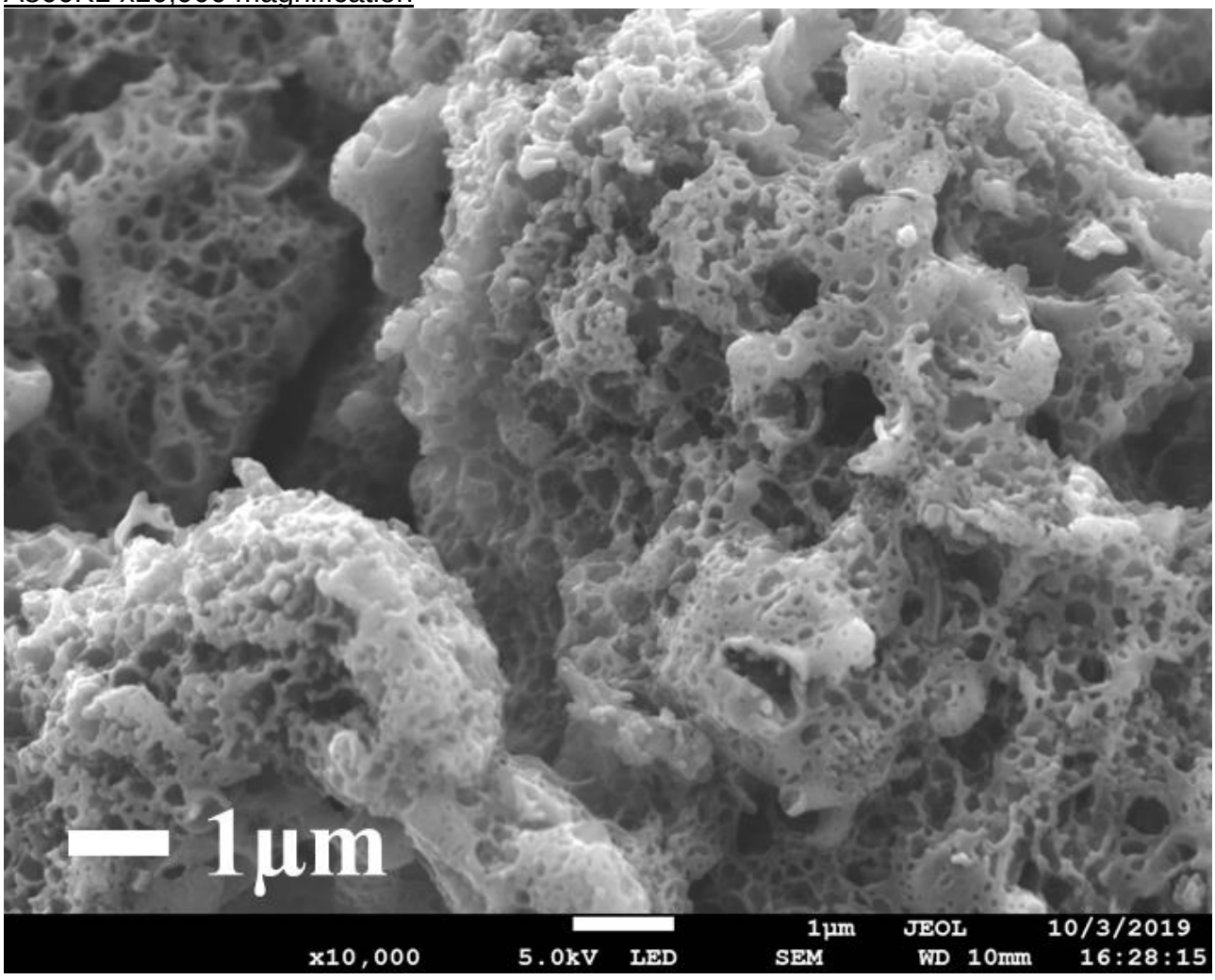

SEM Images for A800K2

A800K2 x500 magnification and particle size distribution plot

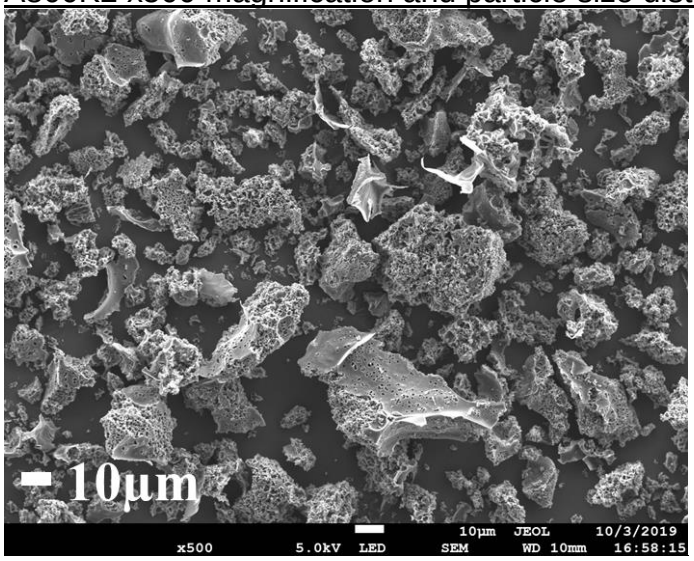

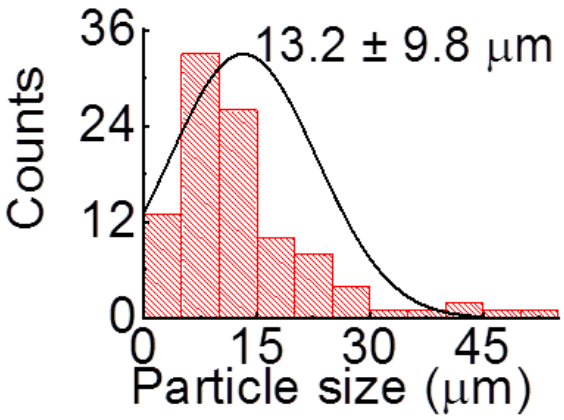

A800K2 x10,000 magnification

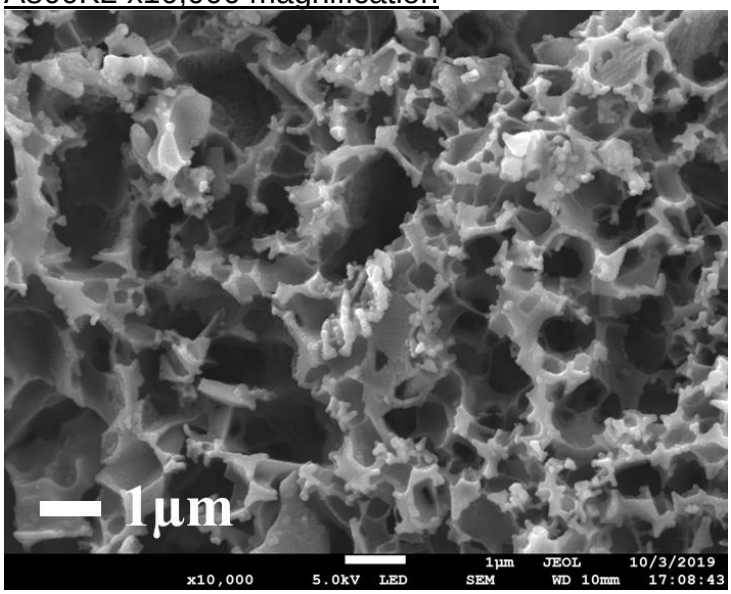

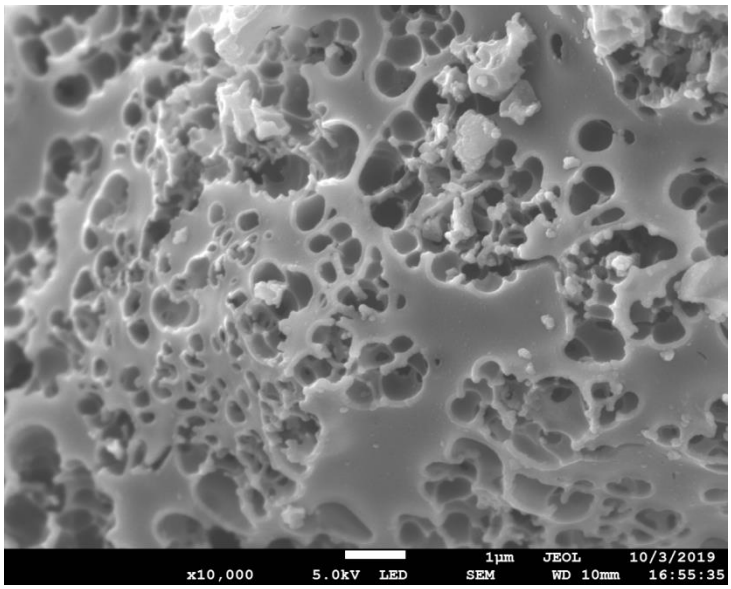

SEM Images for A800K3

A800K x500 magnification and particle size distribution plot

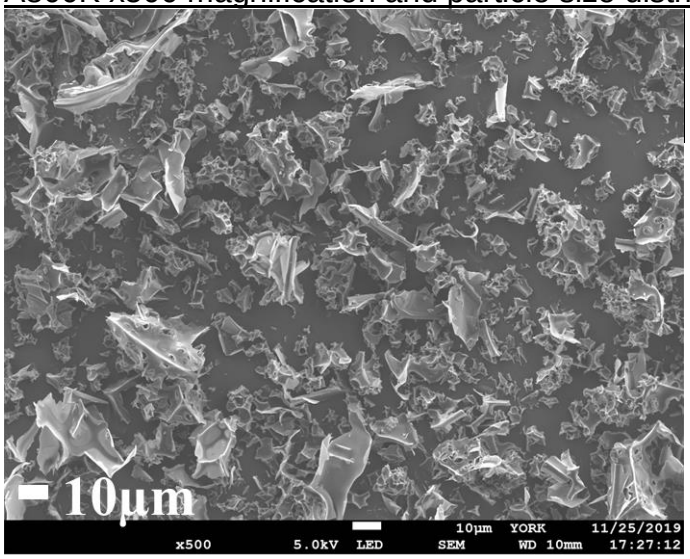

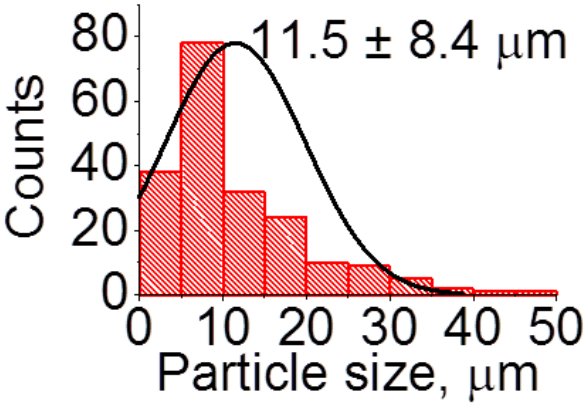

A800K3 x10,000 magnification

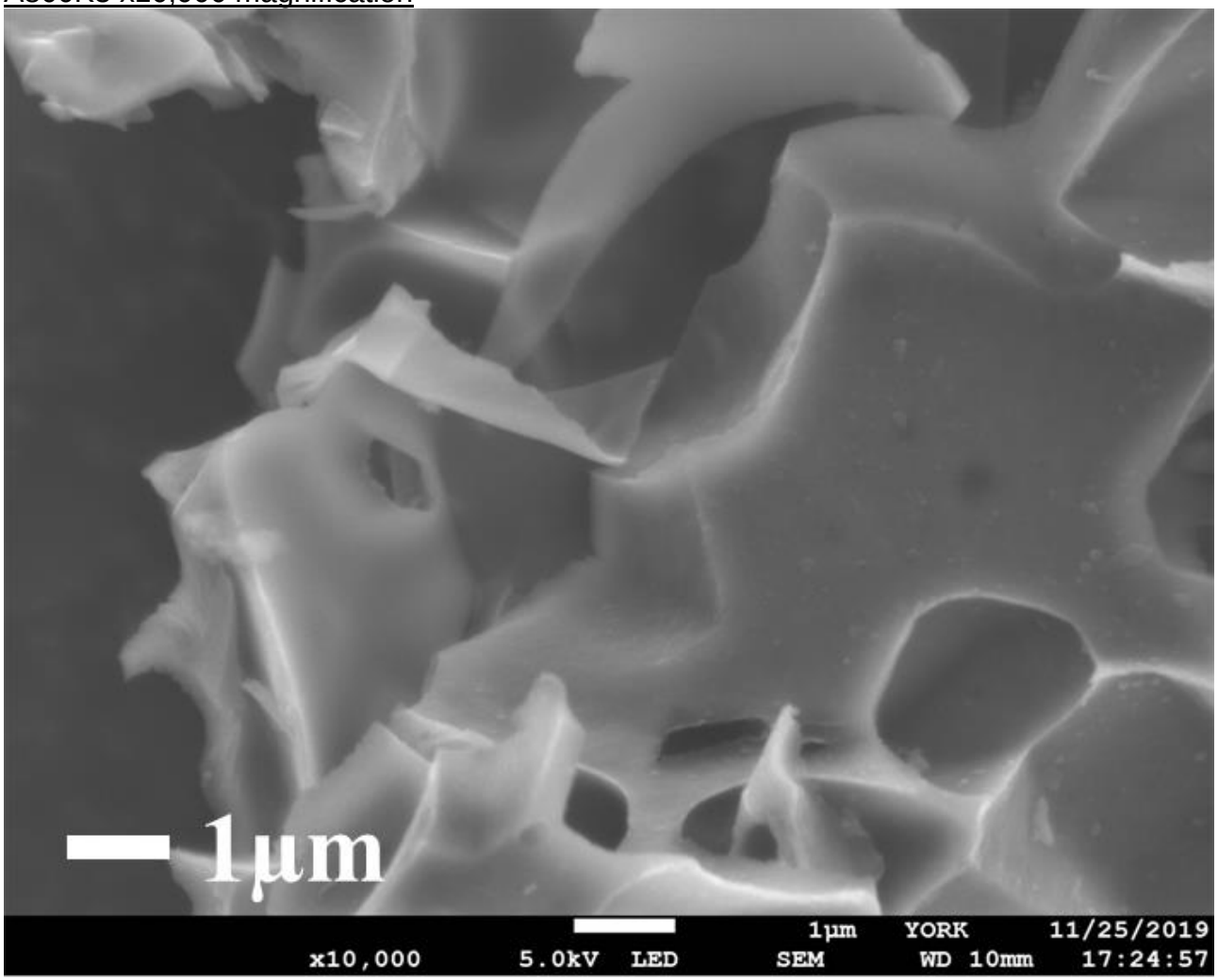

SEM Images for A800K4

A800K4 x500 magnification and particle size distribution plot

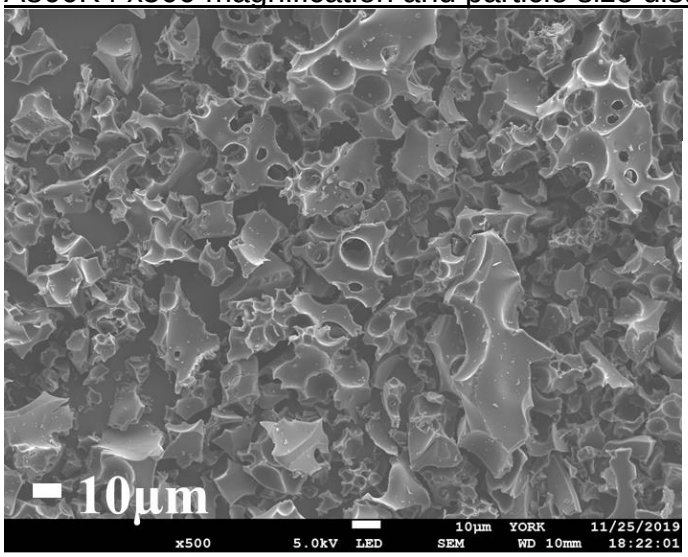

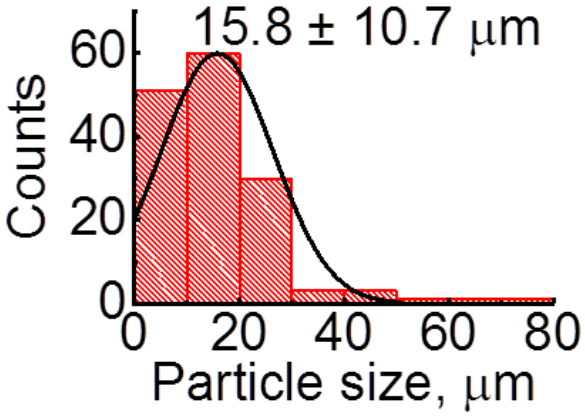

A800K4 x5,000 magnification

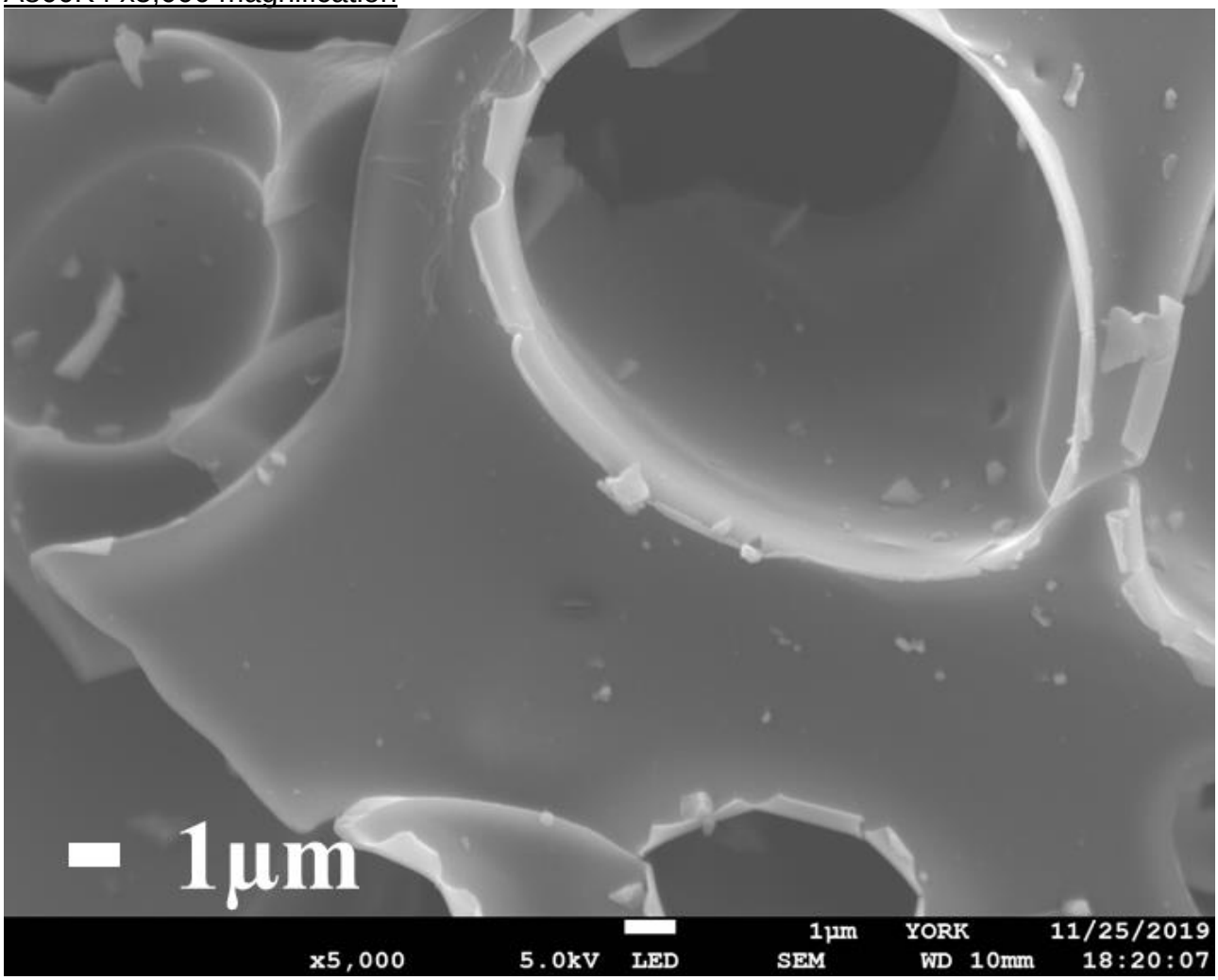

SEM Images for A800K5

A800K5 x100 magnification and particle size distribution plot

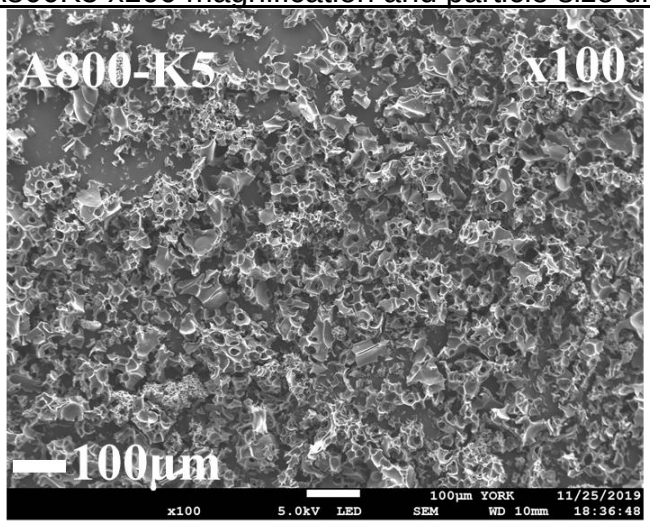

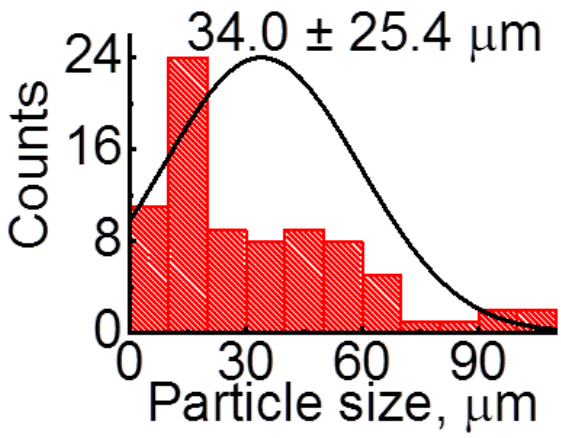

A800K5 x5,000 magnification

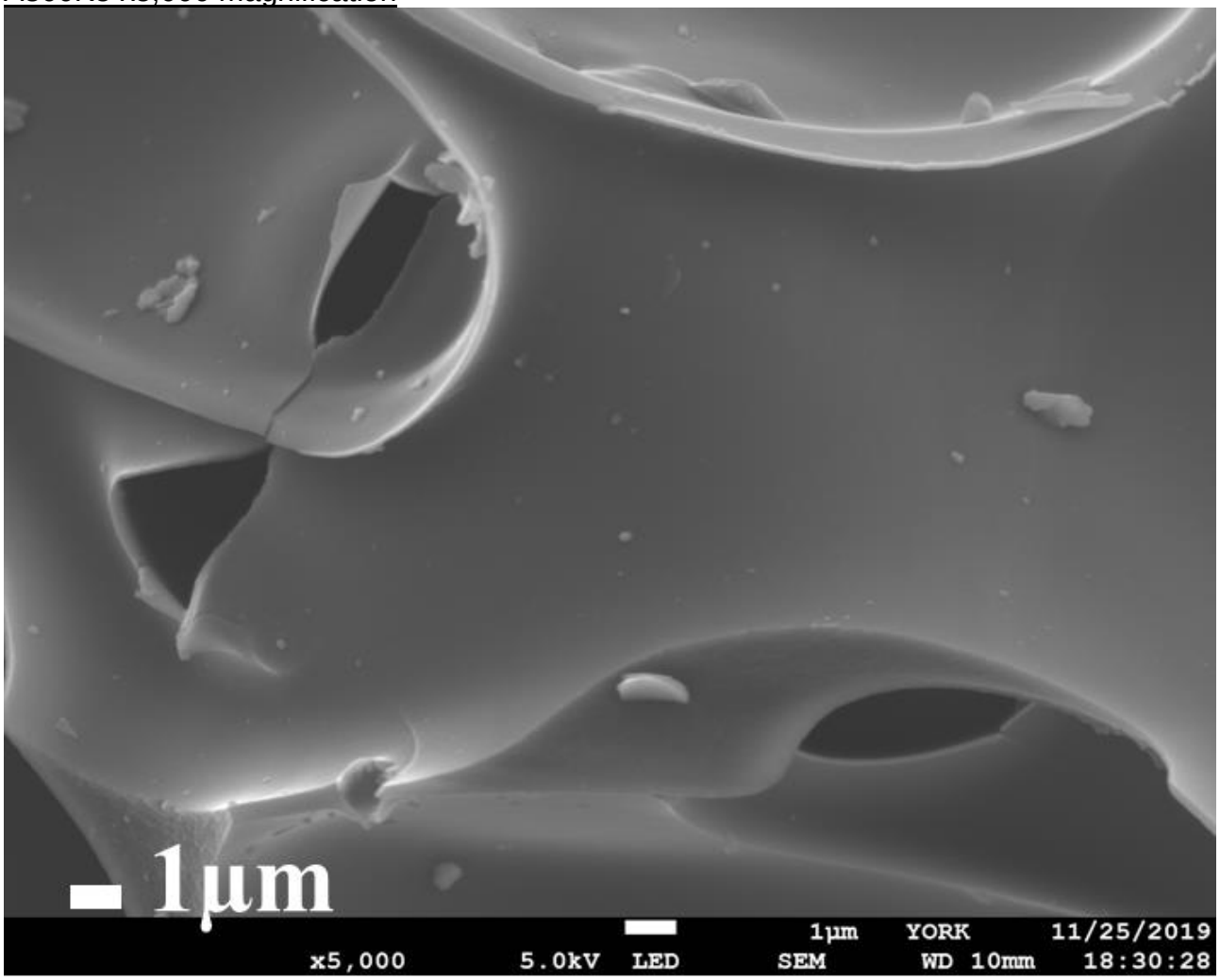

SEM Images for A600K2

A600K2 x100 magnification and particle size distribution plot

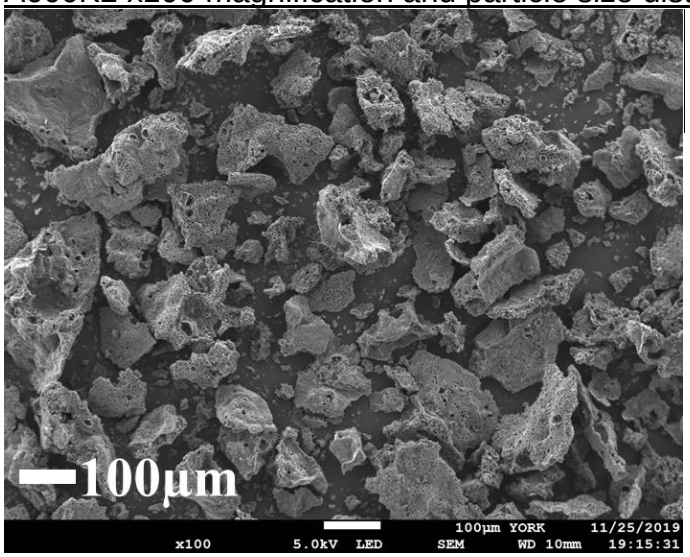

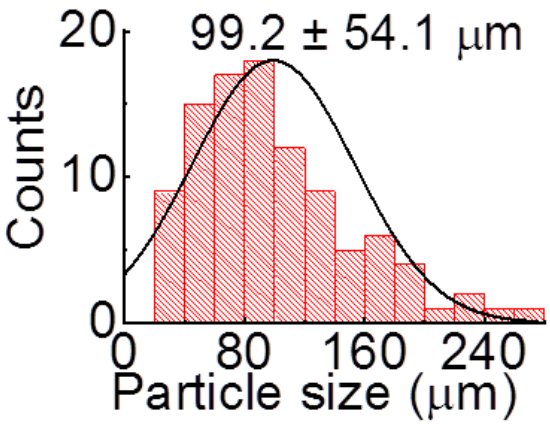

A600K2 x10,000 magnification

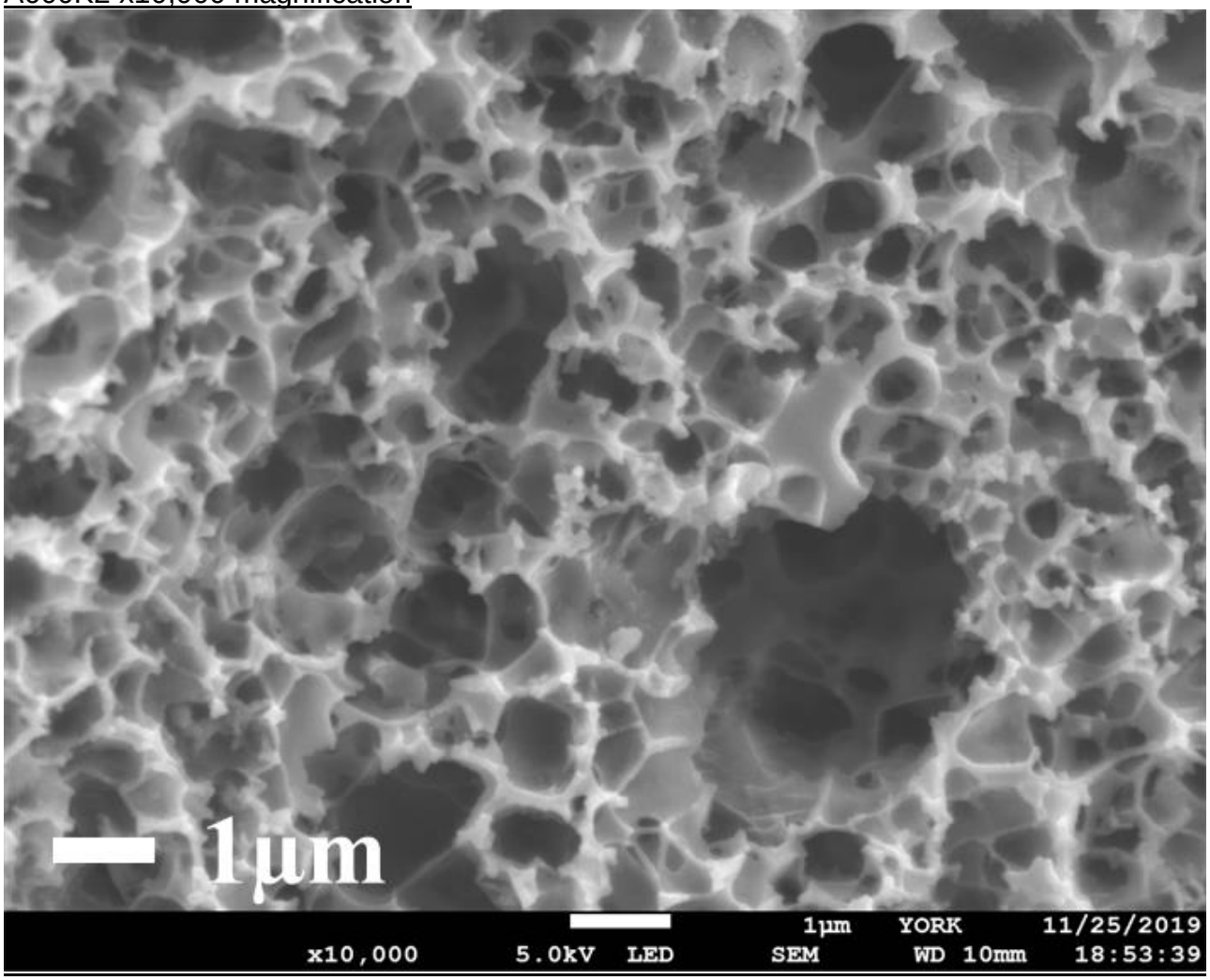

SEM Images for A1000K2

A1000K2 x100 magnification and particle size distribution plot

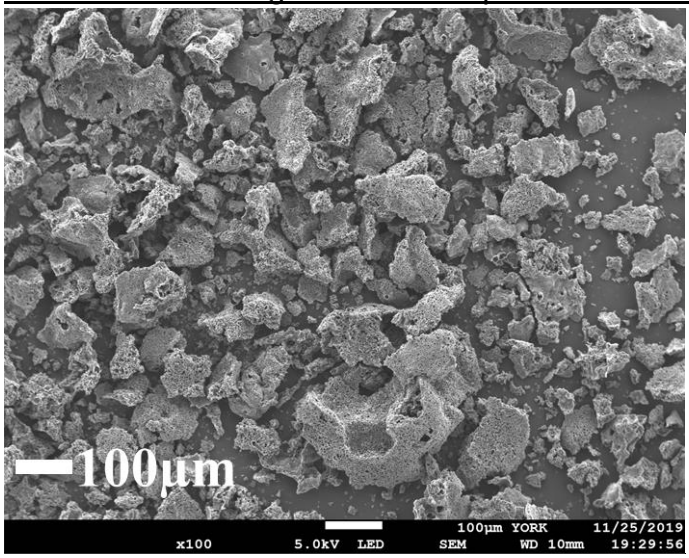

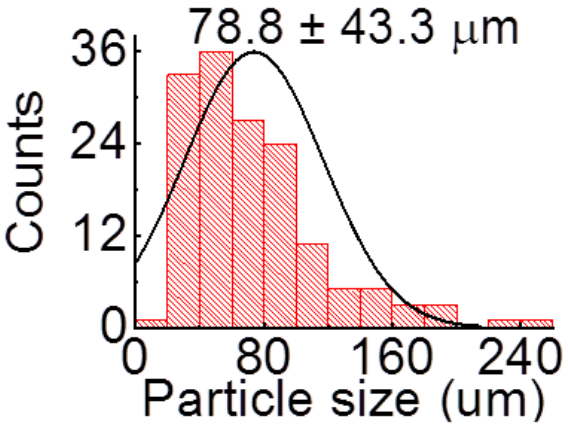

A1000K2 x10,000 magnification

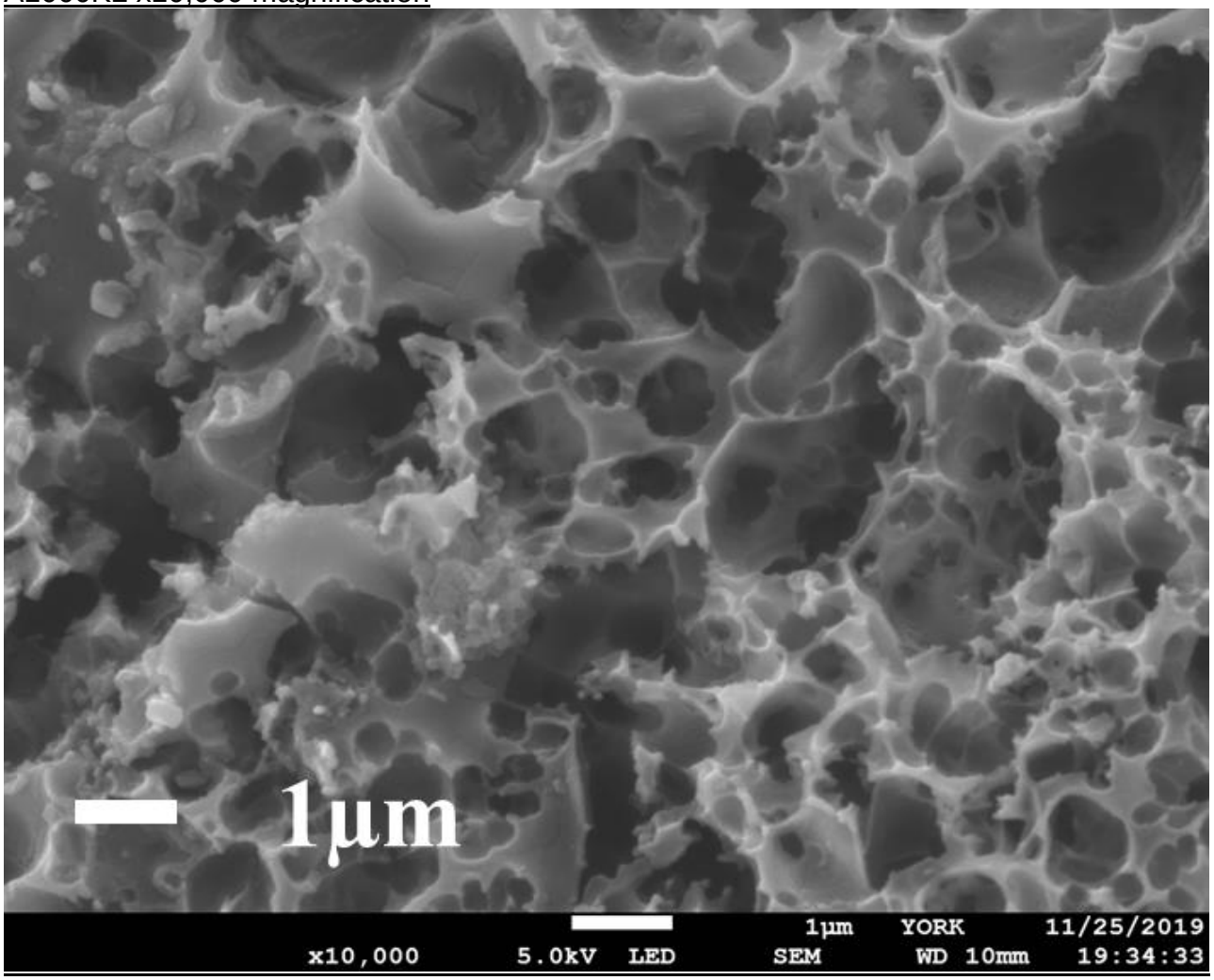

SEM Images for P800K2

P800K2 x200 magnification and particle size distribution plot

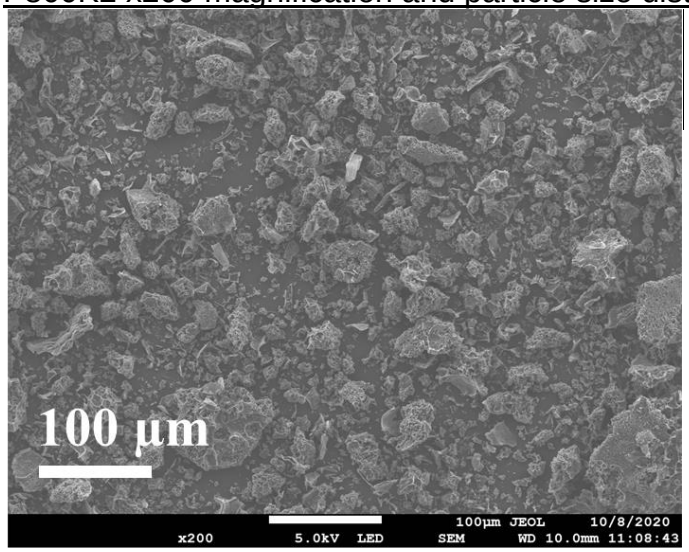

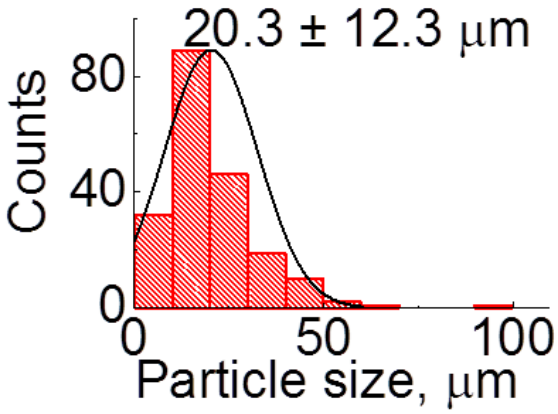

P800K2 x10,000 magnification

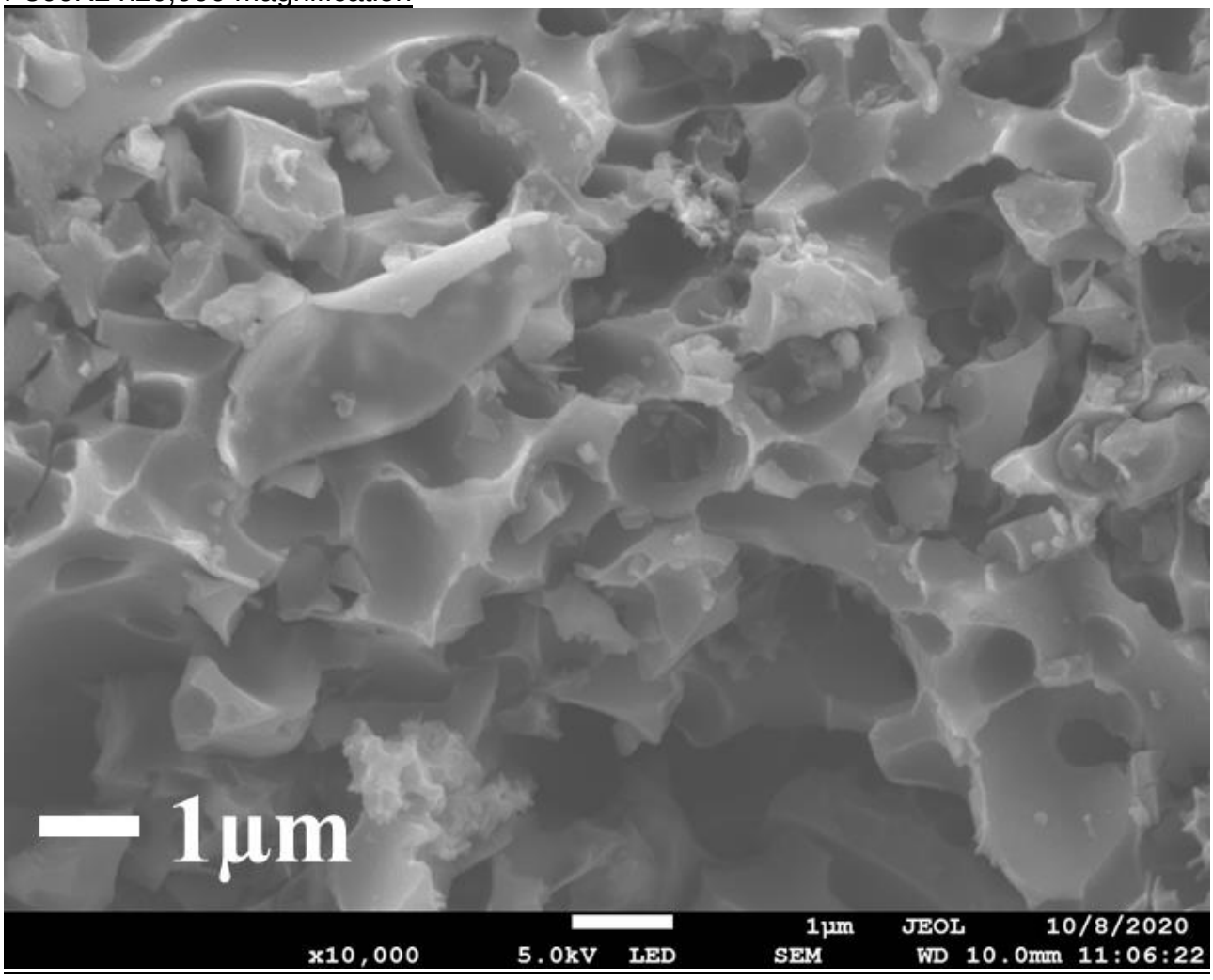

SEM Images for P800K3

P800K3 x200 magnification and particle size distribution plot

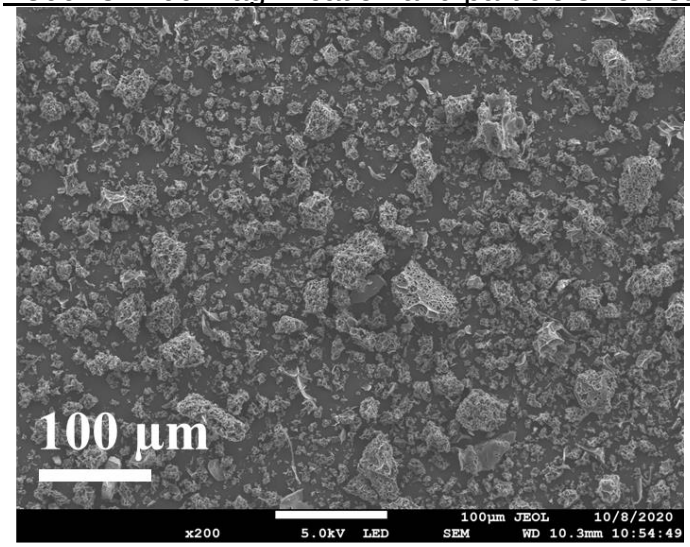

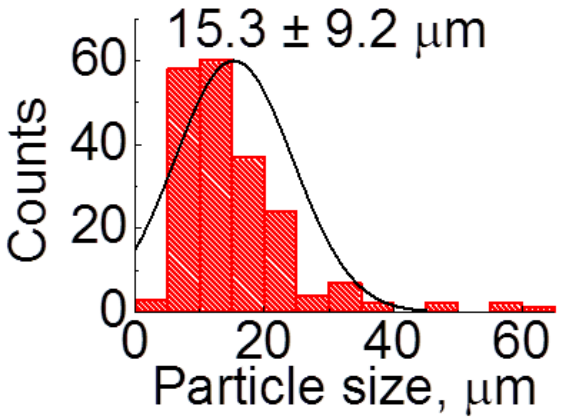

P800K3 x10,000 magnification

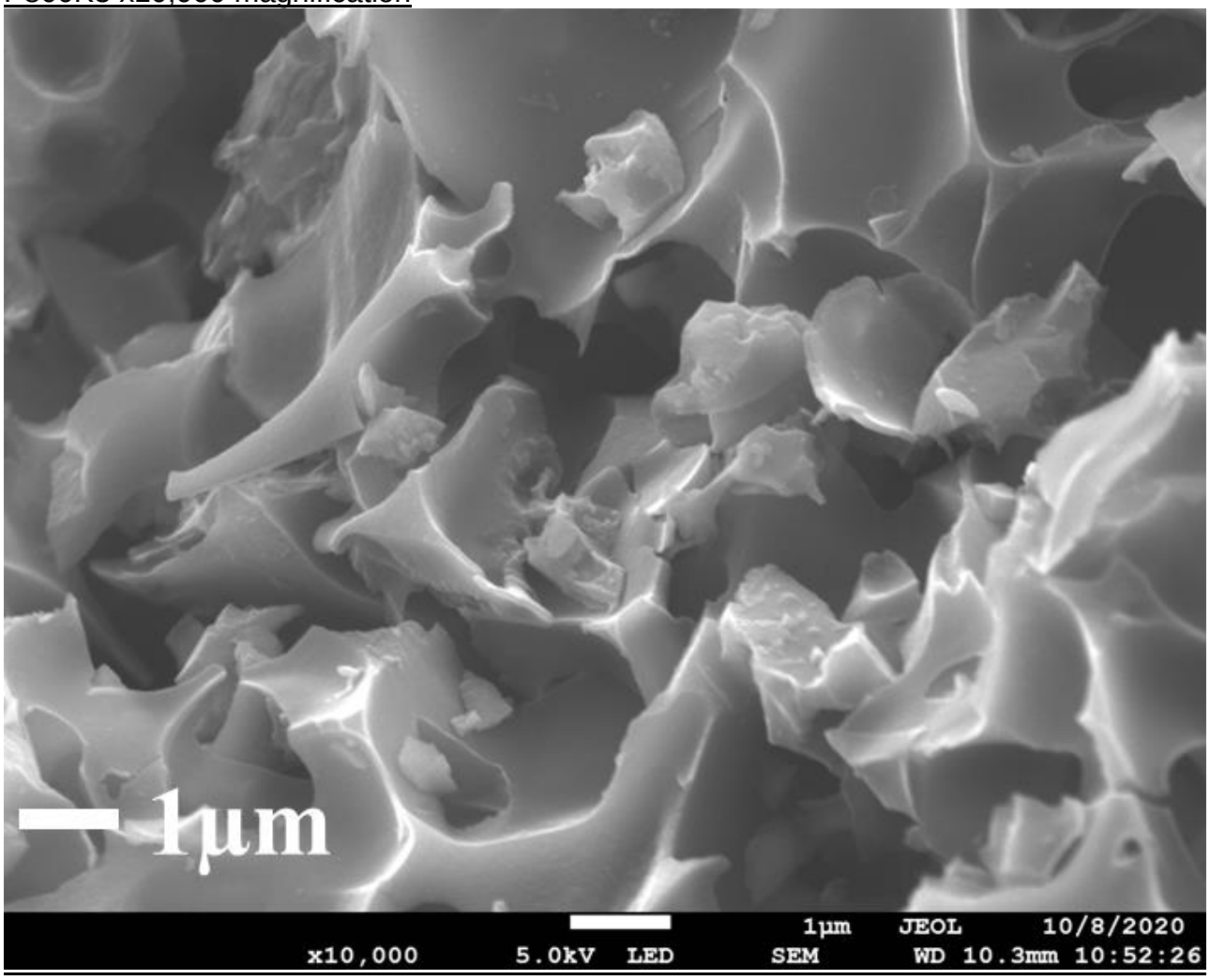

SEM Images for P800K5

P800K5 x200 magnification and particle size distribution plot

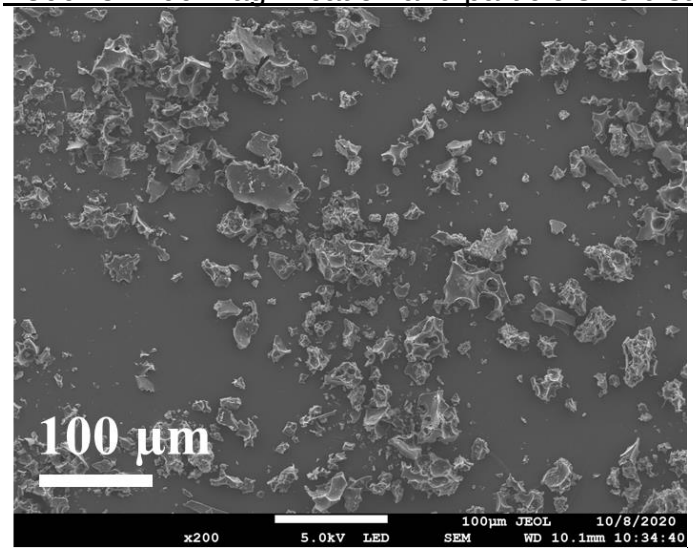

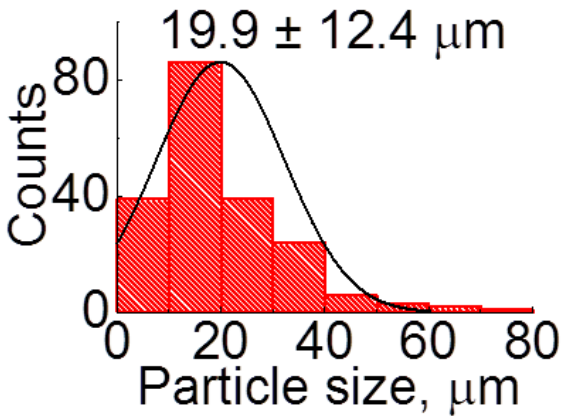

P800K5 x10,000 magnification

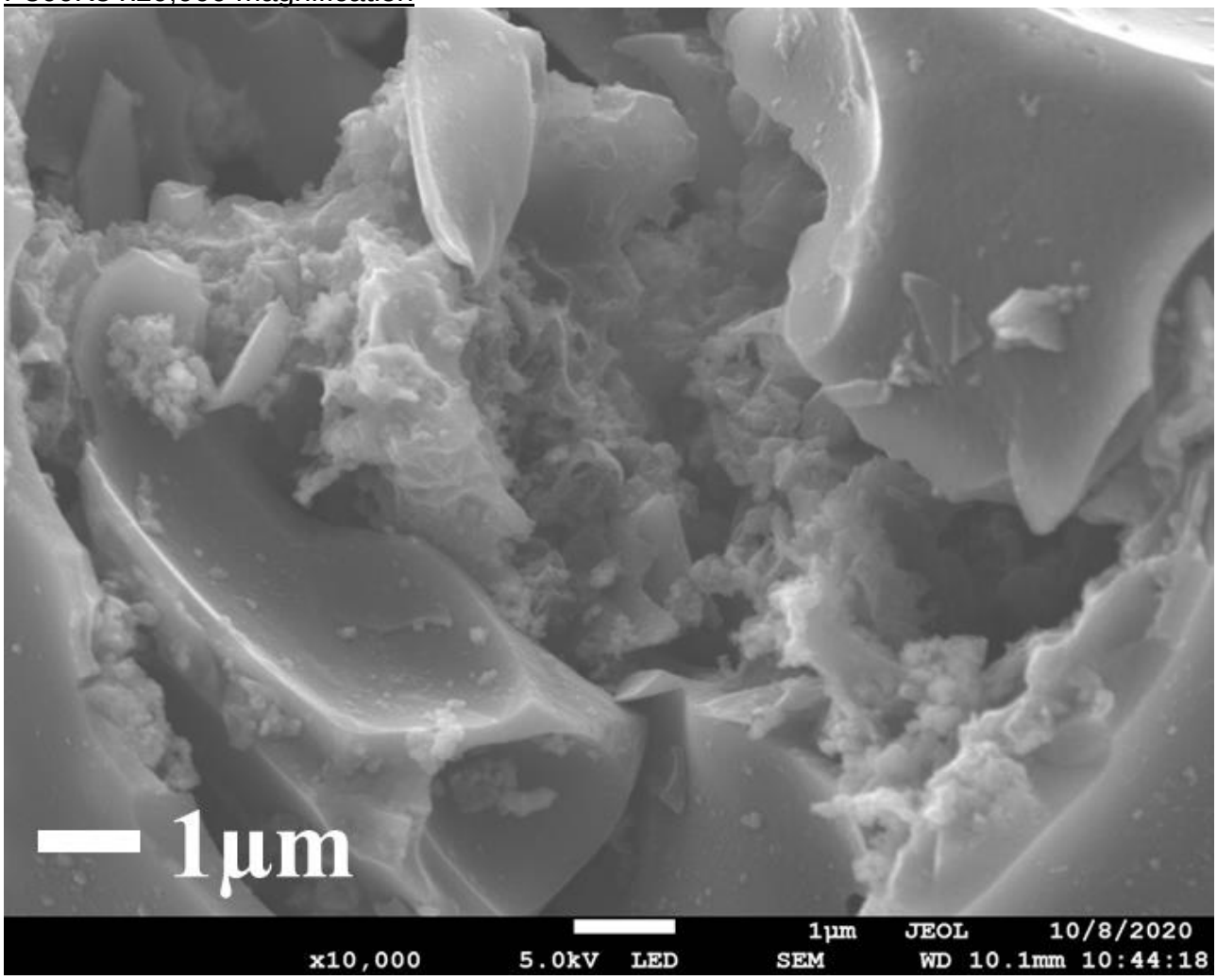

SEM Images for S800C15

S800C15 x500 magnification and particle size distribution plot

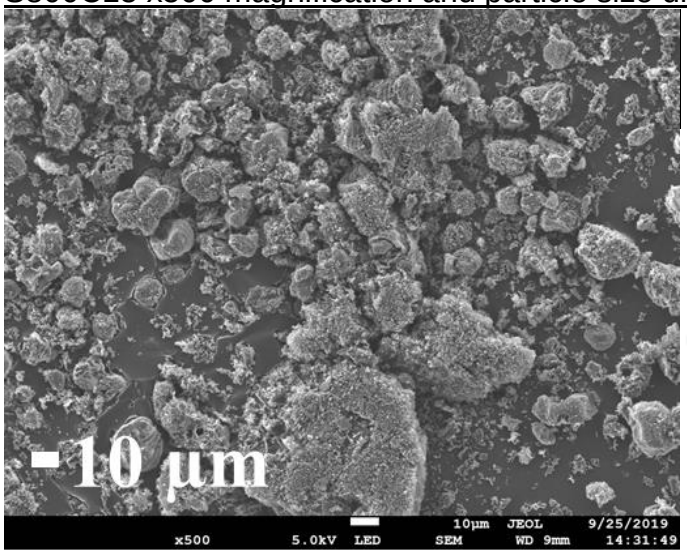

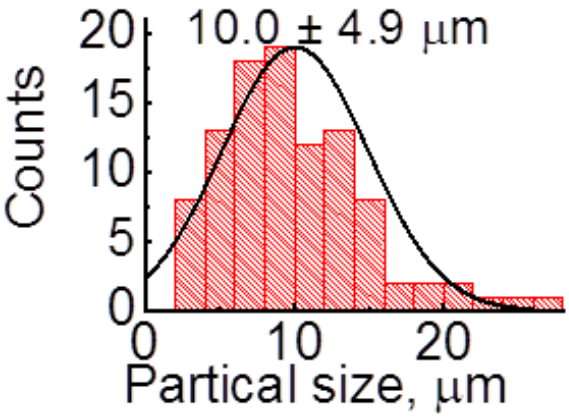

S800C15 x10,000 magnification

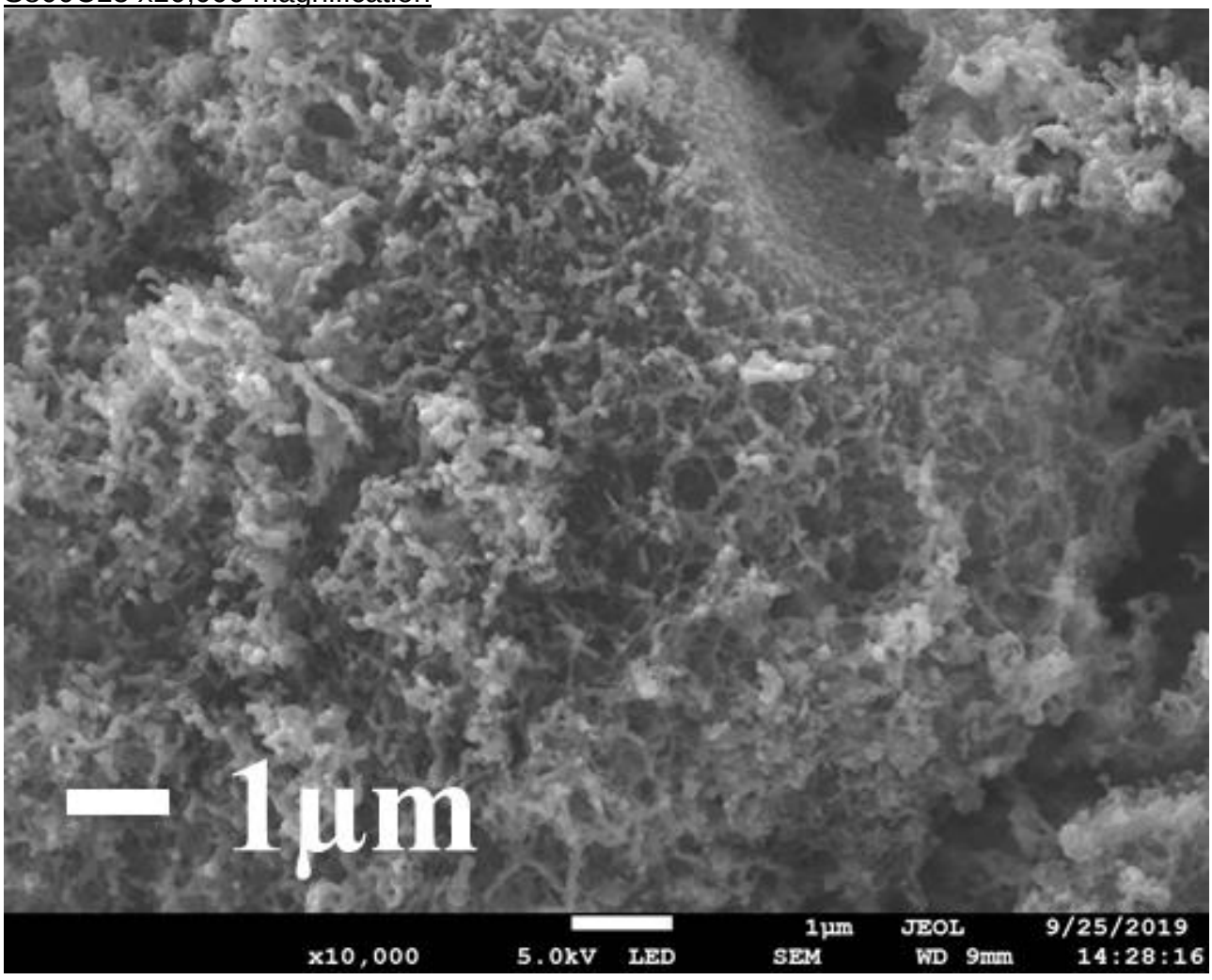

SEM Images for S900C15

S900C15 x500 magnification and particle size distribution plot

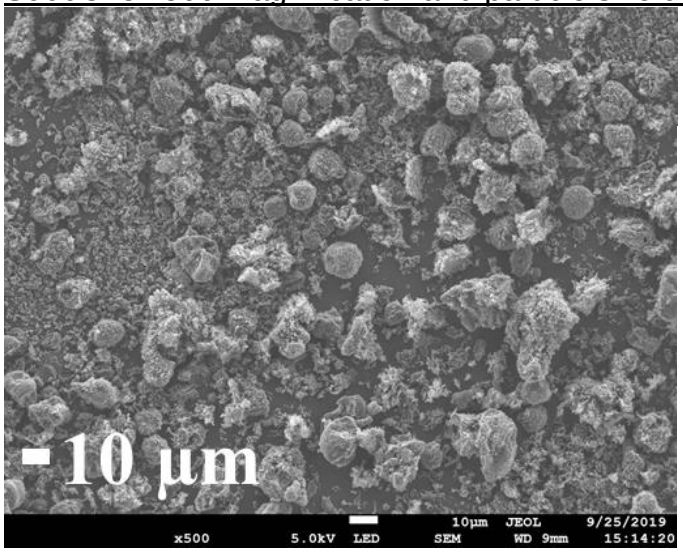

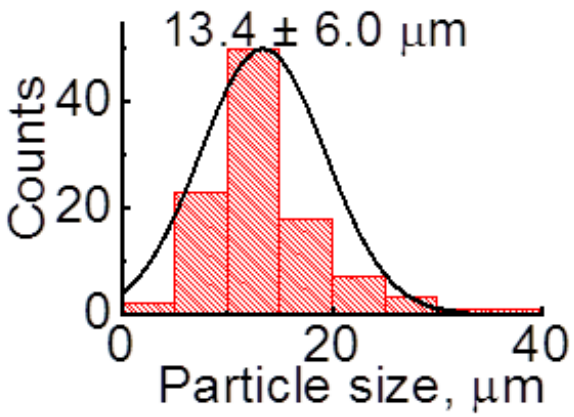

S900C15 x10,000 magnification

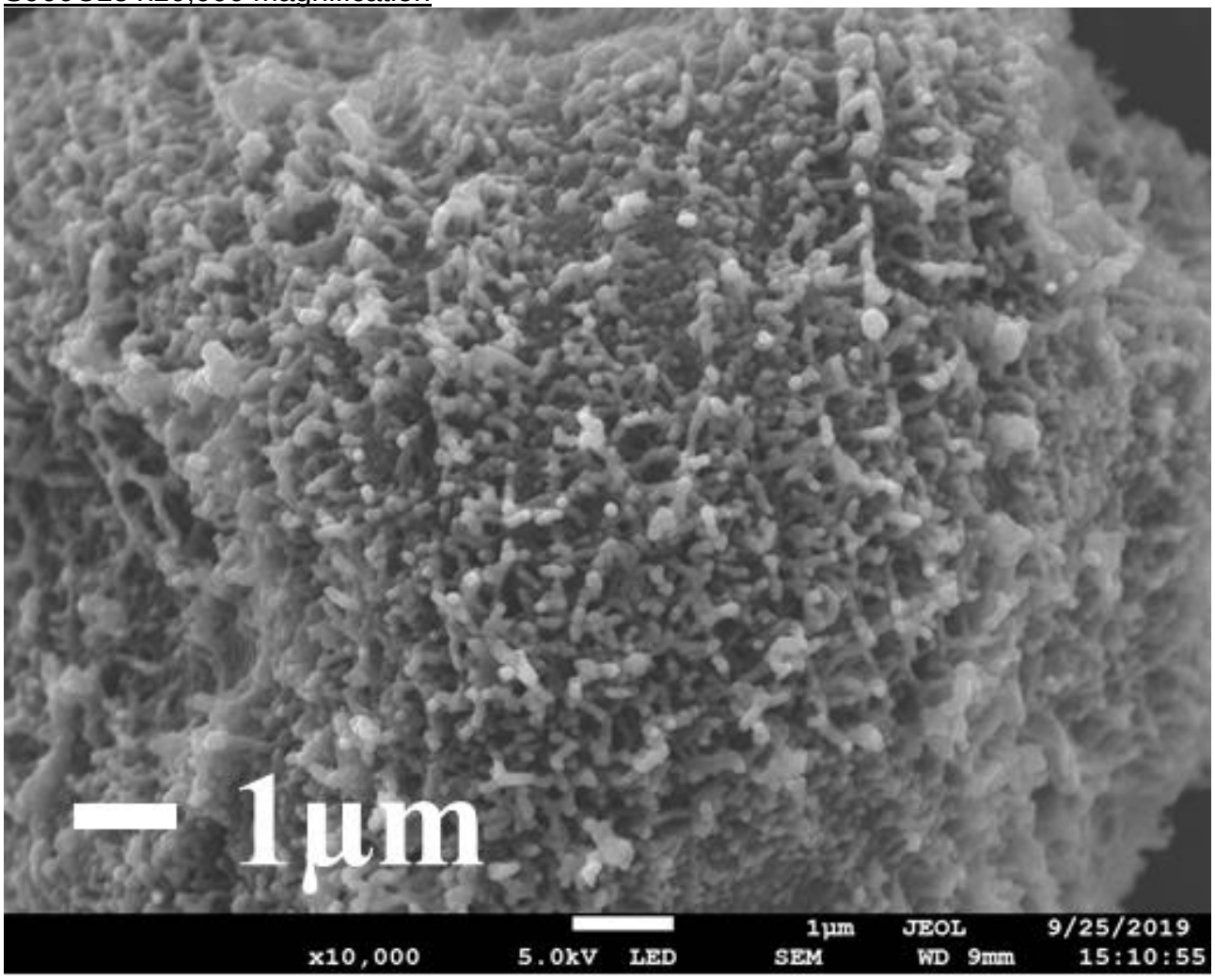

SEM Images for S950C15

S950C15 x500 magnification and particle size distribution plot

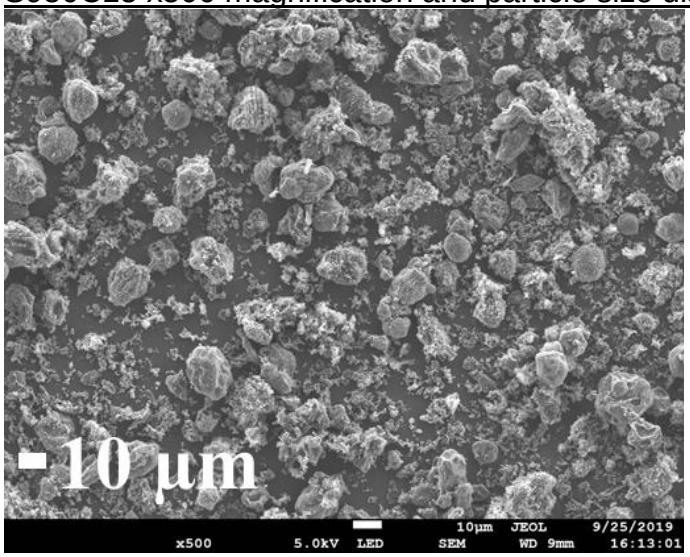

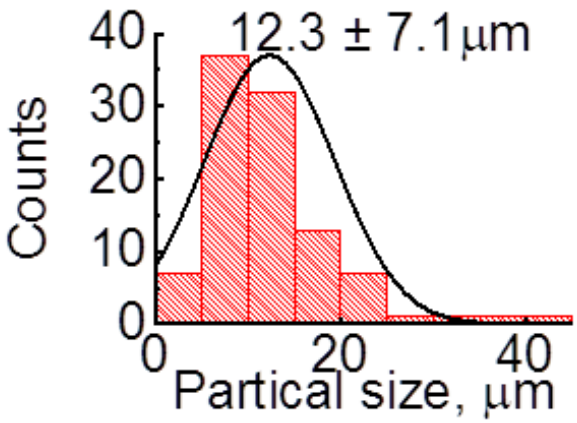

S950C15 x10,000 magnification

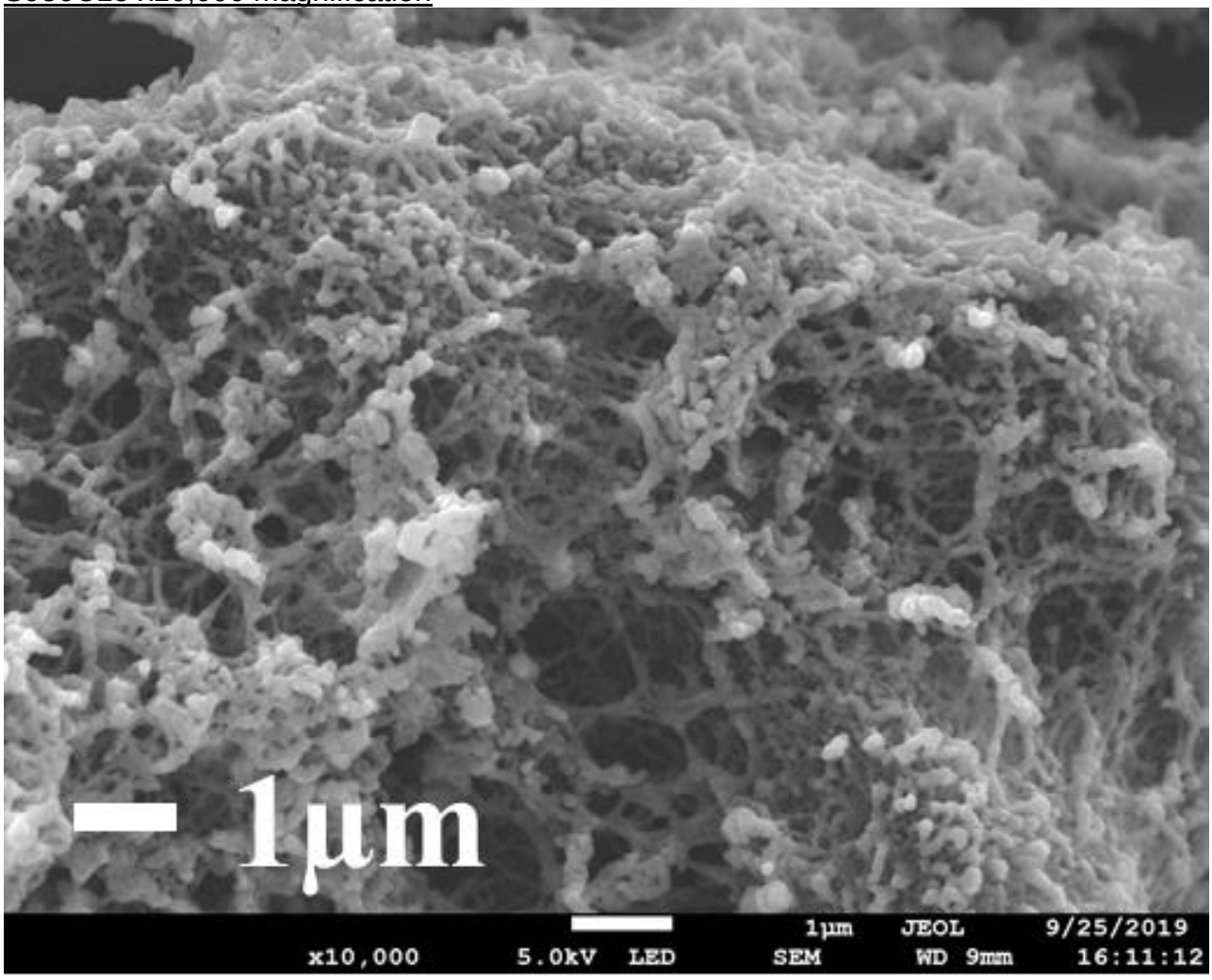

SEM Images for S1000C15

S1000C15 x500 magnification and particle size distribution plot

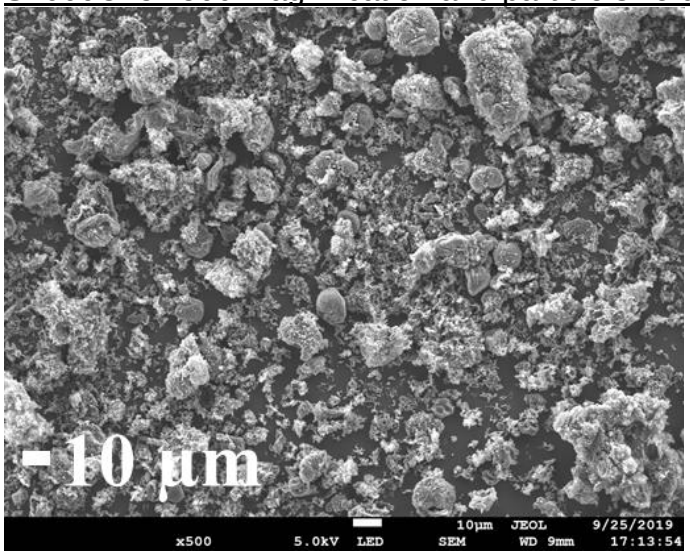

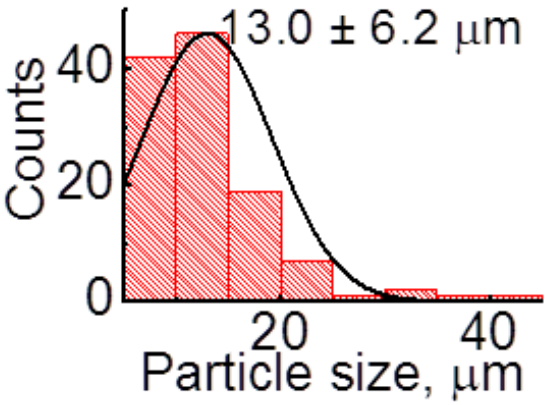

S1000C15 x10,000 magnification

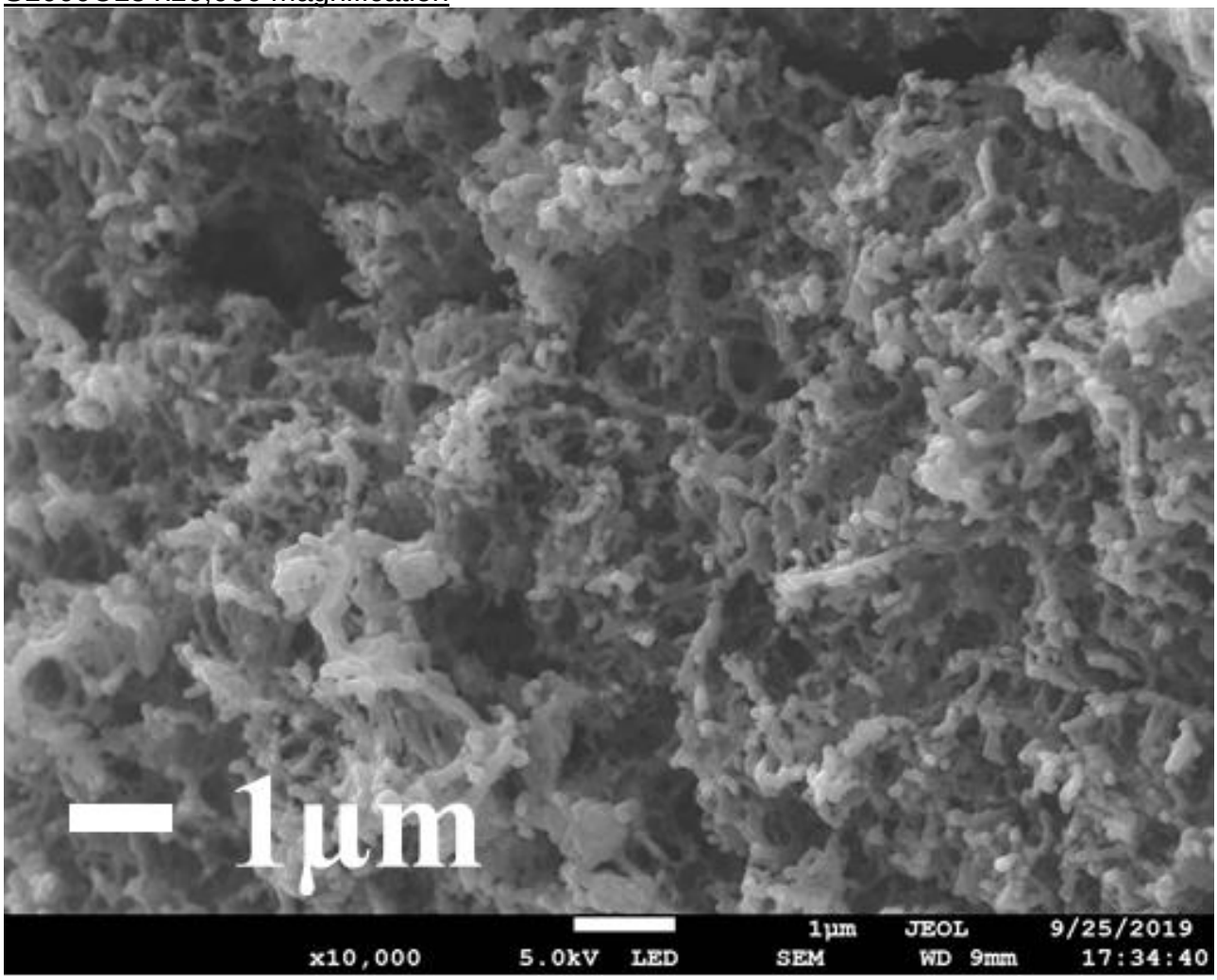

SEM Images for S900C30

S900C30 x500 magnification and particle size distribution plot

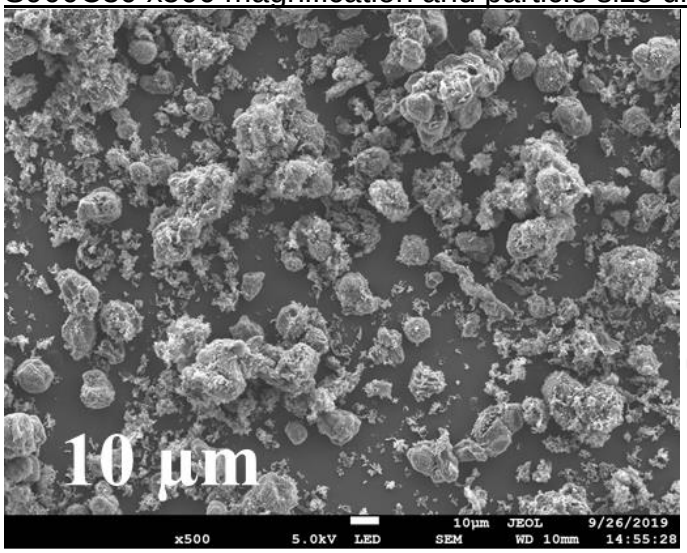

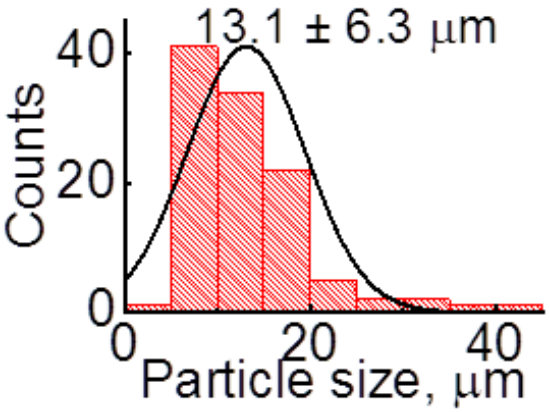

S900C30 x10,000 magnification

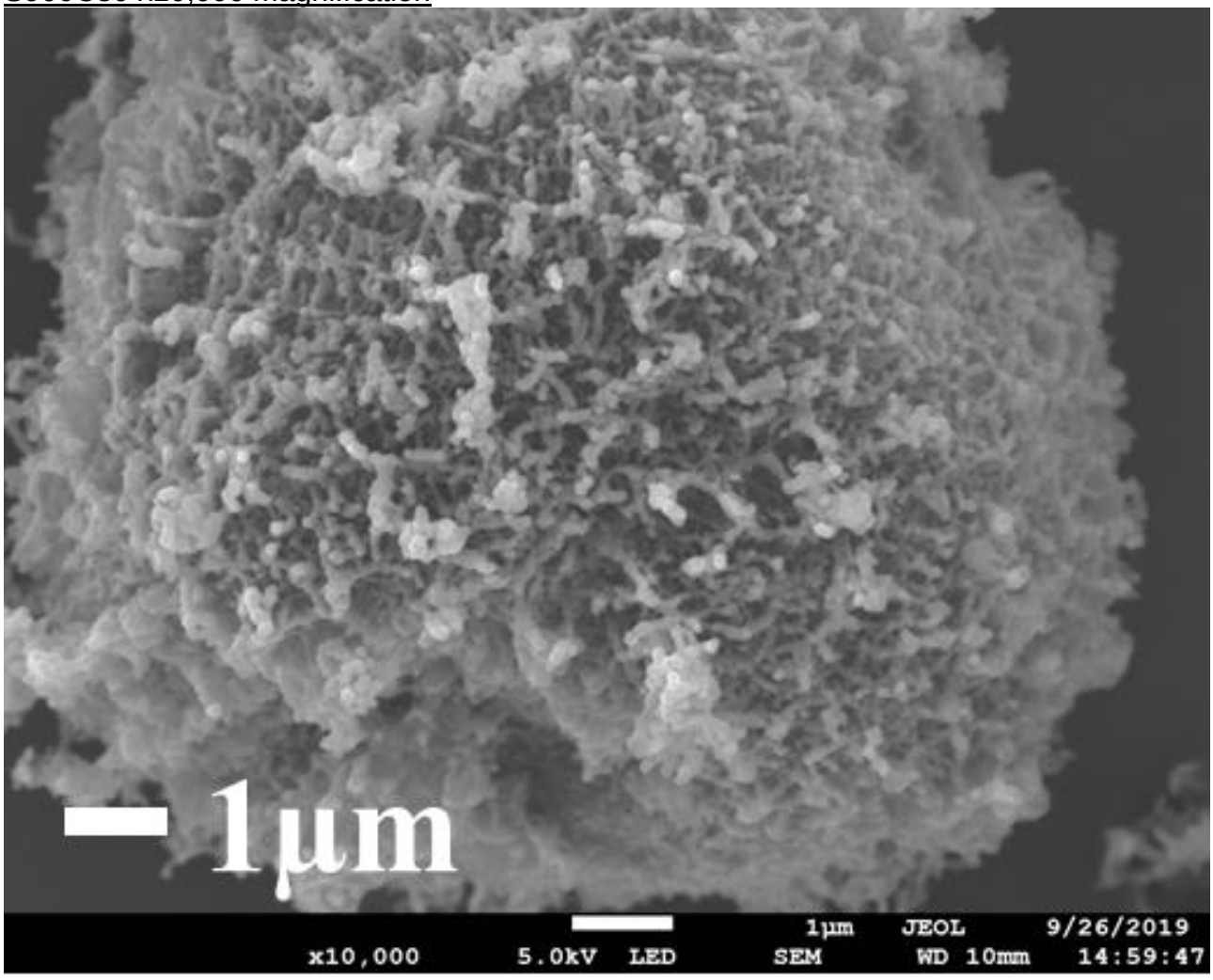

SEM Images for S900C60

S900C60 x500 magnification and particle size distribution plot

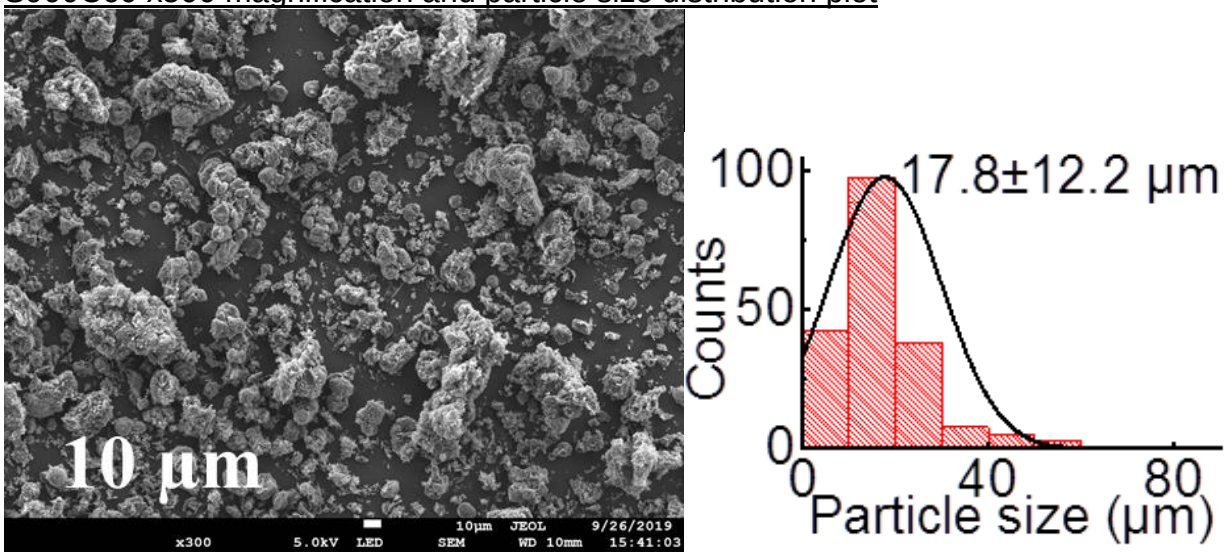

S900C60 x10,000 magnification

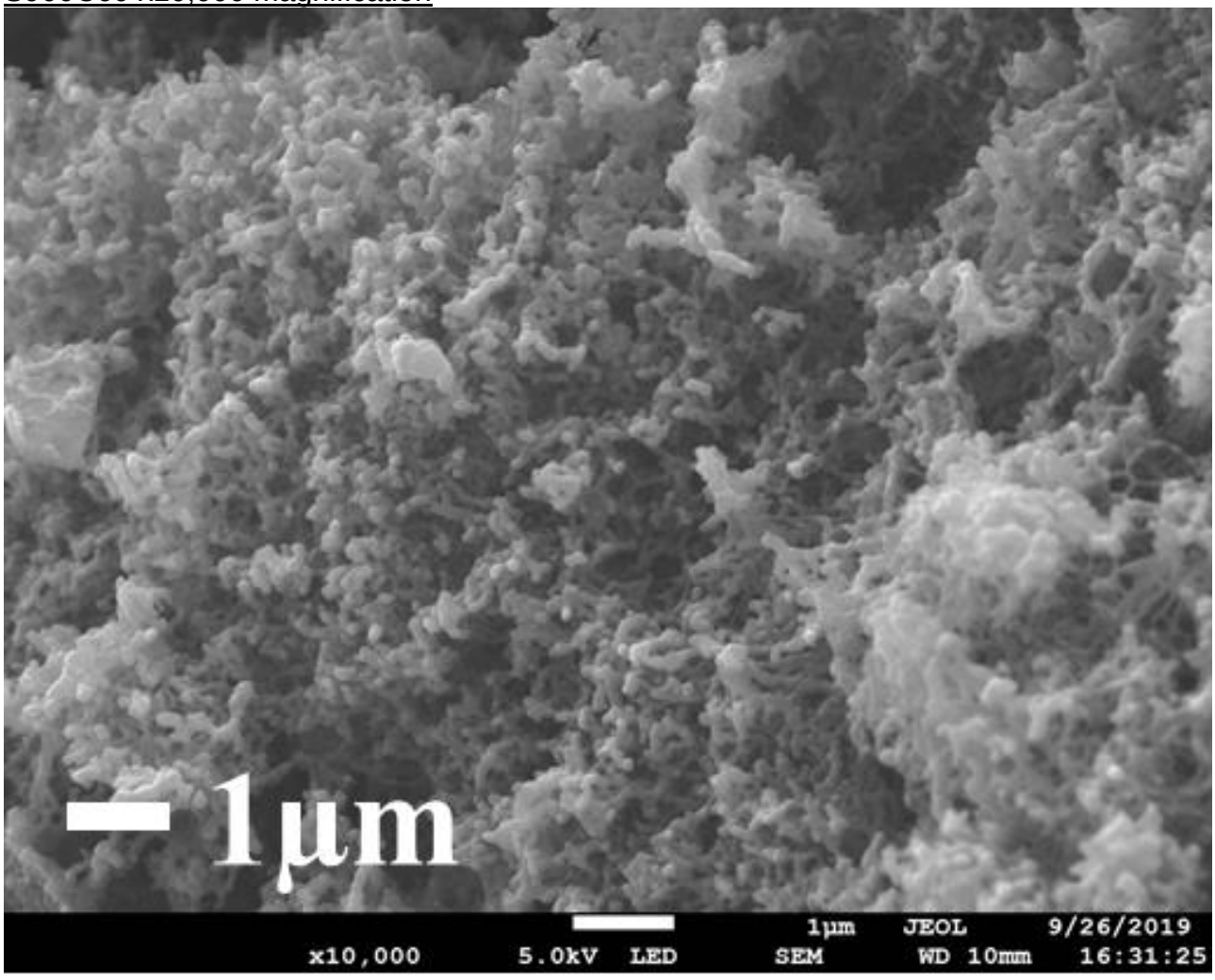

SEM Images for S900C90

S900C90 x500 magnification and particle size distribution plot

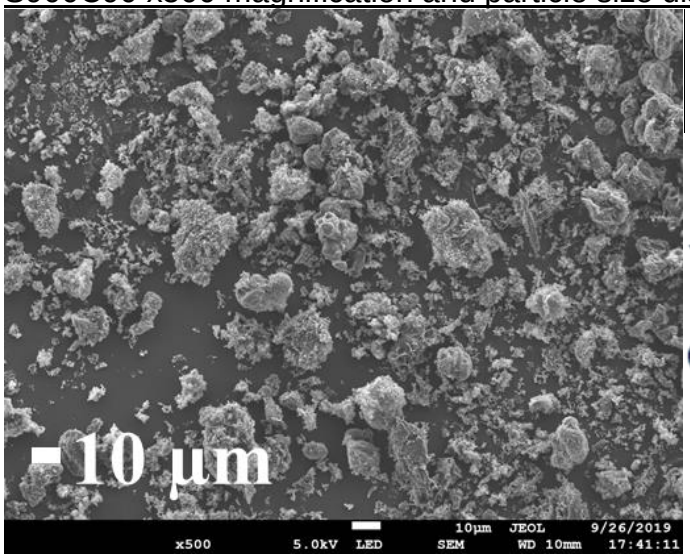

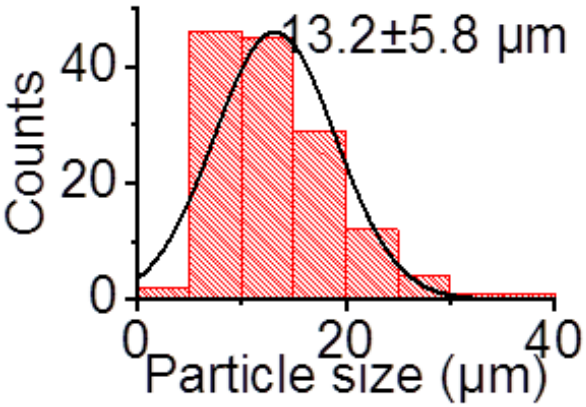

S900C90 x10,000 magnification

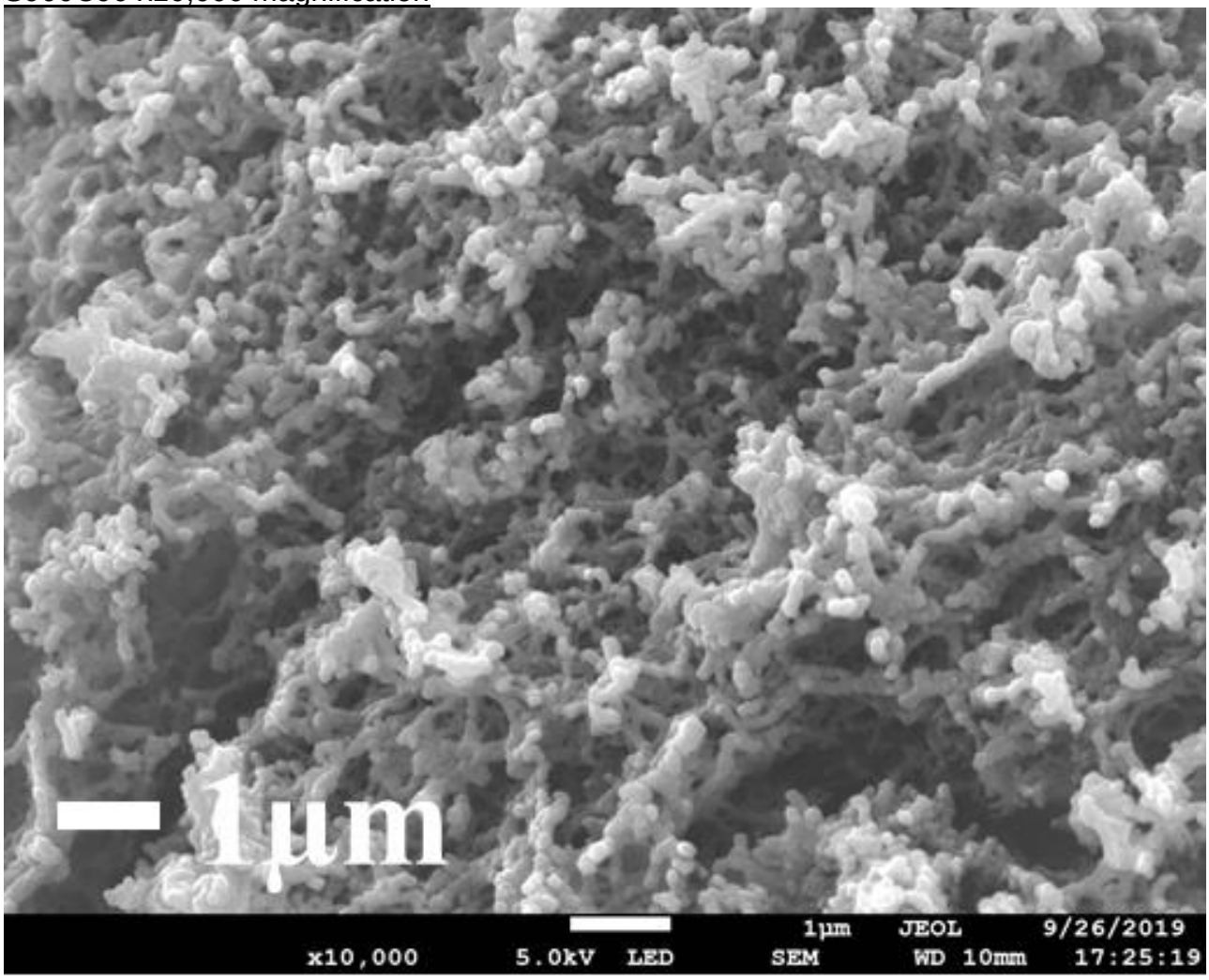

SEM Images for S900C120

S900C120 x500 magnification and particle size distribution plot

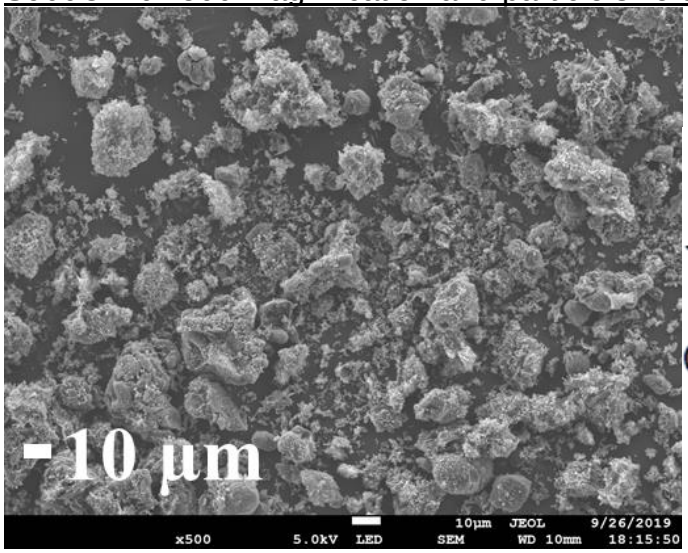

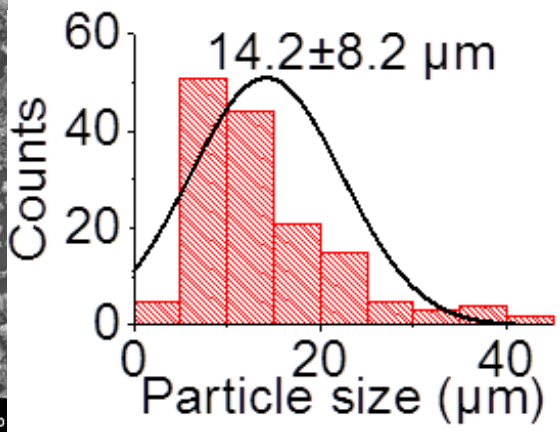

S900C120 x10,000 magnification

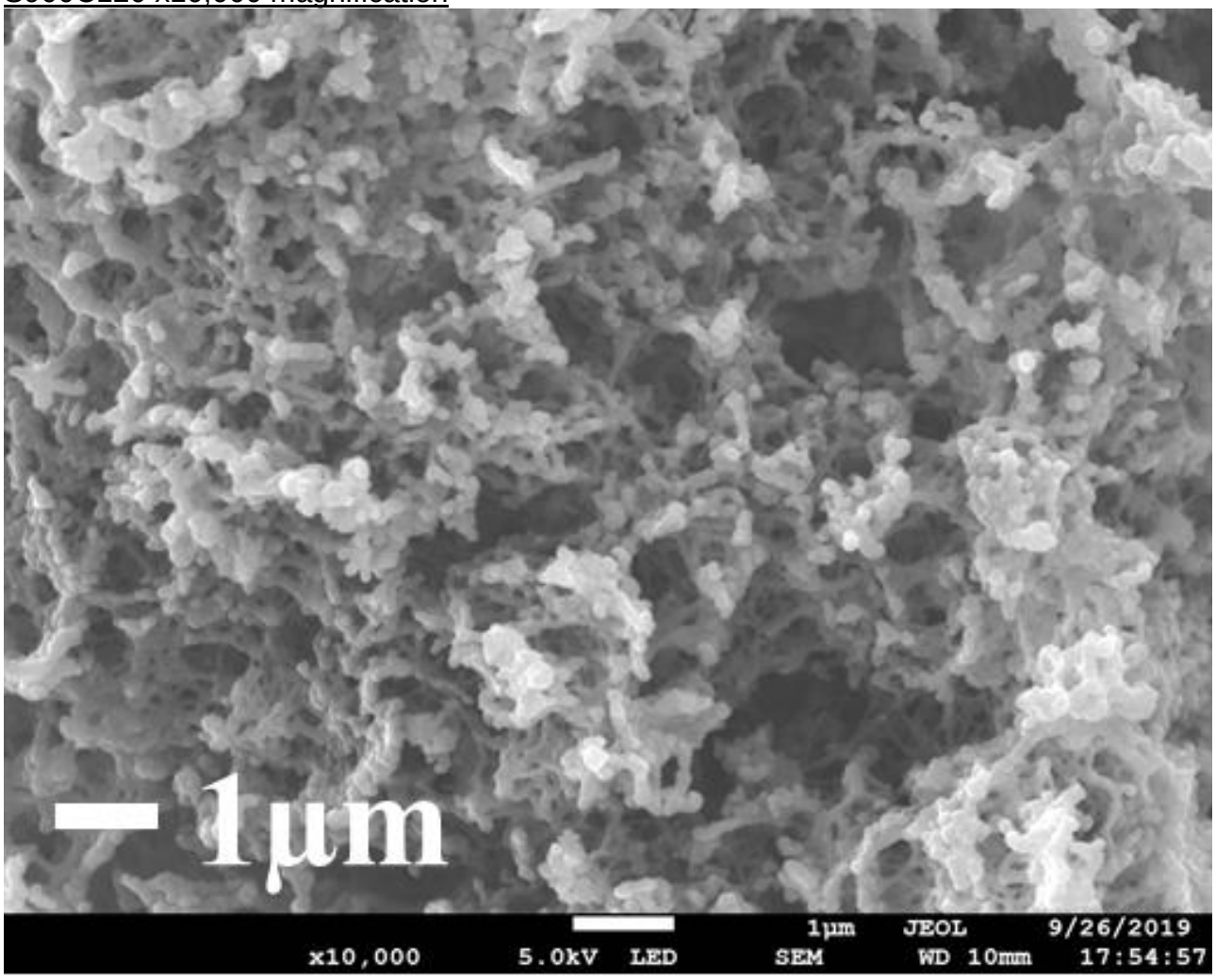

SEM Images for A750C45

A750C45 x100 magnification and particle size distribution plot

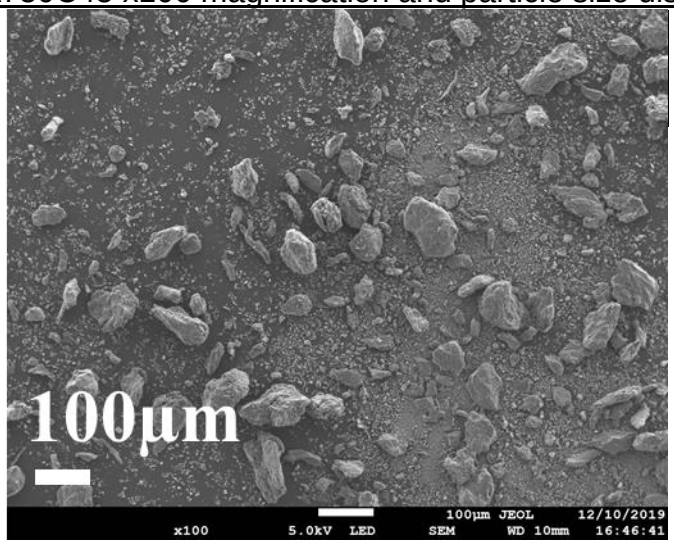

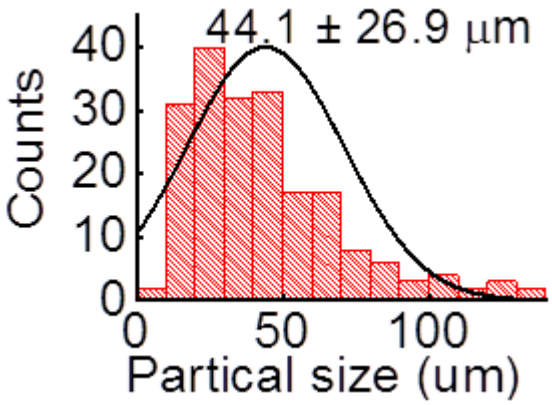

A750C45 x10,000 magnification

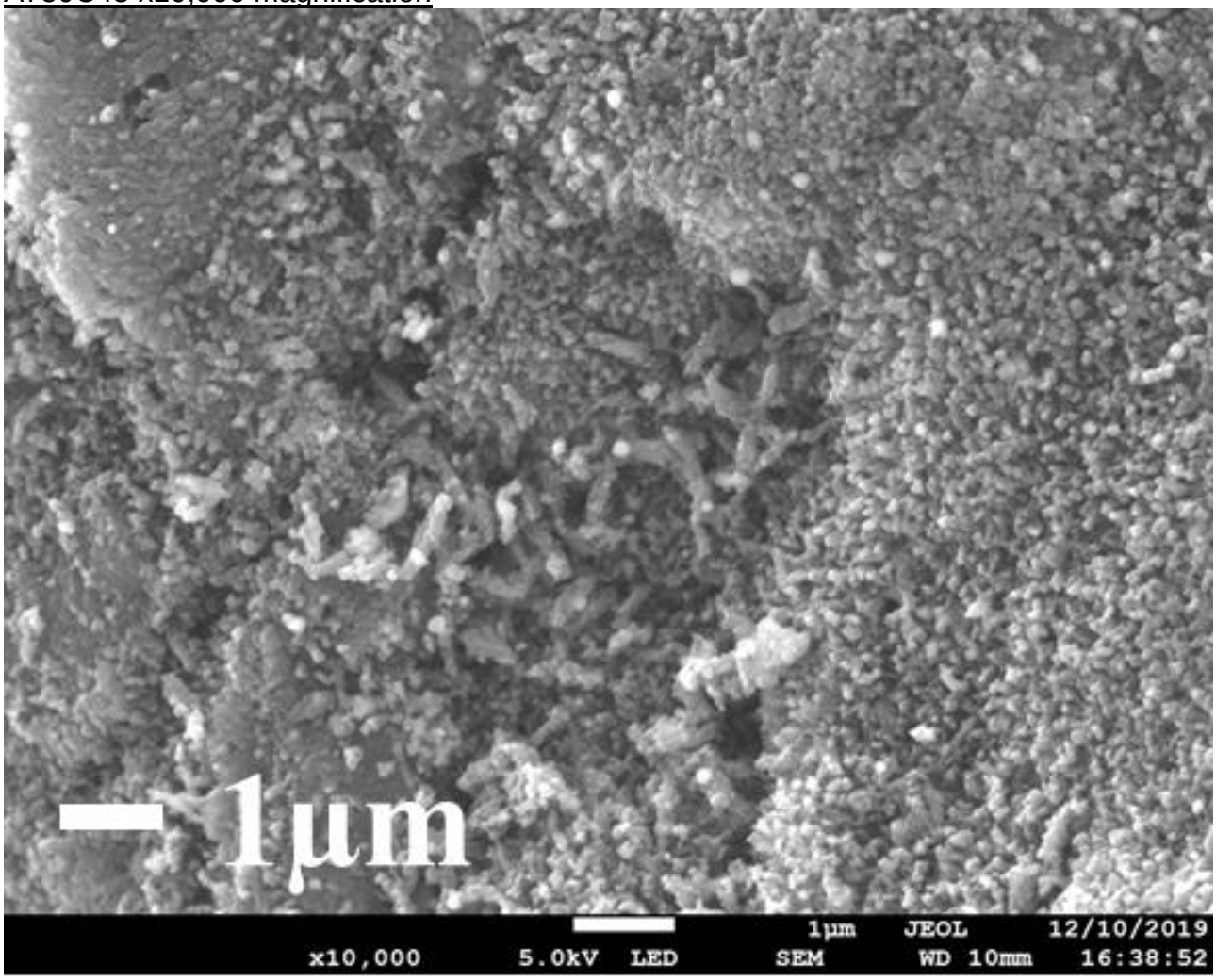

SEM Images for A750C60

A750C60 x100 magnification and particle size distribution plot

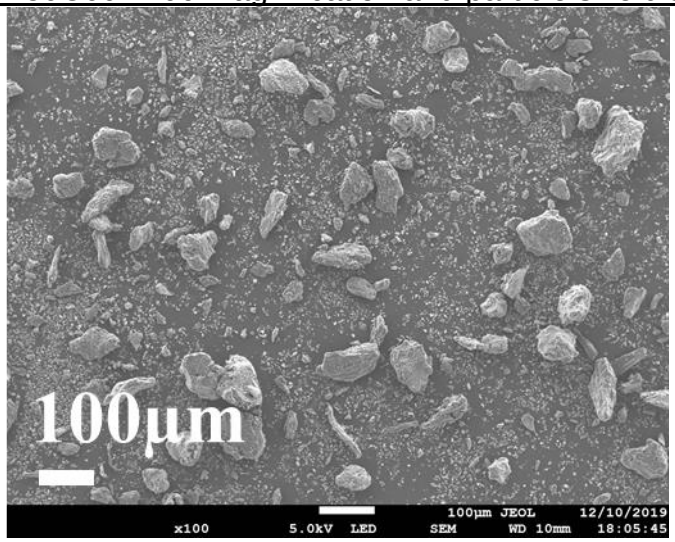

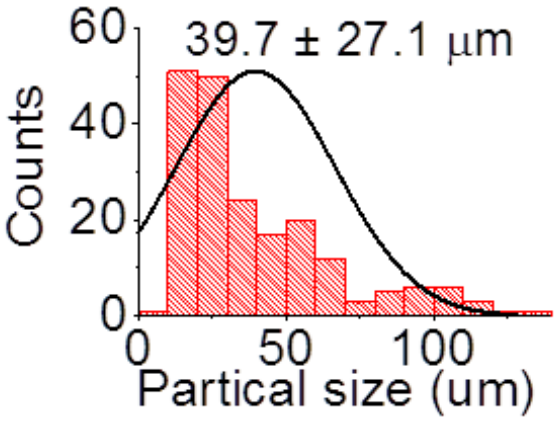

A750C60 x10,000 magnification

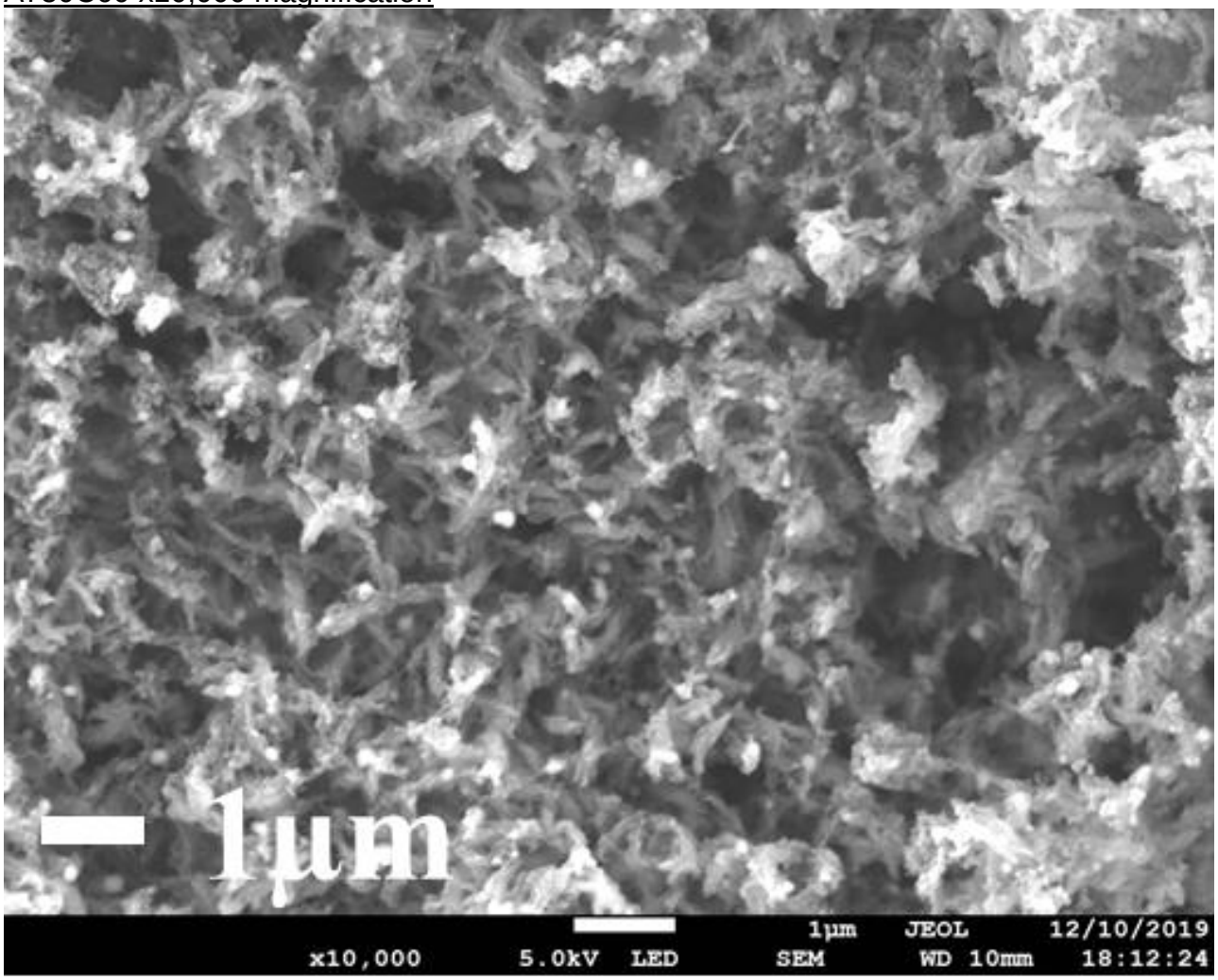

SEM Images for A750C90

A750C90 x100 magnification and particle size distribution plot

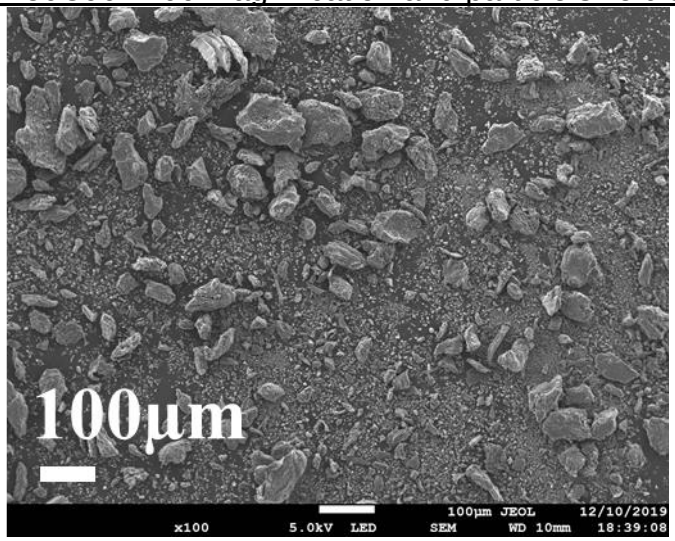

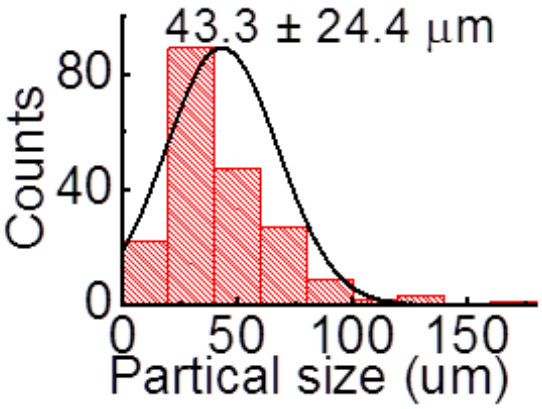

A750C90 x10,000 magnification

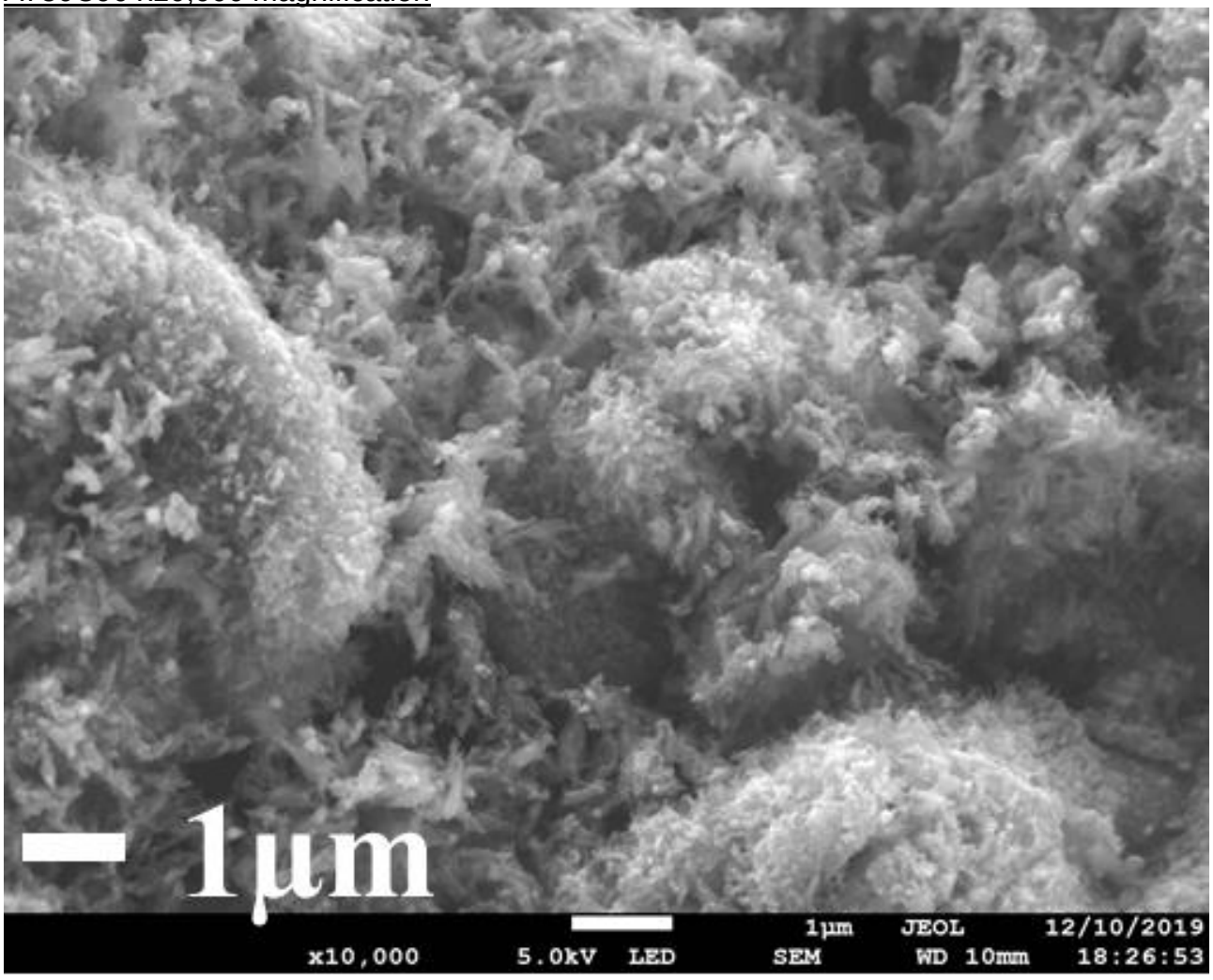

SEM Images for A900C0

A900C0 x100 magnification and particle size distribution plot

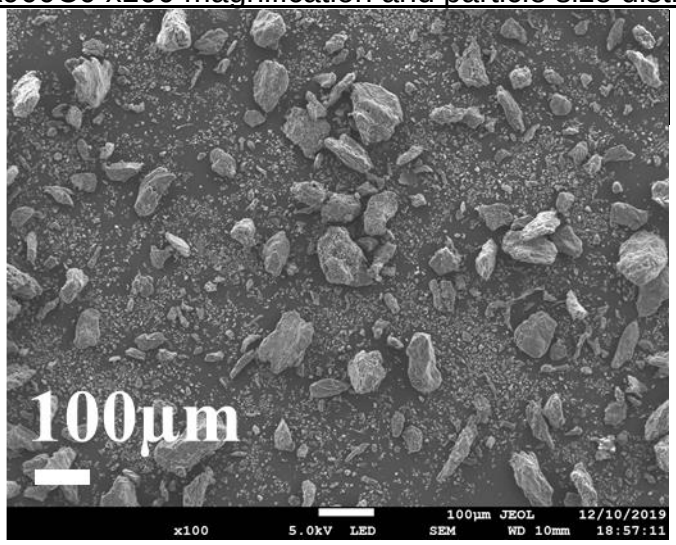

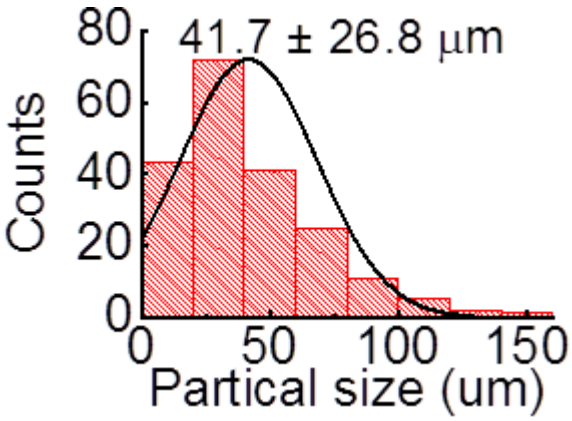

A900C0 x10,000 magnification

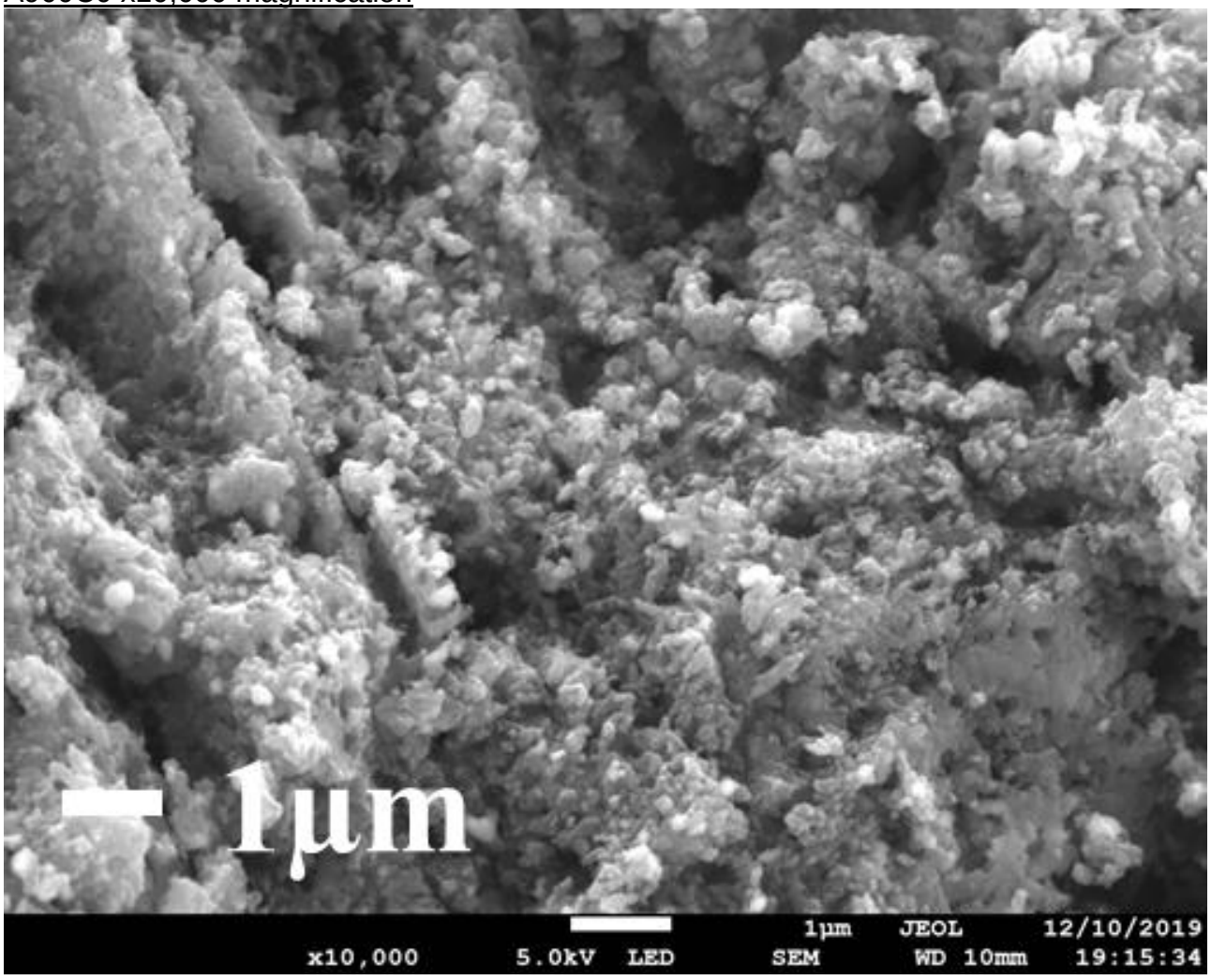

SEM Images for A900C10

A900C10 x100 magnification and particle size distribution plot

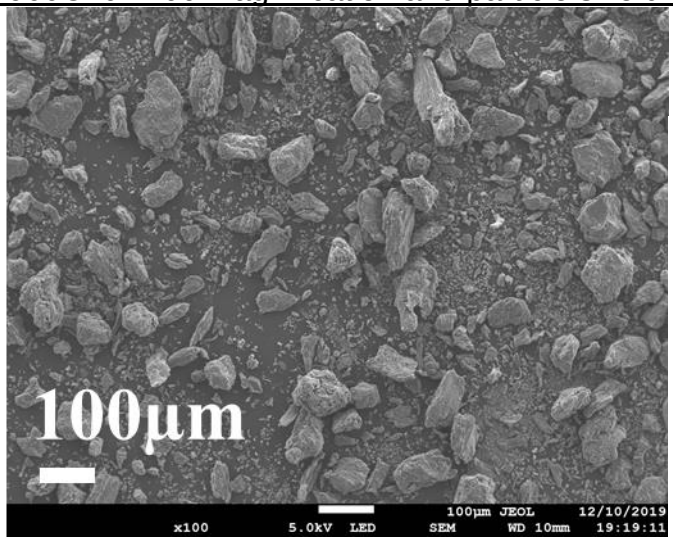

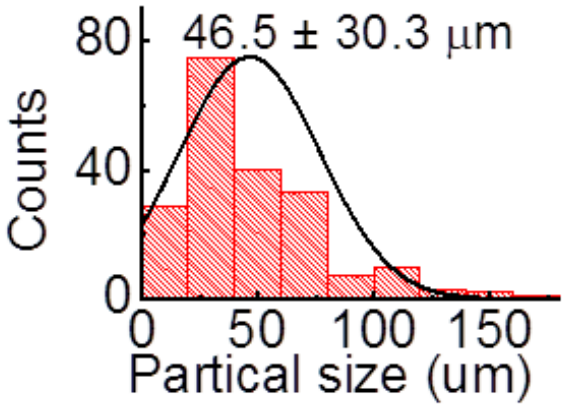

A900C10 x10,000 magnification

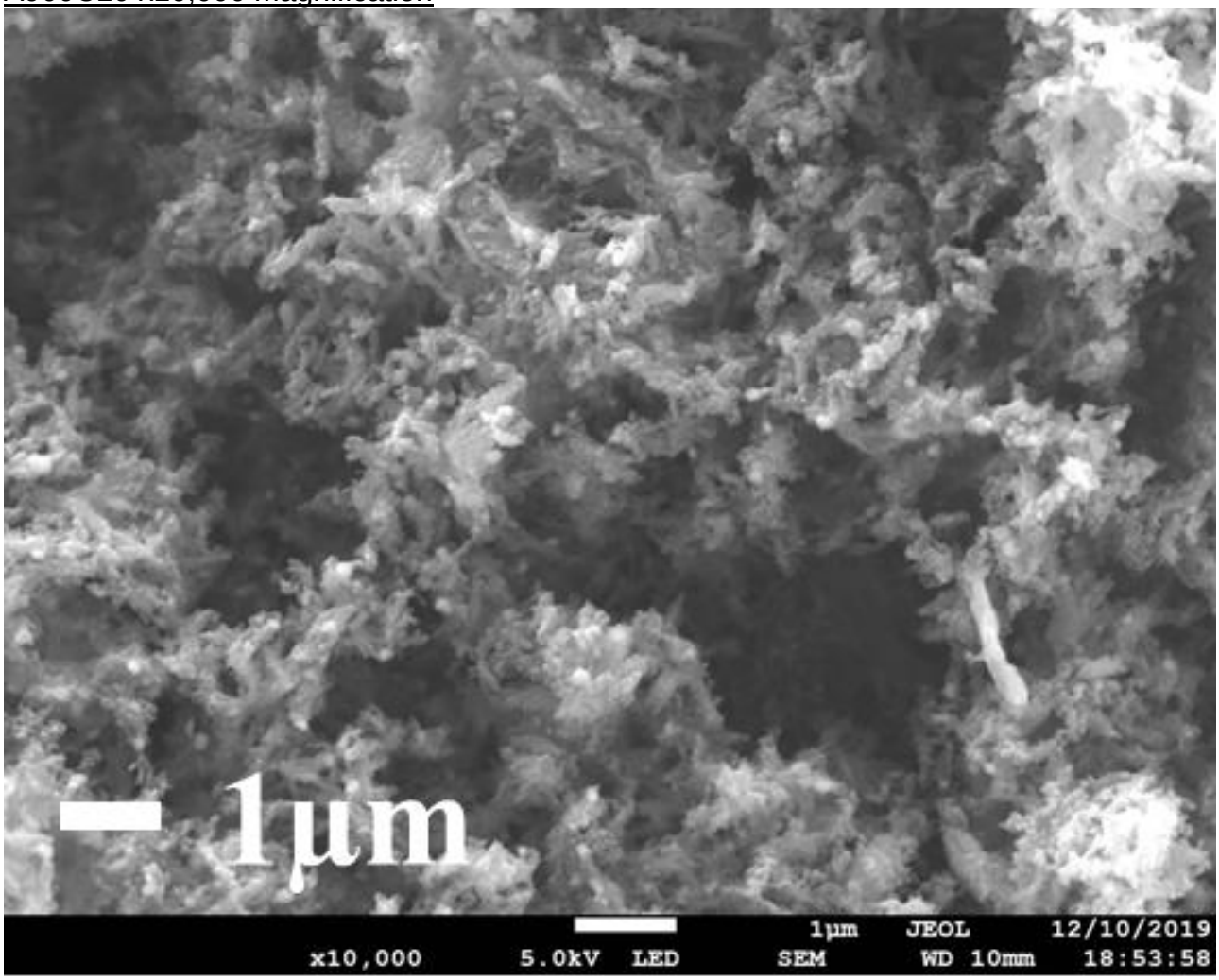

SEM Images for P900C0

P900C0 x200 magnification and particle size distribution plot

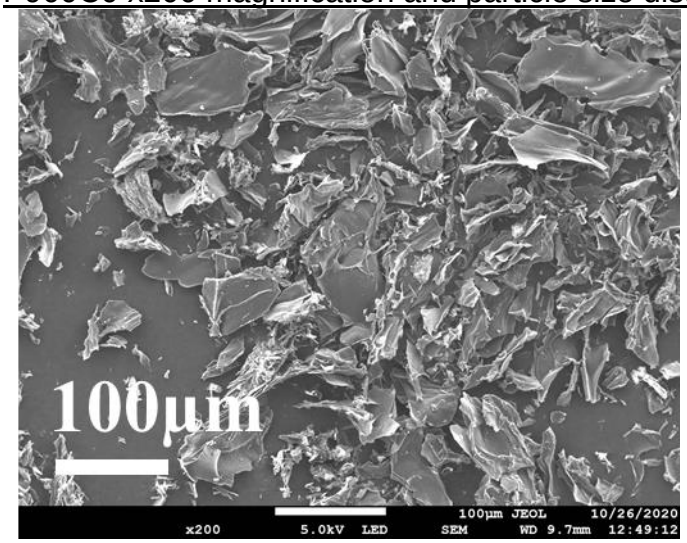

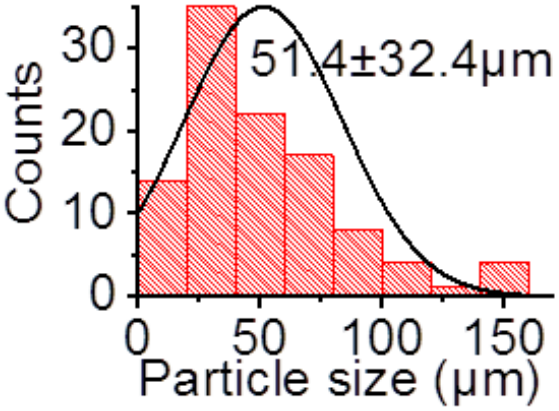

P900C0 x10,000 magnification

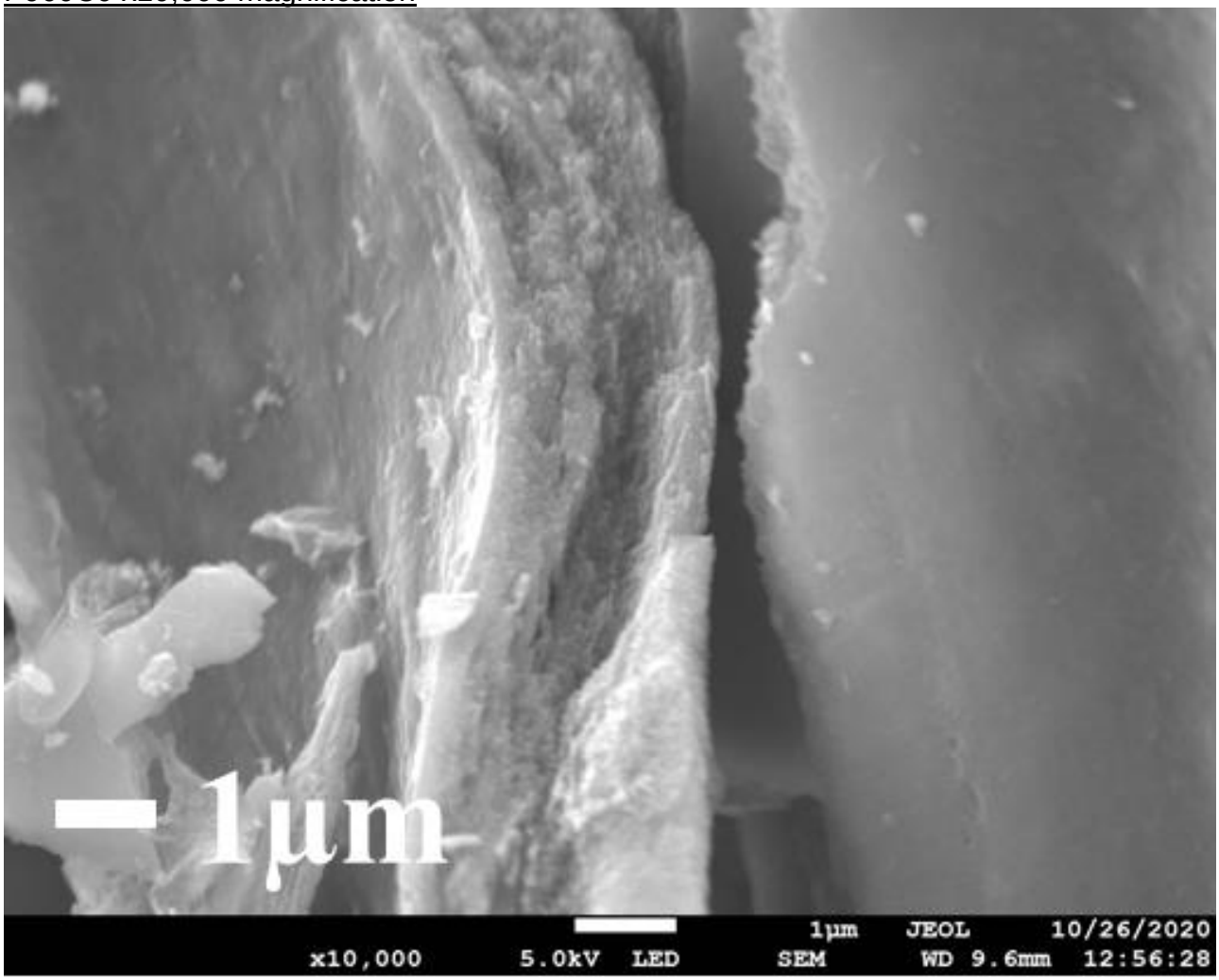

SEM Images for S700O0

S700O0 x500 magnification and particle size distribution plot

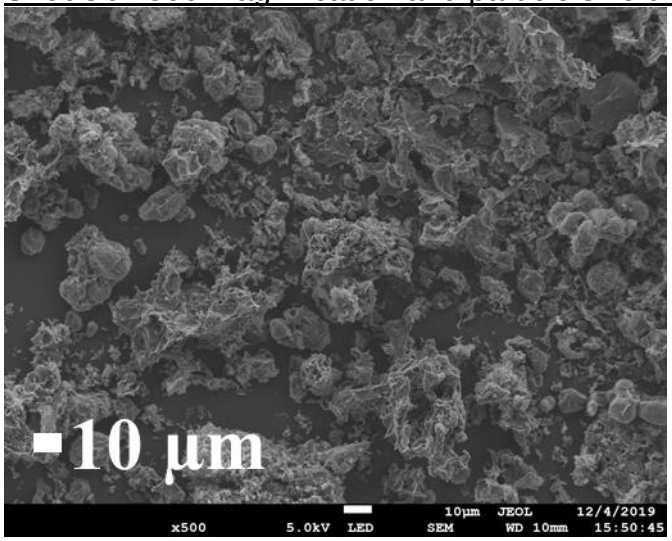

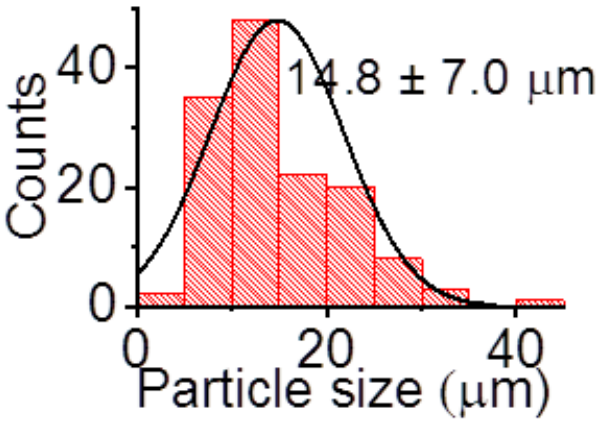

S700O0 x5,000 magnification

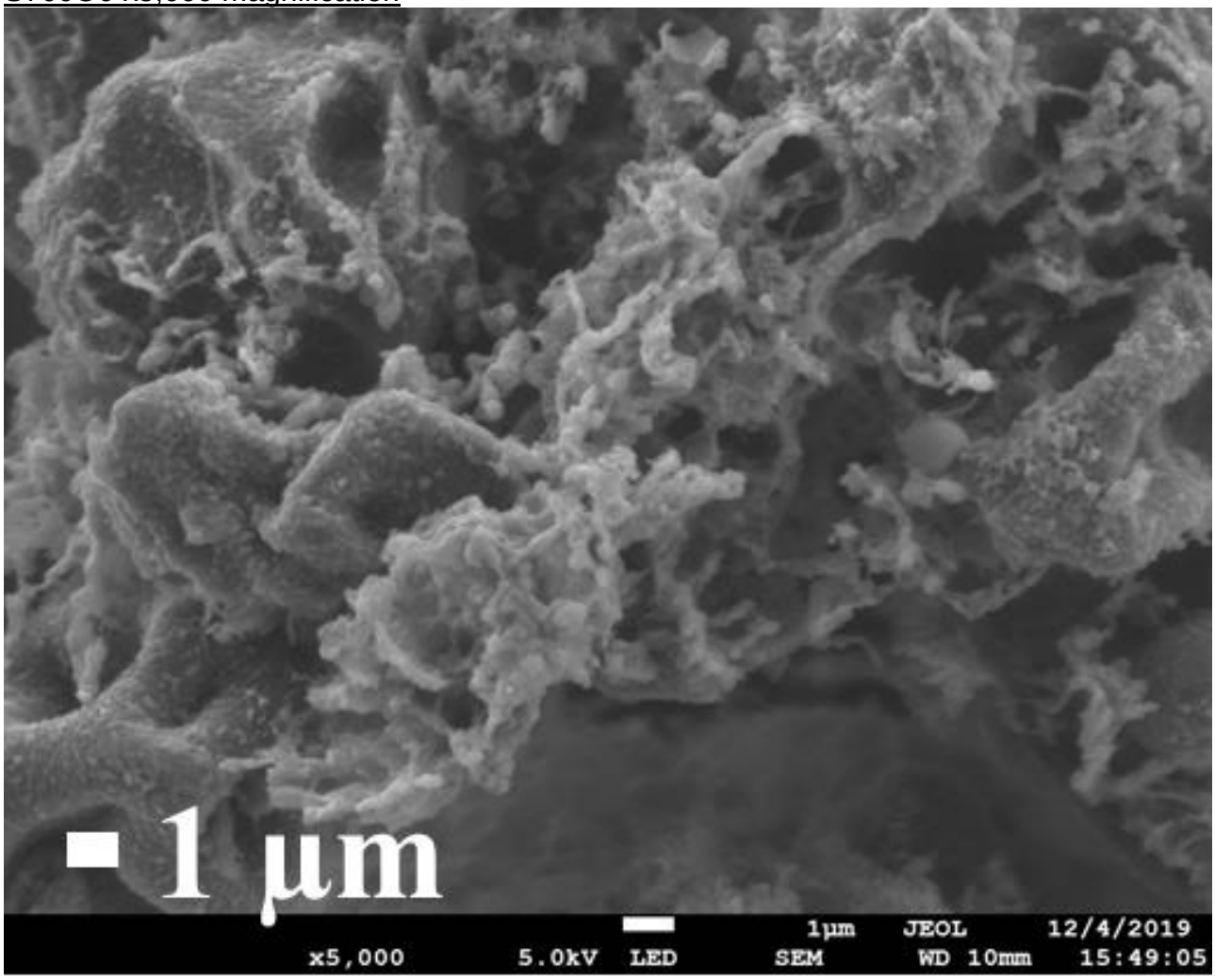

SEM Images for S750O0

S750O0 x500 magnification and particle size distribution plot

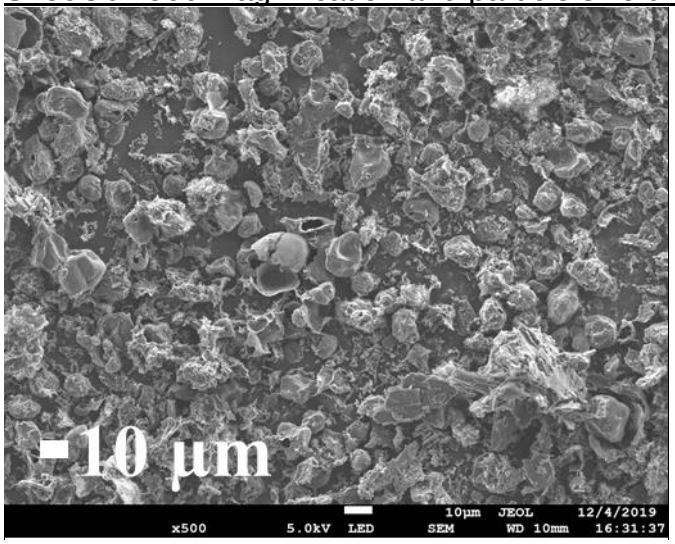

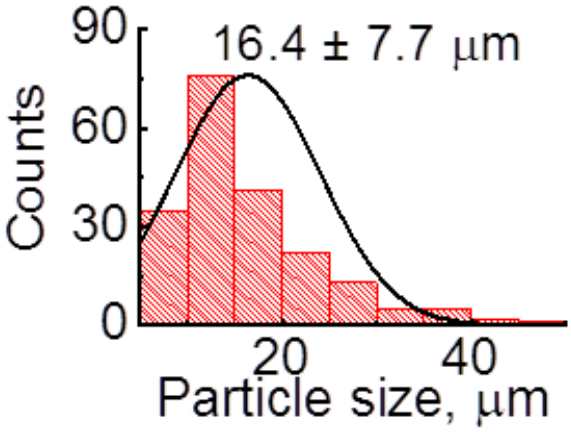

S750O0 x5,000 magnification

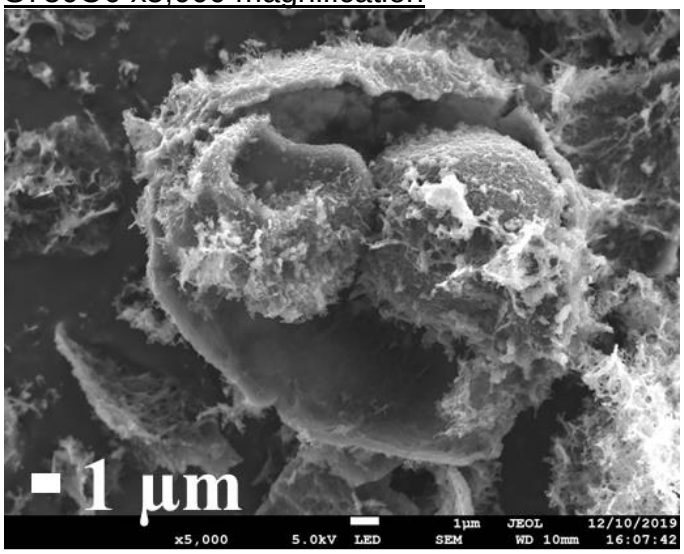

S750O0 x10,000 magnification

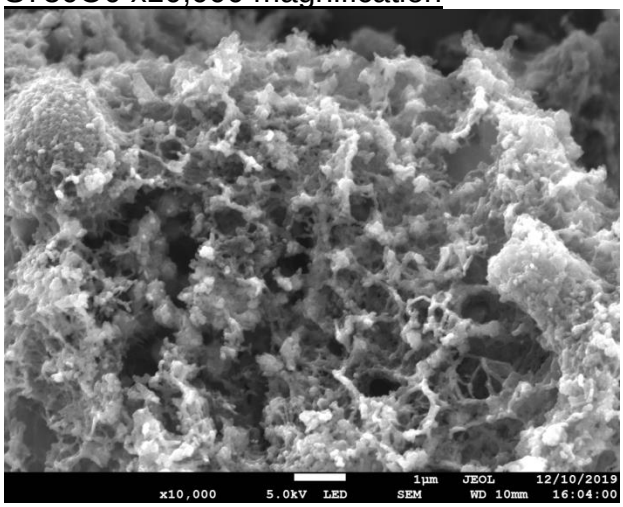

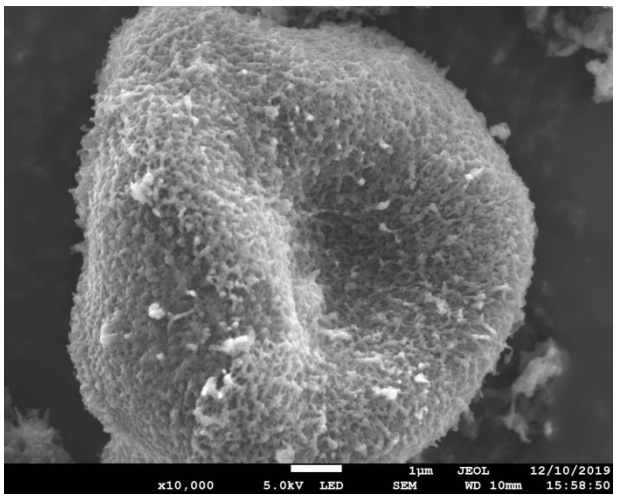

SEM Images for S800O0

S800O0 x500 magnification and particle size distribution plot

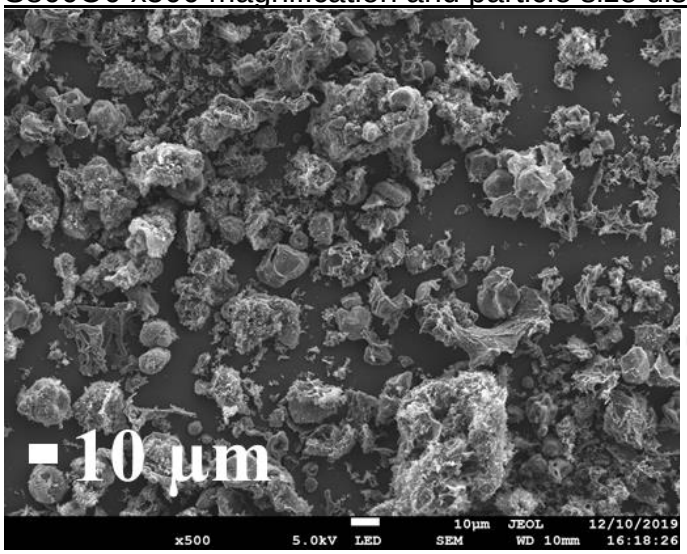

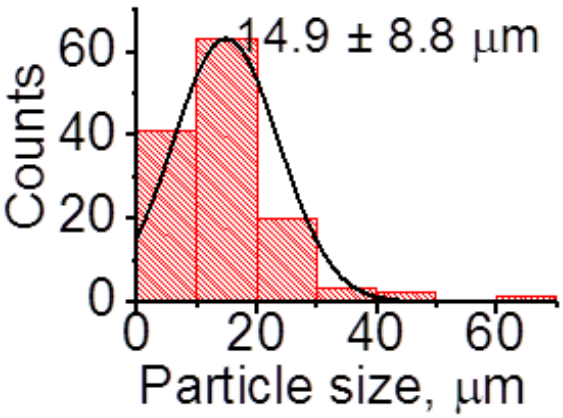

S800O0 x5,000 magnification

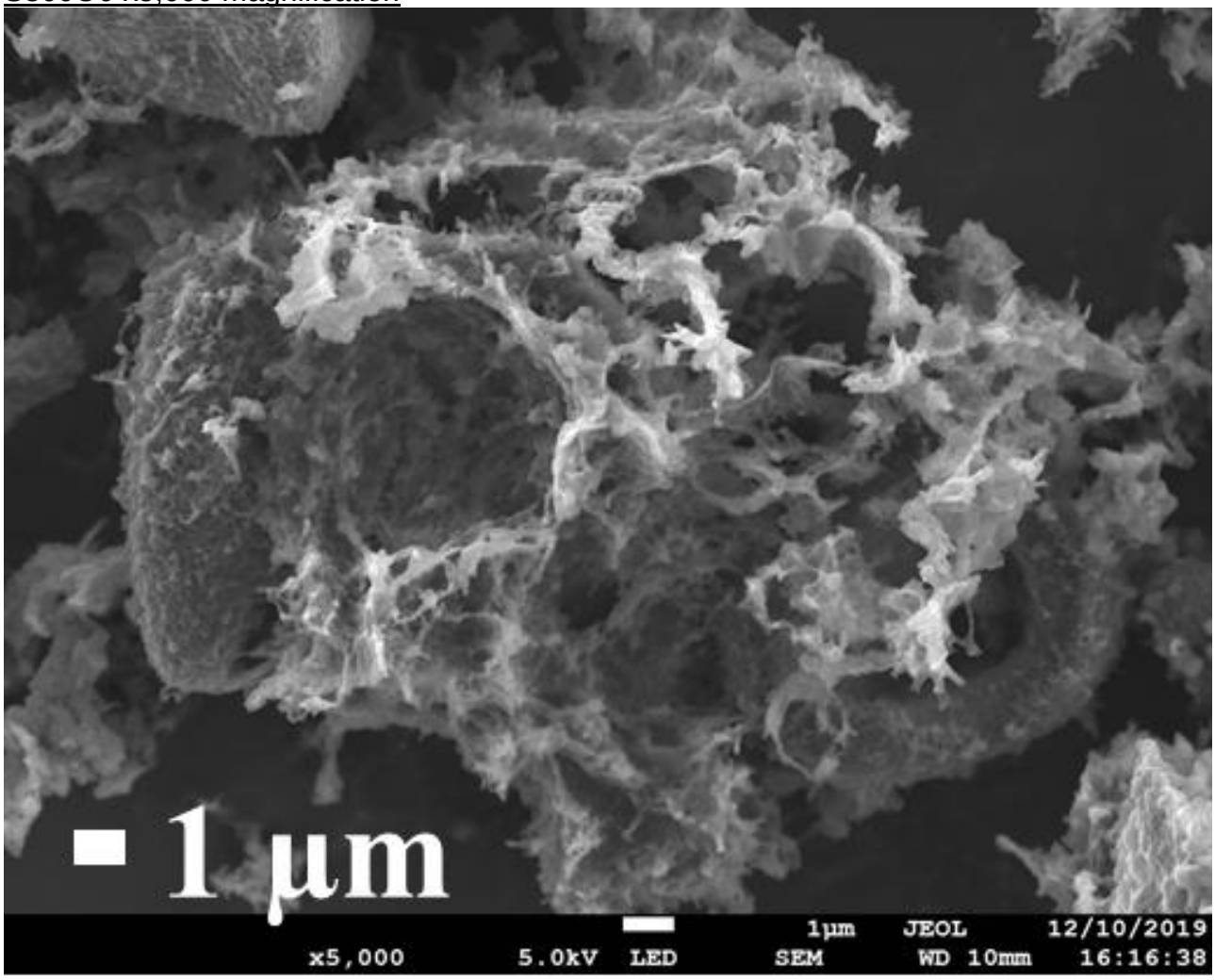

SEM Images for S750O40

S750O40 x500 magnification and particle size distribution plot

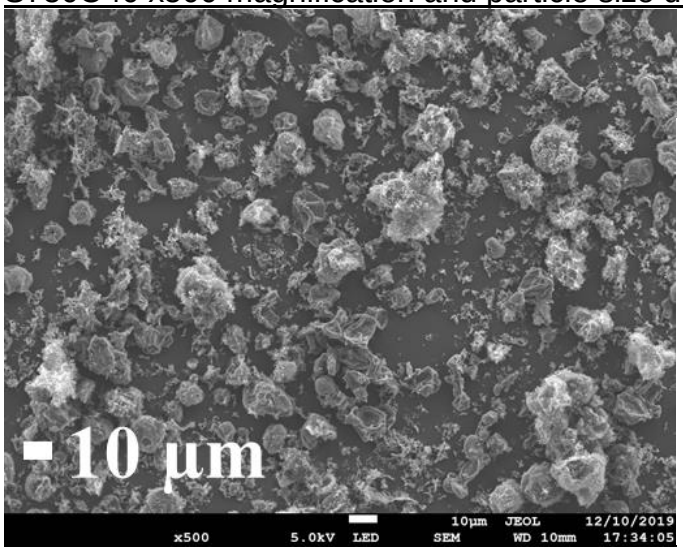

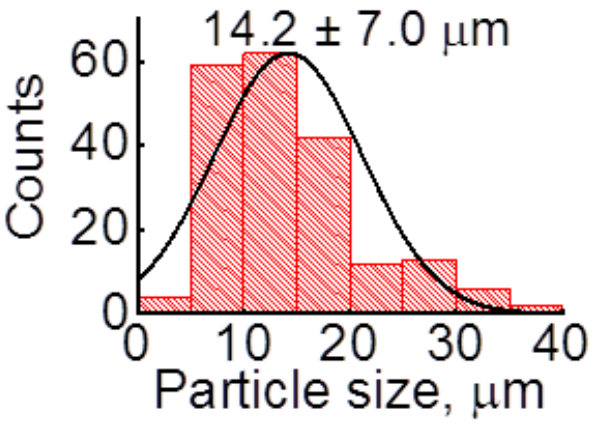

S750O40 x5,000 magnification

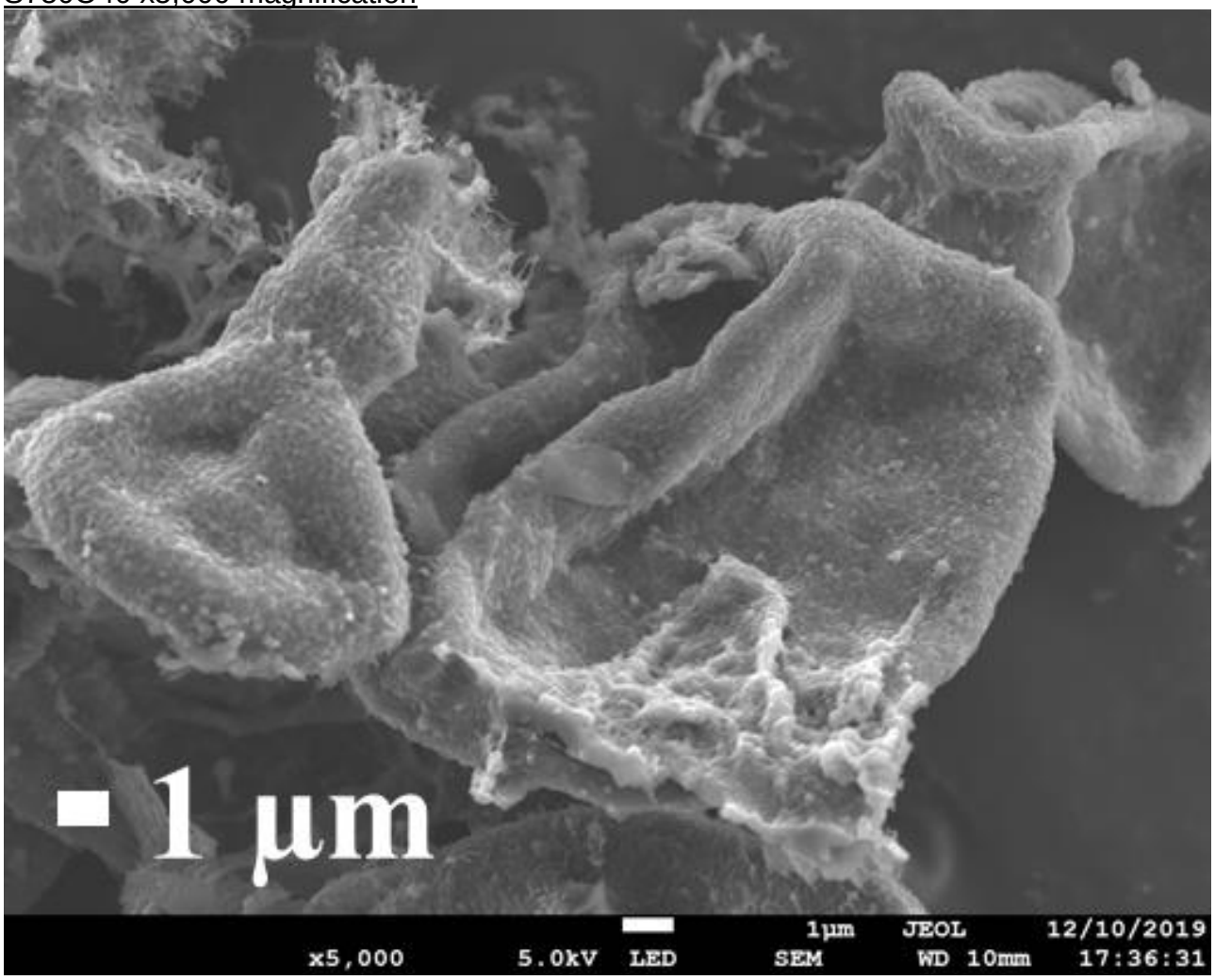

SEM Images for S750O56

S750O56 x500 magnification and particle size distribution plot

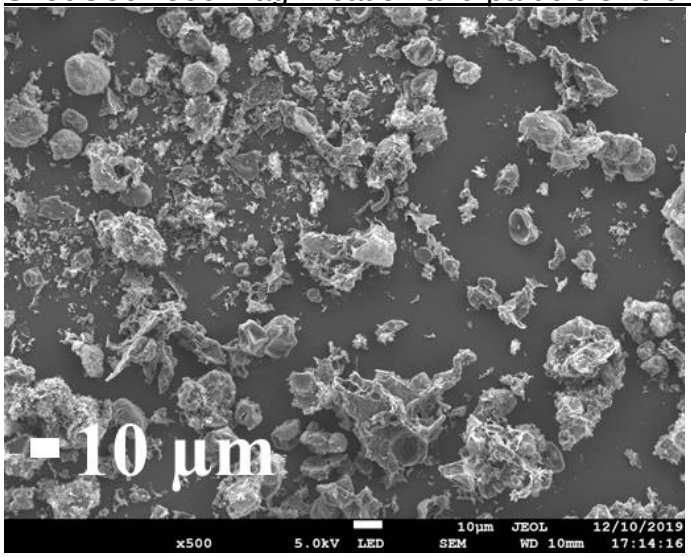

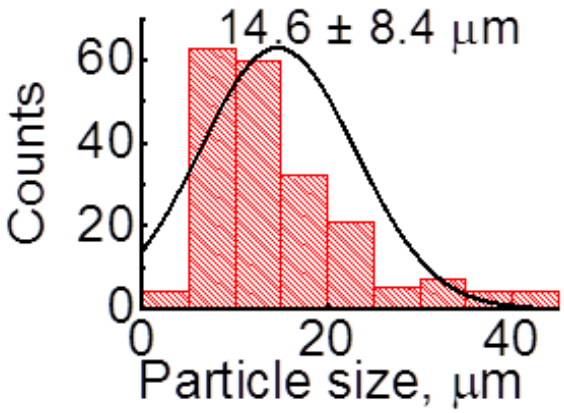

S750O56 x5,000 magnification

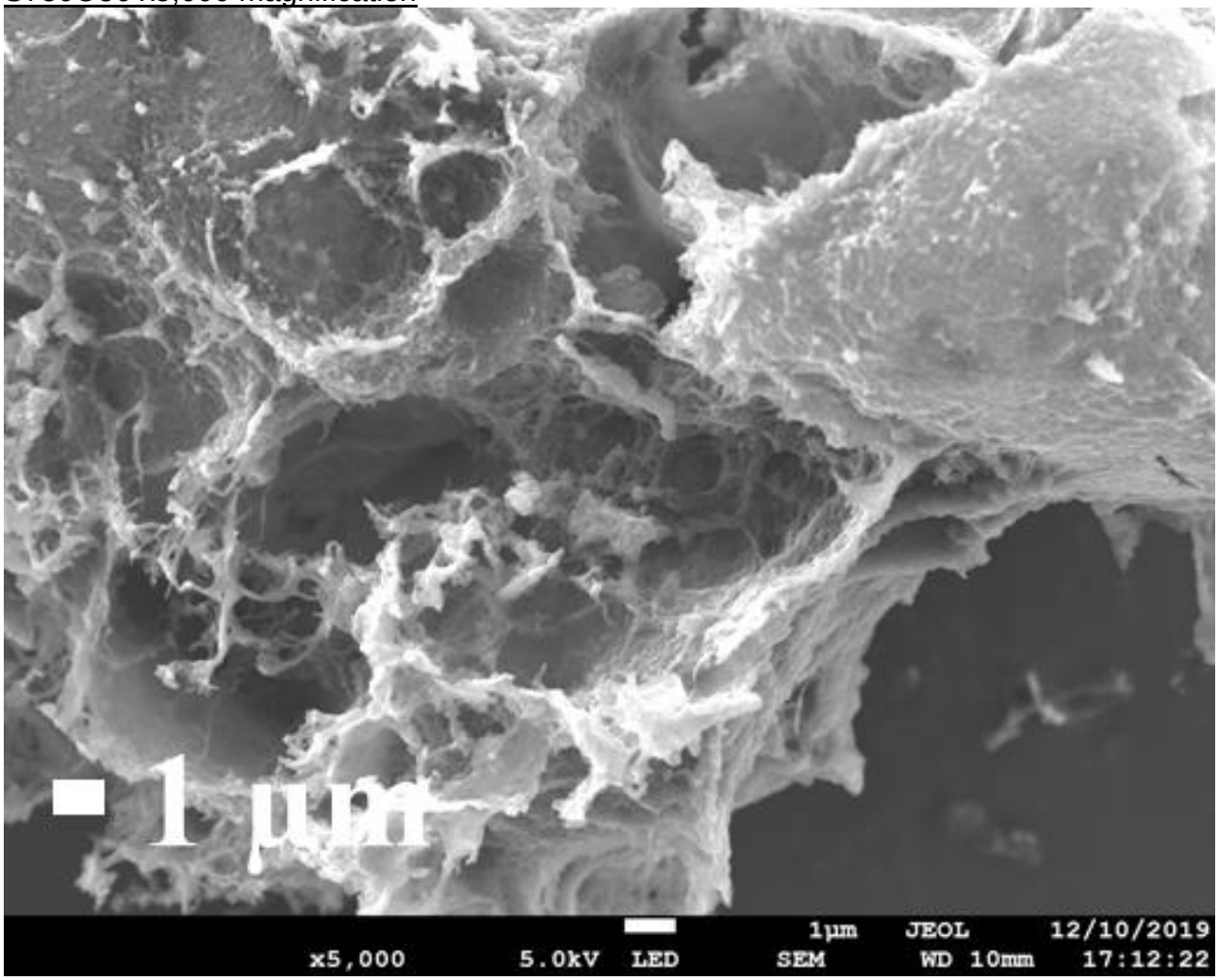

SEM Images for A500O30

A500O30 x100 magnification and particle size distribution plot

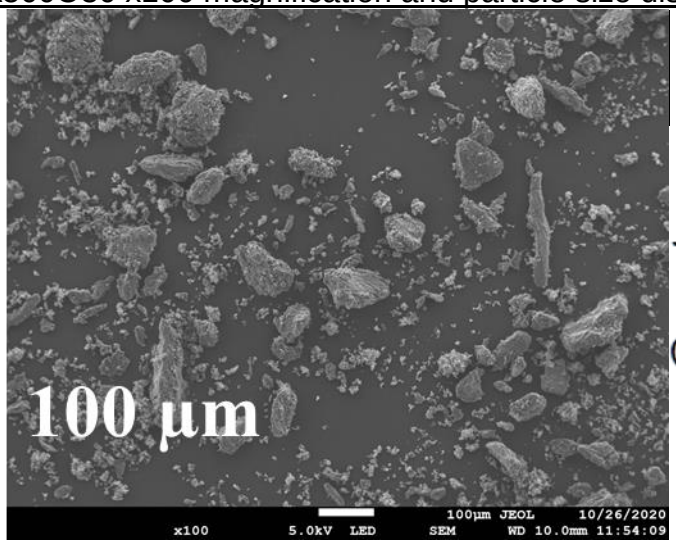

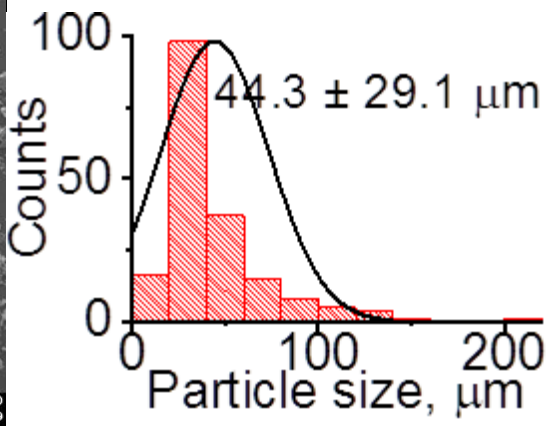

A500O30 x10,000 magnification

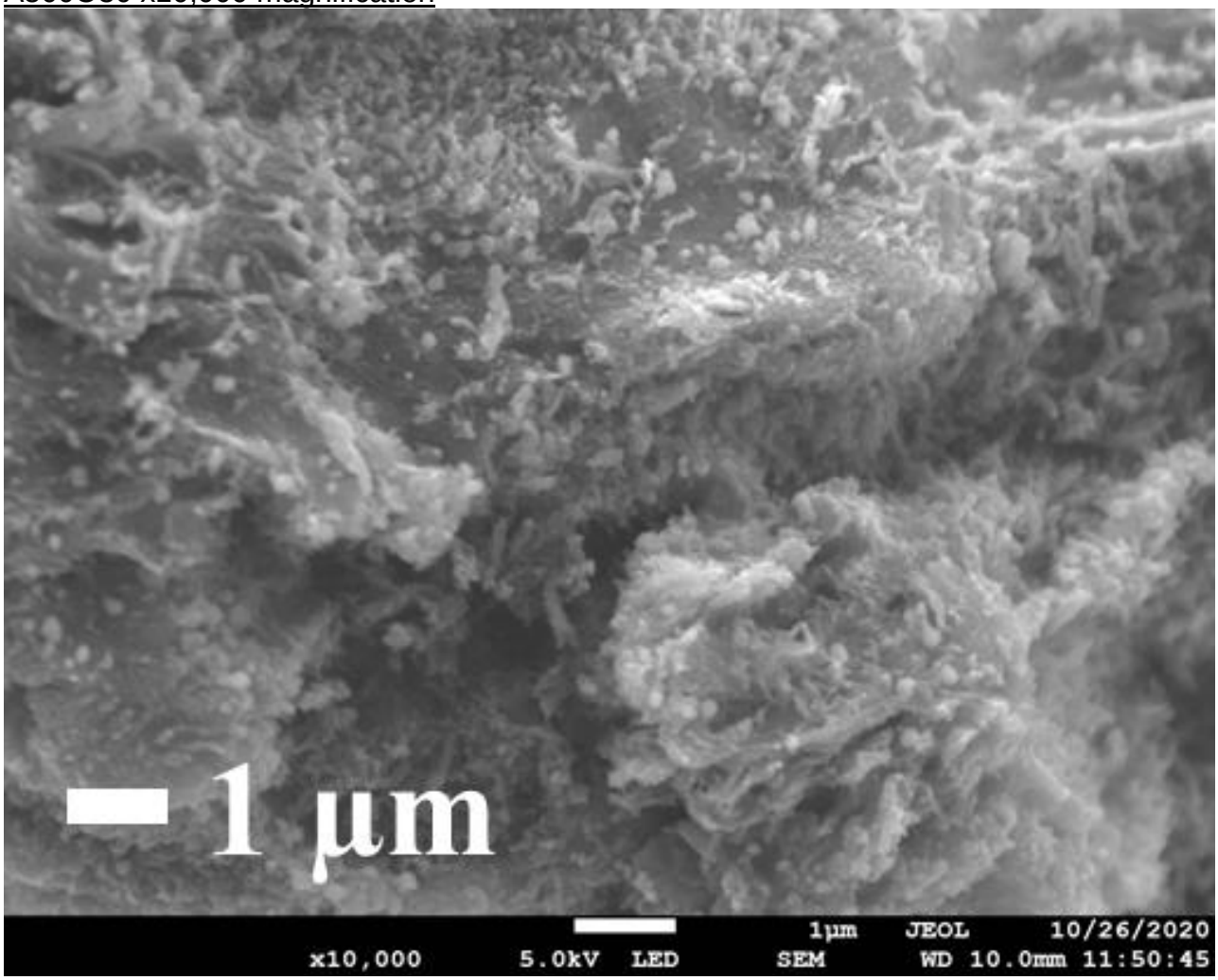

SEM Images for A500O60

A500O60 x100 magnification and particle size distribution plot

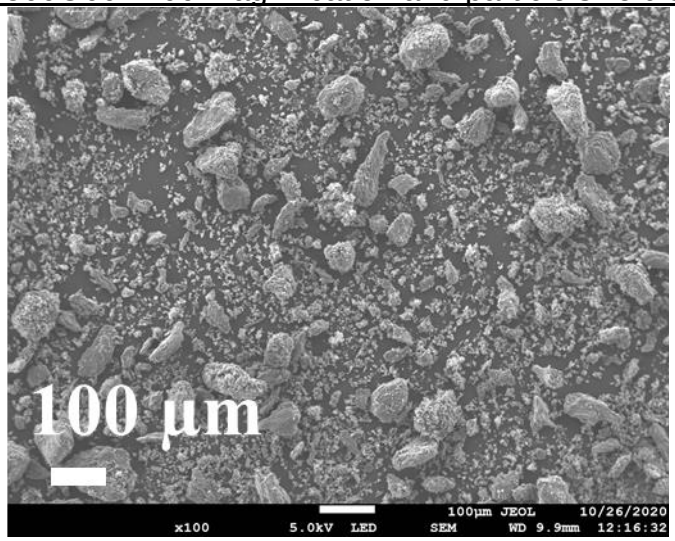

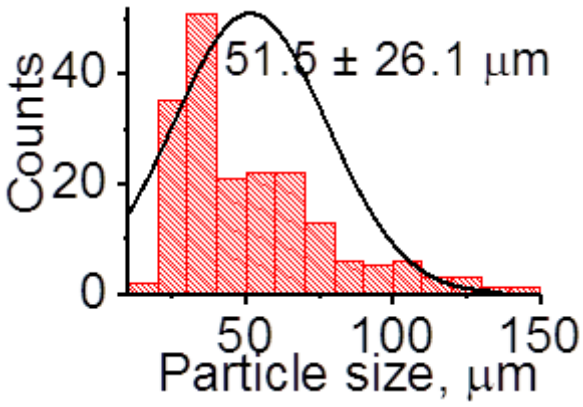

A500O60 x10,000 magnification

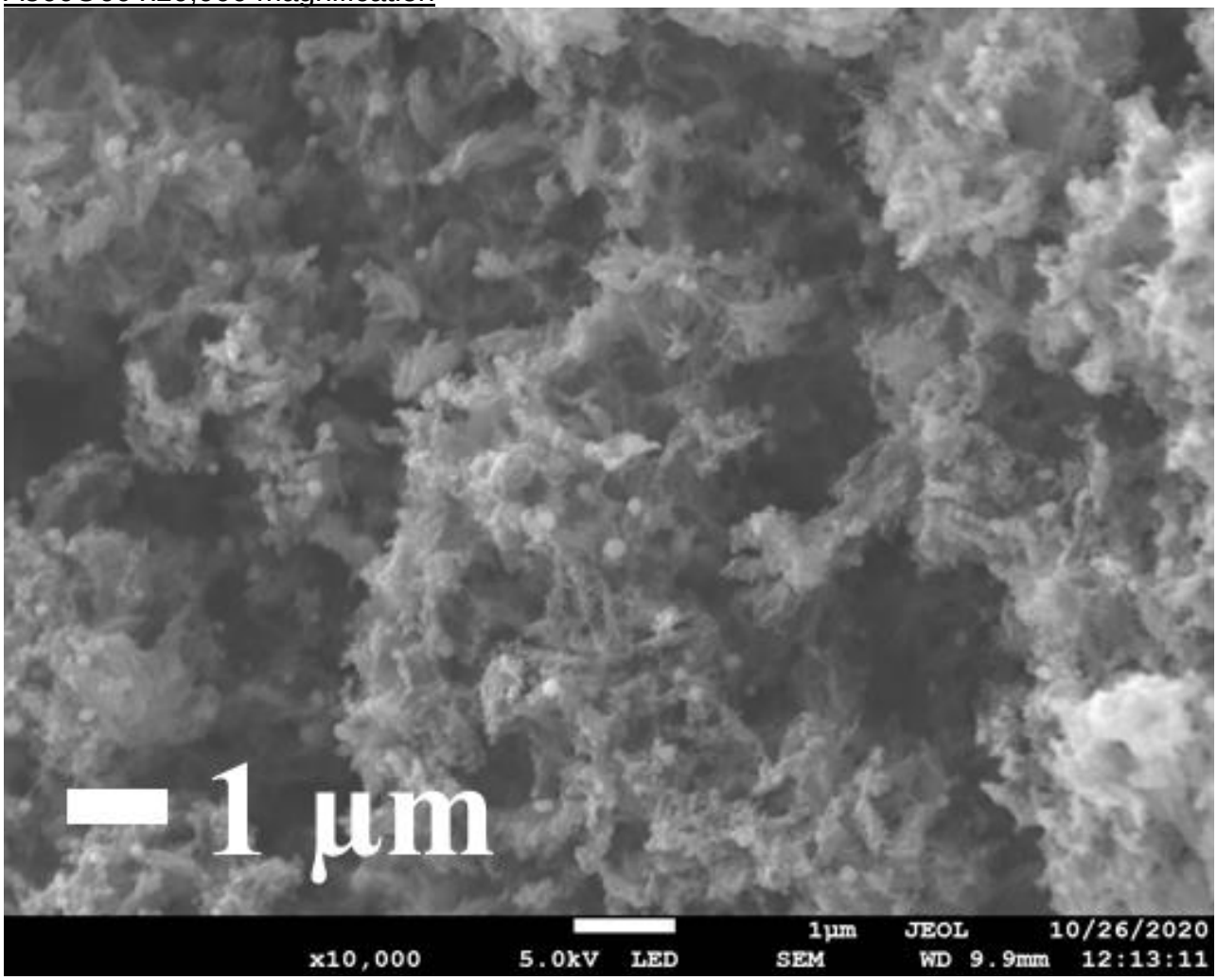

SEM Images for A750O0

A750O0 x100 magnification and particle size distribution plot

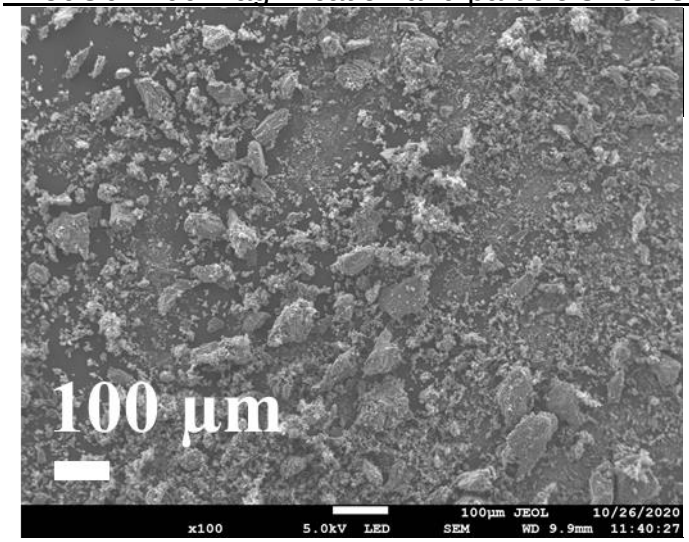

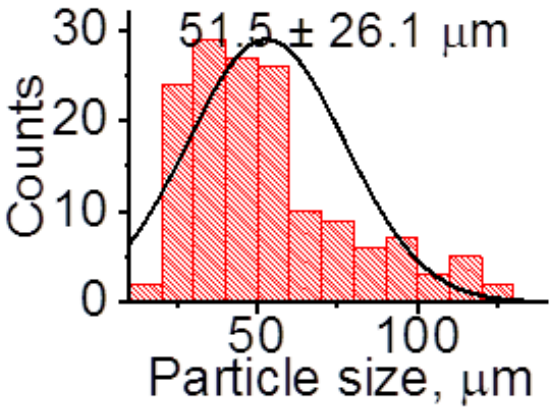

A750O0 x10,000 magnification

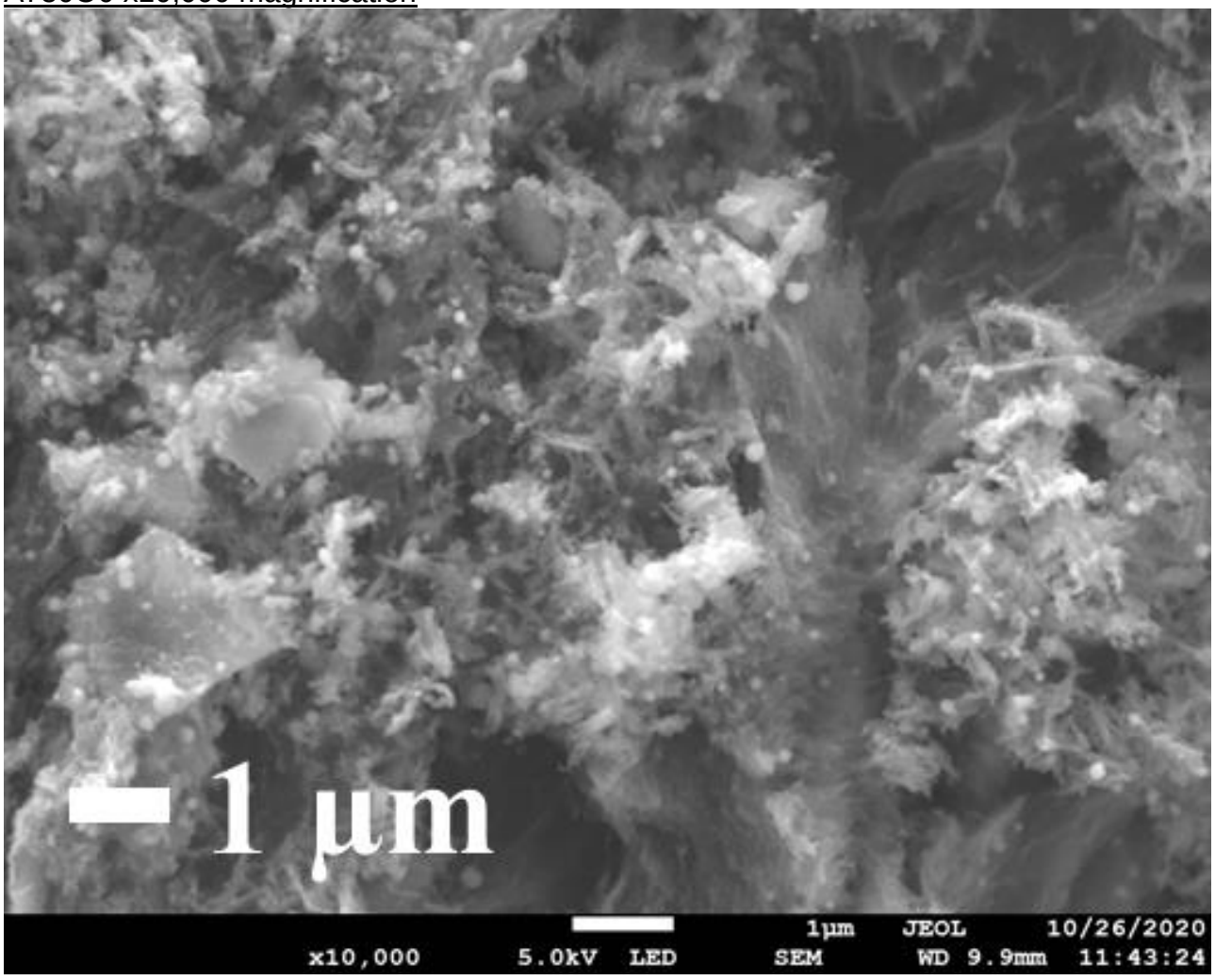

SEM Images for P400O50

P400O50 x100 magnification and particle size distribution plot

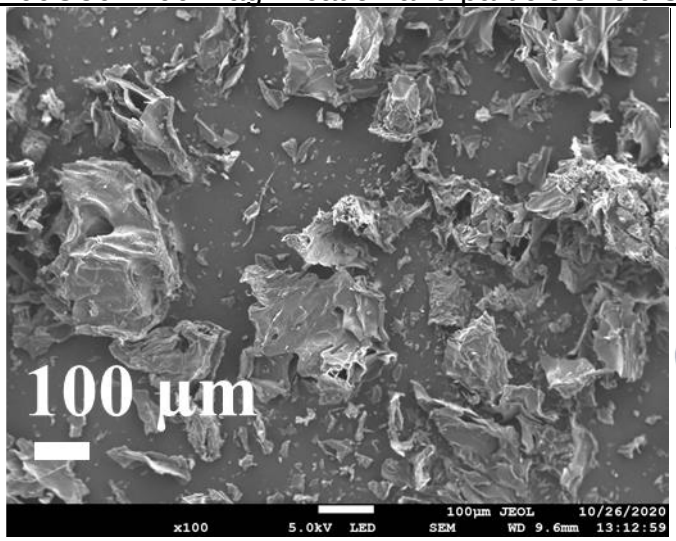

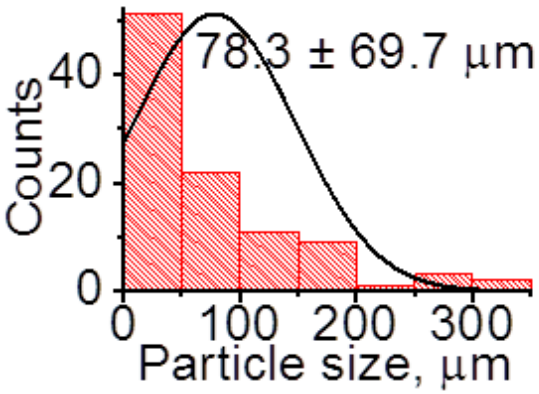

P400O50 x10,000 magnification

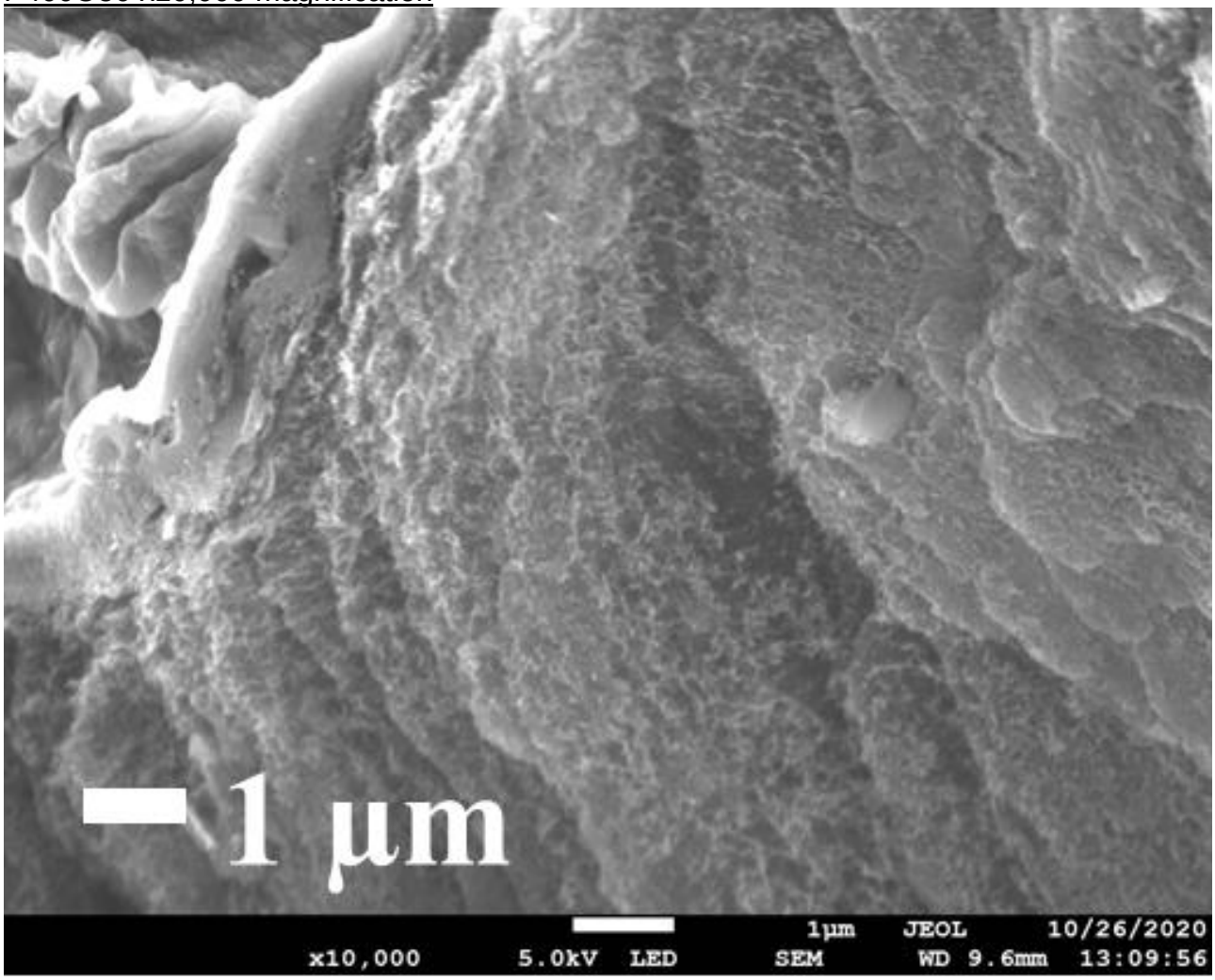

TEM Images

S800

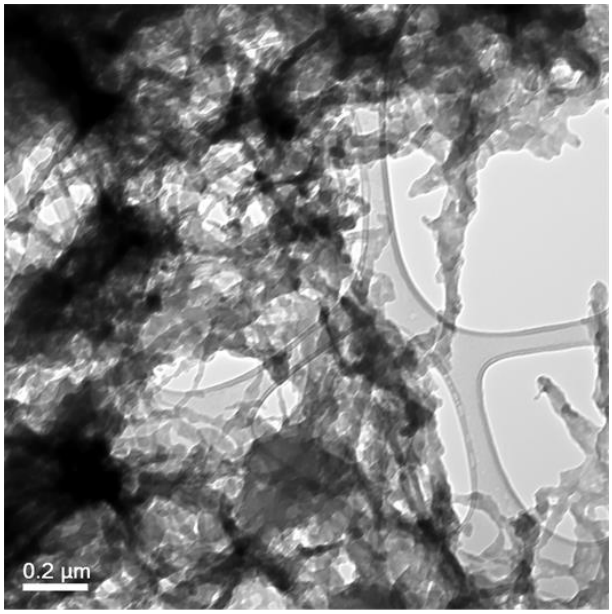

The grey curved lines visible to the right and centre of this image are the carbon film on copper grid that the sample is supported on.

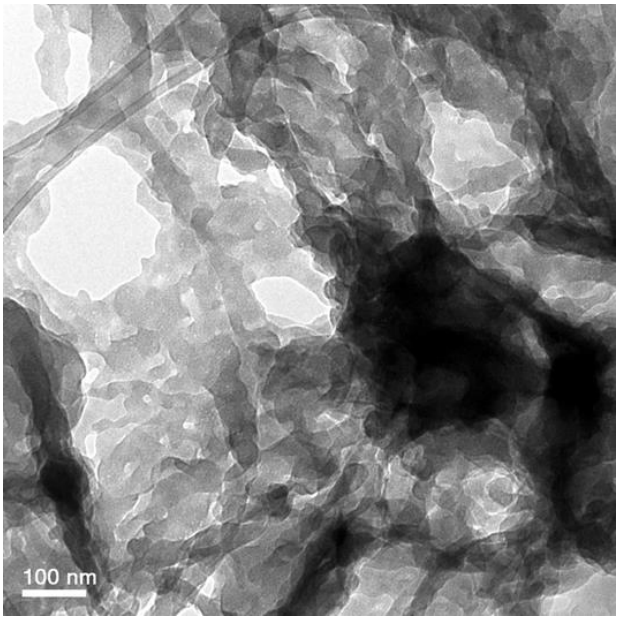

The grey curved lines visible to the top left of this image are the carbon film on copper grid that the sample is supported on.

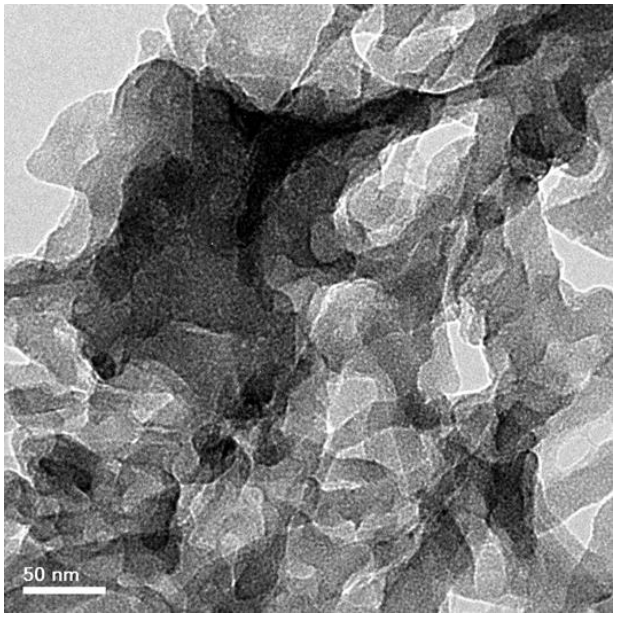

Mesopores are visible as pale grey areas and micropores as white dots in this image.

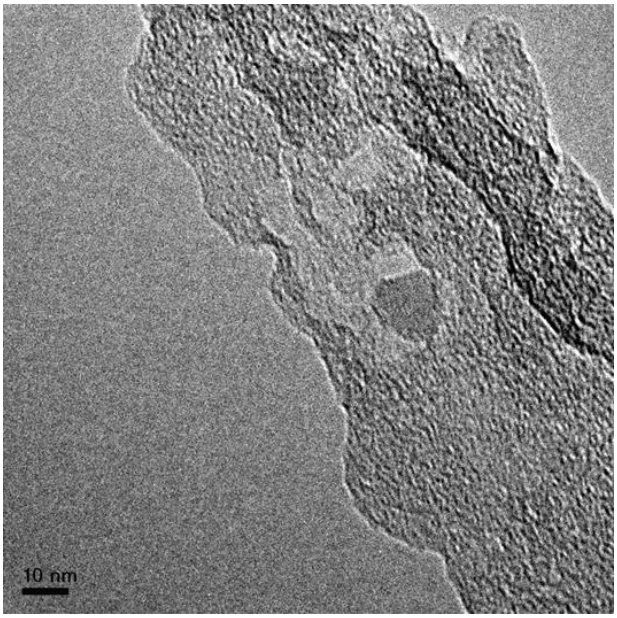

The smooth grey areas to the left and top right of this image are areas where there is no sample. Mesopores are visible as pale grey areas and micropores are visible as white dots in the sample.

A800

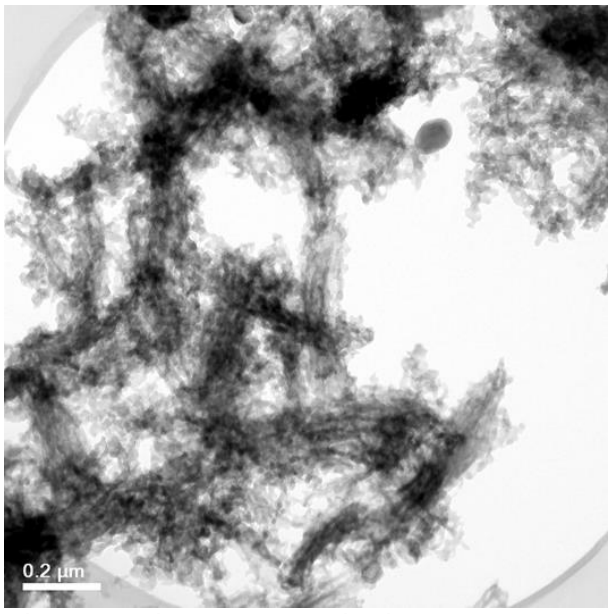

The smooth grey areas in the corners of this image are the carbon film that the supported on.

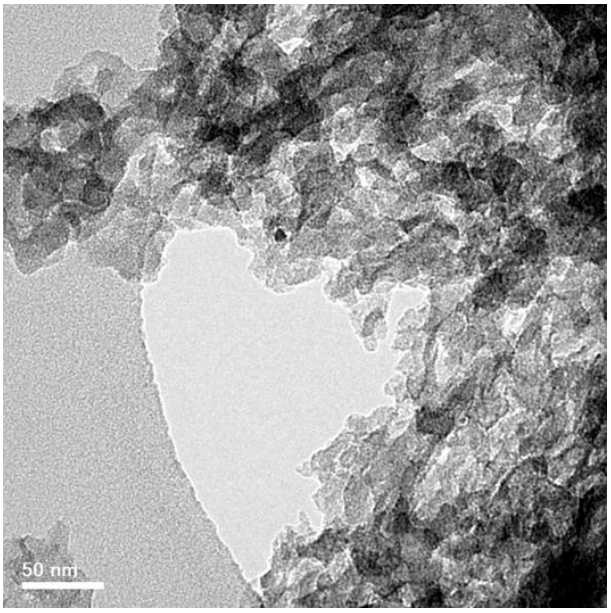

The smooth grey area to the left of this image is the carbon film that the sample is supported on. Mesopores are visible as pale areas within the sample.

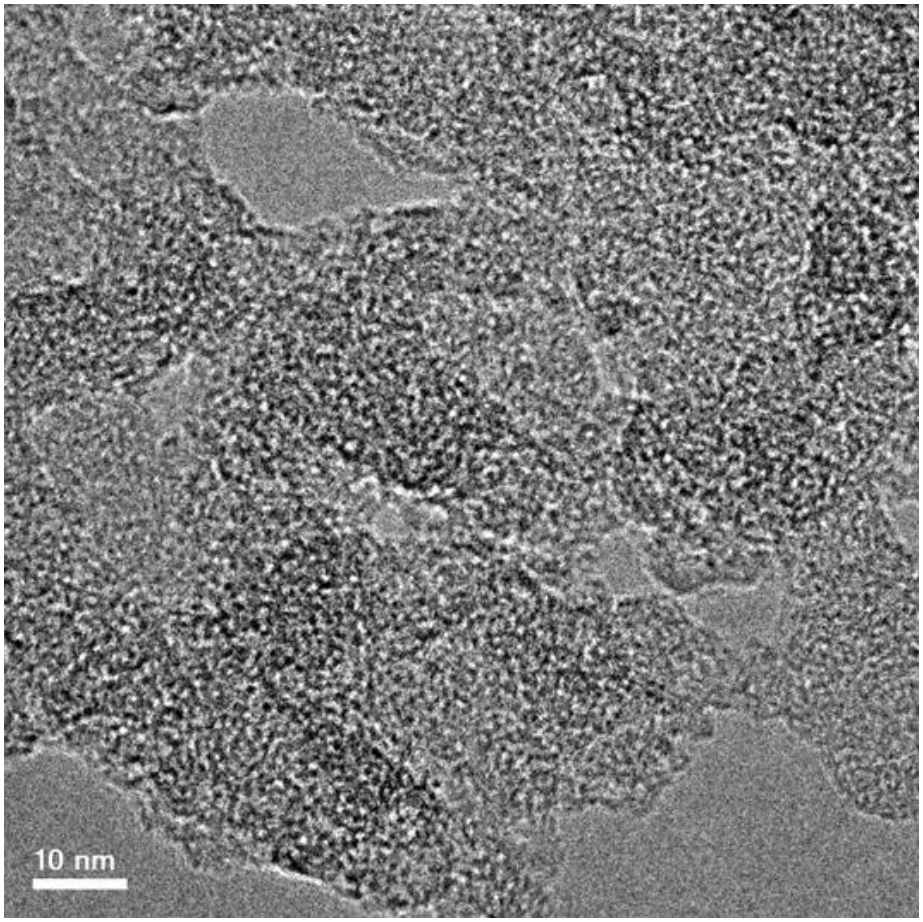

The smooth grey areas in this image are areas where there is no sample. Those at the bottom are beyond the edge of the particle, those surrounded by sample are mesopores. Micropores are visible as white dots in the sample.

S800K2

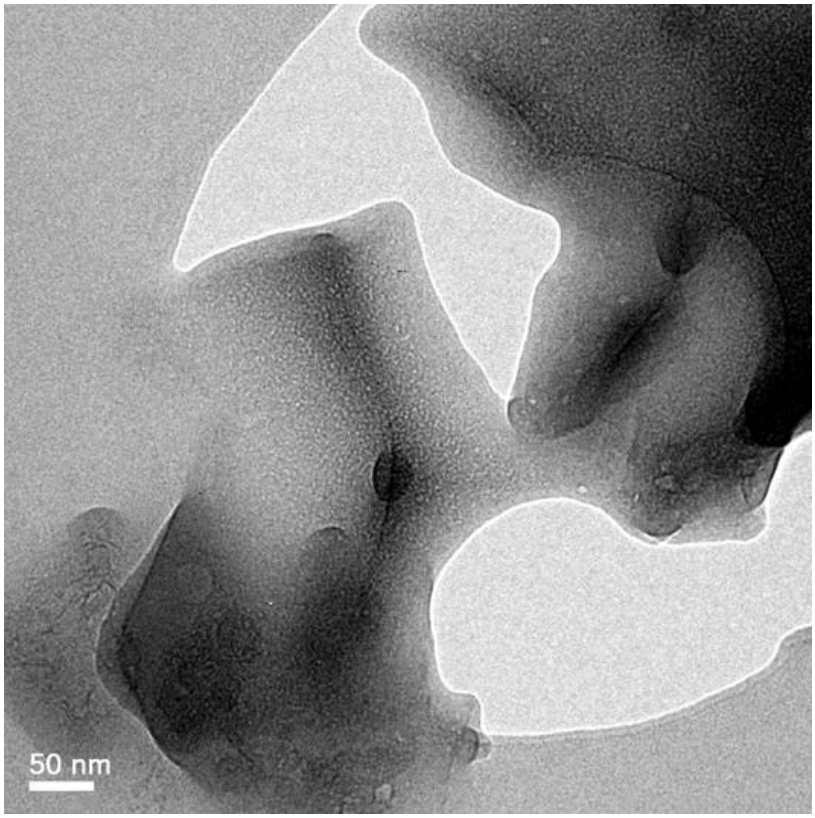

The palest areas in this image are two macropores and mesopores are also visible within the sample.

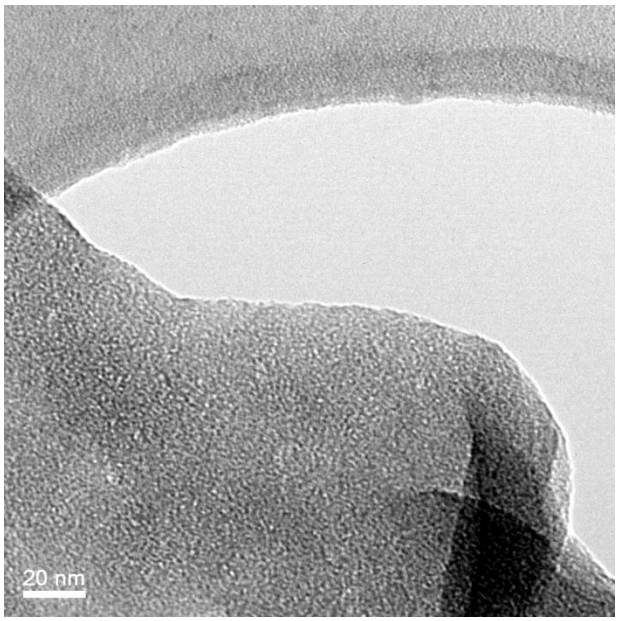

The slightly rough grey area at the top of this image is the carbon film supported on a copper grid. The smoother grey area below it is an area where there is no sample. Micropores are visible as white dots in the sample.

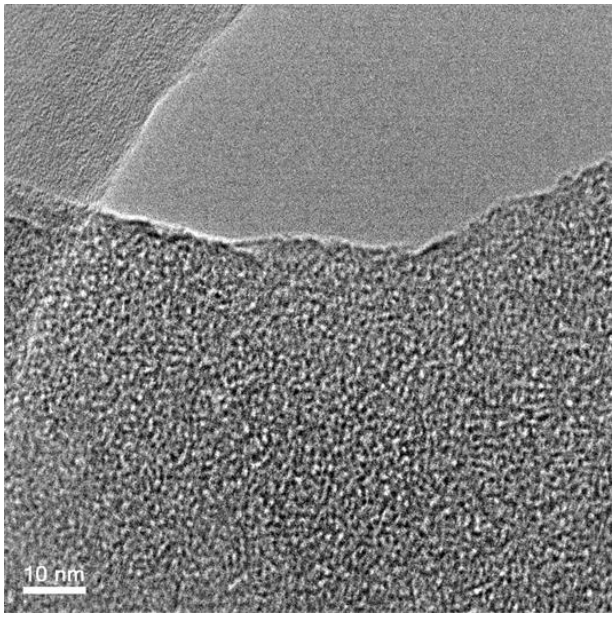

The slightly rough grey area at the top left of this image is the carbon film supported on a copper grid. The smoother grey area in the top right is an area where there is no sample. Micropores are visible as white dots in the sample.

A800K2

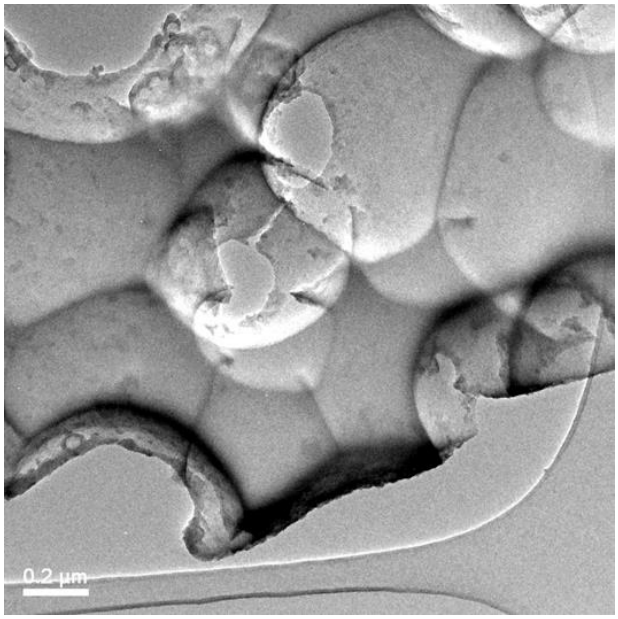

The smooth grey curve at the bottom and lower right of this image is the carbon film that the sample is supported on.

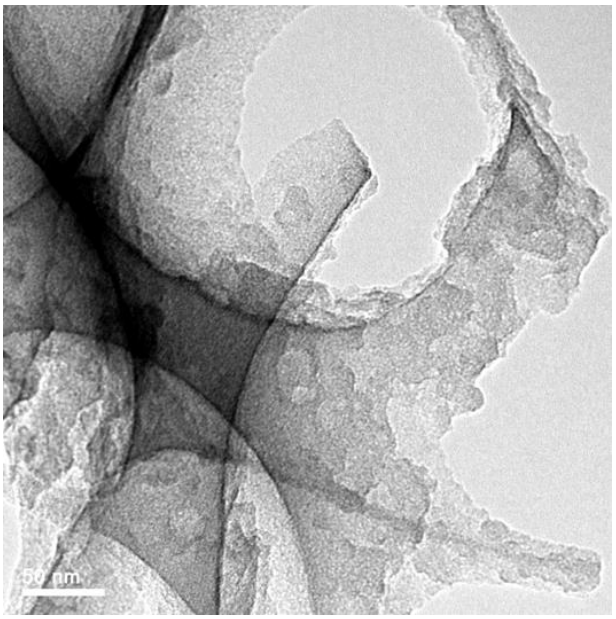

This image shows mesopores within the sample.

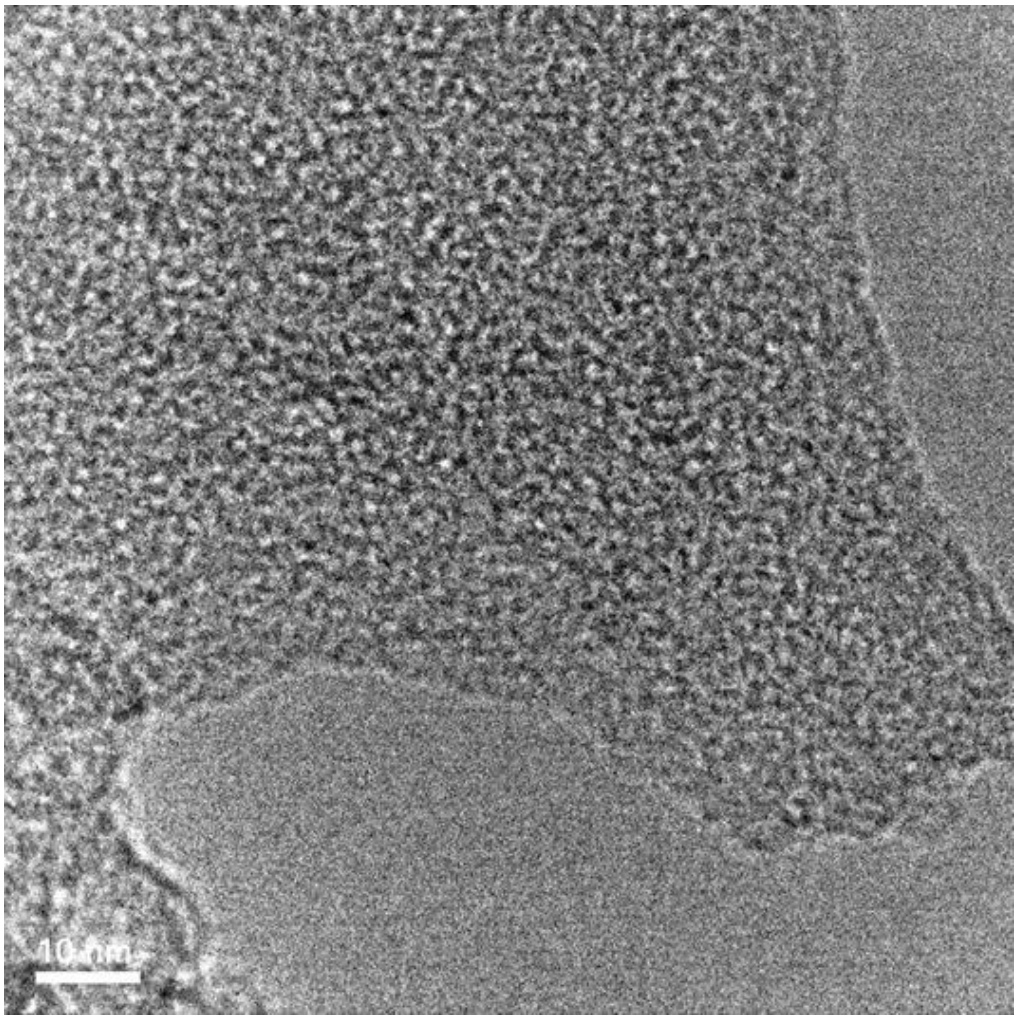

The smooth grey area at the bottom of this image is an area with no sample. Micropores are visible as white dots in the sample.

S950C90

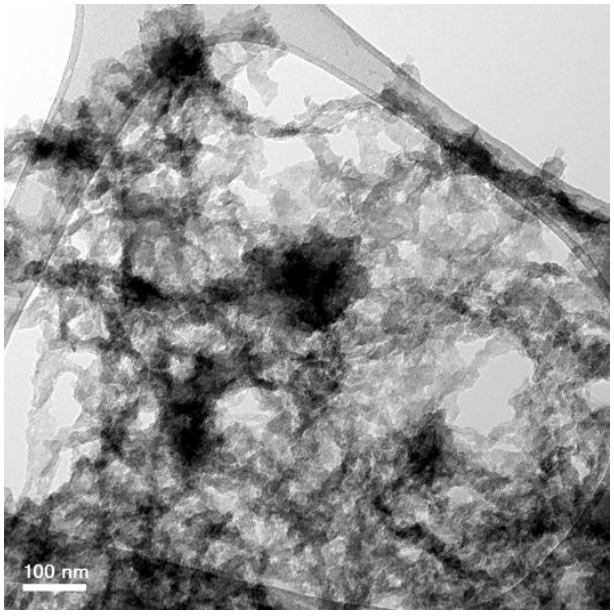

The grey curve at the top of this image is the carbon film that the sample is supported on.

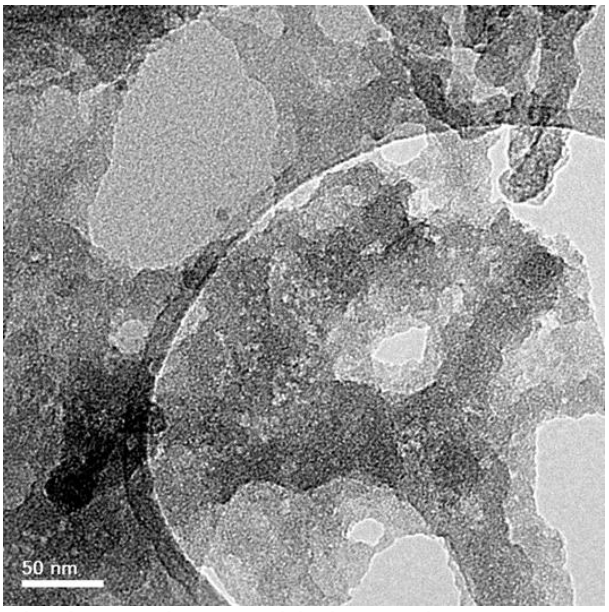

The left and top of this image is sample sitting on top of the carbon film. The right side is sample not on the film. Various sizes of mesopores are visible.

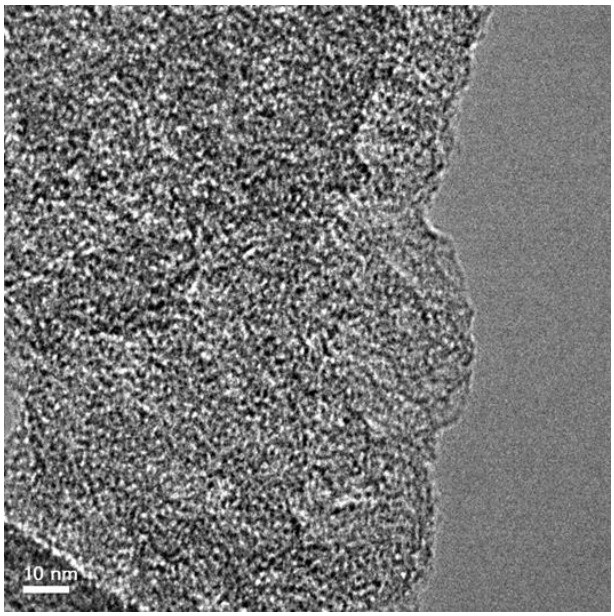

The smooth grey area at the right of this image is an area with no sample. Micropores are visible as white dots in the sample.

ICP-OES data for unactivated and KOH activated starch derived Starbons®

Element	S800 (ppm)	S800K1 (ppm)	S800K2 (ppm)	S800K3 (ppm)	S800K4 (ppm)	S800K5 (ppm)	S600K4 (ppm)	S1000K4 (ppm)
Ag	0.92	<LOQ	<LOQ	0.04	0.29	<LOQ	0.55	1.95
Al	46.11	7.03	13.30	5.20	77.60	33.68	73.63	128.95
As	53.96	<LOQ	<LOQ	<LOQ	<LOQ	<LOQ	14.10	3.36
Au	0.99	4.33	<LOQ	5.33	0.26	<LOQ	1.50	1.42
B	3.96	23.23	15.98	17.24	16.49	26.71	18.26	50.29
Ba	5.71	3.82	4.26	3.39	13.60	4.48	9.21	19.61
Be	<LOQ	<LOQ	<LOQ	<LOQ	<LOQ	<LOQ	<LOQ	<LOQ
Bi	22.85	18.53	7.94	8.92	< 1.15	9.41	8.48	1.00
Ca	1986.22	937.41	976.67	1110.57	2190.61	1128.38	2727.20	4656.83
Cd	0.13	<LOQ	<LOQ	<LOQ	<LOQ	<LOQ	<LOQ	<LOQ
Co	1.82	<LOQ	<LOQ	<LOQ	<LOQ	0.55	<LOQ	<LOQ
Cr	1.63	2.39	7.30	5.11	7.13	129.92	11.20	36.89
Cu	16.56	10.72	13.39	8.85	21.72	28.47	51.05	74.94
Fe	133.75	95.82	274.51	65.91	191.20	1351.97	249.35	336.82
Hg	12.10	1.60	1.83	1.28	0.49	<LOQ	6.68	1.12
K	66.01	218.91	202.17	231.48	366.96	427.90	116.75	305.46
La	3.27	0.44	<LOQ	0.39	1.24	0.33	5.55	5.89
Li	<LOQ	0.05	0.19	0.10	0.46	0.33	<LOQ	<LOQ
Mg	174.32	90.32	91.30	112.36	181.20	107.37	215.25	324.13
Mn	2.87	2.77	2.69	1.76	28.38	54.85	4.02	11.98
Mo	3.85	1.05	2.71	0.83	<LOQ	24.71	2.68	3.10
Na	695.18	195.28	191.93	255.39	327.93	257.90	424.03	692.25
Ni	9.06	<LOQ	2.22	2.14	6.52	19.97	4.79	15.35
P	330.37	13.28	29.29	<LOQ	0.28	31.73	79.87	25.07
Pb	13.89	<LOQ	<LOQ	0.07	<LOQ	<LOQ	<LOQ	<LOQ
Pd	0.66	3.14	3.68	2.67	0.19	1.18	3.69	<LOQ
Pt	<LOQ	<LOQ	<LOQ	<LOQ	<LOQ	<LOQ	<LOQ	<LOQ
Rb	<LOQ	26.98	24.97	24.66	<LOQ	29.32	<LOQ	<LOQ
S	2968.00	405.00	844.00	1109.00	1400.00	958.00	3785.00	8674.00
Sb	7.56	<LOQ	<LOQ	<LOQ	<LOQ	<LOQ	6.76	9.79
Sc	0.25	0.26	0.36	0.13	0.27	0.39	0.36	0.61
Se	48.73	<LOQ	<LOQ	4.85	<LOQ	<LOQ	<LOQ	<LOQ
Si	189.51	209.35	155.78	95.48	771.94	164.22	570.15	1403.61
Sn	23.80	<LOQ	<LOQ	<LOQ	<LOQ	8.98	<LOQ	<LOQ
Sr	34.81	15.35	15.82	19.80	29.96	18.55	46.20	69.21
Te	<LOQ	<LOQ	<LOQ	<LOQ	<LOQ	<LOQ	<LOQ	<LOQ
Ti	43.33	30.69	50.42	9.04	14.71	29.13	190.01	131.54
Tl	26.26	<LOQ	<LOQ	<LOQ	<LOQ	5.74	<LOQ	<LOQ
V	2.18	0.46	1.05	1.38	2.58	24.71	3.59	4.80
W	14.25	<LOQ	<LOQ	<LOQ	<LOQ	2.28	13.33	0.55
Zn	9.42	3.02	2.81	2.19	6.58	13.56	216.57	109.78
Zr	7.40	2.07	1.08	3.34	3.95	3.06	13.92	28.43
Total %	**0.70**	**0.23**	**0.29**	**0.31**	**0.57**	**0.49**	**0.89**	**1.71**

LOQ is the limit of quantification which is three times the limit of detection. These elements were assumed to have a concentration of 0 in calculating the total.

ICP-OES data for CO_2 and O_2 activated starch derived Starbons®

Element	S950C90 (ppm)	S750O0 (ppm)
Ag	<LOQ	69632.89
Al	972.84	284.52
As	1.15	<LOQ
Au	1.11	0.58
B	81.43	197.51
Ba	15.17	4.29
Be	<LOQ	<LOQ
Bi	5.86	22.95
Ca	2076.32	849.48
Cd	1.97	9.42
Co	1.09	1.33
Cr	27.78	1.08
Cu	29.64	7.36
Fe	7654.31	752.16
Hg	<LOQ	0.56
K	1217.87	534.68
La	0.73	0.18
Li	<LOQ	<LOQ
Mg	407.60	308.21
Mn	17.71	5.49
Mo	41.90	<LOQ
Na	1738.85	1567.46
Ni	33.29	16.53
P	9292.77	<LOQ
Pb	40.35	117.86
Pd	1.88	<LOQ
Pt	0.19	3.04
Rb	1.83	<LOQ
S	17338.36	17338.36
Sb	0.27	0.76
Sc	<LOQ	<LOQ
Se	<LOQ	<LOQ
Si	<LOQ	<LOQ
Sn	<LOQ	<LOQ
Sr	6.06	2.45
Te	<LOQ	<LOQ
Ti	34.33	<LOQ
Tl	<LOQ	<LOQ
V	1.06	0.91
W	1.56	1.14
Zn	115.52	97.89
Zr	<LOQ	83.84
Total %	**4.12**	**9.18**

LOQ is the limit of quantification which is three times the limit of detection. These elements were assumed to have a concentration of 0 in calculating the total.

ICP-OES data for alginic acid and pectin derived Starbons®

Element	A800 (ppm)	A800K2 (ppm)	A750C60 (ppm)	A750O0 (ppm)	P800 (ppm)	P800K2 (ppm)	P700C50 (ppm)	P400O50 (ppm)
Ag	0.29	0.06	<LOQ	<LOQ	<LOQ	8.14	<LOQ	<LOQ
Al	775.51	14.11	530.75	441.71	183.76	1315.95	809.18	128.98
As	4.41	0.59	0.87	0.68	<LOQ	1.32	1.10	<LOQ
Au	15.71	7.44	0.03	0.41	3.02	3.05	21.64	3.84
B	<LOQ	15.54	22.10	23.15	6.31	14.95	85.95	100.90
Ba	513.28	2.17	386.17	309.68	10.68	14.65	18.45	6.48
Be	<LOQ	<LOQ	<LOQ	<LOQ	<LOQ	<LOQ	<LOQ	<LOQ
Bi	16.51	18.68	0.98	0.61	13.32	115.96	<LOQ	1.09
Ca	53668.26	336.60	33755.13	27424.69	2838.49	254.88	5526.43	2037.26
Cd	0.43	0.51	<LOQ	0.04	<LOQ	0.74	4.55	<LOQ
Co	0.62	0.53	0.27	0.27	0.27	2.65	1.86	0.19
Cr	15.18	14.80	9.92	8.38	24.60	40.76	63.98	18.81
Cu	10.55	15.54	3.19	3.84	22.98	8.36	54.19	18.00
Fe	1108.85	1201.33	749.32	613.34	450.60	245.53	561.60	130.62
Hg	<LOQ	<LOQ	<LOQ	<LOQ	<LOQ	<LOQ	<LOQ	<LOQ
K	861.13	392.60	1895.14	815.18	431.08	380.12	15862.25	8087.16
La	1.53	<LOQ	1.03	0.68	0.09	0.31	1.23	0.18
Li	<LOQ	<LOQ	7.66	<LOQ	<LOQ	<LOQ	<LOQ	<LOQ
Mg	1398.24	10.93	879.41	722.32	796.12	35.63	1558.88	602.36
Mn	19.25	4.35	12.93	10.32	14.60	1.37	25.94	9.66
Mo	3.03	135.92	<LOQ	9.76	<LOQ	<LOQ	<LOQ	<LOQ
Na	5669.44	173.56	3662.93	3244.67	50109.90	239.63	92553.72	38083.53
Ni	37.82	407.38	3.56	5.77	15.39	12.41	37.91	10.21
P	1858.65	<LOQ	1521.39	1383.82	1030.84	106.47	2802.42	<LOQ
Pb	9.40	2.90	<LOQ	0.67	2.80	4.47	34.61	<LOQ
Pd	0.86	0.67	0.09	<LOQ	0.47	0.47	<LOQ	2.04
Pt	0.00	<LOQ	0.10	0.16	<LOQ	<LOQ	0.61	0.84
Rb	0.93	3.34	1.16	0.39	5.31	0.80	10.63	6.24
S	5892.63	5516.81	<LOQ	5915.10	4483.56	6779.44	<LOQ	<LOQ
Sb	0.46	1.41	<LOQ	0.06	0.80	2.40	0.78	<LOQ
Sc	15.23	14.56	<LOQ	<LOQ	11.66	16.49	<LOQ	<LOQ
Se	<LOQ	<LOQ	<LOQ	<LOQ	<LOQ	5.55	<LOQ	<LOQ
Si	8119.84	8796.03	<LOQ	<LOQ	6741.60	7950.26	<LOQ	<LOQ
Sn	2.48	1.95	<LOQ	<LOQ	1.72	11.35	<LOQ	<LOQ
Sr	898.51	1.87	875.60	721.56	14.60	0.69	33.43	15.87
Te	<LOQ	<LOQ	<LOQ	<LOQ	<LOQ	<LOQ	<LOQ	<LOQ
Ti	25.65	26.70	31.06	24.40	5.62	25.70	<LOQ	<LOQ
Tl	7.15	2.27	<LOQ	<LOQ	1.12	1.01	<LOQ	<LOQ
V	1.72	1.33	0.96	0.90	<LOQ	<LOQ	1.47	0.04
W	1.35	1.46	0.76	0.53	0.26	4.53	0.17	<LOQ
Zn	30.15	21.36	<LOQ	25.94	5.13	18.02	117.50	<LOQ
Zr	1.48	10.80	<LOQ	<LOQ	1.12	9.09	<LOQ	<LOQ
Total %	**8.10**	**1.72**	**4.44**	**4.17**	**6.72**	**1.76**	**12.02**	**4.93**

LOQ is the limit of quantification which is three times the limit of detection. These elements were assumed to have a concentration of 0 in calculating the total.

Surface compositions determined by XPS

Sample	C%	O%	Ca%	K%	N%	Na%	Si%	S%
S800	94.8 (91.6)	5.2						
A800	87.4 (80.9)	9.3	2.0		0.4	0.6		0.4
P800	76.2 (72.1)	14.4	0.2	0.6	0.7	7.7		0.2
S800K2	86.3 (83.8)	13.5				0.2		
A800K2	84.8 (70)	14.4			0.4	0.2		0.1
P800K2	91.0 (68.6)	8.8				0.2		
S950C90	98.5 (88.7)	1.3						0.1
A750C60	90.9 (74.7)	6.8	1.5		0.2	0.4		0.2
P700C50	77.2 (62.7)	13.8	0.1	0.4	0.9	7.5		0.1
S750O0	98.2 (84.6)	1.5				0.1	0.2	0.1
A750O0	90.4 (78.3)	7.1	1.4		0.4	0.4		0.2
P400O50	72.1 (66.8)	17.2	0.2	0.4	1.0	9.2		

The figure in brackets is the % carbon in the bulk material determined by combustion analysis.

XPS plots

S800

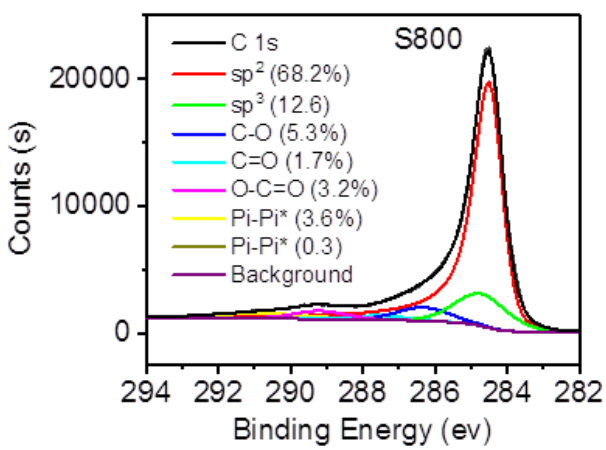

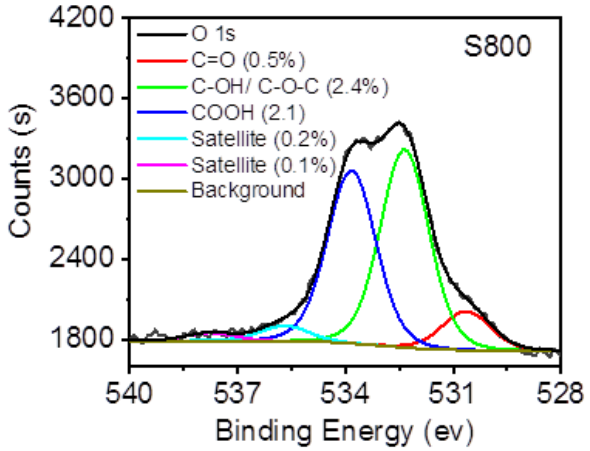

A800

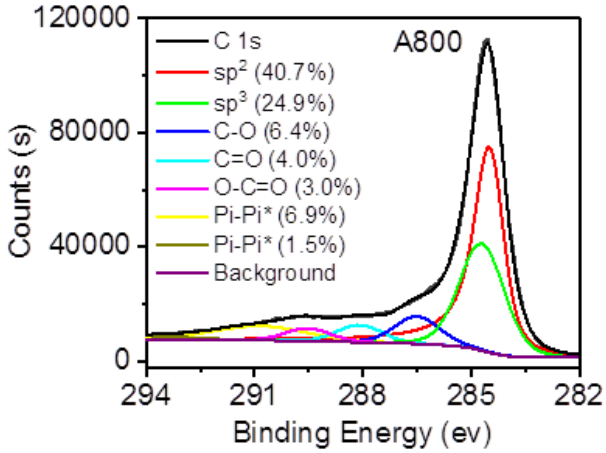

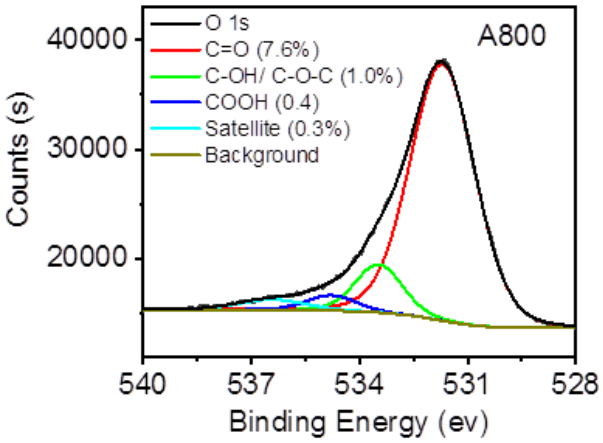

P800

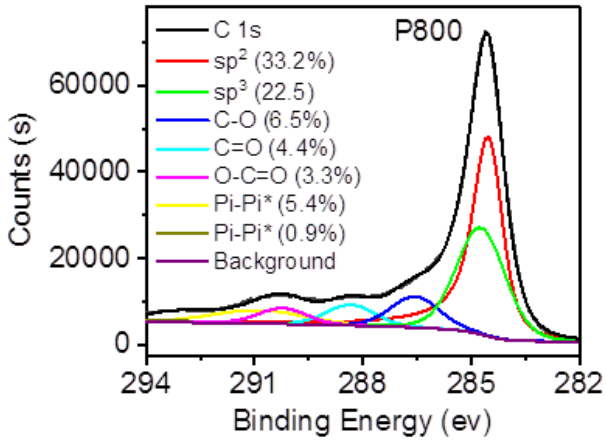

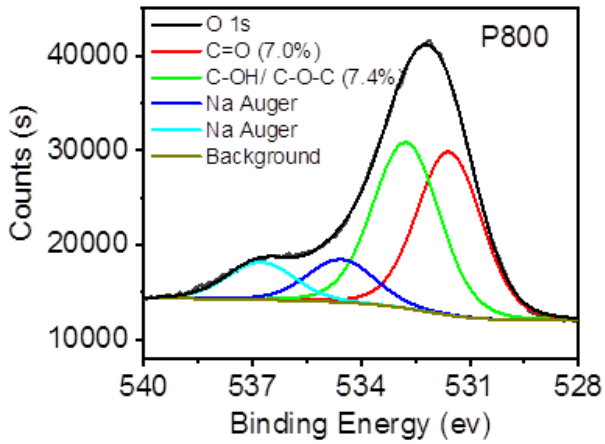

S800K2

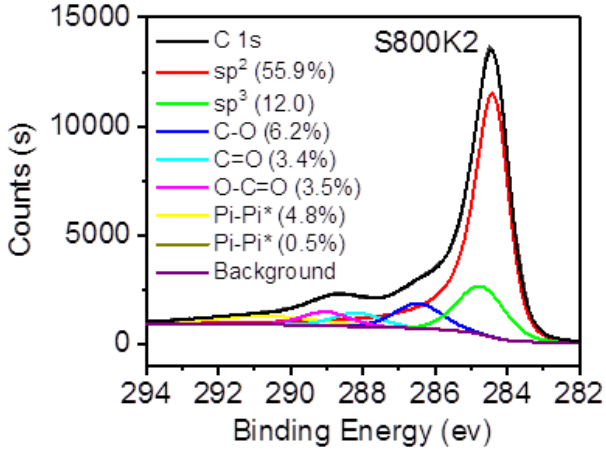

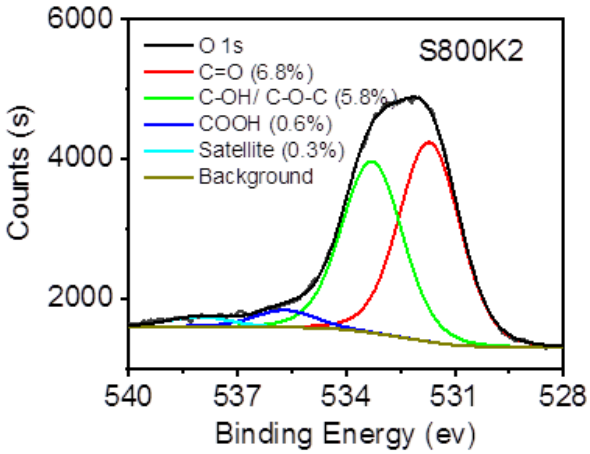

A800K2

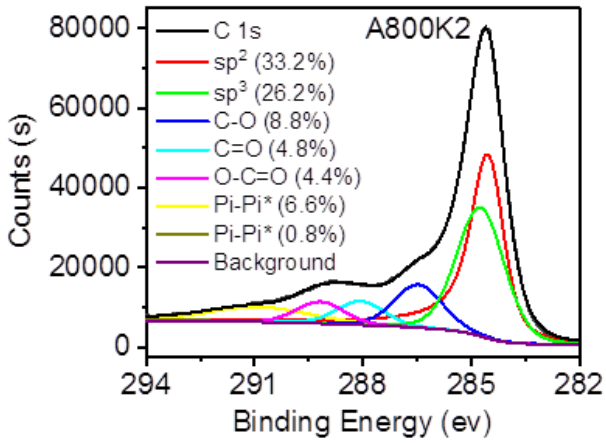

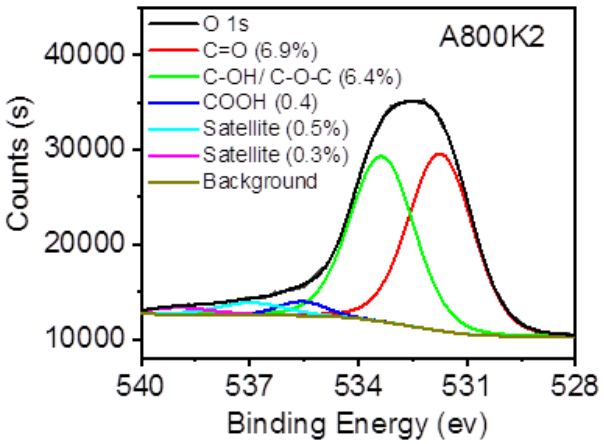

P800K2

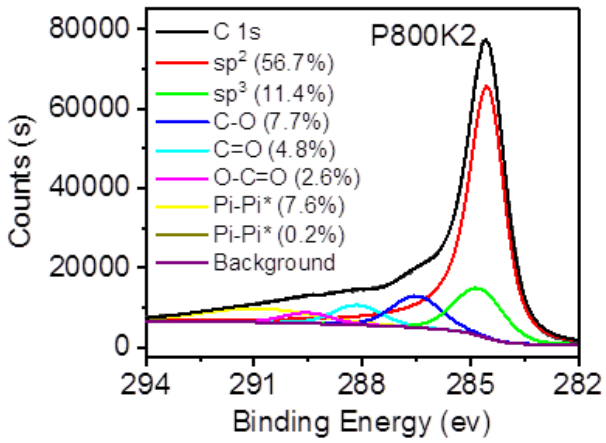

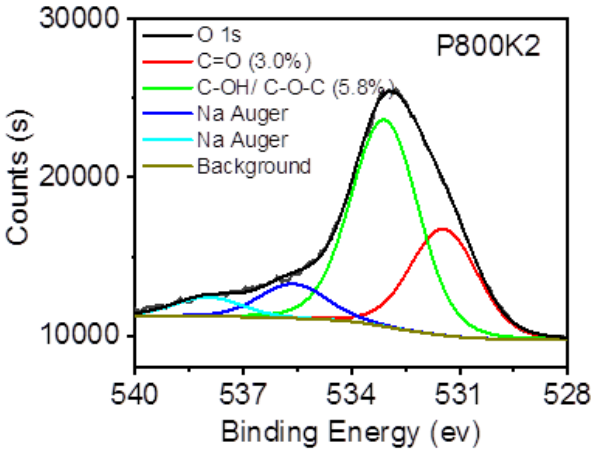

S950C90

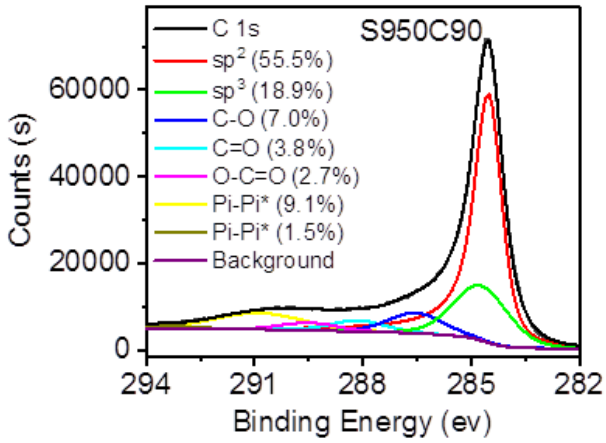

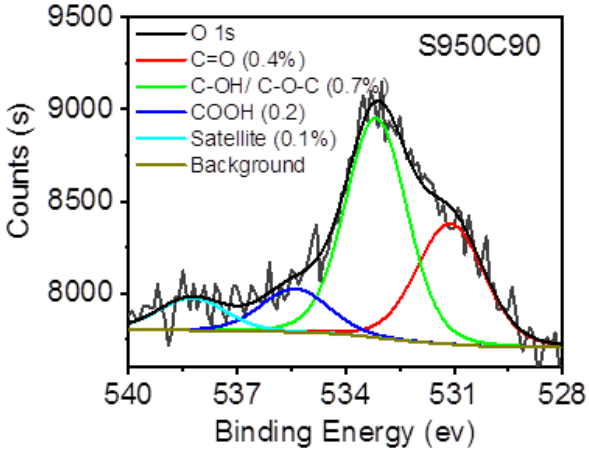

A750C60

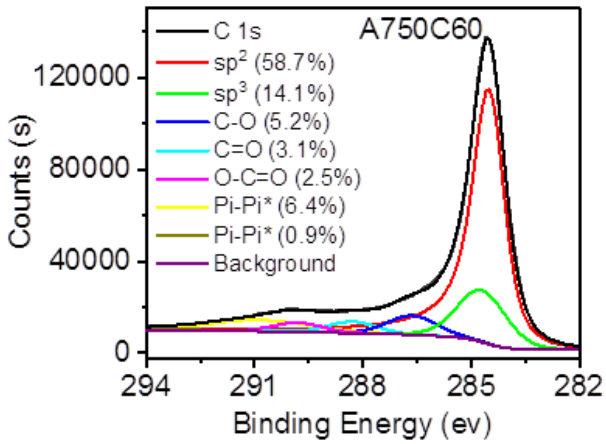

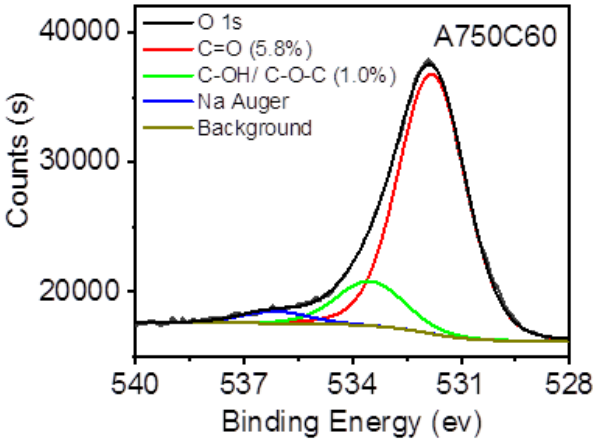

P700C50

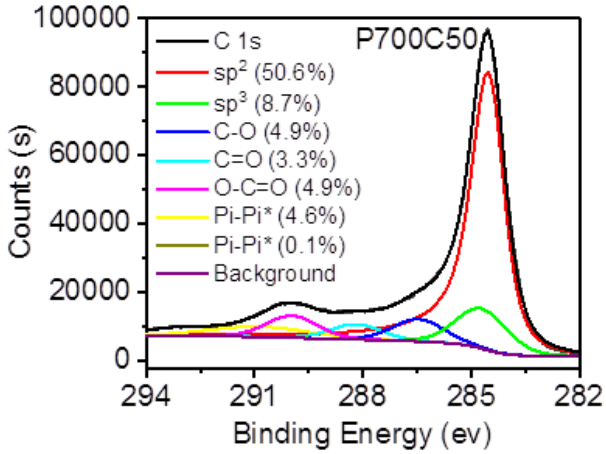

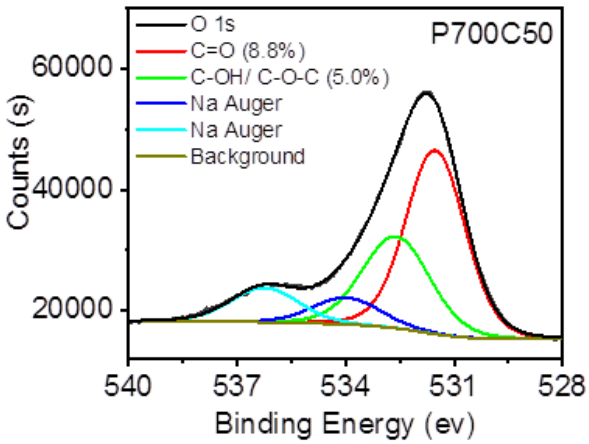

S750O0

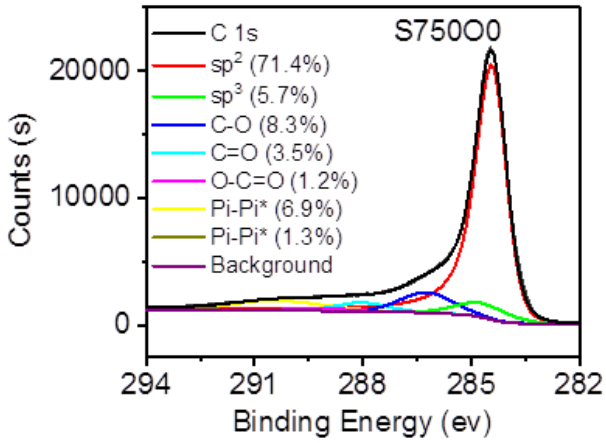

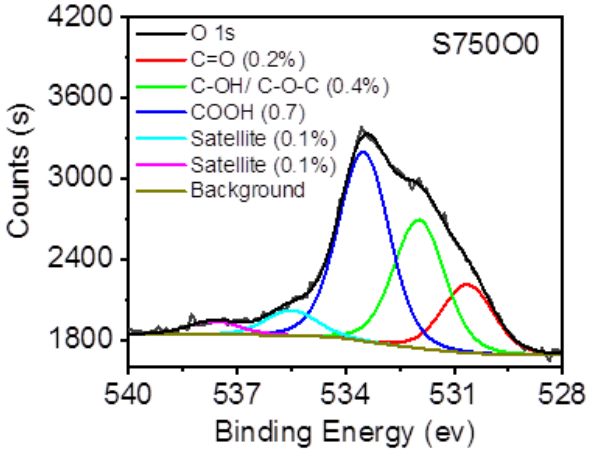

A750O0

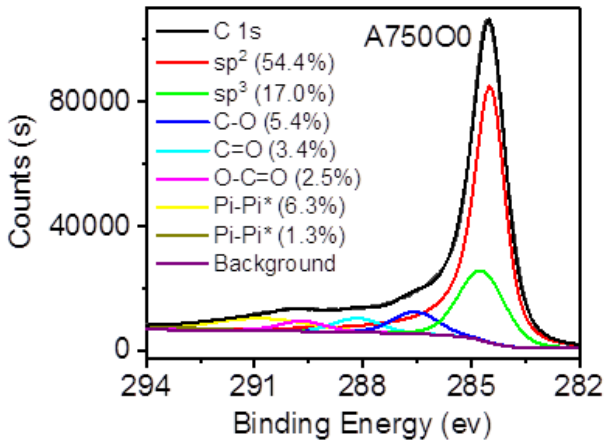

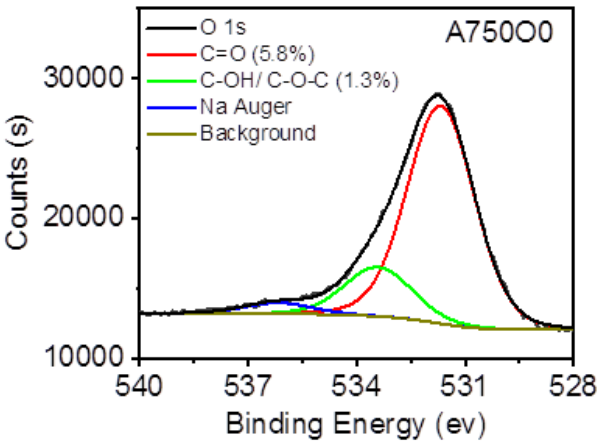

P400O50

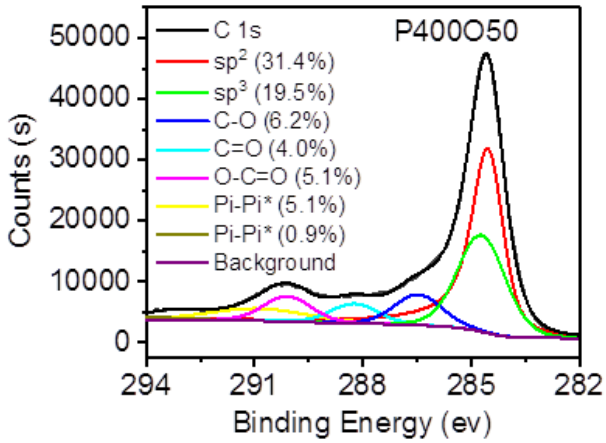

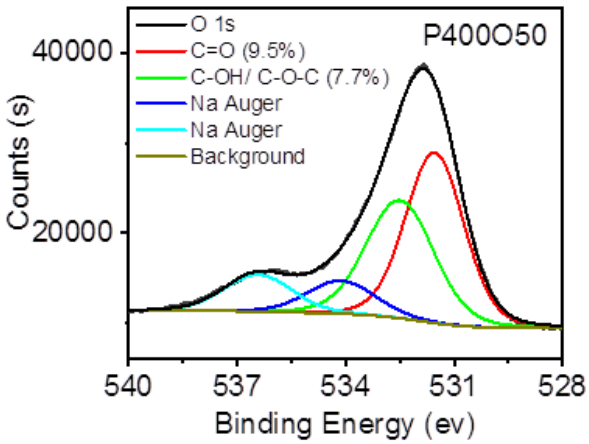

Mass and heat flow changes during CO_2 adsorption at 35 ^oC and 1 bar pressure

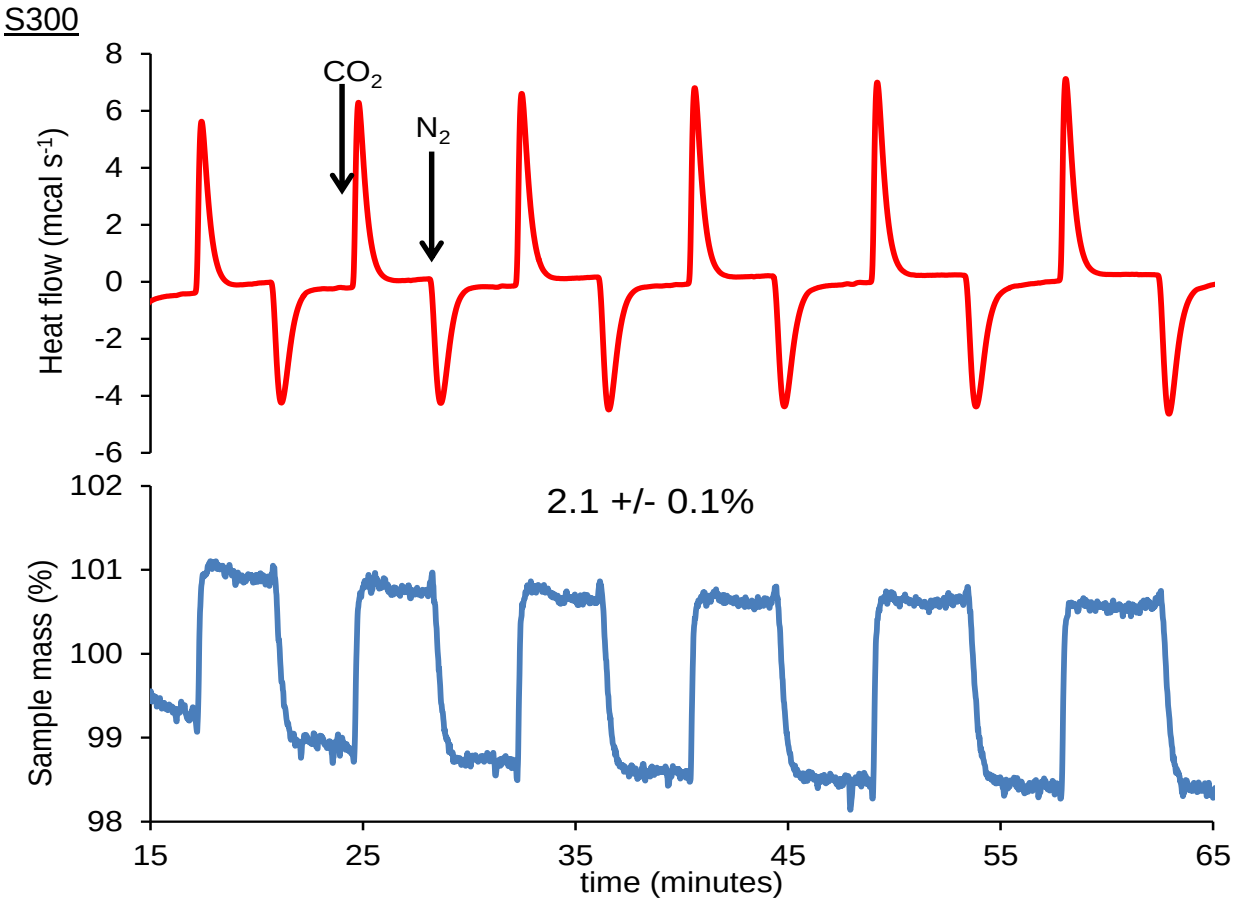

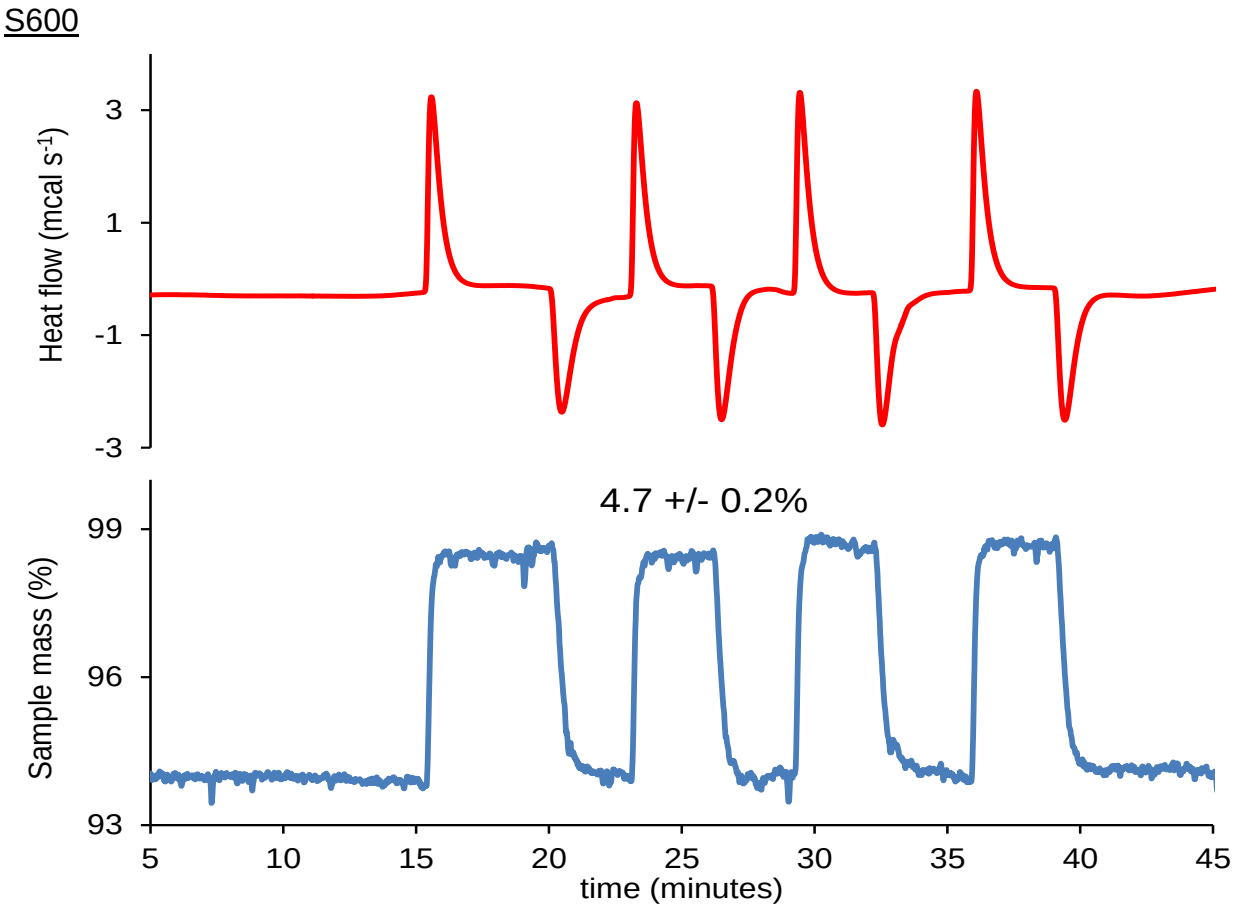

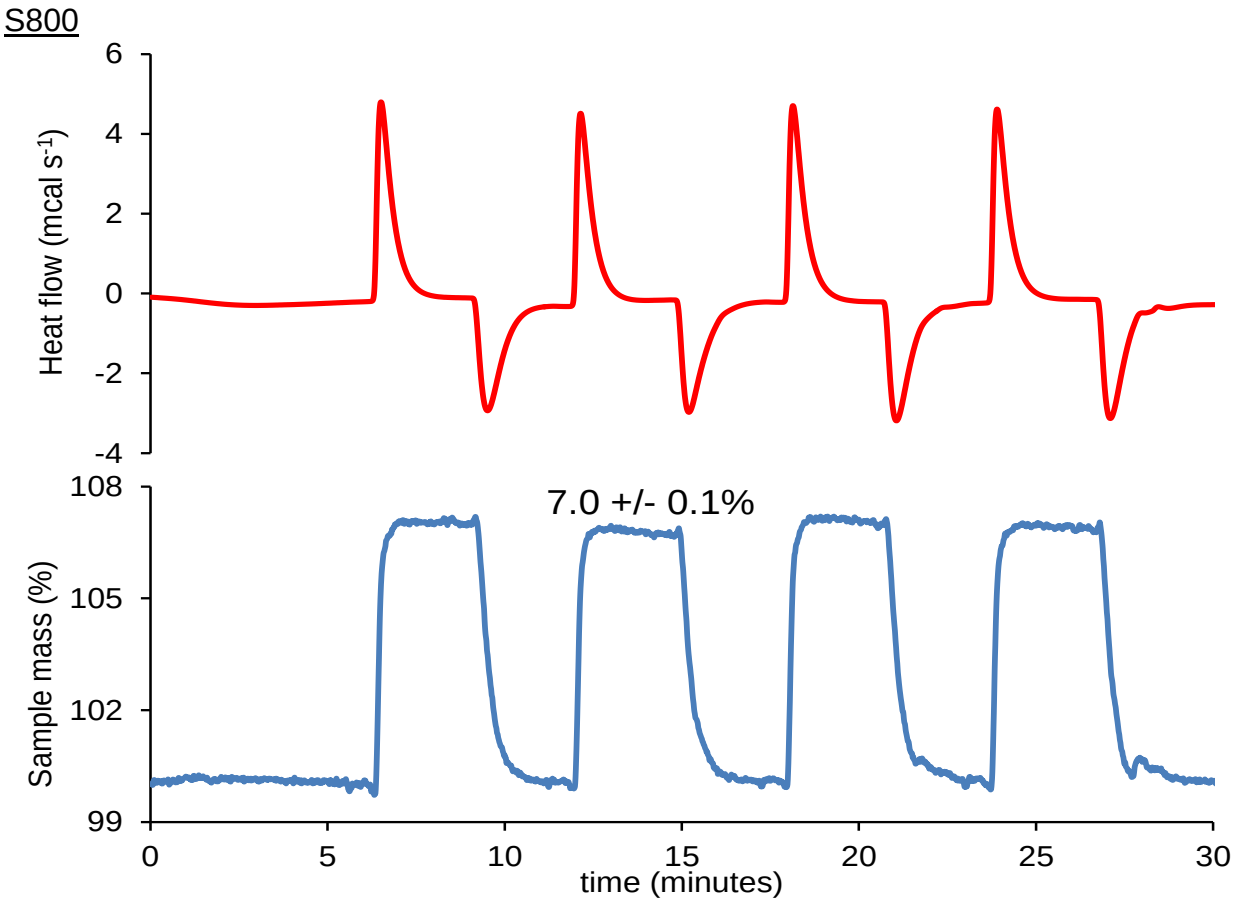
S800
Heat flow (mcal s-1)
6
4
2
0
-2
-4
7.0 +/- 0.1%
Sample mass (%)
108
105
102
99
0
5
10
15
20
25
30
time (minutes)

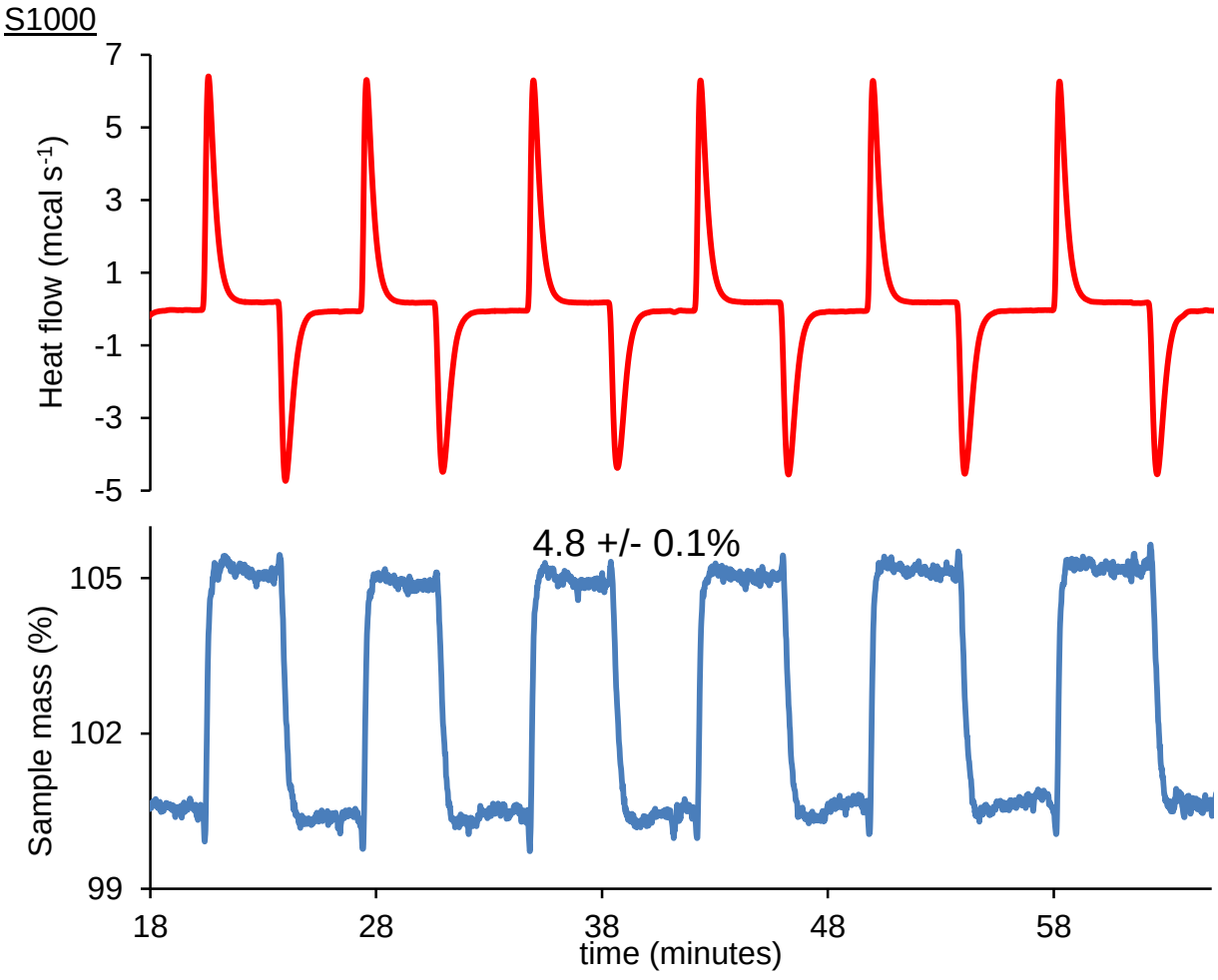
S1000
Heat flow (mcal s-1)
7
5
3
1
-1
-3
-5
4.8 +/- 0.1%
Sample mass (%)
105
102
99
18
28
38
48
58
time (minutes)

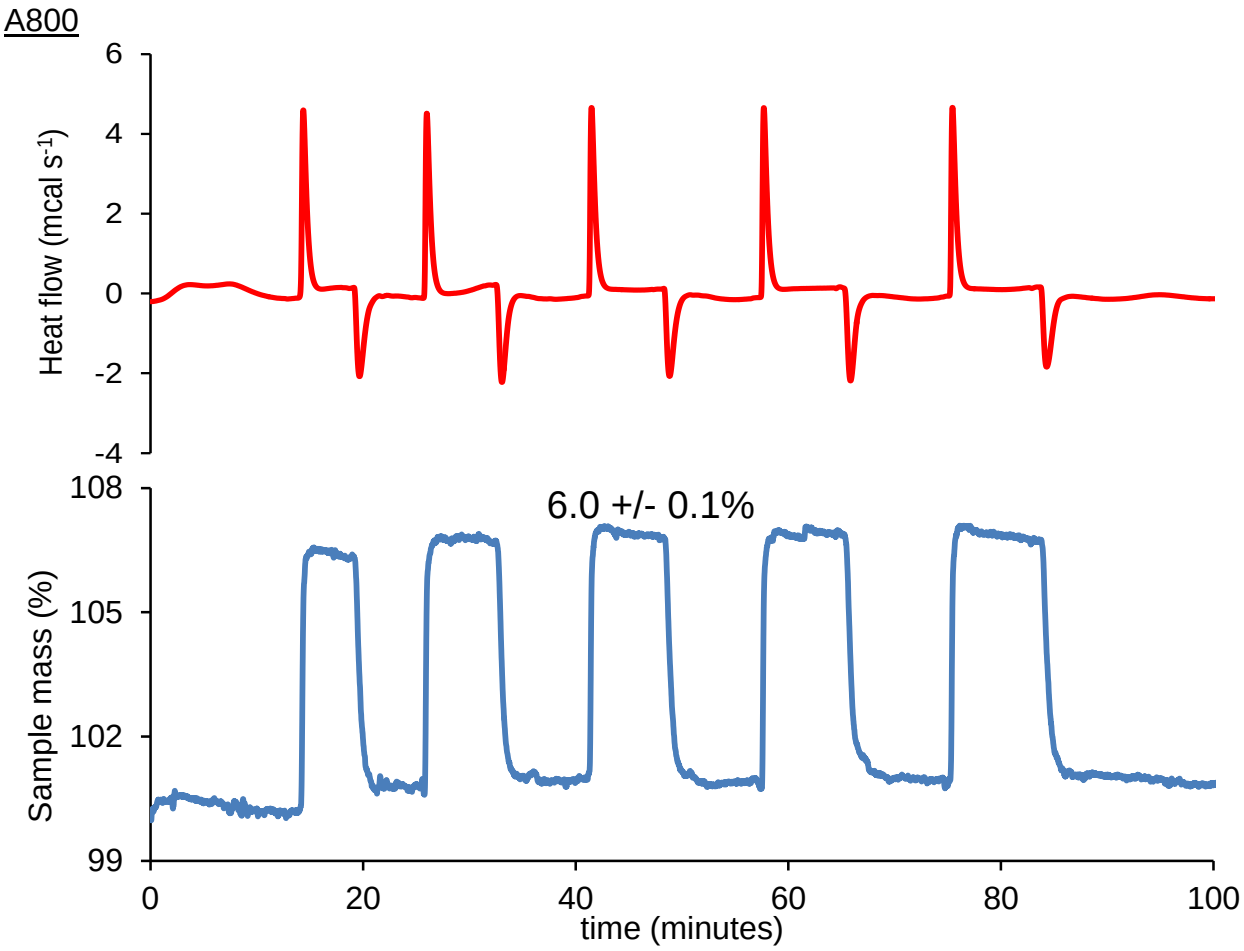
A800
Heat flow (mcal s-1)
6
4
2
0
-2
-4
Sample mass (%)
108
105
102
99
6.0 +/- 0.1%
0
20
40
60
80
100
time (minutes)

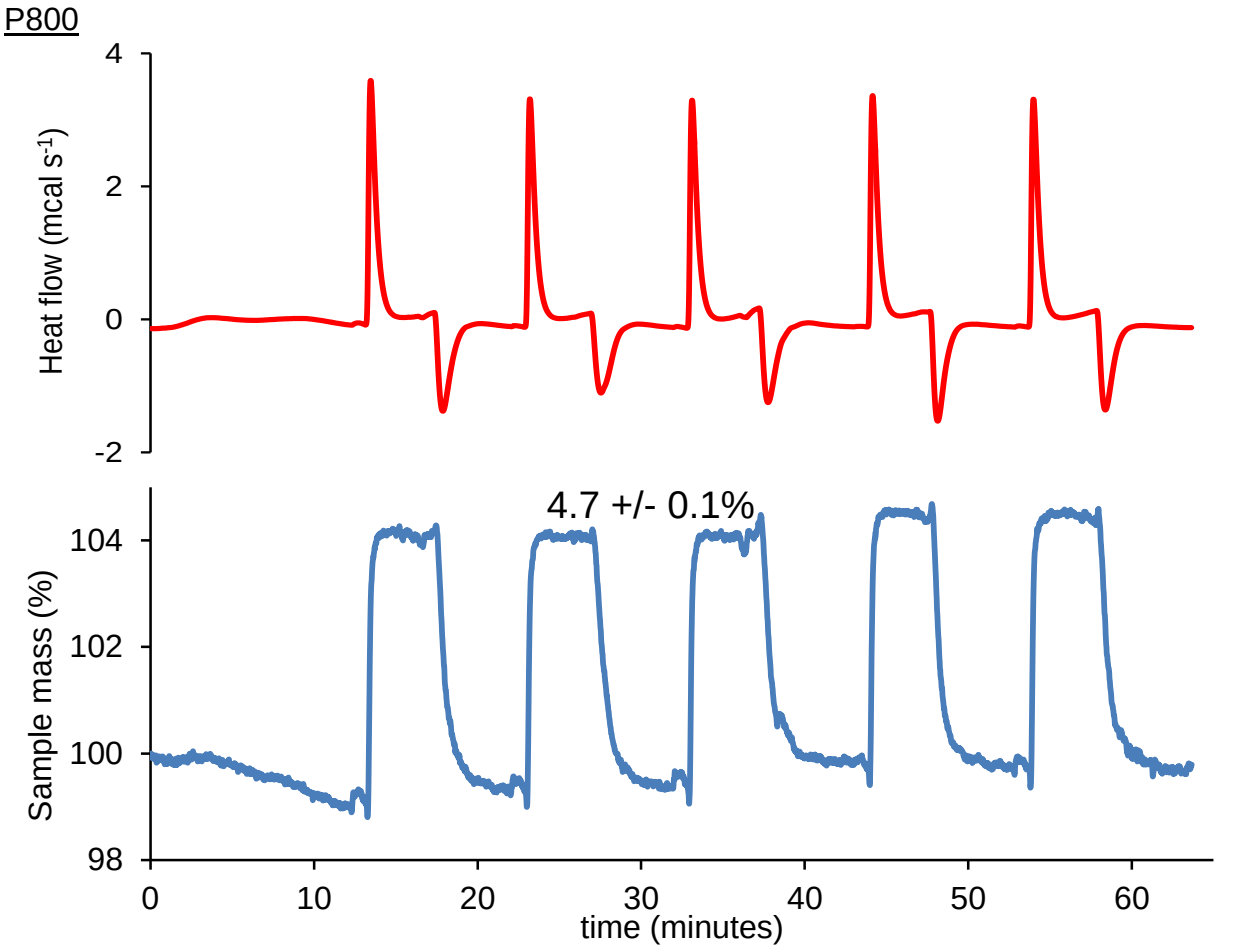
P800
Heat flow (mcal s-1)
4
2
0
-2
Sample mass (%)
104
102
100
98
4.7 +/- 0.1%
0
10
20
30
40
50
60
time (minutes)

S800K1

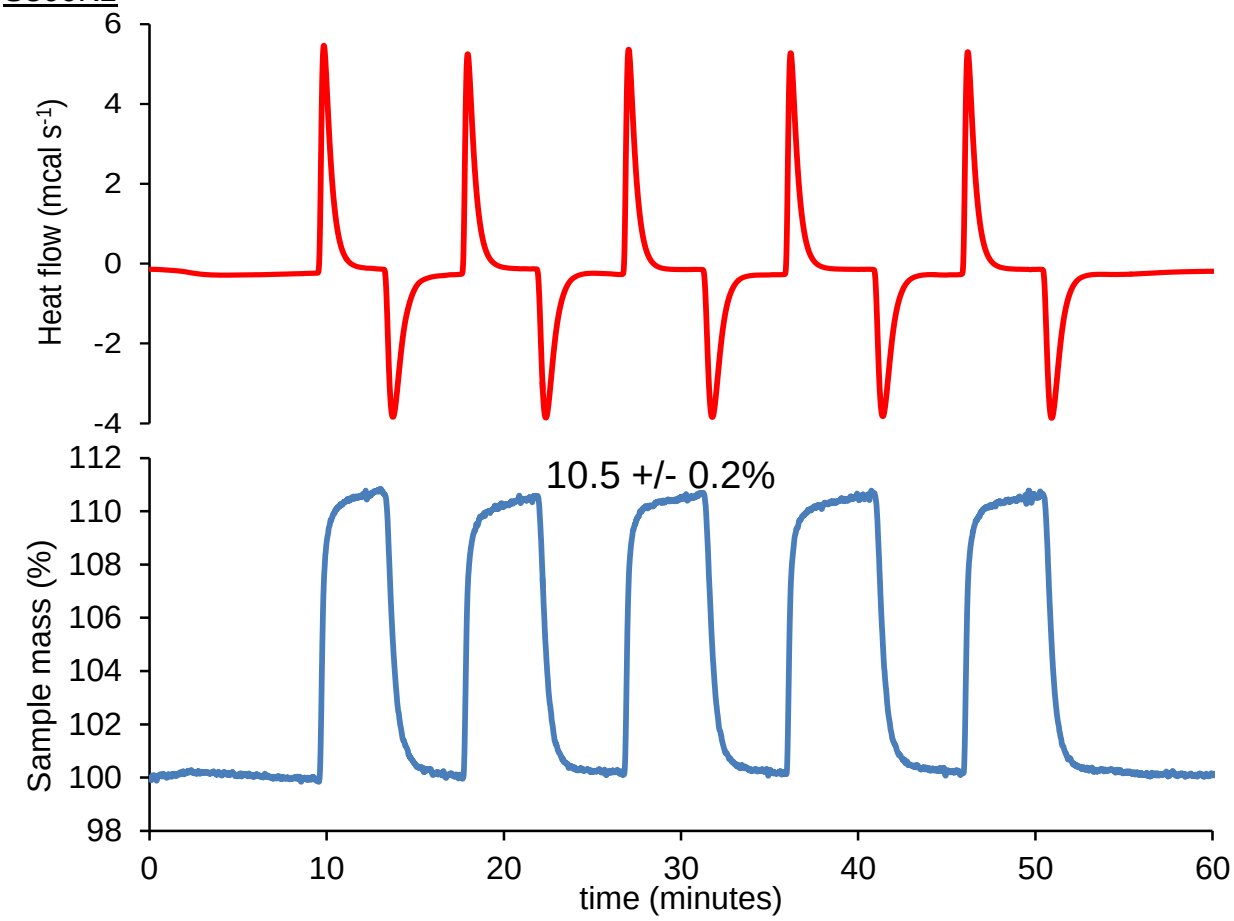

S800K2

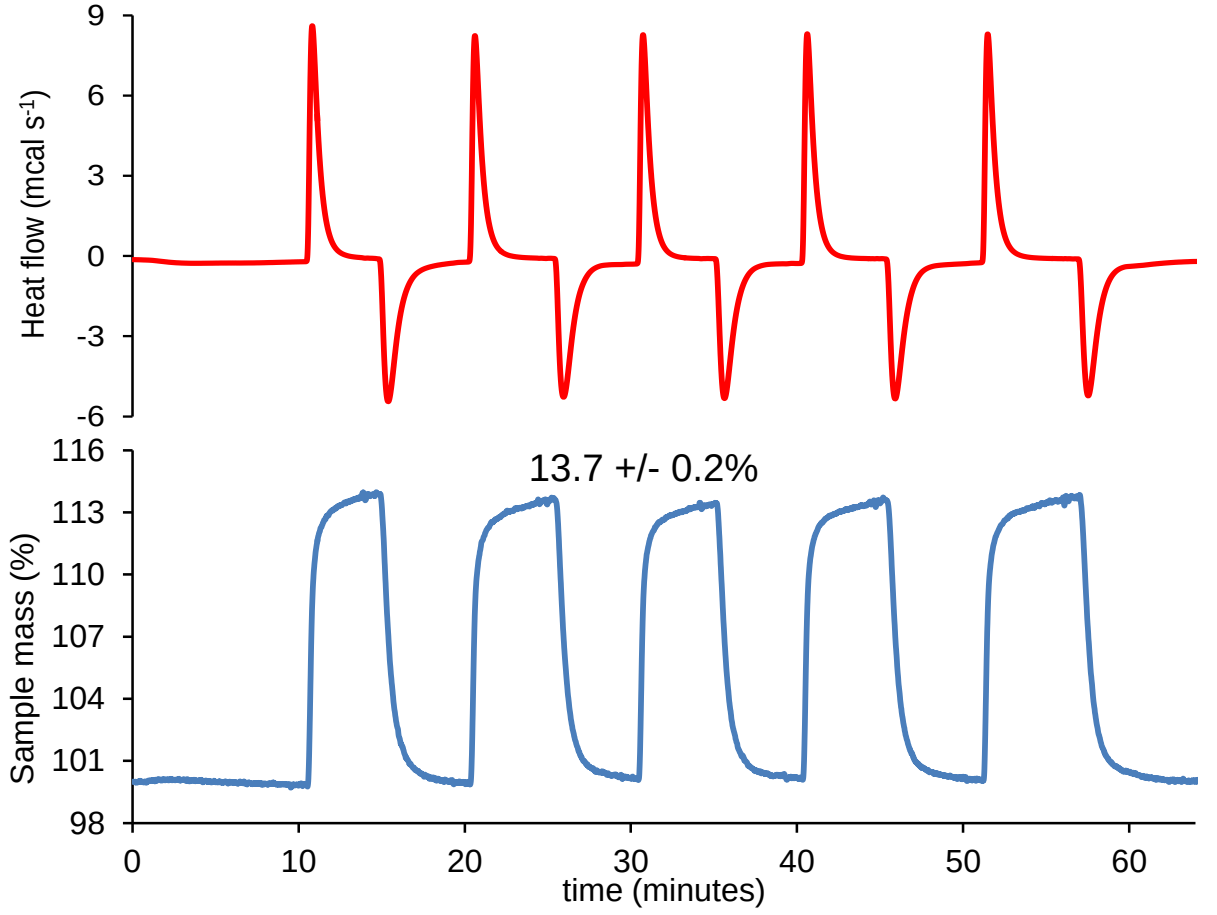

S800K3

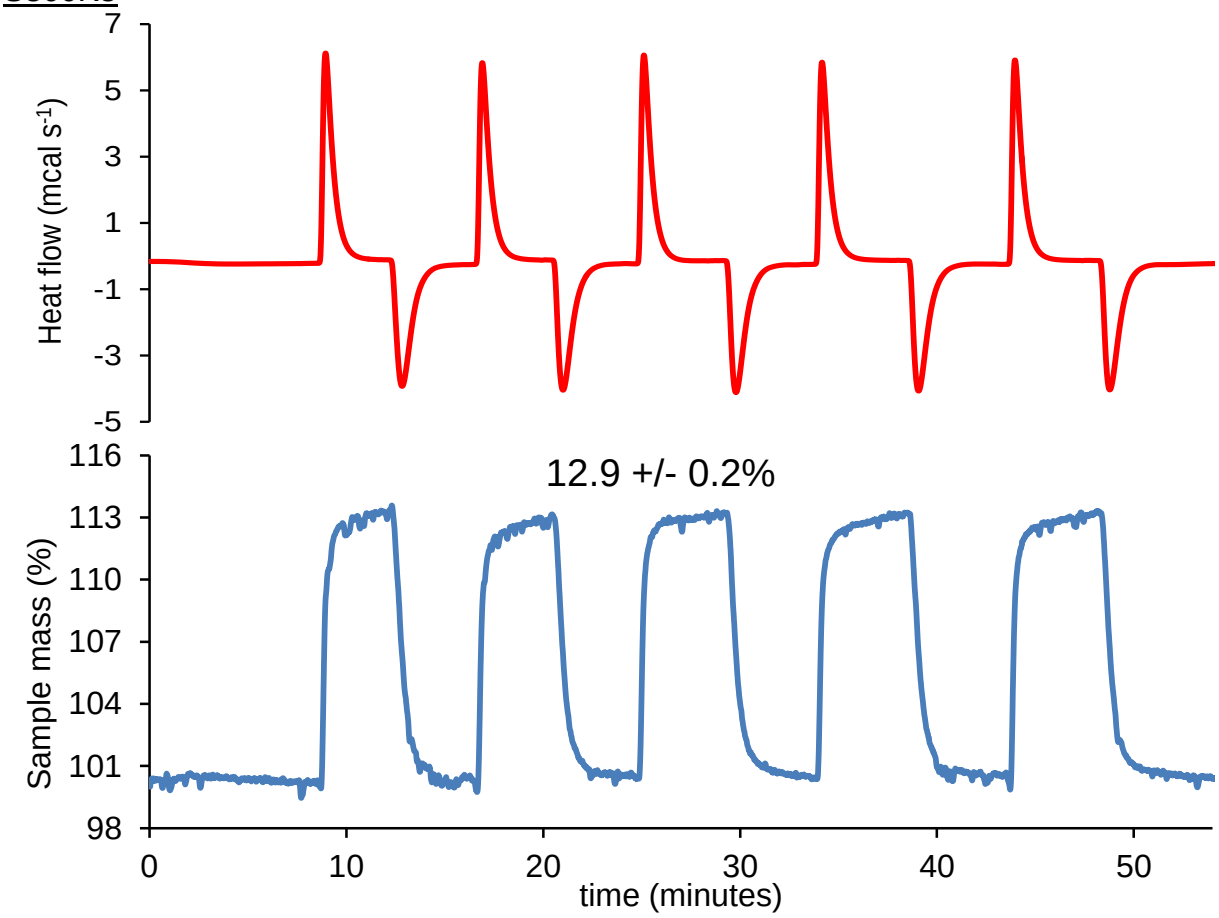

S800K4

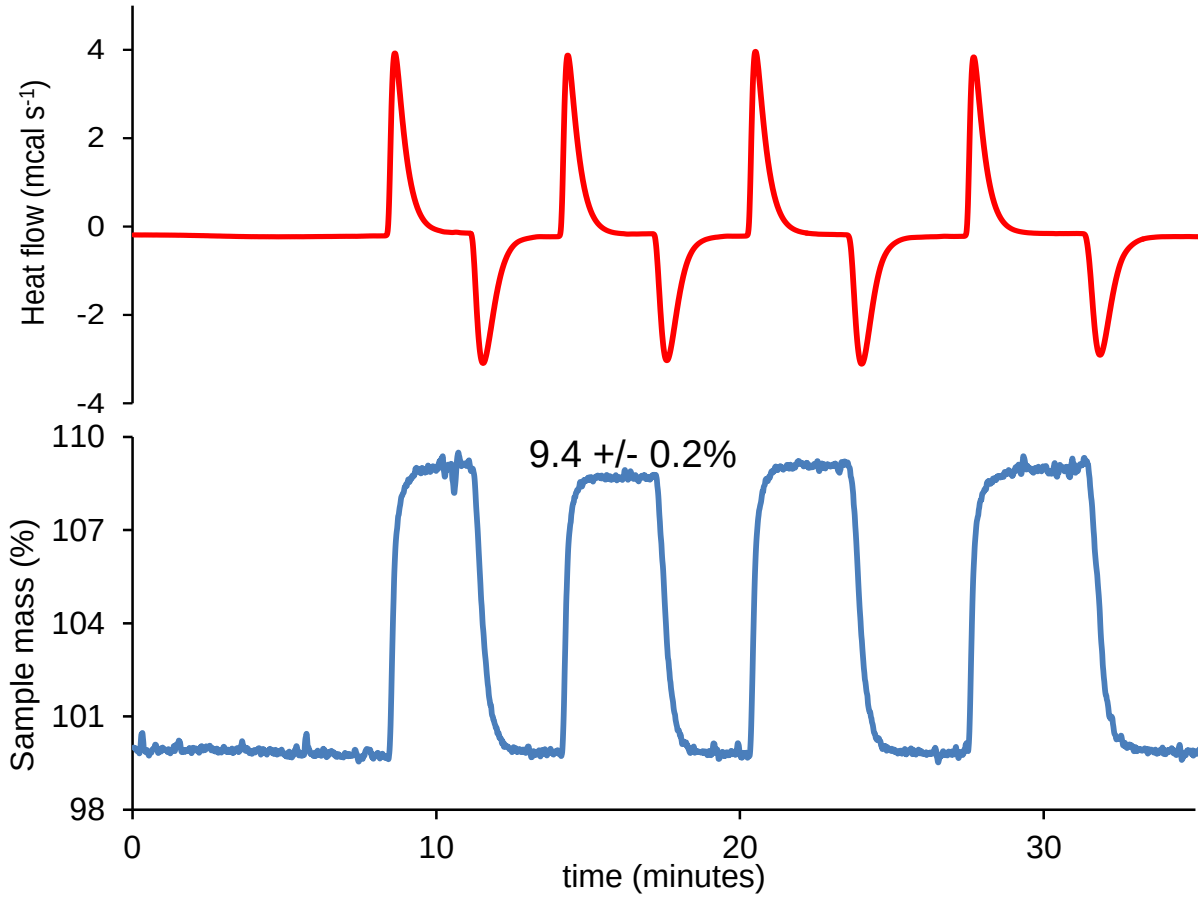

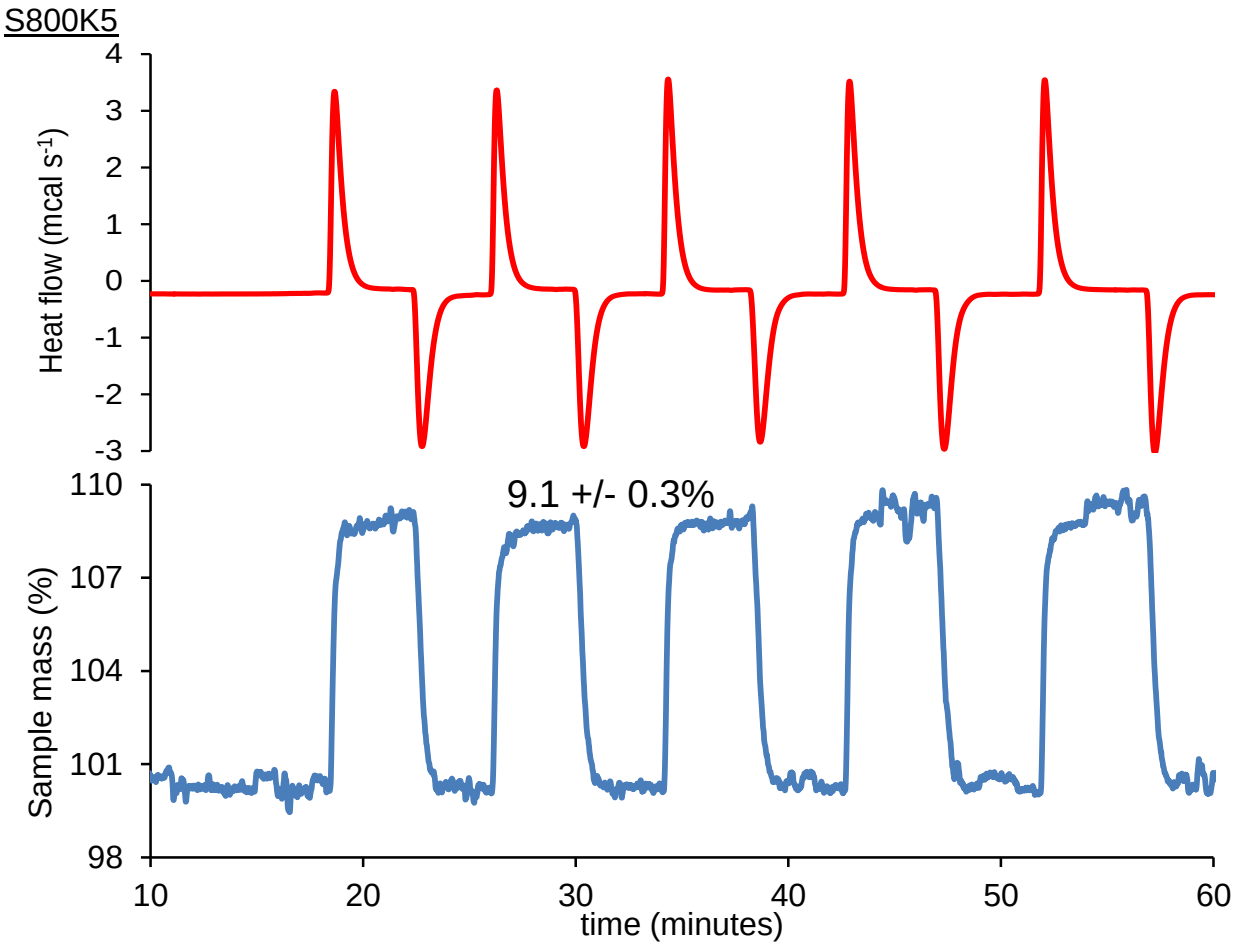
S800K5
Heat flow (mcal s-1)
4
3
2
1
0
-1
-2
-3
9.1 +/- 0.3%
Sample mass (%)
110
107
104
101
98
10
20
30
40
50
60
time (minutes)

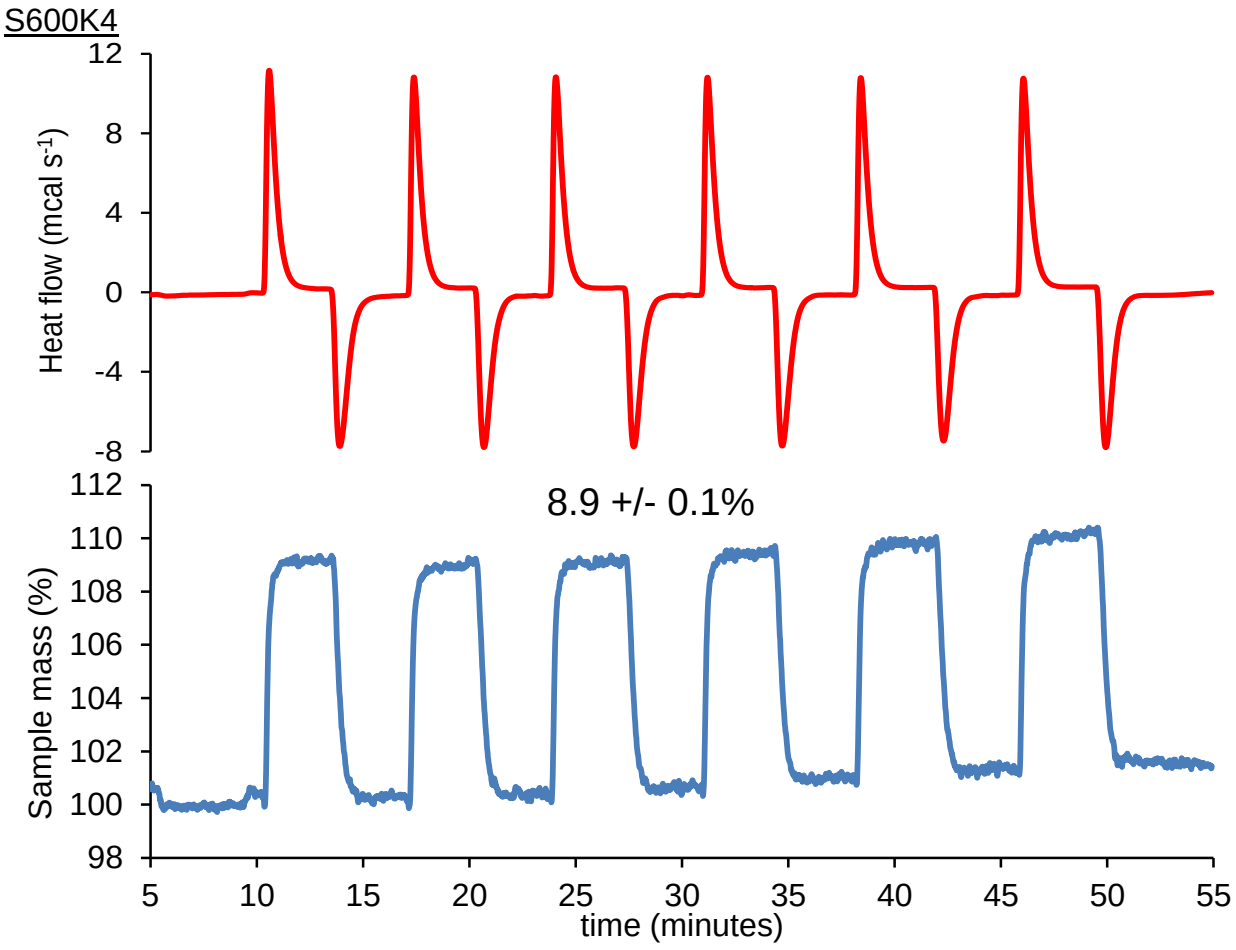
S600K4
Heat flow (mcal s-1)
12
8
4
0
-4
-8
8.9 +/- 0.1%
Sample mass (%)
112
110
108
106
104
102
100
98
5
10
15
20
25
30
35
40
45
50
55
time (minutes)

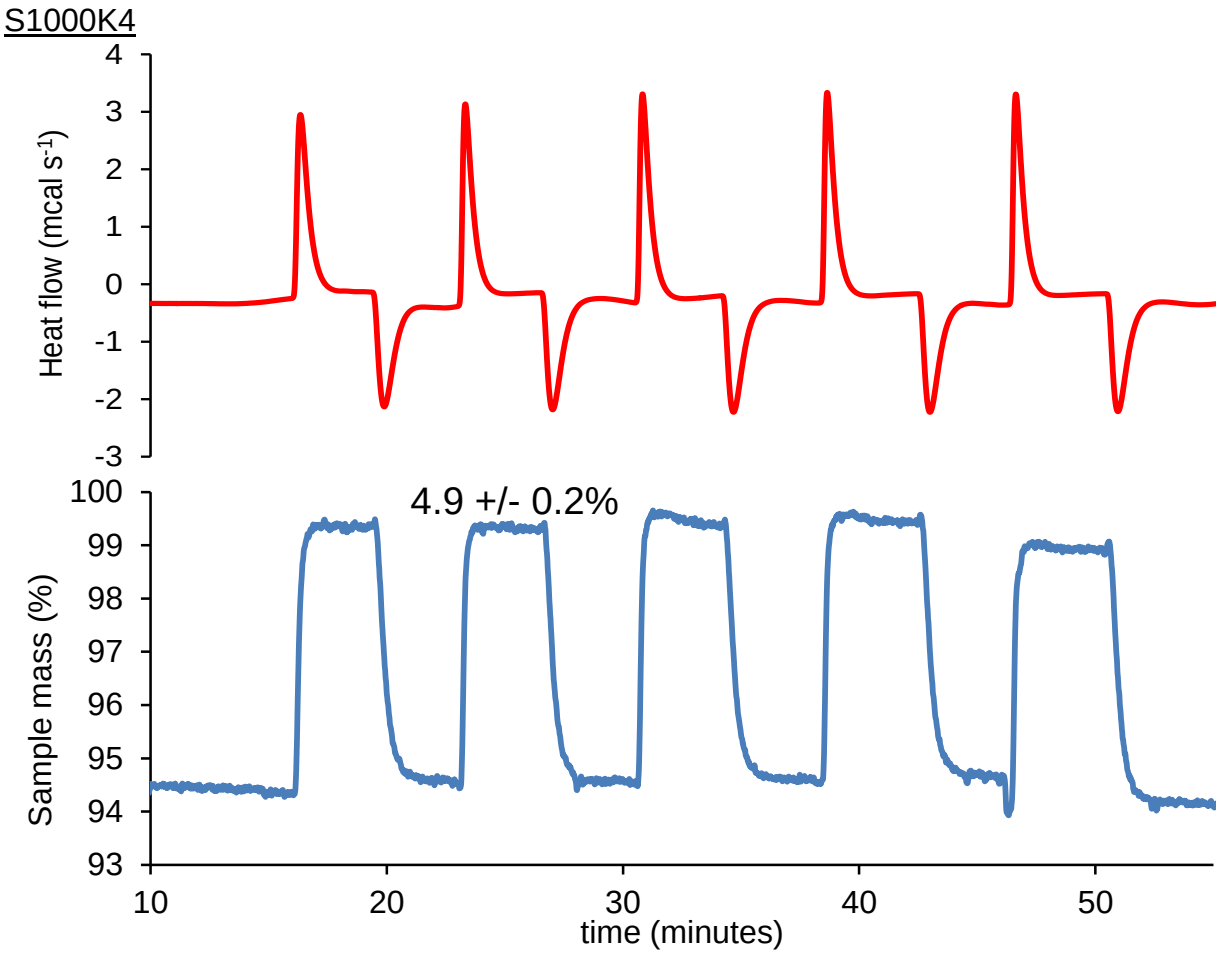
S1000K4
Heat flow (mcal s-1)
4
3
2
1
0
-1
-2
-3
Sample mass (%)
4.9 +/- 0.2%
100
99
98
97
96
95
94
93
10
20
30
40
50
time (minutes)

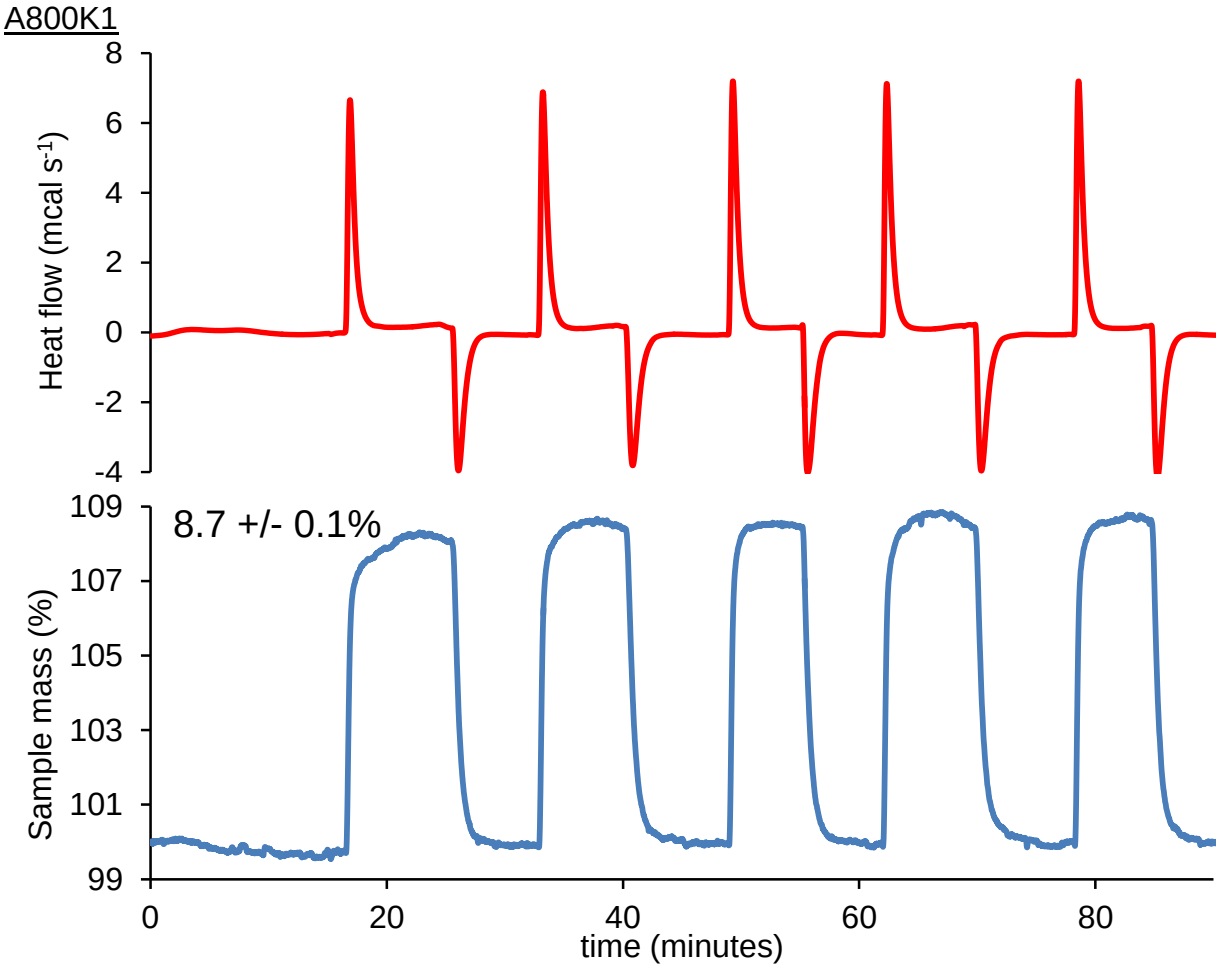
A800K1
Heat flow (mcal s-1)
8
6
4
2
0
-2
-4
Sample mass (%)
8.7 +/- 0.1%
109
107
105
103
101
99
0
20
40
60
80
time (minutes)

A800K2

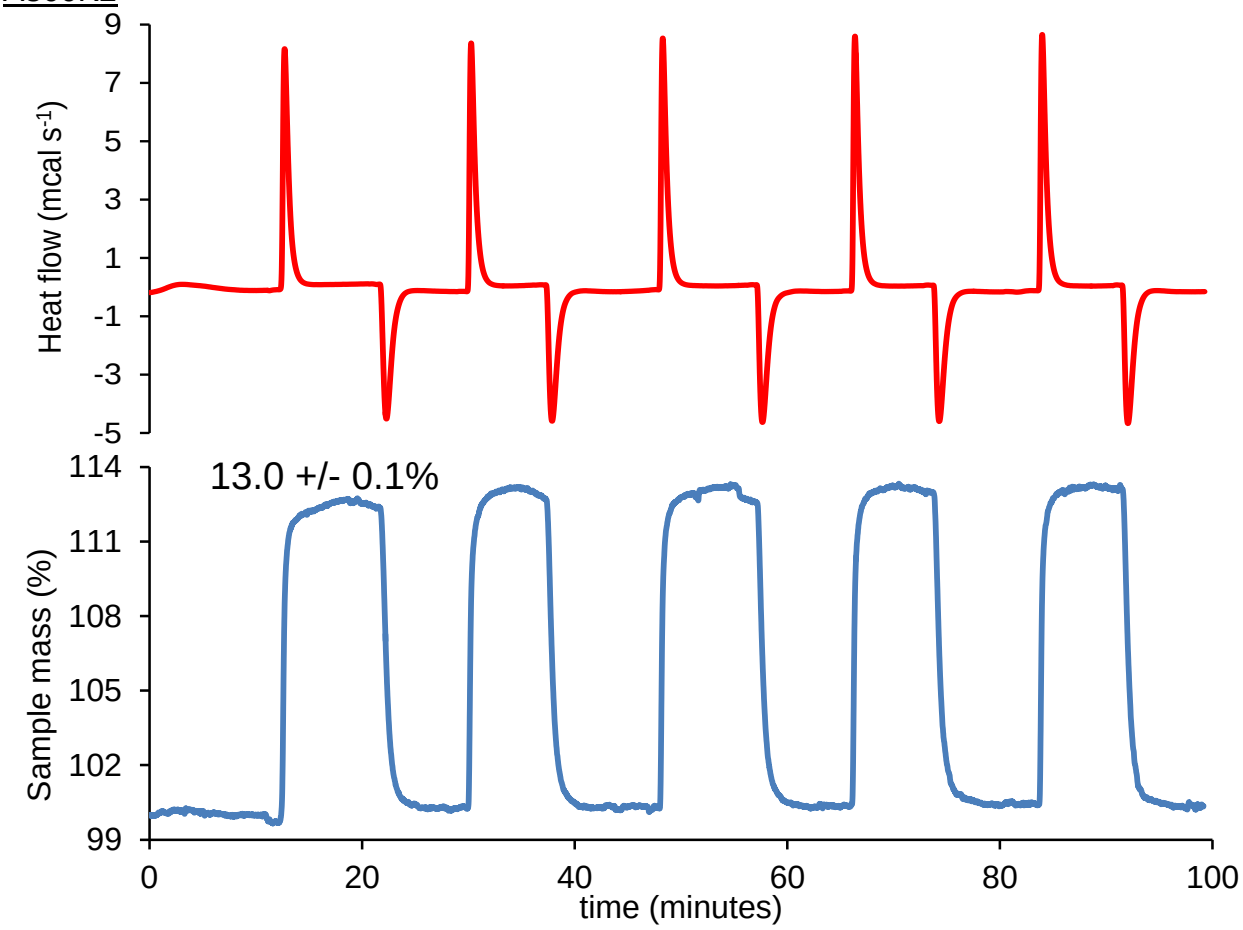

A800K3

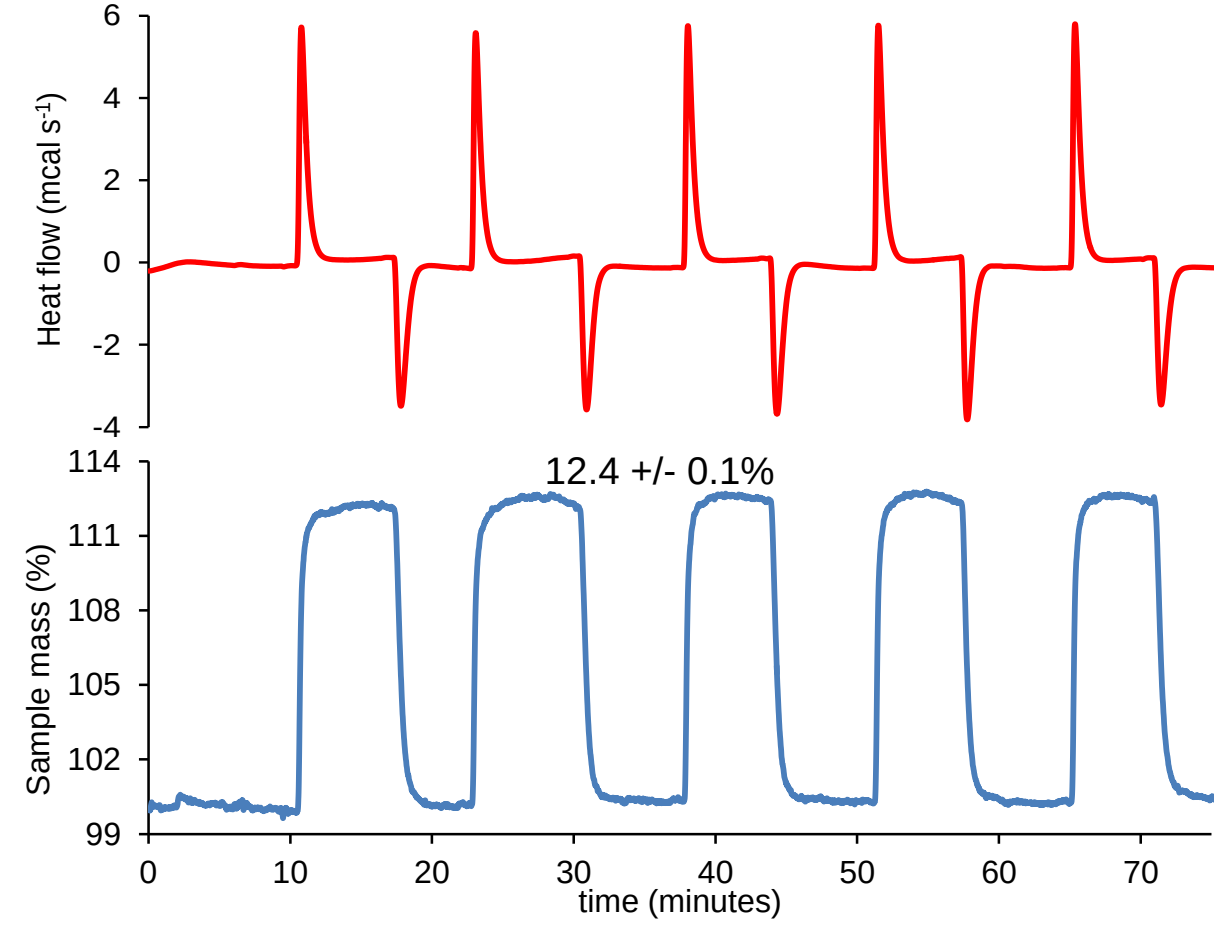

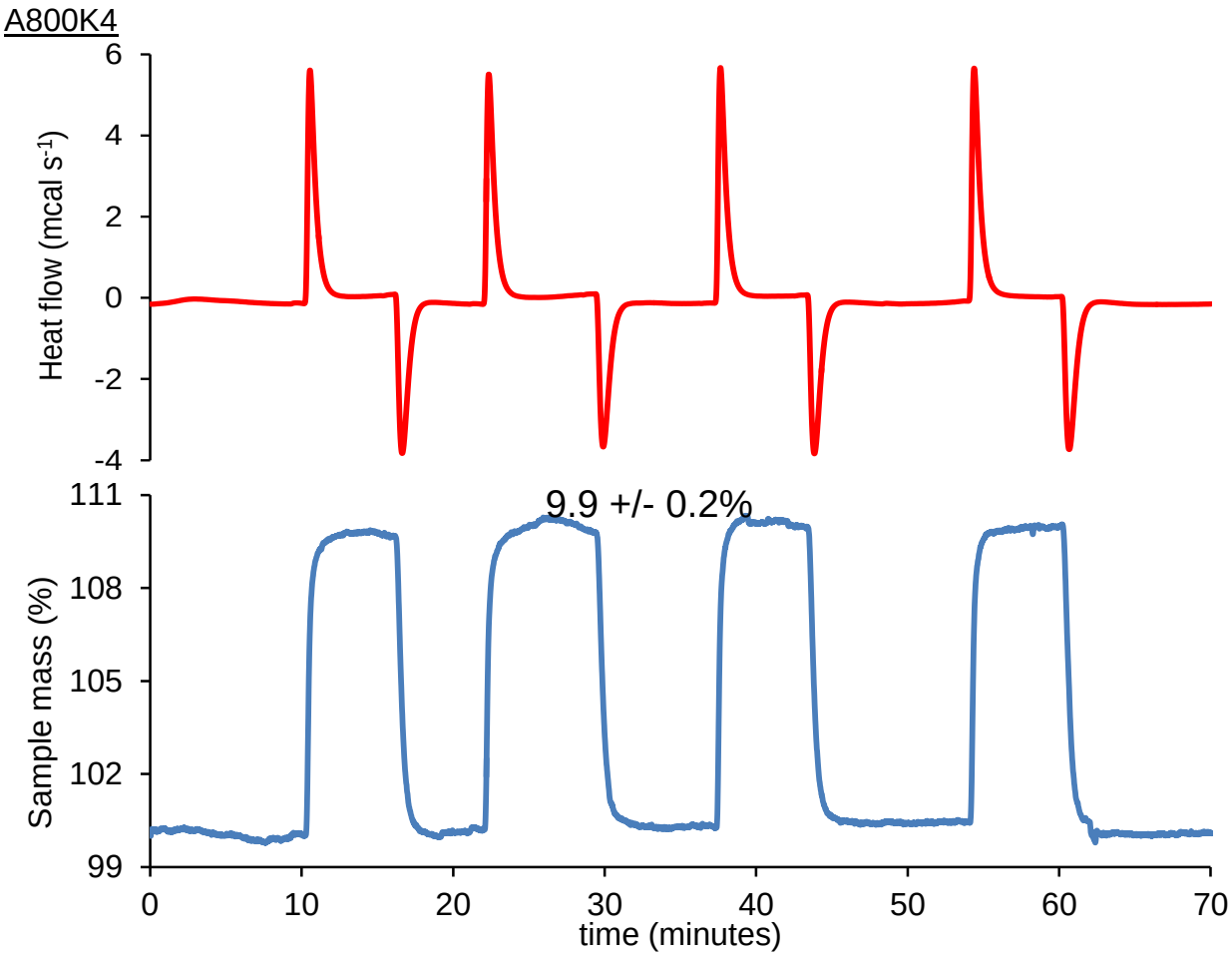
A800K4
Heat flow (mcal s-1)
6
4
2
0
-2
-4
Sample mass (%)
111
108
105
102
99
9.9 +/- 0.2%
0
10
20
30
40
50
60
70
time (minutes)

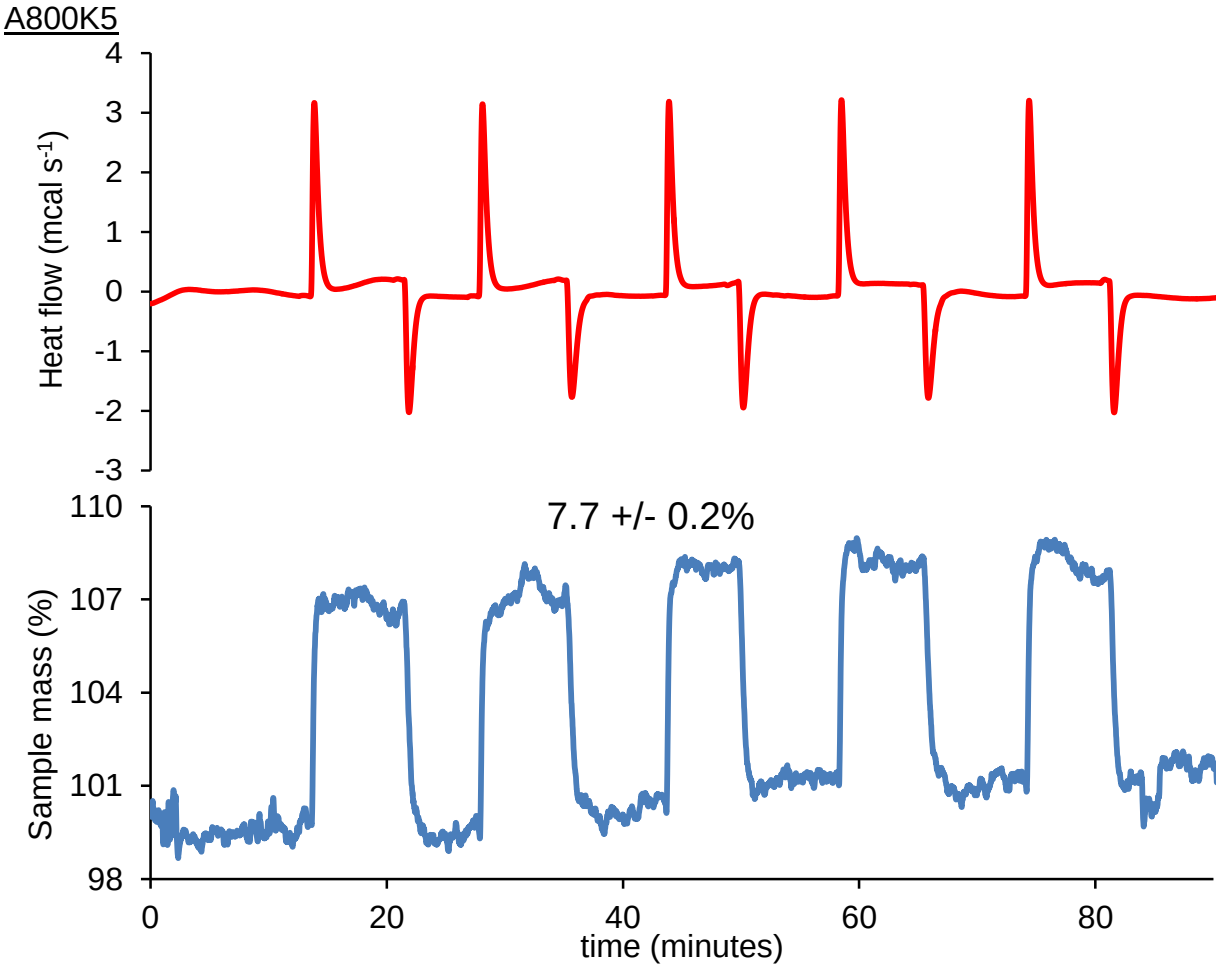
A800K5
Heat flow (mcal s-1)
4
3
2
1
0
-1
-2
-3
Sample mass (%)
110
107
104
101
98
7.7 +/- 0.2%
0
20
40
60
80
time (minutes)

A600K2

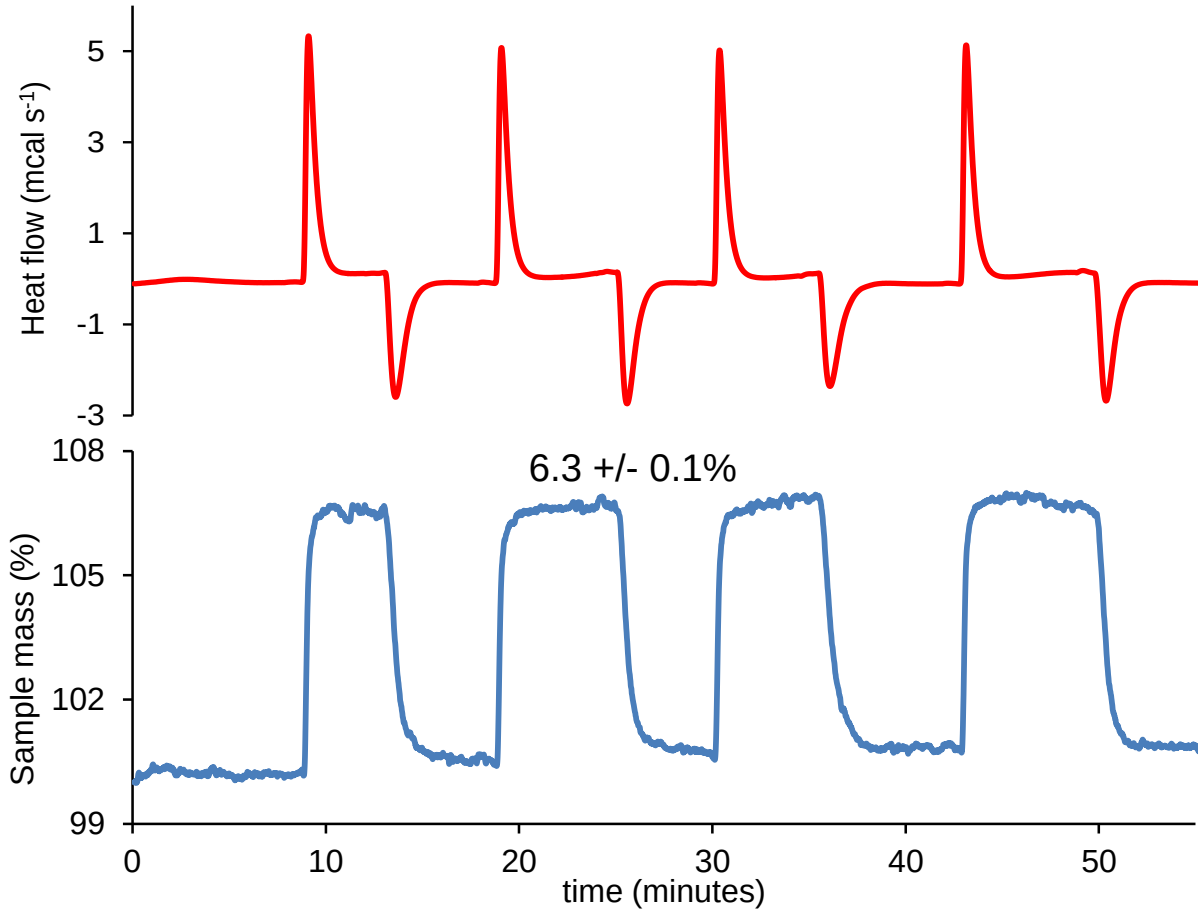

A1000K2

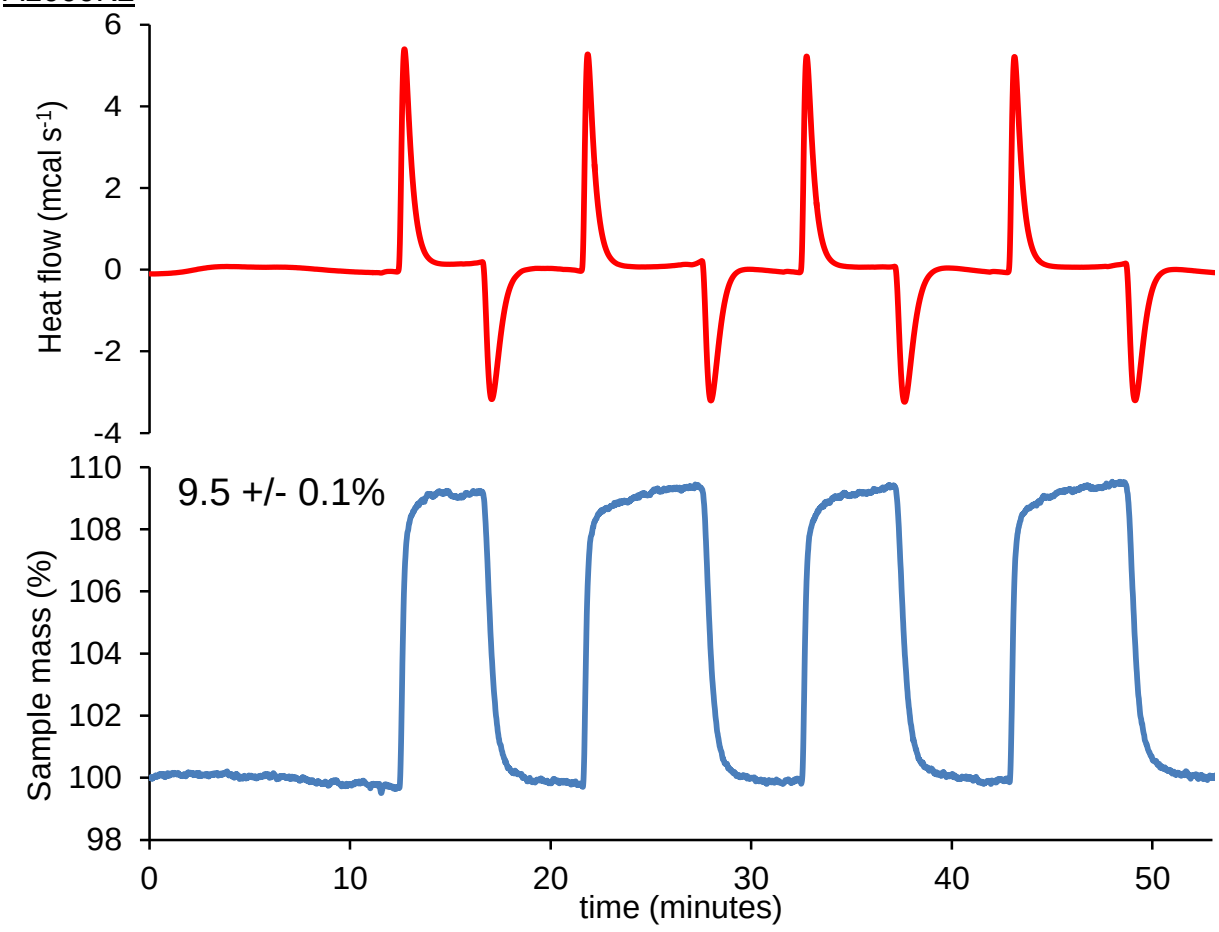

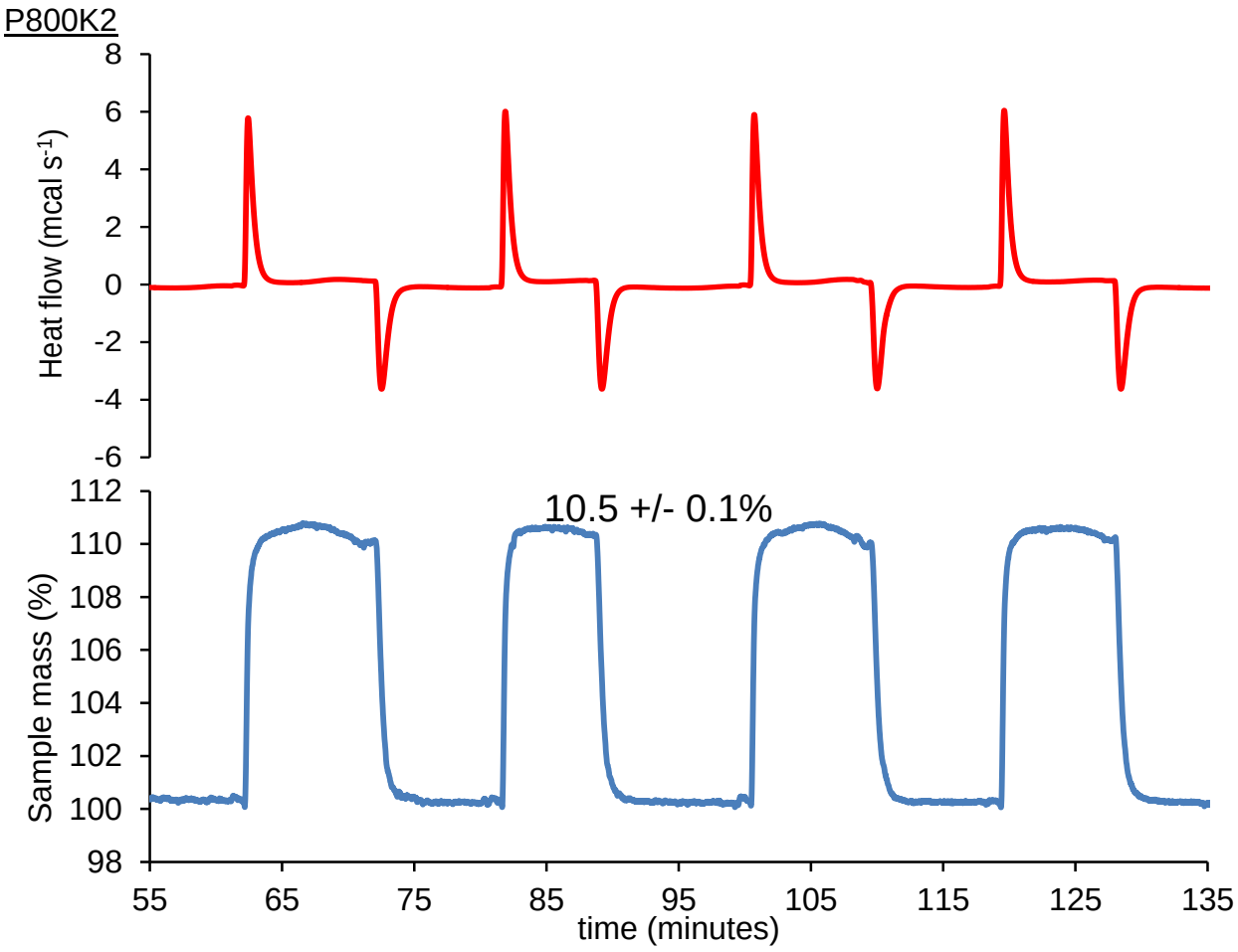
P800K2
Heat flow (mcal s-1)
8
6
4
2
0
-2
-4
-6
Sample mass (%)
112
110
108
106
104
102
100
98
10.5 +/- 0.1%
55
65
75
85
95
105
115
125
135
time (minutes)

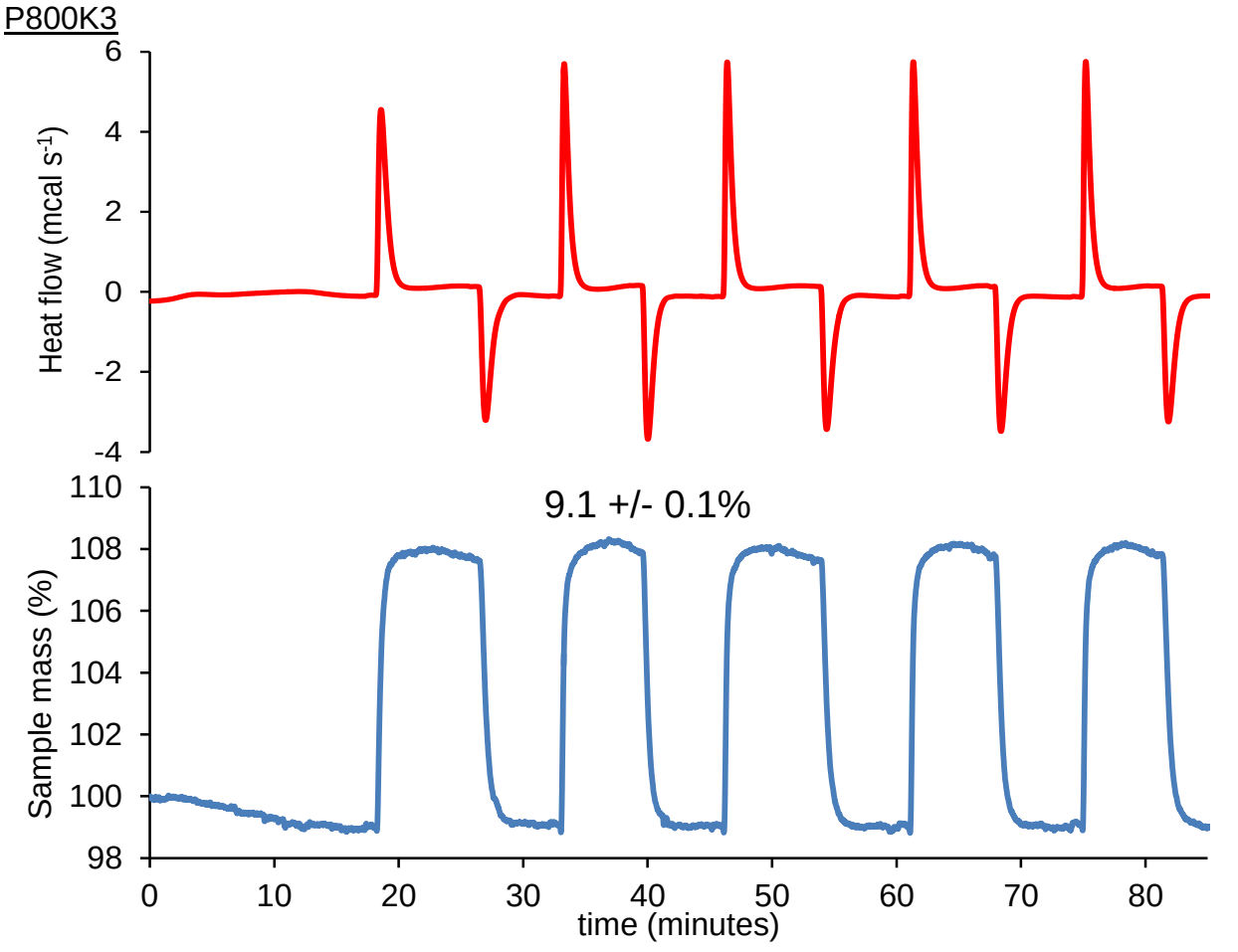
P800K3
Heat flow (mcal s-1)
6
4
2
0
-2
-4
Sample mass (%)
110
108
106
104
102
100
98
9.1 +/- 0.1%
0
10
20
30
40
50
60
70
80
time (minutes)

P800K5

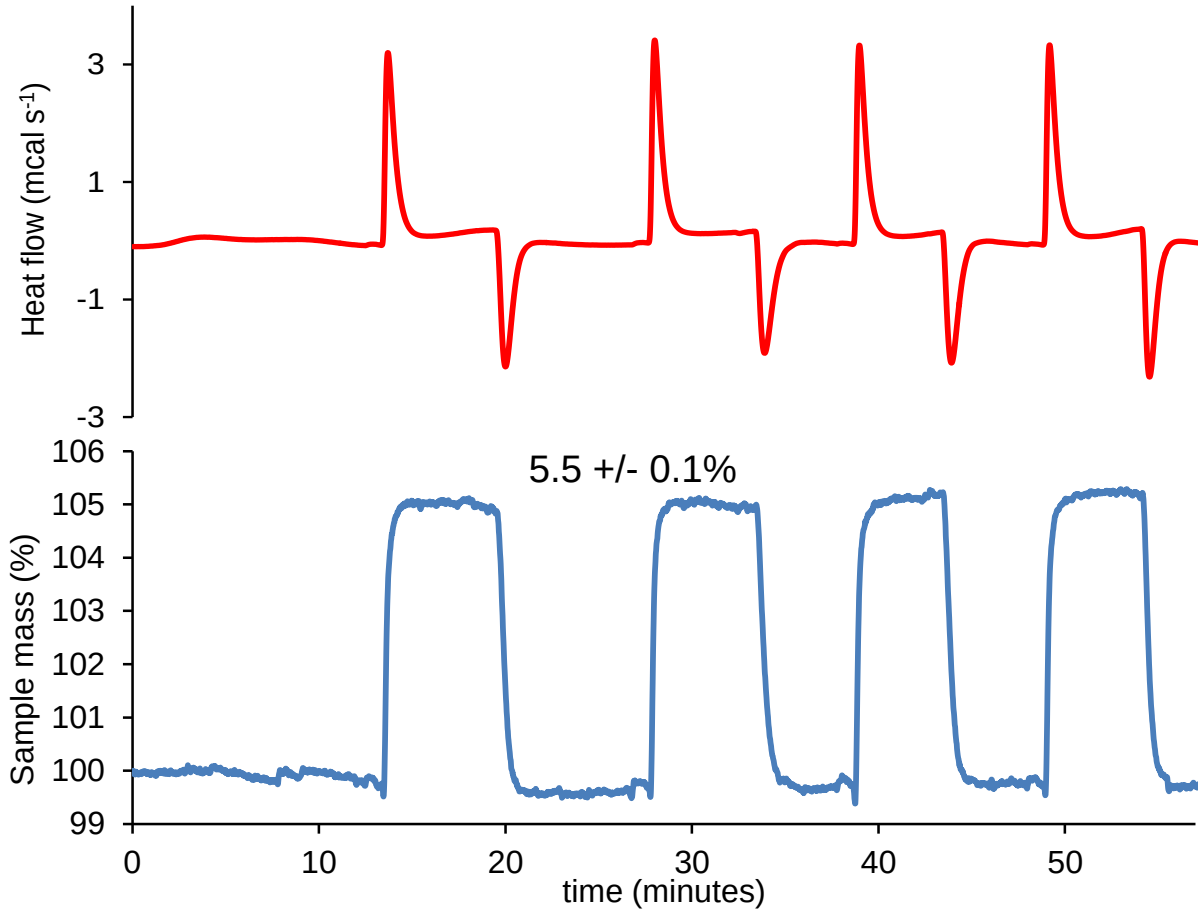

S800C15

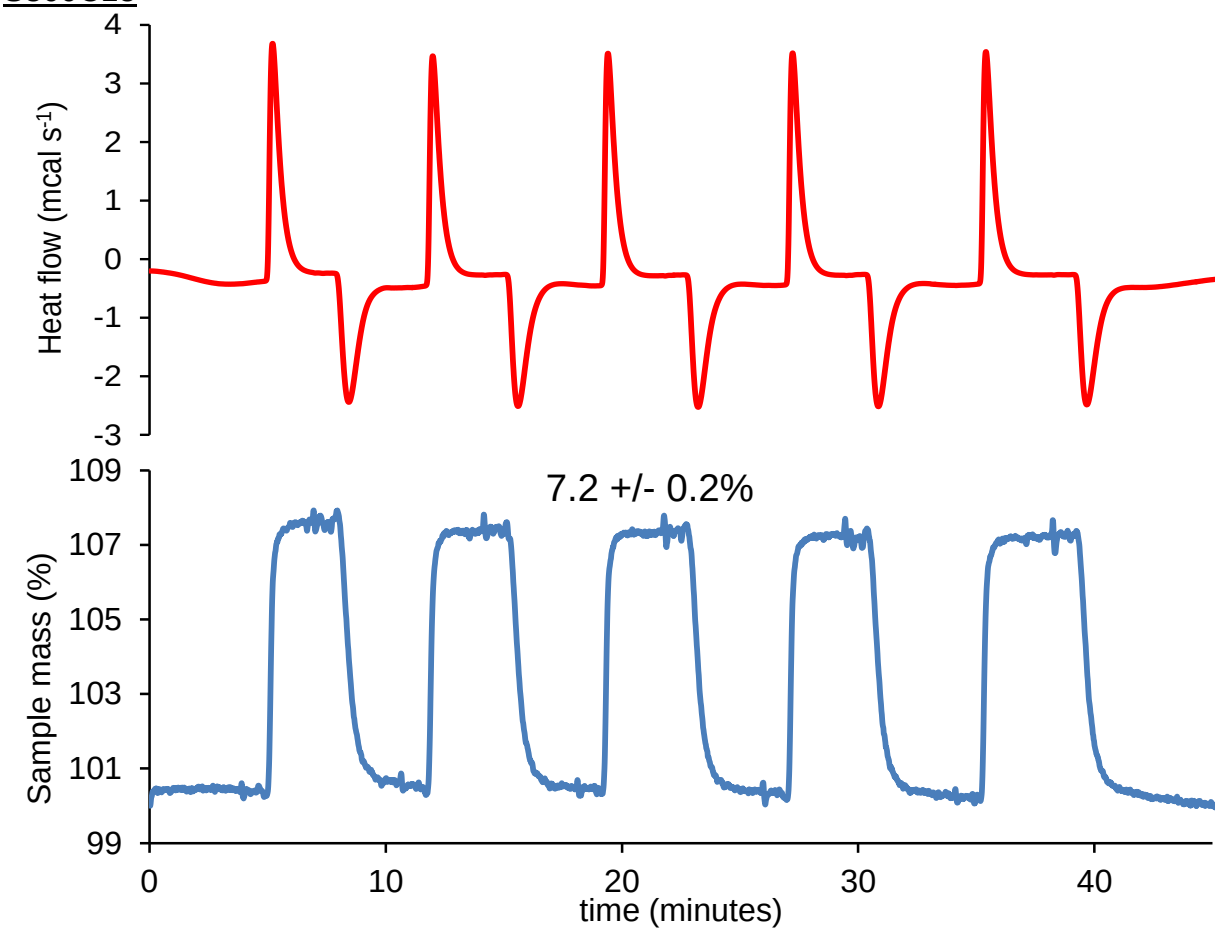

S850C15

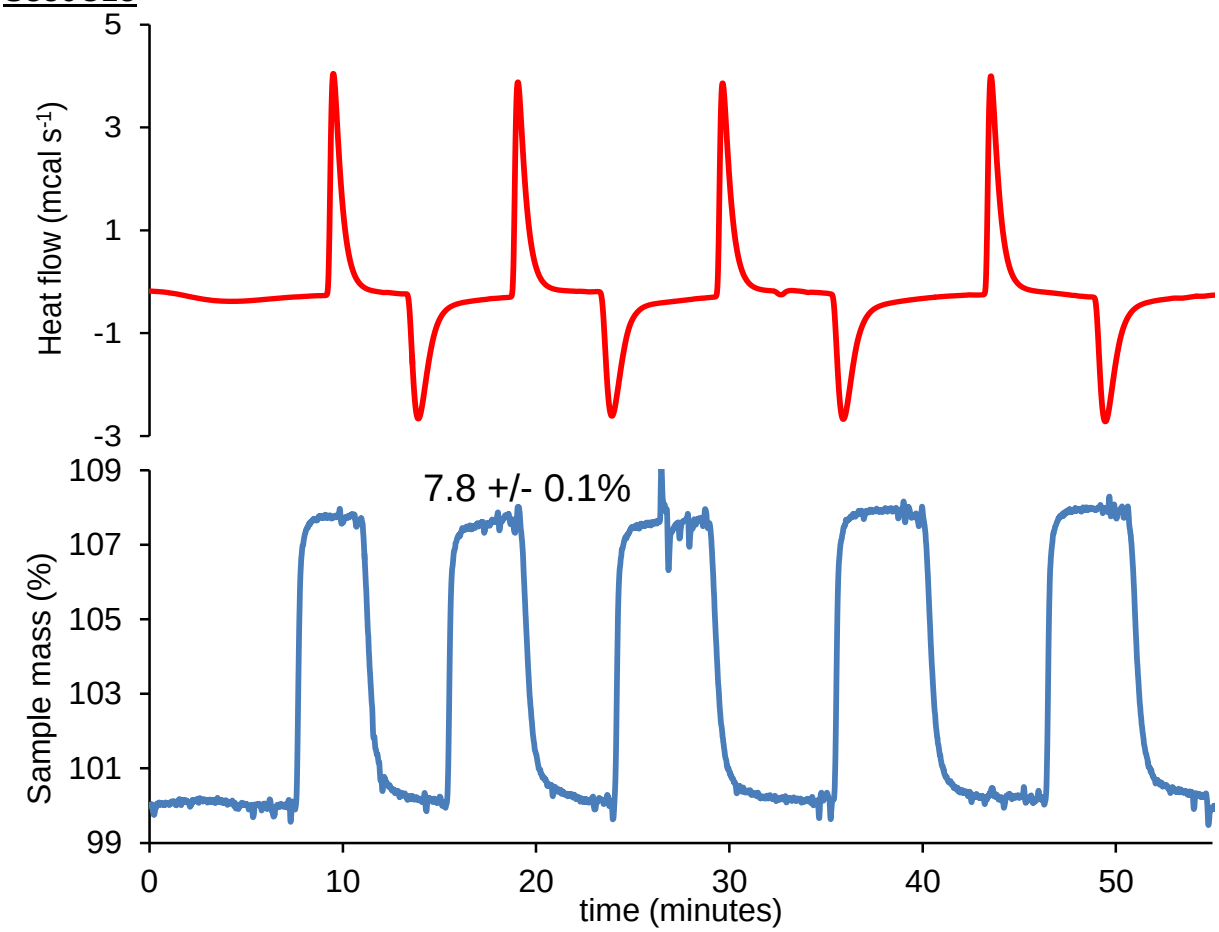

S900C15

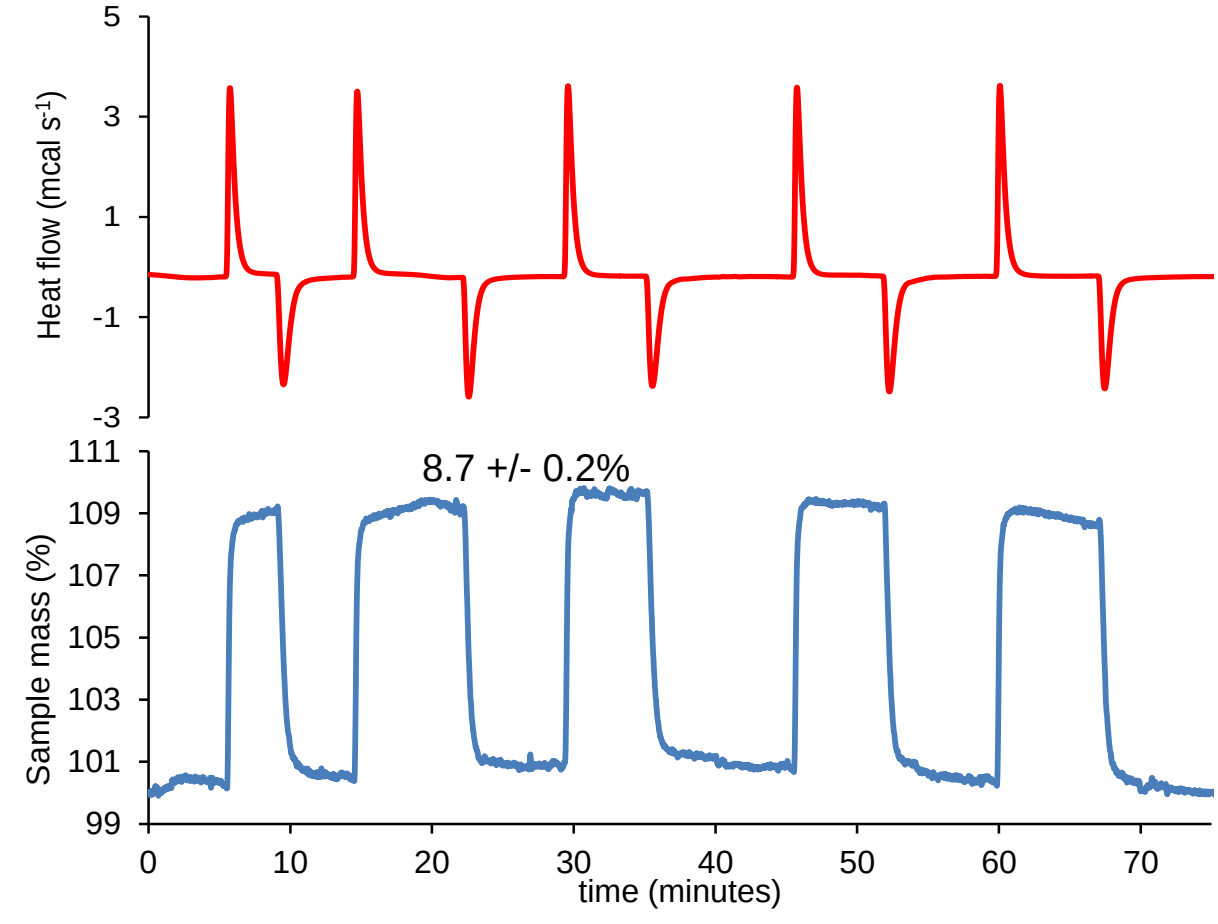

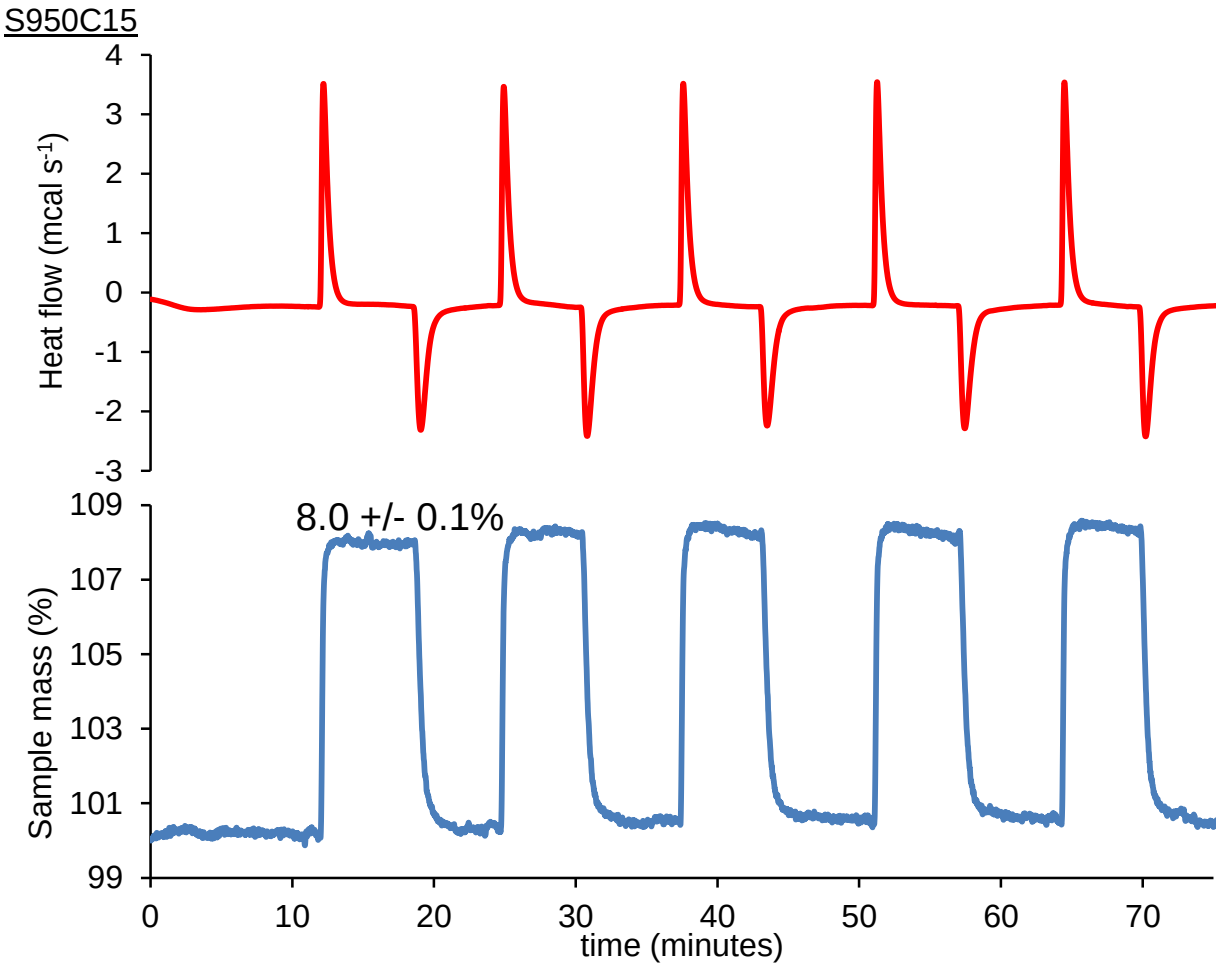
S950C15
Heat flow (mcal s-1)
4
3
2
1
0
-1
-2
-3
8.0 +/- 0.1%
Sample mass (%)
109
107
105
103
101
99
0
10
20
30
40
50
60
70
time (minutes)

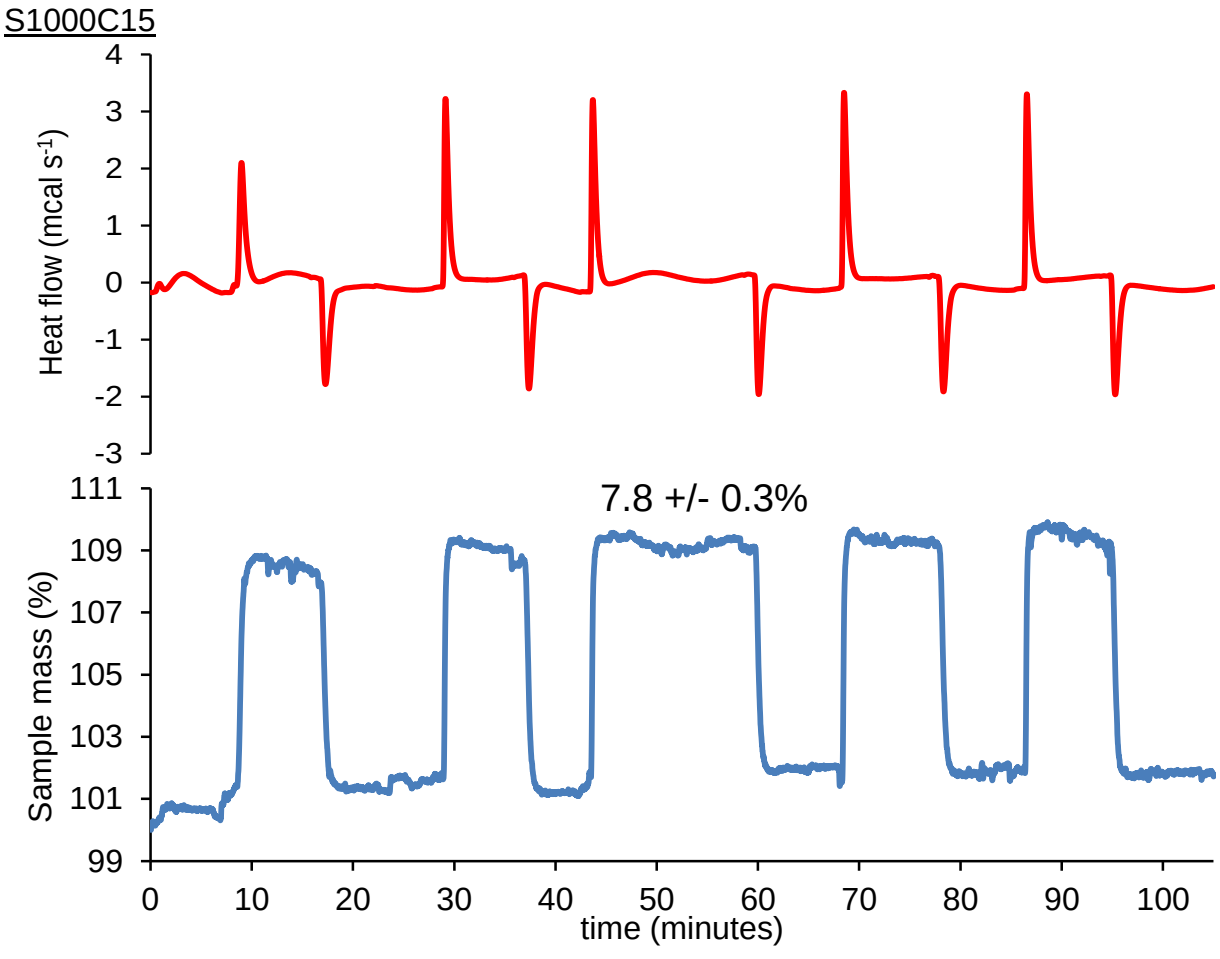
S1000C15
Heat flow (mcal s-1)
4
3
2
1
0
-1
-2
-3
7.8 +/- 0.3%
Sample mass (%)
111
109
107
105
103
101
99
0
10
20
30
40
50
60
70
80
90
100
time (minutes)

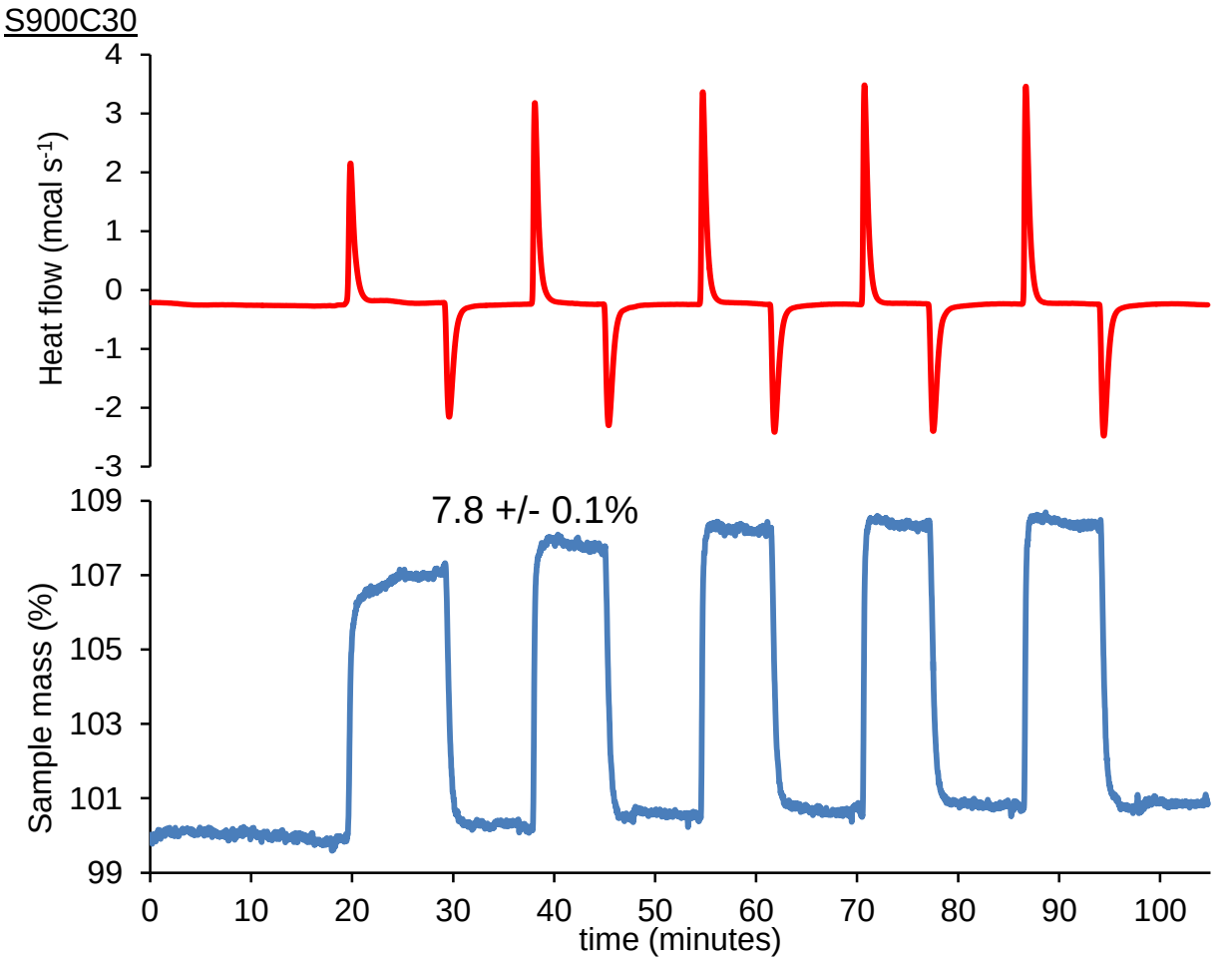
S900C30
Heat flow (mcal s-1)
4
3
2
1
0
-1
-2
-3
7.8 +/- 0.1%
Sample mass (%)
109
107
105
103
101
99
0
10
20
30
40
50
60
70
80
90
100
time (minutes)

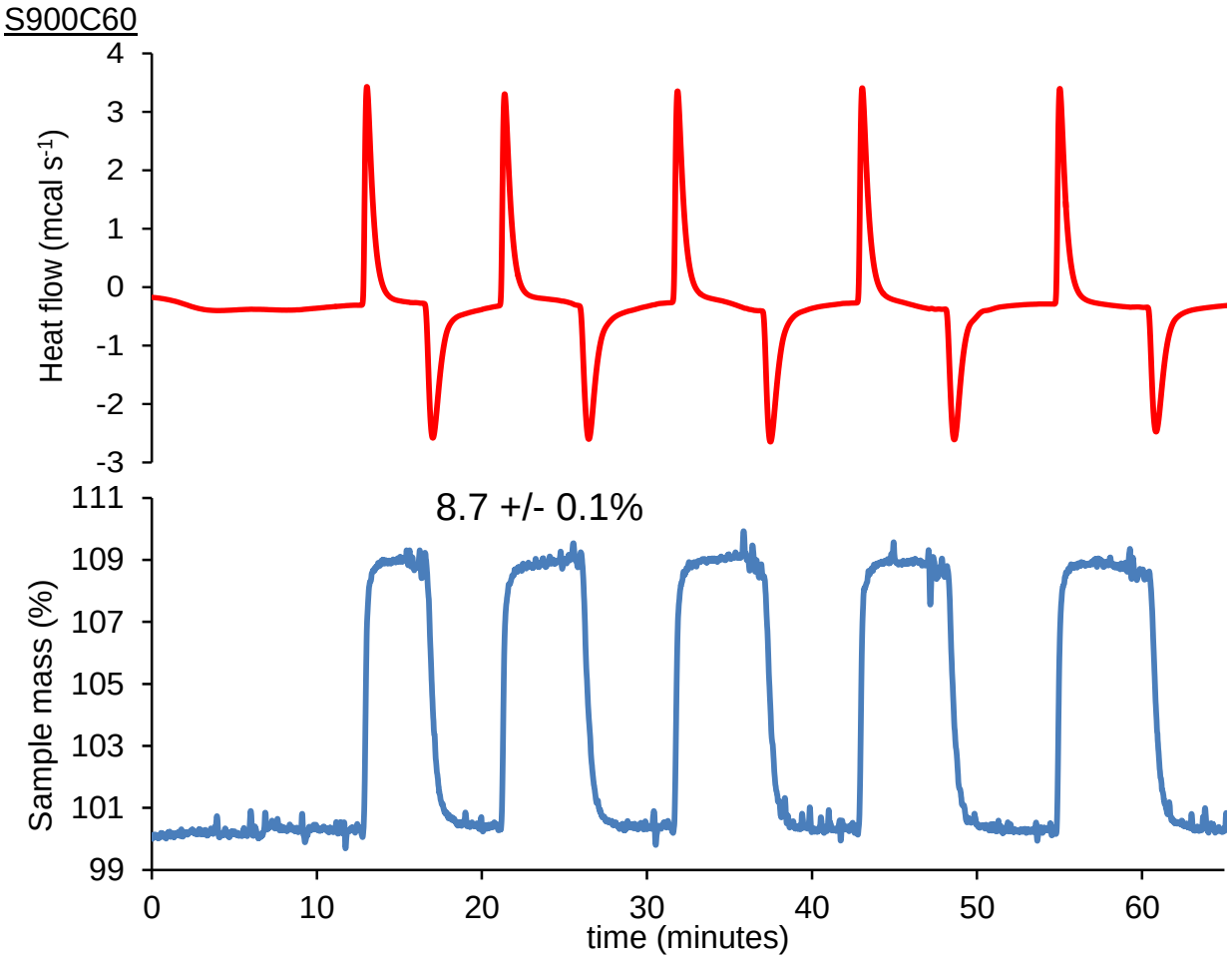
S900C60
Heat flow (mcal s-1)
4
3
2
1
0
-1
-2
-3
8.7 +/- 0.1%
Sample mass (%)
111
109
107
105
103
101
99
0
10
20
30
40
50
60
time (minutes)

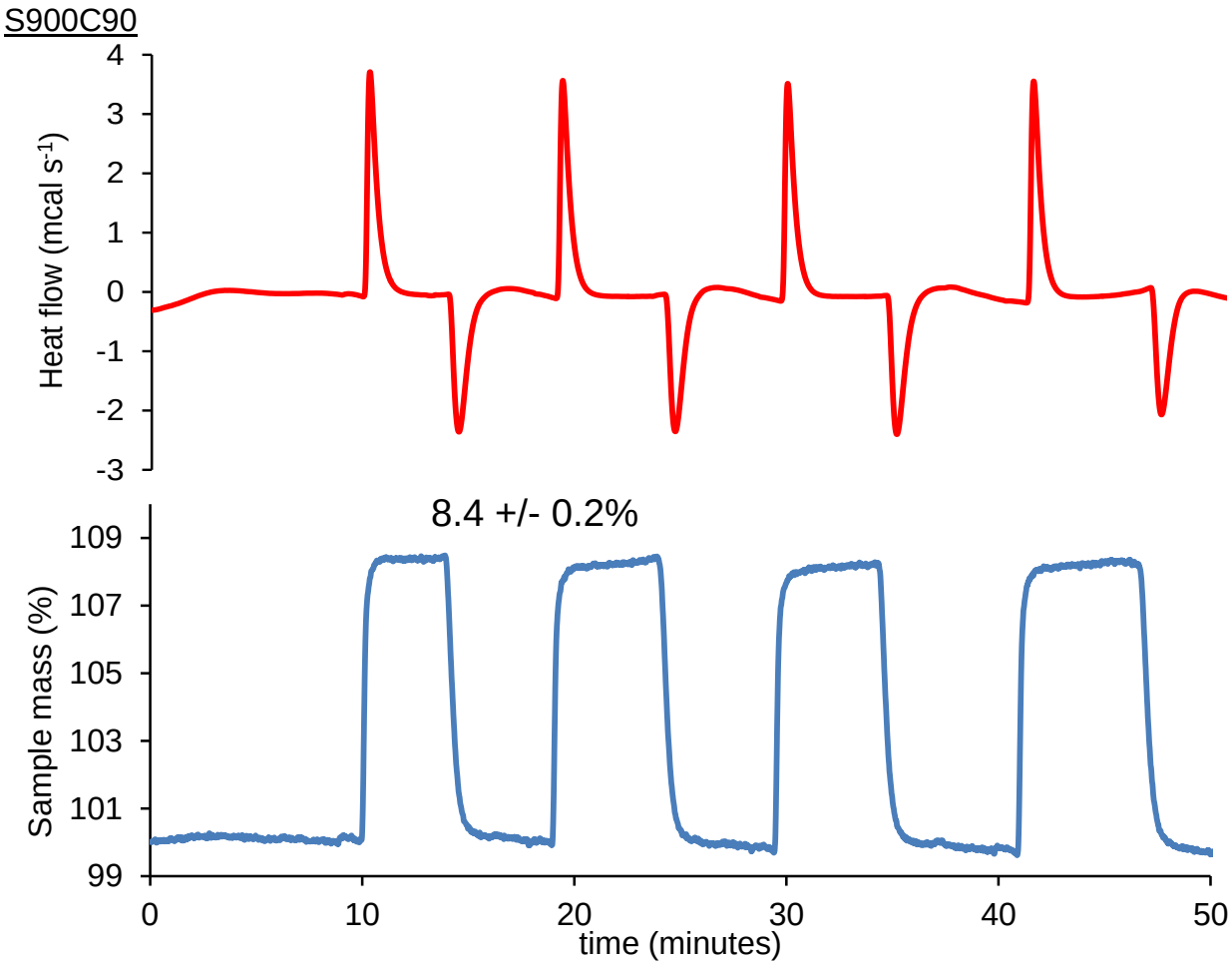
S900C90
Heat flow (mcal s-1)
4
3
2
1
0
-1
-2
-3
8.4 +/- 0.2%
Sample mass (%)
109
107
105
103
101
99
0
10
20
30
40
50
time (minutes)

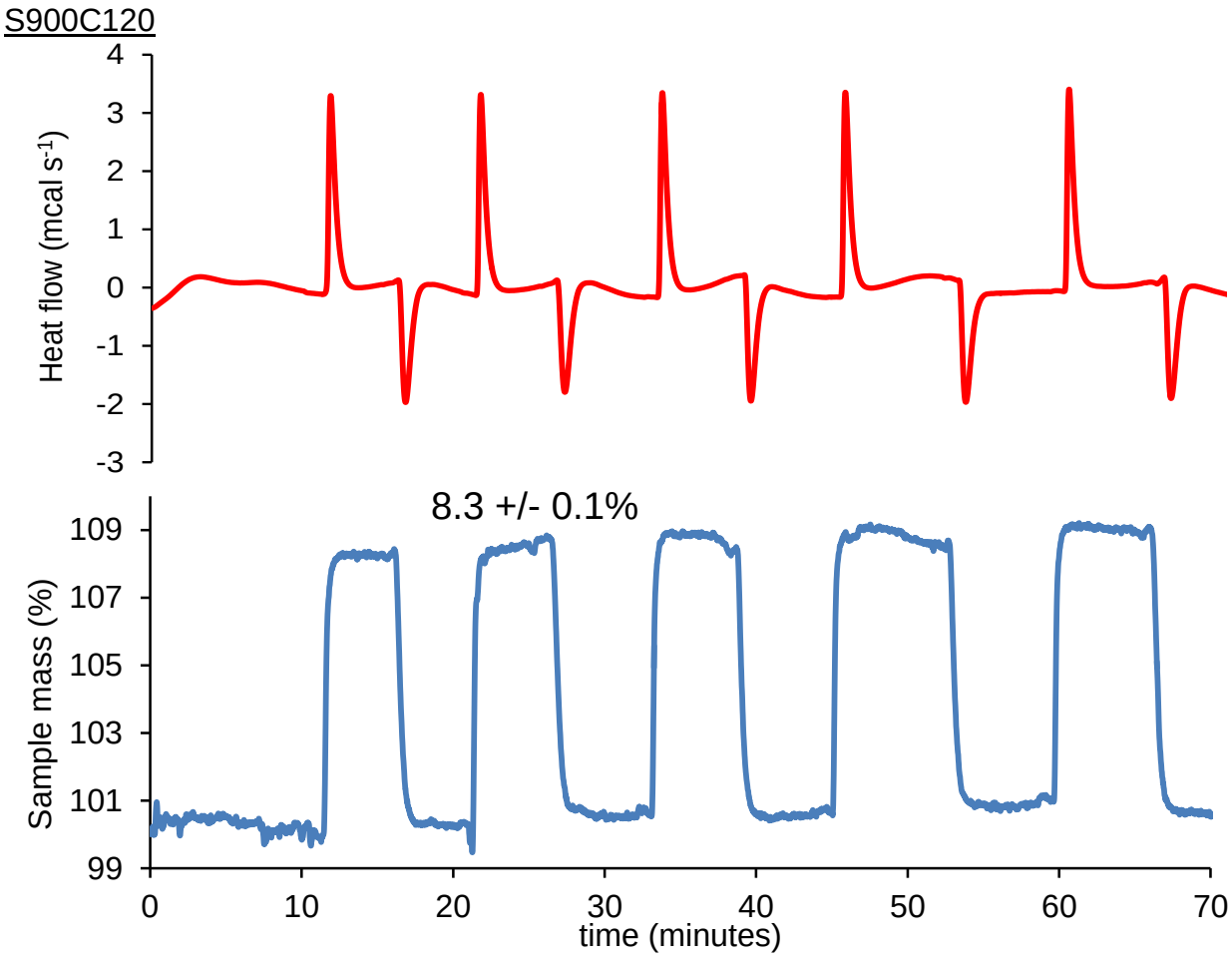
S900C120
Heat flow (mcal s-1)
4
3
2
1
0
-1
-2
-3
8.3 +/- 0.1%
Sample mass (%)
109
107
105
103
101
99
0
10
20
30
40
50
60
70
time (minutes)

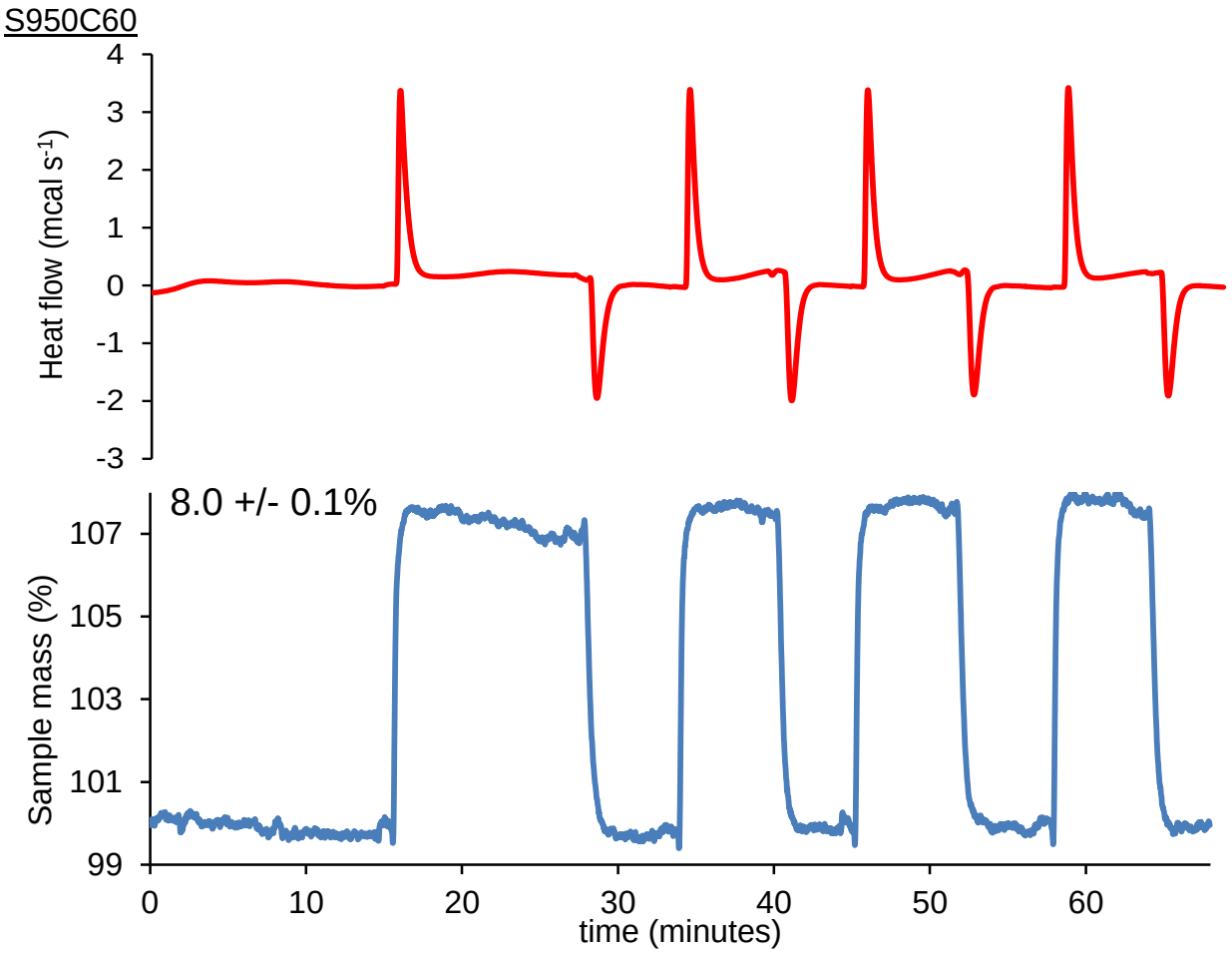
S950C60
Heat flow (mcal s-1)
4
3
2
1
0
-1
-2
-3
8.0 +/- 0.1%
Sample mass (%)
107
105
103
101
99
0
10
20
30
40
50
60
time (minutes)

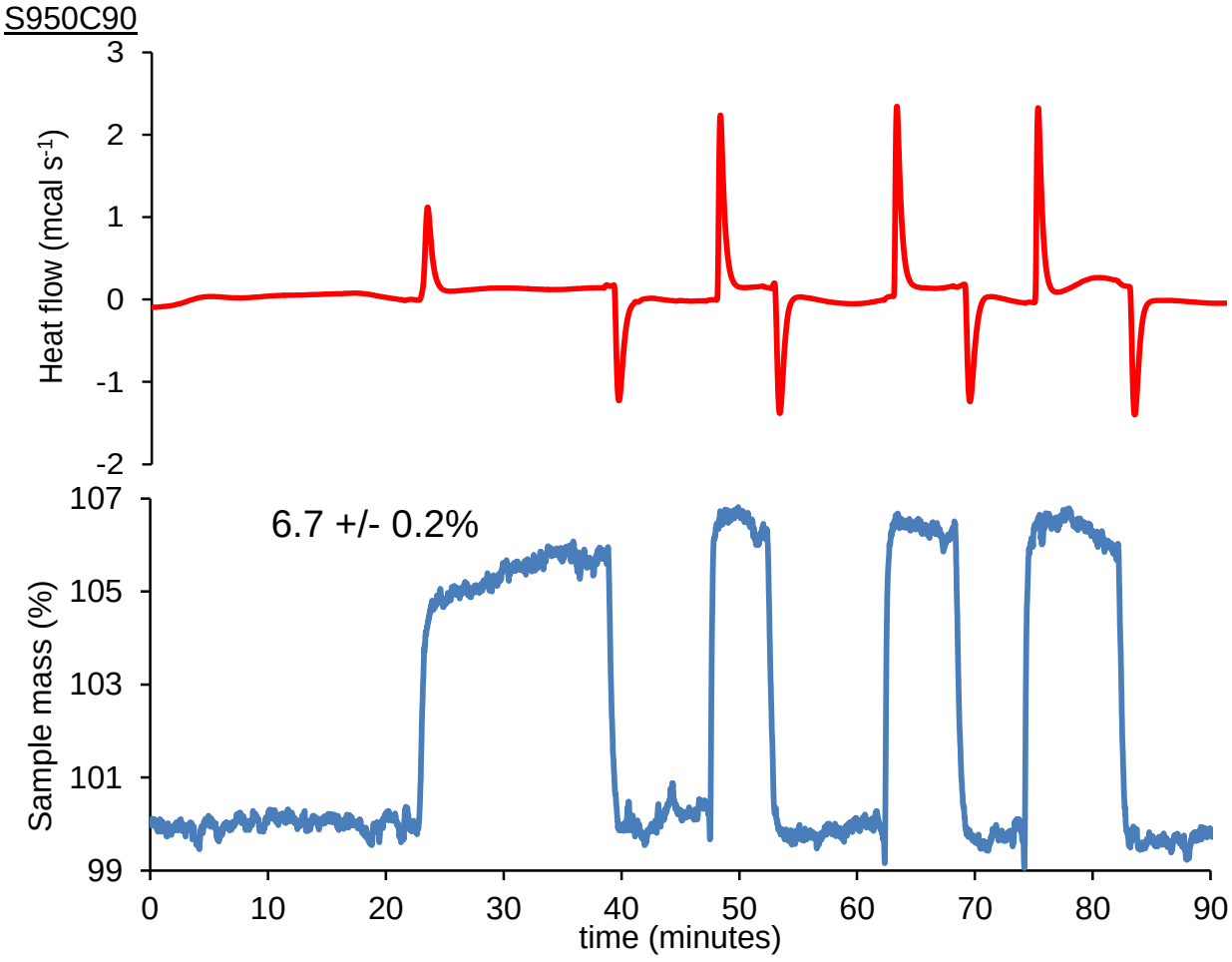
S950C90
Heat flow (mcal s-1)
3
2
1
0
-1
-2
6.7 +/- 0.2%
Sample mass (%)
107
105
103
101
99
0
10
20
30
40
50
60
70
80
90
time (minutes)

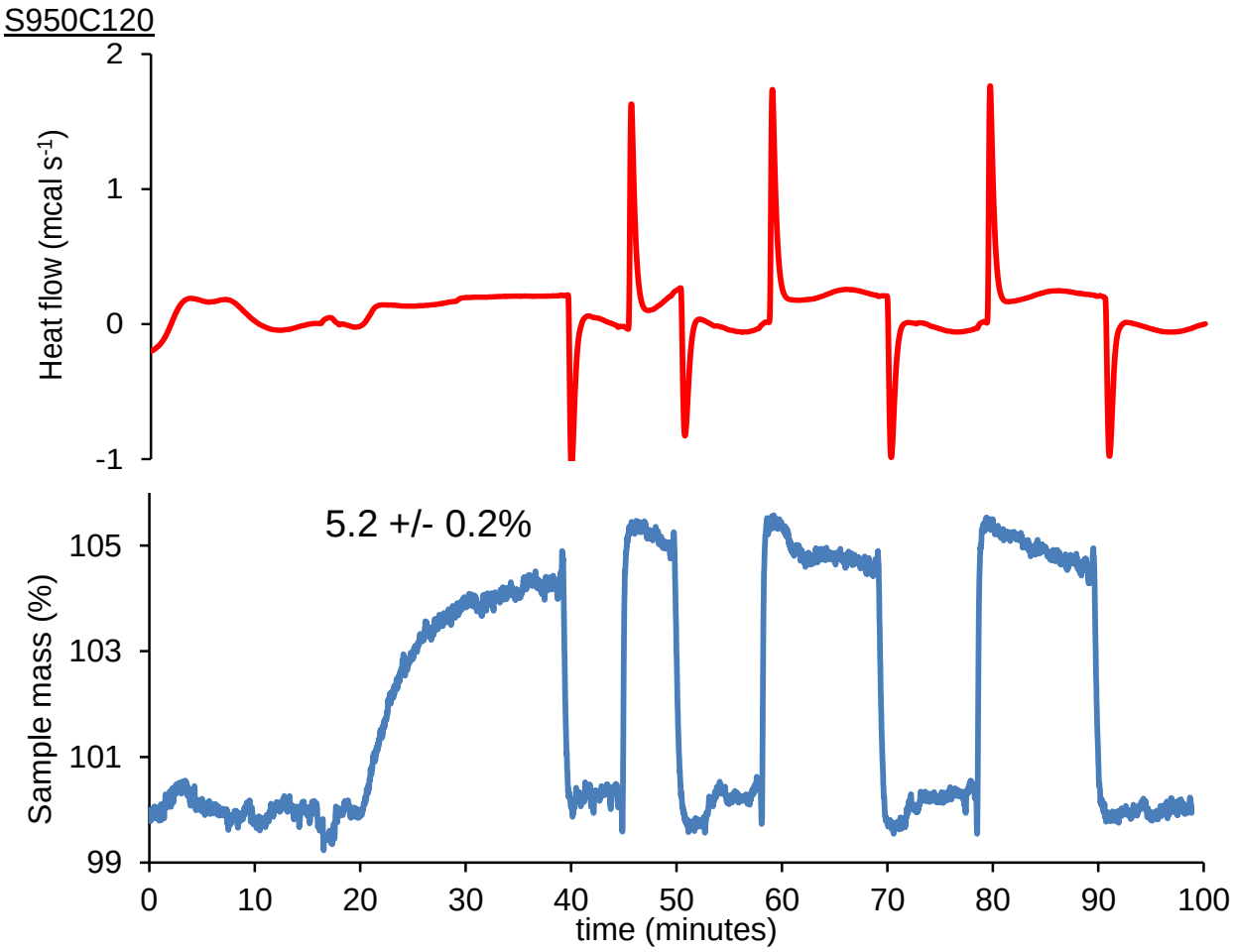
S950C120
Heat flow (mcal s-1)
2
1
0
-1
5.2 +/- 0.2%
Sample mass (%)
105
103
101
99
0
10
20
30
40
50
60
70
80
90
100
time (minutes)

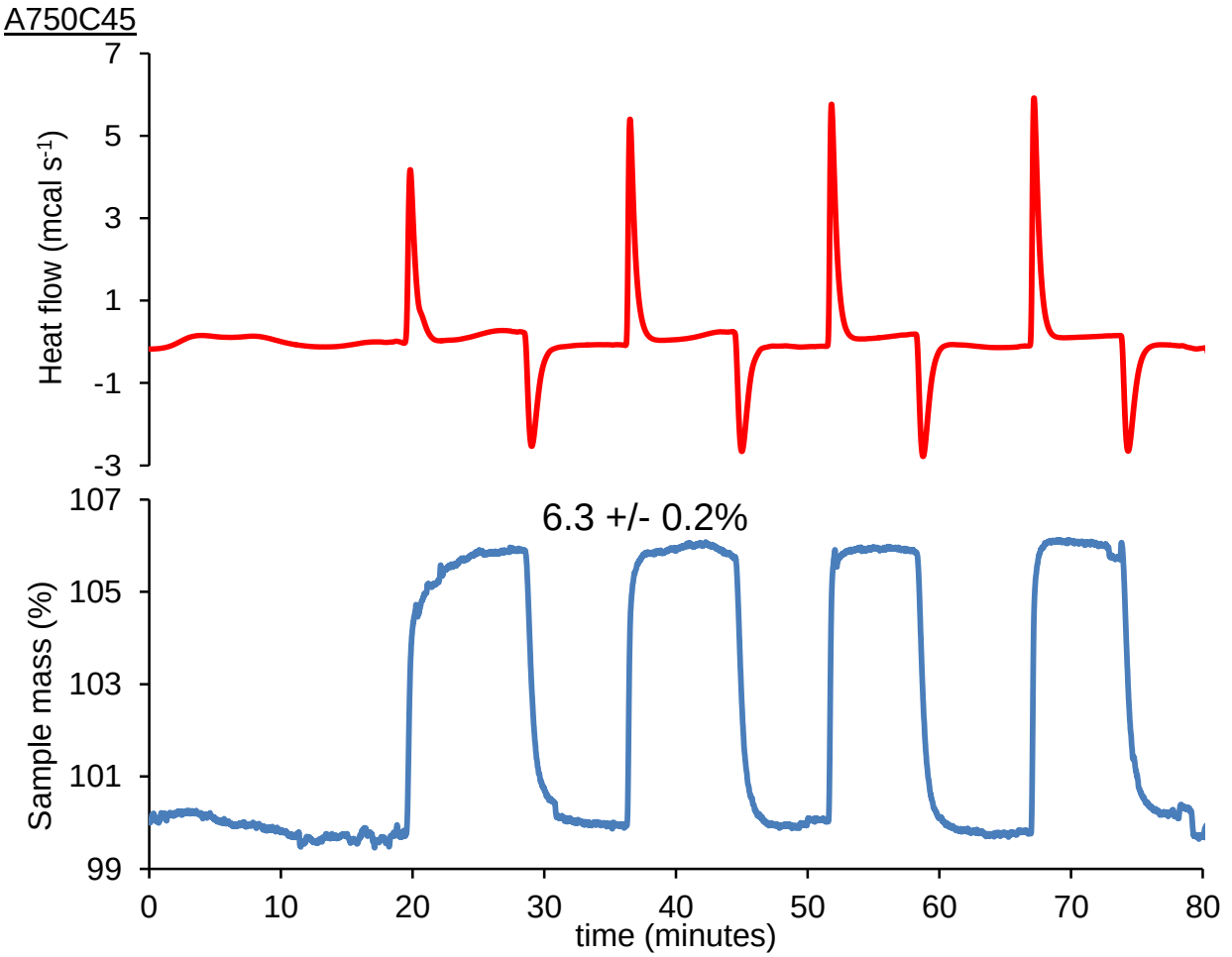
A750C45
Heat flow (mcal s-1)
7
5
3
1
-1
-3
6.3 +/- 0.2%
Sample mass (%)
107
105
103
101
99
0
10
20
30
40
50
60
70
80
time (minutes)

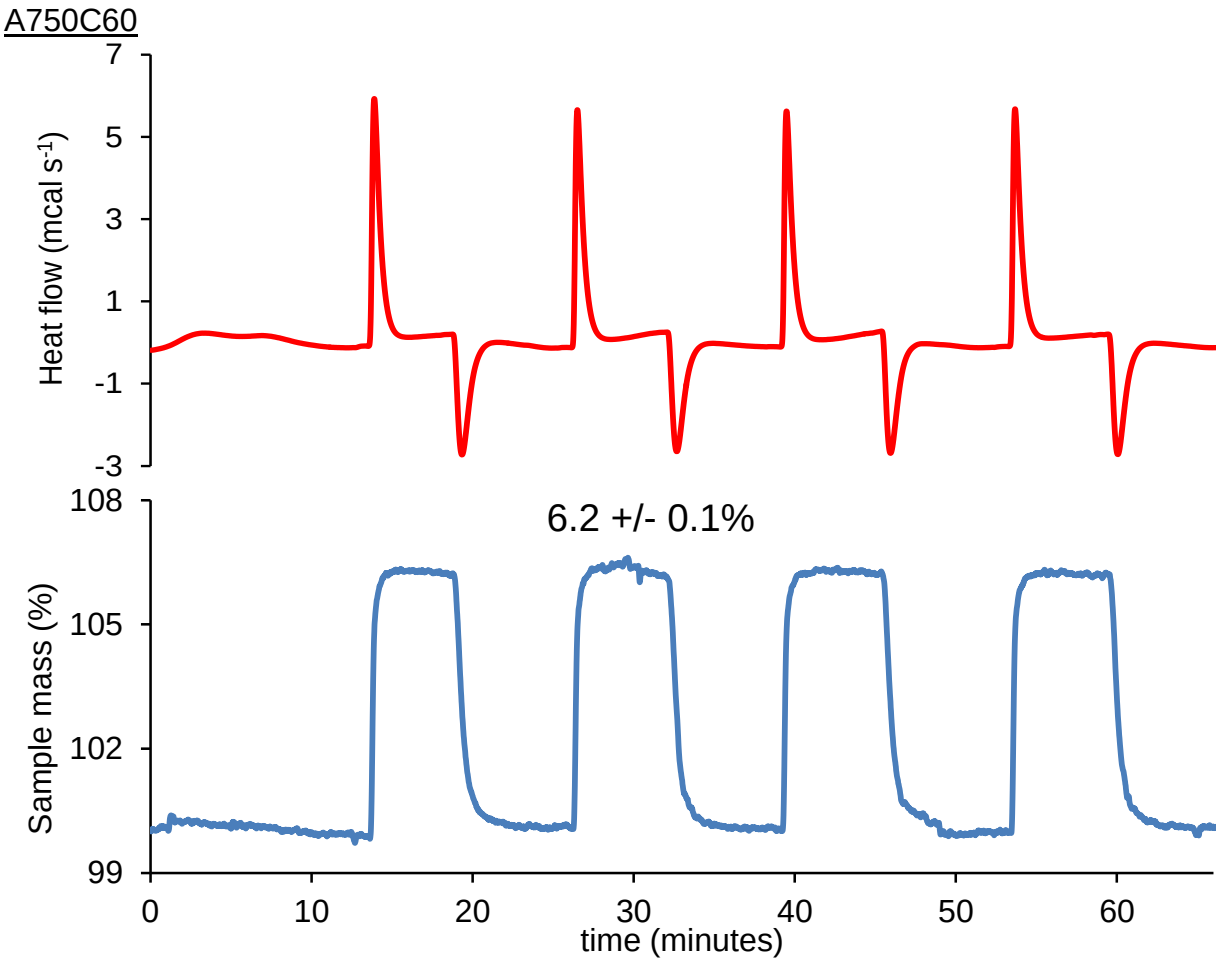
A750C60
Heat flow (mcal s-1)
7
5
3
1
-1
-3
Sample mass (%)
108
105
102
99
6.2 +/- 0.1%
0
10
20
30
40
50
60
time (minutes)

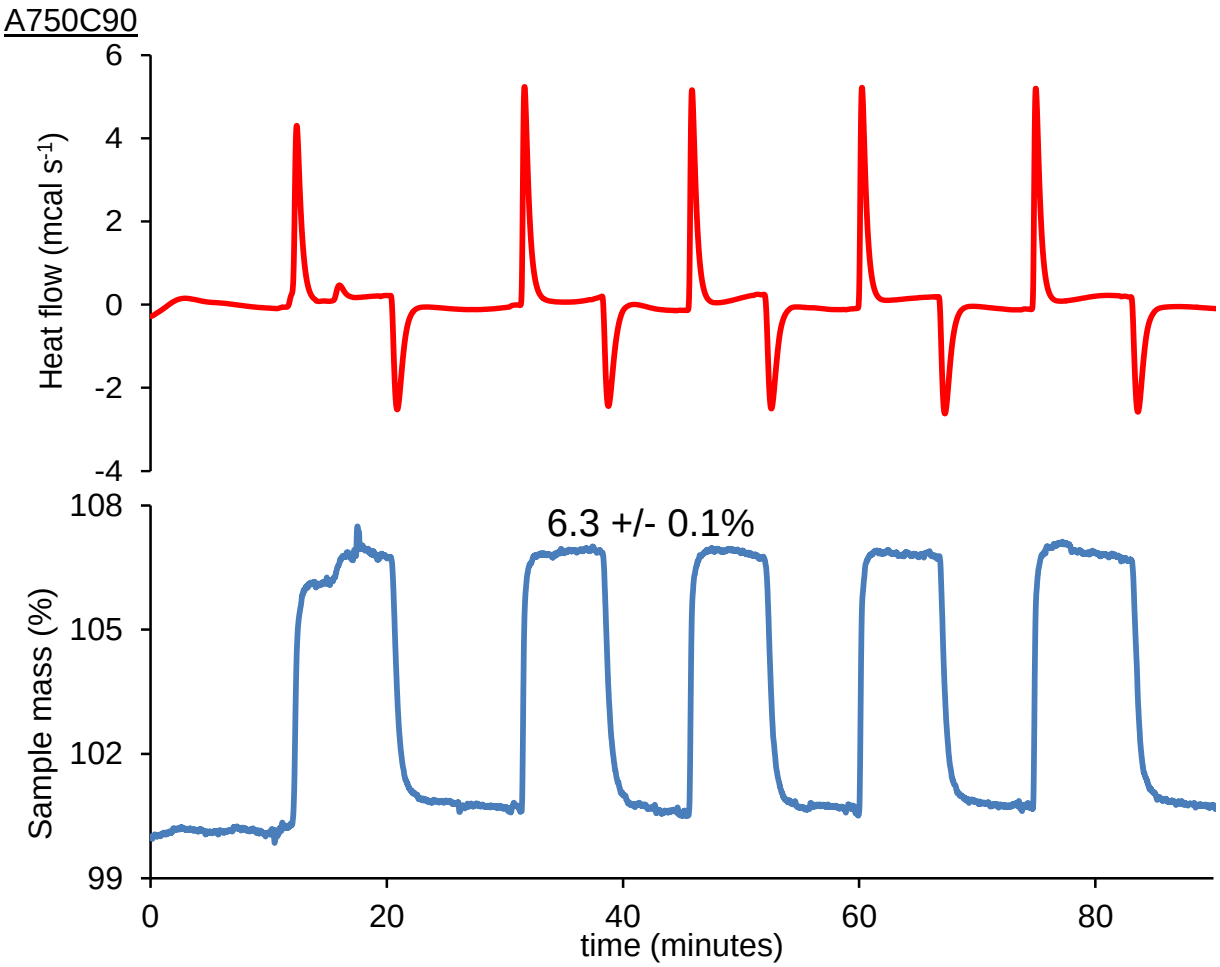
A750C90
Heat flow (mcal s-1)
6
4
2
0
-2
-4
Sample mass (%)
108
105
102
99
6.3 +/- 0.1%
0
20
40
60
80
time (minutes)

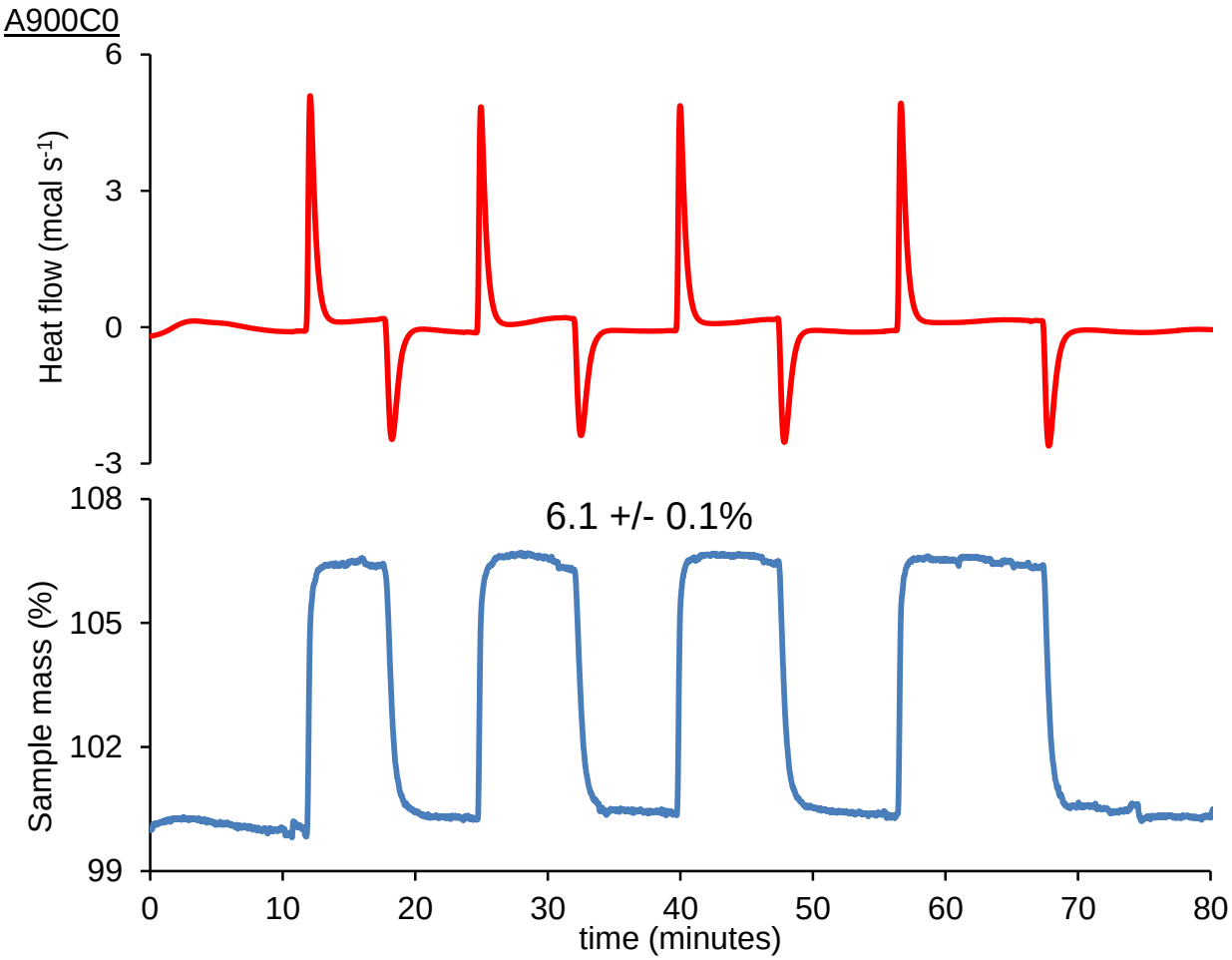
A900C0
Heat flow (mcal s-1)
6
3
0
-3
Sample mass (%)
108
105
102
99
6.1 +/- 0.1%
0
10
20
30
40
50
60
70
80
time (minutes)

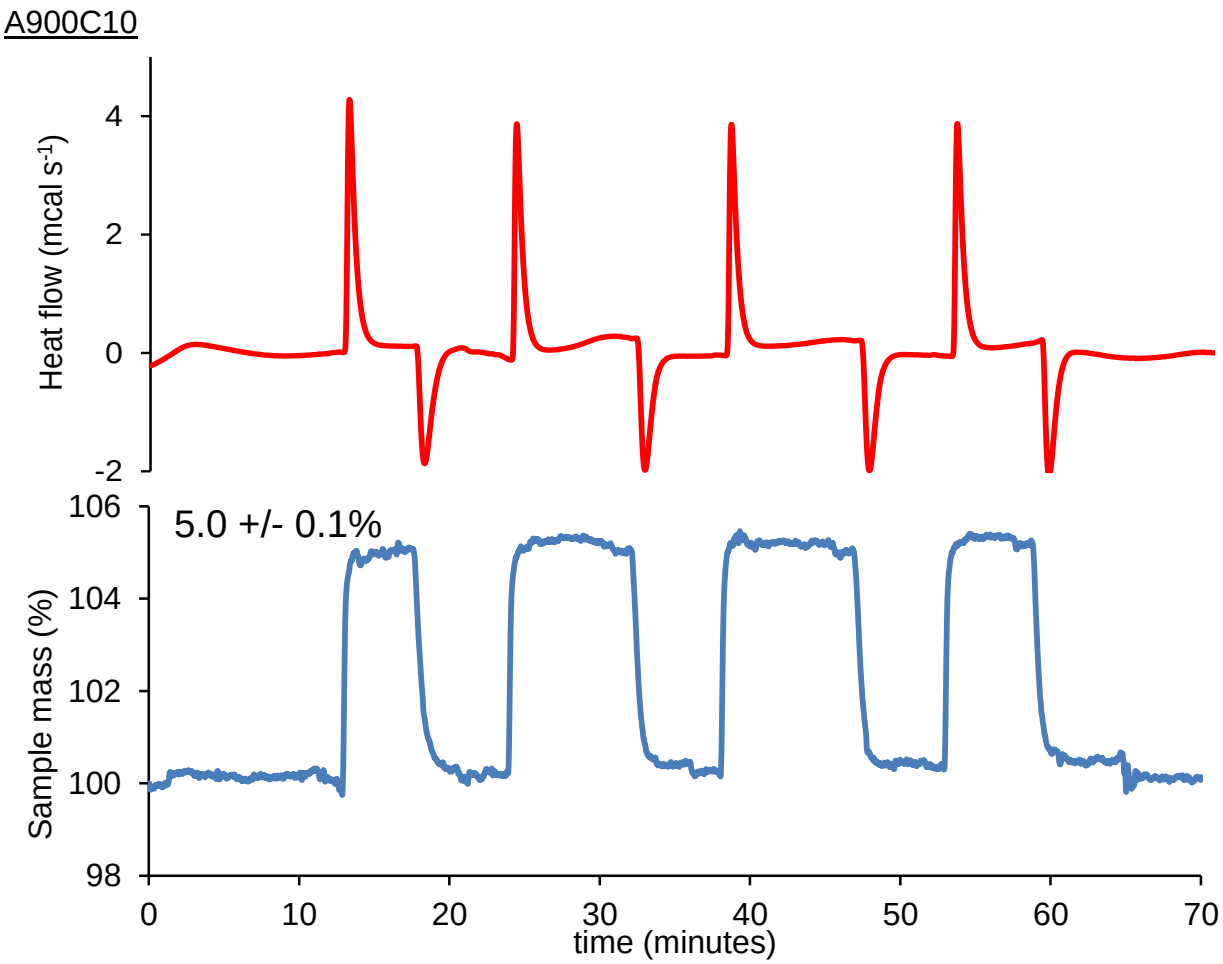
A900C10
Heat flow (mcal s-1)
4
2
0
-2
Sample mass (%)
106
104
102
100
98
5.0 +/- 0.1%
0
10
20
30
40
50
60
70
time (minutes)

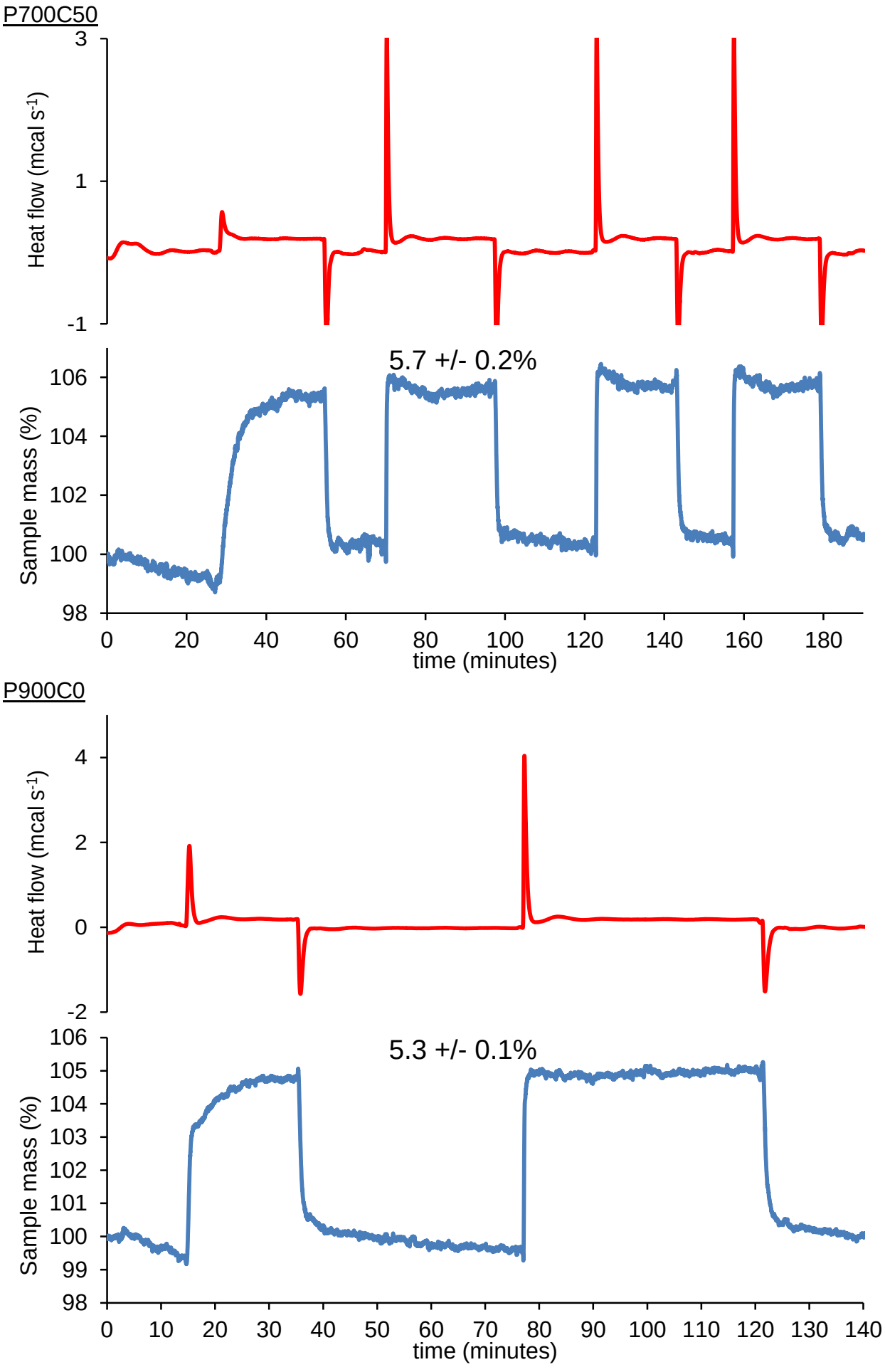
P700C50
Heat flow (mcal s-1)
3
1
-1
5.7 +/- 0.2%
Sample mass (%)
106
104
102
100
98
0
20
40
60
80
100
120
140
160
180
time (minutes)
P900C0
Heat flow (mcal s-1)
4
2
0
-2
5.3 +/- 0.1%
Sample mass (%)
106
105
104
103
102
101
100
99
98
0
10
20
30
40
50
60
70
80
90
100
110
120
130
140
time (minutes)

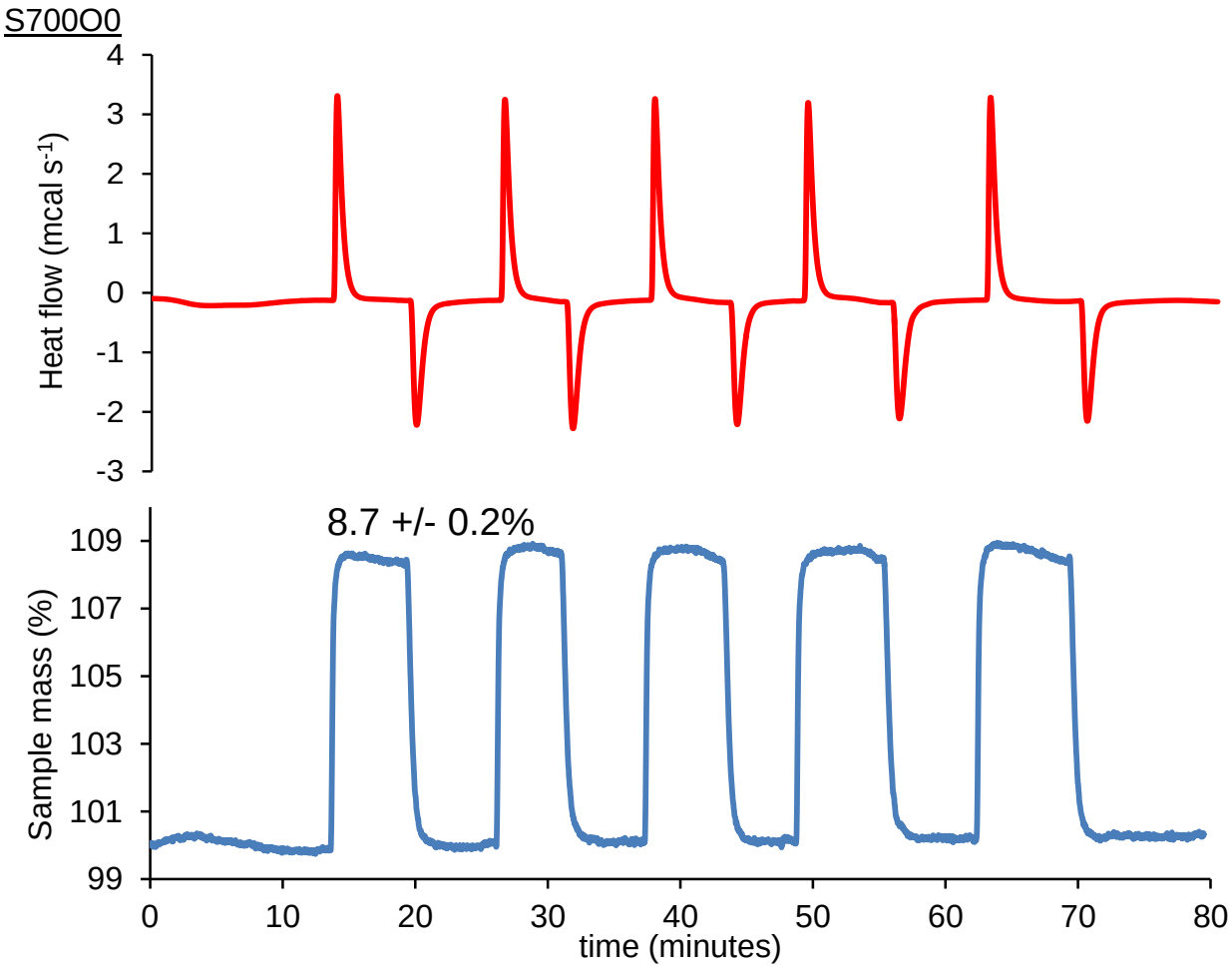
S700O0
Heat flow (mcal s-1)
4
3
2
1
0
-1
-2
-3
8.7 +/- 0.2%
Sample mass (%)
109
107
105
103
101
99
0
10
20
30
40
50
60
70
80
time (minutes)

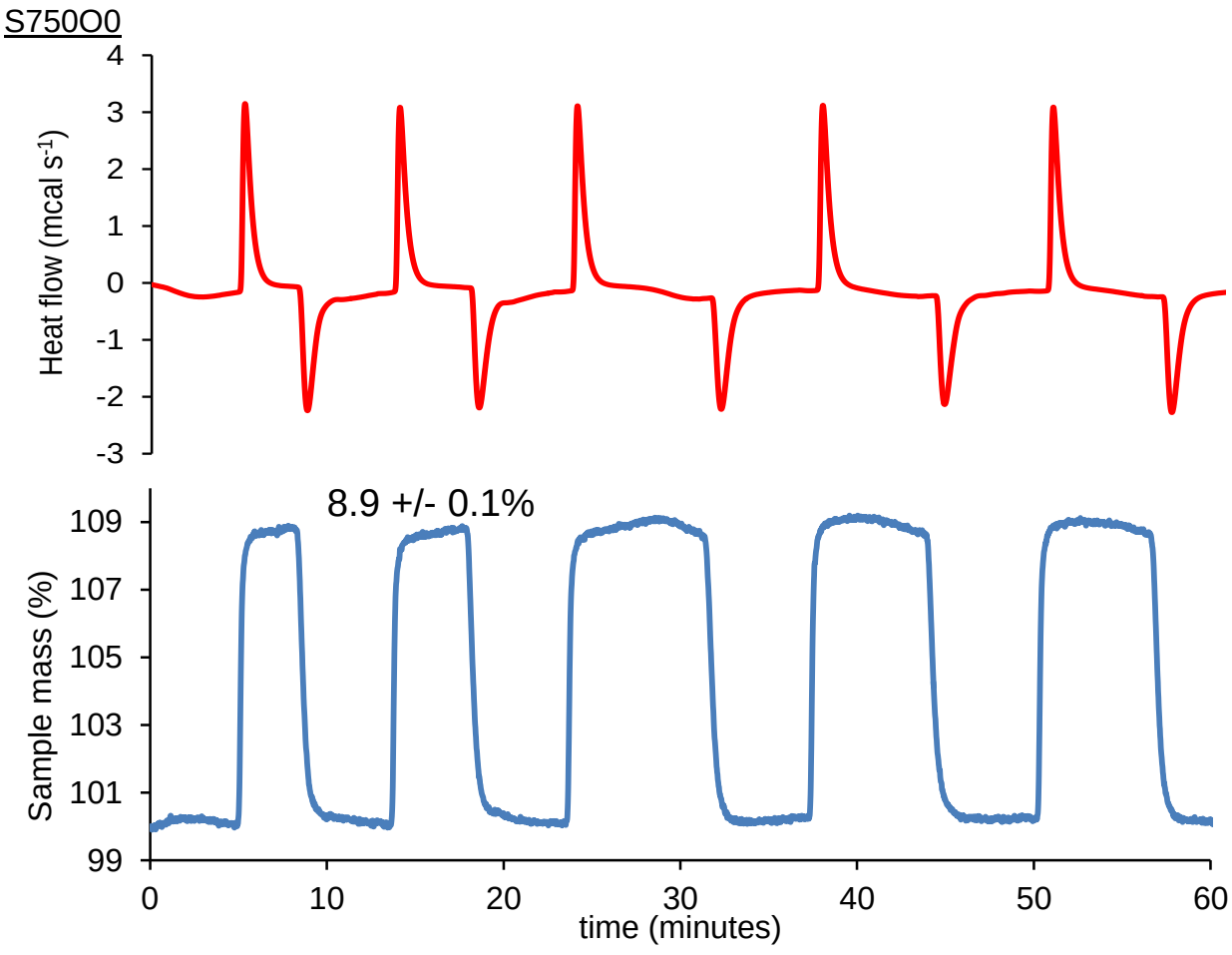
S750O0
Heat flow (mcal s-1)
4
3
2
1
0
-1
-2
-3
8.9 +/- 0.1%
Sample mass (%)
109
107
105
103
101
99
0
10
20
30
40
50
60
time (minutes)

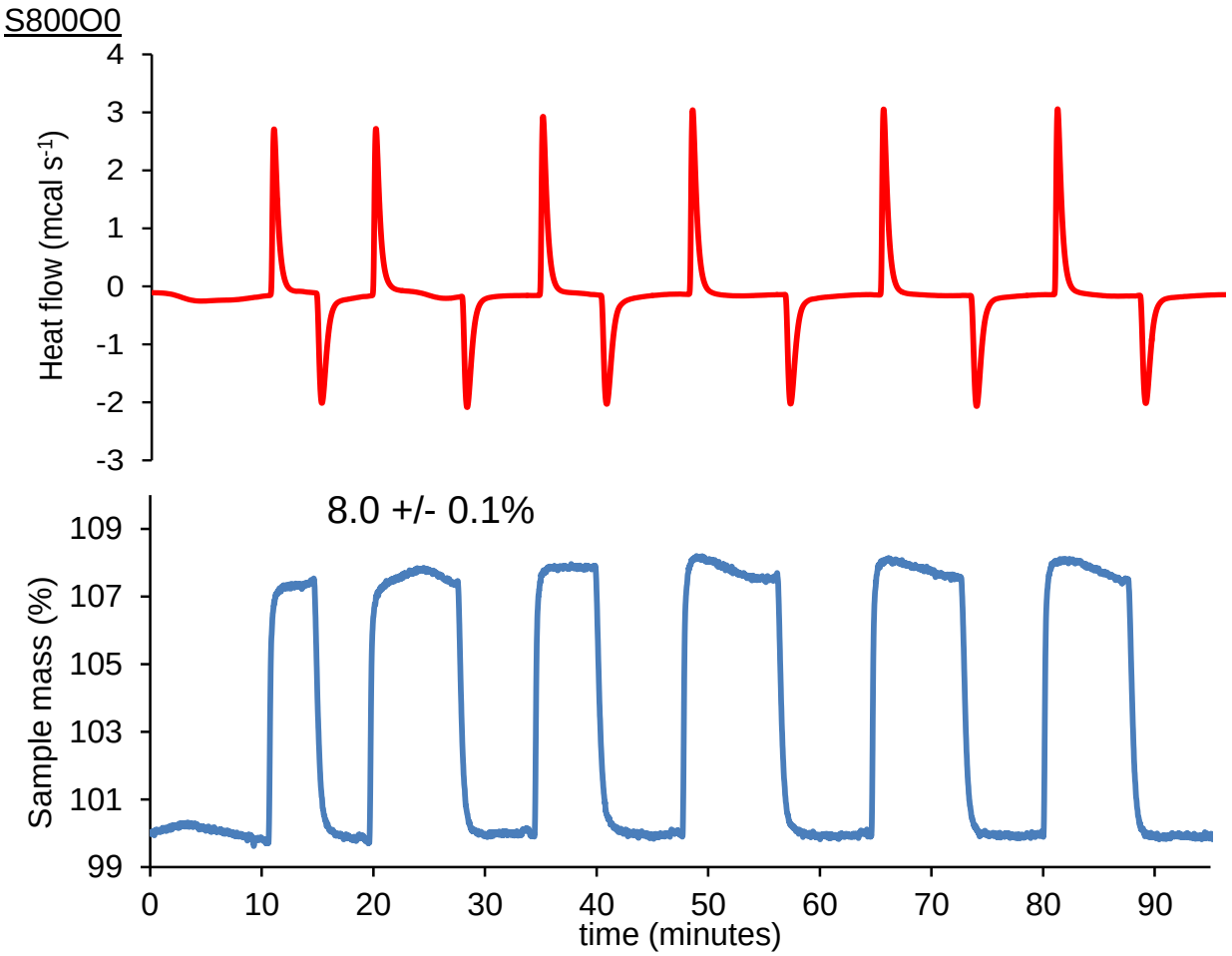
S800O0
Heat flow (mcal s-1)
4
3
2
1
0
-1
-2
-3
8.0 +/- 0.1%
Sample mass (%)
109
107
105
103
101
99
0
10
20
30
40
50
60
70
80
90
time (minutes)

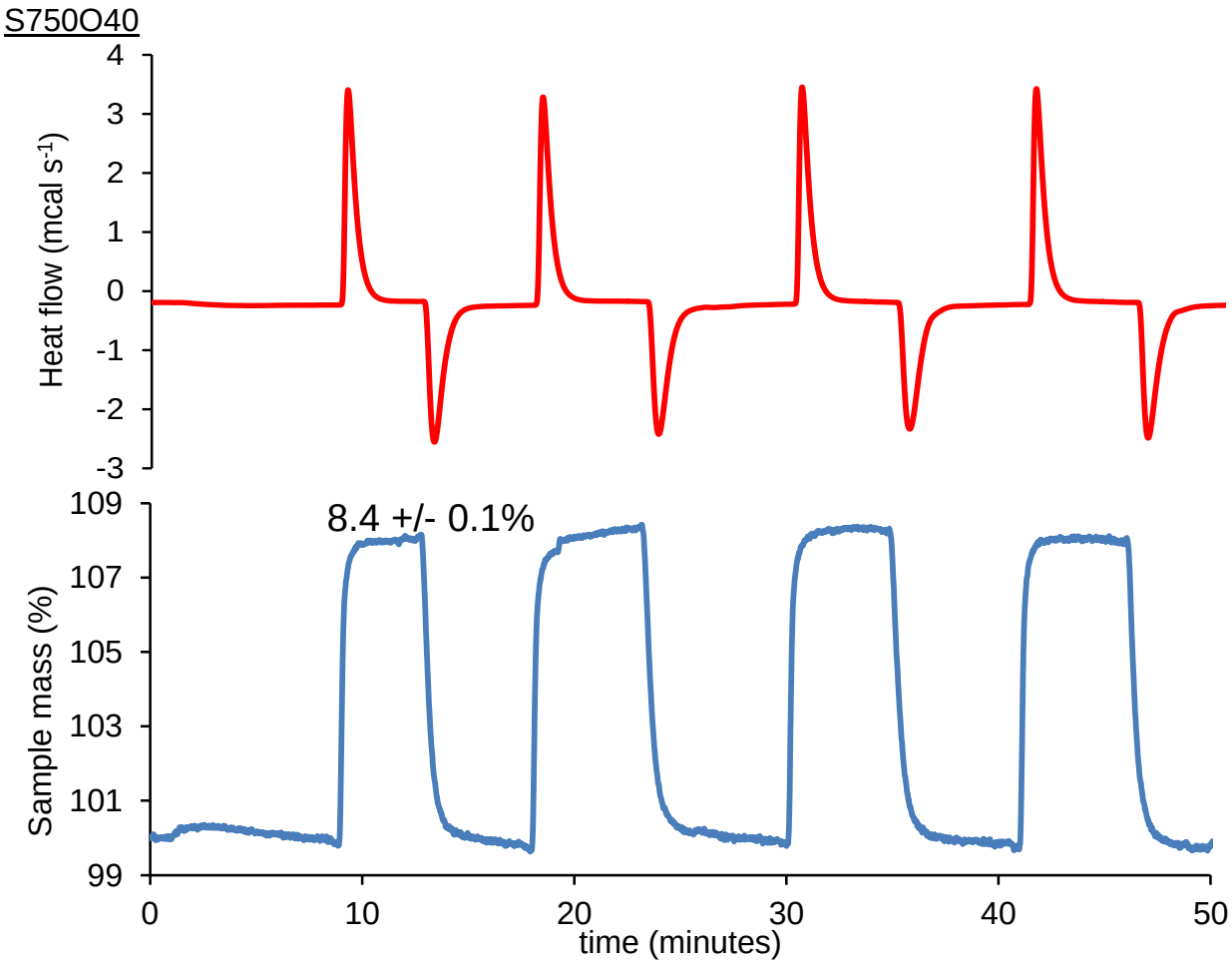
S750O40
Heat flow (mcal s-1)
4
3
2
1
0
-1
-2
-3
8.4 +/- 0.1%
Sample mass (%)
109
107
105
103
101
99
0
10
20
30
40
50
time (minutes)

S750O56

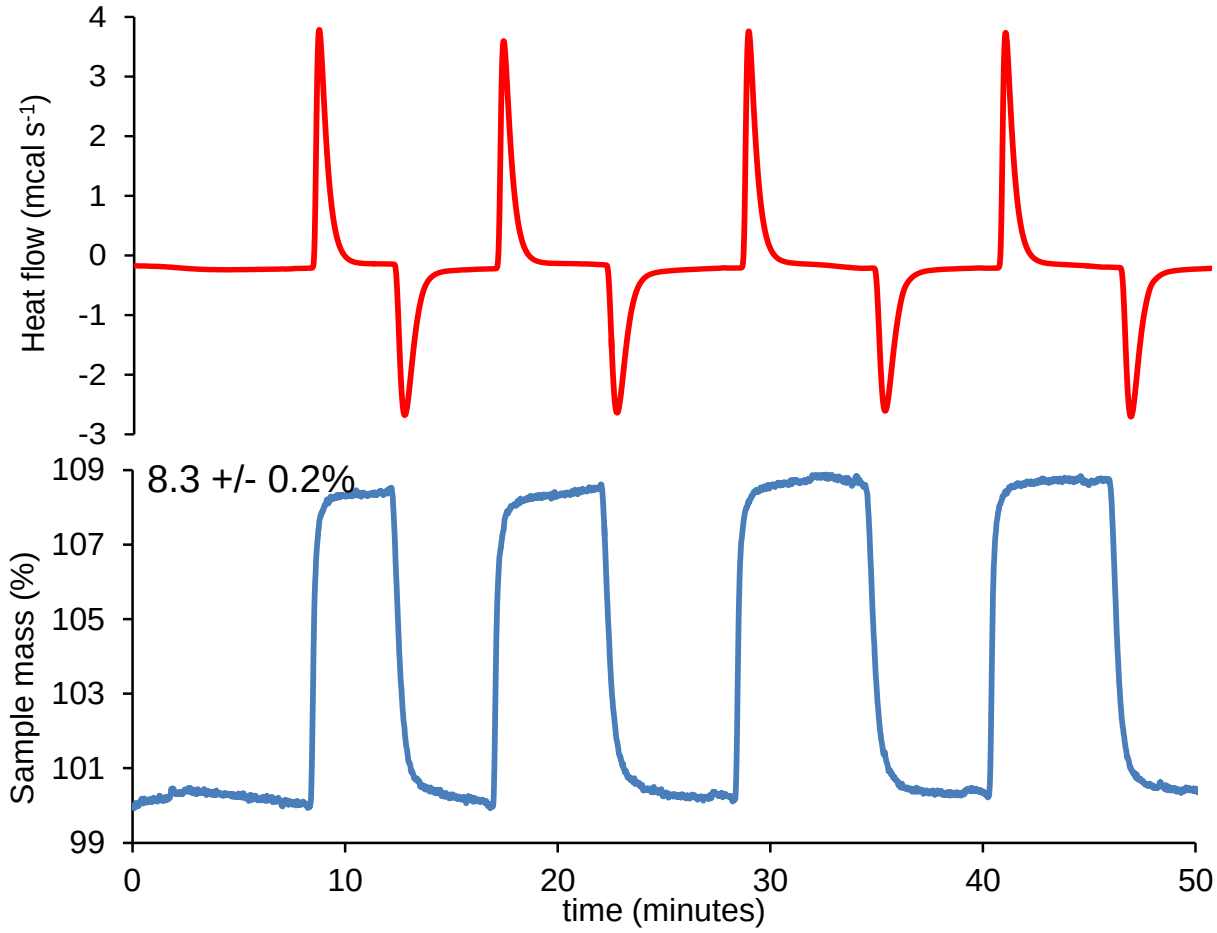

A500O30

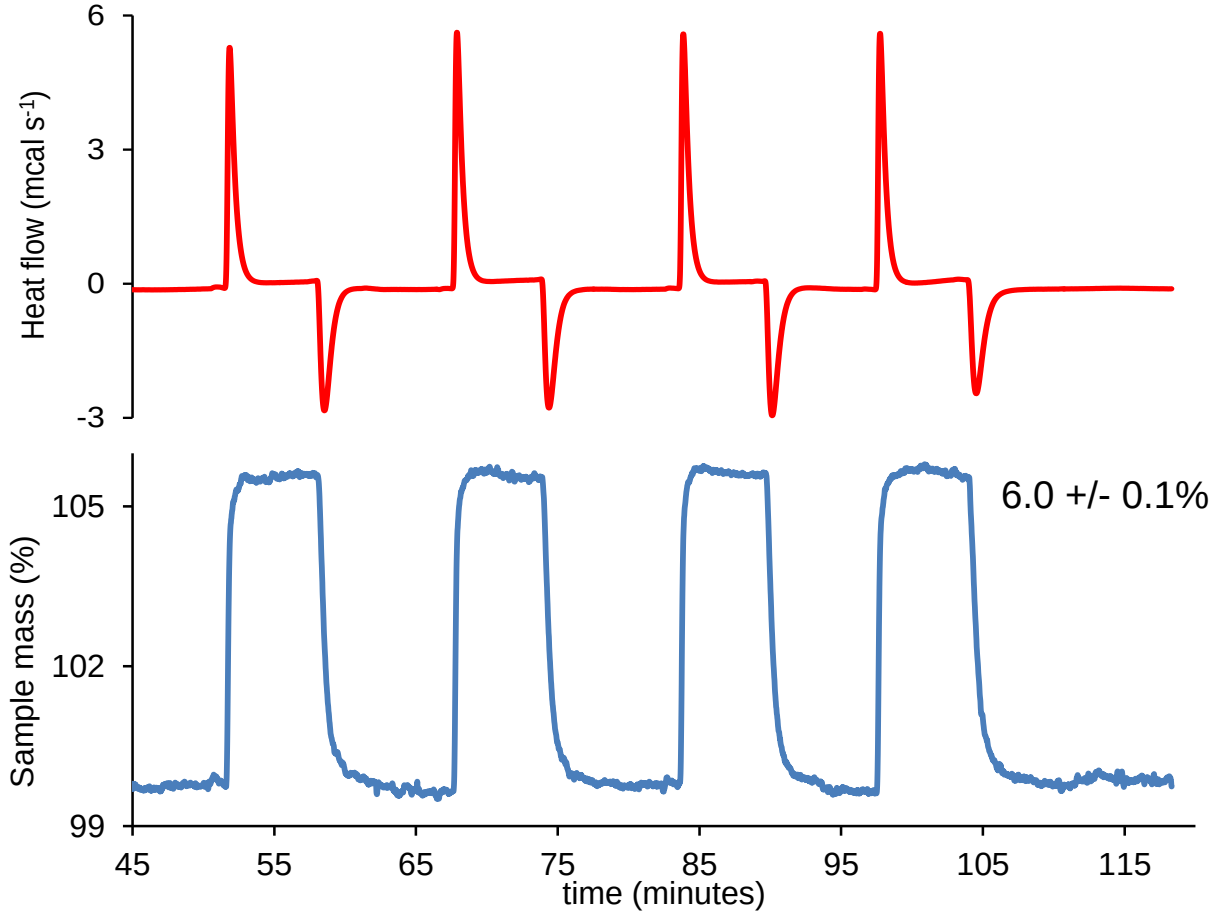

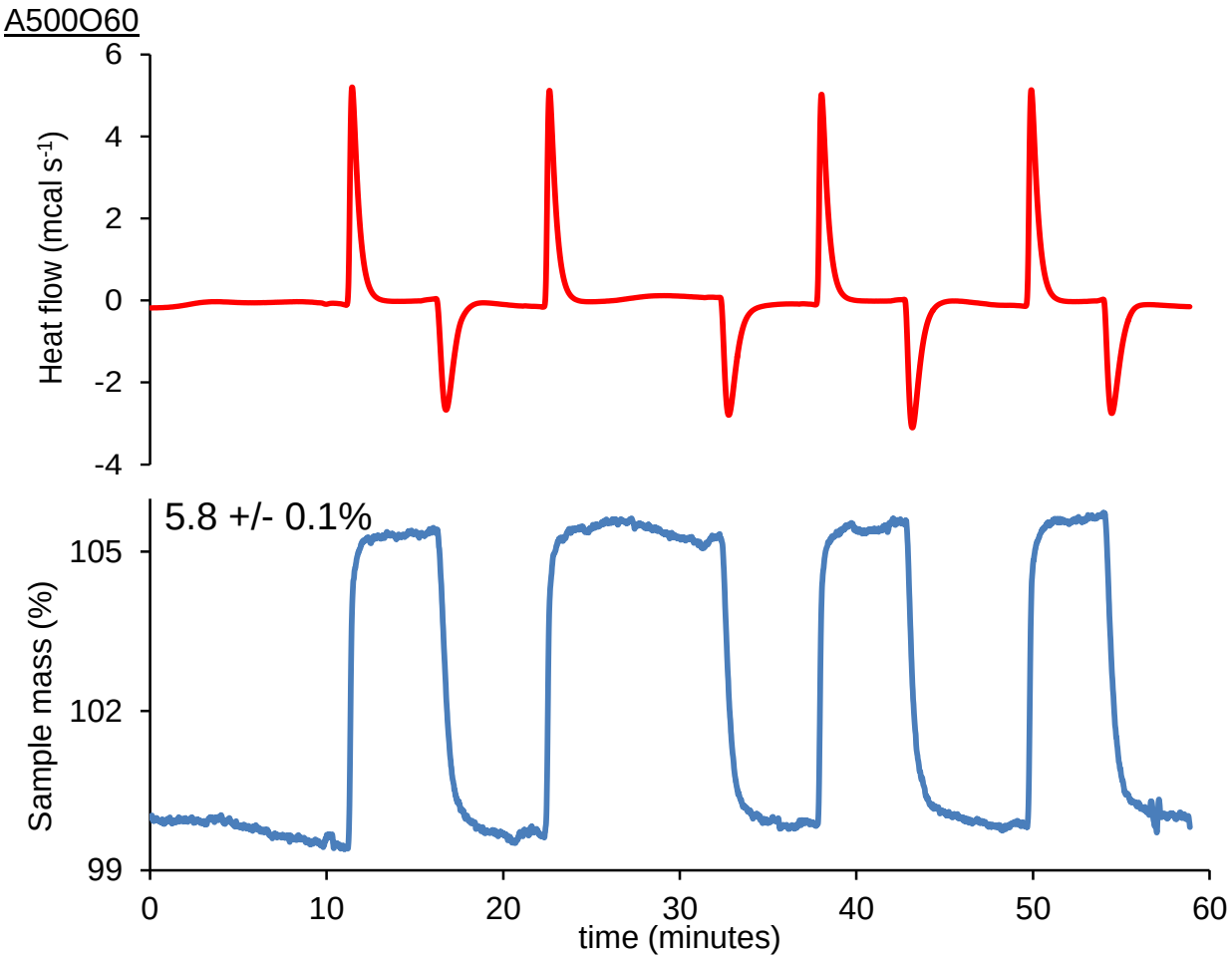
A500O60
Heat flow (mcal s-1)
6
4
2
0
-2
-4
5.8 +/- 0.1%
Sample mass (%)
105
102
99
0
10
20
30
40
50
60
time (minutes)

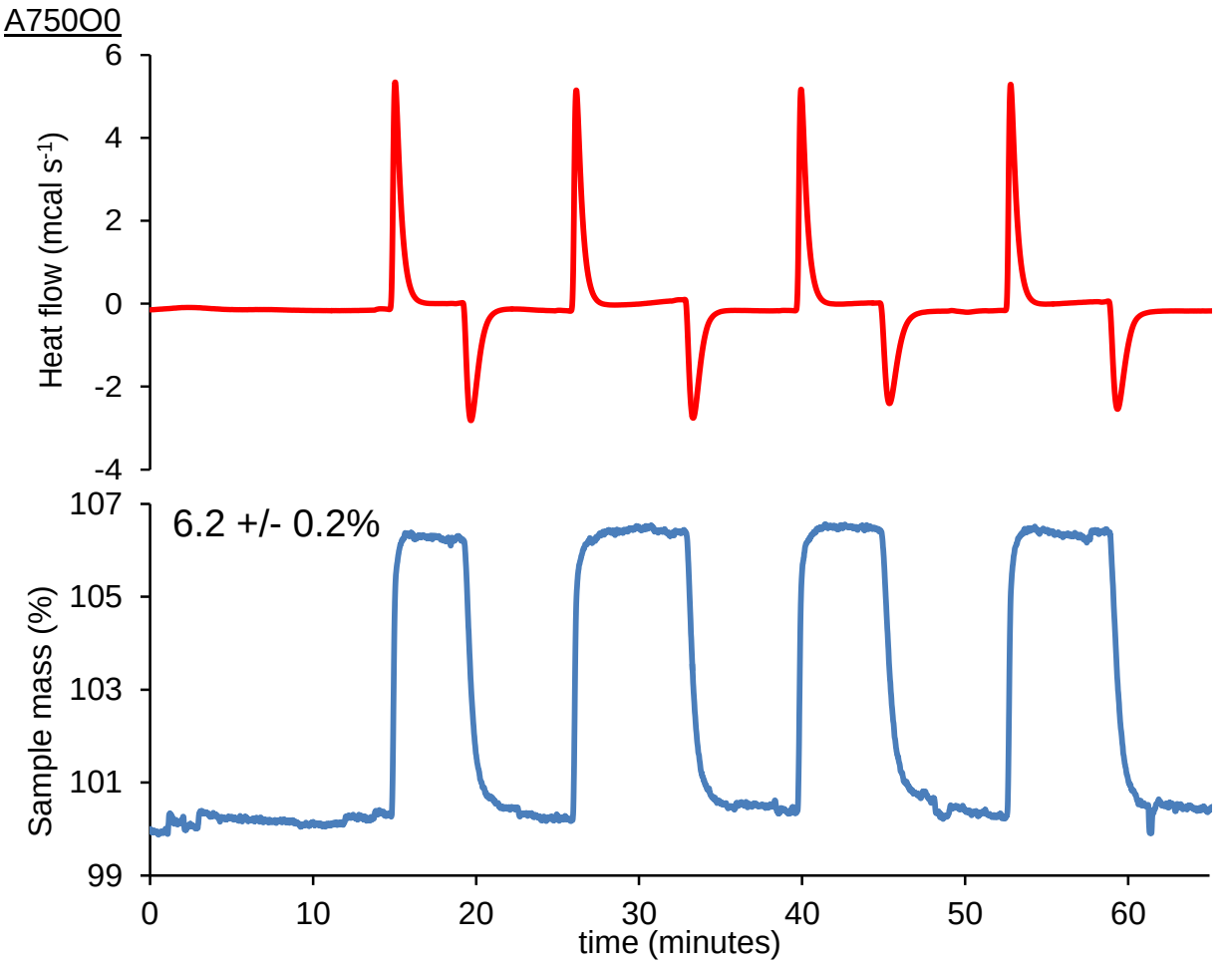
A750O0
Heat flow (mcal s-1)
6
4
2
0
-2
-4
6.2 +/- 0.2%
Sample mass (%)
107
105
103
101
99
0
10
20
30
40
50
60
time (minutes)

P400O50

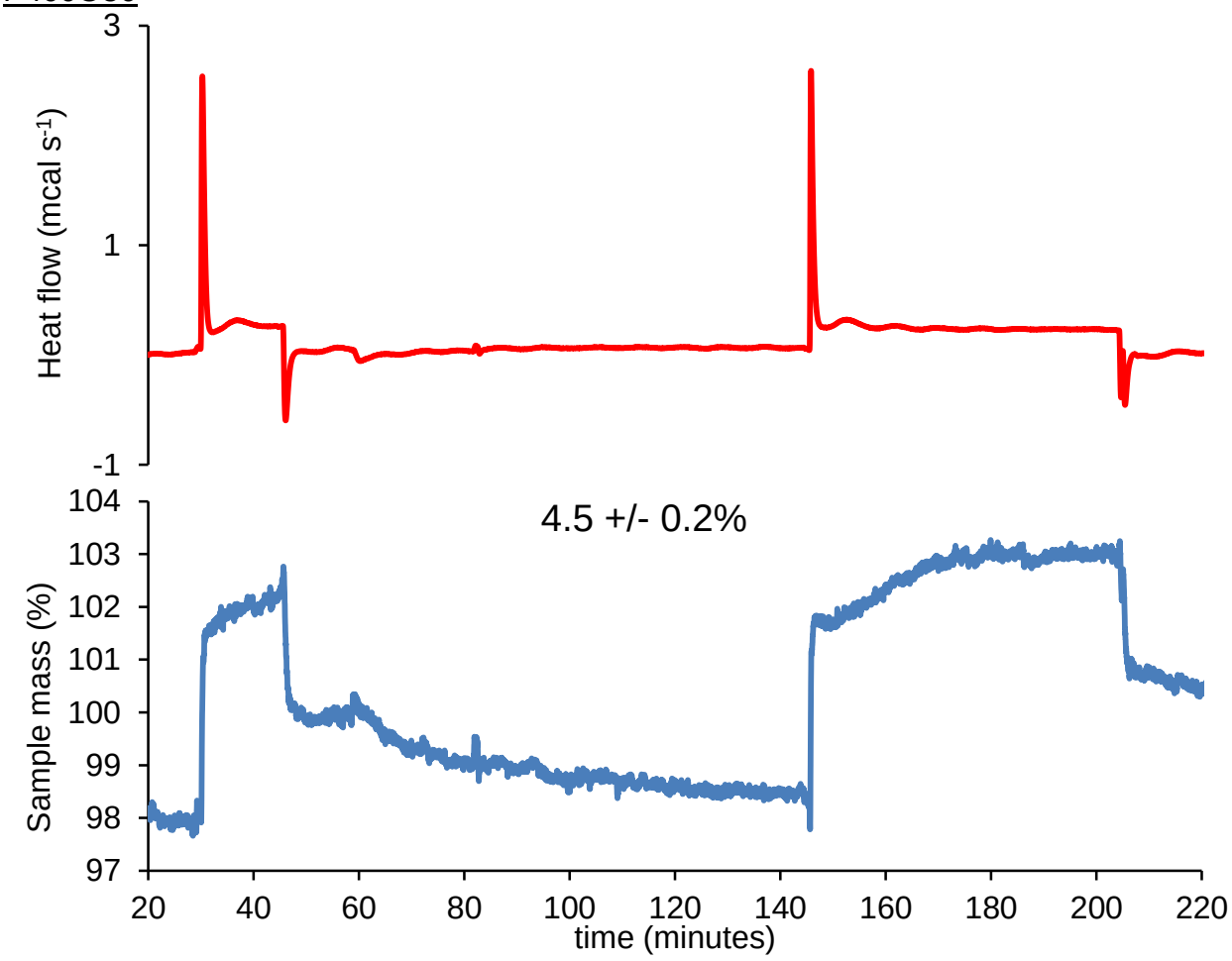
Heat flow (mcal s-1)
3
1
-1
4.5 +/- 0.2%
Sample mass (%)
104
103
102
101
100
99
98
97
20
40
60
80
100
120
140
160
180
200
220
time (minutes)

CO_2 adsorption capacities and heats of CO_2 adsorption at 35 ^oC

Entry	Material	CO_2 uptake (%)[a]	CO_2 uptake (mmol g^{-1})[a]	ΔH_{ads} (KJ mol^{-1})[a]
1	AC[b,c]	1.8 ± 0.4	0.41 ± 0.09	-27.3 ± 0.5
2	S800SE[c]	4.4 ± 0.3	1.00 ± 0.07	-22.7 ± 0.7
3	A800SE[c]	3.4 ± 0.3	0.77 ± 0.07	-27.2 ± 2.4
4	S300	2.1 ± 0.1	0.48 ± 0.02	-40.2 ± 4.8
5	S600	4.7 ± 0.2	1.07 ± 0.05	-42.4 ± 1.3
6	S800	7.0 ± 0.1	1.59 ± 0.02	-35.3 ± 1.9
7	S1000	4.8 ± 0.1	1.09 ± 0.02	-38.3 ± 1.7
8	A800	6.0 ± 0.1	1.36 ± 0.02	-48.6 ± 2.8
9	P800	4.7 ± 0.1	1.07 ± 0.02	-52.9 ± 1.3
10	S800K1	10.5 ± 0.2	2.39 ± 0.05	-31.7 ± 0.7
11	S800K2	13.7 ± 0.2	3.11 ± 0.05	-33.6 ± 0.8
12	S800K3	12.9 ± 0.2	2.93 ± 0.05	-32.7 ± 0.5
13	S800K4	9.4 ± 0.2	2.14 ± 0.05	-30.9 ± 0.4
14	S800K5	9.1 ± 0.3	2.07 ± 0.07	-26.7 ± 1.0
15	S600K4	8.9 ± 0.1	2.02 ± 0.02	-29.1 ± 0.3
16	S1000K4	4.9 ± 0.2	1.11 ± 0.05	-34.5 ± 0.8
17	A800K1	8.7 ± 0.1	1.98 ± 0.02	-38.0 ± 1.1
18	A800K2	13.0 ± 0.1	2.95 ± 0.02	-38.6 ± 0.9
19	A800K3	12.4 ± 0.1	2.82 ± 0.02	-36.1 ± 0.9
20	A800K4	9.9 ± 0.2	2.25 ± 0.05	-33.3 ± 1.5
21	A800K5	7.7 ± 0.2	1.75 ± 0.05	-38.2 ± 2.4
22	A600K2	6.3 ± 0.1	1.64 ± 0.02	-46.0 ± 2.5
23	A1000K2	9.5 ± 0.1	2.16 ± 0.02	-38.5 ± 1.1
24	P800K2	10.5 ± 0.1	2.39 ± 0.02	-36.9 ± 0.4
25	P800K3	9.1 ± 0.1	2.07 ± 0.02	-35.1 ± 0.3
26	P800K5	5.5 ± 0.1	1.25 ± 0.02	-37.6 ± 1.4
27	S800C15	7.2 ± 0.2	1.64 ± 0.05	-25.0 ± 5.1
28	S850C15	7.8 ± 0.1	1.77 ± 0.02	-36.3 ± 2.0
29	S900C15	8.7 ± 0.2	1.98 ± 0.05	-35.8 ± 0.4
30	S950C15	8.0 ± 0.1	1.82 ± 0.02	-34.9 ± 0.4
31	S1000C15	7.8 ± 0.3	1.77 ± 0.07	-40.2 ± 2.7
32	S900C30	7.8 ± 0.1	1.77 ± 0.02	-31.9 ± 1.0
33	S900C60	8.7 ± 0.1	1.98 ± 0.02	-36.4 ± 3.5
34	S900C90	8.4 ± 0.2	1.91 ± 0.05	-37.4 ± 2.7
35	S900C120	8.3 ± 0.1	1.89 ± 0.02	-35.9 ± 3.2
36	S950C60	8.0 ± 0.1	1.82 ± 0.02	-42.7 ± 2.9
37	S950C90	6.7 ± 0.2	1.52 ± 0.05	-46.7 ± 4.4
38	S950C120	5.2 ± 0.2	1.18 ± 0.05	-53.7 ± 4.7

Entry	Material	CO_2 uptake (%)	CO_2 uptake (mmol g^{-1})	ΔH_{ads} (KJ mol^{-1})
39	A750C45	6.3 ± 0.2	1.43 ± 0.05	-45.7 ± 2.0
40	A750C60	6.2 ± 0.1	1.41 ± 0.02	-47.5 ± 1.4
41	A750C90	6.3 ± 0.1	1.43 ± 0.02	-43.7 ± 1.8
42	A900C0	6.1 ± 0.1	1.39 ± 0.02	-46.4 ± 2.0
43	A900C10	5.0 ± 0.1	1.14 ± 0.02	-48.2 ± 4.5
44	P700C50	5.7 ± 0.1	1.30 ± 0.02	-68.5 ± 2.2
45	P900C0	5.3 ± 0.1	1.20 ± 0.02	-69.0 ± 7.1
46	S700O0	8.7 ± 0.2	1.98 ± 0.05	-32.2 ± 0.1
47	S750O0	8.9 ± 0.1	2.02 ± 0.02	-34.6 ± 0.9
48	S800O0	8.0 ± 0.1	1.82 ± 0.02	-30.0 ± 1.1
49	S750O40	8.4 ± 0.1	1.91 ± 0.02	-30.8 ± 0.5
50	S750O56	8.3 ± 0.2	1.89 ± 0.05	-36.7 ± 0.9
51	A500O30	6.0 ± 0.1	1.36 ± 0.02	-47.0 ± 1.4
52	A500O60	5.8 ± 0.1	1.32 ± 0.02	-46.3 ± 1.2
53	A750O0	6.2 ± 0.2	1.41 ± 0.05	-30.6 ± 1.4
54	P400O50	4.5 ± 0.2	1.02 ± 0.05	-73.5 ± 1.0

a) Measured at 1 bar pressure during gas composition swing between pure nitrogen and pure carbon dioxide. Each value is the mean ± one standard deviation. b) AC = Norit activated carbon. c) Materials prepared by the older solvent exchange method and data taken from: G. Dura, V. L. Budarin, J. A. Castro-Osma, P. S. Shuttleworth, S. C. Z. Quek, J. H. Clark and M. North, *Angew. Chem. Int. Ed.* 2016, **55**, 9173–9177.

Influence of water on CO_2 adsorption at 1 bar pressure

S800

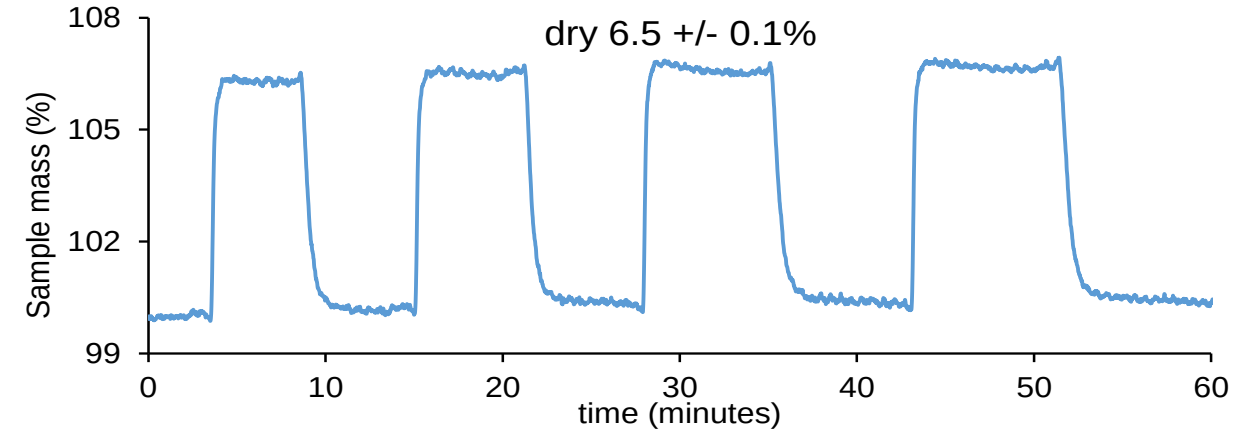

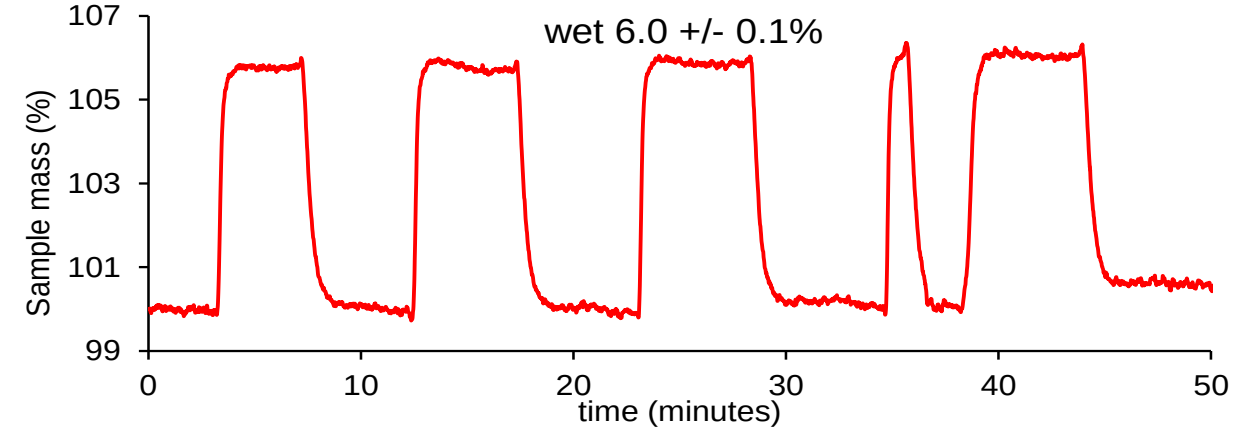

S800K2

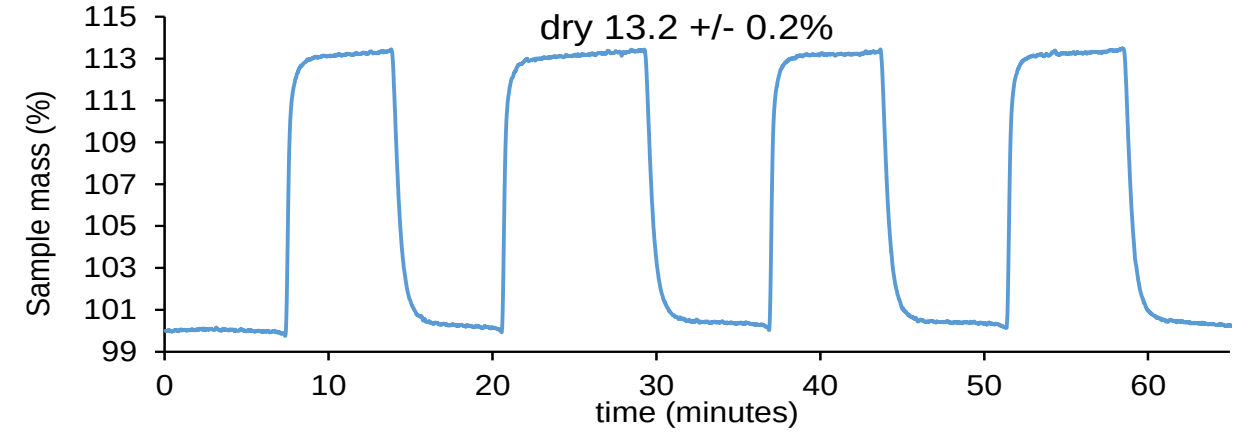

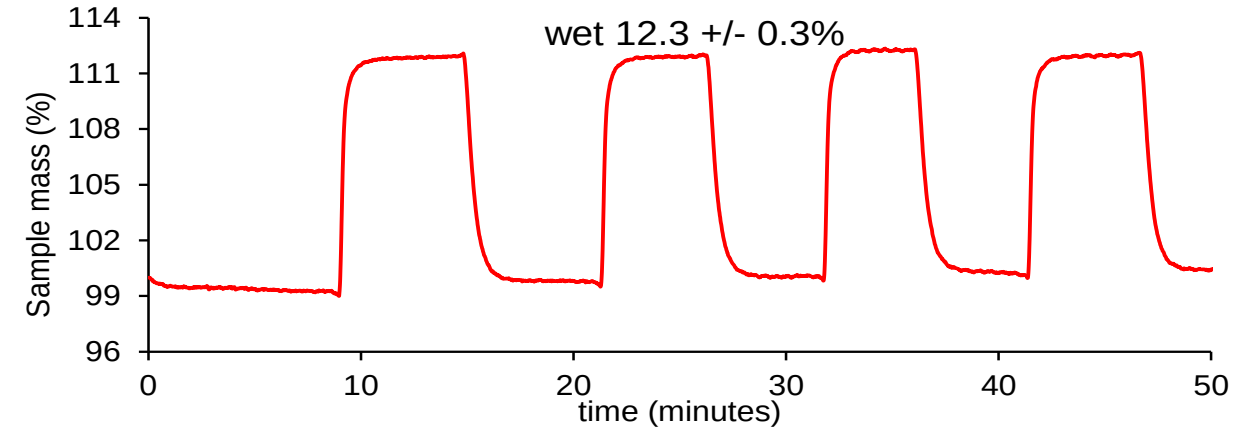

S800K5

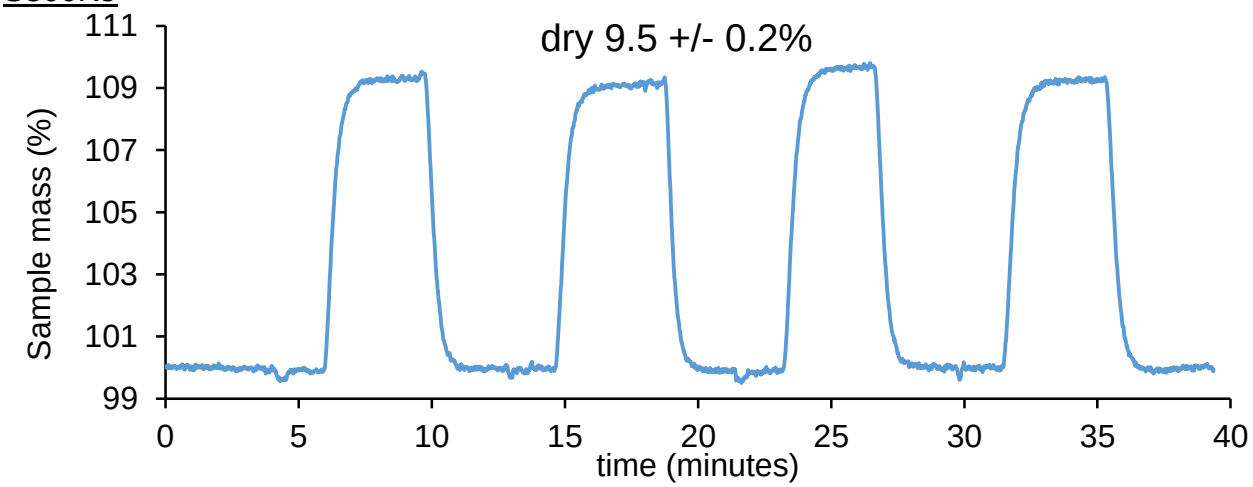
dry 9.5 +/- 0.2%
Sample mass (%)
111
109
107
105
103
101
99
0
5
10
15
20
25
30
35
40
time (minutes)

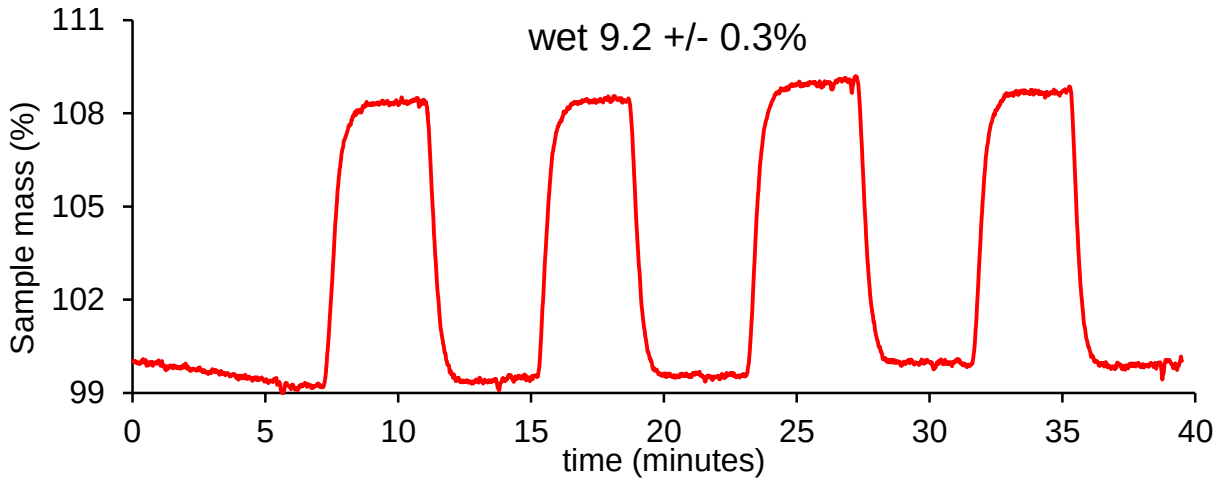
wet 9.2 +/- 0.3%
Sample mass (%)
111
108
105
102
99
0
5
10
15
20
25
30
35
40
time (minutes)

Kinetics of CO_2 adsorption at 1 bar and 35 ^oC

The pseudo-first order plot is obtained by plotting $q_t = q_e(1-e^{-K_1 t})$.

The pseudo-second order plot is obtained by plotting $q_t = K_2 q_e^2 t/(1+K_2 q_e t)$

The Sum of Squared Errors (SSE) is calculated as $\sum[(q_{t,exp} - q_{t,cal})]^2$

where q_t is the amount of CO_2 adsorbed at time t; q_e is the amount of CO_2 adsorbed at equilibrium; and K_1 (min^{-1}) and K_2 (g $mmol^{-1}$ min^{-1}) are the first and second order rate constants. $q_{t,exp}$ and $q_{t,cal}$ are the experimental and calculated adsorption capacity. The experimetal and modelled plots and the best fit parameters are below. A higher value of linear regression correlation coefficient (R^2) and a lower value of SSE represent a goodness of fit.

S300

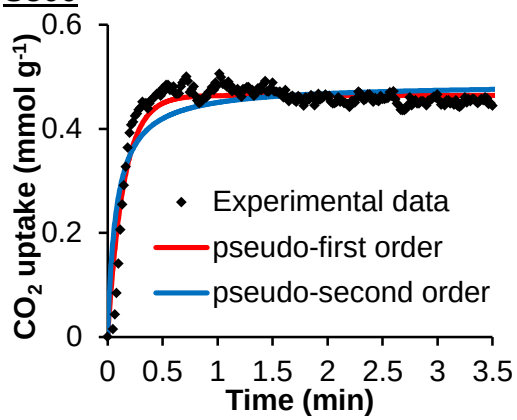

Pseudo-first order model				
q_e(exp) (mmol g^{-1})	K_1 (min^{-1})	q_e(calc) (mmol g^{-1})	R^2	SSE
0.44	6.81	0.46	0.91	0.13

Pseudo-second order model				
q_e(exp) (mmol g^{-1})	K_2 (g min^{-1} $mmol^{-1}$)	q_e(calc) (mmol g^{-1})	R^2	SSE
0.44	25.75	0.49	0.78	0.31

S600

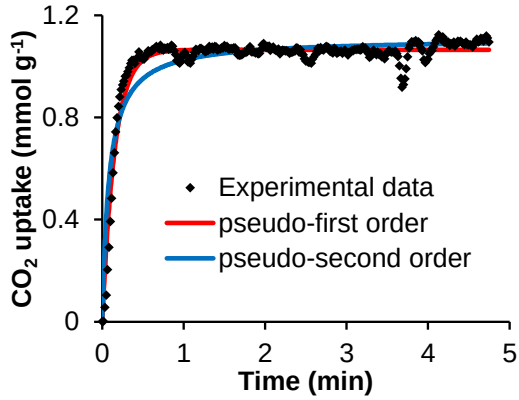

Pseudo-first order model				
q_e(exp) (mmol g^{-1})	K_1 (min^{-1})	q_e(calc) (mmol g^{-1})	R^2	SSE
1.07	6.55	1.07	0.94	0.40

Pseudo-second order model				
q_e(exp) (mmol g^{-1})	K_2 (g min^{-1} $mmol^{-1}$)	q_e(calc) (mmol g^{-1})	R^2	SSE
1.07	10.90	1.11	0.86	0.99

S800

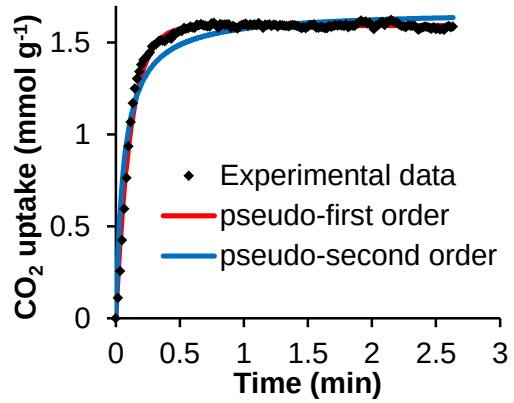

Pseudo-first order model				
q_e(exp) (mmol g^{-1})	K_1 (min^{-1})	q_e(calc) (mmol g^{-1})	R^2	SSE
1.62	8.85	1.59	0.99	1.99
Pseudo-second order model				
q_e(exp) (mmol g^{-1})	K_2 (g min^{-1} $mmol^{-1}$)	q_e(calc) (mmol g^{-1})	R^2	SSE
1.62	9.50	1.67	0.93	8.67

S1000

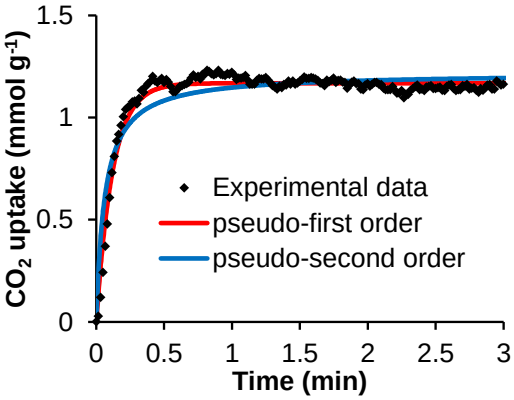

Pseudo-first order model				
q_e(exp) (mmol g^{-1})	K_1 (min^{-1})	q_e(calc) (mmol g^{-1})	R^2	SSE
1.09	8.32	1.17	0.96	0.26
Pseudo-second order model				
q_e(exp) (mmol g^{-1})	K_2 (g min^{-1} $mmol^{-1}$)	q_e(calc) (mmol g^{-1})	R^2	SSE
1.09	13.13	1.21	0.86	0.91

A800

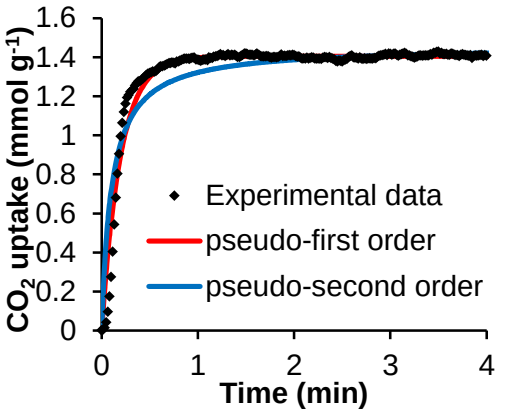

Pseudo-first order model				
q_e(exp) (mmol g^{-1})	K_1 (min^{-1})	q_e(calc) (mmol g^{-1})	R^2	SSE
1.36	5.16	1.41	0.95	0.70
Pseudo-second order model				
q_e(exp) (mmol g^{-1})	K_2 (g min^{-1} $mmol^{-1}$)	q_e(calc) (mmol g^{-1})	R^2	SSE
1.36	6.66	1.46	0.86	2.08

P800

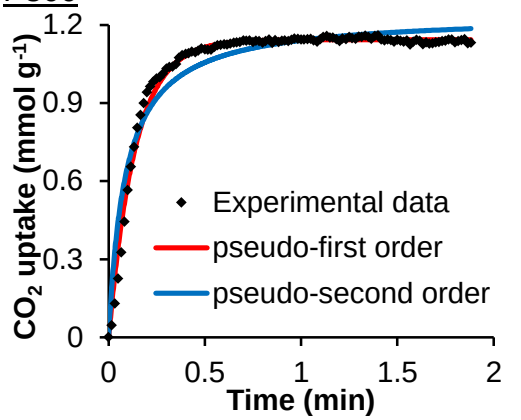

Pseudo-first order model				
q_e(exp) (mmol g^{-1})	K_1 (min^{-1})	q_e(calc) (mmol g^{-1})	R^2	SSE
1.07	7.33	1.14	0.99	0.08
Pseudo-second order model				
q_e(exp) (mmol g^{-1})	K_2 (g min^{-1} $mmol^{-1}$)	q_e(calc) (mmol g^{-1})	R^2	SSE
1.07	9.21	1.24	0.94	0.37

S800K1

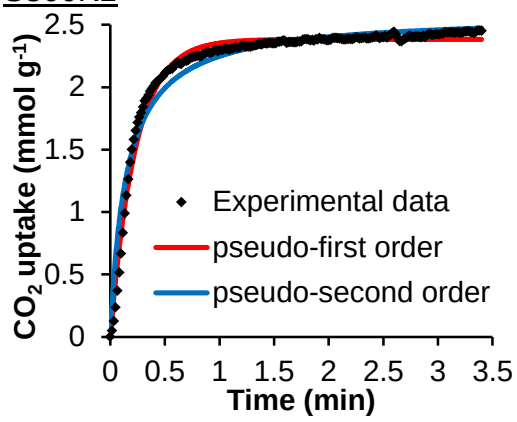

Pseudo-first order model				
q_e(exp) (mmol g^{-1})	K_1 (min^{-1})	q_e(calc) (mmol g^{-1})	R^2	SSE
2.4	4.36	2.38	0.98	0.66
Pseudo-second order model				
q_e(exp) (mmol g^{-1})	K_2 (g min^{-1} $mmol^{-1}$)	q_e(calc) (mmol g^{-1})	R^2	SSE
2.4	2.63	2.58	0.96	1.60

S800K2

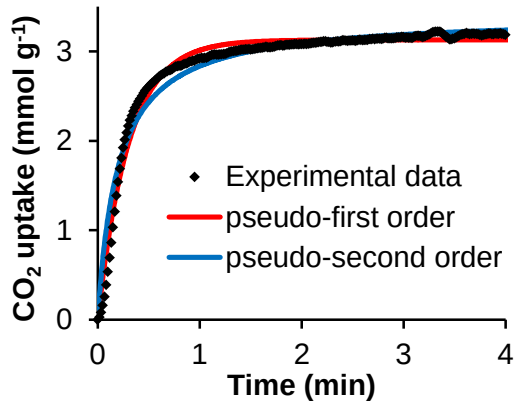

Pseudo-first order model				
q_e(exp) (mmol g^{-1})	K_1 (min^{-1})	q_e(calc) (mmol g^{-1})	R^2	SSE
3.22	3.30	3.13	0.98	3.24
Pseudo-second order model				
q_e(exp) (mmol g^{-1})	K_2 (g min^{-1} $mmol^{-1}$)	q_e(calc) (mmol g^{-1})	R^2	SSE
3.22	1.48	3.40	0.96	12.11

S800K3

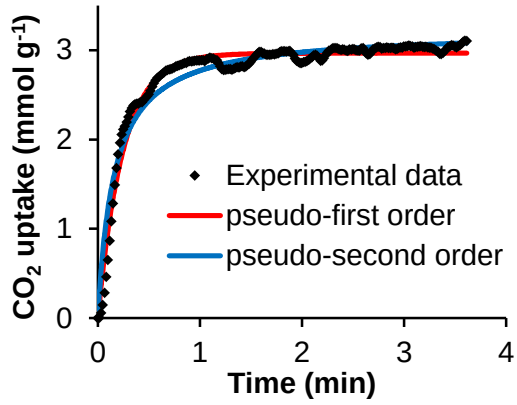

Pseudo-first order model				
q_e(exp) (mmol g^{-1})	K_1 (min^{-1})	q_e(calc) (mmol g^{-1})	R^2	SSE
2.93	4.05	2.97	0.97	2.11
Pseudo-second order model				
q_e(exp) (mmol g^{-1})	K_2 (g min^{-1} $mmol^{-1}$)	q_e(calc) (mmol g^{-1})	R^2	SSE
2.93	1.93	3.22	0.94	3.86

S800K4

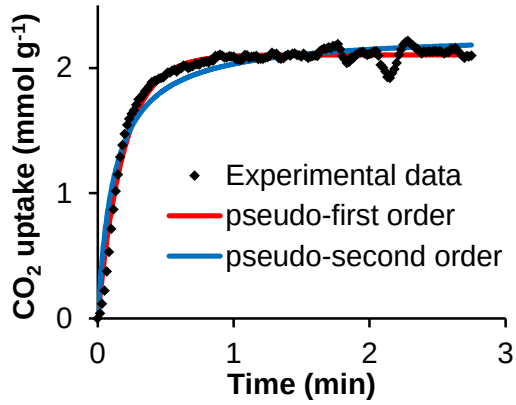

Pseudo-first order model				
q_e(exp) (mmol g^{-1})	K_1 (min^{-1})	q_e(calc) (mmol g^{-1})	R^2	SSE
2.14	5.25	2.10	0.98	0.64
Pseudo-second order model				
q_e(exp) (mmol g^{-1})	K_2 (g min^{-1} $mmol^{-1}$)	q_e(calc) (mmol g^{-1})	R^2	SSE
2.14	3.60	2.28	0.93	1.82

S800K5

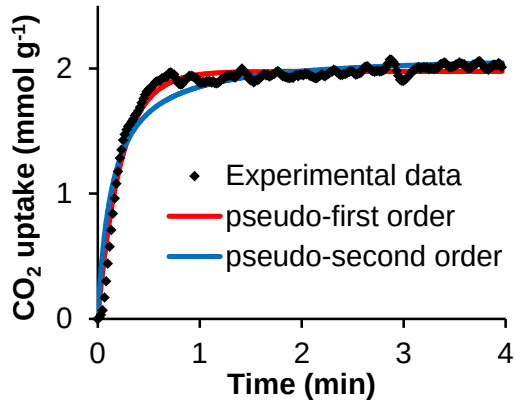

Pseudo-first order model				
q_e(exp) (mmol g^{-1})	K_1 (min^{-1})	q_e(calc) (mmol g^{-1})	R^2	SSE
2.06	4.38	1.98	0.97	1.04

Pseudo-second order model				
q_e(exp) (mmol g^{-1})	K_2 (g min^{-1} $mmol^{-1}$)	q_e(calc) (mmol g^{-1})	R^2	SSE
2.06	3.29	2.12	0.92	2.57

S600K4

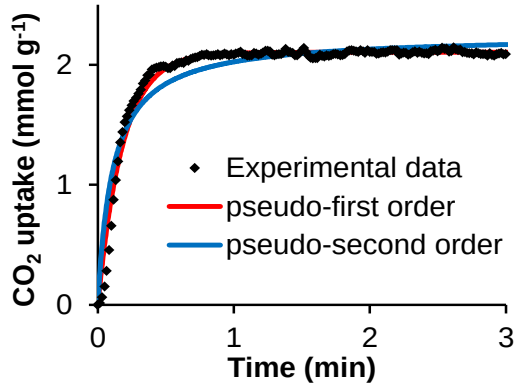

Pseudo-first order model				
q_e(exp) (mmol g^{-1})	K_1 (min^{-1})	q_e(calc) (mmol g^{-1})	R^2	SSE
2.02	5.51	2.10	0.97	0.71

Pseudo-second order model				
q_e(exp) (mmol g^{-1})	K_2 (g min^{-1} $mmol^{-1}$)	q_e(calc) (mmol g^{-1})	R^2	SSE
2.02	4.03	2.25	0.91	2.44

S1000K4

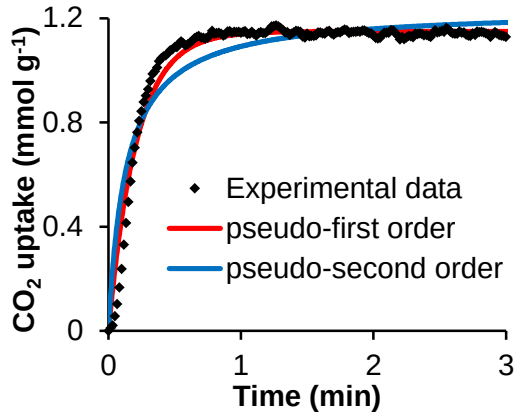

Pseudo-first order model				
q_e(exp) (mmol g^{-1})	K_1 (min^{-1})	q_e(calc) (mmol g^{-1})	R^2	SSE
1.11	4.74	1.15	0.97	0.33

Pseudo-second order model				
q_e(exp) (mmol g^{-1})	K_2 (g min^{-1} $mmol^{-1}$)	q_e(calc) (mmol g^{-1})	R^2	SSE
1.11	6.16	1.24	0.89	1.10

A800K1

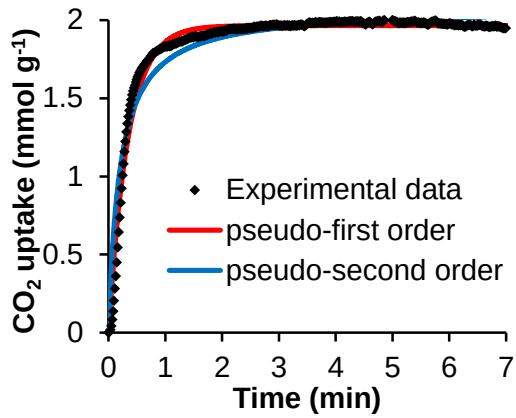

Pseudo-first order model				
q_e(exp) (mmol g^{-1})	K_1 (min^{-1})	q_e(calc) (mmol g^{-1})	R^2	SSE
1.98	2.92	1.96	0.97	1.15

Pseudo-second order model				
q_e(exp) (mmol g^{-1})	K_2 (g min^{-1} $mmol^{-1}$)	q_e(calc) (mmol g^{-1})	R^2	SSE
1.98	2.39	2.08	0.93	3.26

A800K2

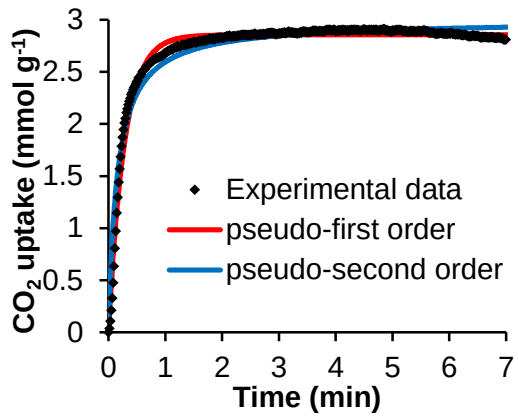

Pseudo-first order model				
q_e(exp) (mmol g^{-1})	K_1 (min^{-1})	q_e(calc) (mmol g^{-1})	R^2	SSE
2.90	3.60	2.85	0.98	1.42
Pseudo-second order model				
q_e(exp) (mmol g^{-1})	K_2 (g min^{-1} $mmol^{-1}$)	q_e(calc) (mmol g^{-1})	R^2	SSE
2.90	2.18	2.99	0.95	3.80

A800K3

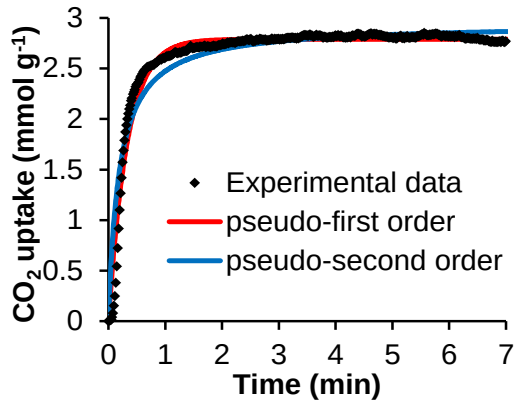

Pseudo-first order model				
q_e(exp) (mmol g^{-1})	K_1 (min^{-1})	q_e(calc) (mmol g^{-1})	R^2	SSE
2.82	3.06	2.79	0.96	3.49
Pseudo-second order model				
q_e(exp) (mmol g^{-1})	K_2 (g min^{-1} $mmol^{-1}$)	q_e(calc) (mmol g^{-1})	R^2	SSE
2.82	1.79	2.94	0.91	8.54

A800K4

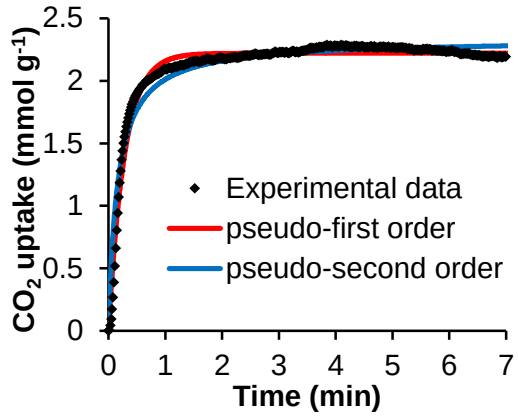

Pseudo-first order model				
q_e(exp) (mmol g^{-1})	K_1 (min^{-1})	q_e(calc) (mmol g^{-1})	R^2	SSE
2.25	3.55	2.22	0.97	1.39
Pseudo-second order model				
q_e(exp) (mmol g^{-1})	K_2 (g min^{-1} $mmol^{-1}$)	q_e(calc) (mmol g^{-1})	R^2	SSE
2.25	2.70	2.33	0.93	3.02

A800K5

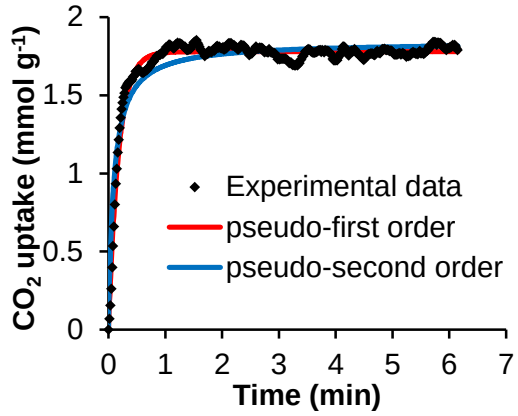

Pseudo-first order model				
q_e(exp) (mmol g^{-1})	K_1 (min^{-1})	q_e(calc) (mmol g^{-1})	R^2	SSE
1.75	5.68	1.78	0.97	0.61
Pseudo-second order model				
q_e(exp) (mmol g^{-1})	K_2 (g min^{-1} $mmol^{-1}$)	q_e(calc) (mmol g^{-1})	R^2	SSE
1.75	6.06	1.84	0.90	1.93

A600K2

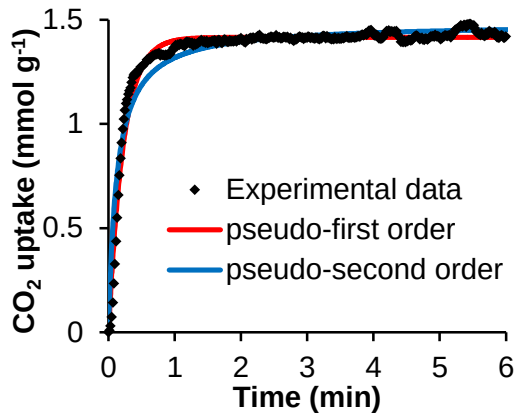

Pseudo-first order model				
q_e(exp) (mmol g^{-1})	K_1 (min^{-1})	q_e(calc) (mmol g^{-1})	R^2	SSE
1.48	4.52	1.42	0.97	0.50
Pseudo-second order model				
q_e(exp) (mmol g^{-1})	K_2 (g min^{-1} $mmol^{-1}$)	q_e(calc) (mmol g^{-1})	R^2	SSE
1.48	5.39	1.48	0.92	1.22

A1000K2

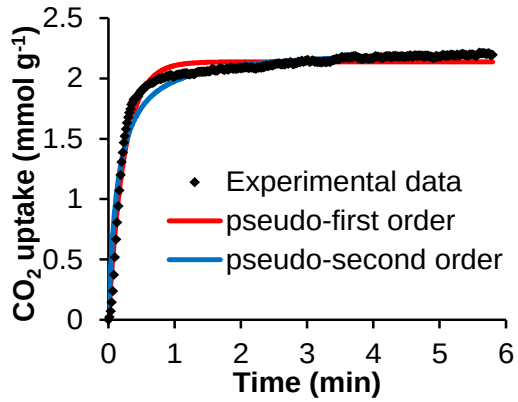

Pseudo-first order model				
q_e(exp) (mmol g^{-1})	K_1 (min^{-1})	q_e(calc) (mmol g^{-1})	R^2	SSE
2.16	4.22	2.14	0.96	1.39
Pseudo-second order model				
q_e(exp) (mmol g^{-1})	K_2 (g min^{-1} $mmol^{-1}$)	q_e(calc) (mmol g^{-1})	R^2	SSE
2.16	3.12	2.26	0.95	2.00

P800K2

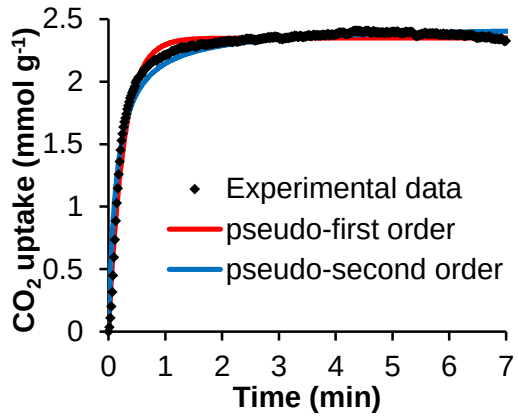

Pseudo-first order model				
q_e(exp) (mmol g^{-1})	K_1 (min^{-1})	q_e(calc) (mmol g^{-1})	R^2	SSE
2.39	3.79	2.35	0.98	1.01
Pseudo-second order model				
q_e(exp) (mmol g^{-1})	K_2 (g min^{-1} $mmol^{-1}$)	q_e(calc) (mmol g^{-1})	R^2	SSE
2.39	2.84	2.45	0.95	2.22

P800K3

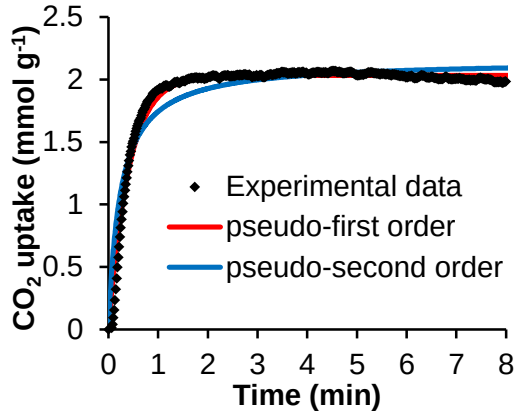

Pseudo-first order model				
q_e(exp) (mmol g^{-1})	K_1 (min^{-1})	q_e(calc) (mmol g^{-1})	R^2	SSE
2.06	2.46	2.03	0.97	1.46
Pseudo-second order model				
q_e(exp) (mmol g^{-1})	K_2 (g min^{-1} $mmol^{-1}$)	q_e(calc) (mmol g^{-1})	R^2	SSE
2.06	1.98	2.15	0.89	6.06

P800K5

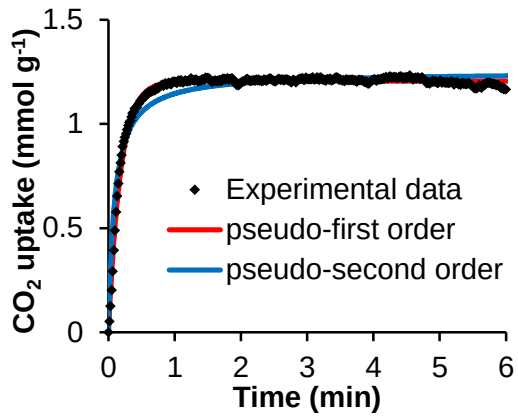

Pseudo-first order model				
q_e(exp) (mmol g^{-1})	K_1 (min^{-1})	q_e(calc) (mmol g^{-1})	R^2	SSE
1.22	5.57	1.21	0.99	0.09

Pseudo-second order model				
q_e(exp) (mmol g^{-1})	K_2 (g min^{-1} $mmol^{-1}$)	q_e(calc) (mmol g^{-1})	R^2	SSE
1.22	8.80	1.25	0.93	0.62

S800C15

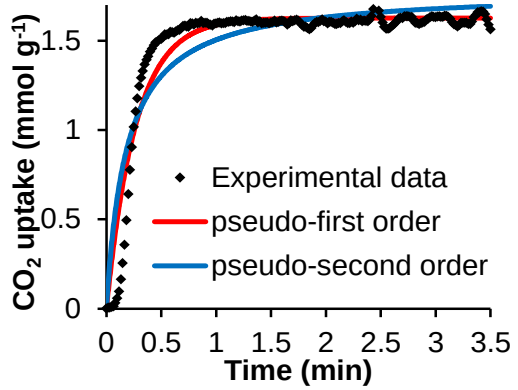

Pseudo-first order model				
q_e(exp) (mmol g^{-1})	K_1 (min^{-1})	q_e(calc) (mmol g^{-1})	R^2	SSE
1.64	3.74	1.63	0.92	2.19

Pseudo-second order model				
q_e(exp) (mmol g^{-1})	K_2 (g min^{-1} $mmol^{-1}$)	q_e(calc) (mmol g^{-1})	R^2	SSE
1.64	3.04	1.78	0.84	4.27

S850C15

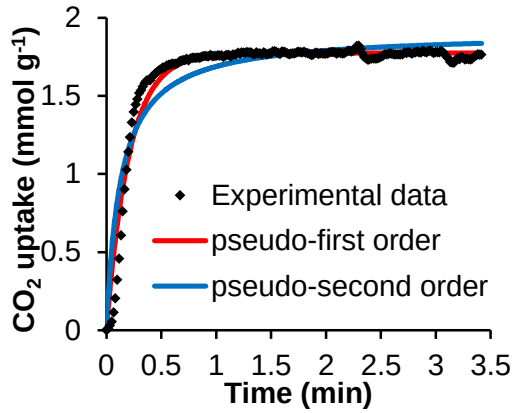

Pseudo-first order model				
q_e(exp) (mmol g^{-1})	K_1 (min^{-1})	q_e(calc) (mmol g^{-1})	R^2	SSE
1.77	4.85	1.78	0.95	1.08

Pseudo-second order model				
q_e(exp) (mmol g^{-1})	K_2 (g min^{-1} $mmol^{-1}$)	q_e(calc) (mmol g^{-1})	R^2	SSE
1.77	4.07	1.91	0.88	2.91

S900C15

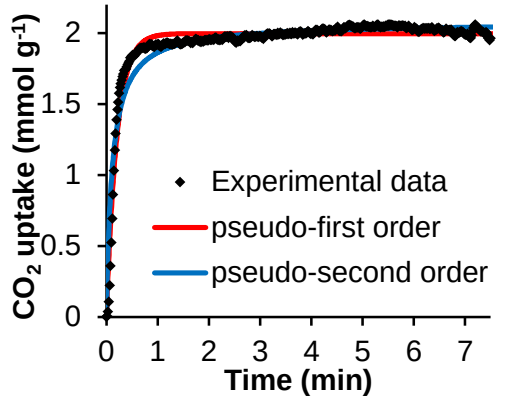

Pseudo-first order model				
q_e(exp) (mmol g^{-1})	K_1 (min^{-1})	q_e(calc) (mmol g^{-1})	R^2	SSE
1.98	4.93	2.00	0.95	1.40

Pseudo-second order model				
q_e(exp) (mmol g^{-1})	K_2 (g min^{-1} $mmol^{-1}$)	q_e(calc) (mmol g^{-1})	R^2	SSE
1.98	4.27	2.07	0.92	2.49

S950C15

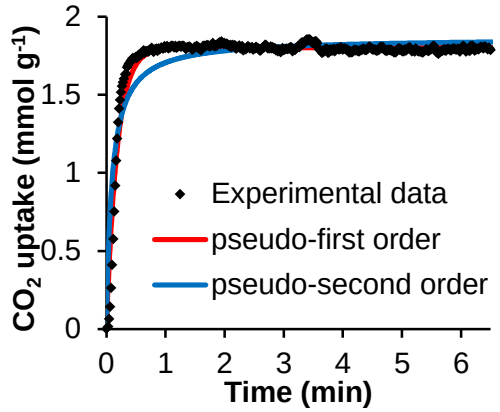

Pseudo-first order model				
q_e(exp) (mmol g^{-1})	K_1 (min^{-1})	q_e(calc) (mmol g^{-1})	R^2	SSE
1.82	5.59	1.80	0.95	1.23
Pseudo-second order model				
q_e(exp) (mmol g^{-1})	K_2 (g min^{-1} $mmol^{-1}$)	q_e(calc) (mmol g^{-1})	R^2	SSE
1.82	5.77	1.86	0.84	3.81

S1000C15

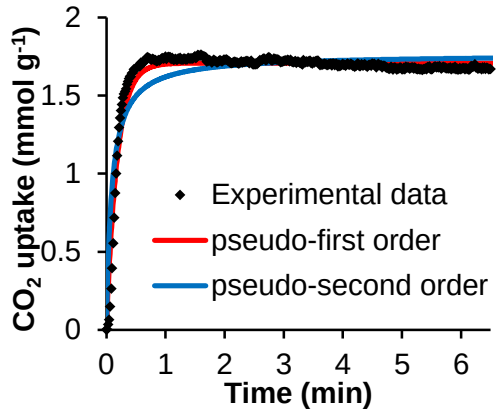

Pseudo-first order model				
q_e(exp) (mmol g^{-1})	K_1 (min^{-1})	q_e(calc) (mmol g^{-1})	R^2	SSE
1.74	5.58	1.71	0.94	1.21
Pseudo-second order model				
q_e(exp) (mmol g^{-1})	K_2 (g min^{-1} $mmol^{-1}$)	q_e(calc) (mmol g^{-1})	R^2	SSE
1.74	6.36	1.76	0.81	4.03

S900C30

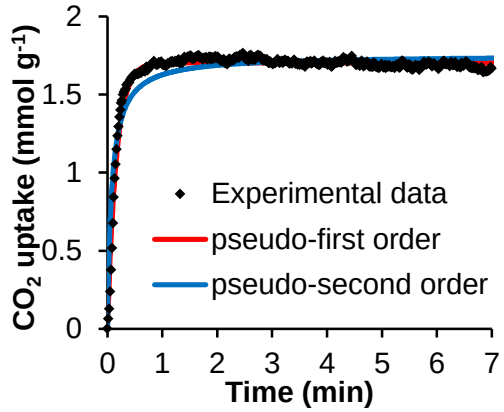

Pseudo-first order model				
q_e(exp) (mmol g^{-1})	K_1 (min^{-1})	q_e(calc) (mmol g^{-1})	R^2	SSE
1.74	6.29	1.70	0.97	0.48
Pseudo-second order model				
q_e(exp) (mmol g^{-1})	K_2 (g min^{-1} $mmol^{-1}$)	q_e(calc) (mmol g^{-1})	R^2	SSE
1.74	7.41	1.75	0.88	2.11

S900C60

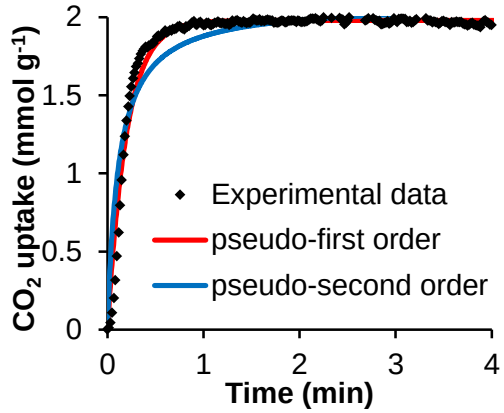

Pseudo-first order model				
q_e(exp) (mmol g^{-1})	K_1 (min^{-1})	q_e(calc) (mmol g^{-1})	R^2	SSE
1.98	5.08	1.98	0.97	0.95
Pseudo-second order model				
q_e(exp) (mmol g^{-1})	K_2 (g min^{-1} $mmol^{-1}$)	q_e(calc) (mmol g^{-1})	R^2	SSE
1.98	4.15	2.10	0.89	3.09

S900C90

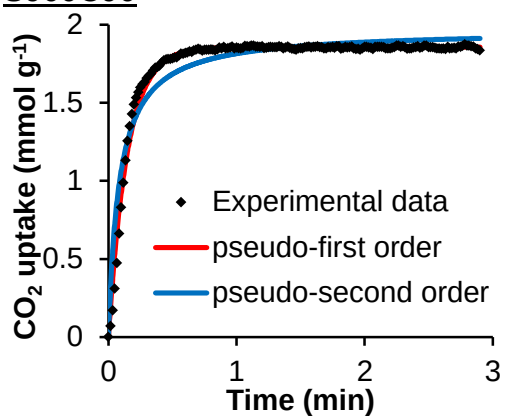

Pseudo-first order model				
q_e(exp) (mmol g^{-1})	K_1 (min^{-1})	q_e(calc) (mmol g^{-1})	R^2	SSE
1.86	6.90	1.86	0.99	0.25
Pseudo-second order model				
q_e(exp) (mmol g^{-1})	K_2 (g min^{-1} $mmol^{-1}$)	q_e(calc) (mmol g^{-1})	R^2	SSE
1.86	6.03	1.97	0.92	1.31

S900C120

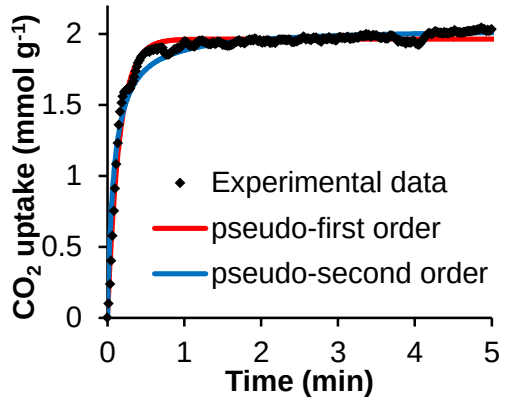

Pseudo-first order model				
q_e(exp) (mmol g^{-1})	K_1 (min^{-1})	q_e(calc) (mmol g^{-1})	R^2	SSE
1.89	6.50	1.96	0.97	0.57
Pseudo-second order model				
q_e(exp) (mmol g^{-1})	K_2 (g min^{-1} $mmol^{-1}$)	q_e(calc) (mmol g^{-1})	R^2	SSE
1.89	5.85	2.04	0.95	1.02

S950C60

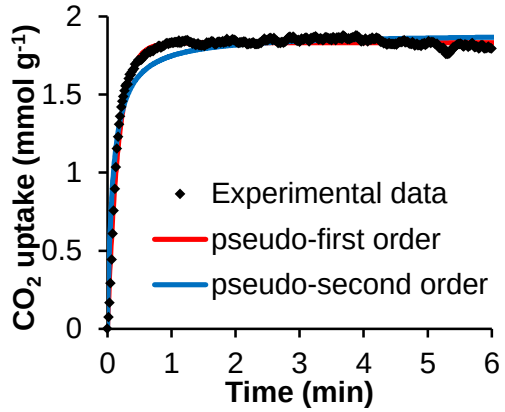

Pseudo-first order model				
q_e(exp) (mmol g^{-1})	K_1 (min^{-1})	q_e(calc) (mmol g^{-1})	R^2	SSE
1.82	6.04	1.83	0.98	0.34
Pseudo-second order model				
q_e(exp) (mmol g^{-1})	K_2 (g min^{-1} $mmol^{-1}$)	q_e(calc) (mmol g^{-1})	R^2	SSE
1.82	6.36	1.89	0.91	1.68

S950C90

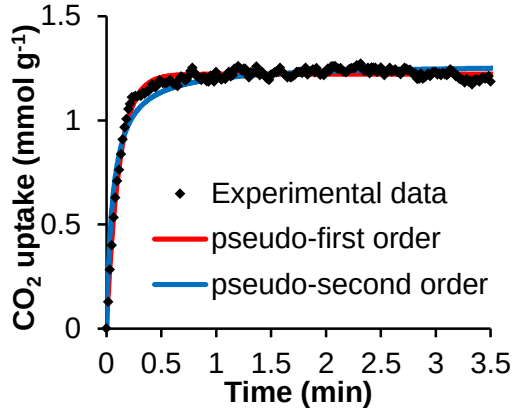

Pseudo-first order model				
q_e(exp) (mmol g^{-1})	K_1 (min^{-1})	q_e(calc) (mmol g^{-1})	R^2	SSE
1.52	8.71	1.22	0.98	0.11
Pseudo-second order model				
q_e(exp) (mmol g^{-1})	K_2 (g min^{-1} $mmol^{-1}$)	q_e(calc) (mmol g^{-1})	R^2	SSE
1.52	13.06	1.27	0.94	0.33

S950C120

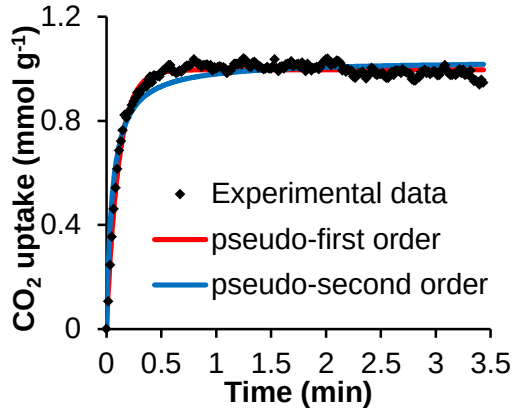

Pseudo-first order model				
q_e(exp) (mmol g^{-1})	K_1 (min^{-1})	q_e(calc) (mmol g^{-1})	R^2	SSE
1.04	9.10	1.00	0.98	0.09
Pseudo-second order model				
q_e(exp) (mmol g^{-1})	K_2 (g min^{-1} $mmol^{-1}$)	q_e(calc) (mmol g^{-1})	R^2	SSE
1.04	17.91	1.03	0.91	0.31

A750C45

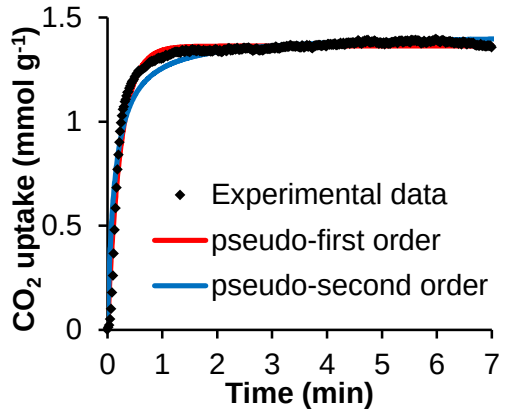

Pseudo-first order model				
q_e(exp) (mmol g^{-1})	K_1 (min^{-1})	q_e(calc) (mmol g^{-1})	R^2	SSE
1.39	4.23	1.36	0.97	0.50
Pseudo-second order model				
q_e(exp) (mmol g^{-1})	K_2 (g min^{-1} $mmol^{-1}$)	q_e(calc) (mmol g^{-1})	R^2	SSE
1.39	5.32	1.42	0.92	1.21

A750C60

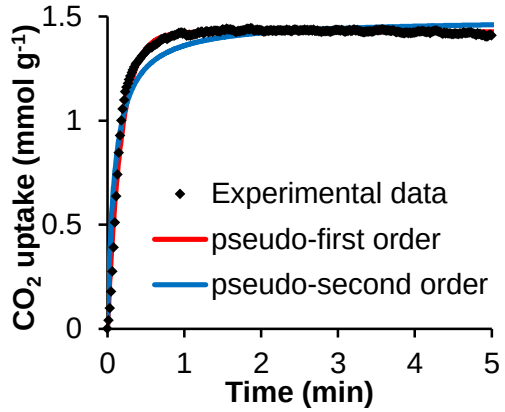

Pseudo-first order model				
q_e(exp) (mmol g^{-1})	K_1 (min^{-1})	q_e(calc) (mmol g^{-1})	R^2	SSE
1.41	5.71	1.43	0.98	0.20
Pseudo-second order model				
q_e(exp) (mmol g^{-1})	K_2 (g min^{-1} $mmol^{-1}$)	q_e(calc) (mmol g^{-1})	R^2	SSE
1.41	7.18	1.49	0.92	1.03

A750C90

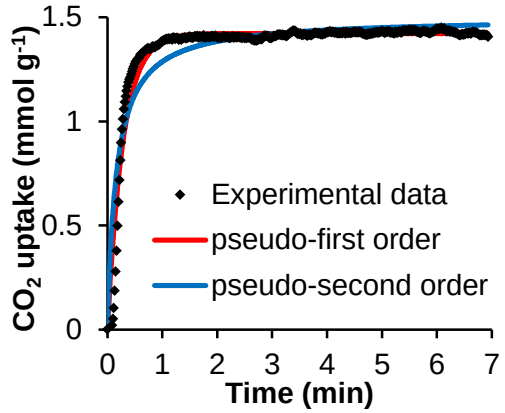

Pseudo-first order model				
q_e(exp) (mmol g^{-1})	K_1 (min^{-1})	q_e(calc) (mmol g^{-1})	R^2	SSE
1.43	3.57	1.42	0.94	1.23
Pseudo-second order model				
q_e(exp) (mmol g^{-1})	K_2 (g min^{-1} $mmol^{-1}$)	q_e(calc) (mmol g^{-1})	R^2	SSE
1.43	4.07	1.50	0.87	2.94

A900C0

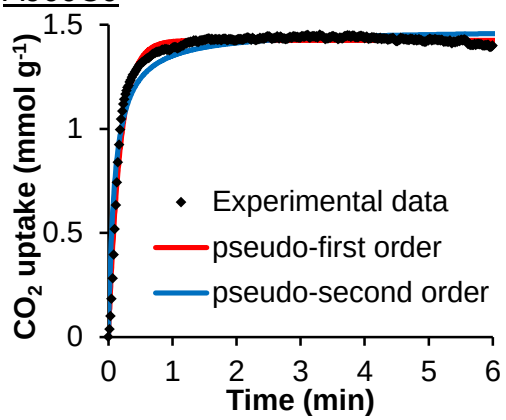

Pseudo-first order model				
q_e(exp) (mmol g^{-1})	K_1 (min^{-1})	q_e(calc) (mmol g^{-1})	R^2	SSE
1.39	5.49	1.43	0.98	0.26

Pseudo-second order model				
q_e(exp) (mmol g^{-1})	K_2 (g min^{-1} $mmol^{-1}$)	q_e(calc) (mmol g^{-1})	R^2	SSE
1.39	7.03	1.48	0.93	0.93

A900C10

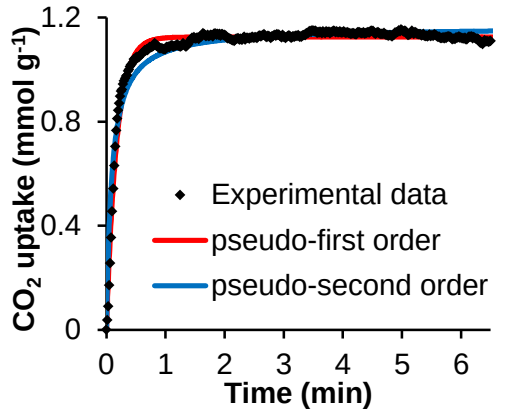

Pseudo-first order model				
q_e(exp) (mmol g^{-1})	K_1 (min^{-1})	q_e(calc) (mmol g^{-1})	R^2	SSE
1.14	5.85	1.13	0.98	0.19

Pseudo-second order model				
q_e(exp) (mmol g^{-1})	K_2 (g min^{-1} $mmol^{-1}$)	q_e(calc) (mmol g^{-1})	R^2	SSE
1.14	9.61	1.16	0.93	0.50

P700C50

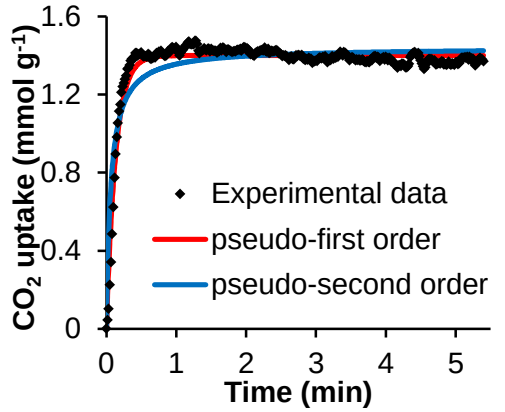

Pseudo-first order model				
q_e(exp) (mmol g^{-1})	K_1 (min^{-1})	q_e(calc) (mmol g^{-1})	R^2	SSE
1.30	6.60	1.40	0.95	0.53

Pseudo-second order model				
q_e(exp) (mmol g^{-1})	K_2 (g min^{-1} $mmol^{-1}$)	q_e(calc) (mmol g^{-1})	R^2	SSE
1.30	11.08	1.44	0.82	1.85

P900C0

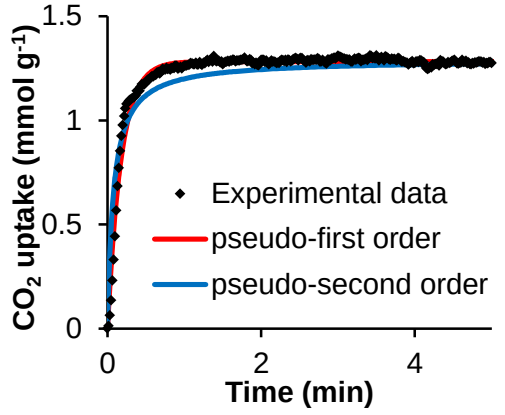

Pseudo-first order model				
q_e(exp) (mmol g^{-1})	K_1 (min^{-1})	q_e(calc) (mmol g^{-1})	R^2	SSE
1.20	5.71	1.28	0.90	1.18

Pseudo-second order model				
q_e(exp) (mmol g^{-1})	K_2 (g min^{-1} $mmol^{-1}$)	q_e(calc) (mmol g^{-1})	R^2	SSE
1.20	10.07	1.29	0.83	2.05

S700O0

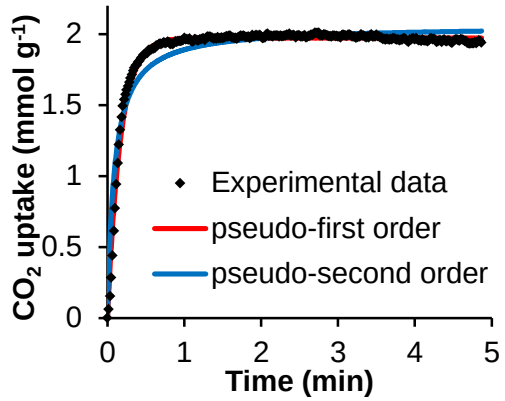

Pseudo-first order model				
q_e(exp) (mmol g^{-1})	K_1 (min^{-1})	q_e(calc) (mmol g^{-1})	R^2	SSE
1.98	6.00	1.97	0.98	0.34

Pseudo-second order model				
q_e(exp) (mmol g^{-1})	K_2 (g min^{-1} $mmol^{-1}$)	q_e(calc) (mmol g^{-1})	R^2	SSE
1.98	5.48	2.06	0.92	1.87

S750O0

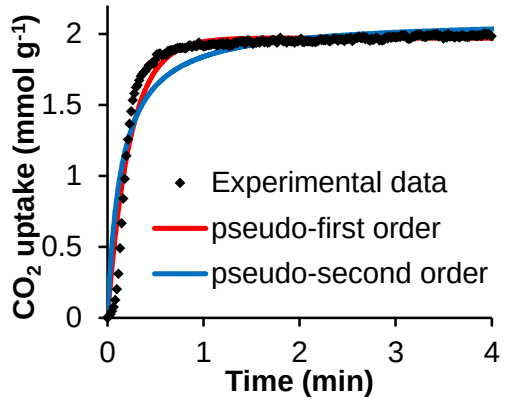

Pseudo-first order model				
q_e(exp) (mmol g^{-1})	K_1 (min^{-1})	q_e(calc) (mmol g^{-1})	R^2	SSE
2.01	4.29	1.97	0.95	1.75

Pseudo-second order model				
q_e(exp) (mmol g^{-1})	K_2 (g min^{-1} $mmol^{-1}$)	q_e(calc) (mmol g^{-1})	R^2	SSE
2.01	3.25	2.11	0.88	3.96

S800O0

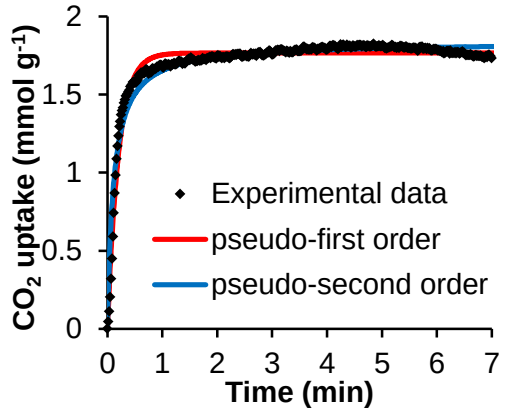

Pseudo-first order model				
q_e(exp) (mmol g^{-1})	K_1 (min^{-1})	q_e(calc) (mmol g^{-1})	R^2	SSE
1.82	4.98	1.77	0.96	0.81

Pseudo-second order model				
q_e(exp) (mmol g^{-1})	K_2 (g min^{-1} $mmol^{-1}$)	q_e(calc) (mmol g^{-1})	R^2	SSE
1.82	4.95	1.84	0.95	1.16

S750O40

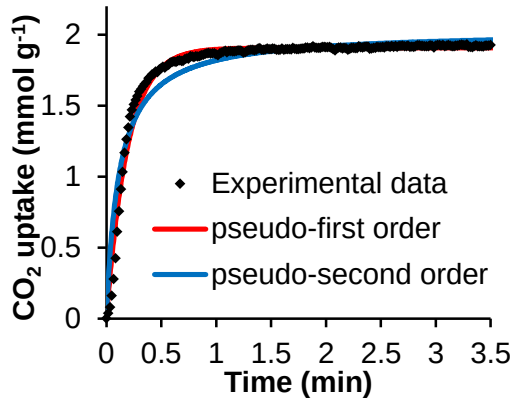

Pseudo-first order model				
q_e(exp) (mmol g^{-1})	K_1 (min^{-1})	q_e(calc) (mmol g^{-1})	R^2	SSE
1.91	5.22	1.91	0.98	0.50

Pseudo-second order model				
q_e(exp) (mmol g^{-1})	K_2 (g min^{-1} $mmol^{-1}$)	q_e(calc) (mmol g^{-1})	R^2	SSE
1.91	4.30	2.03	0.93	1.66

S750O56

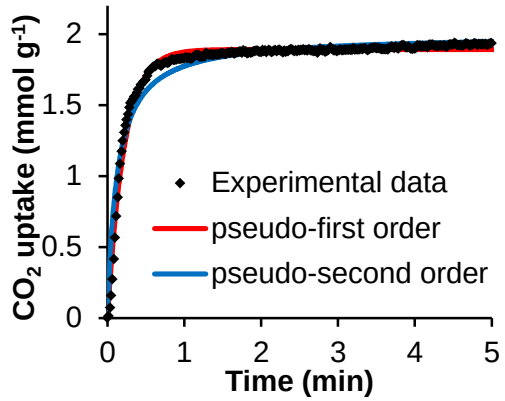

Pseudo-first order model				
q_e(exp) (mmol g^{-1})	K_1 (min^{-1})	q_e(calc) (mmol g^{-1})	R^2	SSE
1.89	4.65	1.89	0.98	0.51

Pseudo-second order model				
q_e(exp) (mmol g^{-1})	K_2 (g min^{-1} $mmol^{-1}$)	q_e(calc) (mmol g^{-1})	R^2	SSE
1.89	4.04	2.00	0.95	1.40

A500O30

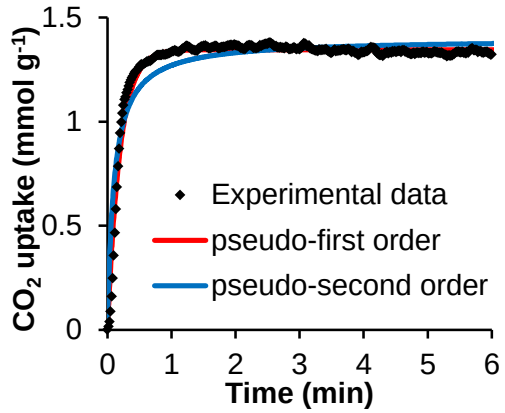

Pseudo-first order model				
q_e(exp) (mmol g^{-1})	K_1 (min^{-1})	q_e(calc) (mmol g^{-1})	R^2	SSE
1.34	5.20	1.35	0.97	0.41

Pseudo-second order model				
q_e(exp) (mmol g^{-1})	K_2 (g min^{-1} $mmol^{-1}$)	q_e(calc) (mmol g^{-1})	R^2	SSE
1.34	7.11	1.40	0.88	1.59

A500O60

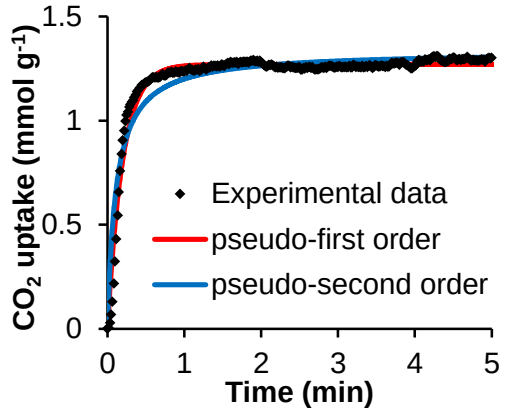

Pseudo-first order model				
q_e(exp) (mmol g^{-1})	K_1 (min^{-1})	q_e(calc) (mmol g^{-1})	R^2	SSE
1.32	5.14	1.27	0.96	0.43

Pseudo-second order model				
q_e(exp) (mmol g^{-1})	K_2 (g min^{-1} $mmol^{-1}$)	q_e(calc) (mmol g^{-1})	R^2	SSE
1.32	6.73	1.33	0.90	1.14

A750O0

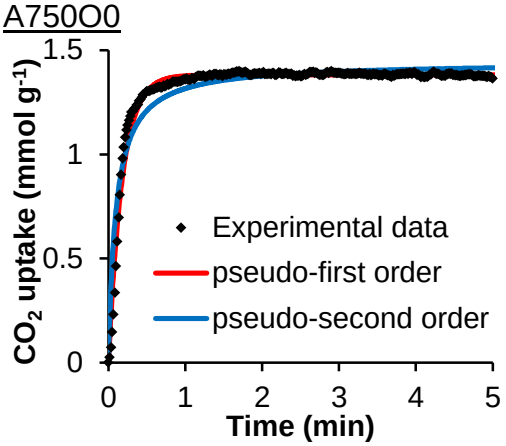

Pseudo-first order model				
q_e(exp) (mmol g^{-1})	K_1 (min^{-1})	q_e(calc) (mmol g^{-1})	R^2	SSE
1.39	5.69	1.38	0.98	0.29

Pseudo-second order model				
q_e(exp) (mmol g^{-1})	K_2 (g min^{-1} $mmol^{-1}$)	q_e(calc) (mmol g^{-1})	R^2	SSE
1.39	7.22	1.44	0.91	1.08

CO_2 adsorption isotherms (0.1-10 bar)

S800, S800K2, S800K3 and S800K5 at 0 ^{o}C

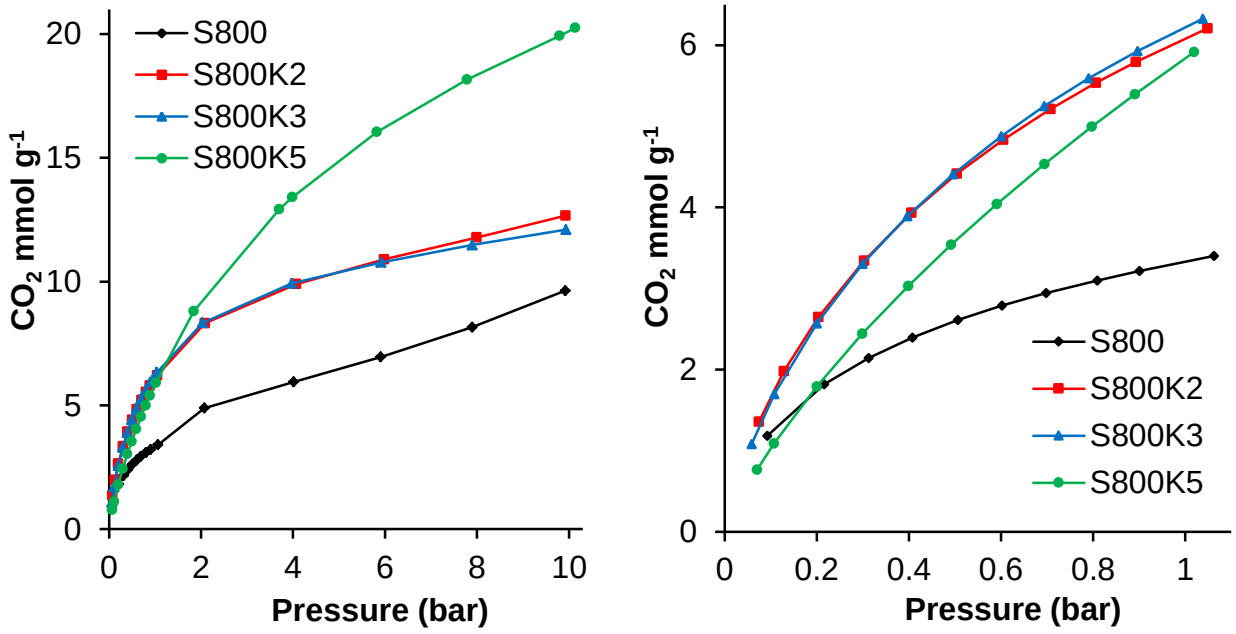

S800 and S800K2 at 25 ^{o}C

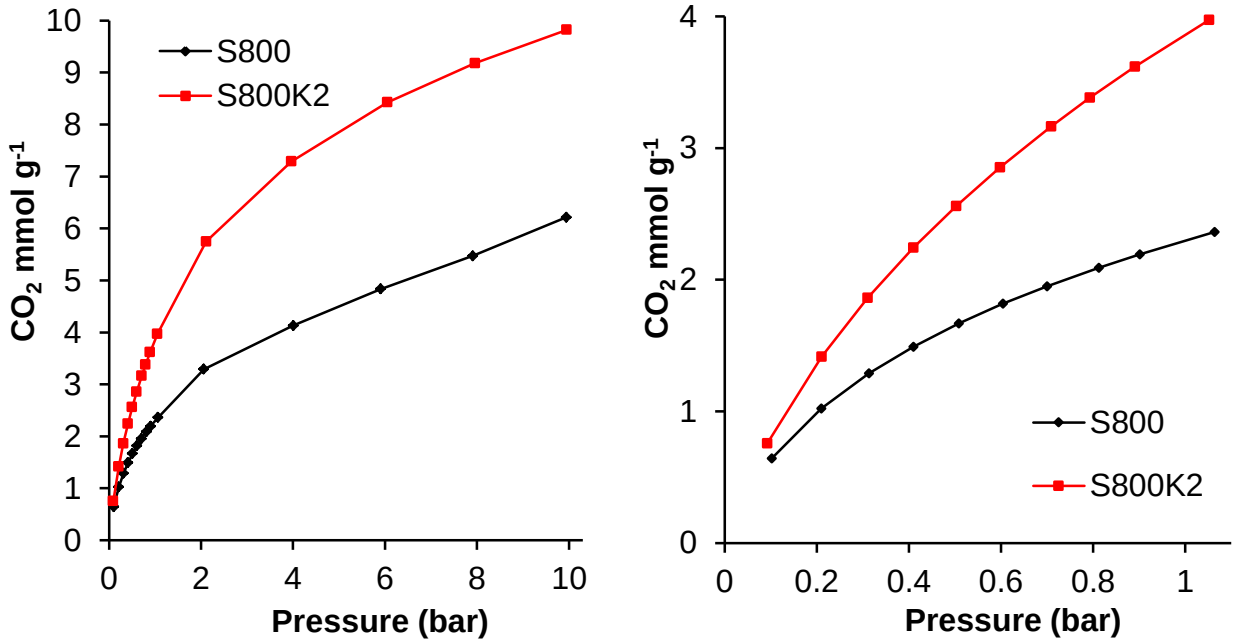

S800 and S800K2 at 50 °C

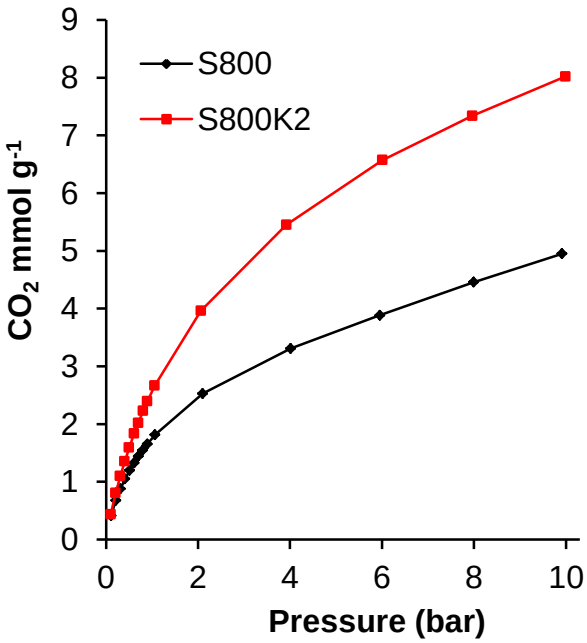

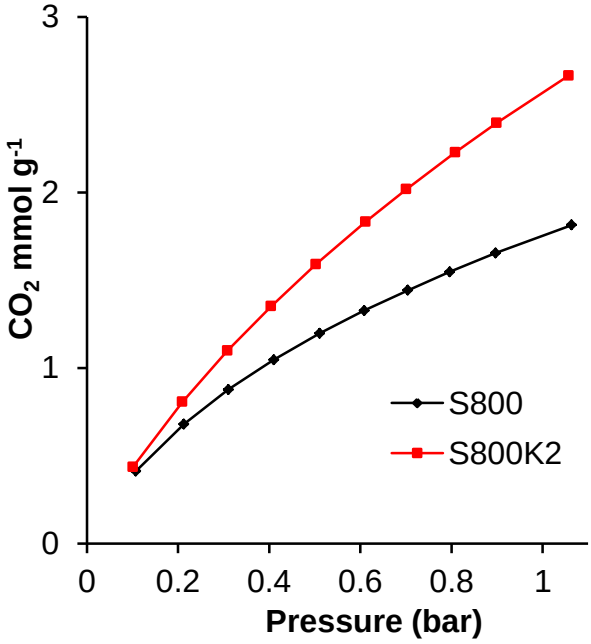

S800 at 0-50 °C

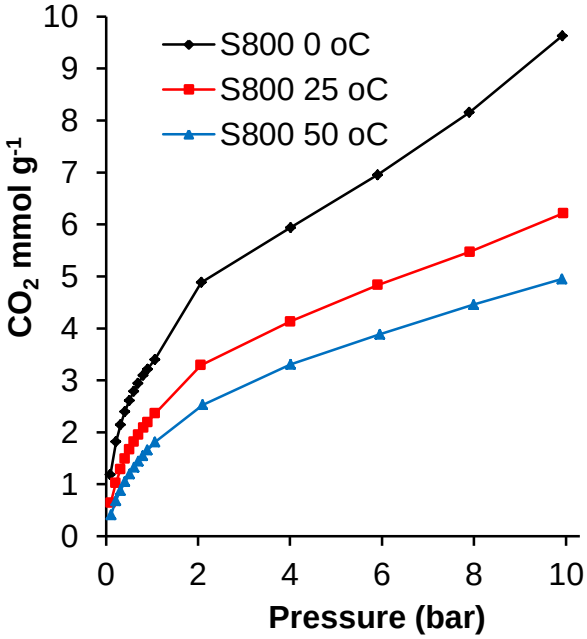

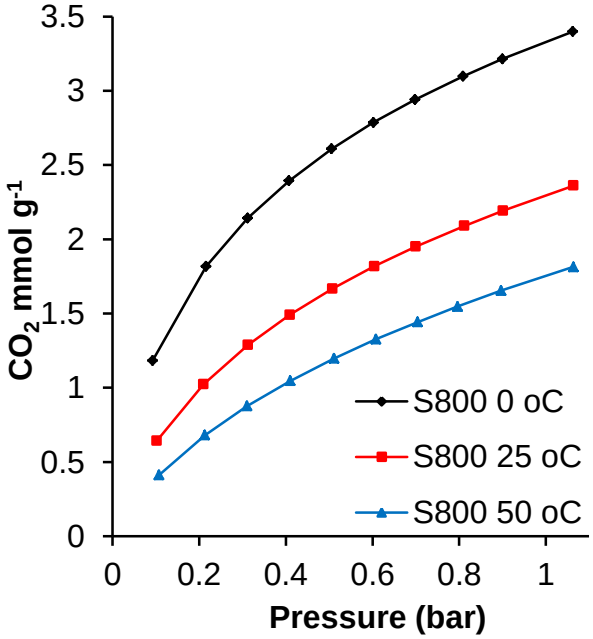

S800K2 at 0-50 ^{o}C

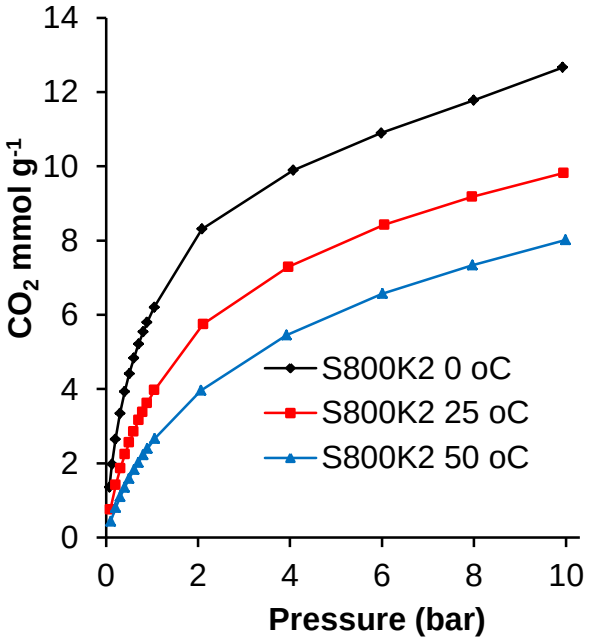

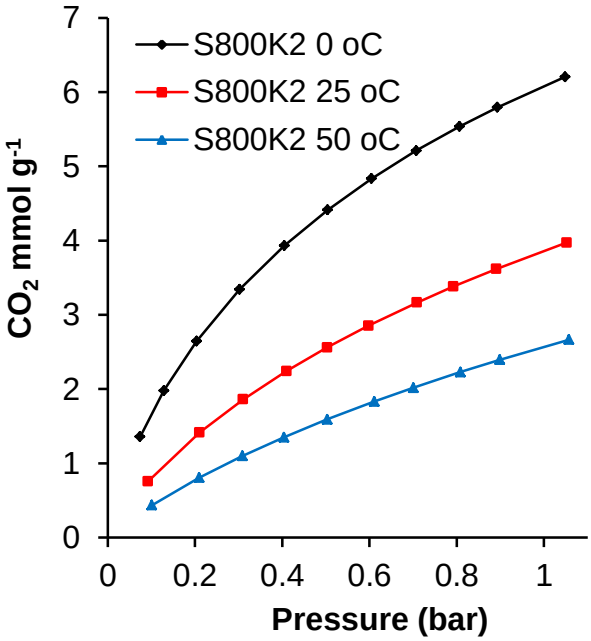

Fitting of isotherm models to the experimental data

Three isotherm models (Langmuir, Freundlich and Temkin) were used to analyse the equilibrium adsorption of CO_2 and N_2 on S800, S00K2, S800K3 and S800K5. The models are represented by the following equations:

Langmuir: $q_e=q_mK_LP/(1+K_LP)$ Freundlich: $q_e=K_FP^{1/n}$ Temkin: $q_e=Bln(K_TP)$

q_m (mmol g^{-1}) is the maximum adsorption capacity, q_e (mmol g^{-1}) is the amount adsorbed at equilibrium, P (atm) is the pressure at equilibrium, K_L (atm^{-1}) is the Langmuir constant, K_F (mmol g^{-1} $atm^{-1/n}$) and n are Freundlich constants indicating the adsorption intensity, and K_T (atm^{-1}) is the Temkin constant.

S800

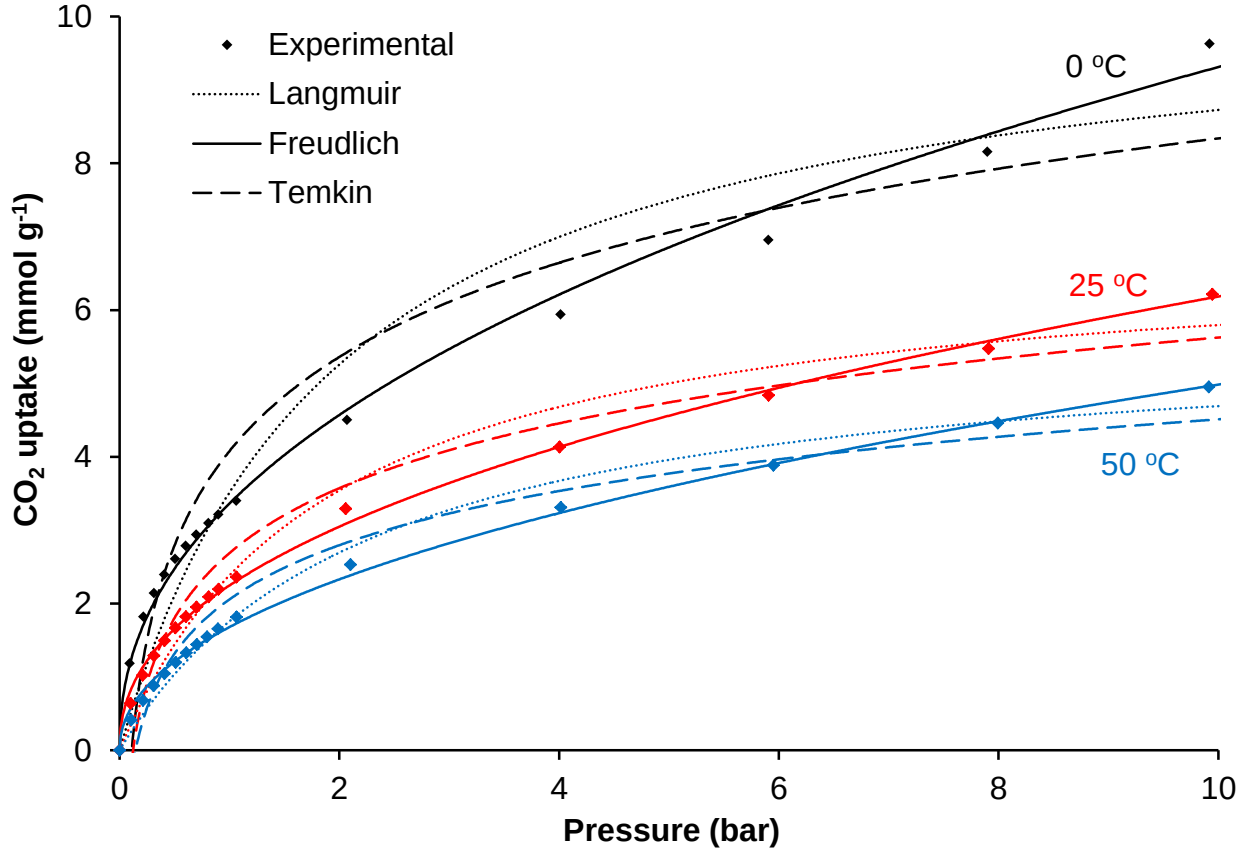

Optimised parameters for isotherm fitting

Model	Parameters	Temperature (°C)		
		0	25	50
Langmuir	q_m (mmol g^{-1})	10.4	6.9	5.8
	K_L(atm^{-1})	0.51	0.53	0.44
	R^2	0.950	0.978	0.986
Freundlich	K_F (mmol g^{-1} $atm^{-1/n}$)	3.36	2.25	1.68
	1/n	0.44	0.44	0.47
	R^2	0.995	0.998	0.998
Temkin	B (KJ mol^{-1})	1.85	1.28	1.07
	K_T (atm^{-1})	9.06	8.24	6.90
	R^2	0.930	0.961	0.962

S800K2

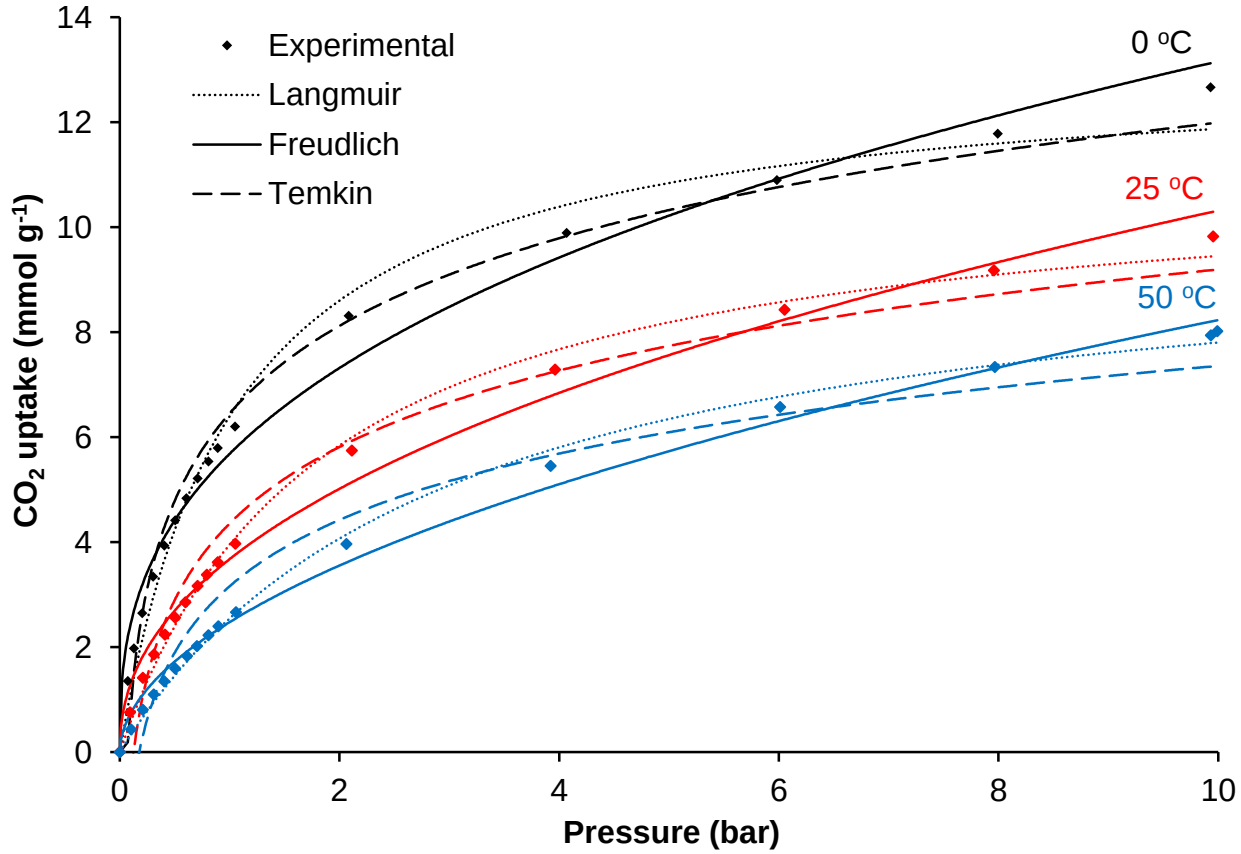

Optimised parameters for isotherm fitting

Model	Parameters	Temperature (°C)		
		0	25	50
Langmuir	q_m (mmol g^{-1})	13.1	11.2	10.1
	K_L(atm^{-1})	0.95	0.55	0.34
	R^2	0.989	0.996	0.997
Freundlich	K_F (mmol g^{-1} $atm^{-1/n}$)	5.68	3.68	2.45
	1/n	0.36	0.45	0.52
	R^2	0.985	0.989	0.993
Temkin	B (KJ mol^{-1})	2.41	2.10	1.82
	K_T (atm^{-1})	14.64	7.94	5.66
	R^2	0.985	0.968	0.956

S800K3

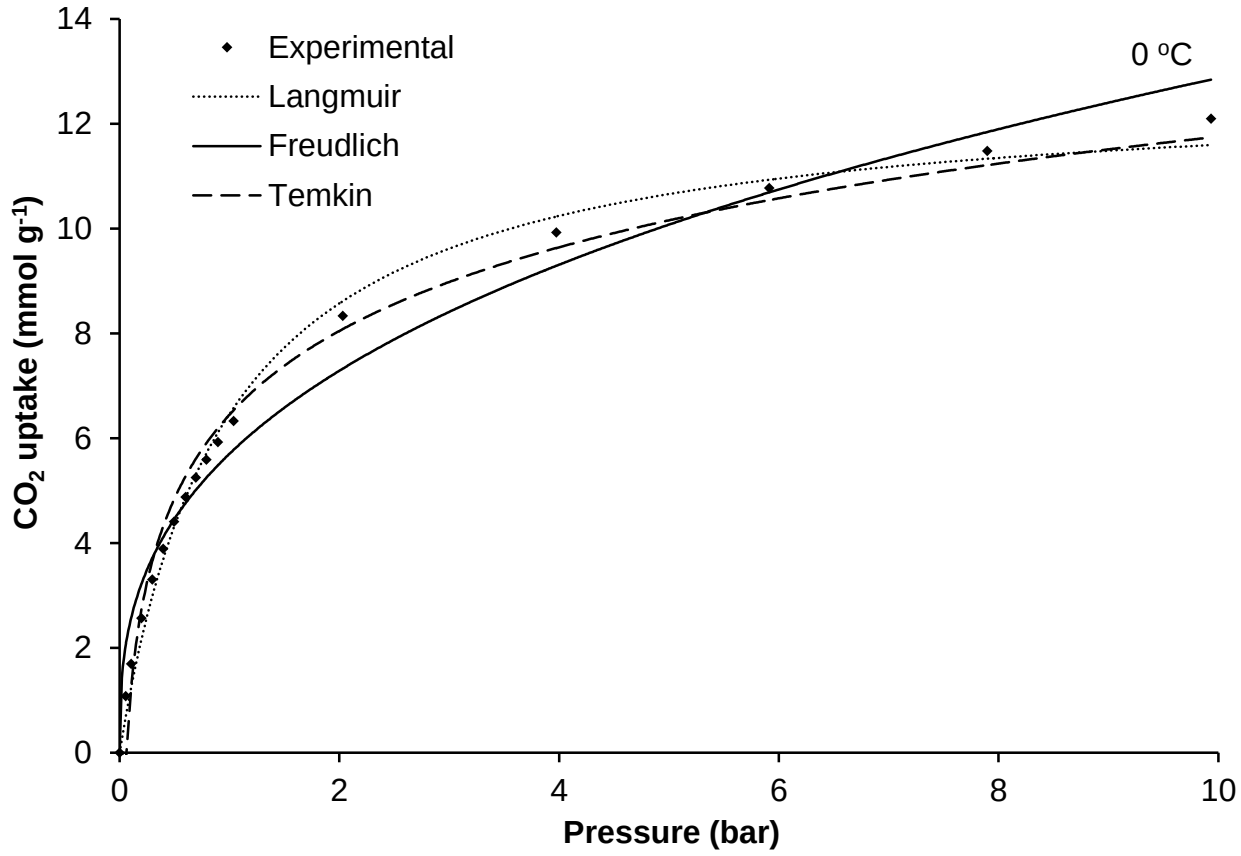

Optimised parameters for isotherm fitting

Model	Parameters	Temperature (0 °C)
Langmuir	q_m (mmol g^{-1})	12.7
	K_L(atm^{-1})	1.03
	R^2	0.995
Freundlich	K_F (mmol g^{-1} $atm^{-1/n}$)	5.71
	1/n	0.35
	R^2	0.988
Temkin	B (KJ mol^{-1})	2.30
	K_T (atm^{-1})	16.45
	R^2	0.986

S800K5

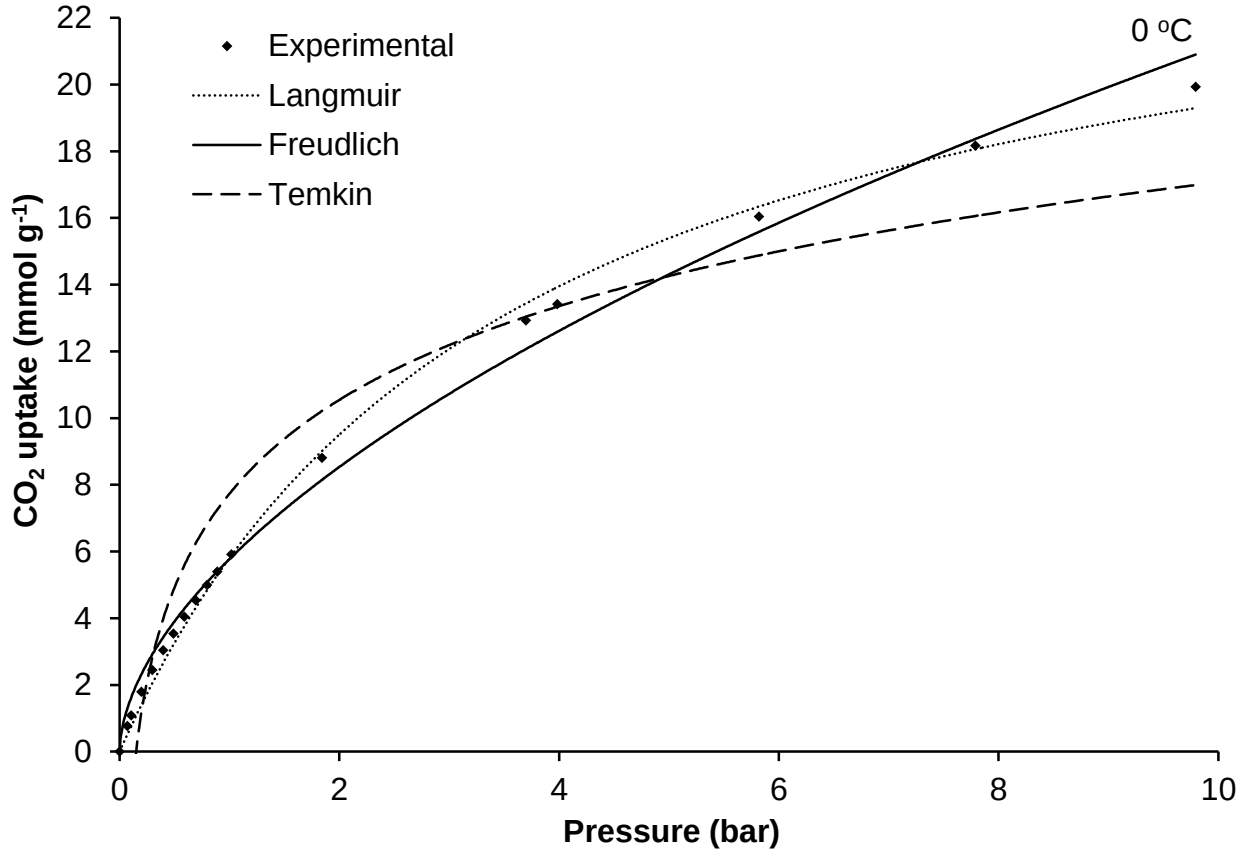

Optimised parameters for isotherm fitting

Model	Parameters	Temperature (0 °C)
Langmuir	q_m (mmol g^{-1})	26.2
	K_L(atm^{-1})	0.284
	R^2	0.997
Freundlich	K_F (mmol g^{-1} $atm^{-1/n}$)	5.78
	1/n	0.564
	R^2	0.993
Temkin	B (KJ mol^{-1})	4.06
	K_T (atm^{-1})	6.74
	R^2	0.917

Van't Hoff plots

The change in Gibbs free energy ΔG^o (KJ mol^{-1}), standard molar adsorption enthalpy ΔH^o (KJ mol^{-1}) and entropy ΔS^o (J mol^{-1} K^{-1}) were calculated using the equations:

$\Delta G^o = -RT \ln K_F$
$\ln K_F = \Delta S^o / R - \Delta H^o / RT$

where, K_F is the Freundlich equilibrium constant and ΔH^o and ΔS^o can be obtained from the slope and intercept of van't Hoff plot.

S800

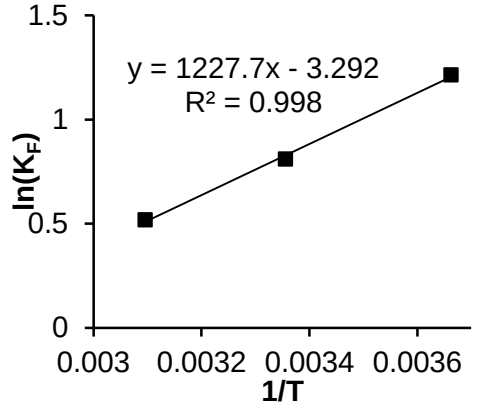

T (K)	1/T	K_F	ln(K_F)
273	0.003663	3.36428	1.213214
298	0.003356	2.2477	0.809907
323	0.003096	1.67964	0.518579

R = 8.314
Slope (= $-\Delta H^o/R$) = 1227.7
ΔH^o (KJ mol^{-1}) = -10.21

Intercept (= $\Delta S^o/R$) = -3.292
ΔS^o (J mol^{-1} K^{-1}) = -27.37

S800K2

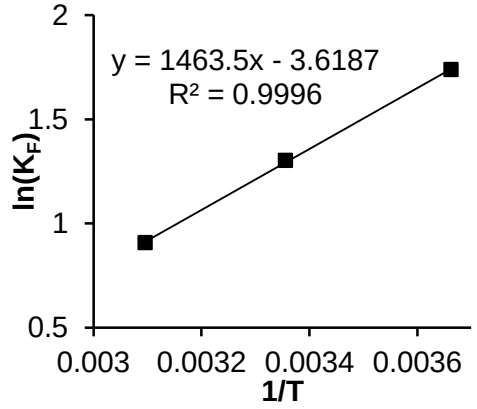

T (K)	1/T	K_F	ln(K_F)
273	0.003663	5.68403	1.73766
298	0.003356	3.67787	1.302334
323	0.003096	2.47682	0.906975

R = 8.314
Slope (= $-\Delta H^o/R$) = 1463.5
ΔH^o (KJ mol^{-1}) = -12.17

Intercept (= $\Delta S^o/R$) = -3.6187
ΔS^o (J mol^{-1} K^{-1}) = -30.09

N_2 adsorption isotherms (0.1-10 bar)

S800 at 25 ^oC

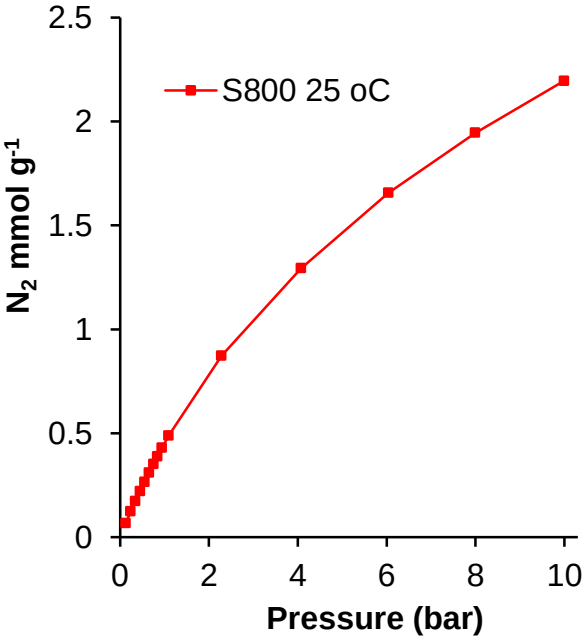

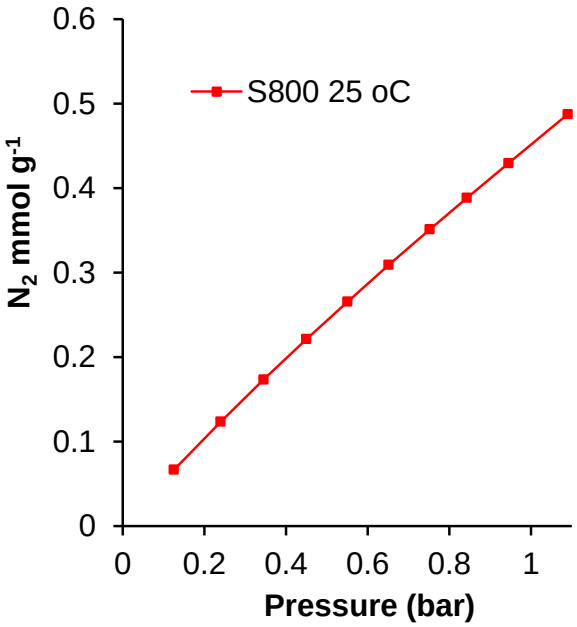

S800K2 at 25 ^oC

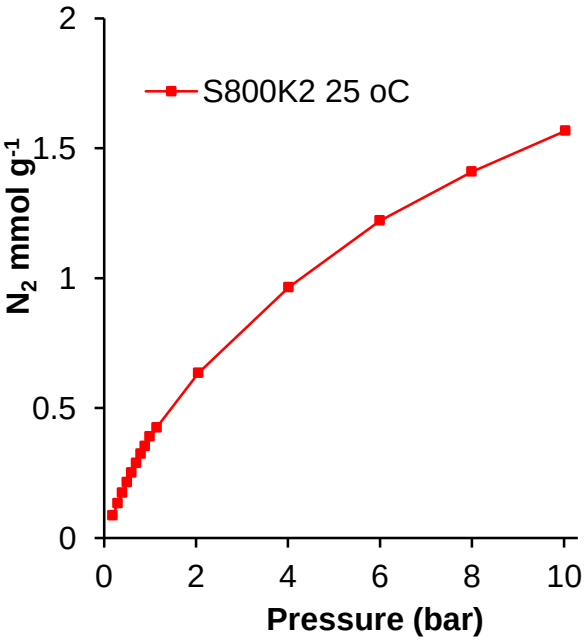

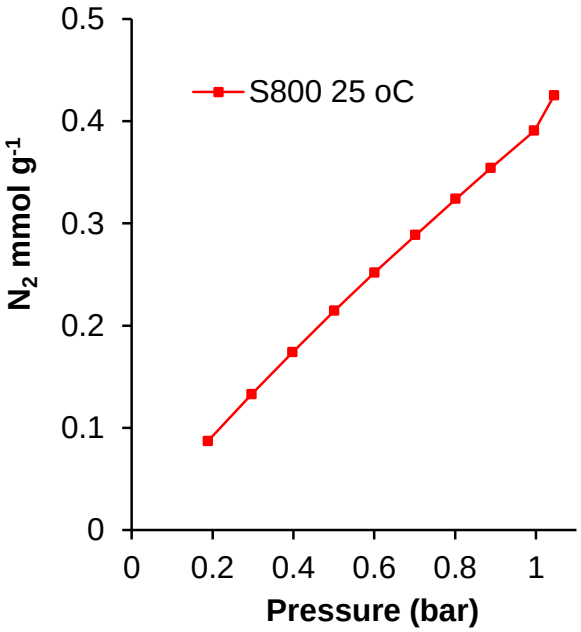

S800K2 at 0 °C

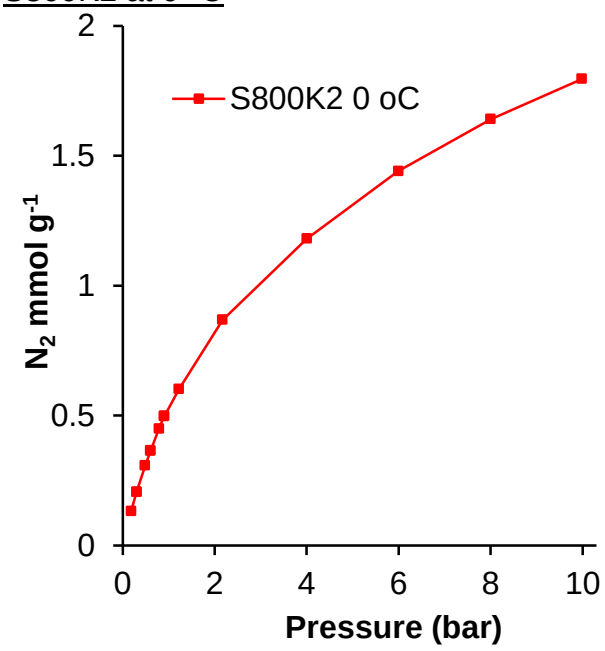

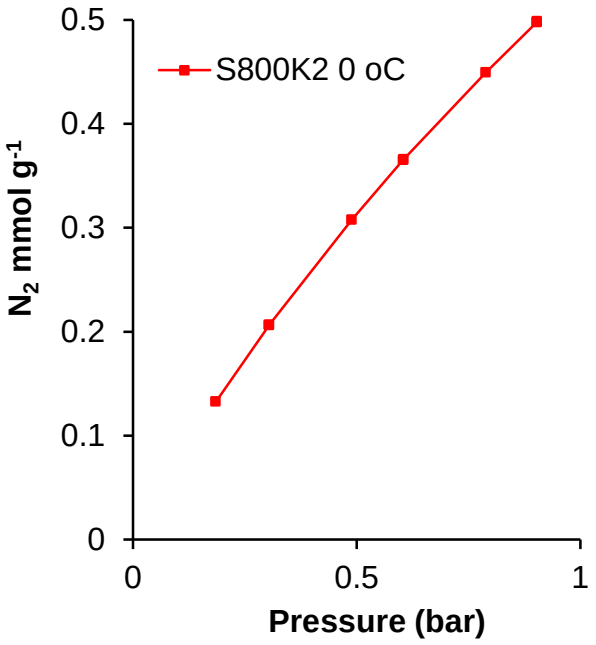

S800K5 at 0 °C

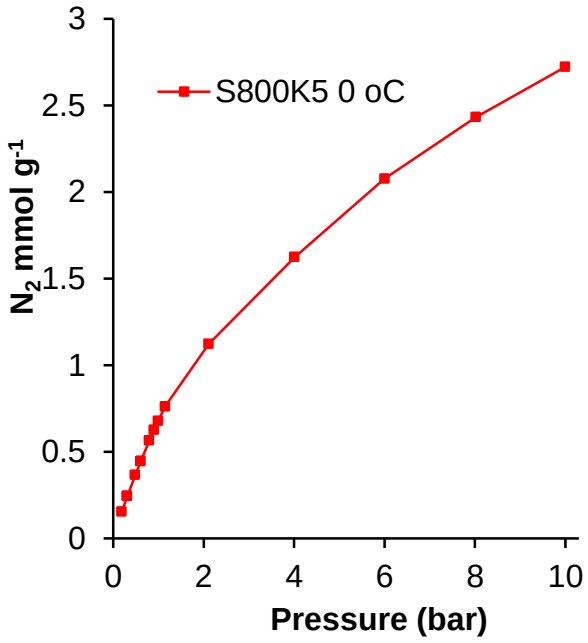

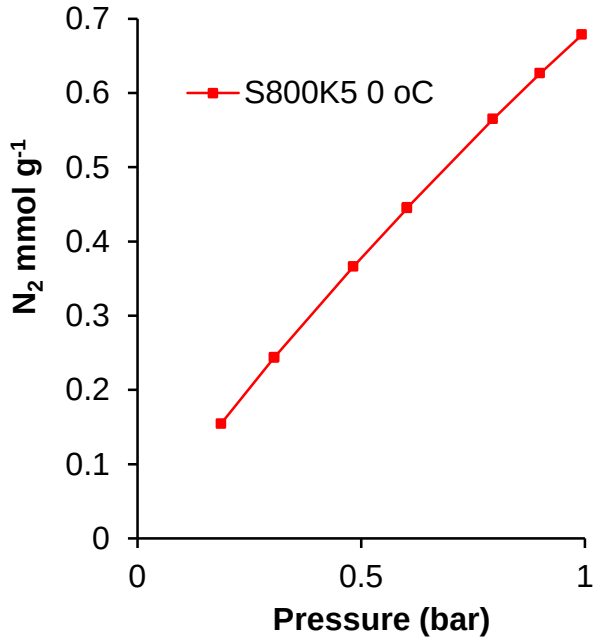

Fitting of isotherm models to the experimental N_2 adsorption data

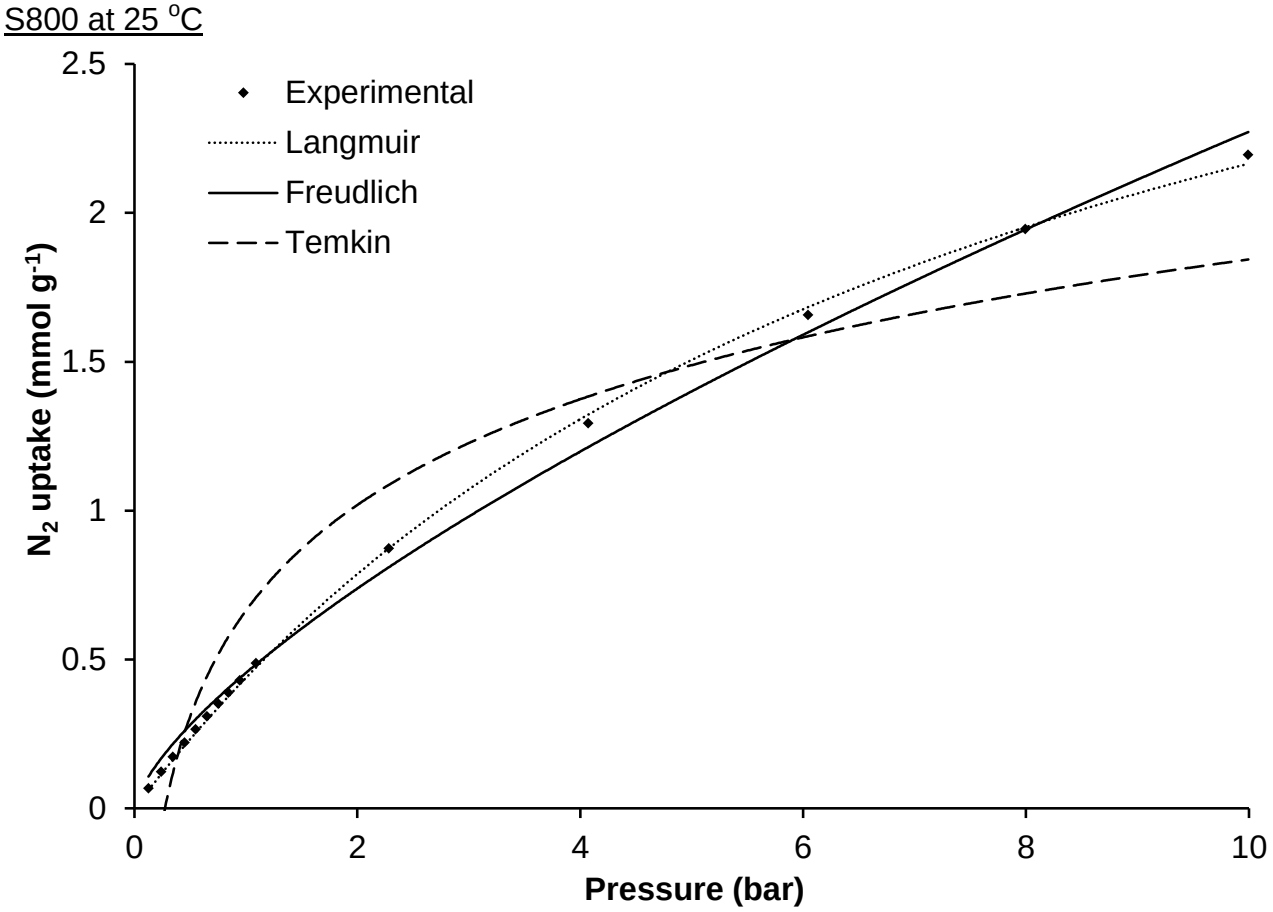

Optimised parameters for isotherm fitting

Model	Parameters	Value
Langmuir	q_m (mmol g^{-1})	3.9
	K_L(atm^{-1})	0.13
	R^2	0.999
Freundlich	K_F (mmol g^{-1} $atm^{-1/n}$)	0.46
	1/n	0.70
	R^2	0.996
Temkin	B (KJ mol^{-1})	0.51
	K_T (atm^{-1})	3.67
	R^2	0.905

S800K2 at 0 and 25 ^{o}C

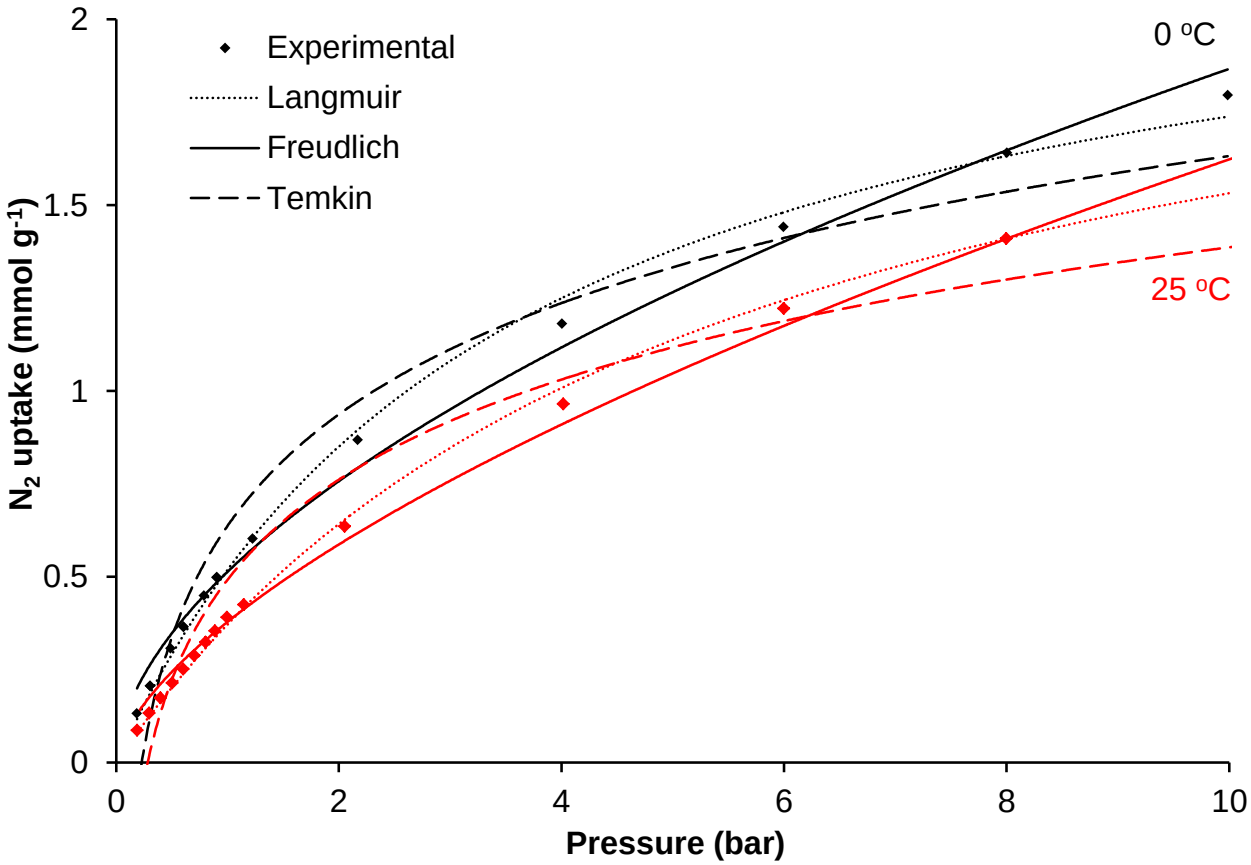

Optimised parameters for isotherm fitting

Model	Parameters	Temperature (^{o}C)	
		0	**25**
Langmuir	q_m (mmol g^{-1})	2.4	2.4
	K_L(atm^{-1})	0.28	0.19
	R^2	0.997	0.998
Freundlich	K_F (mmol g^{-1} atm$^{-1/n}$)	0.51	0.38
	1/n	056	0.63
	R^2	0.993	0.995
Temkin	B (KJ mol^{-1})	0.40	0.39
	K_T (atm^{-1})	4.37	3.55
	R^2	0.961	0.944

S800K5 at 0 ^{o}C

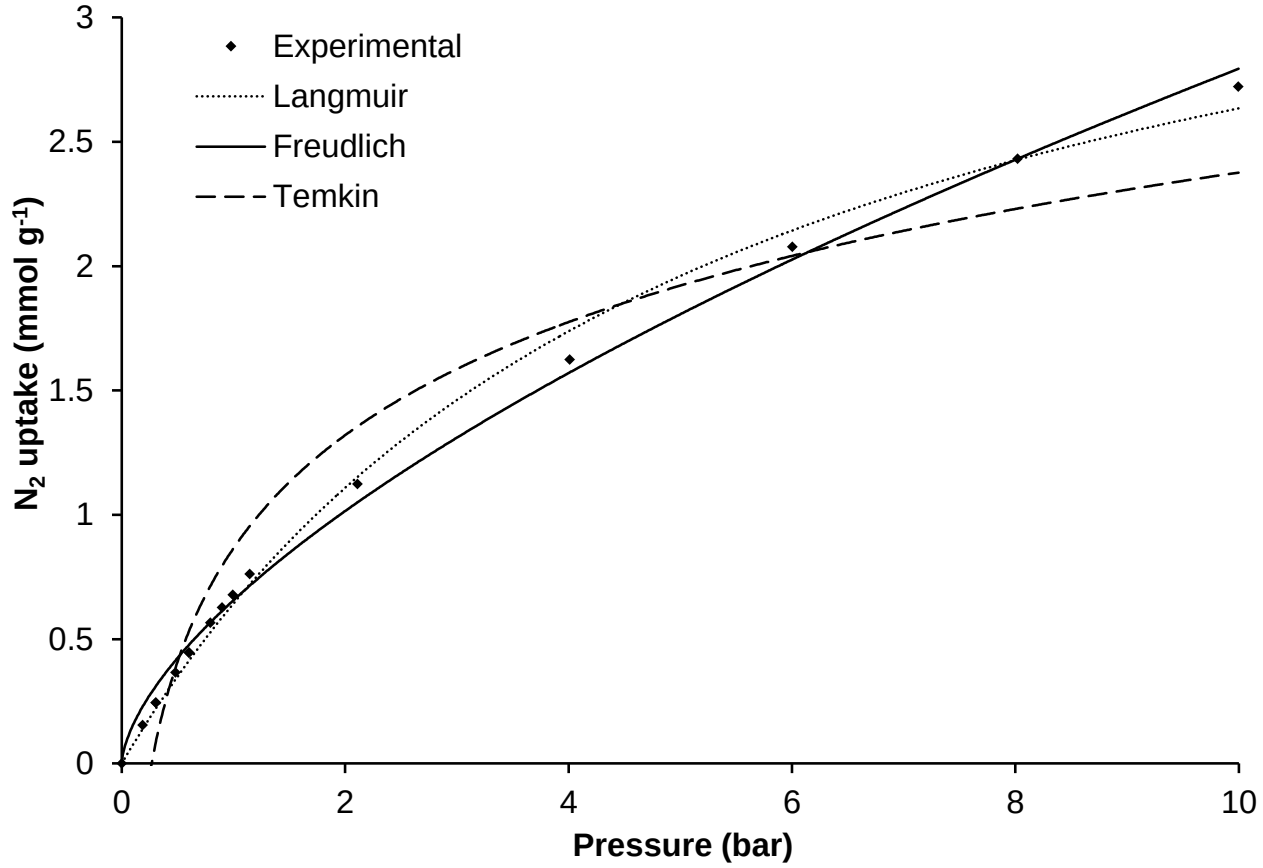

Optimised parameters for isotherm fitting

Model	Parameters	Value
Langmuir	q_m (mmol g^{-1})	4.0
	K_L(atm^{-1})	0.19
	R^2	0.997
Freundlich	K_F (mmol g^{-1} $atm^{-1/n}$)	0.66
	1/n	0.63
	R^2	0.997
Temkin	B (KJ mol^{-1})	0.60
	K_T (atm^{-1})	3.74
	R^2	0.947

Selectivities of CO_2 versus N_2 adsorption

The selectivity of CO_2 versus N_2 adsorption was calculated based on the single component adsorption isotherms by applying Ideal Adsorbed Solutions Theory (IAST): $S=(q_1p_2)/(q_2p_1)$ where q_1 (mmol g^{-1}) and q_2 (mmol g^{-1}) are the amount of CO_2 adsorbed at the equilibrium partial pressures of p_1 (bar) and p_2 (bar), respectively. The typical composition of post-combustion flue gas is 15% CO_2 and 85% N_2 by volume. Therefore, the equilibrium partial pressures of N_2 and CO_2 in the bulk phase were deemed to be 0.85 bar and 0.15 bar.

S800 and S800K2 at 25 °C

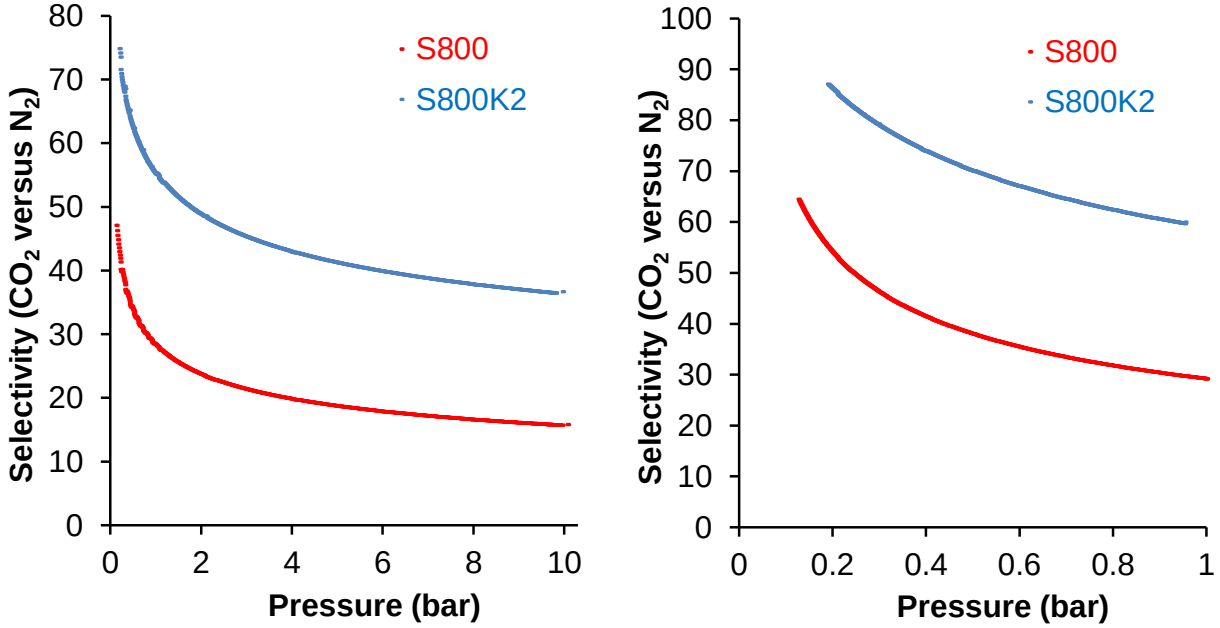

The 0-1 bar graph is plotted using data calculated using only the 0-1 bar adsorption isotherms. This will give low pressure selectivities (0-1 bar) that are more accurate than those calculated using the whole 0-10 bar adsorption isotherms.

S800K2 and S800K5 at 0 °C

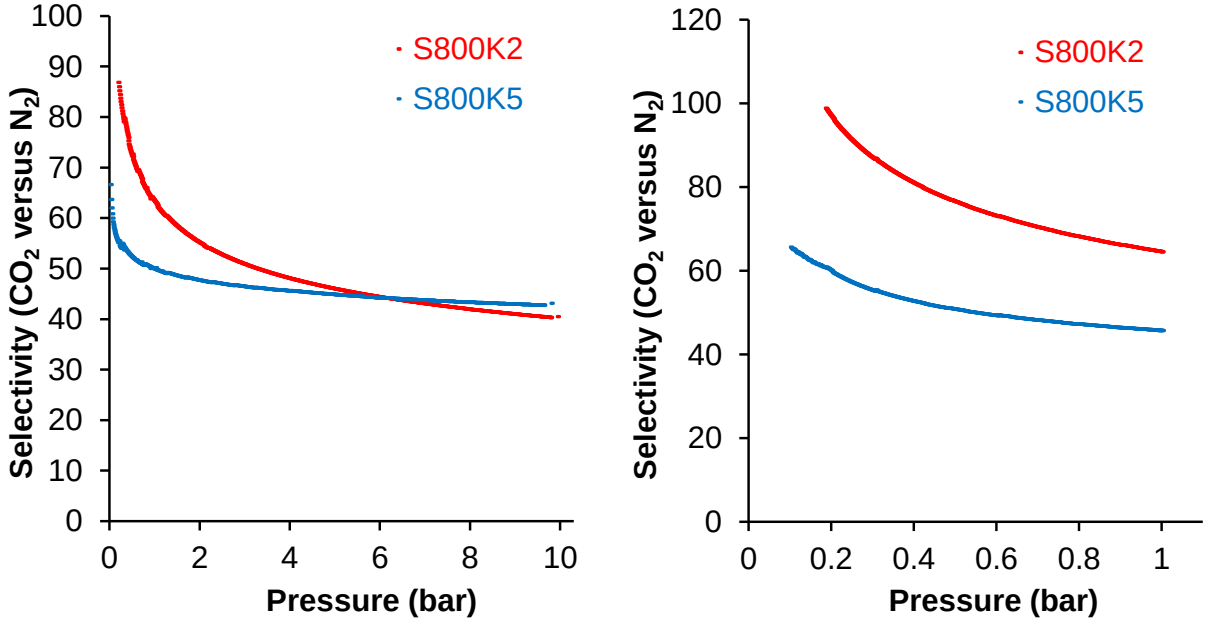

The 0.1-1 bar graph is plotted using data calculated using only the 0.1-1 bar adsorption isotherms. This will give low pressure selectivities (0.1-1 bar) that are more accurate than those calculated using the whole 0.1-10 bar adsorption isotherms.

Norit activated carbon, S800SE and S800 at 25 ^{o}C

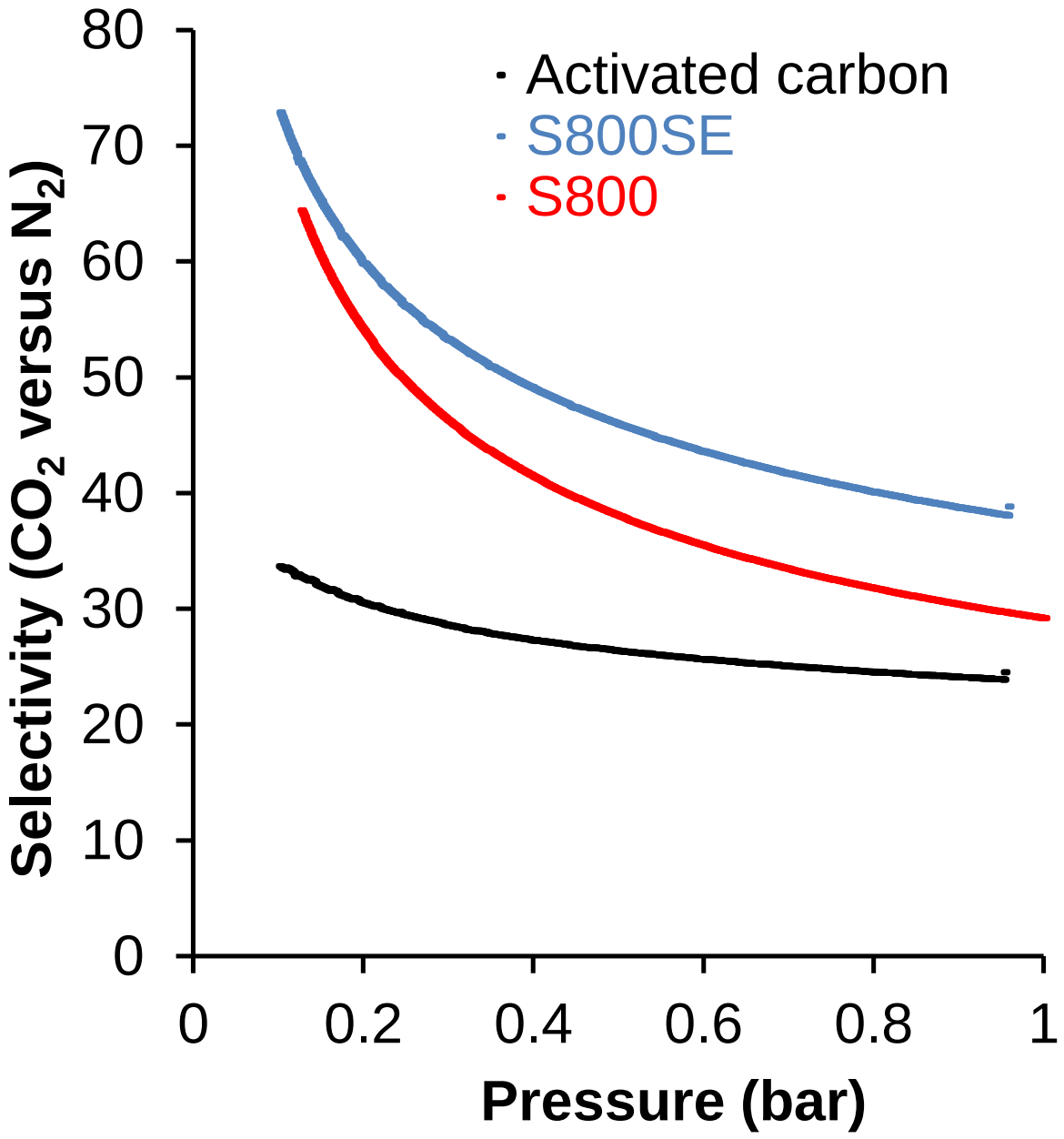

CO_2 and N_2 adsorption isotherm data for Norit activated carbon and S800SE (prepared by the solvent exchange method) are taken from (*Angew. Chem. Int. Ed.* **2016**, *55*, 9173–9177) and compared with the data obtained in this work for S800. As the Norit activated carbon and S800SE data was measured by porosimetry, only 0.1-1 bar data is available.

Tabulation of selectivities

SAMPLE	Selectivity at 1 bar	Selectivity at 10 bar
Activated Carbon 25 ^{o}C	24.5	
S800SE	38.7	
S800 25 ^{o}C	29.1	15.7
S800K2 25 ^{o}C	59.9	36.6
S800K2 0 ^{o}C	64.5	40.5
S800K5 0 ^{o}C	45.6	43.1

Tabulation of material physical properties and CO_2 uptake parameters

Material	Ultramicropore surface area ($m^2 g^{-1}$)	Micropore surface area ($m^2 g^{-1}$)	External surface area ($m^2 g^{-1}$)	BET surface area ($m^2 g^{-1}$)	Ultramicropore volume$_{<0.7\ nm}$ ($cm^3 g^{-1}$)	CO_2 uptake (mmol g^{-1})	CO_2 adsorption enthalpy (-KJ mol^{-1})	K_1 for CO_2 adsorption (min^{-1})
S300		154	151	305		0.48	40.2	6.81
S600		533	94	627	0.18	1.07	42.4	6.55
S800	253	543	76	619	0.19	1.59	35.3	8.85
S1000	210	437	83	520	0.15	1.09	38.3	8.32
A800	161	160	163	322	0.08	1.36	48.6	5.16
P800	142	135	127	262	0.07	1.07	52.9	7.33
S600K4	467	1784	106	1890	0.5	2.02	29.1	5.51
S1000K4	316	1151	353	1503	0.28	1.11	34.5	4.74
S800K1	868	908	306	1214	0.32	2.39	31.7	4.36
S800K2	1225	1177	117	1294	0.39	3.11	33.6	3.3
S800K3	1105	1468	165	1633	0.45	2.93	32.7	4.05
S800K4	727	1781	518	2299	0.46	2.14	30.9	5.25
S800K5	804	1404	1048	2452	0.57	2.07	26.7	4.38
A600K2	718	598	89	687	0.22	1.64	46	4.52
A800K2	837	1249	143	1392	0.43	2.95	38.5	3.6
A1000K2	230	923	311	1233	0.33	2.16	38	4.22
A800K1	271	626	491	1117	0.29	1.98	38.6	2.92
A800K3	1017	1699	253	1952	0.57	2.82	36.1	3.06
A800K4	529	1482	937	2419	0.39	2.25	33.3	3.55
A800K5	669	1102	1311	2414	0.55	1.75	38.2	5.68
P800K2	960	1251	644	1895	0.52	2.39	36.9	3.79
P800K3	705	1152	594	1747	0.47	2.07	35.1	2.46
P800K5	572	812	1142	1954	0.43	1.25	37.6	5.57
S800C15	103	430	99	529	0.17	1.64	25	3.74
S850C15	600	462	175	637	0.2	1.77	36.3	4.85
S900C15	931	745	238	983	0.31	1.98	35.8	4.93

S950C15	738	668	261	930	0.28	1.82	34.9	5.59
S1000C15	803	1033	502	1535	0.42	1.77	40.2	5.58
S900C30	940	827	292	1119	0.34	1.77	31.9	6.29
S900C60	934	805	292	1097	0.33	1.98	36.4	5.08
S900C90	935	1089	386	1475	0.43	1.91	37.4	6.9
S900C120	1022	1331	583	1914	0.52	1.89	35.9	6.5
S950C60	802	1418	761	2180	0.53	1.82	42.7	6.04
S950C90	731	1193	1264	2457	0.56	1.52	46.7	8.71
S950C120	609	703	2030	2733	0.56	1.18	53.7	9.1
A750C45	13	393	344	738	0.21	1.43	45.7	4.23
A750C60	13	385	371	756	0.21	1.41	47.5	5.71
A750C90	544	363	399	762	0.21	1.43	43.7	3.57
A900C0	30	343	479	822	0.22	1.39	46.4	5.49
A900C10	29	237	631	868	0.21	1.14	48.2	5.85
P700C50	586	404	330	734	0.21	1.30	68.5	6.6
P900C0	401	260	686	946	0.22	1.20	69	5.71
S700O0	770	732	165	897	0.27	1.98	32.2	6
S750O0	369	933	168	1100	0.33	2.02	34.6	4.29
S800O0	724	704	230	935	0.28	1.82	30	4.98
S750O40	632	772	118	889	0.27	1.91	30.8	5.22
S750O56	604	590	188	777	0.23	1.89	36.7	4.65
A500O30	23	354	286	640	0.18	1.36	47	5.2
A500O60	123	396	251	647	0.19	1.32	46.3	5.14
A750O0	505	364	265	629	0.17	1.41	30.6	5.69
P400O50	293	209	177	385	0.11	1.02	73.5	

BET surface area = External surface area + micropore surface area
Micropore volume = Ultramicropore volume + supramicropore volume
Ultramicropore surface area is determined by the DFT model

Material	Supramicropore volume$_{0.7\text{-}2\ nm}$ ($cm^3\ g^{-1}$)	Micropore volume$_{<2\ nm}$ ($cm^3\ g^{-1}$)	Mesopore volume ($cm^3\ g^{-1}$)	Total pore volume P/P_0=0.99 ($cm^3\ g^{-1}$)	Ultramicropore volume / total pore volume	CO_2 uptake (mmol g^{-1})	CO_2 adsorption enthalpy (-KJ mol^{-1})	K_1 for CO_2 adsorption (min^{-1})
S300	0.13	0.13	0.22	0.35		0.48	40.2	6.81
S600	0.07	0.25	0.34	0.59	0.31	1.07	42.4	6.55
S800	0.05	0.24	0.35	0.59	0.32	1.59	35.3	8.85
S1000	0.05	0.2	0.39	0.59	0.25	1.09	38.3	8.32
A800	0.05	0.13	0.71	0.81	0.1	1.36	48.6	5.16
P800	0.04	0.11	0.43	0.54	0.13	1.07	52.9	7.33
S600K4	0.23	0.73	0.13	0.84	0.6	2.02	29.1	5.51
S1000K4	0.34	0.62	0.23	0.84	0.33	1.11	34.5	4.74
S800K1	0.16	0.48	0.58	1.06	0.3	2.39	31.7	4.36
S800K2	0.1	0.49	0.1	0.59	0.66	3.11	33.6	3.3
S800K3	0.17	0.62	0.14	0.77	0.58	2.93	32.7	4.05
S800K4	0.45	0.91	0.07	0.98	0.47	2.14	30.9	5.25
S800K5	0.43	1	0.09	1.09	0.52	2.07	26.7	4.38
A600K2	0.05	0.27	0.08	0.36	0.61	1.64	46	4.52
A800K2	0.1	0.53	0.15	0.67	0.64	2.95	38.5	3.6
A1000K2	0.16	0.49	0.3	0.8	0.41	2.16	38	4.22
A800K1	0.17	0.46	0.82	1.31	0.22	1.98	38.6	2.92
A800K3	0.18	0.75	0.09	0.85	0.67	2.82	36.1	3.06
A800K4	0.56	0.95	0.18	1.15	0.34	2.25	33.3	3.55
A800K5	0.46	1.01	0.1	1.09	0.51	1.75	38.2	5.68
P800K2	0.25	0.77	0.18	0.97	0.54	2.39	36.9	3.79
P800K3	0.26	0.73	0.13	0.86	0.55	2.07	35.1	2.46
P800K5	0.39	0.82	0.2	1.02	0.42	1.25	37.6	5.57
S800C15	0.04	0.21	0.37	0.58	0.29	1.64	25	3.74
S850C15	0.06	0.26	0.31	0.6	0.33	1.77	36.3	4.85
S900C15	0.08	0.39	0.38	0.77	0.4	1.98	35.8	4.93
S950C15	0.1	0.38	0.35	0.73	0.38	1.82	34.9	5.59

S1000C15	0.2	0.62	0.52	1.16	0.36	1.77	40.2	5.58
S900C30	0.11	0.45	0.5	0.98	0.35	1.77	31.9	6.29
S900C60	0.11	0.44	0.4	0.89	0.37	1.98	36.4	5.08
S900C90	0.16	0.59	0.45	1.05	0.41	1.91	37.4	6.9
S900C120	0.25	0.77	0.71	1.49	0.35	1.89	35.9	6.5
S950C60	0.36	0.89	0.41	1.32	0.4	1.82	42.7	6.04
S950C90	0.48	1.04	0.59	1.64	0.34	1.52	46.7	8.71
S950C120	0.6	1.16	0.96	2.09	0.27	1.18	53.7	9.1
A750C45	0.1	0.31	0.68	0.99	0.21	1.43	45.7	4.23
A750C60	0.11	0.32	0.76	1.09	0.19	1.41	47.5	5.71
A750C90	0.11	0.32	0.74	1.05	0.2	1.43	43.7	3.57
A900C0	0.13	0.35	0.86	1.18	0.19	1.39	46.4	5.49
A900C10	0.17	0.38	0.98	1.33	0.16	1.14	48.2	5.85
P700C50	0.1	0.31	0.47	0.78	0.27	1.30	68.5	6.6
P900C0	0.18	0.4	0.54	0.93	0.24	1.20	69	5.71
S700O0	0.08	0.35	0.14	0.5	0.54	1.98	32.2	6
S750O0	0.1	0.43	0.14	0.58	0.57	2.02	34.6	4.29
S800O0	0.09	0.37	0.2	0.57	0.49	1.82	30	4.98
S750O40	0.08	0.35	0.09	0.45	0.6	1.91	30.8	5.22
S750O56	0.08	0.31	0.15	0.46	0.5	1.89	36.7	4.65
A500O30	0.09	0.27	0.7	0.97	0.19	1.36	47	5.2
A500O60	0.08	0.27	0.66	0.96	0.2	1.32	46.3	5.14
A750O0	0.09	0.26	0.67	0.94	0.18	1.41	30.6	5.69
P400O50	0.05	0.16	0.44	0.6	0.18	1.02	73.5	

BET surface area = External surface area + micropore surface area
Micropore volume = Ultramicropore volume + supramicropore volume
Ultramicropore surface area is determined by the DFT model

Material	Supramicropore volume / total pore volume	Micropore volume / total pore volume	Mesopore volume / total pore volume	Micropore volume / mesopore volume	CO_2 uptake (mmol g^{-1})	CO_2 adsorption enthalpy (-KJ mol^{-1})	K_1 for CO_2 adsorption (min^{-1})
S300	0.37	0.37	0.63	0.59	0.48	40.2	6.81
S600	0.12	0.42	0.58	0.74	1.07	42.4	6.55
S800	0.08	0.41	0.59	0.69	1.59	35.3	8.85
S1000	0.08	0.34	0.66	0.51	1.09	38.3	8.32
A800	0.06	0.16	0.88	0.18	1.36	48.6	5.16
P800	0.07	0.2	0.80	0.26	1.07	52.9	7.33
S600K4	0.27	0.87	0.15	5.62	2.02	29.1	5.51
S1000K4	0.40	0.74	0.27	2.70	1.11	34.5	4.74
S800K1	0.15	0.45	0.55	0.83	2.39	31.7	4.36
S800K2	0.17	0.83	0.17	4.90	3.11	33.6	3.3
S800K3	0.22	0.81	0.18	4.43	2.93	32.7	4.05
S800K4	0.46	0.93	0.07	13.00	2.14	30.9	5.25
S800K5	0.39	0.92	0.08	11.11	2.07	26.7	4.38
A600K2	0.14	0.75	0.22	3.38	1.64	46	4.52
A800K2	0.15	0.79	0.22	3.53	2.95	38.5	3.6
A1000K2	0.20	0.61	0.38	1.63	2.16	38	4.22
A800K1	0.13	0.35	0.63	0.56	1.98	38.6	2.92
A800K3	0.21	0.88	0.11	8.33	2.82	36.1	3.06
A800K4	0.49	0.83	0.16	5.28	2.25	33.3	3.55
A800K5	0.42	0.93	0.09	10.10	1.75	38.2	5.68
P800K2	0.26	0.79	0.19	4.28	2.39	36.9	3.79
P800K3	0.30	0.85	0.15	5.62	2.07	35.1	2.46
P800K5	0.38	0.8	0.20	4.10	1.25	37.6	5.57
S800C15	0.07	0.36	0.64	0.57	1.64	25	3.74
S850C15	0.10	0.43	0.52	0.84	1.77	36.3	4.85
S900C15	0.10	0.51	0.49	1.03	1.98	35.8	4.93
S950C15	0.14	0.52	0.48	1.09	1.82	34.9	5.59
S1000C15	0.17	0.53	0.45	1.19	1.77	40.2	5.58

S900C30	0.11	0.46	0.51	0.90	1.77	31.9	6.29
S900C60	0.12	0.49	0.45	1.10	1.98	36.4	5.08
S900C90	0.15	0.56	0.43	1.31	1.91	37.4	6.9
S900C120	0.17	0.52	0.48	1.08	1.89	35.9	6.5
S950C60	0.27	0.67	0.31	2.17	1.82	42.7	6.04
S950C90	0.29	0.63	0.36	1.76	1.52	46.7	8.71
S950C120	0.29	0.56	0.46	1.21	1.18	53.7	9.1
A750C45	0.10	0.31	0.69	0.46	1.43	45.7	4.23
A750C60	0.10	0.29	0.70	0.42	1.41	47.5	5.71
A750C90	0.10	0.3	0.70	0.43	1.43	43.7	3.57
A900C0	0.11	0.3	0.73	0.41	1.39	46.4	5.49
A900C10	0.13	0.29	0.74	0.39	1.14	48.2	5.85
P700C50	0.13	0.4	0.60	0.66	1.30	68.5	6.6
P900C0	0.19	0.43	0.58	0.74	1.20	69	5.71
S700O0	0.16	0.7	0.28	2.50	1.98	32.2	6
S750O0	0.17	0.74	0.24	3.07	2.02	34.6	4.29
S800O0	0.16	0.65	0.35	1.85	1.82	30	4.98
S750O40	0.18	0.78	0.20	3.89	1.91	30.8	5.22
S750O56	0.17	0.67	0.33	2.07	1.89	36.7	4.65
A500O30	0.09	0.28	0.72	0.39	1.36	47	5.2
A500O60	0.08	0.28	0.69	0.41	1.32	46.3	5.14
A750O0	0.10	0.28	0.71	0.39	1.41	30.6	5.69
P400O50	0.08	0.27	0.73	0.36	1.02	73.5	

BET surface area = External surface area + micropore surface area
Micropore volume = Ultramicropore volume + supramicropore volume
Ultramicropore surface area is determined by the DFT model

Material	Ultramicropore Volume$_{0.4\text{-}0.7\ nm}$ ($cm^3\ g^{-1}$)	Ultramicropore (0.4-0.7 nm) volume / total pore volume	CO_2 uptake ($mmol\ g^{-1}$)	CO_2 adsorption enthalpy ($-KJ\ mol^{-1}$)	K_1 for CO_2 adsorption (min^{-1})
S300			0.48	40.2	6.81
S600	0.18	0.31	1.07	42.4	6.55
S800	0.18	0.31	1.59	35.3	8.85
S1000	0.14	0.24	1.09	38.3	8.32
A800	0.07	0.09	1.36	48.6	5.16
P800	0.04	0.07	1.07	52.9	7.33
S600K4	0.4	0.48	2.02	29.1	5.51
S1000K4	0.19	0.23	1.11	34.5	4.74
S800K1	0.23	0.22	2.39	31.7	4.36
S800K2	0.29	0.49	3.11	33.6	3.3
S800K3	0.35	0.45	2.93	32.7	4.05
S800K4	0.39	0.40	2.14	30.9	5.25
S800K5	0.46	0.42	2.07	26.7	4.38
A600K2	0.13	0.36	1.64	46	4.52
A800K2	0.36	0.54	2.95	38.5	3.6
A1000K2	0.32	0.40	2.16	38	4.22
A800K1	0.27	0.21	1.98	38.6	2.92
A800K3	0.48	0.56	2.82	36.1	3.06
A800K4	0.33	0.29	2.25	33.3	3.55
A800K5	0.48	0.44	1.75	38.2	5.68
P800K2	0.39	0.40	2.39	36.9	3.79
P800K3	0.43	0.50	2.07	35.1	2.46
P800K5	0.35	0.34	1.25	37.6	5.57
S800C15	0.16	0.28	1.64	25	3.74
S850C15	0.19	0.32	1.77	36.3	4.85
S900C15	0.18	0.23	1.98	35.8	4.93
S950C15	0.17	0.23	1.82	34.9	5.59
S1000C15	0.31	0.27	1.77	40.2	5.58
S900C30	0.23	0.23	1.77	31.9	6.29

S900C60	0.2	0.22	1.98	36.4	5.08
S900C90	0.3	0.29	1.91	37.4	6.9
S900C120	0.4	0.27	1.89	35.9	6.5
S950C60	0.42	0.32	1.82	42.7	6.04
S950C90	0.45	0.27	1.52	46.7	8.71
S950C120	0.47	0.22	1.18	53.7	9.1
A750C45	0.1	0.10	1.43	45.7	4.23
A750C60	0.1	0.09	1.41	47.5	5.71
A750C90	0.11	0.10	1.43	43.7	3.57
A900C0	0.12	0.10	1.39	46.4	5.49
A900C10	0.13	0.10	1.14	48.2	5.85
P700C50	0.11	0.14	1.30	68.5	6.6
P900C0	0.16	0.17	1.20	69	5.71
S700O0	0.14	0.28	1.98	32.2	6
S750O0	0.18	0.31	2.02	34.6	4.29
S800O0	0.17	0.30	1.82	30	4.98
S750O40	0.17	0.38	1.91	30.8	5.22
S750O56	0.13	0.28	1.89	36.7	4.65
A500O30	0.08	0.08	1.36	47	5.2
A500O60	0.09	0.09	1.32	46.3	5.14
A750O0	0.09	0.10	1.41	30.6	5.69
P400O50	0.06	0.10	1.02	73.5	

Plots of textural properties with CO_2 uptake parameters

Plot of CO_2 adsorption capacity against external surface area

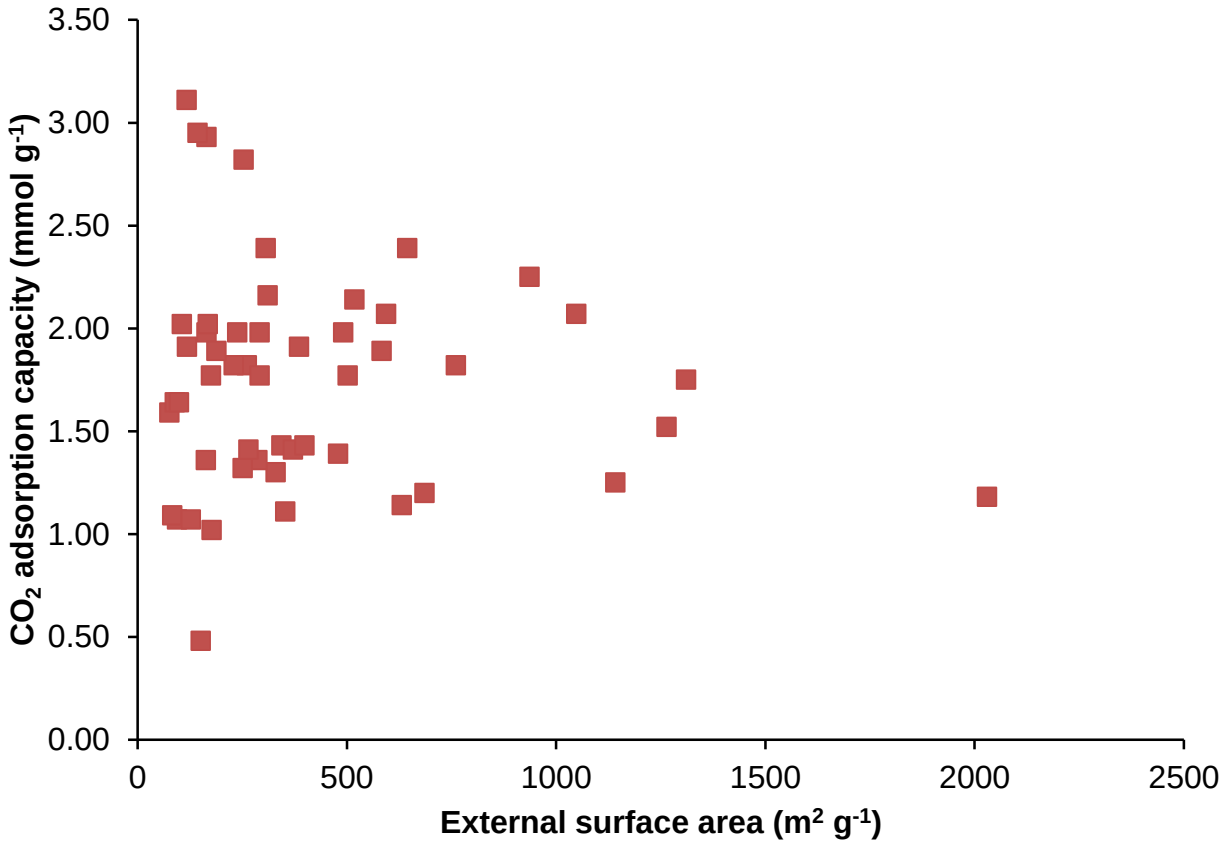

Plot of CO_2 adsorption enthalpy against external surface area

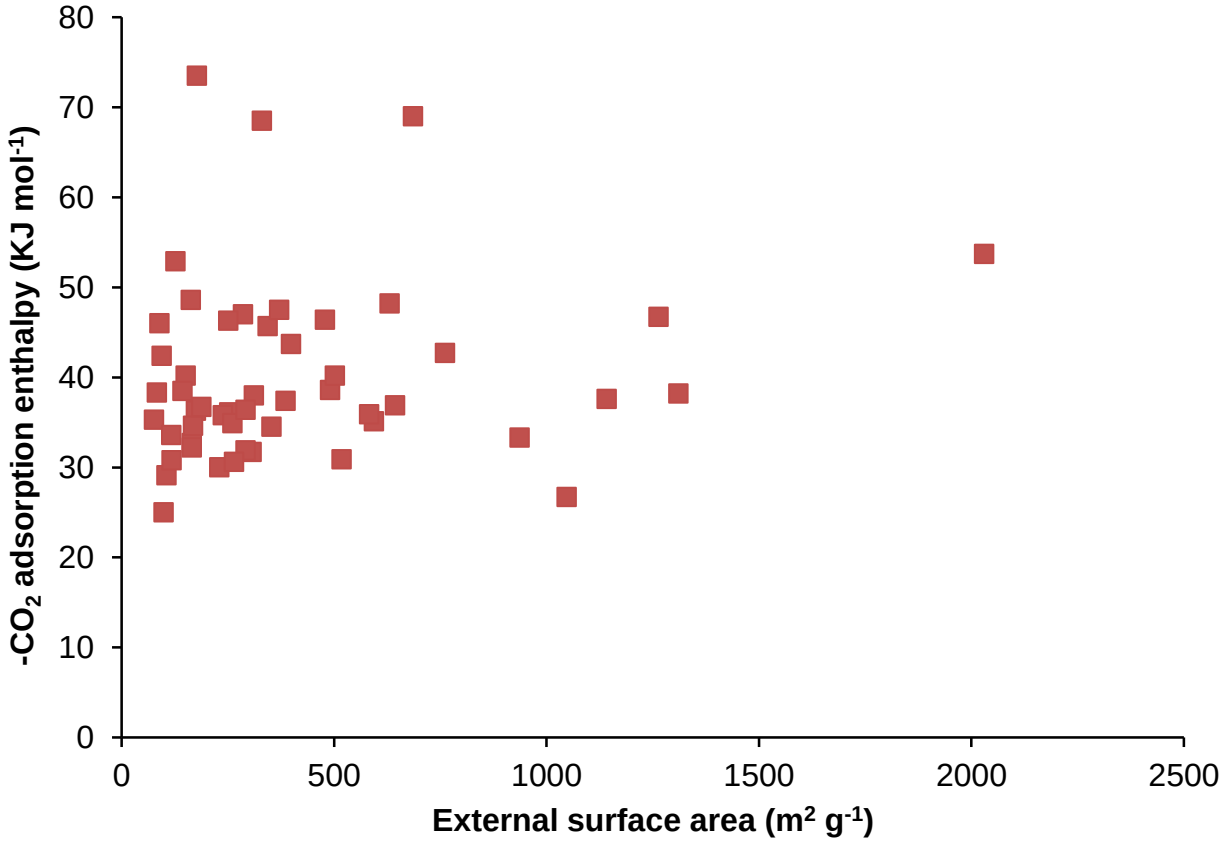

Plot of K_1 for CO_2 adsorption against external surface area

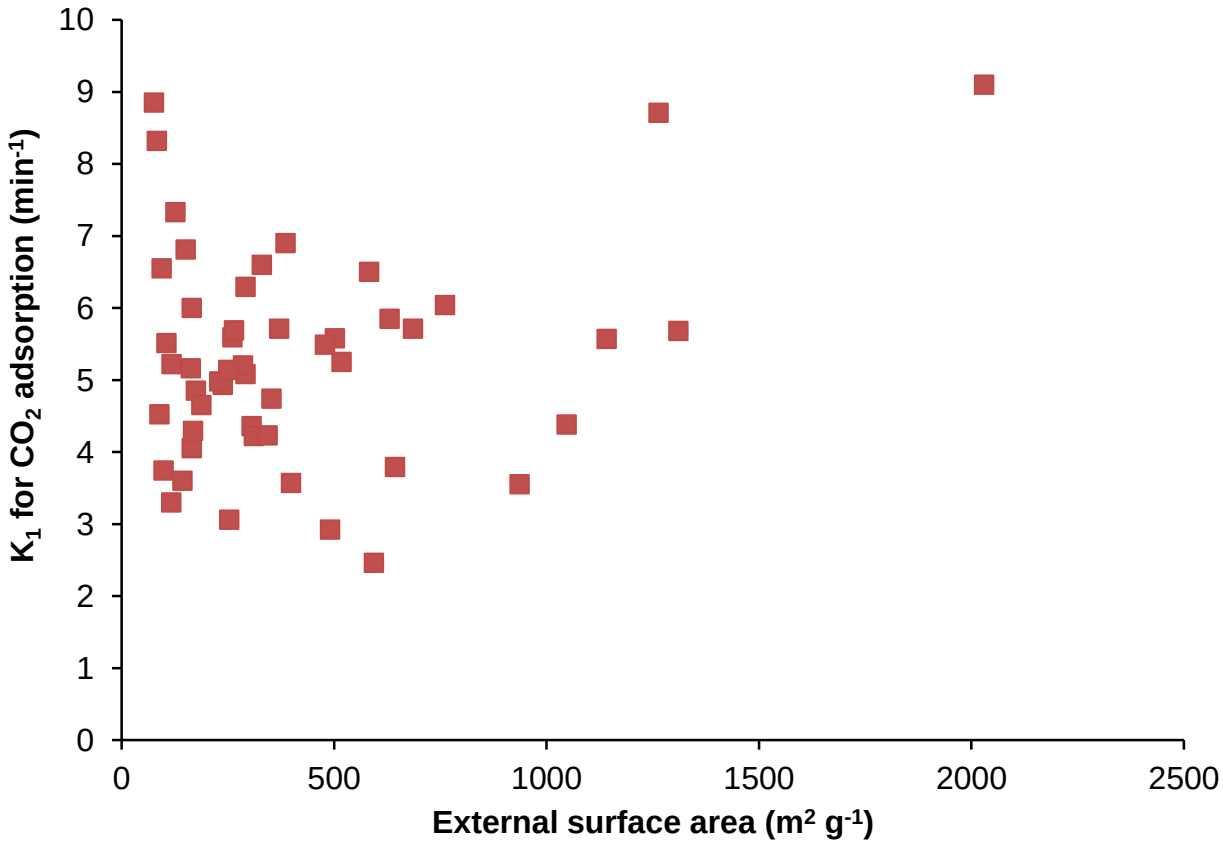

Plot of CO_2 adsorption capacity against ultramicropore surface area

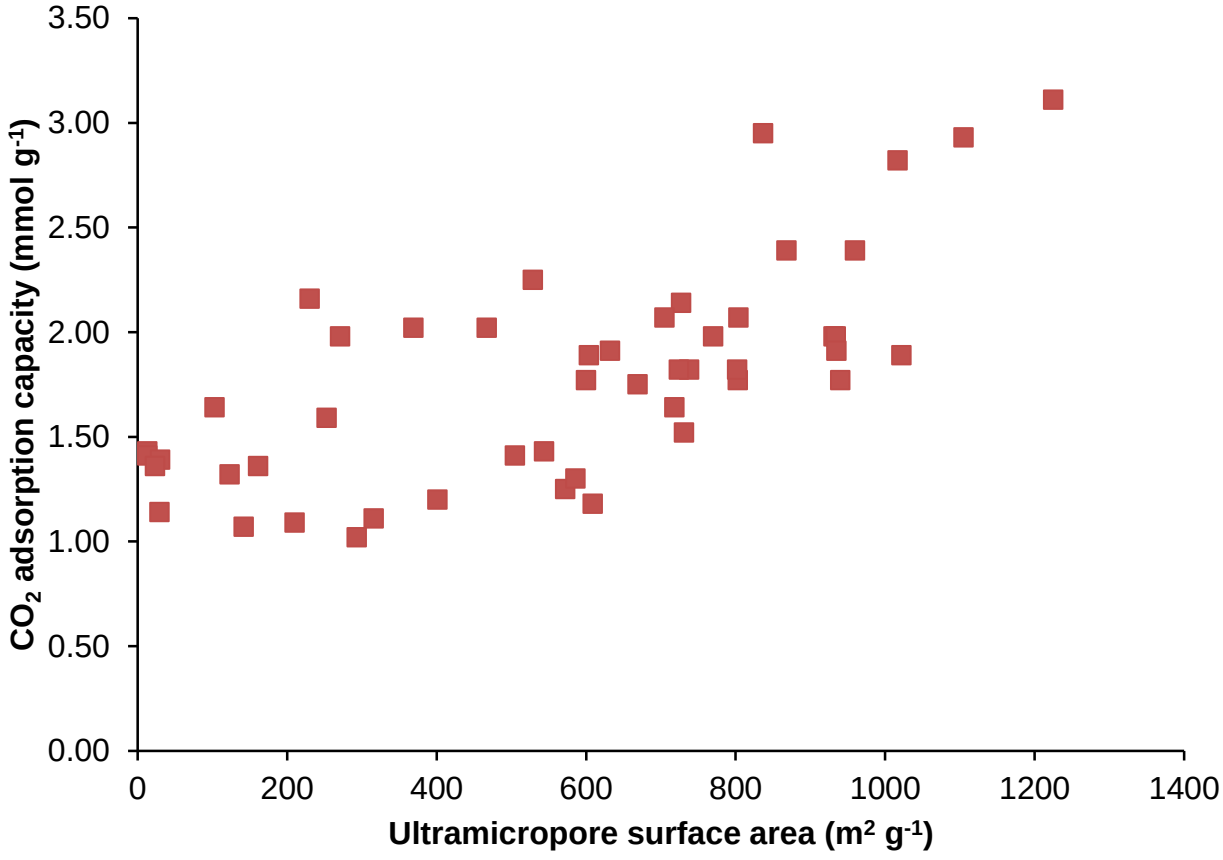

Plot of CO_2 adsorption enthalpy against ultramicropore surface area

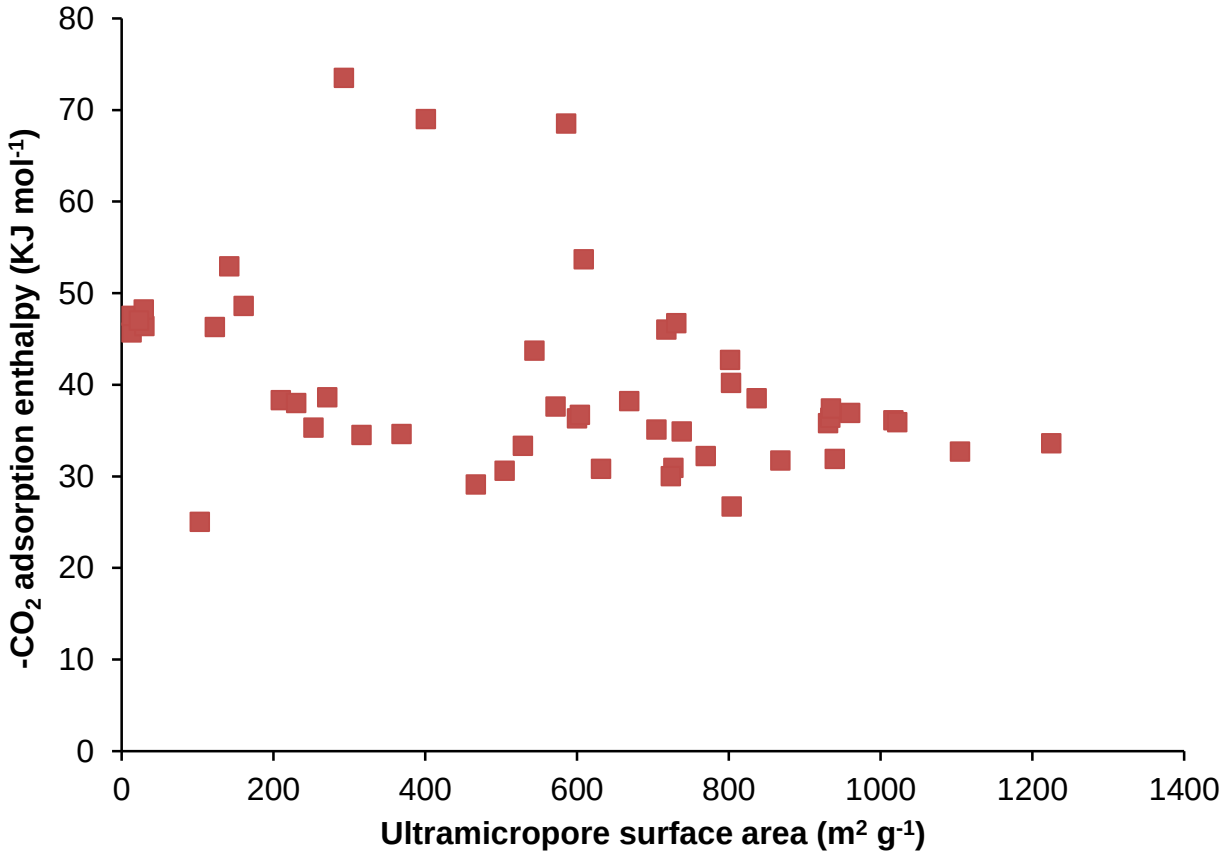

Plot of K_1 for CO_2 adsorption against ultamicropore surface area

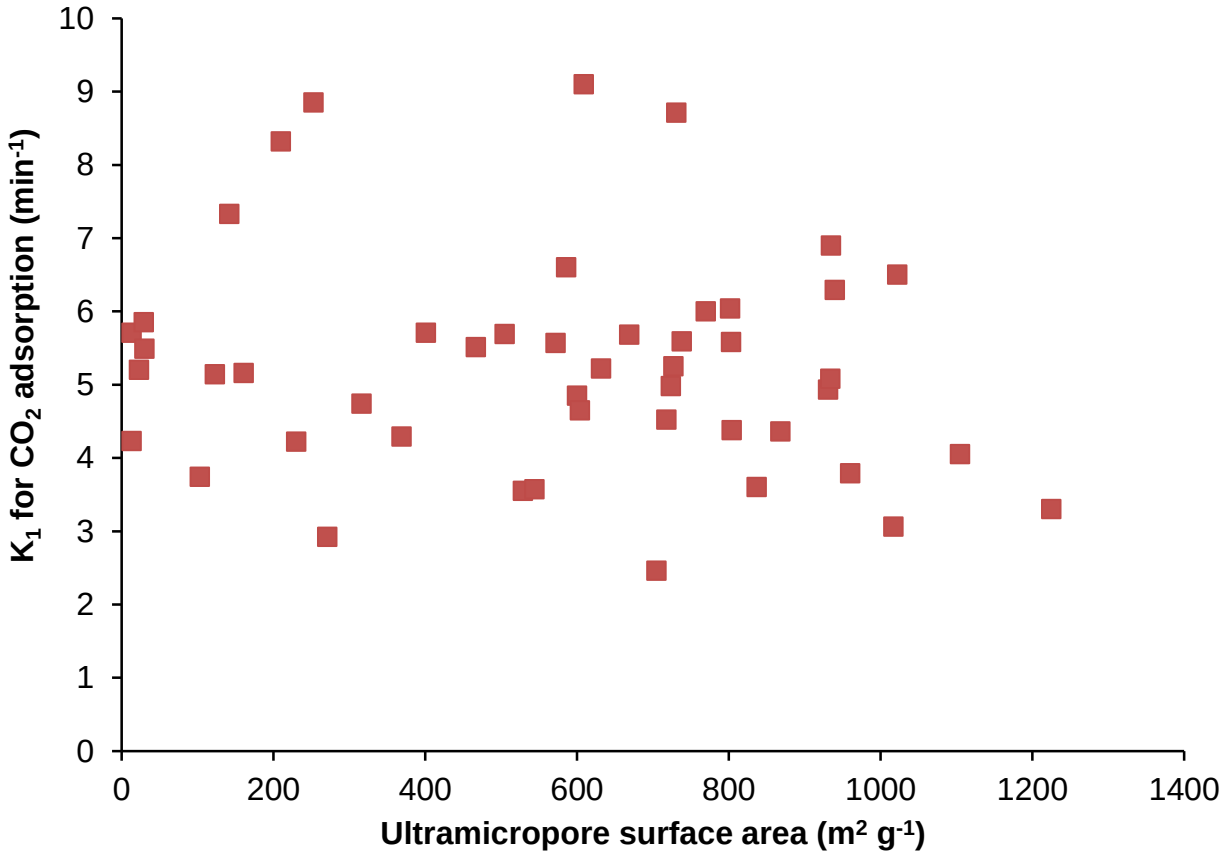

Plot of CO_2 adsorption capacity against micropore surface area

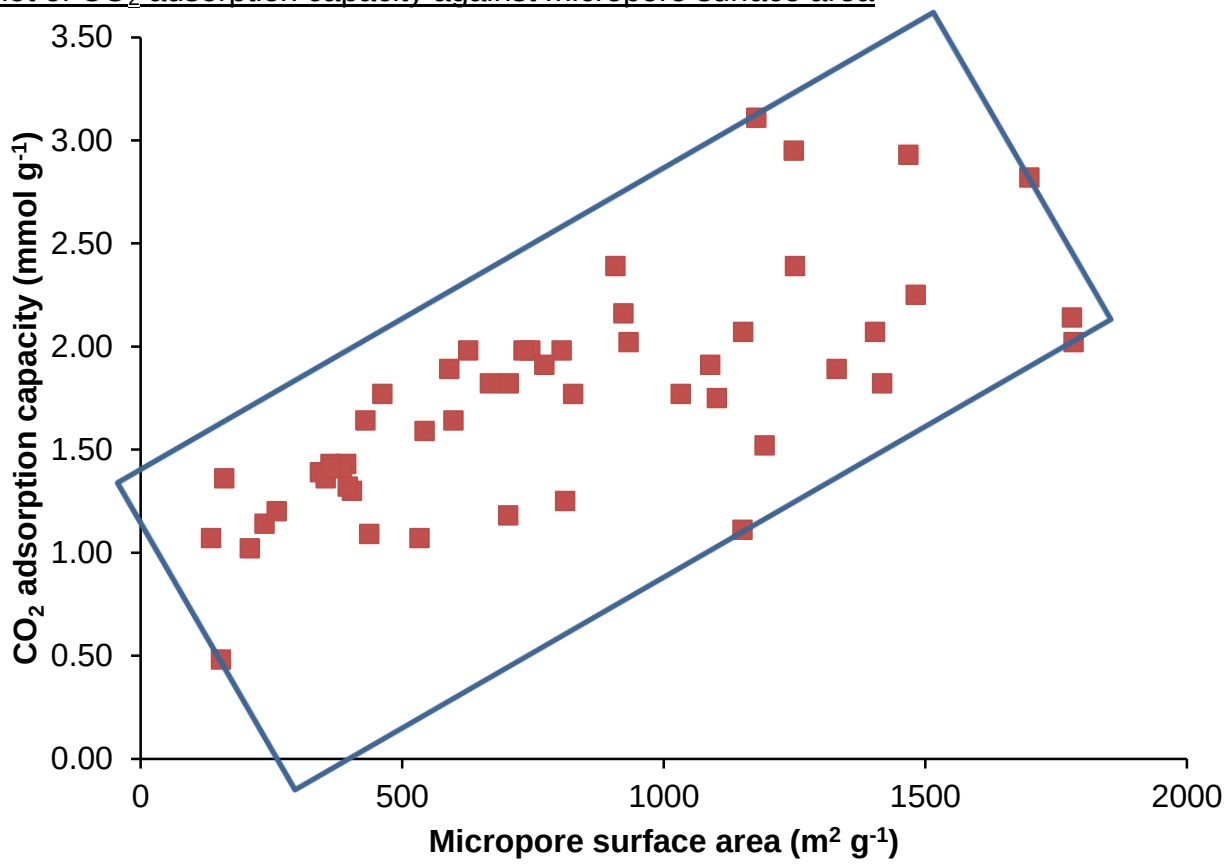

Plot of CO_2 adsorption enthalpy against micropore surface area

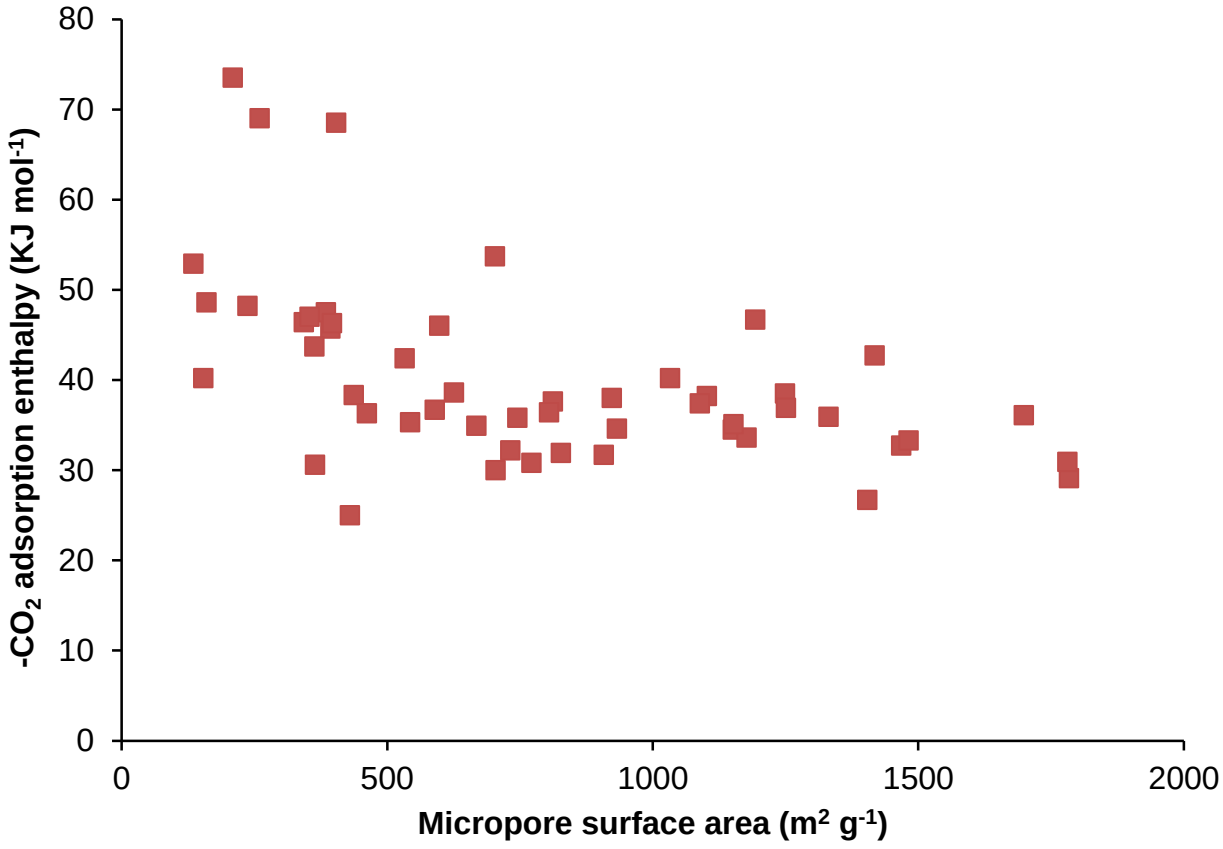

Plot of K_1 for CO_2 adsorption against micropore surface area

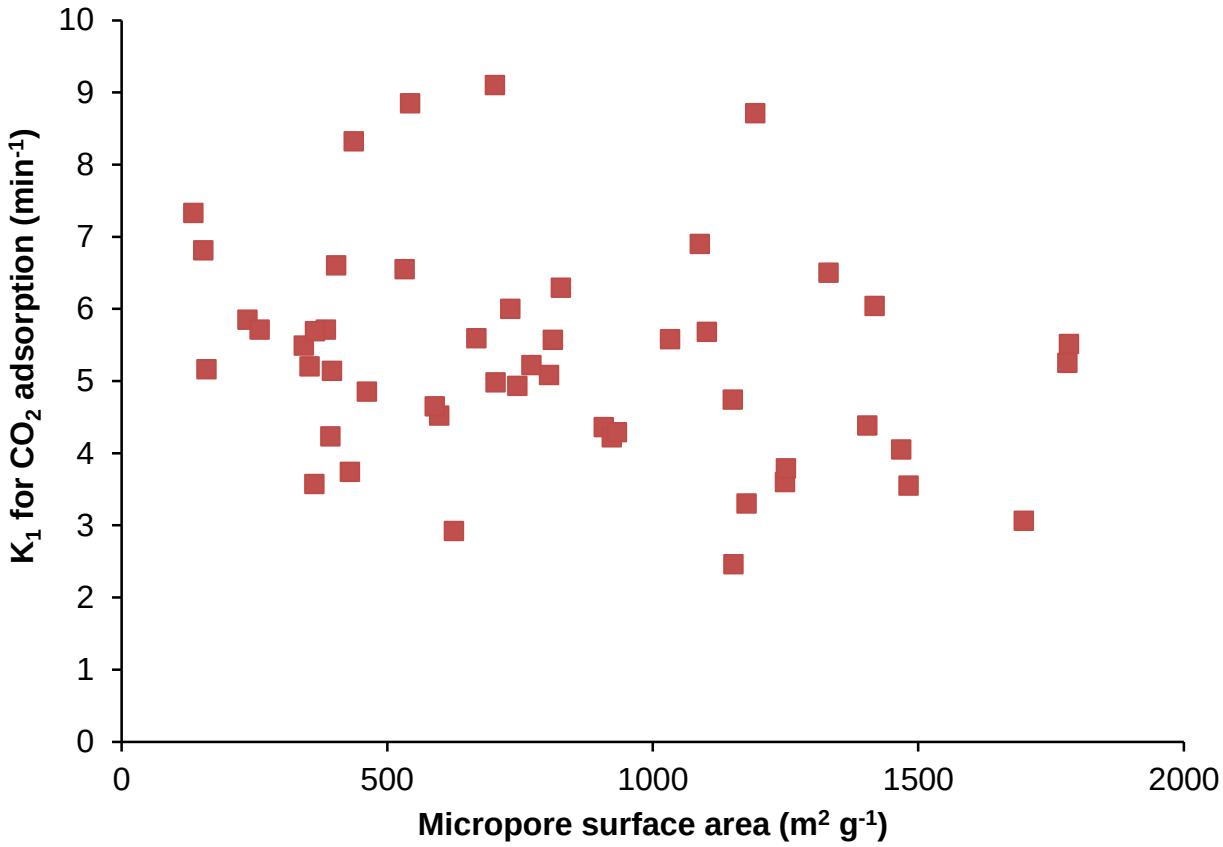

Plot of CO_2 adsorption capacity against BET surface area

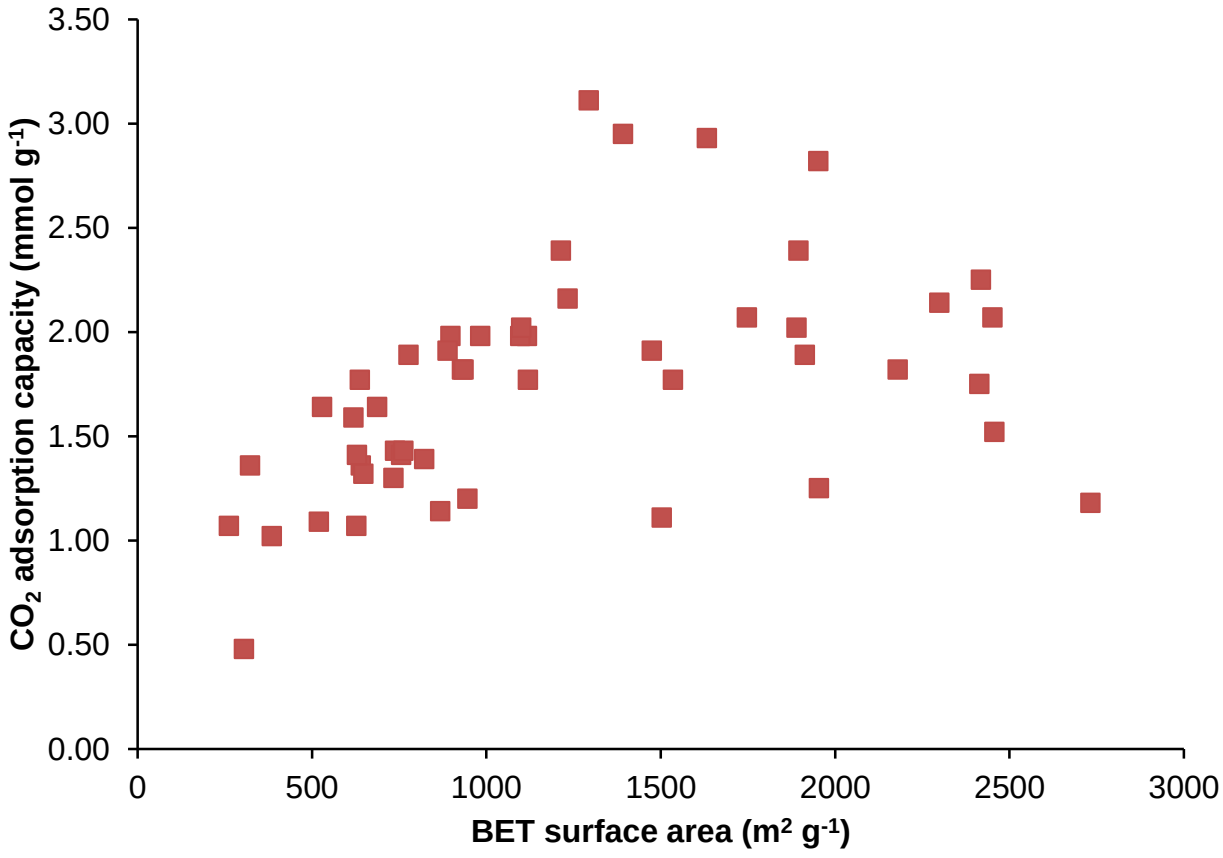

Plot of CO_2 adsorption enthalpy against BET surface area

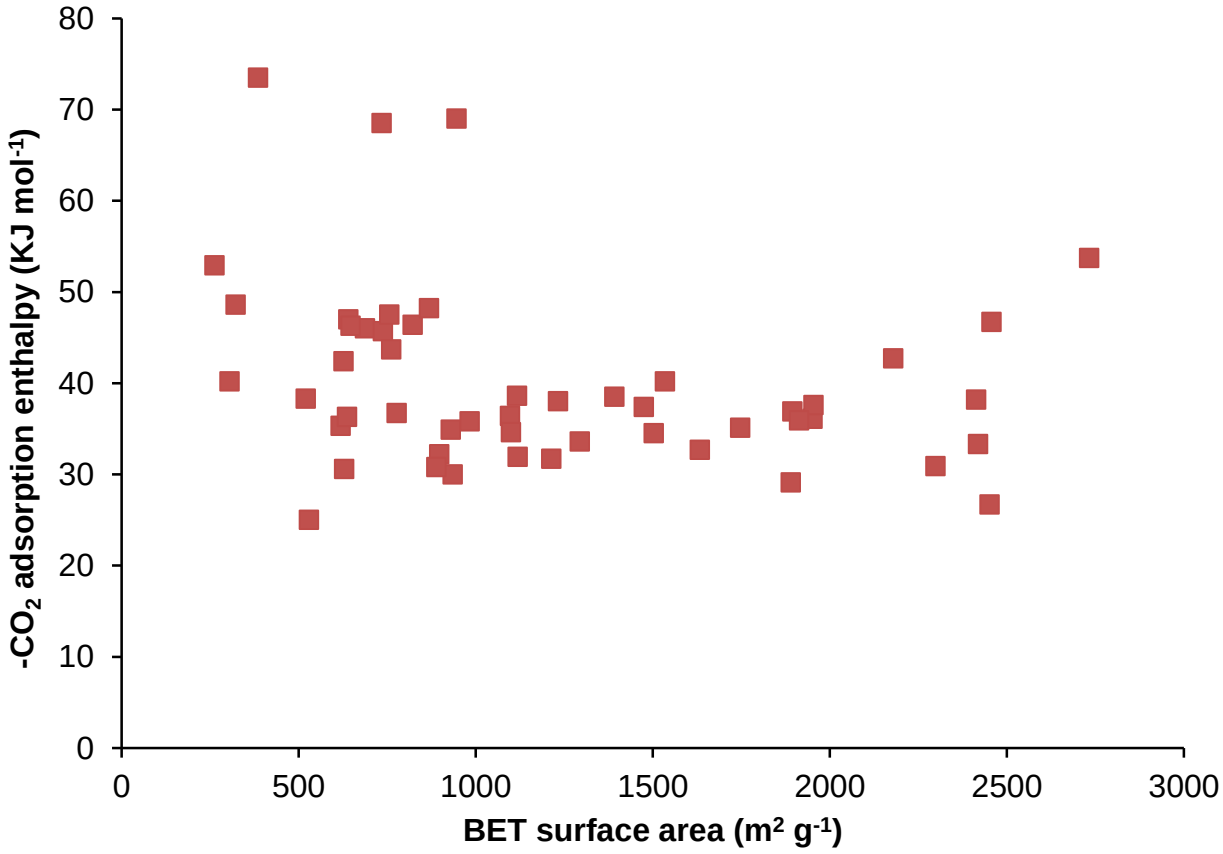

Plot of K_1 for CO_2 adsorption against BET surface area

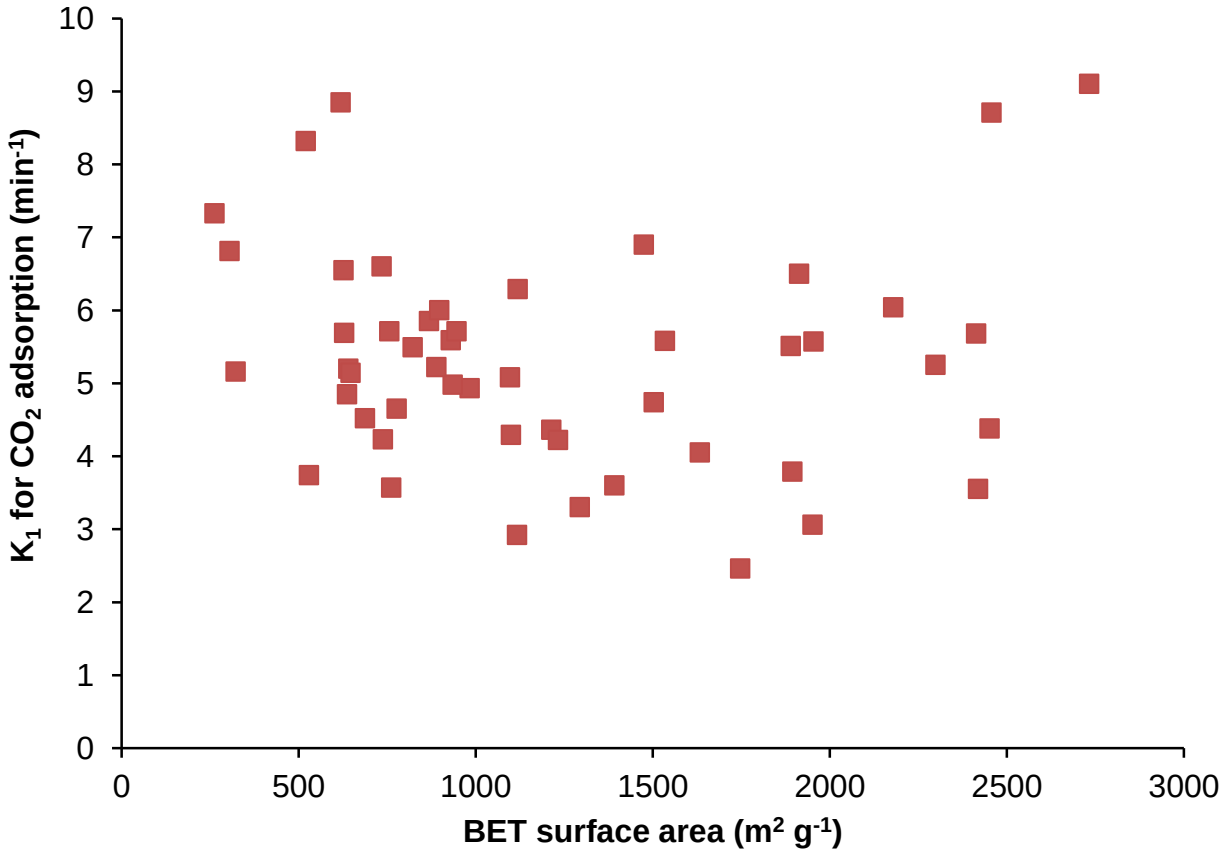

Plot of CO_2 adsorption capacity against ultramicropore volume

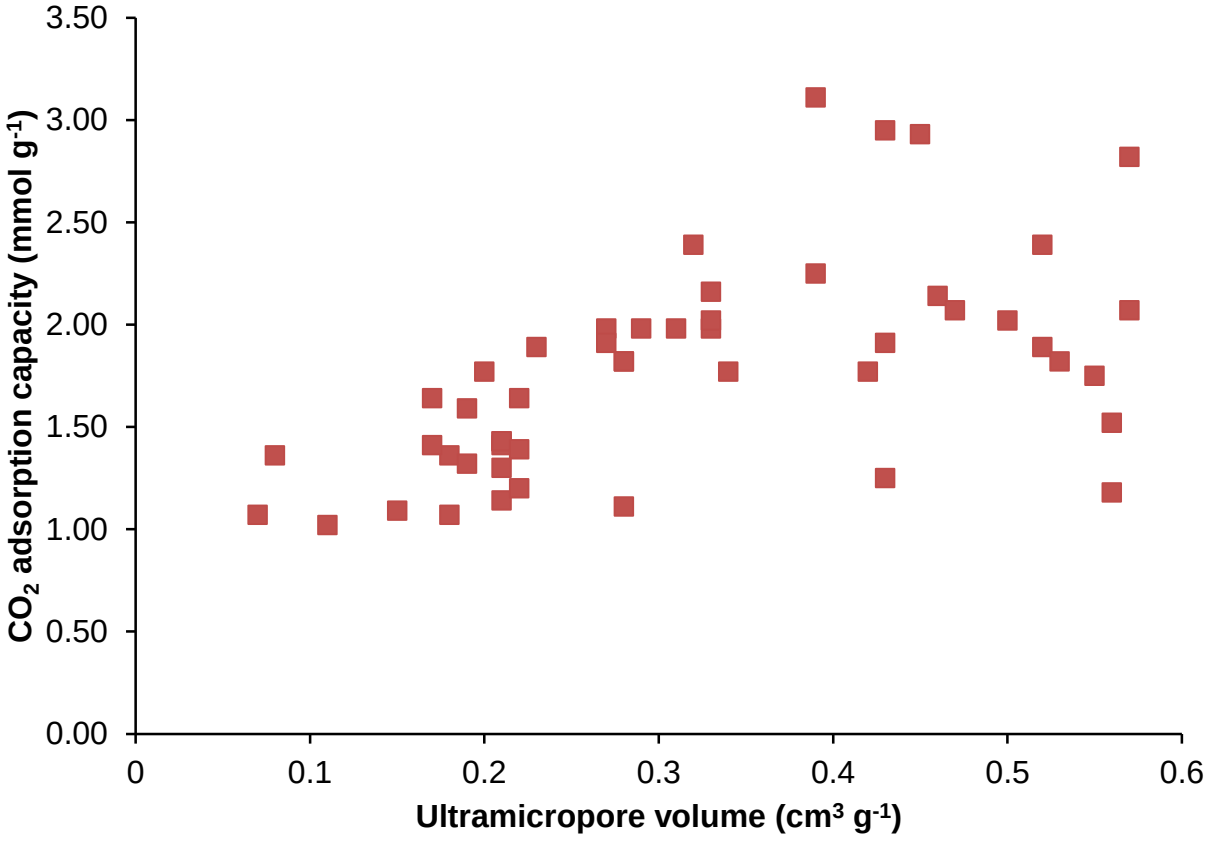

Plot of CO_2 adsorption enthalpy against ultramicropore volume

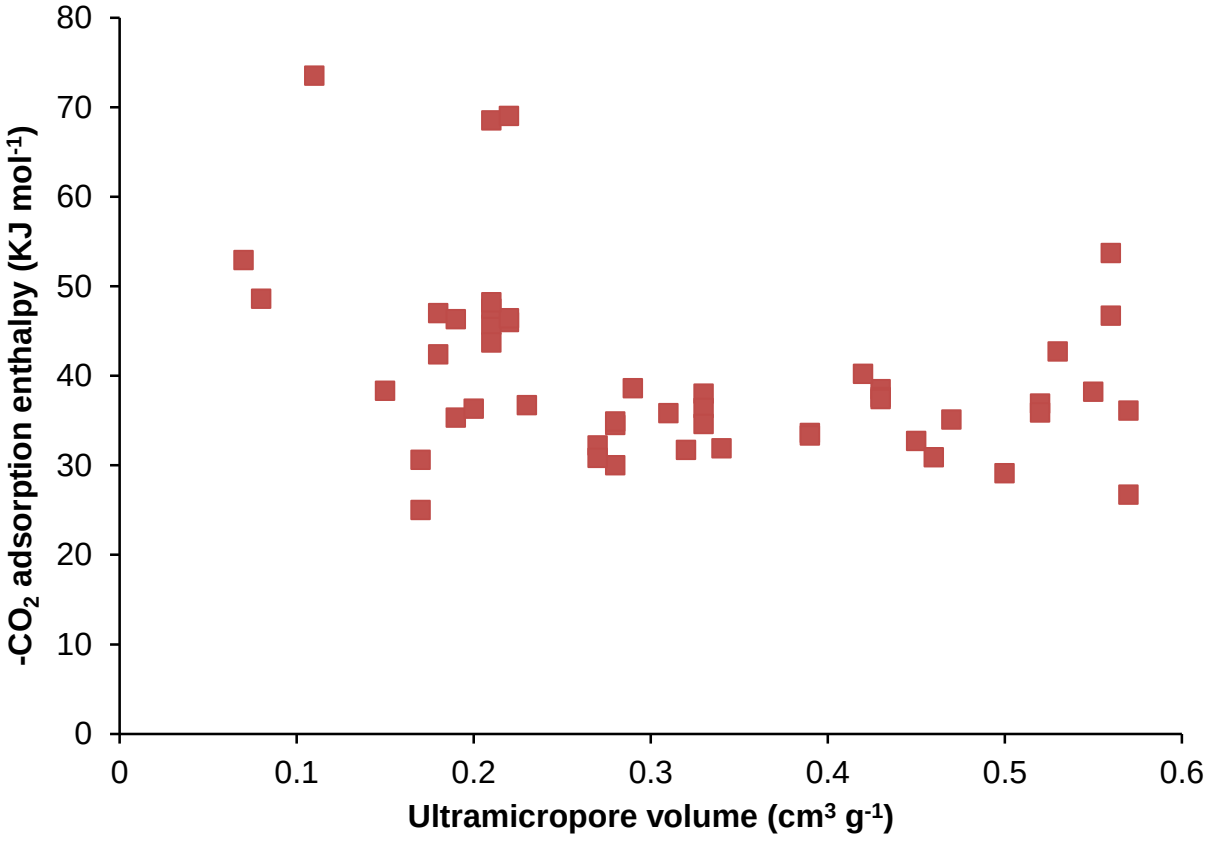

Plot of K_1 for CO_2 adsorption against ultramicropore volume

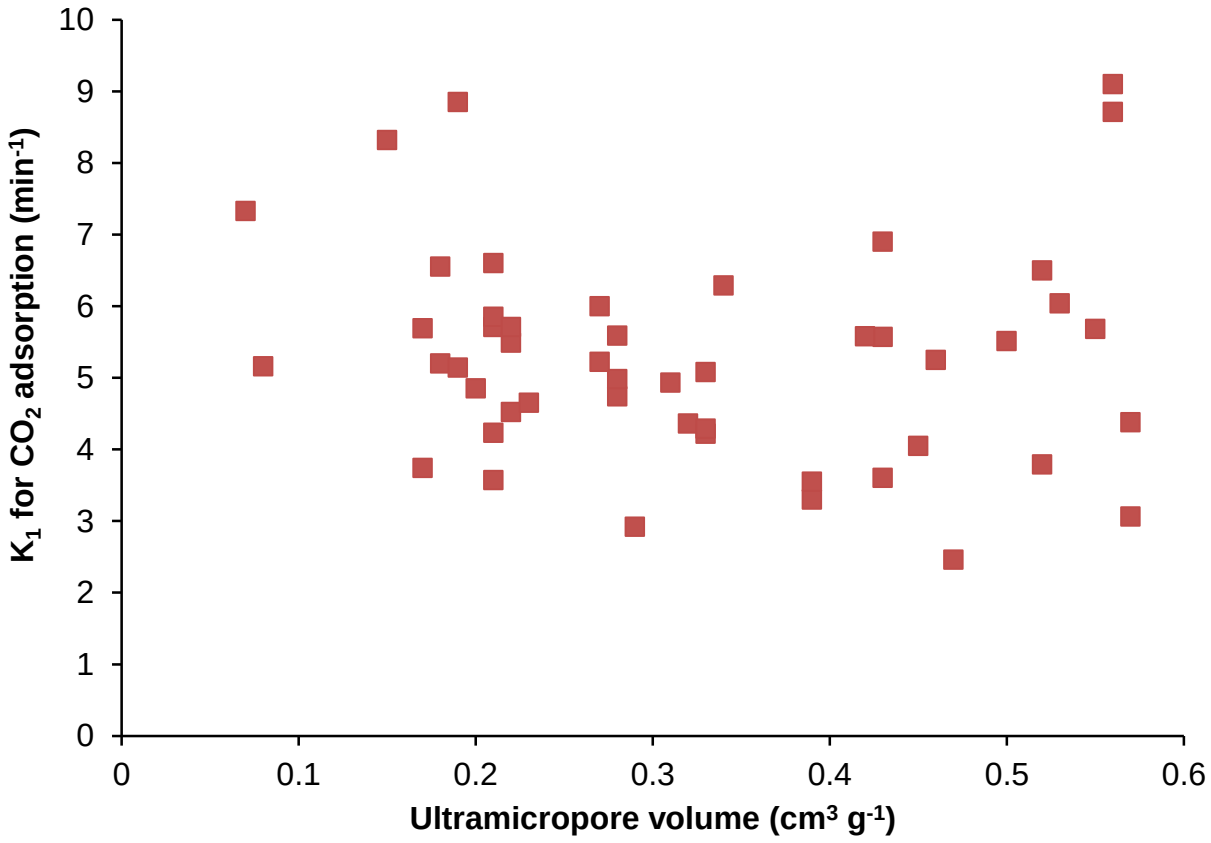

Plot of CO_2 adsorption capacity against ultramicropore (0.4-0.7 nm) volume

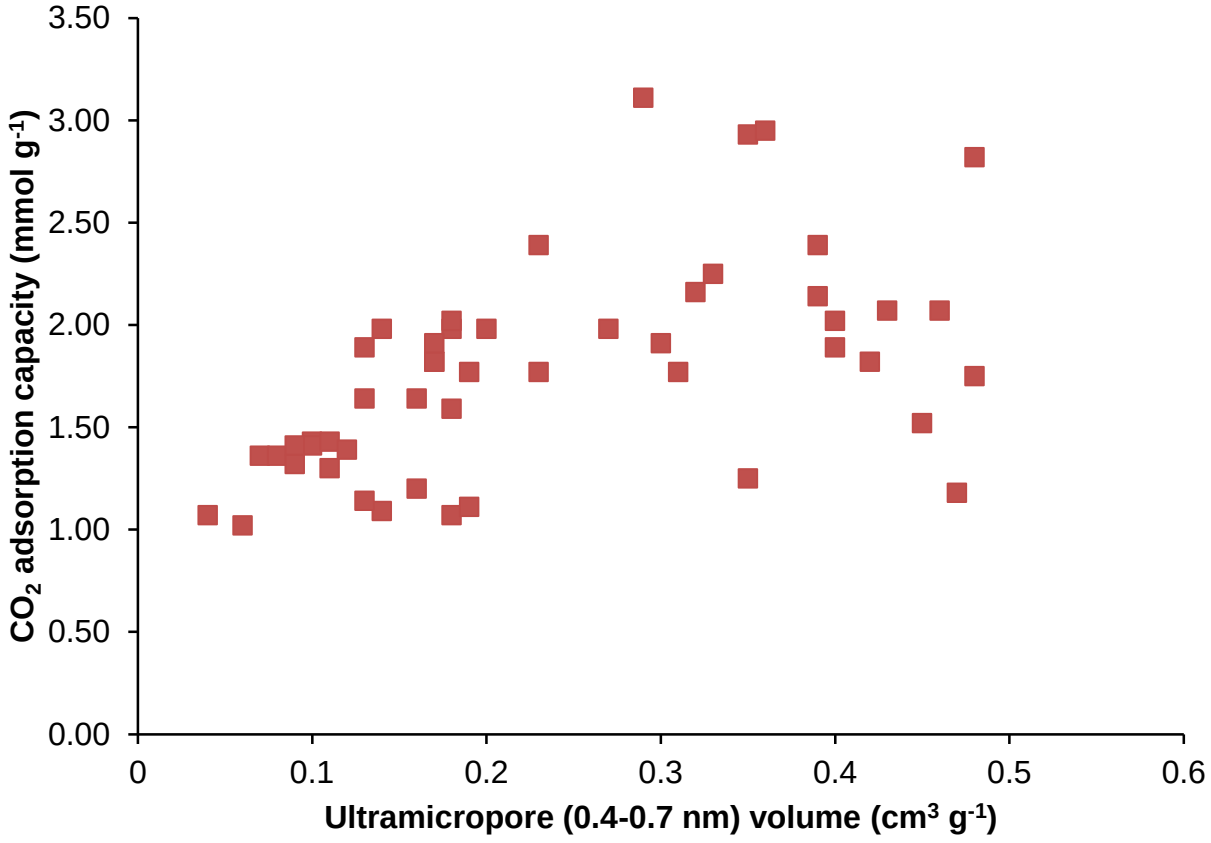

Plot of CO_2 adsorption enthalpy against ultramicropore (0.4-0.7 nm) volume

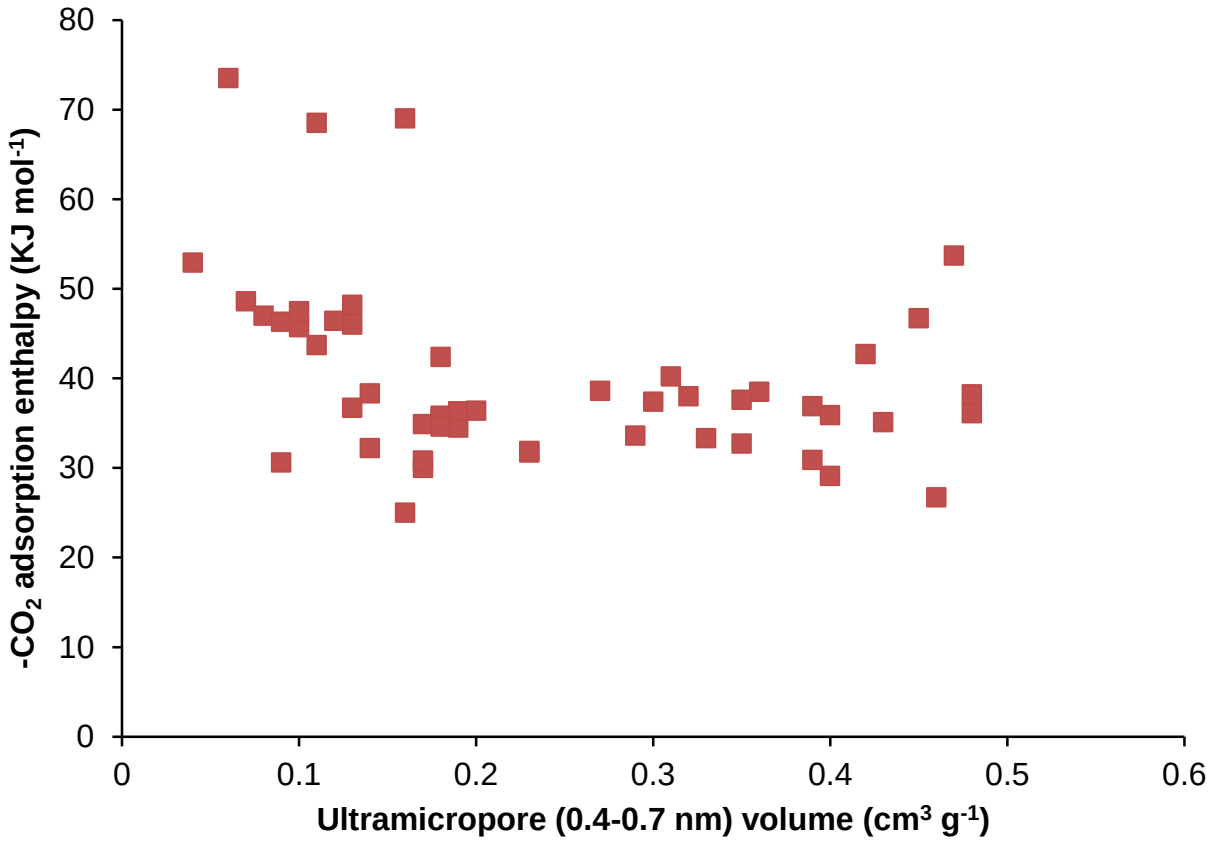

Plot of K_1 for CO_2 adsorption against ultramicropore (0.4-0.7 nm) volume

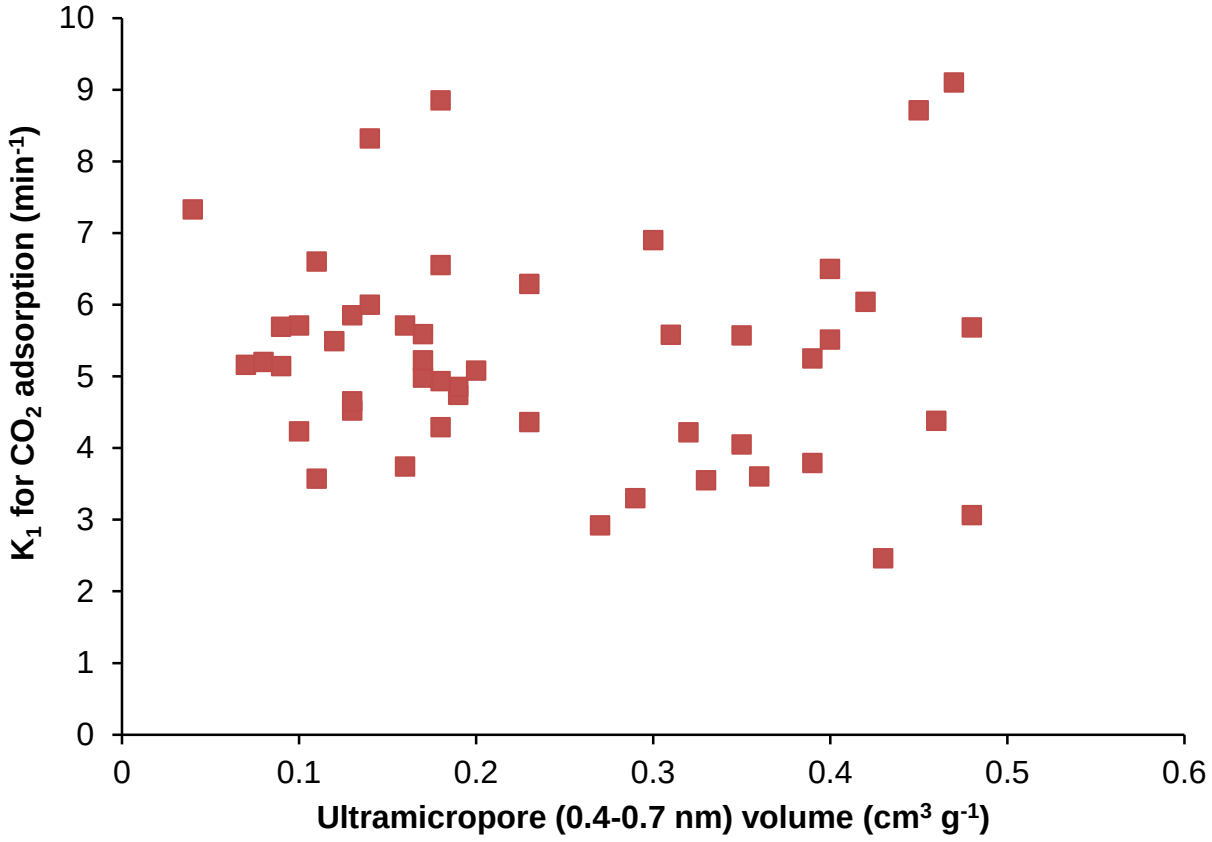

Plot of CO_2 adsorption capacity against supramicropore volume

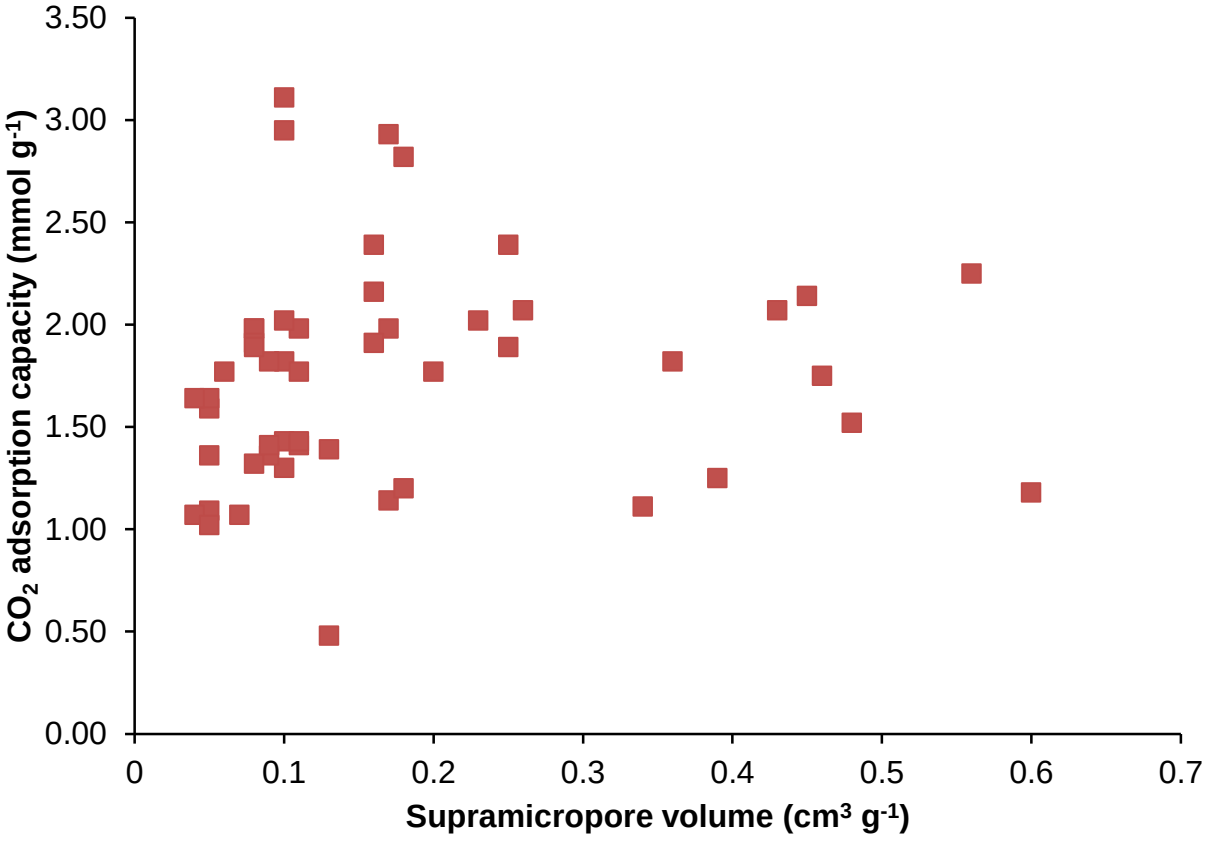

Plot of CO_2 adsorption enthalpy against supramicropore volume

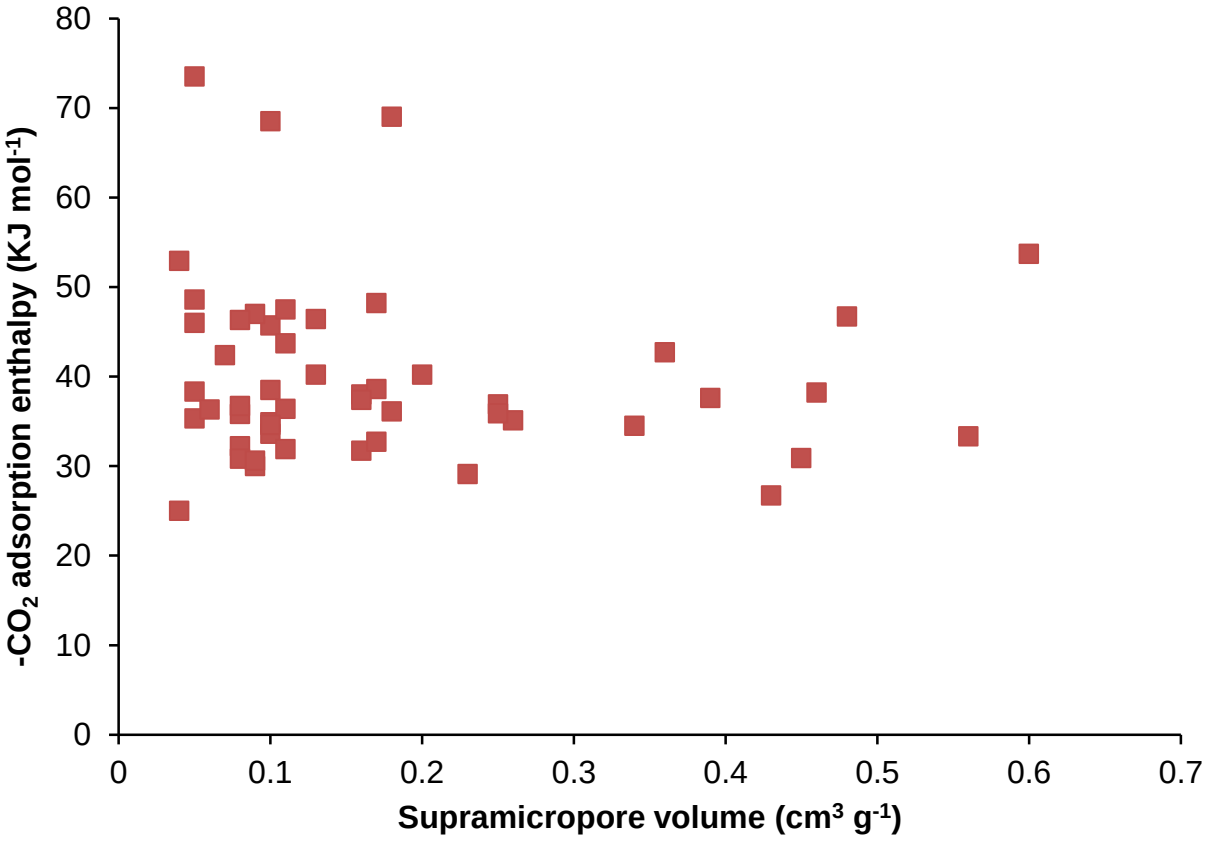

Plot of K_1 for CO_2 adsorption against supramicropore volume

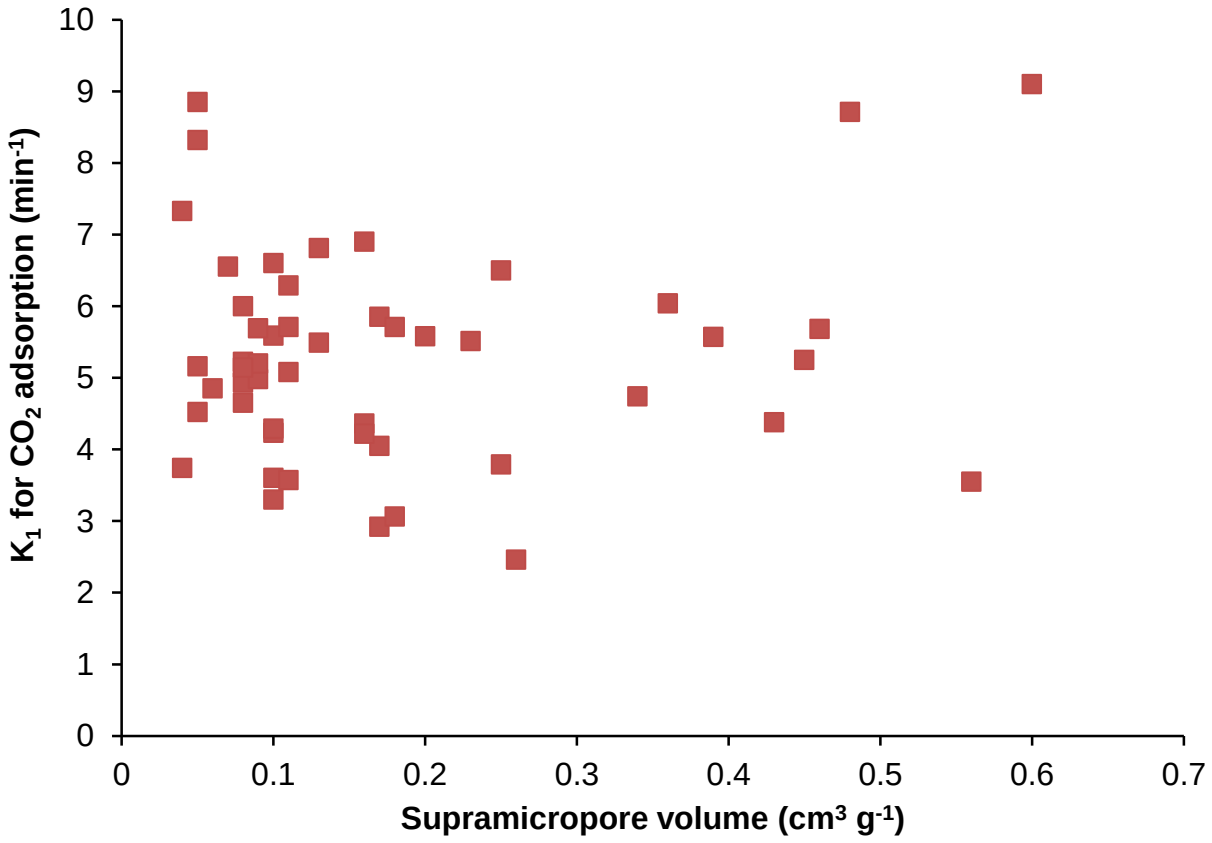

Plot of CO_2 adsorption capacity against micropore volume

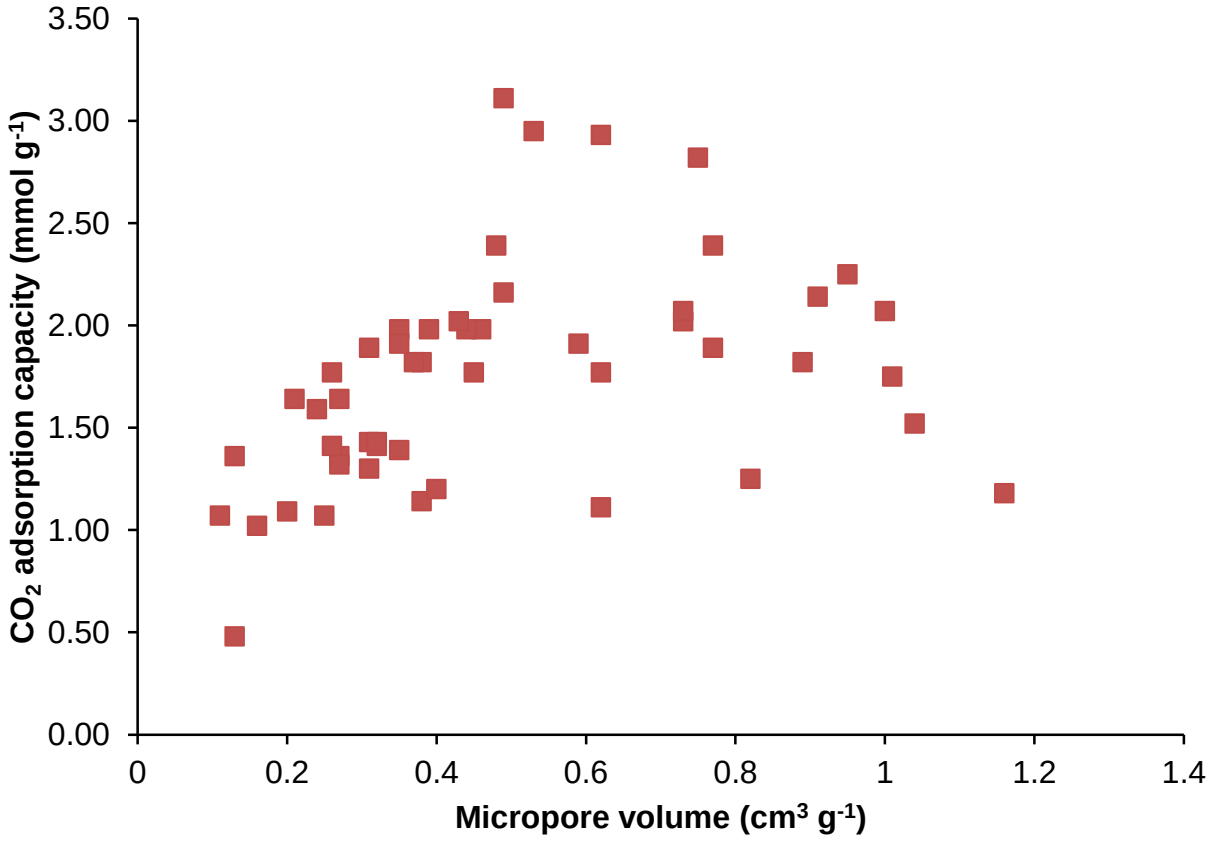

Plot of CO_2 adsorption enthalpy against micropore volume

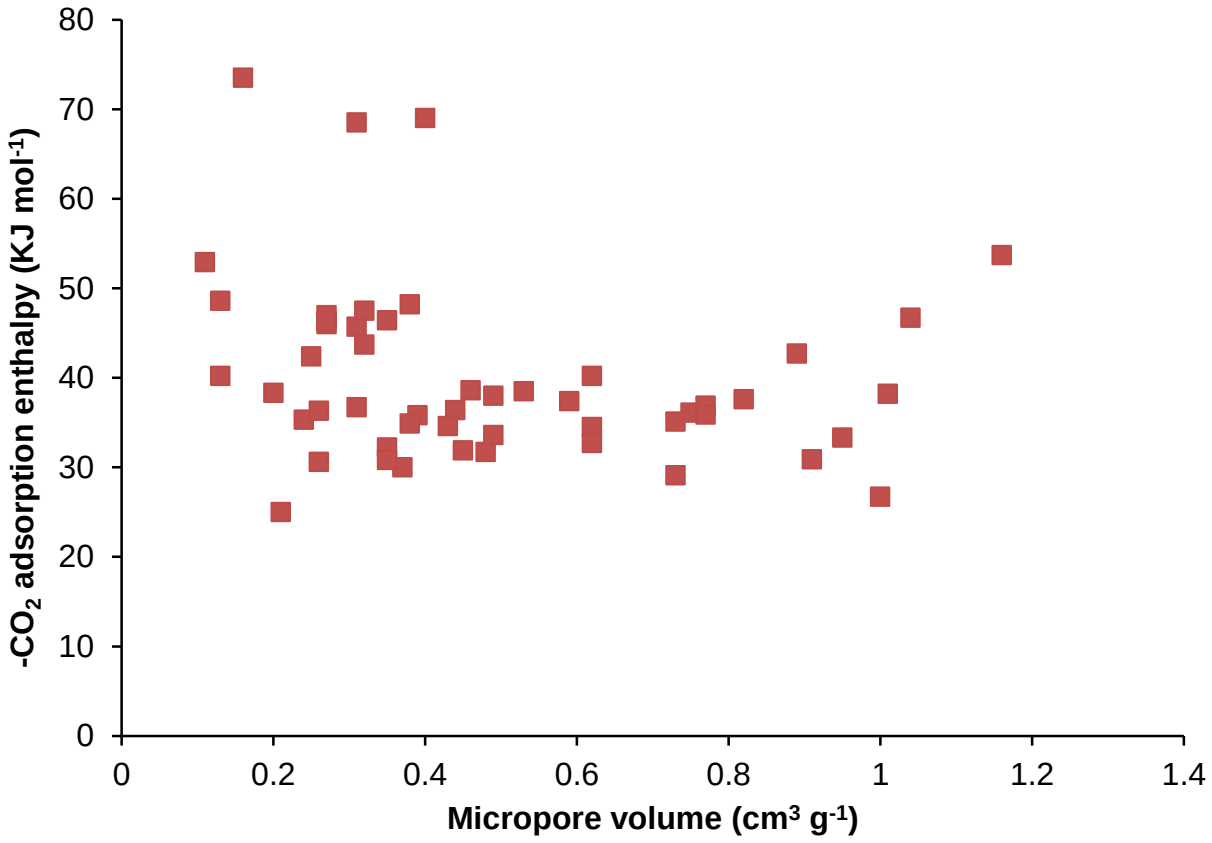

Plot of K_1 for CO_2 adsorption against micropore volume

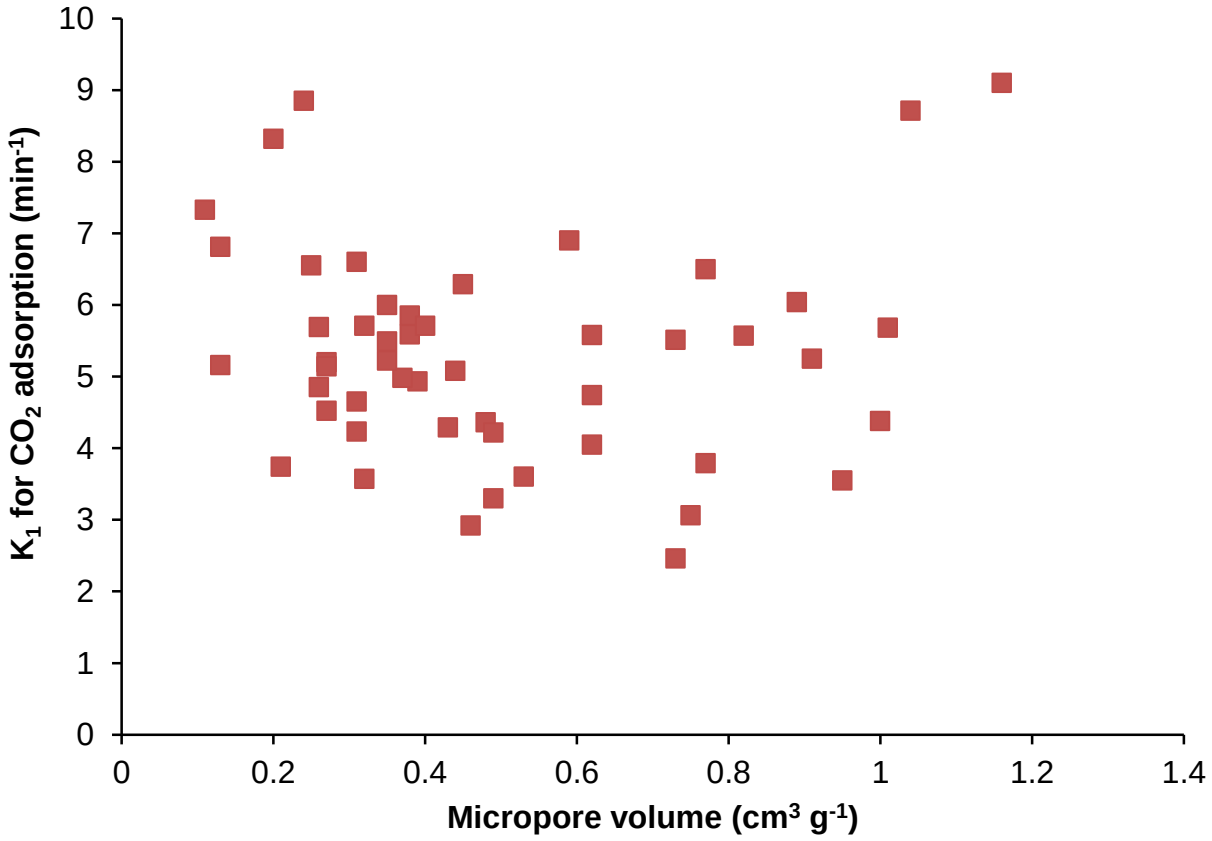

Plot of CO_2 adsorption capacity against mesopore volume

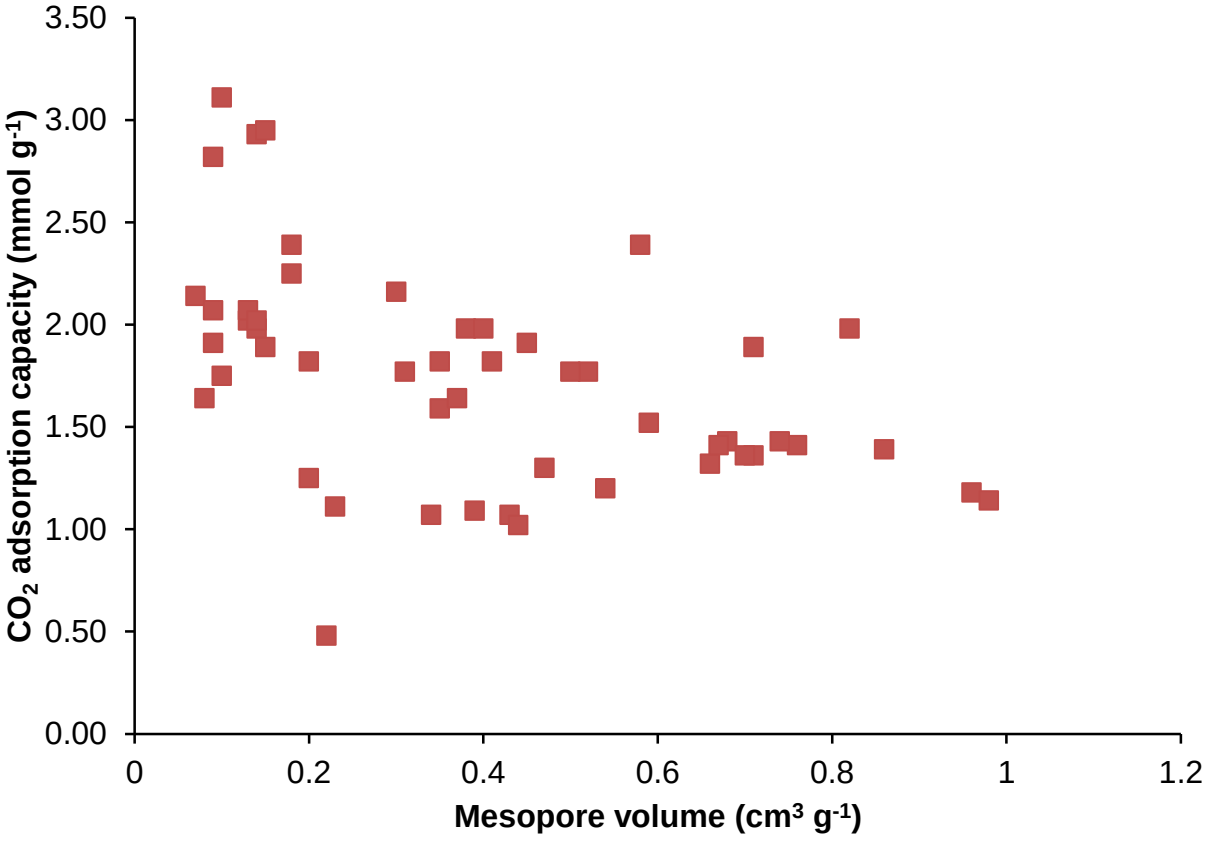

Plot of CO_2 adsorption enthalpy against mesopore volume

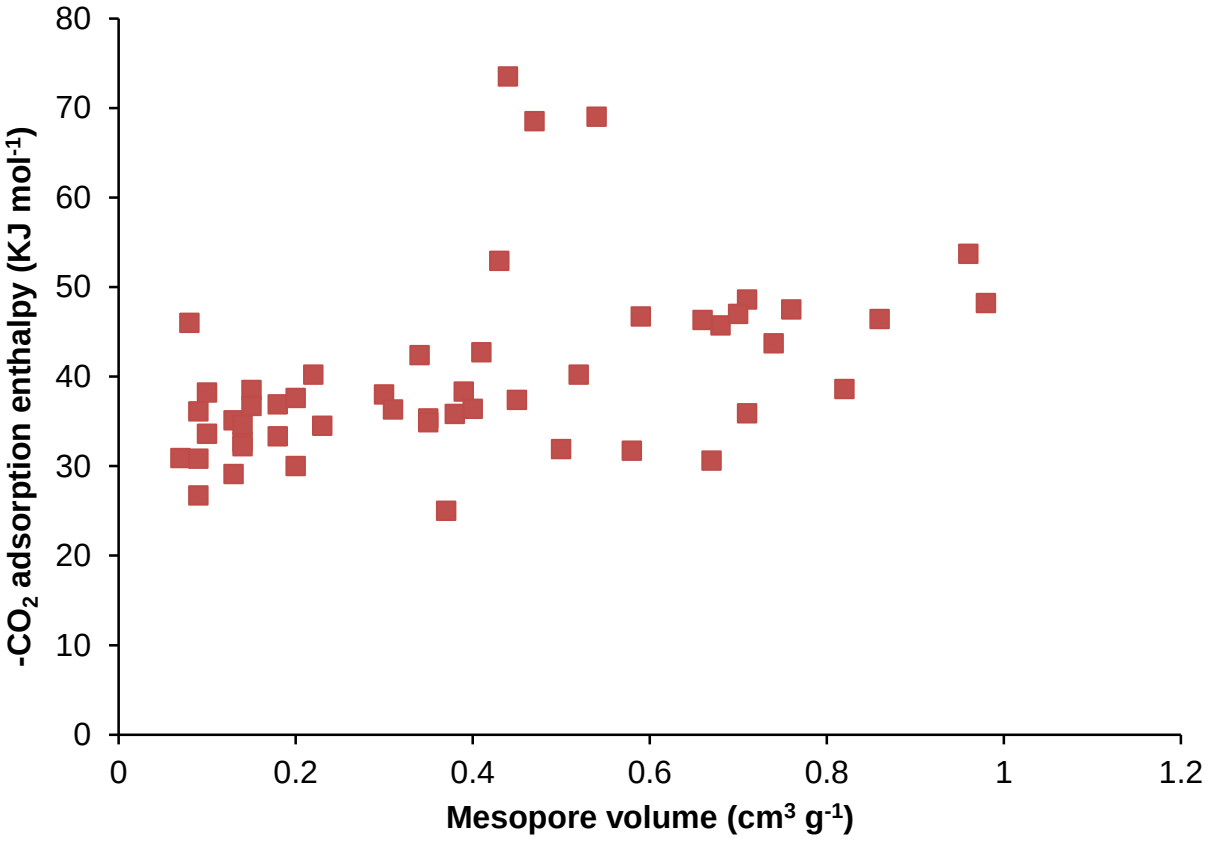

Plot of K_1 for CO_2 adsorption against mesopore volume

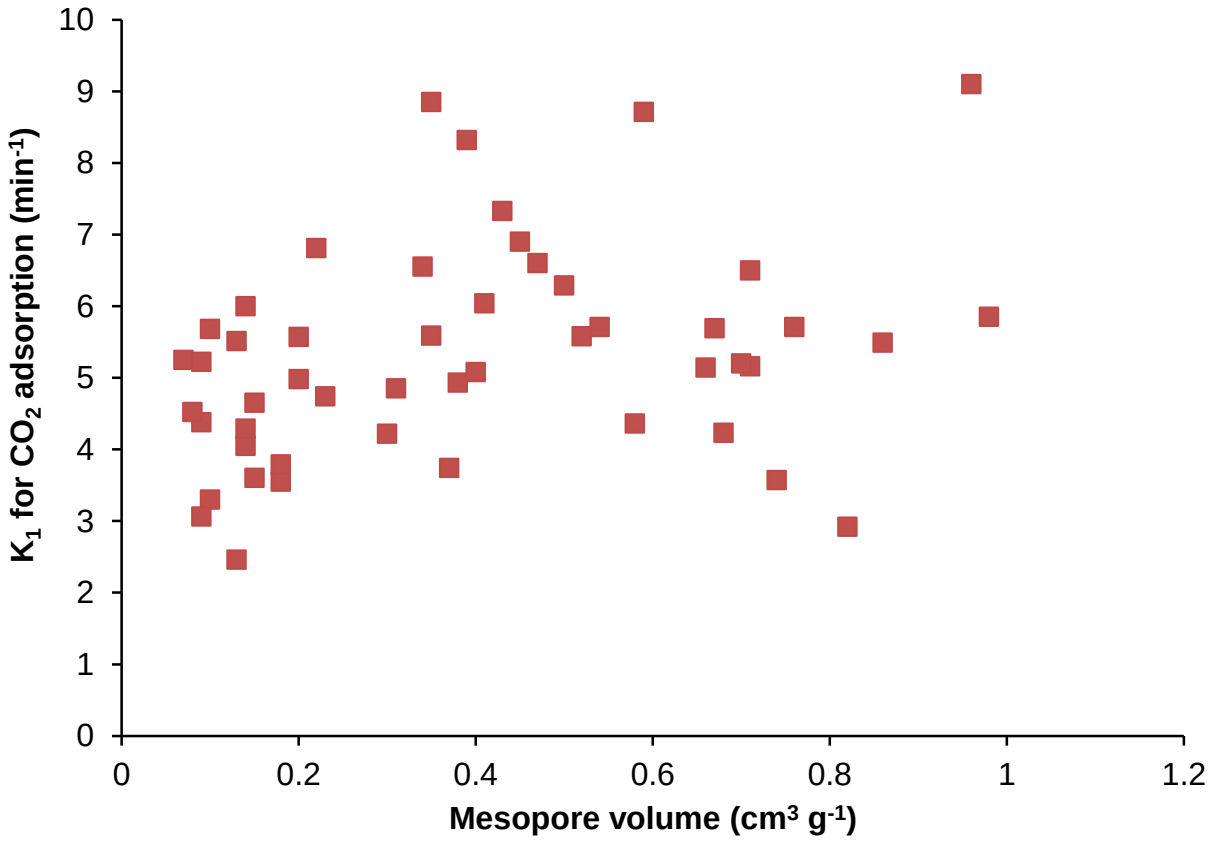

Plot of CO_2 adsorption capacity against total pore volume

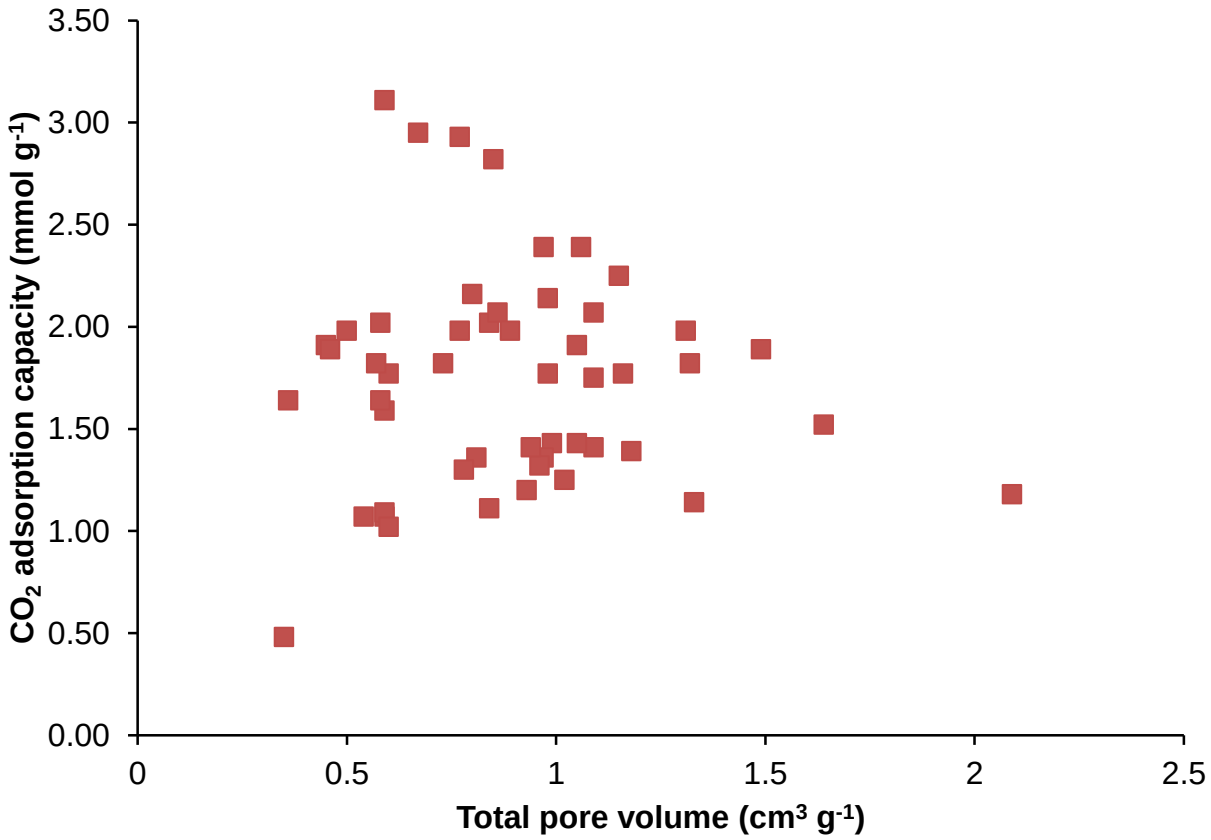

Plot of CO_2 adsorption enthalpy against total pore volume

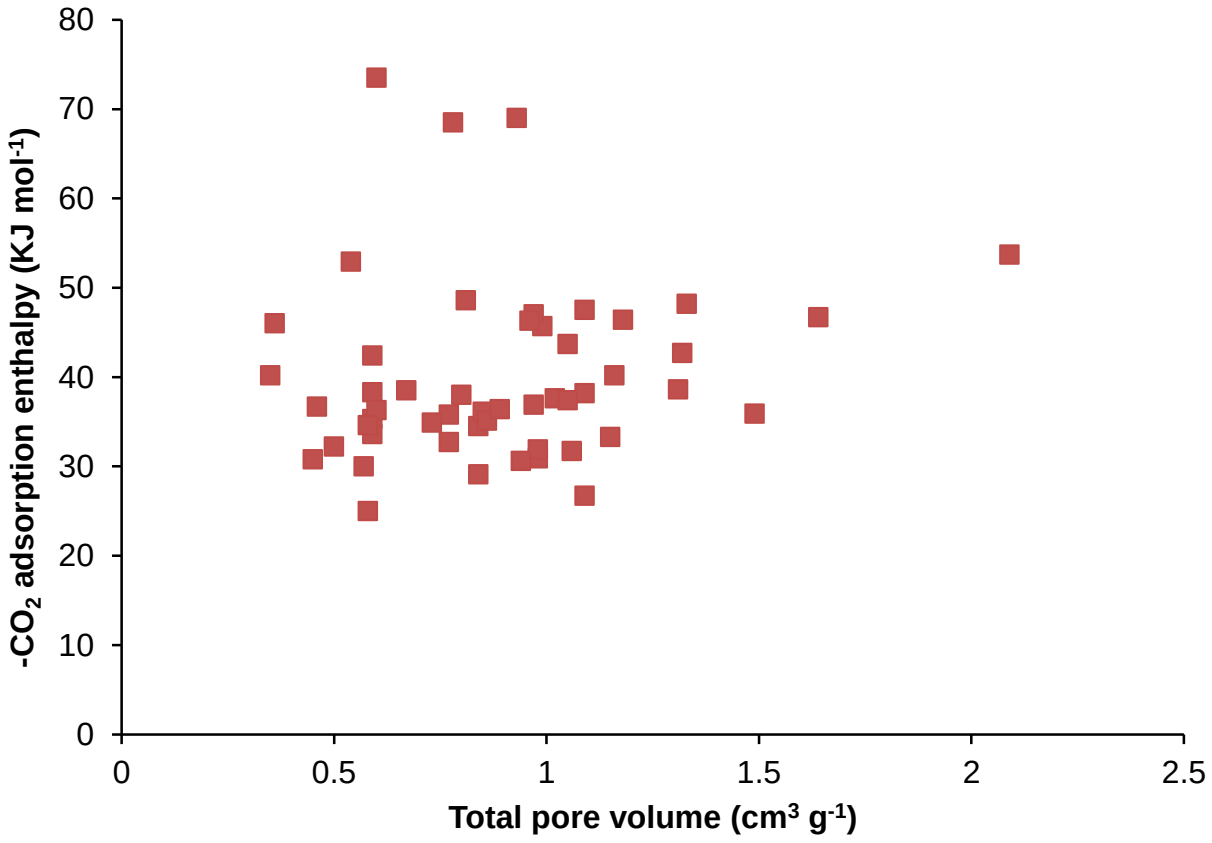

Plot of K_1 for CO_2 adsorption against total pore volume

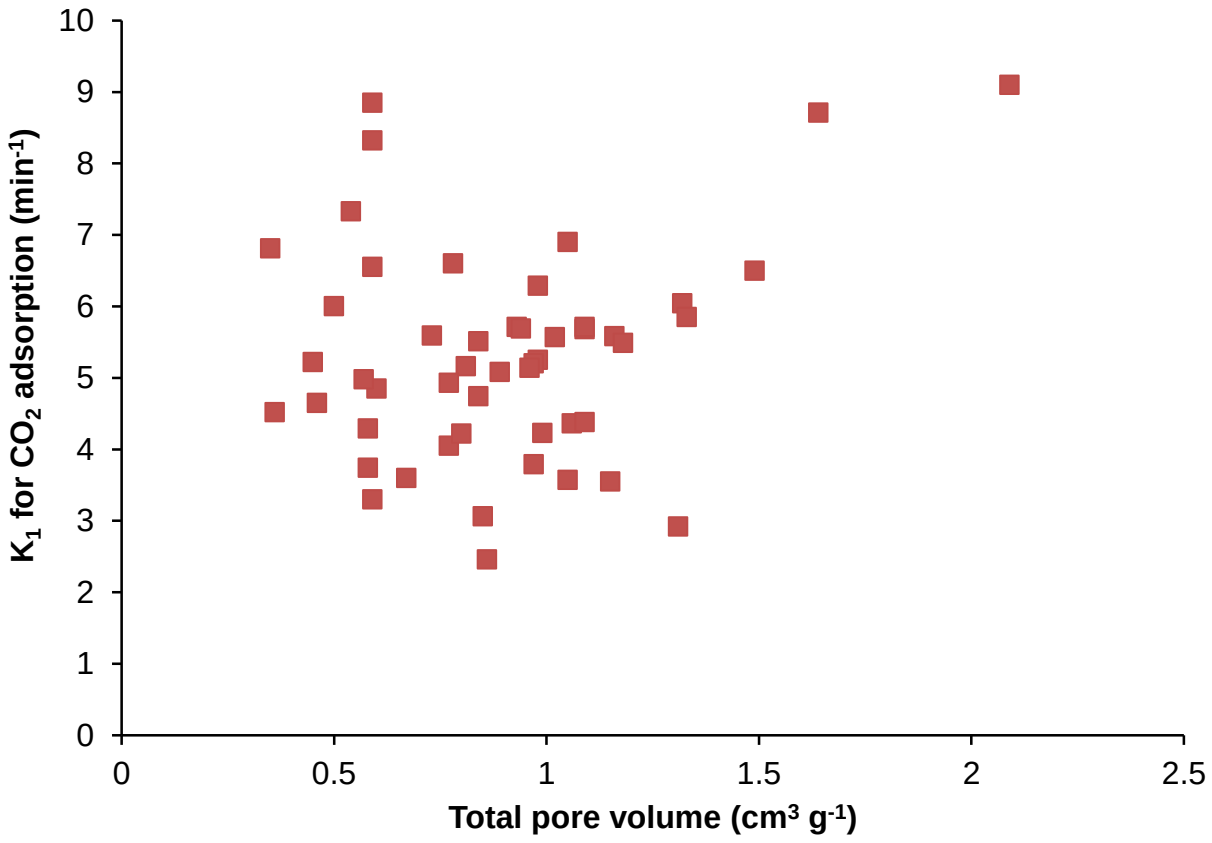

Plot of CO_2 adsorption capacity against ultramicropore volume/total pore volume

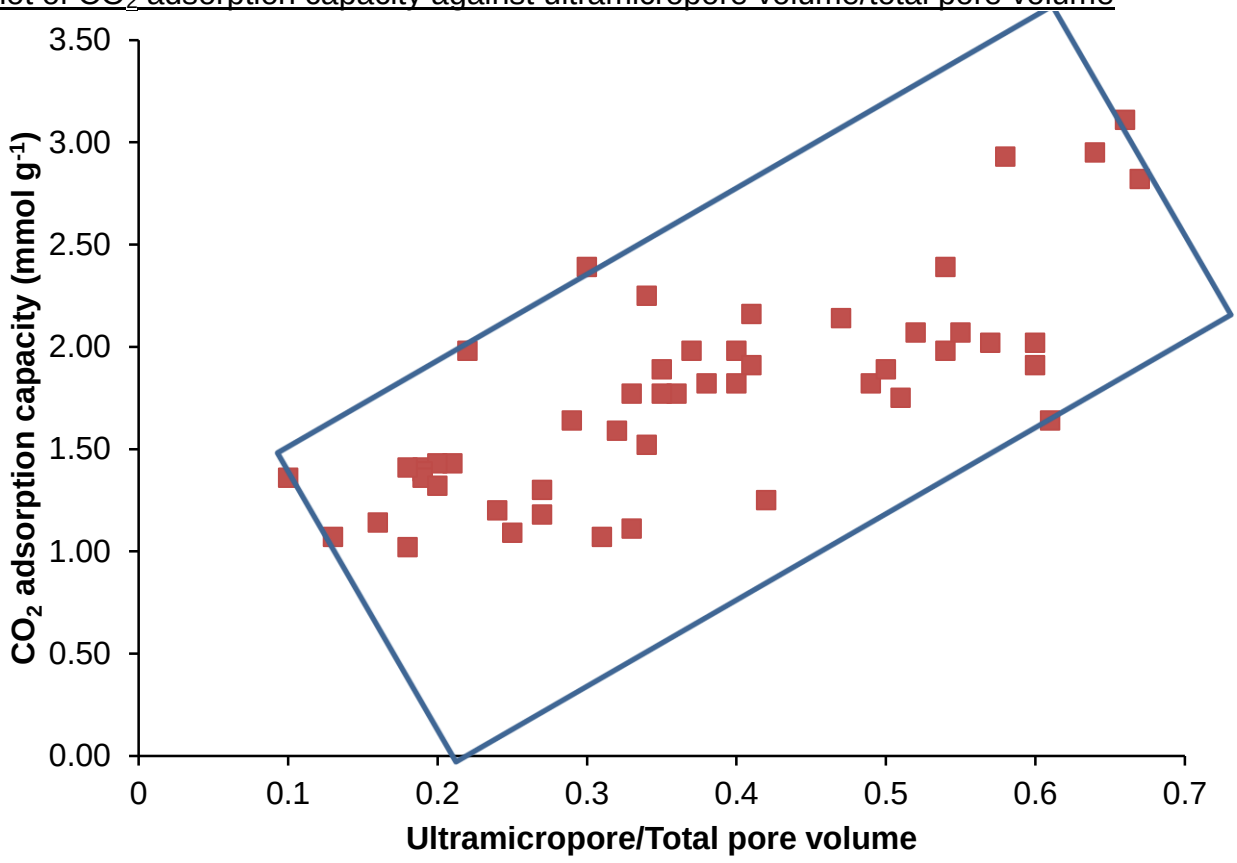

Plot of CO_2 adsorption enthalpy against ultramicropore volume/total pore volume

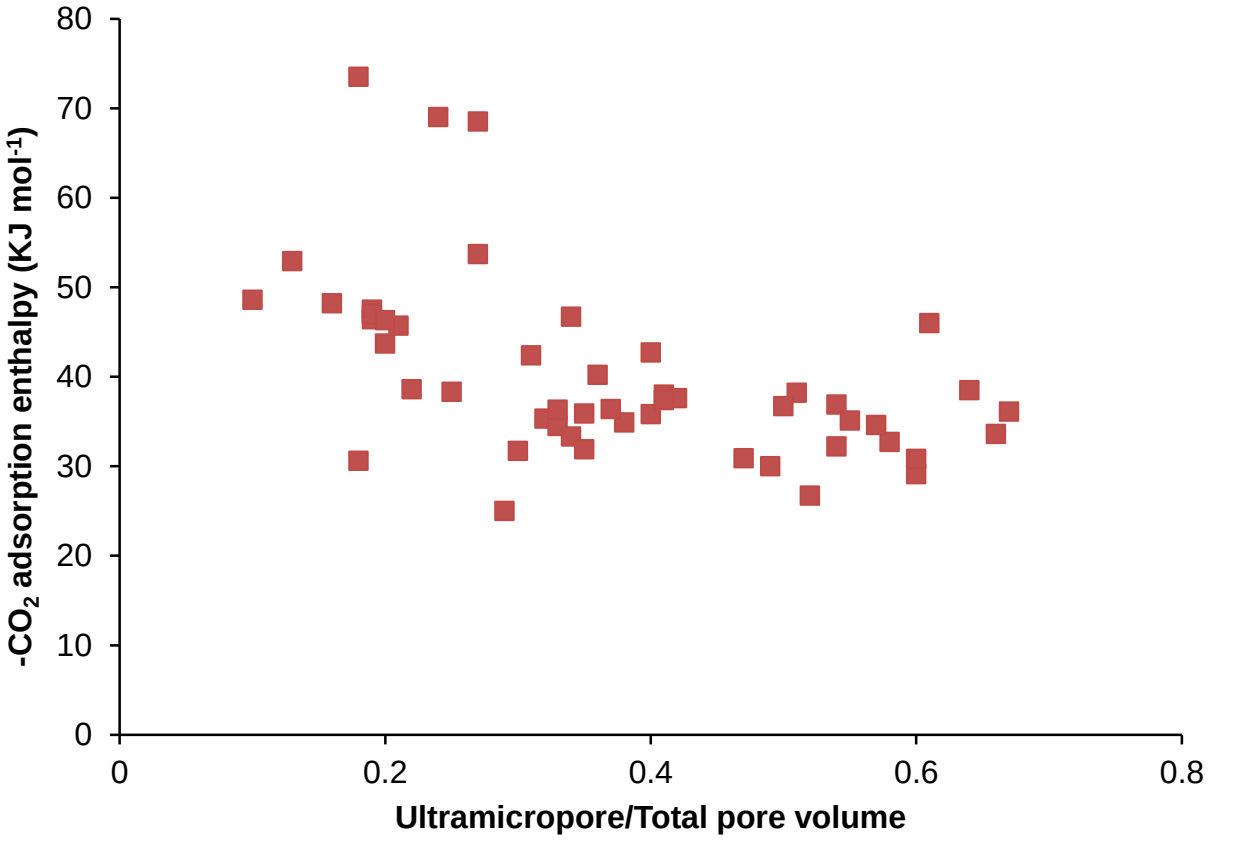

Plot of K_1 for CO_2 adsorption against ultramicropore volume/total pore volume

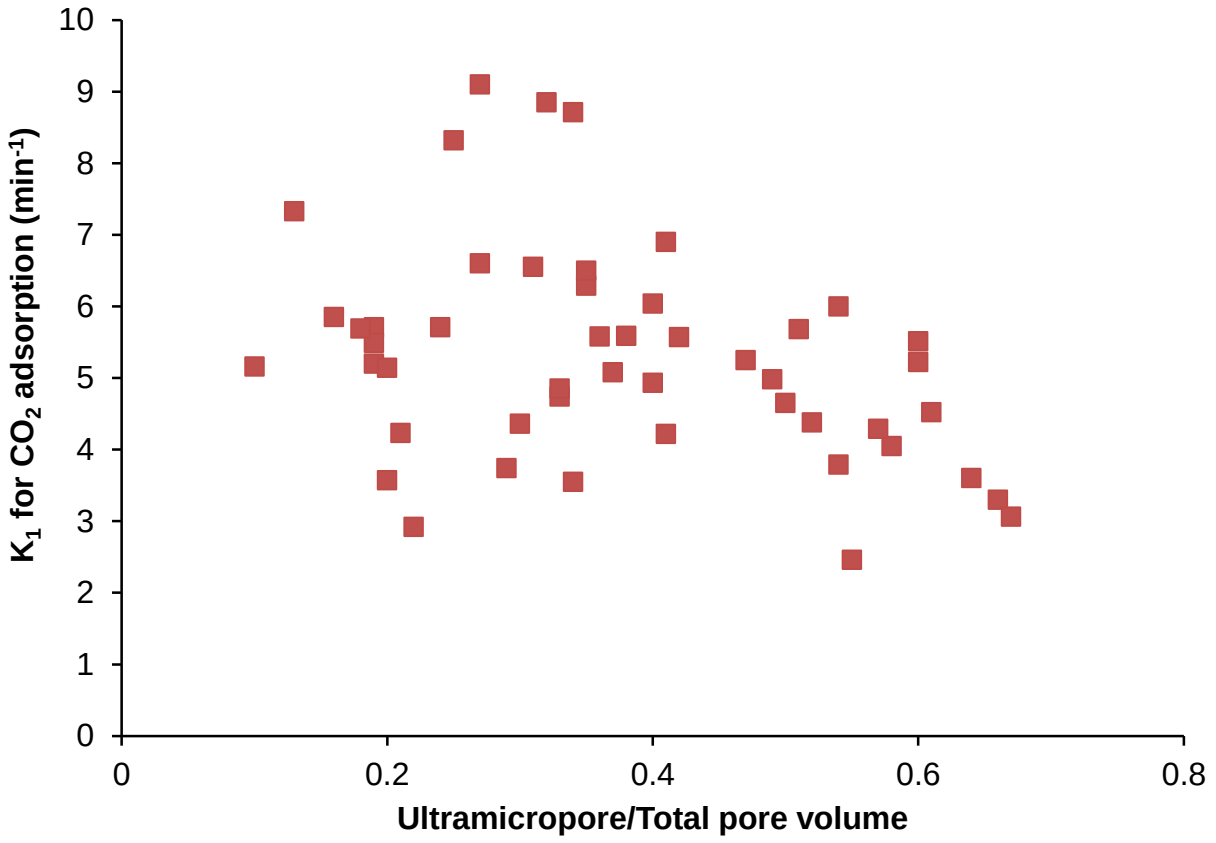

Plot of CO_2 adsorption capacity against ultramicropore (0.4-0.7 nm) volume/total pore volume

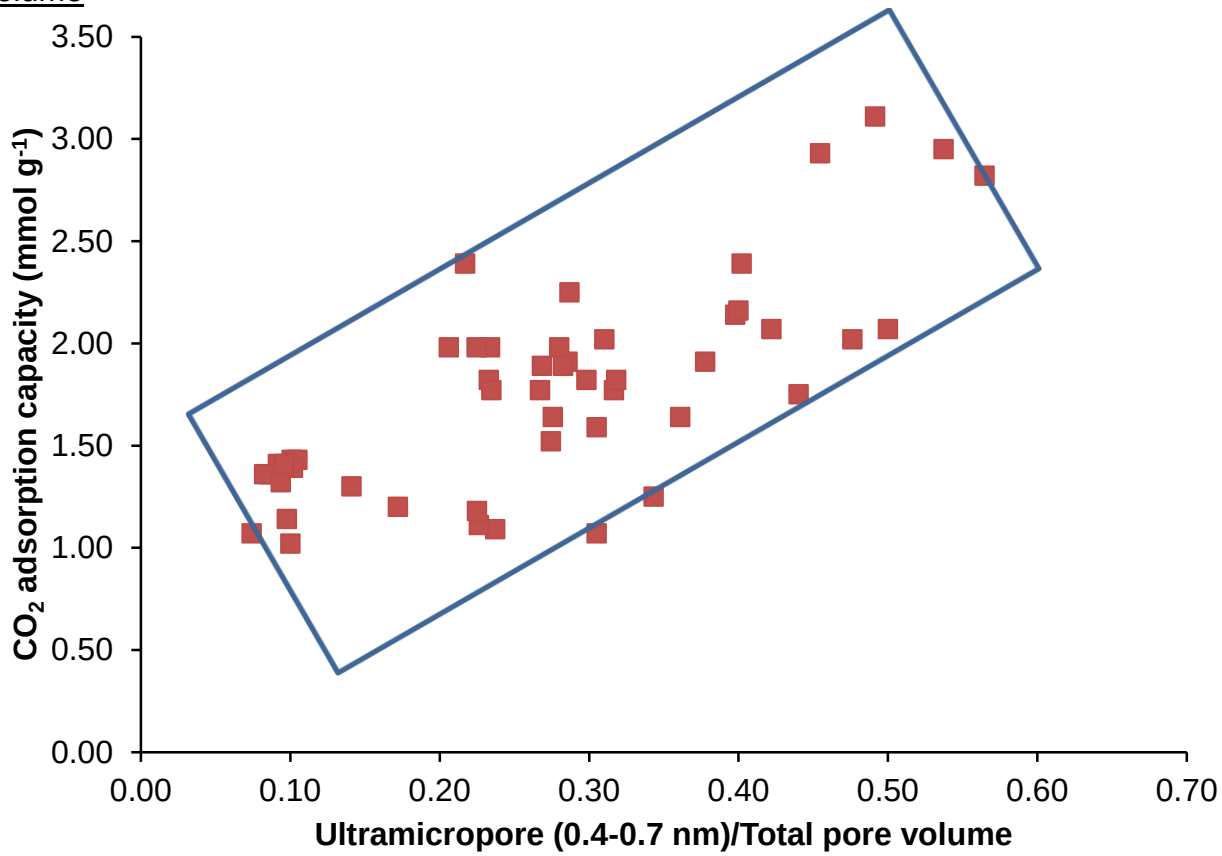

Plot of CO_2 adsorption enthalpy against ultramicropore (0.4-0.7 nm) volume/total pore volume

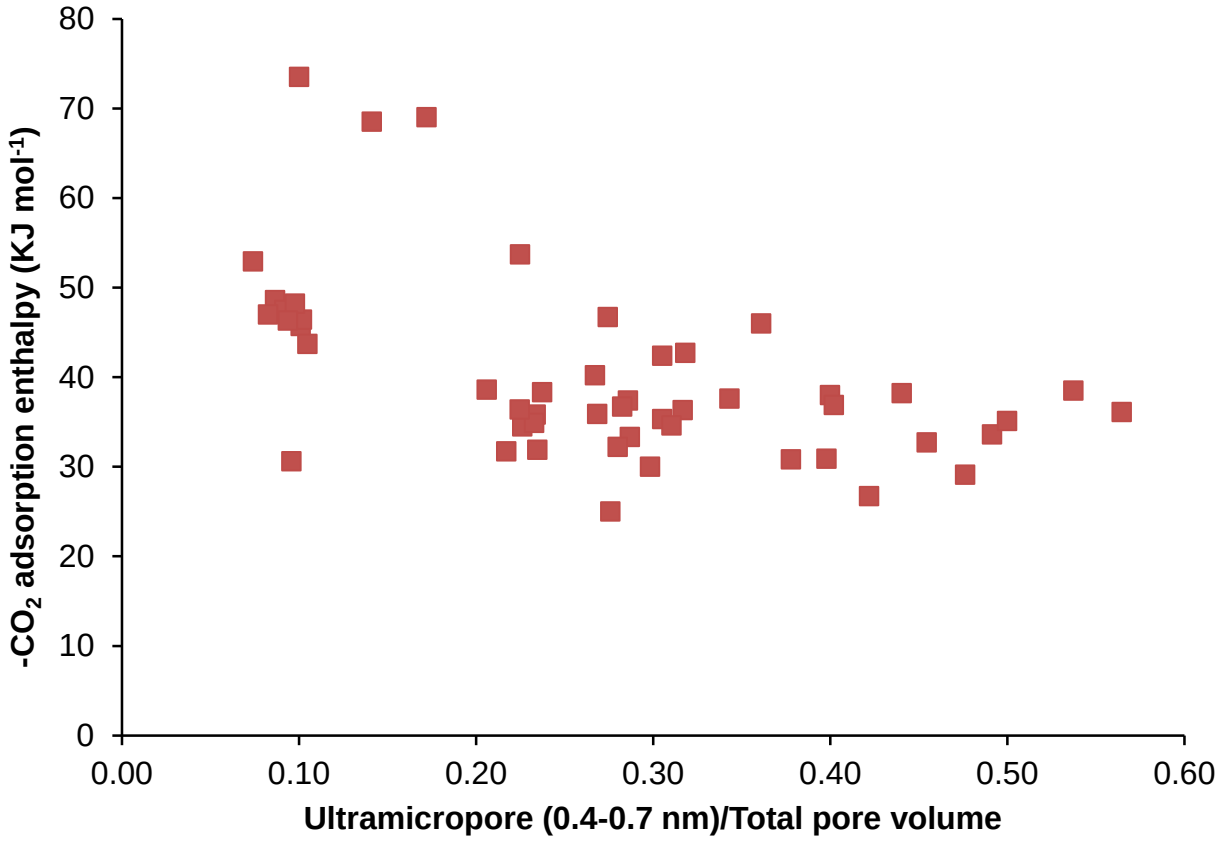

Plot of K_1 for CO_2 adsorption against ultramicropore (0.4-0.7 nm) volume/total pore volume

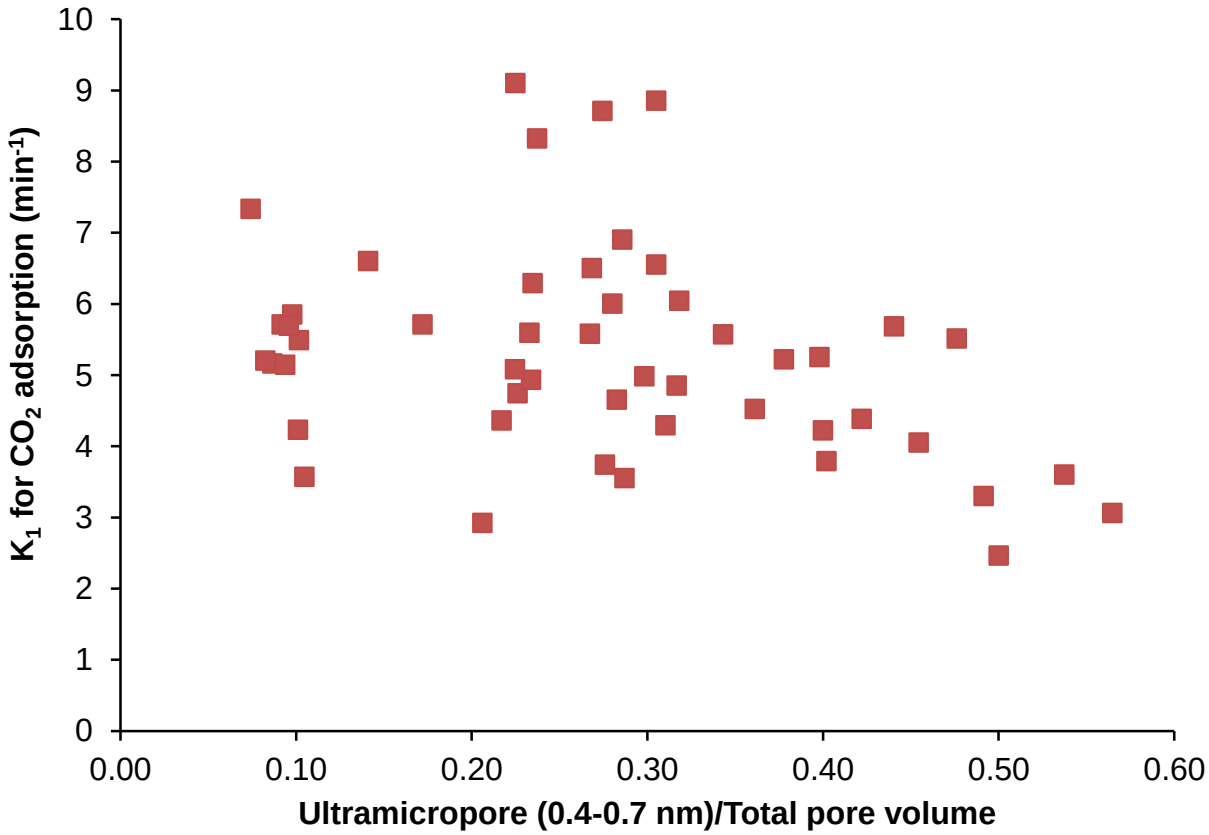

Plot of CO_2 adsorption capacity against supramicropore volume/total pore volume

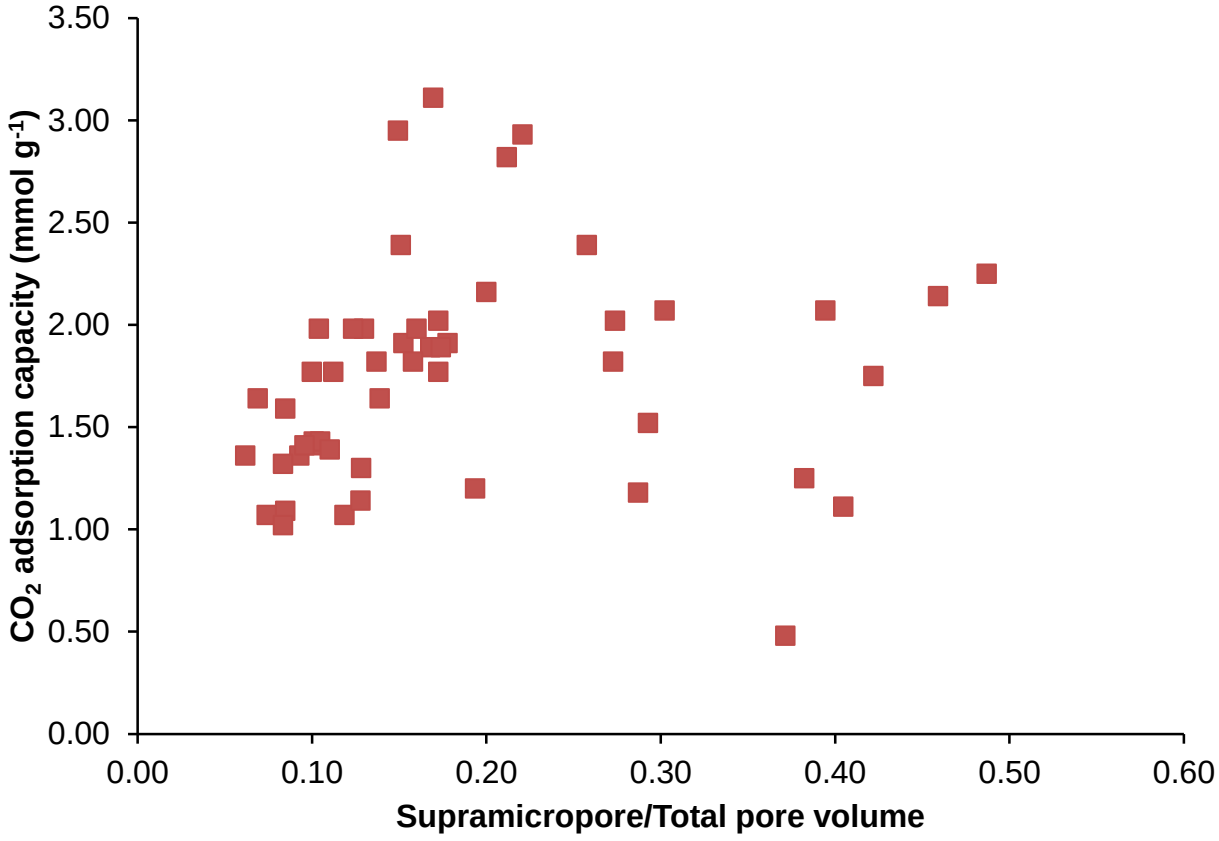

Plot of CO_2 adsorption enthalpy against supramicropore volume/total pore volume

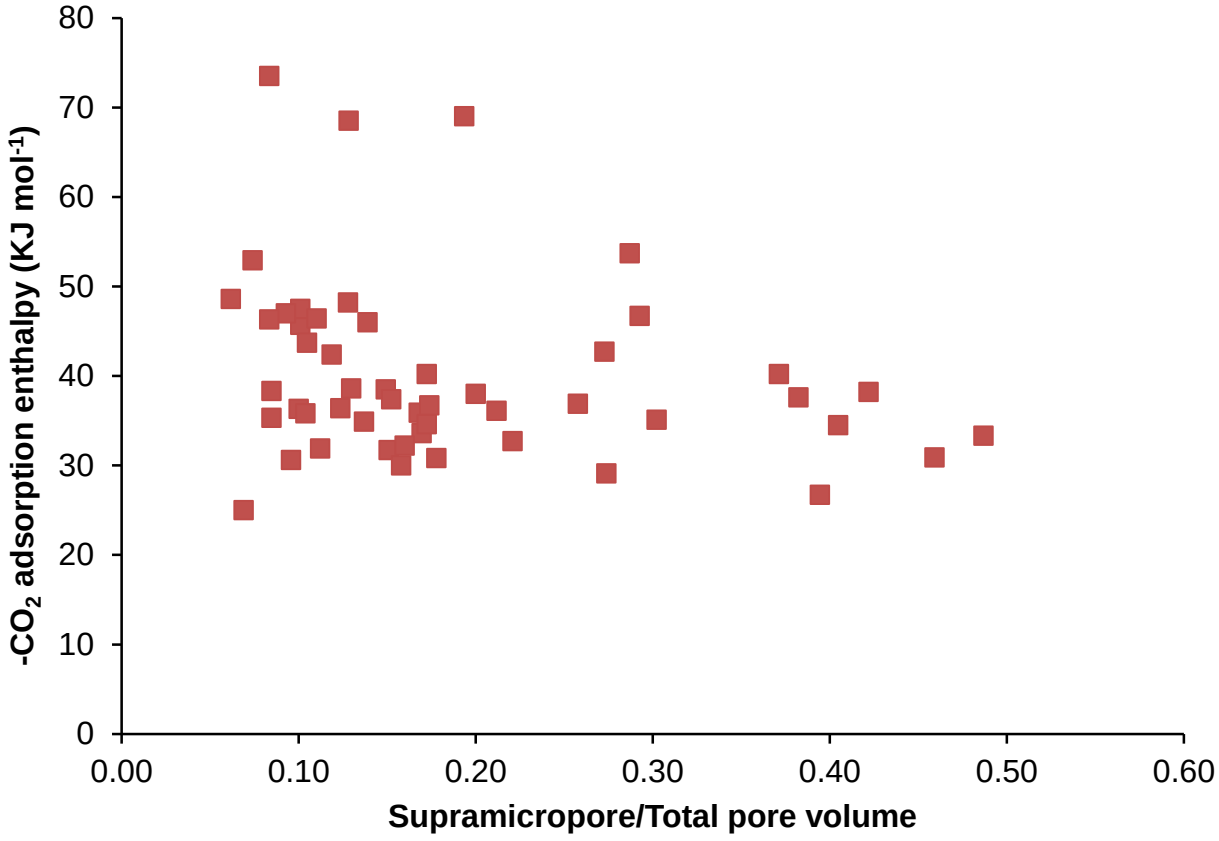

Plot of K_1 for CO_2 adsorption against supramicropore volume/total pore volume

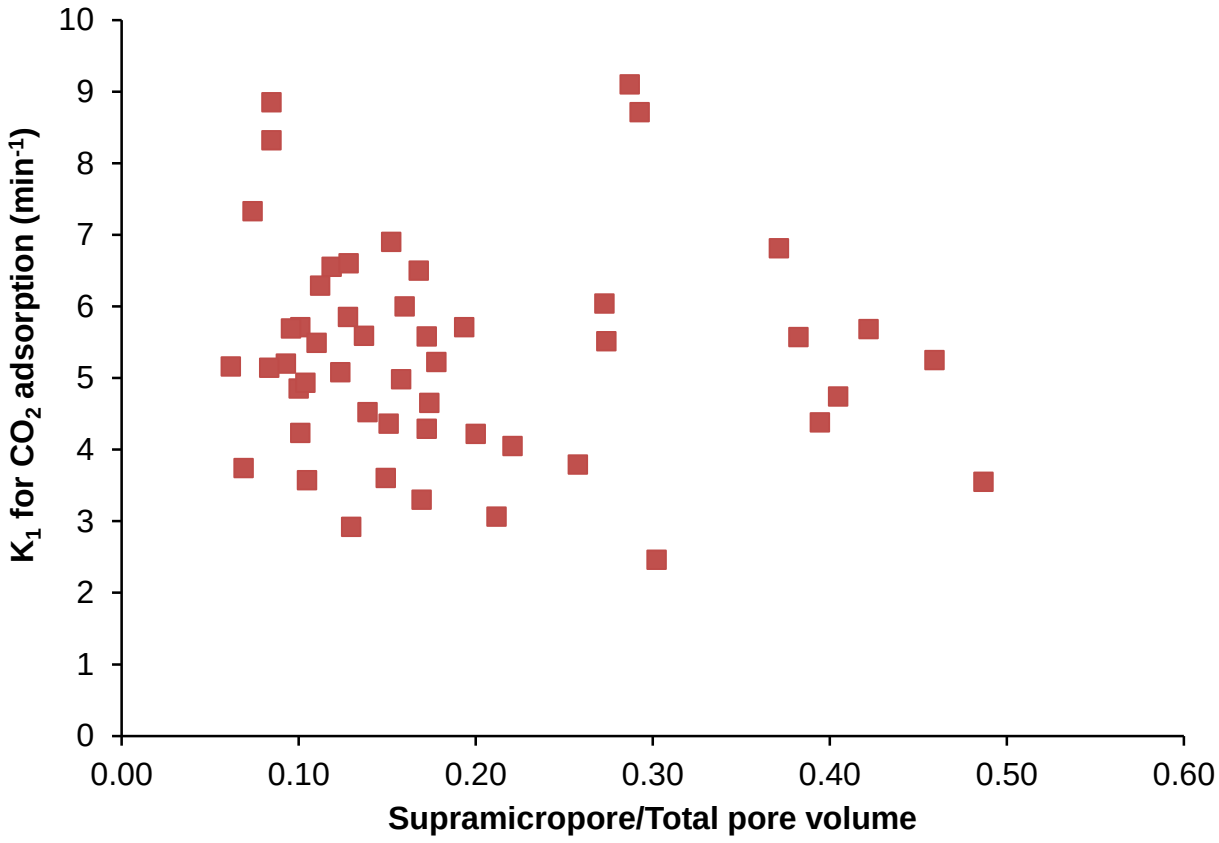

Plot of CO_2 adsorption capacity against micropore volume/total pore volume

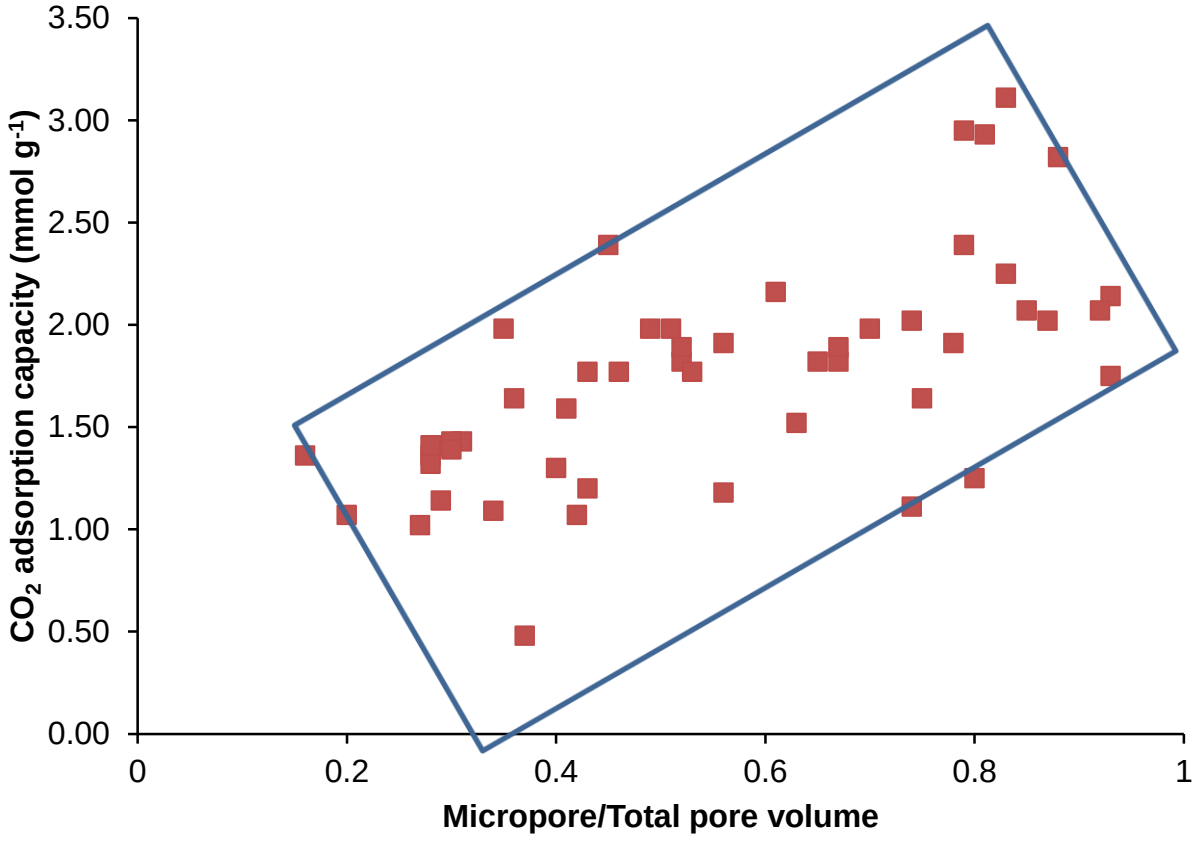

Plot of CO_2 adsorption enthalpy against micropore volume/total pore volume

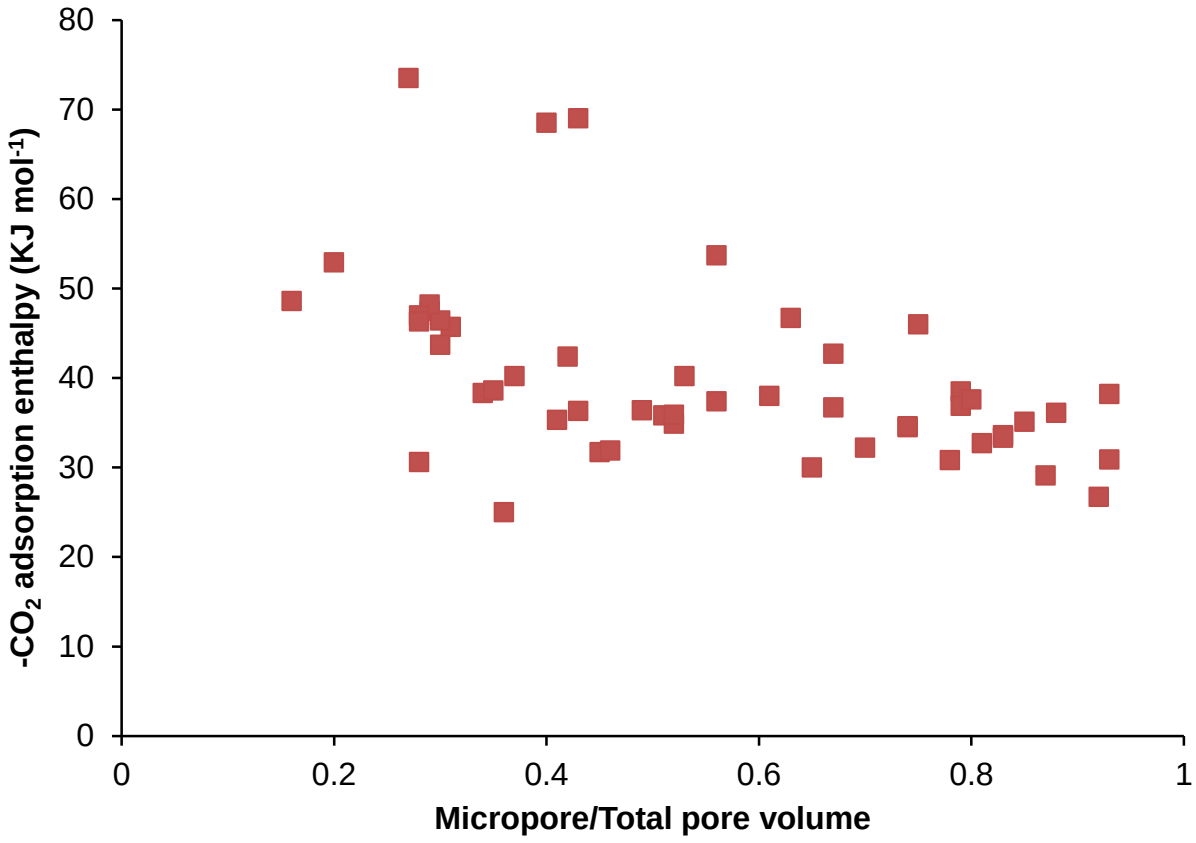

Plot of K_1 for CO_2 adsorption against micropore volume/total pore volume

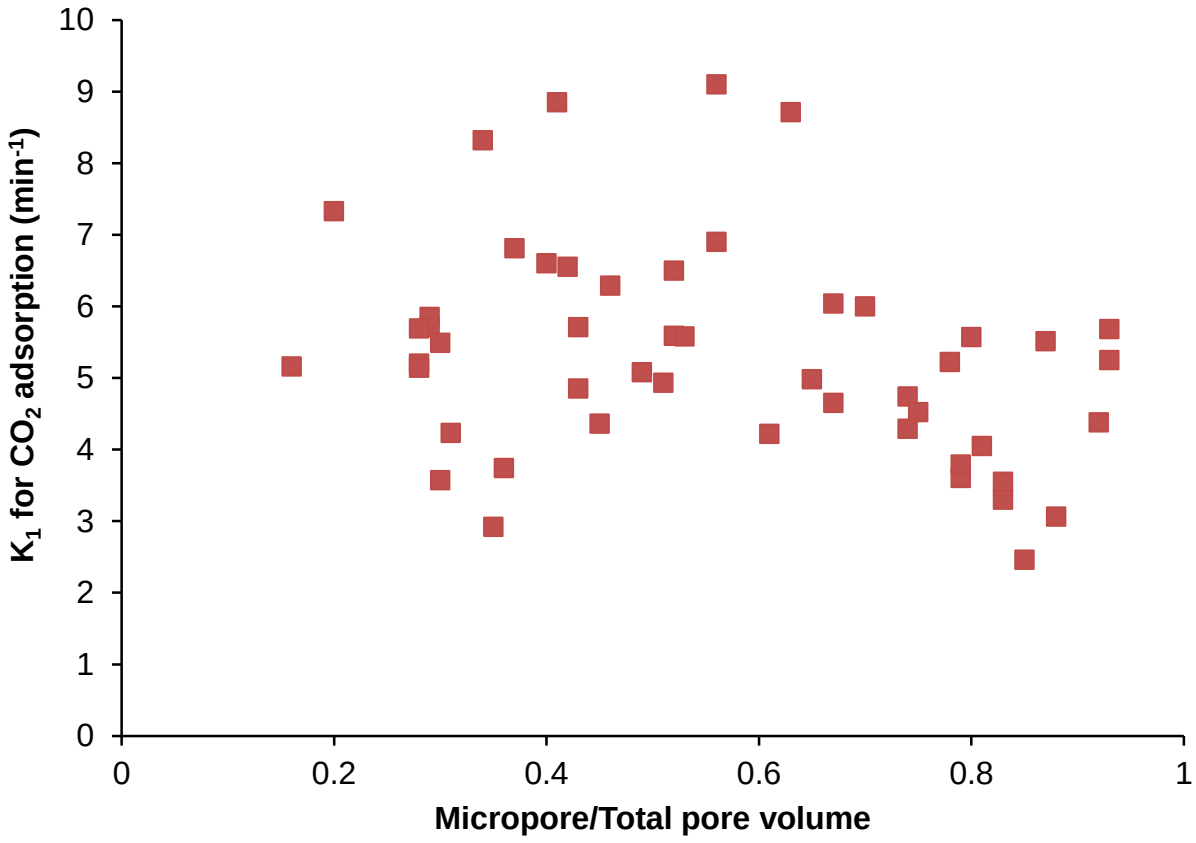

Plot of CO_2 adsorption capacity against mesopore volume/total pore volume

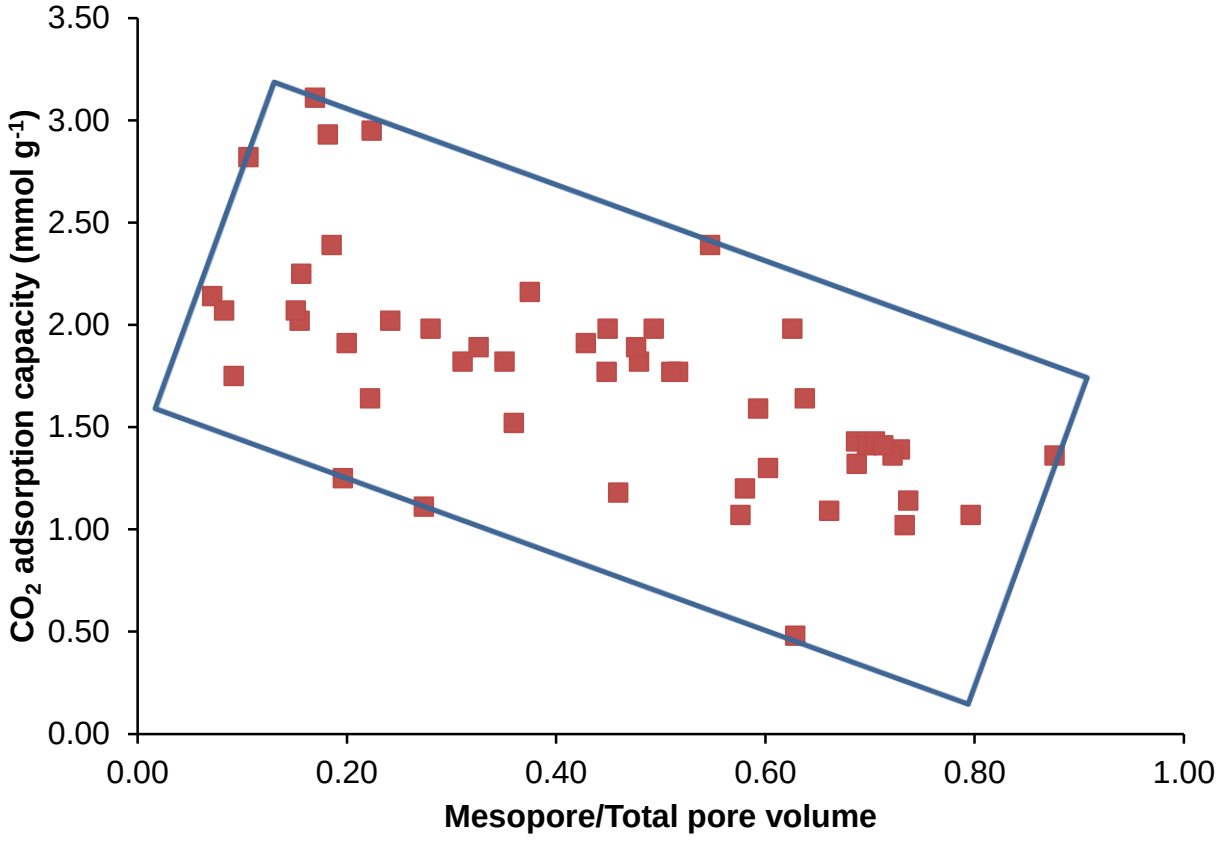

Plot of CO_2 adsorption enthalpy against mesopore volume/total pore volume

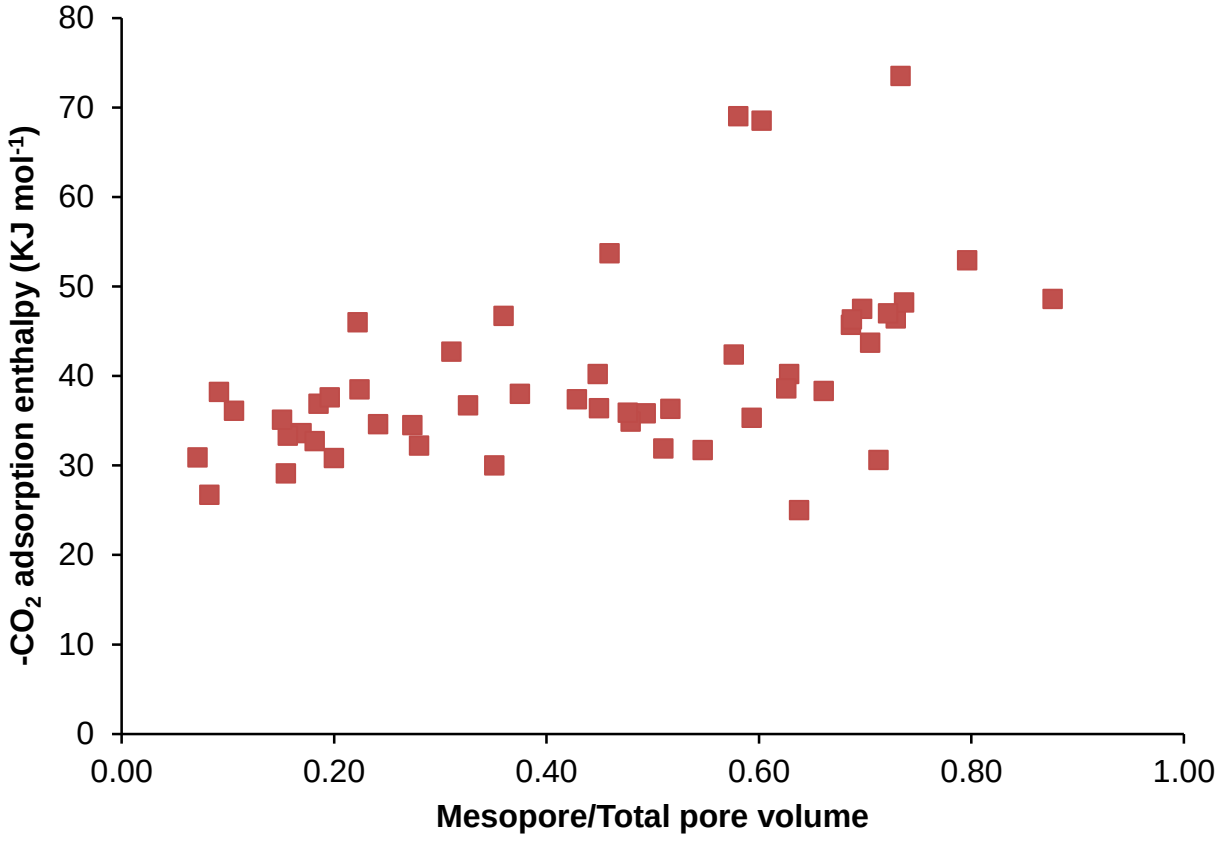

Plot of K_1 for CO_2 adsorption against mesopore volume/total pore volume

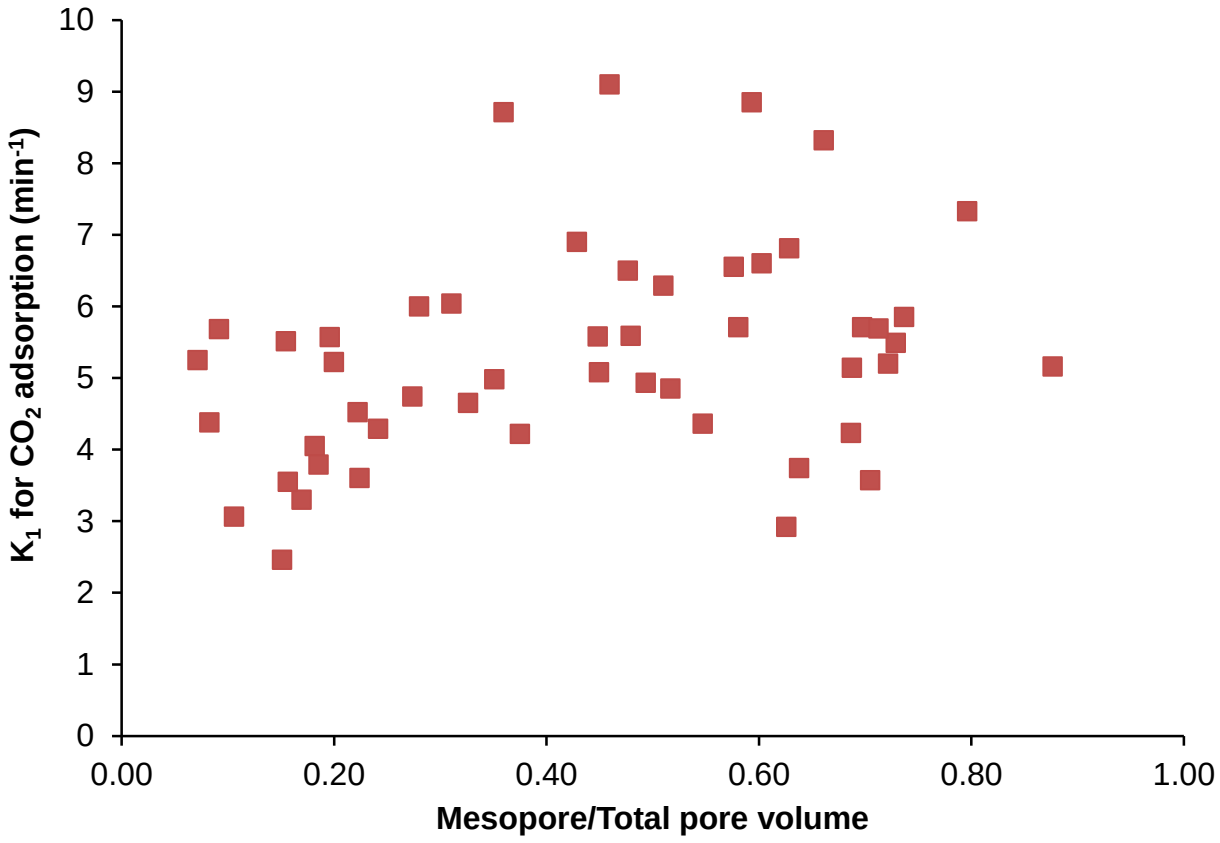

Plot of CO_2 adsorption capacity against micropore volume/mesopore volume

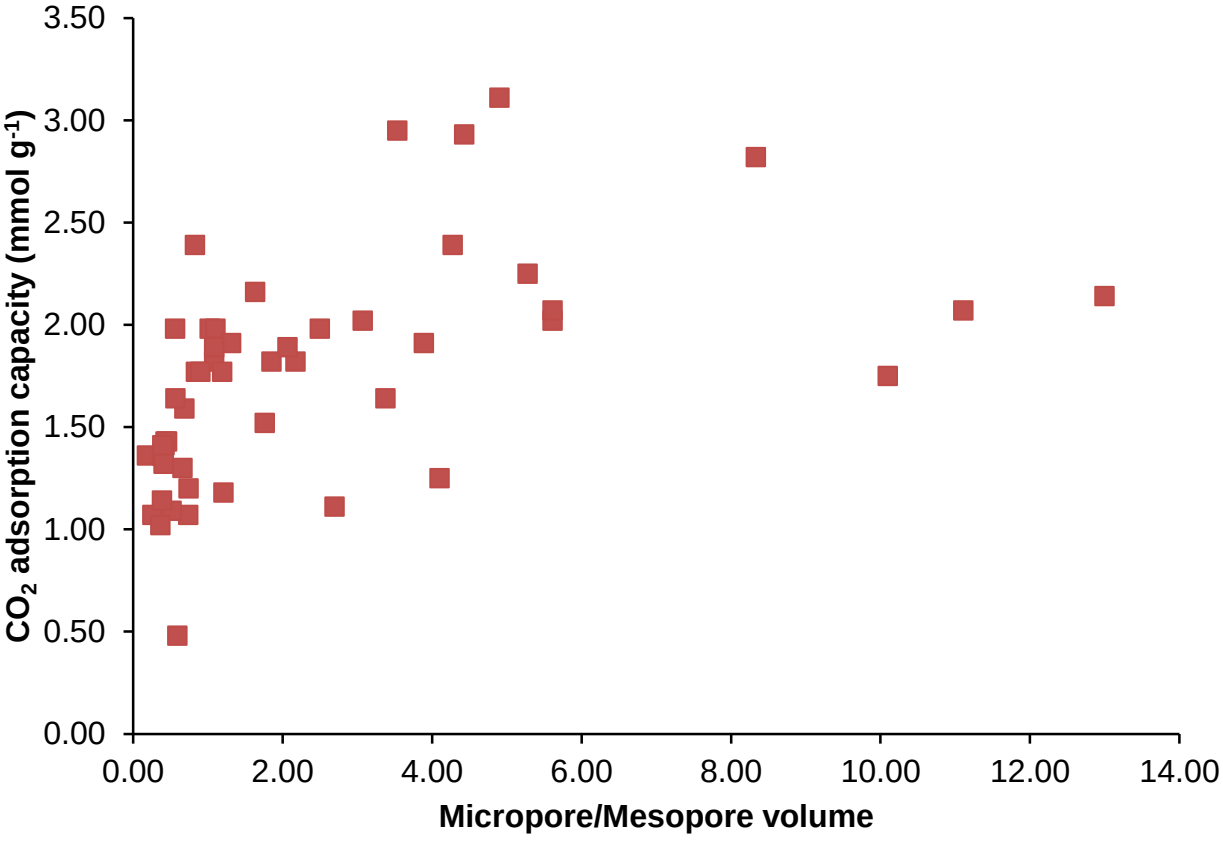

Plot of CO_2 adsorption enthalpy against micropore volume/mesopore volume

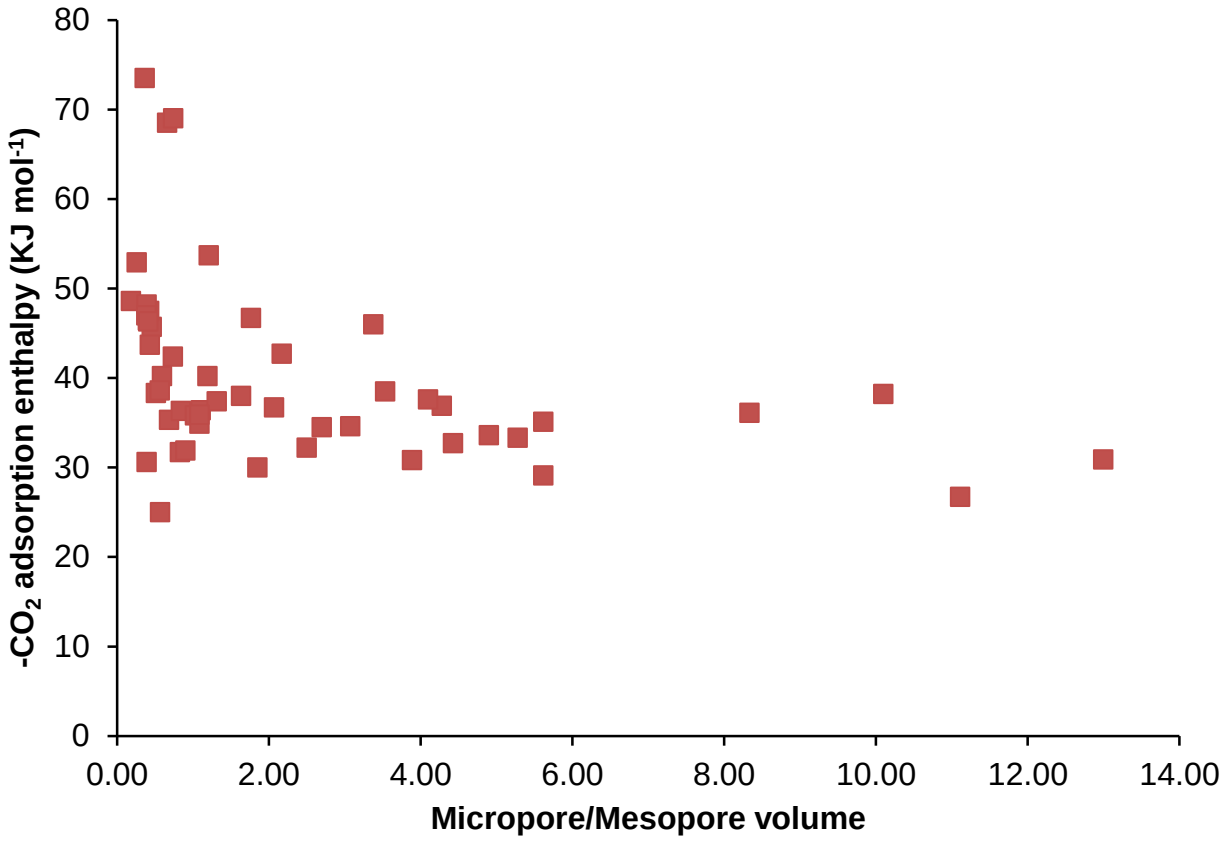

Plot of K_1 for CO_2 adsorption against micropore volume/mesopore volume

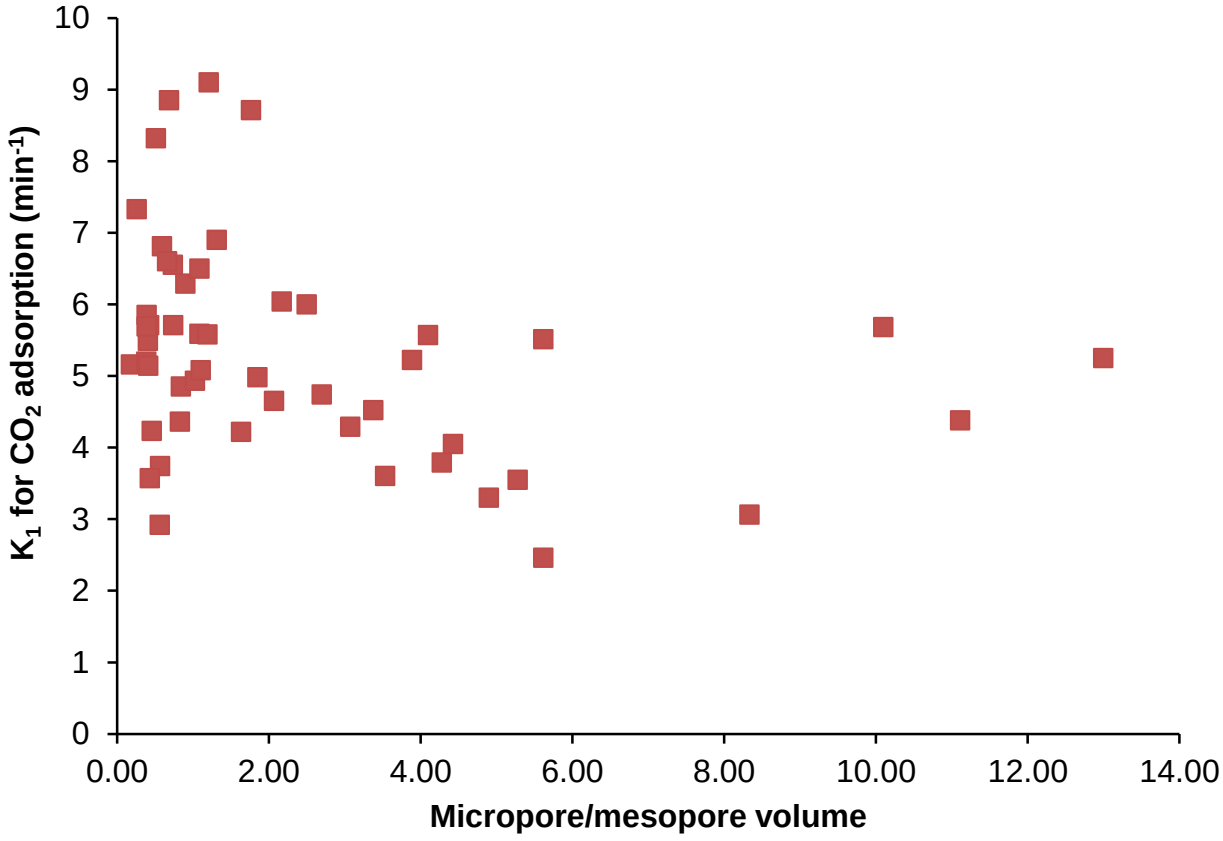

Mass changes during CO_2 adsorption at 35 ^oC and various CO_2 partial pressures

The spikes visble before each CO_2 adsorption are artifacts caused by pressure and flow rate fluctuations as the CO_2 gas supply was opened and the supply of CO_2 and N_2 was rebalanced.

S800 with CO_2 partial pressure = 0.83

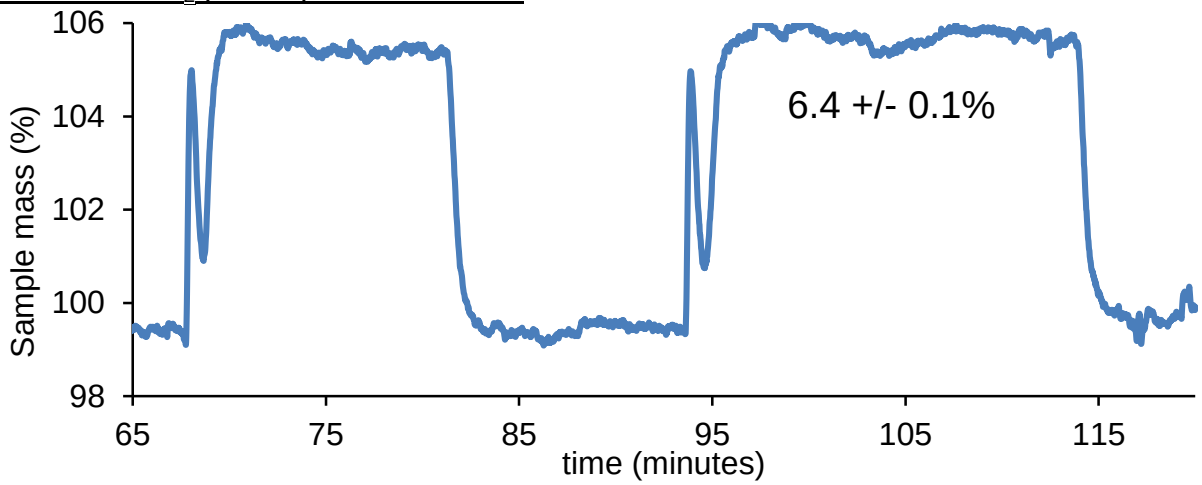

S800 with CO_2 partial pressure = 0.58

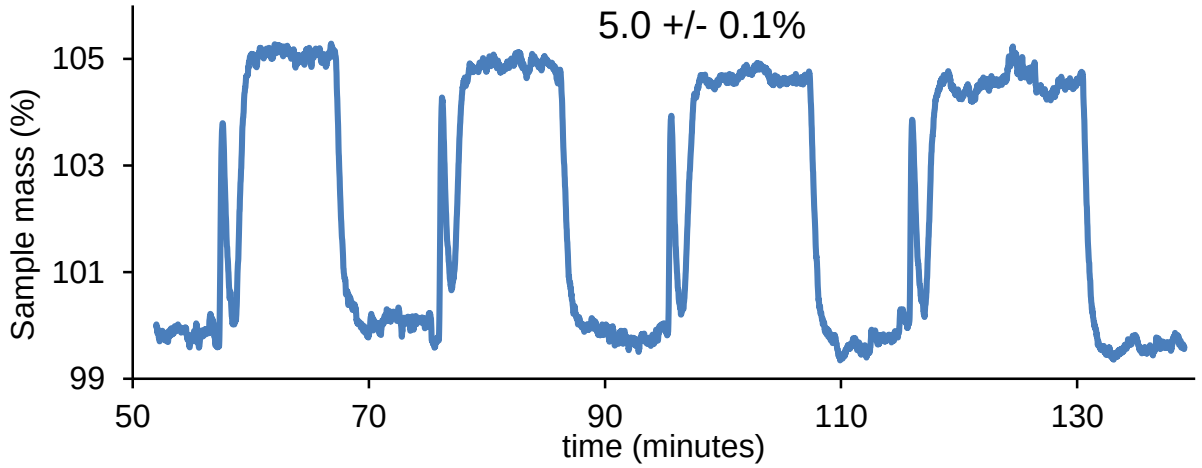

S800 with CO_2 partial pressure = 0.42

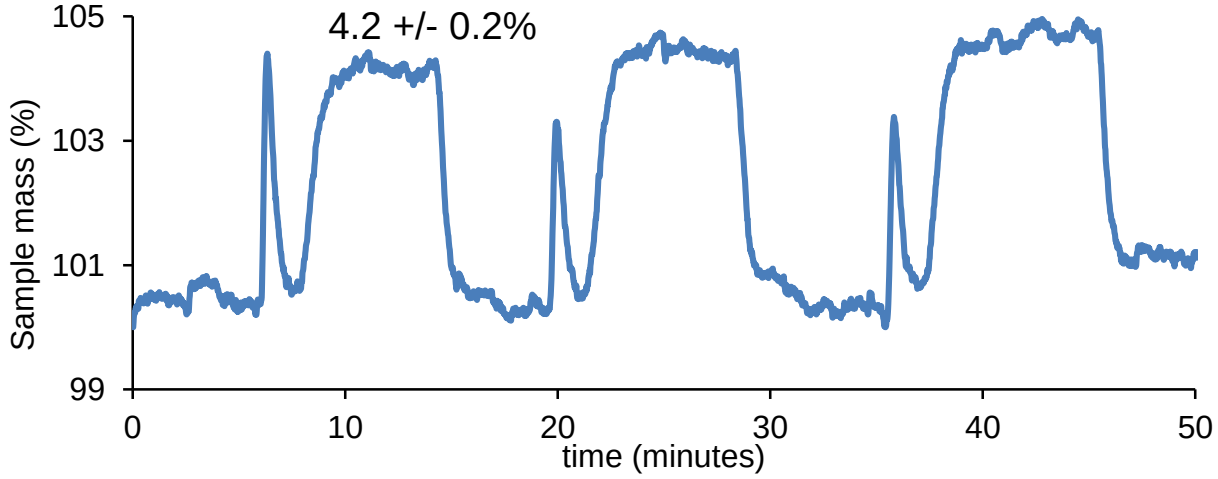

S800 with CO_2 partial pressure = 0.33

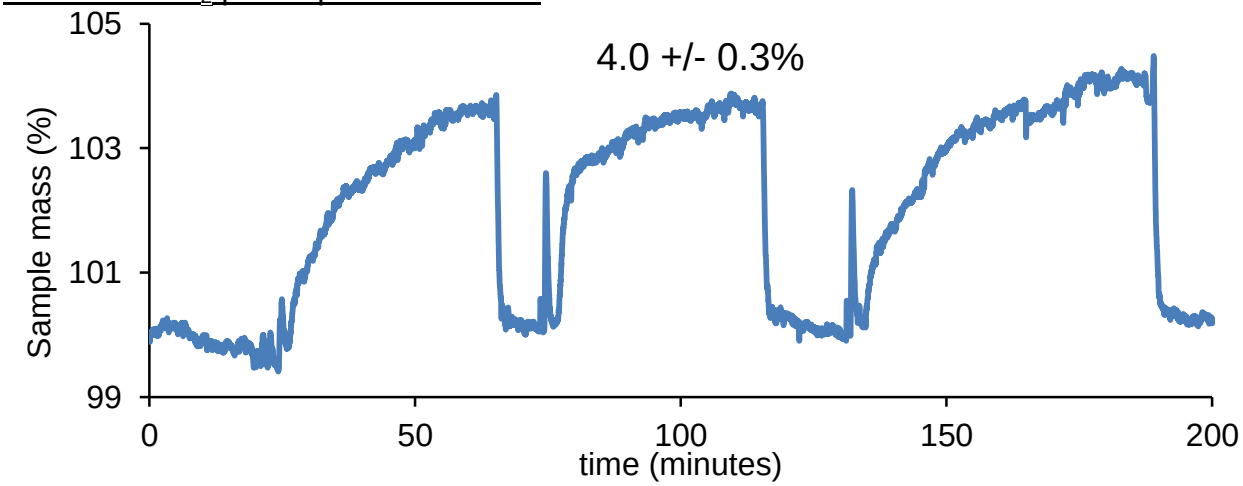

S800 with CO_2 partial pressure = 0.25

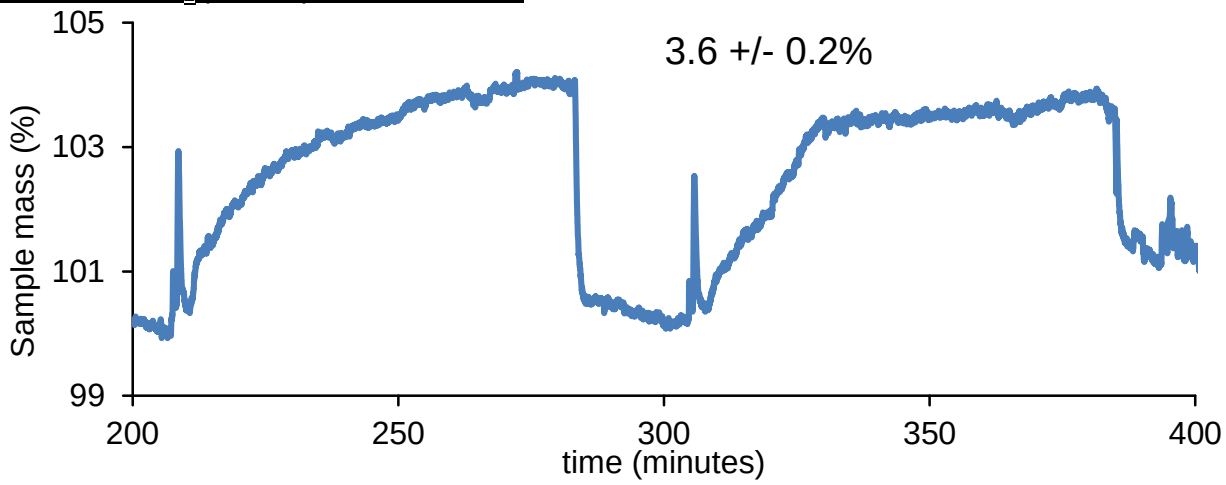

S800 with CO_2 partial pressure = 0.15

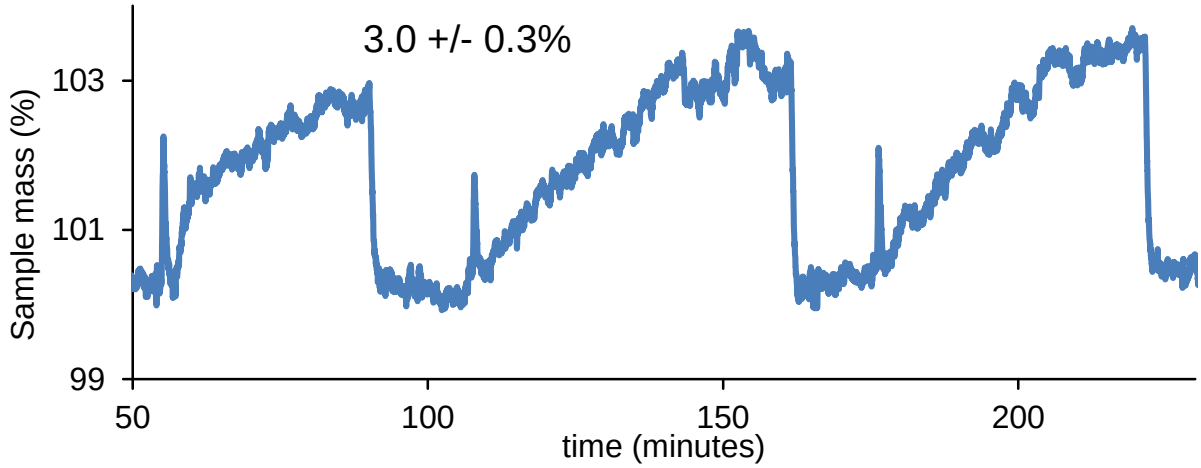

S800K2 with CO_2 partial pressure = 0.83

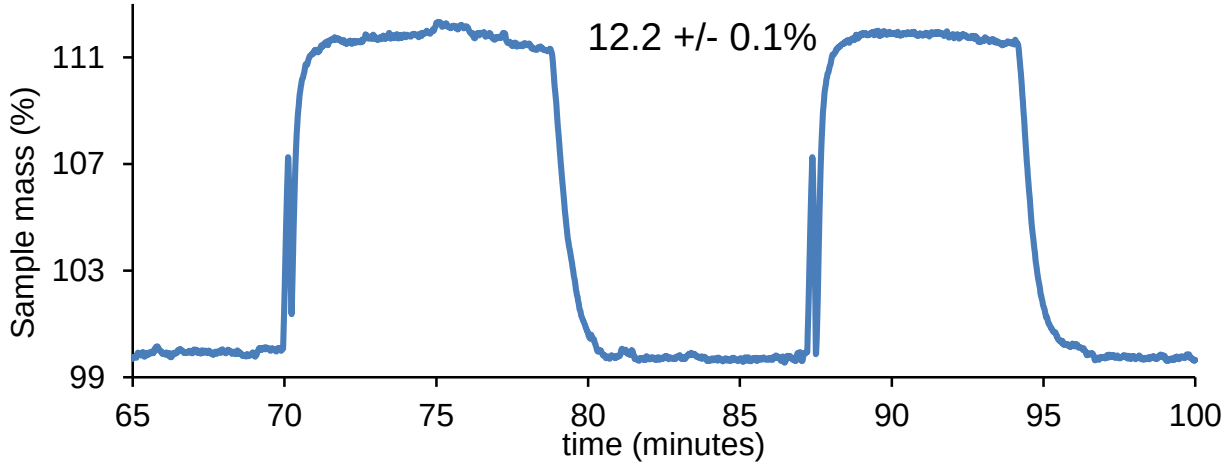

S800K2 with CO_2 partial pressure = 0.58

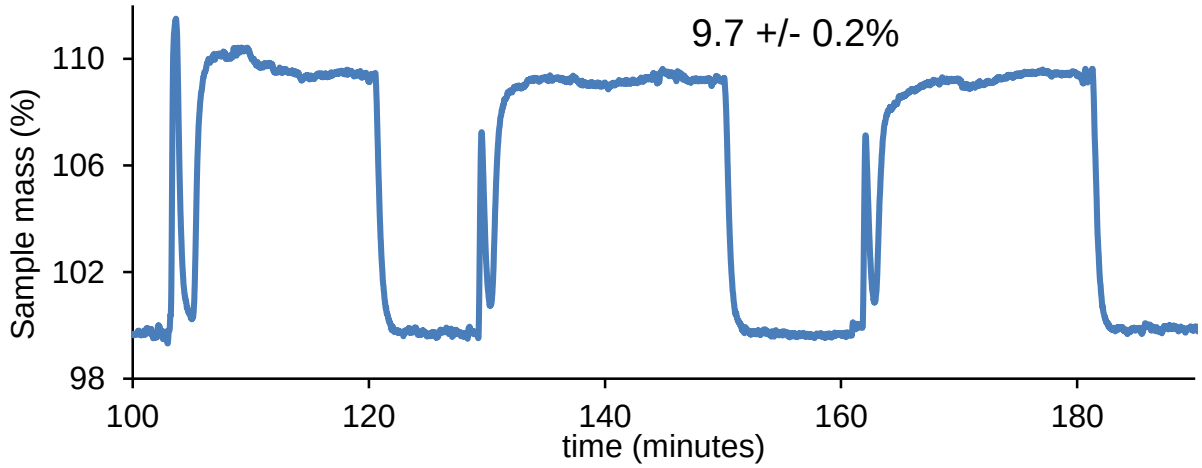

S800K2 with CO_2 partial pressure = 0.42

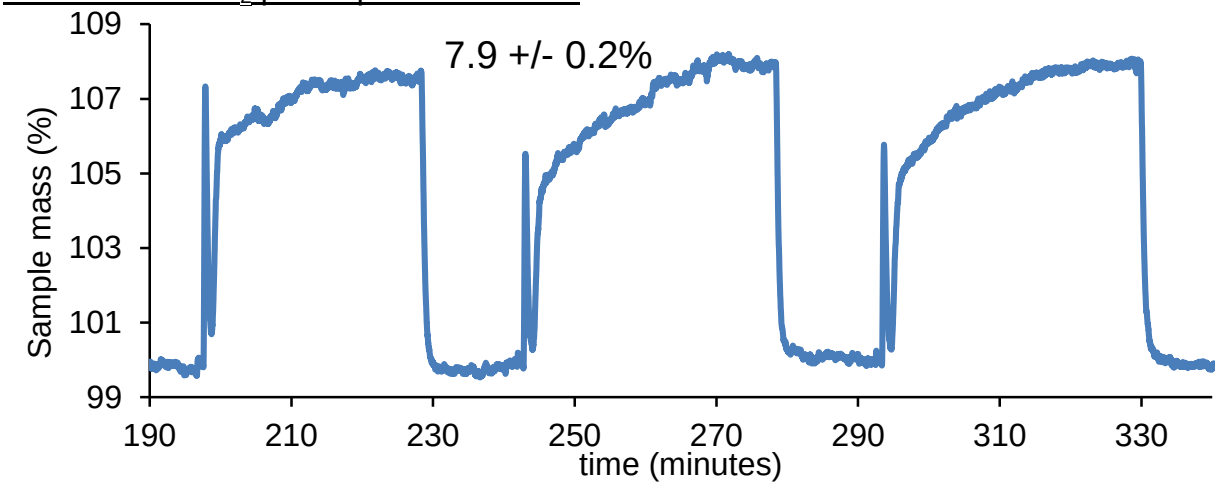

S800K2 with CO_2 partial pressure = 0.33

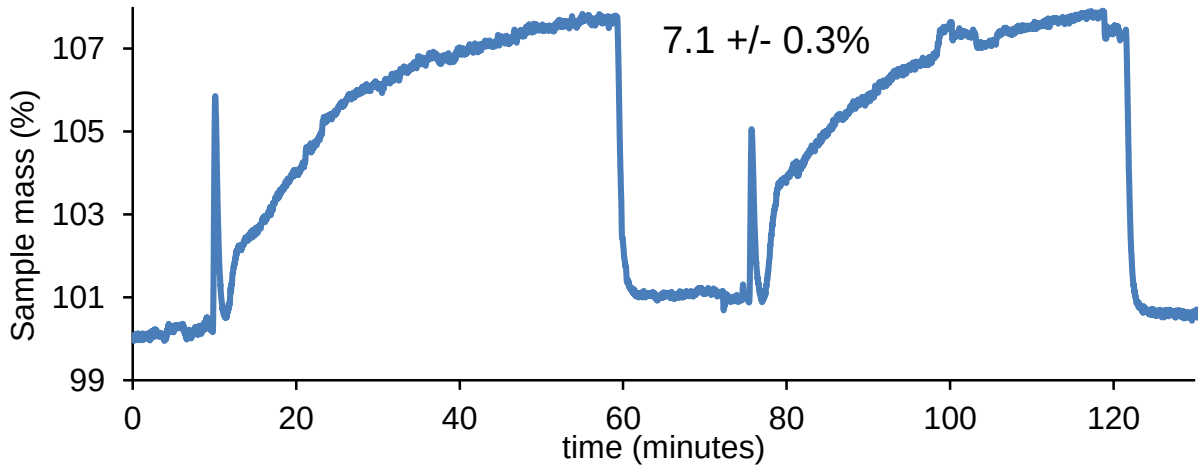

S800K2 with CO_2 partial pressure = 0.25

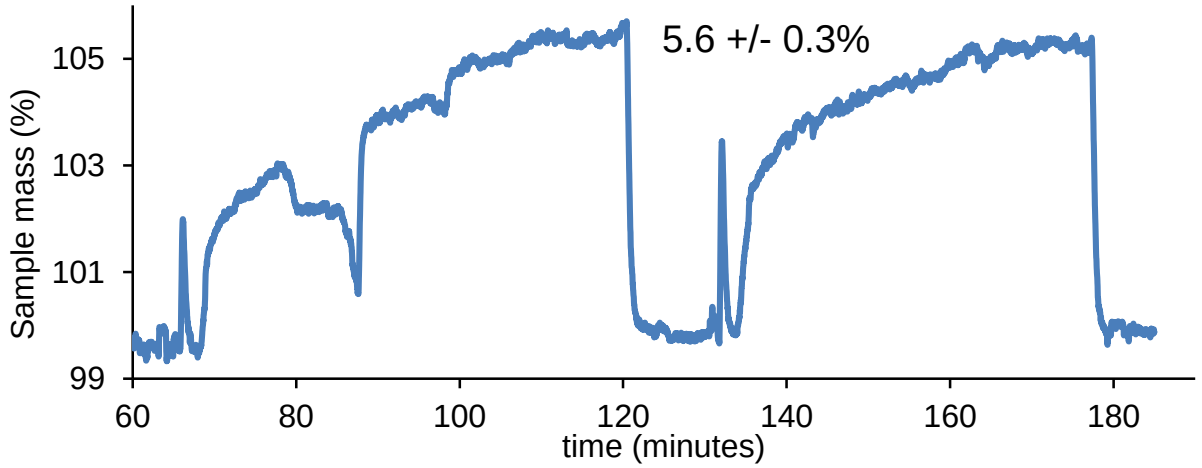

S800K2 with CO_2 partial pressure = 0.15

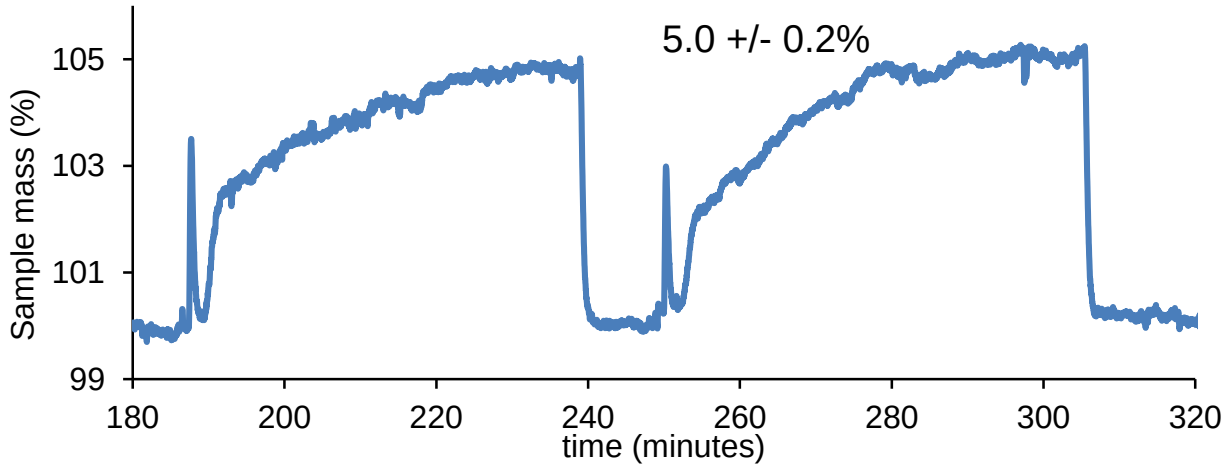

Tabulation of CO_2 adsorption capacities at various CO_2 partial pressures

CO_2 content (%)	CO_2 partial pressure (bar)	CO_2 uptake			
		S800		S800K2	
		%	mmol g^{-1}	%	mmol g^{-1}
100	1	6.7±0.1	1.50±0.02	13.7±0.2	3.11±0.05
83	0.83	6.4±0.1	1.45±0.02	12.2±0.1	2.77±0.02
58	0.58	5.0±0.1	1.14±0.02	9.7±0.2	2.20±0.05
42	0.42	4.2±0.2	0.95±0.05	7.9±0.2	1.80±0.05
33	0.33	4.0±0.3	0.91±0.07	7.1±0.3	1.61±0.07
25	0.25	3.6±0.2	0.82±0.05	5.6±0.3	1.27±0.07
15	0.15	3.0±0.3	0.68±0.07	5.0±0.2	1.14±0.05

Fitting of the Freundlich isotherm to the pressure varied CO_2 adsorption data

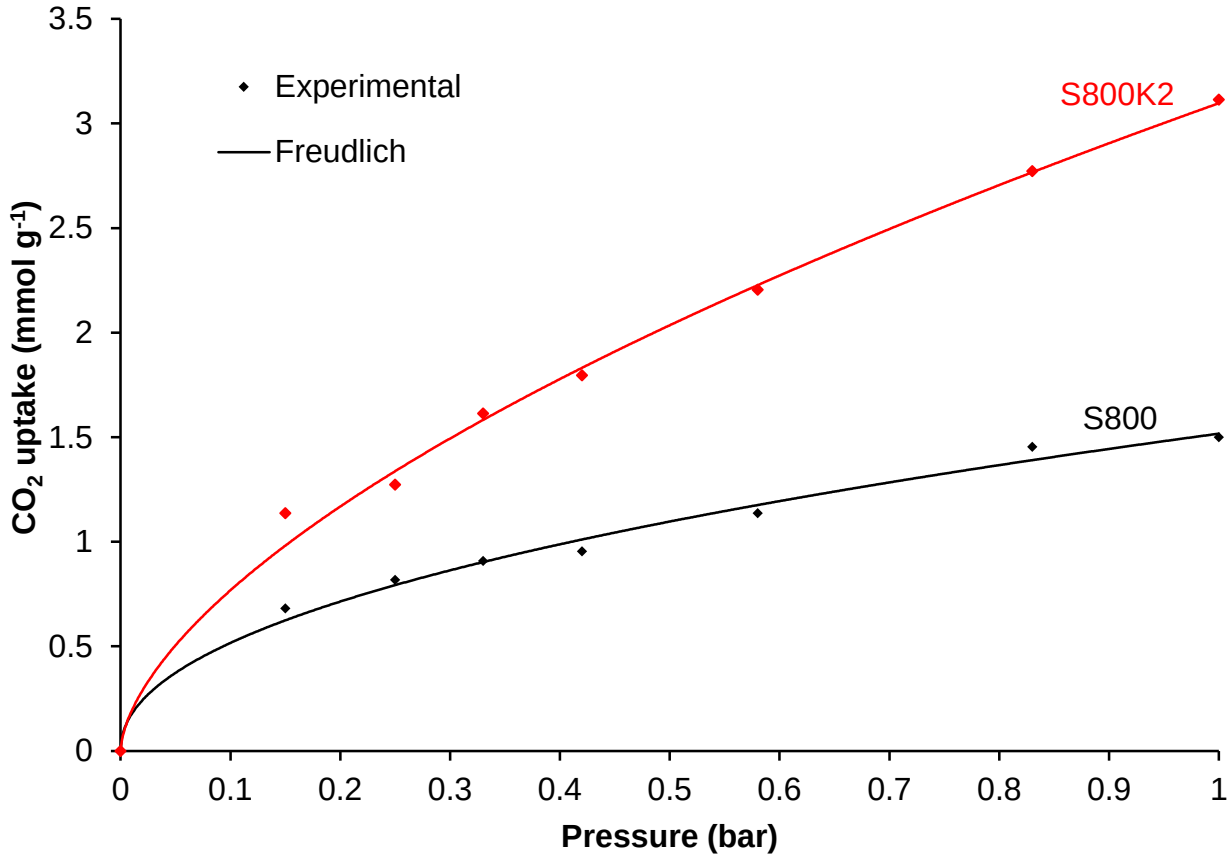

Tabulation of Freundlich parameters for the CO_2 adsorption isotherm

Model	Parameters	S800	S800K2
Freundlich	K_F (mmol g^{-1} $bar^{-1/n}$)	1.757	3.097
	1/n	0.468	0.606
	R^2	0.994	0.998

Gibbs free energies (-1.4 KJ mol^{-1} for S800 and -2.9 KJ mol^{-1} for S800K2) calculated based on the adsorption constant K_F at 308 K ($\Delta G^o = -RT \ln K_F$) are consistent with the values obtained using pure carbon dioxide at 298 K and 323K (-2.1 and -1.4 KJ mol^{-1} for S800; and -3.2 and -2.5 KJ mol^{-1} for S800K2) given in Table 4 of the manuscript.